The Geochemistry of Spitskop and Related Alkaline Complexes

by

R.E. Harmer

Thesis Presented for the Degree
of
DOCTOR OF PHILOSOPHY

in the
Department of Geochemistry
UNIVERSITY OF CAPE TOWN

December 1992

The Geochemistry of Spitskop and Related Alkaline Intrusions

ABSTRACT

The Spitskop Alkaline Complex is part of the Pilanesberg Suite of carbonatite and alkaline complexes which intruded the central Kaapvaal Craton during the time period 1400-1200 Ma.

Spitskop consists of successive intrusions of pyroxenite, ijolite, nepheline syenite and carbonatite and is surrounded by a zone of fenitised granitic country rock. Pyroxenite is preserved as screens and xenoliths within intrusive ijolite and is consists of diopsidic clinopyroxene with minor titanomagnetite and mica. Textures in the pyroxenite suggest a cumulate origin. Two different types of ijolite are distinguishable texturally: a fine to medium-grained variety characterised by euhedral nepheline and fine to acicular interstitial aegerine-augite ("Type-I"); and a variety in which anhedral nepheline and clinopyroxene form "granoblastic" mosaics interspersed with pyroxene aggregates. The field occurrence of Type-I ijolites as intrusive dykes and sheets indicate an essentially magmatic origin for these ijolites. Type-II ijolites appear to have been generated from the "nephelinisation" of the pyroxenite: essentially the addition of felsic components from intrusive ijolite with subsequent recrystallisation. A sub-group of "granoblastic" ijolites with high Ni contents (which correlate with MgO) are not consistent with a derivation from the pyroxenites and it is argued that these ijolites are the products of extensive metasomatism of Bushveld upper zone gabbros.

Nepheline syenites were emplaced into the pyroxenite-ijolite assemblage as a series of sheets. Field, textural and geochemical data suggest that these bodies are not connected and originated from separate magma batches. Nepheline syenites from the sheet on the farm Rietfontein are isotopically equivalent to the magmatic ijolites whereas syenites from the other bodies have different, generally more enriched, isotopic signatures.

Carbonatites form a triangular-shaped plug-like intrusion eccentrically positioned within the silicate units. The carbonatite plug is composite: calcio-carbonatites form an incomplete marginal facies to volumetrically more significant

magnesio-carbonatites. Later magnesio-carbonatite mingled with and possibly transformed portions of the earlier calcio-carbonatitic magma producing a hybrid "dolomitic-sövite" zone. The outer margins of the carbonatite mass are smooth and no evidence is noted of forceful disruption nor of metasomatism of the bounding silicate units by the emplacement of the carbonatite.

Fenitisation processes are well displayed at Spitskop: fluids emanating from the Complex have extensively metasomatised both the Lebowa Granite Suite (LGS) country rocks and a large xenolith of material from the upper zone of the underlying Rustenburg Layered Suite (RLS). Vanadium contents in magnetite seams included in the RLS material indicate that the xenolith is composed of material from two different stratigraphic levels in the upper zone: one from sub-zone A, the other from sub-zone C. Chemical changes noted in the fenitisation of the LGS country rocks indicate that the metasomatising fluids were carbonatitic and introduced Ca, Na, Fe, Al and Sr into the granites while removing Si, K, Rb and LREE.

Despite apparently systematic variations in clinopyroxene composition in the pyroxenites, ijolites and nepheline syenites, whole rock major and trace element variations amongst the silicate units of the Complex argue that the ijolites and nepheline syenites are not related through a simple crystal-liquid fractionation process of the constituent phases of these rocks. A large contrast exists in $\varepsilon_{(Sr)}$ and $\varepsilon_{(Nd)}$ compositions between the silicate and carbonatitic units of the Complex which indicates that the carbonatites cannot have originated as the residues from the differentiation of the silicates, nor can the silicates and carbonatites represent immiscible liquid pairs.

Experimental evidence indicates that magnesio-carbonatite can be produced by direct melting of pargasitic lherzolite in the presence of CO_2 . The evolution from magnesio- to calcio-carbonatite compositions is unlikely to occur through fractionation of olivine and/or dolomite, its known liquidus phases, but can be effected through interaction with mantle wall rocks en route to surface. A compilation of published Sr and Nd isotopic data for world carbonatites shows very limited variation and suggests that carbonatites are derived from mantle sources which bear similarities to those producing ocean island basalts.

New data from the Pilanesberg Suite complexes shows that carbonatites from most of these complexes have isotopic compositions which are similar to the variations established for world carbonatites. Carbonatites from the Spitskop and

Stukpan complexes deviate from this field and indicate contributions from a reservoir with time-integrated enrichment in Nd/Sm. Silicate components of the Spitskop Complex essentially extend the trend defined by the carbonatites to higher $\varepsilon_{(Sr)}$ and more negative $\varepsilon_{(Nd)}$ values.

The preferred model considers carbonatites as primitive mantle melts of carbonated peridotite mantle. Because of the topology of the peridotite-CO_2 solidus ascending carbonatite melts are trapped at depths of about 75km. Repeated influxes of carbonatite transforms the peridotite to the stage that it meltsto produce an undersaturated alkaline silicate melt which ascends to surface. Only once a magma pathway partially sleeved with alkalic melt, is established to surface, can influxes of carbonatite melt ascend to shallow levels. This model satisfies the isotopic and field relationships between components of the Spitskop Complex and satisfactorily explains the universal observation that, when associated in an alkaline complex, carbonatites always post-date the emplacement of silicate magmas.

Acknowledgements

It is a genuine pleasure to gratefully acknowledge the people and institutions who have assisted me in completing this dissertation:

- My thanks to my three supervisors Andy Duncan, the late Tony Erlank and Dave Reid for their help, constructive criticism, encouragement, cajoling and threats; but mostly for their patience over the numerous years and missed deadlines it has taken to finalise this thesis.

- My gratitude to various bosses down the years: Drs. Alwyn Burger, Jan van Zijl and Johann de Beer at the CSIR; and Profs Gerhard von Gruenewaldt and Sybrand de Waal at UP for providing the opportunities and support to persue this research, often when more pressing matters needed attention. The CSIR, in particular, is thanked for their support and for funding most of the analytical work while I was in their employ.

- I thank Bruce Eglington for his moral support, his good humoured readiness to act as a sounding board for new ideas, however hair-brained; but mostly for his unfailing faith that I would actually complete this dissertation! My gratitude, too, to past colleagues at the CSIR for their assistance with technical chores in the laboratory: in particular to Darrell Farrow, Elke Grösser, Malherbe Auret and Yootha Stander. Elijah Nkhosi and Jakob Twala ably assisted with various crushing, mineral separation and filament stringing jobs through the years.

- I thank colleagues at the Bushveld Institute and Geology Department, University of Pretoria for accepting my frequent absences over the past 18 months while this thesis was being written up. Particular thanks are due Marina van Leeuwen for encouragement and for expertly drafting the maps and some figures, often "by yesterday"!

- Many people generously provided hospitality during my visits to UCT: my gratitude to my sister and brother-in-law Judy and Dereck Kirby, to Rich and Brenda Armstrong and family, and to Mike and Lindsay Watkeys who, respectively, are guilty of greatly improving my appréciation of Cape seafood, Cape wine and passage cricket!

- In closing, my deepest gratitude to my wife Barbara: for believing in me, for her support, her strength, her endless encouragement, and for accepting my ill humour for so many years. Thanks, too, to my sons Matthew and Simon for putting up with a part-time daddy: without their efforts this thesis may have been completed sooner!

Thank you all.

Jock Harmer
December 1992

Contents

Appendices

Appendix A: Analytical and Calculation Procedures

Appendix B: Data Tables

Chapter 1: Introduction

1.1. Geological Setting of the Proterozoic Alkaline Intrusions of the Kaapvaal Craton

During the late Proterozoic a number of alkaline and tholeiitic igneous intrusions were emplaced into rocks of the Kaapvaal Craton in central South Africa. Intrusions of tholeiitic affinity include the Timbavati gabbros (SACS, 1980; Bristow *et al.*, 1982) and the Trompsberg intrusion (Davies *et al.*, 1970). More significant are a suite of complexes of alkaline character, many containing carbonatite, which intrude over an area of some 75 000km^2 (Figure 1.1). Most of these complexes fall within the current outcrop region of the Bushveld Complex but also include complexes such as Glenover, to the north west, and Stukpan which sub-outcrops below Karoo cover overlying the south western extremity of the Witwatersrand Basin in the Orange Free State (Verwoerd *et al.*, 1986). Also included within this Proterozoic alkaline suite are the group of kimberlites near Pretoria - the Premier pipe at Cullinan being the best known.

In discussing the relative ages of the carbonatites of the Pilanesberg Suite, Verwoerd (1967) argued that the Spitskop, Tweerivier and Nooitgedacht complexes were significantly younger than the Glenover, Goudini, Kruidfontein and Pienaars River (including the Derdepoort carbonatite) complexes. Verwoerd (1967; table 25, page 284) tentatively assigned an age of approximately 1250 Ma (equivalent to the age of the Pilanesberg Complex : Snelling, 1962; Schreiner and Van Niekerk, 1958) for the latter group of complexes, and a Karoo age of approximately 210 Ma to the Spitskop, Tweerivier and Nooitgedacht complexes. As a result, the South African Geological Survey adopted a Jurassic age for Nooitgedacht and Tweerivier on the 1:250 000 geological map sheet 2526 Rustenburg, yet accepted a Proterozoic age for the Spitskop Complex on the 1:250 000 geological map sheet 2526 Nylstroom. The South African Committee for Stratigraphy (SACS, 1980) publication classifies all of these complexes within the "post-Mokolian" erathem, i.e. post-Bushveld Complex, or post-2.0Ga.

Figure 1.1 : The distribution of alkaline complexes on the Kaapvaal Craton

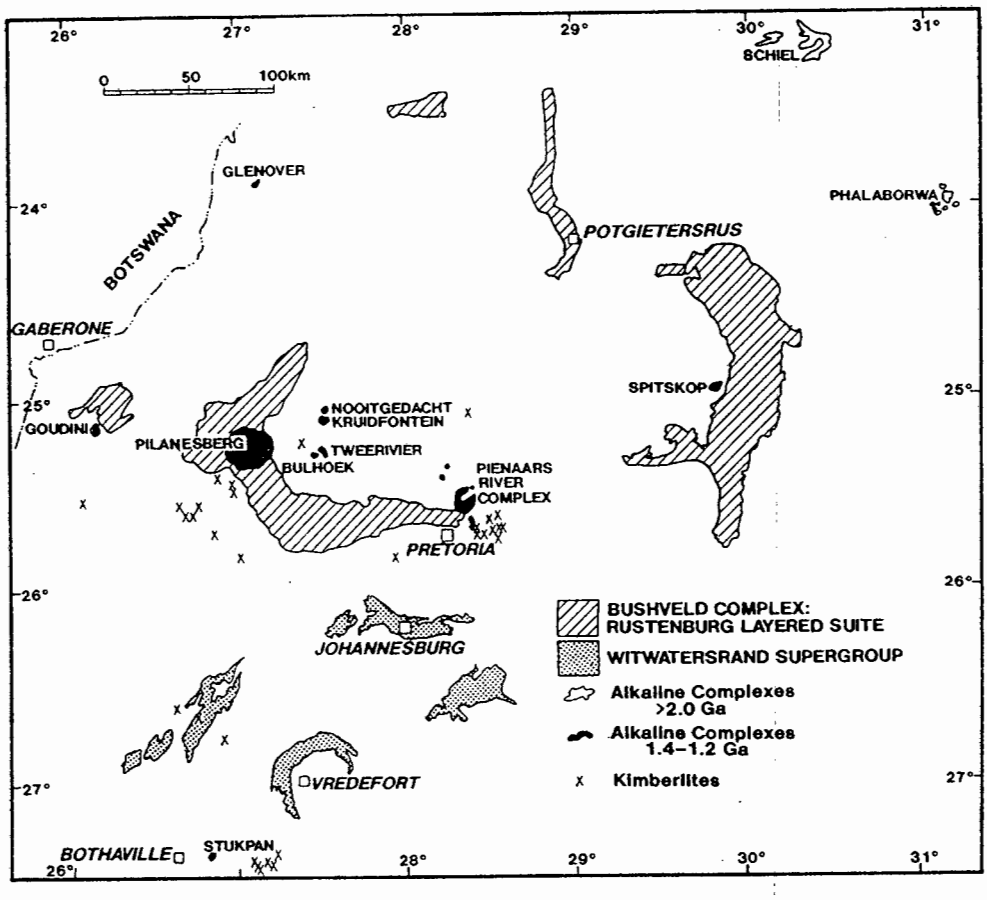

Available age information on these complexes, both published and data accumulated during the current study, is summarised in Table (1.1). The data on which the unpublished dates are based will be presented and discussed in later chapters. From Table (1.1) it may be seen that all the intrusions were apparently emplaced during the period 1420 - 1200Ma. It is worth noting that the Premier kimberlite has been dated at close to 1200Ma (Richardson, 1986; Phillips *et al.*, 1989). (The age reported for the Premier kimberlite by Kramers and Smith (1983) should be viewed with suspicion as their date cannot be reproduced by regressing the data using the uncertainties presented by the authors in their paper.)

These complexes represent the only record of geological activity on the Kaapvaal Craton during the period following the deposition of the Waterberg Group sediments up to the initiation of Karoo sedimentation in the Palaeozoic. While the interior of the Kaapvaal Craton was apparently stable, the period 1420-1200Ma marks the initiation and early phases of the orogeny which produced the Namaqua-Natal metamorphic provinces along the southern and western margins of the Craton (e.g. Reid, 1979; Barton, 1983; Eglington *et al.*, 1989). The largest, and probably the

best known of the alkaline complexes, is the Pilanesberg Complex which comprises some 650 km^2 of syenitic to nepheline-syenitic intrusives and trachytic extrusives (Shand, 1928; Retief, 1963; Lurie, 1973; Lurie and Cawthorn, 1984). Ferguson (1973) proposed that all the alkaline complexes on the Kaapvaal Craton be regarded as the "Pilanesberg Alkaline Province". For ease of reference it is here proposed that the 1400-1200Ma complexes be informally grouped as the "Pilanesberg Suite" to distinguish them from the earlier Proterozoic, ca. 2.05Ga, carbonatite-bearing alkaline complexes of Phalaborwa (Eriksson, 1989) and Schiel (Barton and Ryan, 1977; Barton *et al.*, 1983).

1.2. The Present Study

The present study concentrates on the petrogenetic relationships in the Spitskop Complex and the following four chapters present new data on the distribution, character and isotopic composition of the silicate and carbonatite components of this Complex. These chapters are followed by a description of the metasomatic rocks associated with the Spitskop Complex. The treatment of the Spitskop Complex is concluded with a discussion of the petrogenetic relationships between the different magmatic and metasomatic components. In Chapter 8, a brief review is presented of the geology of the other complexes in the Pilanesberg Suite for which new chemical and isotopic data have been determined. The dissertation closes with a synthesis of the data and a discussion of the implications of the new geochemical and isotopic data from the Pilanesberg Suite complexes for the genesis of carbonatites and associated alkaline silicate igneous rocks in general.

Spitskop was chosen for more detailed study for a number of reasons, the most significant of which are:

(i) the complex contains a well exposed body of carbonatite surrounded by alkalic silicate units and consequently provides an excellent opportunity to investigate the petrogenetic relationships between carbonate and silicate magmatic systems;

(ii) although large portions of the silicate units are poorly exposed, where outcrops are found the rocks are extremely fresh and so suitable samples could be obtained for petrological study;

(iii) the Complex had been well mapped (Strauss and Truter, 1950; Verwoerd, 1967) and petrographic and preliminary chemical information was available for the major components of the complex.

Table 1.1: Summary of age information for the late Proterozoic Kaapvaal Alkaline Complexes.

Complex,Unit	*Age(Ma)*	*Method*	*Ref*
Spitskop			
Rietfontein nepheline syenites	1326 ±35	Rb/Sr,E	2
Ijolites	1357 ±67	Rb/Sr,E	2
combined ijolites & nepheline syenites	1341 ±37	Rb/Sr,E	2
Pienaars River Complex			
Leeuwfontein	1430 ±50	Rb/Sr,I	1
	1420 ±70	U/Pb min	3
Leeuwkraal	1334 ±26	Rb/Sr,I	1
Rondawel	1361 ±142	Rb/Sr,I	1
Franspoort, Buffelsdrift, Klipdrift, Haakdoornfontein	1306 ±11	Rb/Sr,I	1
Premier kimberlite			
mineral-whole rock	1202 ±72	Pb/Pb,"I"	7
di,garn megacrysts	1180 ±30	Rb/Sr, Sm/Nd	8
Pilanesberg Complex			
green foyaite	1193 ±98	Rb/Sr,I	2
"foyaite" biotite	1250 ±60	K/Ar	4
Kruidfontein Complex			
carbonatite dykes	1246 ±26	Sm/Nd,C	2
Goudini Complex			
carbonatite	1190 ±80	Sm/Nd,I	5,2
Kruidfontein, Goudini, Tweerivier, Bulhoek and Derdepoort	1269 ±171	Sm/Nd,E	2
Stukpan Complex			
carbonatite-mica	1354 ±11	Rb/Sr,I	2,6

I: regressed isochron; E: regressed "errorchron"; C: averaged model T_{CHUR} age.
Sources of data: 1:Harmer (1985); 2:Harmer - this study; 3:Oosthuyzen and Burger (1964); 4:Snelling (1963); 5:Nelson *et al.*(1988); 6:Verwoerd *et al.*(1986); 7:Kramers and Smith (1983); 8:Richardson (1986).

1.3. *Introduction to the Spitskop Complex*

1.3.1. *Location of the Complex and General Physiography*

The Spitskop Complex occupies parts of the farms Eenzaam 875KS, Rietfontein 876KS and Spitskop 874KS in the Malaita district of the Sekukhune plateau in Lebowa, 50 km north east of Groblersdal (Figure 1.2). Access to the complex was greatly improved in the middle 1980's through the construction of the tarred Groblersdal (and Stofberg) - Nebo - Magnet Heights road.

As shown in the regional geological map in Figure (1.3) components of the Complex intrude the sheeted granite of the Lebowa Granite Suite of the Bushveld Complex less than 2 km from the edge of the western escarpment bounding the valley of the Steelpoort River which has incised into the underlying Rustenburg Layered Suite components of the Bushveld Complex. The Spitskop Complex lies just north of the Steelpoort fault which is thought to have been active during the emplacement of the Rustenburg Suite and also displaces granites of the Lebowa Suite. Geophysical modelling in this area (Meyer and De Beer, 1987) indicates that the Bushveld Granites on the Sekukhune Plateau are underlain by the mafic units of the Rustenburg Layered Suite, together with at least the Pretoria Group component of the Transvaal Sequence. Magmatic components of the Spitskop Complex thus passed through at least 18 km of supra-basement successions *en route* to the surface.

Because of a lack of cadastral information on early maps of the Spitskop area, Shand (1921a) and Strauss and Truter (1950) devised their own names for the rivers and hills in the area. The significant river which flows through the centre of the Complex was called the Spitskop Spruit in these reports. On the current 1:50 000 scale topographical map of the area this is named the "Tshweneng" River. None of the tributaries are named, however, so those used in the early geological reports are retained and are shown on the map in Figure (1.4) . A number of the topographic features and place names have been changed since the reports of Shand (1921a) and Strauss and Truter (1950), most notably the adoption of the local name "Mare" for the hill and farm Eenzaamkop. For consistency the tributary to the Tshweneng River west of Mare hill has been renamed the Mare Spruit. Since the formation of the Lebowa "national state", the original farms have disappeared from the Spitskop area. Because the farm boundaries are still shown on the topographical maps of the area, and some of the original fences still remain, they remain useful for describing the distribution of the geology.

Figure 1.2: Location of the Spitskop Complex relative to major access roads.

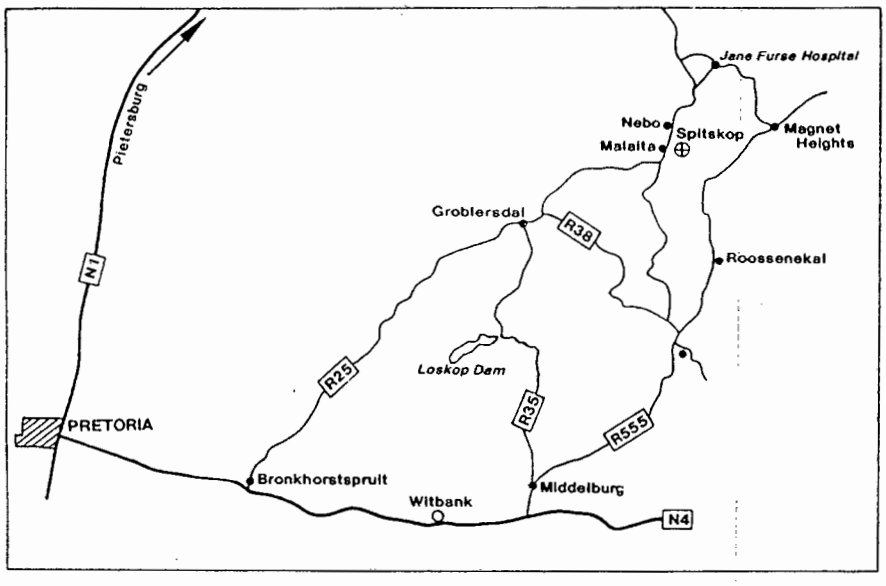

Figure 1.3: Geological Setting of the Spitskop Complex.

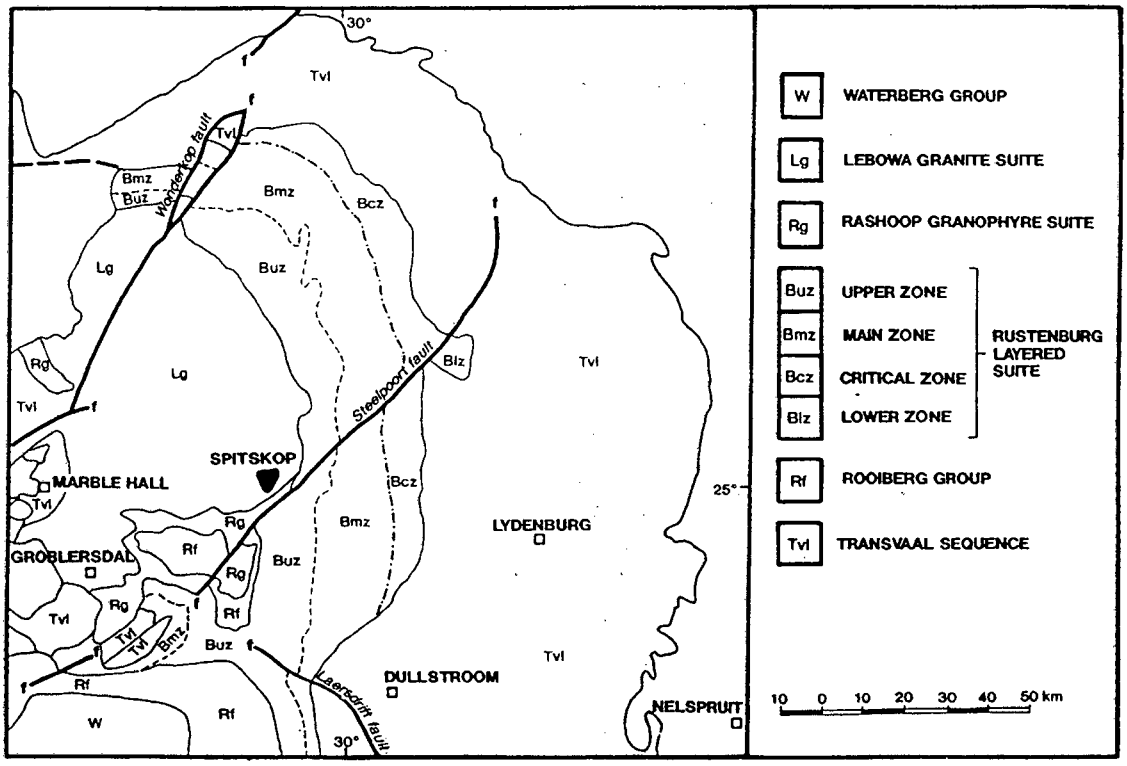

Units of the Complex form a shallow basin (ca. 1385 m above sea level) in the granite plateau, tilted gently to the south east: the regularity of the basin is broken by three prominent hills: Spitskop in the south west (1596 m), Mare (previously Eenzaamkop) in the north (1540 m), and Mahlolong in the south east (Figure 1.4). The basin has been sculpted by a perennial stream, the Tshweneng River, and its major tributaries the Rietfontein, Mare and Makpopeng Spruits, which rises some 3.5 km upstream of the complex and drains over the escarpment to join the Steelpoort River to the south east. To simplify locality descriptions, the Tshweneng River has been arbitrarily segmented into "upper", "middle" and "lower" sections, as shown in Figure (1.4).

1.3.2. *Previous Work*

Undersaturated alkaline igneous rocks at Spitskop were first mapped, as part of a regional survey, by A.L. Hall (1911) and Brouwer (1910) included descriptions of Spitskop material in his treatise on the nepheline syenites of the Transvaal. These works concentrate largely on the nepheline syenites, and contain only passing mention of ijolite and urtite.

The first thorough investigation of Spitskop was published by Shand (1921a) and was based on one week's mapping and sampling at the Complex in 1919. A comment made by Shand (p 112) is worth quoting: "One might think that [one week] would be more than sufficient for the study of some ten square miles of country, but the variety of rocks in the area is such that the time allocated was barely sufficient for the purpose of locating and collecting them all."!

Shand recognised components of both the foyaite and ijolite "compositional ranges", classing sphene-rich pyroxenite ("pienaarite") with the latter group. The carbonatite was considered a "limestone inclusion" within the complex brought up from the Transvaal dolomites at depth by the rising magma. Shand, furthermore, was of the opinion that the rocks of the complex were not emplaced as successive intrusions, but were part of "..the same streaky mass and graduate into one another."

Figure 1.4: Map showing the general physiography of the Spitskop Complex

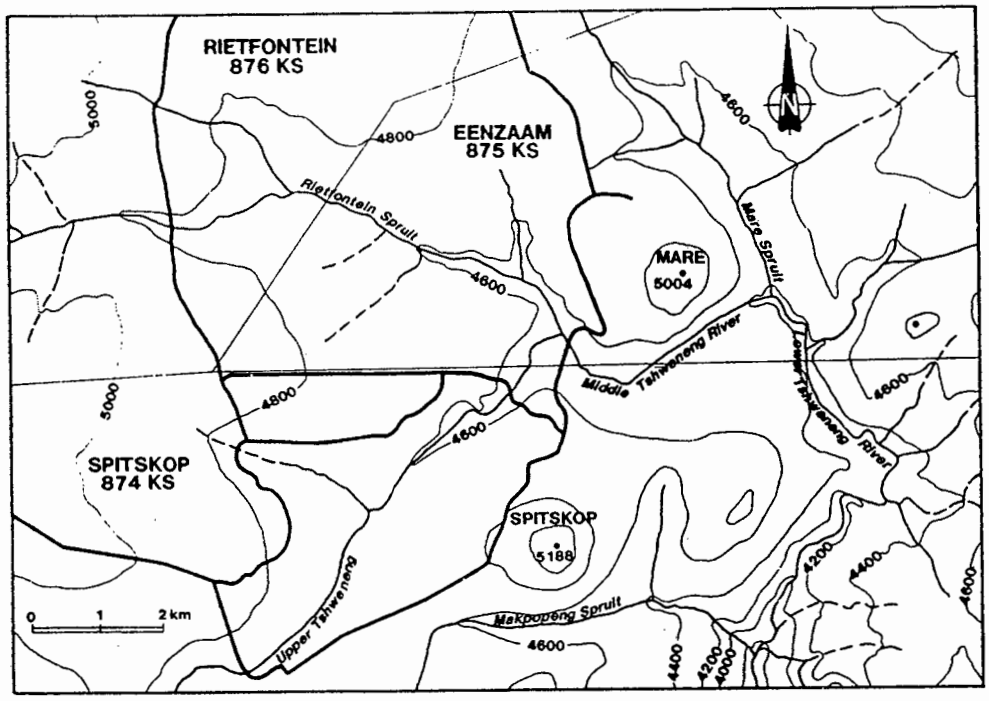

As a result, the observed mineralogical variation "..must therefore have resulted either from a spontaneous differentiation of the magma in place or from assimilation of country rock." He concluded, therefore, that the ijolite components were derived from the foyaite magma through desilication reactions with the "limestone inclusion". As such, Spitskop was regarded as a most convincing demonstration of R.A. Daly's "limestone syntexis" hypothesis for the generation of undersaturated alkaline rocks. Shand proposed that both the foyaite and ijolite groups could represent progressive stages in the desilication of the surrounding Bushveld granite magma by the limestone. As an alternative, he suggested that the original foyaite magma could be the residue ("haplosyenite") from the crystallisation of the noritic magma of the Bushveld Complex.

A detailed and thorough field and petrological study was published by Strauss and Truter (1950) who argued forcefully that the "limestone" was rather a composite intrusion of igneous carbonatite. All the lithological units now considered to comprise the complex were recognised and, in particular, the true extent of the pyroxenite and ijolite relative to the foyaites was clearly established: the foyaites were described as "ring-dyke" intrusions and the complex was thought to consist mainly of a plug of ijolite. The metasomatic effects of the complex on the granitic country rocks were also described. In addition, Strauss and Truter recognised a suite of enigmatic "theralites", "melteigites", and olivine-bearing diorites, from the eastern and southern margins of the complex: along the Makpopeng Spruit, and lower Tshweneng River and Mare Spruit. These units were described as containing bands of massive titaniferous magnetite "microscopically indistinguishable" from the magnetitites of the Bushveld Complex. The genesis of these units was considered to be "..best left open..", although arguments supporting either extreme fenitisation of the country rocks or true magmatic intrusion were presented.

Tribute must be paid to the quality of both the mapping and field observation presented in Strauss and Truter's communication, which must rank as a benchmark publication in South African geology. Few modifications have been necessary to the outcrop positions on Strauss and Truter's original map - the most significant necessitated only by inaccuracies in their topographical base map!

Baertshi (1957) determined oxygen isotope ratios on samples of carbonatite from Spitskop and sedimentary dolomite from the Transvaal Supergroup and the isotopic contrast was used by Holmes (1958) to assert that "..the Spitskop crystalline

limestone is a carbonatite and *not*, as has been supposed, an enormous mass of the "Dolomite" floated up by a hypothetical magma."

The next significant contribution to knowledge of the Complex came in the following decade with the work of Verwoerd (1964, 1966, 1967).

In his earliest communication, Verwoerd addressed the question of the origin of the enigmatic "theralites" and olivine-diorites at Spitskop and observed that these mafic rocks are cut by aegerine-syenite pegmatites exhibiting a graphic texture. Noting that graphic-textured granite pegmatites of similar dimension are often seen elsewhere intruding mafic rocks of the Bushveld Complex (e.g. at Magnet Heights), Verwoerd proposed that the graphic aegerine-syenites were simply fenitised equivalents (aegerine replacing quartz) of such pegmatites. Consequently, the mafic units cut by the pegmatites must also pre-date the emplacement of the alkaline complex, and Verwoerd thus concluded that the "theralites", "melteigites", olivine-diorites and titaniferous magnetite all represent xenoliths of Bushveld Complex material fenitised to varying degrees by the alkaline magmas and associated fluids.

As part of an extensive survey of South African carbonatites, Verwoerd (1967) mapped the carbonatite component of the Spitskop Complex in detail and demonstrated that the carbonatite was compositionally zoned: an incomplete outer zone of calcite carbonatite was followed inwards by a greater volume of dolomitic carbonatites. Concentric, near vertical, flow fabric was mapped in the carbonatite. Although primarily concerned with the carbonatite, Verwoerd (1967) also made a number of highly pertinent observations on the character of, and relationships between, the silicate units of the Complex. It was suggested that previous workers had underestimated the volume of the readily weathered pyroxenitic material in the complex relative to the more resistant ijolite and proposed that Spitskop essentially comprised a pyroxenitic plug, into which the ijolite was emplaced as pervasive sheeted intrusions.

Subsequent drilling by the Geological Survey (Nel, 1976) in the poorly-exposed central parts of the Complex (between the upper Tshweneng River and Rietfontein Spruits) showed that ijolite indeed occurred largely as narrow sheets within extensive and massive pyroxenite. Microprobe analyses of clinopyroxenes from the "theralites" and related units revealed tholeiitic, Bushveld-like, evolution trends, clearly distinguishable from the alkaline trends detected in the foyaites, again implying that these mafic units are xenolithic.

Chapter 2: Field Relationships of Units of the Spitskop Complex.

2.1. *Introduction*

The Spitskop Complex is crudely circular in form, with a diameter of approximately 8 km and covers a surface area of some 50 km^2. It is built of successive intrusions of pyroxenite, ijolite, nepheline syenite (foyaite) and carbonatite; igneous activity closed with the emplacement of small plugs and dykes of very fine-grained "basalt". Fluids emanating from the intrusion have formed a metasomatised border zone in the granitic country rocks.

The distribution of the components of the Spitskop Complex are shown on the geological map in Figure (2.1) which is a modification of the outcrop map of Strauss and Truter (1950) and the detailed map of the carbonatite published by Verwoerd (1967). Outcrops defined by Strauss and Truter (1950) have been interpolated and the relationships between the various fenite units along the lower Tshweneng River were re-mapped. Outcrop limits within the areas of ijolite and nepheline syenite, as defined by Strauss and Truter, are shown as solid lines in Figure (2.1).

Exposures of the nepheline syenites and the carbonatite are generally excellent, whereas good outcrops of ijolite are only found along stream beds. The pyroxenite is very poorly exposed. The superior resistance to weathering of the nepheline syenites is demonstrated by the fact that this rock type underlies each of the three prominent hills previously mentioned.

In the following sections the field relationships of the components of Spitskop Complex will be treated in their relative order of emplacement.

Figure 2.1: Geological Map of the Spitskop Complex.

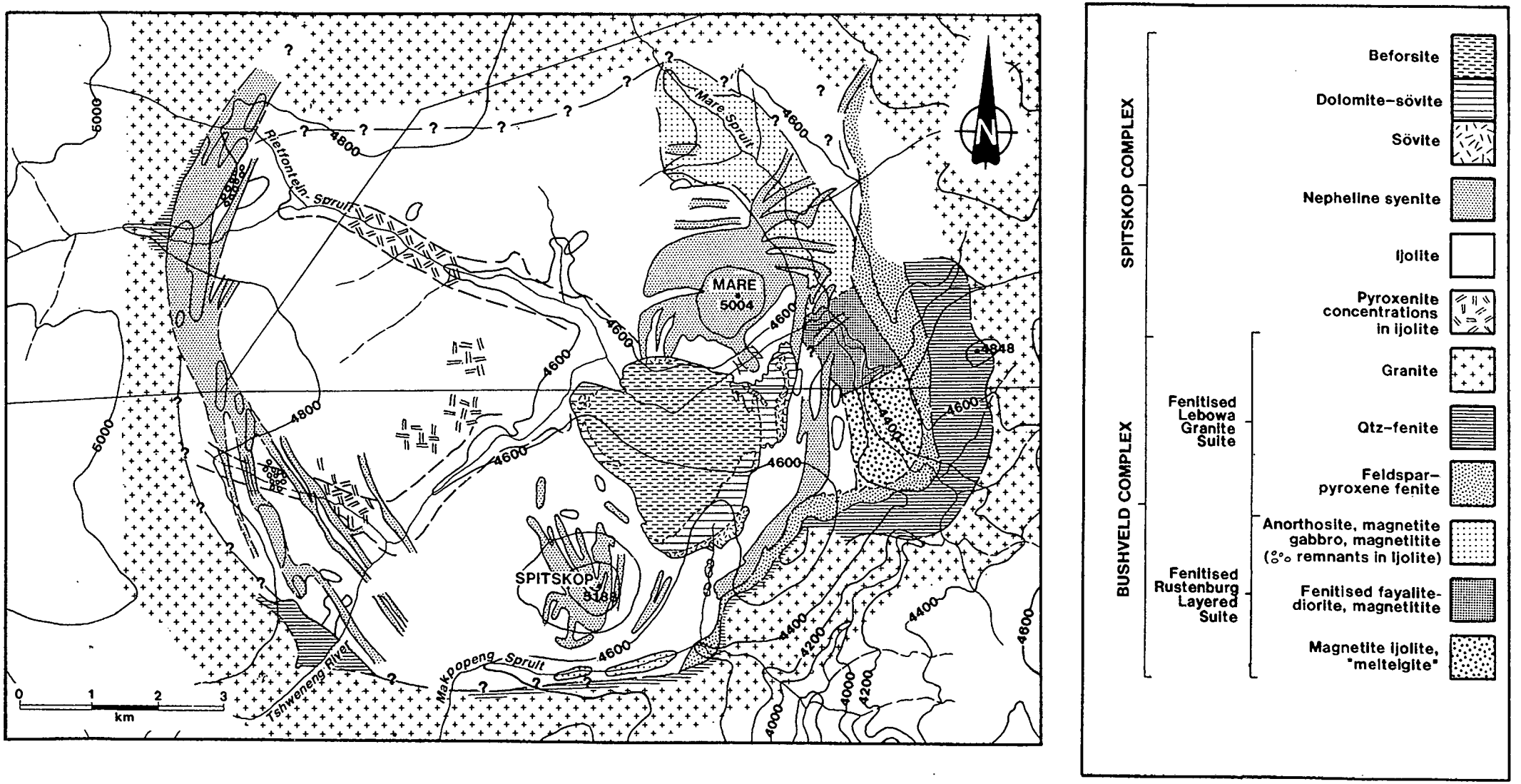

2.2. *Pyroxenites*

Coarse pyroxenite, micaceous and/or magnetiferous in places, is the earliest recognisable component of the alkaline complex.

Easily weathered pyroxenite is only seldom preserved in outcrop and fresh pyroxenite was only observed in the bed of the Rietfontein Spruit, on Mare farm near the boundary with Riet-fontein. At this locality blocks of pyroxenite, up to 50 cm in diameter, are preserved in a matrix of different textural and compositional variants of ijolite (Plate 2.1a, 2.1b) . In these exposures fragments 20 to 30 cm across of pure biotite ("glimmerite") occur in which the mica forms aggregates of coarse grains, 5 to 10 cm in diameter. Alongside these outcrops the pyroxenite rapidly becomes friable and ultimately decomposes to an olive-green soil in which mica flakes are clearly discernible. The 1.5 km river section downstream from this locality contains the best exposures to study the relationships between the pyrox-enite and the later intrusions. Along this stretch, the river banks are composed of olive green, weathered pyroxenite in which variably altered sheets of ijolite, 5-50 cm in width, stand out in relief (see Plate 2.1c). The relative proportion of ijolite increases progressively downstream: ijolite comprises an estimated 20 percent of the outcrops near the old farm boundary; increasing to over 75 percent downstream and within about 500 m of the spruit's confluence, pyroxenite is identifiable only as rare inclusions less than 10 cm across in heterogeneous ijolite.

Recognisable pyroxenite is also seen amongst the exposures along the tributary to the upper Tshweneng River. Again, ijolite increases in relative abundance towards the Tshweneng River confluence.

Plate 2.1

2.1a: Blocks of pyroxenite and "glimmerite" within a complex mixture of ijolite. Upper Rietfontein Spruit.

2.1b: Xenolith of massive pyroxenite in urtitic ijolite. Note the pyroxene-rich patches (pyroxenite remnants) within the ijolite. Upper Rietfontein Spruit.

2.1c: Weathered pyroxenite with ijolite sheets (lighter coloured). Upper Rietfontein Spruit.

2.1d: Ijolite dyke with sharp, finer-grained ("chilled"?) margin. Lower Tshweneng River.

2.1e: Coarse, homogeneous leucocratic ijolite or urtite. Nepheline is flesh coloured. The white mineral is cancrinite. On Tshweneng River upstream of the Rietfontein Spruit confluence.

2.1f: Heterogeneous mixture of ijolite types with relics of nephelinised pyroxenite (see detail in Plate 2.1h) . Upper Rietfontein Spruit.

2.1g: Zoned urtite veinlets (white) cutting across melanocratic ijolite. Note the diffuse margins to the veinlets. Tshweneng River.

2.1h: Nephelinisation of pyroxenite. "Spotted" texture developed through the growth of nepheline within enclave of pyroxenite. Upper Rietfontein Spruit (detail of area near pen in Plate 2.1f).

PLATE 2.1

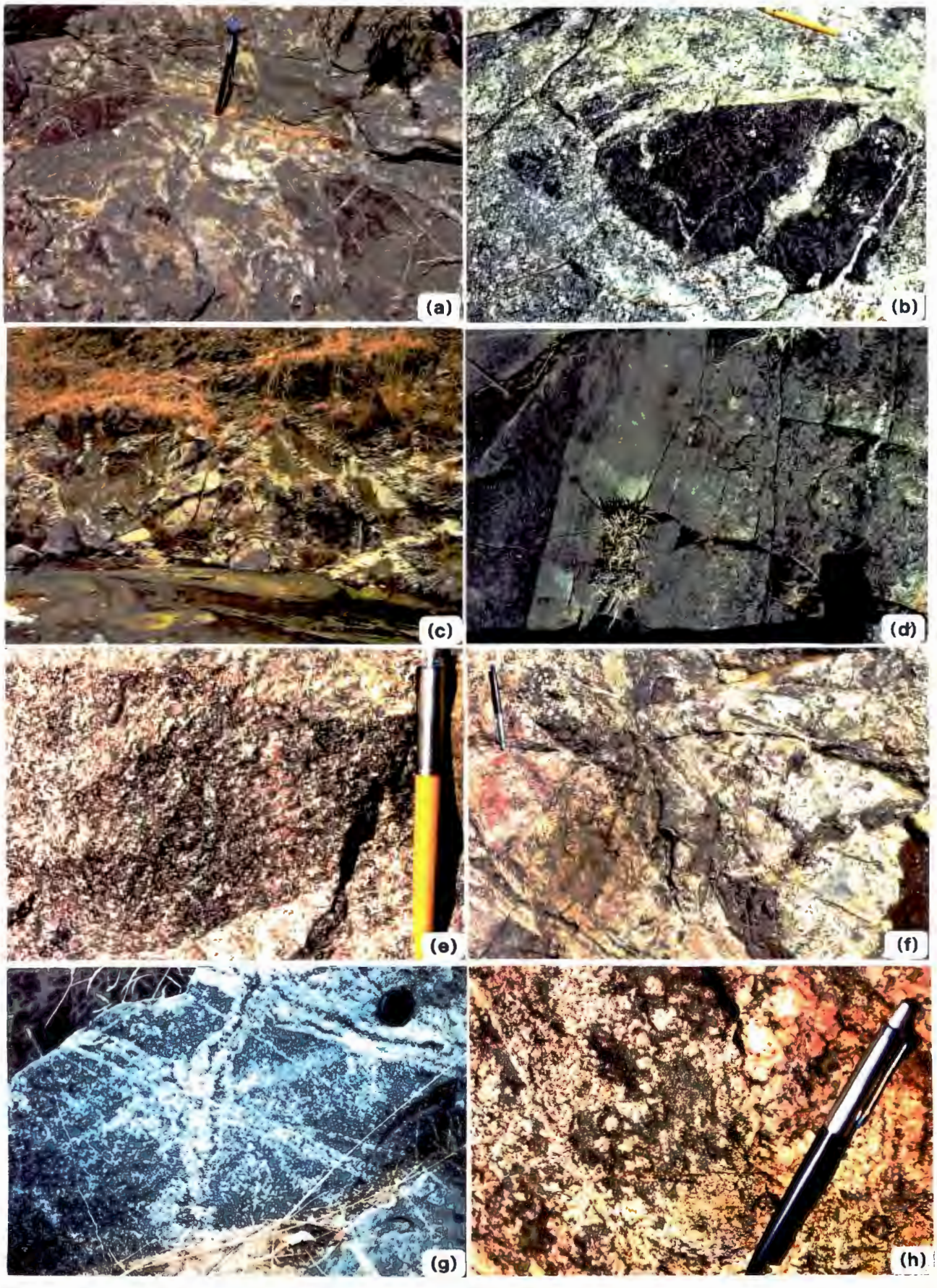

Strauss and Truter (1950) linked the latter concentrat-ions of pyroxenite on their map, interpreting the pyroxenite as an elongate, sheet-like body. The intervening area is underlain by deep soil in which ijolite and nepheline syenite boulders and pebbles are conspicuous as float. Erosion gullies (dongas) do not completely penetrate the overburden in this area but careful examination revealed that the deeper parts of the gully sides are dominantly composed of the micaceous, olive-green soil character-istic of deeply altered pyroxenite. Partially-weathered ijolite sheets are common in the dongas and the donga floors are littered with ijolite cobbles. Taking these observations in association with the drilling results described by Nel (1976), one cannot escape the conclusion that pyroxenite underlies much of the complex to the north west of the carbonatite, and possibly represents a plug-shaped mass, as argued by Verwoerd (1967). Nel (1976) estimated that the relative abundances of pyroxenite and ijolite in this area were 60-70% and 40-30% by volume, respectively.

Although clearly the earliest recognisable lithological unit in the Complex, it is difficult to ascertain from the available exposures whether the pyroxenite is definitely intrusive at its current level of occurrence, or whether the pyroxenite represents a xenolith (possibly cognate) transported from deeper levels by subsequent magma upwellings. It is nowhere seen in contact with the granitic country rocks. Strauss and Truter (1950) describe, and present a photograph (their Plate 18) of, a small outcrop of "mixed rocks" at the foot of Mare just down-stream of the carbonatite, in which a dyke of micaceous pyroxenite is seen to intrude "theralites" (fenitised Bushveld fayalite diorites) and is itself invaded by sheets and veins of ijolite and urtite. This outcrop is also marked on Verwoerd's (1966) detailed map of the carbonatite body. Despite several attempts over a number of years, this outcrop could not be found and has presumably been buried by bank collapse! On the basis of Strauss and Truter's (1950) descriptions and photograph, it must be assumed that at least part of the pyroxenite did indeed intrude as a magma and hence that the pyroxenite represents the earliest magmatic phase of the Spitskop Complex.

It remains somewhat enigmatic that if the pyroxenite is indeed the earliest intrusive phase of the Complex, why it is never seen intruding the mafic fenites which are very well exposed along the lower Tshweneng River, nor does pyroxenite occur as dykes in the surrounding granites.

2.3. *Ijolites*

Bailey (1974a) referred to ijolites, and the compositionally-related nephelinitic volcanics, as "probably the most perplexing groups of alkaline rocks"! "Ijolite" is here used to encompass all the feldspar-free, essentially nepheline-clino-pyroxene, lithologies at Spitskop and includes nepheline-rich leuco-ijolite, or urtite, and nepheline-poor, mela-ijolite varieties.

At Spitskop the ijolites are extremely heterogeneous and occur in such a bewildering range of textures that there is little doubt that all the ijolite varieties could not have been derived through a single phase of igneous activity. Being more resistant to weathering than the pyroxenite, they persist as float cobbles throughout the poorly-exposed central parts of the Complex.

Strauss and Truter (1950) distinguished three textural types of ijolite:

1: coarse-grained, red ijolite with local urtite facies;
2: fine-grained, black ijolite; and
3: very fine-grained, very dark ijolite (also termed melteigite).

As discussed in an earlier section, the "fayalite diorites", "theralites" and "melteigites" of Strauss and Truter (1950) are now regarded as fenitised xenoliths (Verwoerd, 1964; Nel, 1976) and are specifically excluded from the current group: they are discussed later (see Chapter 6). Ijolite types (1) and (2) were described by Strauss and Truter as being intrusive into pyroxenite. Type (1) is "..confined mostly to to the core.." of the Complex, the "..fine-grained variety [occurs] mostly as a broad zone around the coarse-grained.."; with the fine-grained being "..distinctly intrusive.." into the coarser. Confusingly, out-crops are also described of "..injection breccia with fragments of fine-grained ijolite in a groundmass of coarse-grained ijolite"!

Heterogeneity at outcrop scale is expressed as alternations of different textural varieties as well as variations in grain size and modal proportions within a single textural type: e.g. fine-grained, mesocratic ijolite dykelets often contain streaks of coarser grain size. A single macroscropically-defined texture may occur in different associations implying generation through more than one process or at more than one time. Furthermore, it is seldom possible to trace a textural zone for any distance across an outcrop. As a result it is doubtful whether macroscopically-defined textural subdivisions represent correlatable, "mappable units" of petrogenetically distinct varieties of ijolite.

To facilitate discussion, it is useful to define and describe some "end member" components identifiable in outcrop.

2.3.1. *Ijolites displaying intrusive features:*

Dark, fine-grained ijolite dykes: In rare exposures, especially amongst the "melteigites" of the lower Tshweneng River, discrete fine-grained ijolite dykes are noted with sharp, finer grained contacts against earlier units (Plate 2.1d). These ijolites appear dark in hand specimen although the nepheline is recognisable as small, chalky white squares on weathered surfaces. Discrete sheets of mesocratic, medium-grained ijolite are also common within ijolite outcrops. Although one of the later phases of ijolite injection, these sheets are sometimes displaced by diffuse urtite veins.

Coarse-grained ijolite and urtite: Large exposures of coarse-grained ijolite and leuco-ijolite, or urtite, are found along the mid-Tshweneng River, particularly just upstream of the confluence of the Rietfontein Spruit, and also form a sheeted body in the "theralites" of the lower Tshweneng River. These handsome rocks are composed of a mosaic of flesh-coloured nepheline and green-black pyroxene prisms rimmed with white cancrinite (Plate 2.1e). Urtites are those portions of the coarser ijolite having less than 10 modal percent pyroxene. Yellow apatite grains of more than 1mm in length are often distinguishable in hand specimen. The urtitic fractions are generally medium-grained (average grain size ca 2-3 mm) and uniform, whereas pegmatoid patches are common in the more pyroxene-rich types where bladed pyroxenes reach 4 cms in length. Although more texturally uniform than the other ijolites, the urtites do sometimes contain pyroxene stringers. Rounded to sub-rounded clasts of finer-grained ijolite, 10-15 cms in diameter, are sporadic.

2.3.2. *Texturally heterogeneous ijolites:*

Most exposures of ijolite are composed of a complex, "migmatitic", mixture of ijolite of varying textures, modal composition, and macroscopic form.

Mixed ijolite outcrops are generally composed of a "host" of medium-grained ijolite in which wisps, streaks, patches or bands of pyroxene-rich material are heterogeneously distributed. Diffuse leucocratic veins (typically 1-2 cms across) and ijolite sheets (typically 2-10 cms thick) of various ages cut irregularly across this variation (Plate 2.1f). The veins are sometimes longitudinally zoned: central parts

having increased concentrations (streaks) of mafic minerals (Plate 2.1g). The impression gained is that the ijolite exposures were constructed of several pulses of magma, later intrusions mixing with and/or metasomatising earlier, partially consolidated, material. The diffuse margins to many of the ijolite sheets testify to the transfer of constituents between later and earlier phases of intrusion.

The texturally complex and heterogeneous nature of the Spitskop ijolites is apparently typical of ijolites from complexes elsewhere. King and Sutherland's (1966) descriptions and illustrations (pp 98-108; Fig. 15 on p.104) of the ijolite complex in the eroded Napak volcano in Uganda are very similar to the Spitskop ijolites. Comparable features may also be found in the descriptions by Le Bas (1977) of the field relationships of the ijolites in the Kenyan Usaki and Kisingiri complexes.

Blocks of plagioclase-rich material were found in the ijolites exposed along the upper reaches of the tributary to the upper Tshweneng River, in the dongas to the west of this occurrence, and amongst the ijolites which form a screen splitting the inner margin of the foyaite sheet on Rietfontein (see Figure 2.1). These rocks represent relics of partially metasomatised Rustenburg Layered Suite anorthosite and are discussed more fully in Chapter 6.

2.3.3. "Nephelinisation" of the Pyroxenite

As described above, the pyroxenite is extensively invaded by sheets of ijolite. The margins of these ijolite sheets are characteristically nepheline-rich ("urtitic") and diffuse where felsic components from the ijolite have infiltrated into the adjacent pyroxenite. Strauss and Truter (1950) referred to this process as "nephelinisation" of the pyroxenite.

An early manifestation of this process as seen in hand specimen is the growth of subhedral nepheline grains and patches within the pyroxenite, producing a "spotted" appearance (Plate 2.1h). Further infiltration leads to a disaggregation of the pyroxenite texture giving rise to a heterogeneous ijolite in which wisps, stringers and patches of pyroxene-rich material are irregularly distributed. Patchy, pyroxene-rich lenses and zones which persist in many ijolite outcrops remote from identifiable pyroxenite probably represent "ghost" relics of nephelinised pyroxenite.

Plate 2.2

2.2a: Fragment of ijolite in porphyritic nepheline syenite. Note alignment of trachytic fabric around xenolith. Southern slope of Mare hill.

2.2b: Typical schistose nepheline syenite showing some small scale, assymetric fold structures. Rietfontein sheet.

2.2c: Felsic vein in nepheline syenite. Rietfontein.

2.2d: Porphyritic nepheline syenite. Mare.

2.2e: Macroporhyritic nepheline syenite. Diameter of coin in 30mm. Rietfontein.

2.2f: Banded nepheline syenite. Note the grading of phase proportions in many of the bands. Rietfontein.

2.2g: Intrusion of fine-grained nepheline syenite into banded nepheline syenite. Note the sinuous banding in the intrusive sheet and the increased concentration of felsic material along contact. Rietfontein.

2.2h: Banding in macro-porphyritic nepheline syenite. Mare.

PLATE 2.2

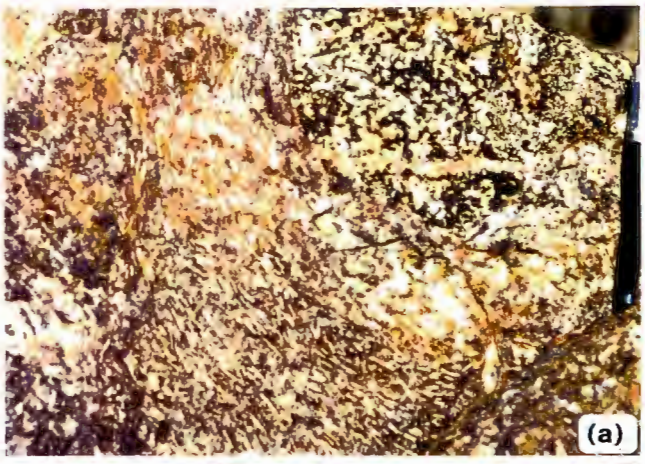
(a)


(b)


(c)

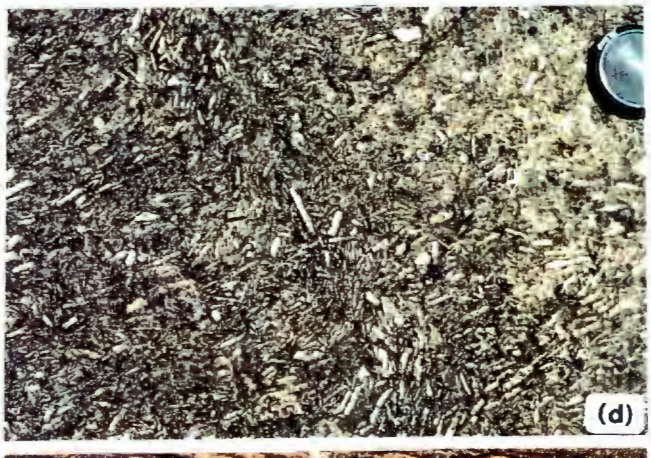
(d)


(e)


(f)


(g)


(h)

2.4. *Nepheline Syenites*

Bodies of nepheline syenite at Spitskop are essentially composed of varying proportions of alkali feldspar (usually perthitic), nepheline and sodic clinopyroxene and were termed "foyaite" by Strauss and Truter (1950). Nepheline syenites weather less readily than the other lithologies in the Complex and hence tend to produce the positive topographical features within the complex, underlying the prominent hills of Spitskop and Mare (Eenzaamkop), and they also support the north western "rim" of the topographic basin on Rietfontein. Because of this resistance to weathering, nepheline syenite boulder float is widely dispersed, often far from its point of outcrop, and care must be exercised in mapping these units.

Nepheline syenites commonly occur as laterally extensive sheets intrusive into the pyroxenite and ijolite and generally have steep to vertical dips - usually trending away from the centre of the intrusion. As a result these bodies were referred to as "ring-dykes" by Strauss and Truter (1950); disturbance of the orientation of the nepheline syenite fabric at intrusive contacts by successive magma pulses renders any strict distinction between "ring-dyke" or "cone-sheet" difficult and so the non-genetic terms "dyke" or "sheet" will be used in the following descriptions.

The nepheline syenites crop out in four major bodies: as broad, somewhat formless masses underlying the koppies of Spitskop and Mare; and as more clearly defined dyke features along the western margin of the complex on Rietfontein and in the east, between the carbonatite and the granitic country rocks. For ease of reference these occurrences will be referred to as the Spitskop, Mare, Rietfontein and "eastern" bodies (or sheets) respectively.

Nel (1976) curiously suggested that the age relationships between ijolite and nepheline syenite in the Mare and Spitskop bodies were equivocal. During the present investigation, examples of ijolite xenoliths in nepheline syenite were found at both these occurrences. A particularly fine example was noted on the south eastern flank of Mare where feldspar phenocrysts in porphyritic nepheline syenite were aligned by flow around an ijolite fragment 20cm in diameter (Plate 2.1a). Furthermore, the forms of many of the nepheline syenite bodies (particularly the branching southern portions of the Rietfontein sheet) are not consistent with the nepheline syenite being emplaced earlier than the ijolites. There can be no doubt, therefore, that the nepheline syenites were injected after consolidation of the ijolite.

Both Strauss and Truter (1950) and Nel (1976) suggest that the different nepheline syenite occurrences are connected at depth, implying that they represent a single, multiply injected, magmatic body. As will be seen, petrographic and geochemical features suggest that this is unlikely.

Four macroscopically identifiable textural varieties of nepheline syenite were described by Strauss and Truter (1950, p104-105): (a) coarsely porphyritic; (b) medium-grained, massive, equigranular; (c) banded to schistose; and (d) nodular. Nel (1976) considered the nodular nepheline syenite, in which rosettes of pyroxene comprise the "nodules" and which always forms as inclusions in the other types, to be the result of "accidental crystallisation around phenocrysts" of each of the other varieties and hence should not be regarded a separate textural type. During the present investigation it was found that nodular porphyritic varieties with pyroxene rosettes were rare and that feldspar rosettes are, in fact, more common.

2.4.1. Macroscopic textural variation

To facilitate the discussion of the distribution and internal structure of each of the nepheline syenite bodies, a number of distinct textural varieties are defined. Gradations between these types, sometimes over a distance of less than a metre, are often noted suggesting that they do not necessarily relate to discrete magma types or injection episodes but rather reflect local crystallisation conditions.

Schistose: This type is developed to some extent in all the syenite bodies and is extremely fine-grained and compact with a well developed planar, "schistose" fabric. In hand specimen the schistose type appears waxy, grey-green in colour and weathers to a khaki-brown surface (Plate 2.2b). In outcrop this variety closely resembles the chlorite-actinolite schists of low grade metamorphic terrains. This analogy is reinforced by the common occurrence of white to flesh-coloured veins and stringers of feldspathic material (Plate 2.2c), giving some outcrops a marked "migmatitic" appearance. On freshly-broken surfaces the rock has a lustrous appearance due to densely packed, oriented acicular pyroxene grains.

Strauss and Truter (1950) included this variety with the other foliated types, and used the terms schistose and trachytic interchangeably to describe nepheline syenites with planar fabrics. It is useful, however, to distinguish between this distinctive, very fine-grained, schistose, variety described above and the variations of

the coarser porphyritic types below, which have developed planar, "trachytic", fabrics of oriented feldspar phenocrysts.

Porphyritic: Porphyritic nepheline syenites are common and vary from "tinguaitic" textural types with tabular feldspars 10-15 mm in length set in a medium-grained, grey groundmass (Plate 2.2d), to macro-porphyritic varieties where the feldspar phenocrysts reach 30 mm and more in length (Plate 2.2e).

Phenocrysts are almost exclusively of alkali feldspar and are usually aligned into a "trachytic" texture. Less commonly, feldspar phenocrysts form clusters or rosettes and develop the "nodular" texture referred to above. Pyroxene-phyric nodular nepheline syenite was found at only one locality in a small exposure near the earth dam to the north of the main Rietfontein outcrop.

In the macro-porphyritic type, the large feldspar phenocrysts characteristically appear "pitted" on weathered surface through the preferential etching of small prisms of early nepheline poikilitically included in the feldspar grains. Larger feldspar phenocrysts tend to lose their rectangular form, the edges becoming somewhat rounded to form "augen"-shaped crystals (Plate 2.2e). The interstitial material is fine-grained, pyroxene and nepheline-rich and may have a distinct preferred orientation.

Porphyritic nepheline syenite exposures sometimes exhibit compositional banding of mineral components at varying scales, and taking different forms. Banding is invariably sub-vertical. Laminated structures have repetitive compositional banding with bands approximately 10 mm in width, individual bands usually characterised by one gradational and one sharp margin (Plate 2.2f). Planar fabrics may also comprise 10-20 mm wide aggregations of randomly-oriented feldspar laths interspersed with 20-30 cm wide zones of normal, porphyritic nepheline syenite. Banding also develops in the macro-porphyritic varieties where bands are defined by differing sizes of the feldspar phenocrysts and as segregations of pyroxene-rich material (Plate 2.2g).

Massive: Nepheline syenites with massive, uniform textures are less common. Grey and waxy in hand specimen, this variety is characteristically equigranular, and the pyroxene typically forms larger, discrete grains, rather than as aggregates as in the other varieties. Nel (1976) referred to this variety as "hypidiomorphic". The central portions of the Mare body are exclusively of this type.

Pegmatoidal: Pegmatoidal facies are restricted to the margins of some nepheline syenite sheets, typically where they abut against massive xenolithic

Bushveld materials (along the Mare Spruit) or ijolite (along the inner contact of the Rietfontein sheet). Large chalky white feldspars, sometimes reaching 20 cm in length, are randomly set in a fine-grained, granular, generally melanocratic matrix (Plate 2.3a). These pegmatoidal zones are clearly distinguished from the macro-porphyritic type in the that the feldspars are free of the nepheline insets which characterise the latter type, by the variation in size and orientation of the feldspars, and by their patchy development.

2.4.2. Rietfontein nepheline syenite sheet

The Rietfontein sheet forms an arcuate body, concave to the centre of the intrusion, traceable for some 2 km from the north western margin of the Spitskop Complex on Rietfontein to the upper reaches of the Makpopeng Spruit in the south. In the north, on Rietfontein, the sheet was emplaced along the contact between fenitised granite and ijolite. Passing southward onto the farm Spitskop, the dyke trends more to the south east, away from the contact, and splits into several sheets varying from 20 to 50m in width which are enclosed entirely within ijolite. Dips throughout the body are subvertical, dominantly away from the centre of the complex (i.e. to the west and north west) although opposing dips are locally noted.

Most of the southern part of the body is comprised of porphyritic, generally trachytic, nepheline syenite. Scattered outcrops south of the stream on Rietfontein are largely composed of porphyritic to macro-porphyritic varieties that exhibit compositional banding in places. Here, the coarse nepheline syenite is cut by dykelets, usually less than 10cm wide, of fine-grained nepheline syenite intruded at high angle to the banding in the coarser variety. The margins of these dykes are sharp but the porphyritic nepheline syenite is deformed in places where the phenocrysts are drawn out along the contact implying that the porphyritic variety had not completely solidified when the later magma pulse was emplaced.

Outcrops between the upper arms of the Rietfontein Spruit display a range of the textural varieties of nepheline syenite noted in the previous section, interleaved in a highly complex fashion.

The outer, north-western contact of the nepheline syenite with fenitised granite is not well exposed but is almost cert-ainly sharp, evidenced by the abrupt transition from flat, grass-covered, sandy granite soils to the broken, vegetated (thorn trees and aloe), angular boulder-strewn outcrops of nepheline syenite. Outer parts of the sheet are composed of fine, compact, schistose nepheline syenite with abundant veinlets

and patches of feldspathic material usually, but not invariably, concordant with the foliation. Widths range from stringers in the order of 1 mm across to veins typically 10 to 15 mm in size. Small amplitude (typically 5-20cm), asymmetric folds are commonly seen through-out this zone (Plate 2.3b) while symmetrical, chevron-shaped folds are noted but are less abundant. These features clearly represent "drag" folds generated through the shear effects of multiple emplacement of nepheline syenitic magma into a restricted conduit. Interestingly, the axes of the asymmetric folds are not always horizontal which indicates that the magma had a significant component of lateral movement.

Within 10-20m of the outer contact, zones of porphyritic nepheline syenite are noted, sometimes macroporphyritic, mixed with areas of schistose nepheline syenite. The porphyritic zones are always totally surrounded by heterogeneous schistose nepheline syenite frequently showing irregular, sinuous fabrics with wildly oriented folds. Vein segregations are common and generally increase in abundance close to the contact between the textural types. Careful examination of the schistose nepheline syenite reveals stringers of porphyritic material and scattered individual feldspar phenocrysts disposed along the foliation. It would appear, then, that the coarser material was sufficiently competent to retain its texture in the larger "xenoliths", but not yet totally solid, enabling crystals to be prised loose and partially incorporated by the intruding magma. The south-east facing slope of the ridge on Rietfontein is largely composed of areas of porphyritic surrounded by schistose nepheline syenite.

Amongst the porphyritic nepheline syenite in this area is a zone which displays well developed rhythmic layering (Plate 2.2f). Because of the abundant fine-grained intrusive material, the layered zone could not be traced laterally for more than 20m (Plate 2.2g). Individual bands are 20 to 30mm wide and are always steeply disposed. Two variations of banding may be distinguished. Firstly, and less common, the bands are defined by concentrations of feldspar phenocrysts with totally random arrangement, i.e. the relative concentration of feldspar is essentially the same across the width of the band. More common, though, are bands which are compositionally graded. These start with a sharp margin of feldspar-rich, almost mono-minerallic, syenite, grade through a zone rich in nepheline and pyroxene with sparse feldspar to end with a pyroxene-rich assemblage. Minerals in these compositional zones do not display any orientation: the feldspars in particular are always randomly aligned.

Towards the centre of the Rietfontein outcrop, where the topography flattens markedly, more massive porphyritic textures dominate though sheets of veined, schistose nepheline syenites are never totally absent.

Considering the disposition of the textural types within the Rietfontein outcrops, it is apparent that the schistose textural type does not represent a simple chilled facies of the intrusion as in many cases it is demonstrably later than the coarse, porphyritic variants. It is clear that the Rietfontein sheet was built from at least two distinct periods of magma injection. It is also evident that different magma compositions are not responsible for the crystallisation of the different textural types. In places a transition has been observed from fine, trachytic nepheline syenite through medium porphyritic to macrocrystic nepheline syenite over a distance of 20cm. It would appear, then, that the different textural types reflect differing conditions of crystallisation rather than radically different magma compositions. Schistose varieties always display significant quantities of felsic veins whereas the coarser variants are more homogeneous.

2.4.3. Mare nepheline syenite body

As mapped by Strauss and Truter (1950), the nepheline syenite underlying the hill Mare is somewhat formless, and is schematically depicted by these authors as a mass of syenite containing large blocks of ijolite. Outcrops are generally masked by scree and boulder float in this area so it is difficult to compile a precise map. It would appear that this body comprises an intrusion centred somewhat to the west of the hill top with sheets trending out from this point. Ijolite and gabbroic fenite material forms screens between the sheets emanat-ing from the intrusion. Sheets of nepheline syenite 10 to 20m in width are well exposed in the mafic fenites along the Mare spruit but cannot be traced for any distance into the soil-covered area to the east.

Most of the nepheline syenites exposed on the flanks of Mare are porphyritic (often trachytic where flow aligned) or massive textured and no true schistose type, as described above, was found. Towards the margins of the body, and particularly in the narrow sheets in the spruit, the nepheline syenite appears to be a finer-grained equivalent of the more massive variety. Banding has been noted in some of the more coarsely porphyritic varieties (Plate 2.2h). Feldspar-rich "schlieren" are noted in places. These feldspathic patches are typically 5 to 15mm wide, seldom longer than 50cm, and tend to have diffuse margins, often with narrow "selvedges" enriched in mafic constituents. These observations suggest that the streaks represent pockets of felsic material squeezed from the surrounding nepheline syenite.

Unlike the Rietfontein sheet, it appears that the Mare body was emplaced largely as a single magma pulse although one cross cutting sheet was observed. It is significant that the finer-grained material in this case is generally slightly porphyritic, shows very little foliation and the margin is free of the leucocratic veining so characteristic of injections of schistose syenite in the Rietfontein outcrops.

Plate 2.3

2.3a: Pegmatoidal nepheline syenite developed along inner (south eastern) margin of Rietfontein sheet on Rietfontein.

2.3b: Assymetric fold structure in schistose nepheline syenite. Note thin felsic veinlets. Rietfontein.

2.3c: View across the carbonatite from the north-eastern margin to Spitskop hill to the south west. Note the sparse vegetation over the carbonatite.

2.3d: Vertical flow structure in beforsite defined by apatite-magnetite concentrations. Tshweneng River.

2.3e: Part of the north eastern contact of the carbonatite. Brownish upstanding rocks on left are beforsitic carbonatite; the grassy surface to the right is underlain by ijolite. Southern slope of Mare hill.

2.3f: Bladed crystal texture ("Spinifex") in carbonatite. Southern slope of Mare hill.

2.3g: The outcrop of the western plug of basalt (see locality in Figure 2.3).

2.3h: Dyke of basalt in carbonatite. Photograph taken in the disused pit of the Spitkalk Quarry.

PLATE 2.3


(a)


(b)


(c)


(d)


(e)


(f)


(g)


(h)

The dyke offshoots which cut the fenites along the upper Mare spruit are characterised by greater abundance of felsic veinlets and, at the margins of the dykes, spectacular feldspar pegmatites have developed.

2.4.4. *Spitskop nepheline syenite body*

The nepheline syenite body underlying Spitskop would also appear to be a single body with sheet-like extremities separated by screens of ijolite. The south-western margin of the body is composed of very fine-grained, grey-green schistose foyaite in which felsic veinlets are typical. Towards the centre of the body, porphyritic to massive textures are common.

2.4.5. *Eastern nepheline syenite sheet*

A sheet of fine-grained nepheline syenite forms an arcuate outcrop around the eastern and south-eastern margin of the Complex. Along its southern extent it abuts directly against granitic country rocks whereas it is bounded within ijolite to the north. Most of the body consists of grey-green schistose nepheline syenite in which felsic stringers are typical and it bears a marked resemblance to the schistose material on Rietfon-tein. Boulder float of coarser porphyritic varieties of nepheline syenite is commonly encountered in this area but outcrop of this rock type was not seen.

2.5. *Carbonatites*

Carbonatite forms a heart- or triangle-shaped outcrop, some 1.1 km^2 in size, eccentrically positioned somewhat east of centre in the Complex. Being more readily eroded than the bounding silicates, the carbonatite occupies the lower-lying central parts of a topographic bowl. Soils overlying the carbonatite are poor and as a result the position of the carbonatite is marked by a scarcity of vegetation, with short grasses dominating (Plate 2.3c).

Verwoerd (1967) refined the original mapping of Strauss and Truter (1950) and described the field relationships and petrography of the carbonatite in greater detail. The carbonatite is not homogeneous and comprises an essentially concentrically-arranged alternation of compositional types: calcitic carbonatite (sövite) occurs along the southern rim and in the eastern apex of the triangular outcrop area; most of the central part is occupied by dolomitic varieties (beforsite) with some hybrid types

Figure 2.2: Geological map of the Spitskop Carbonatite.

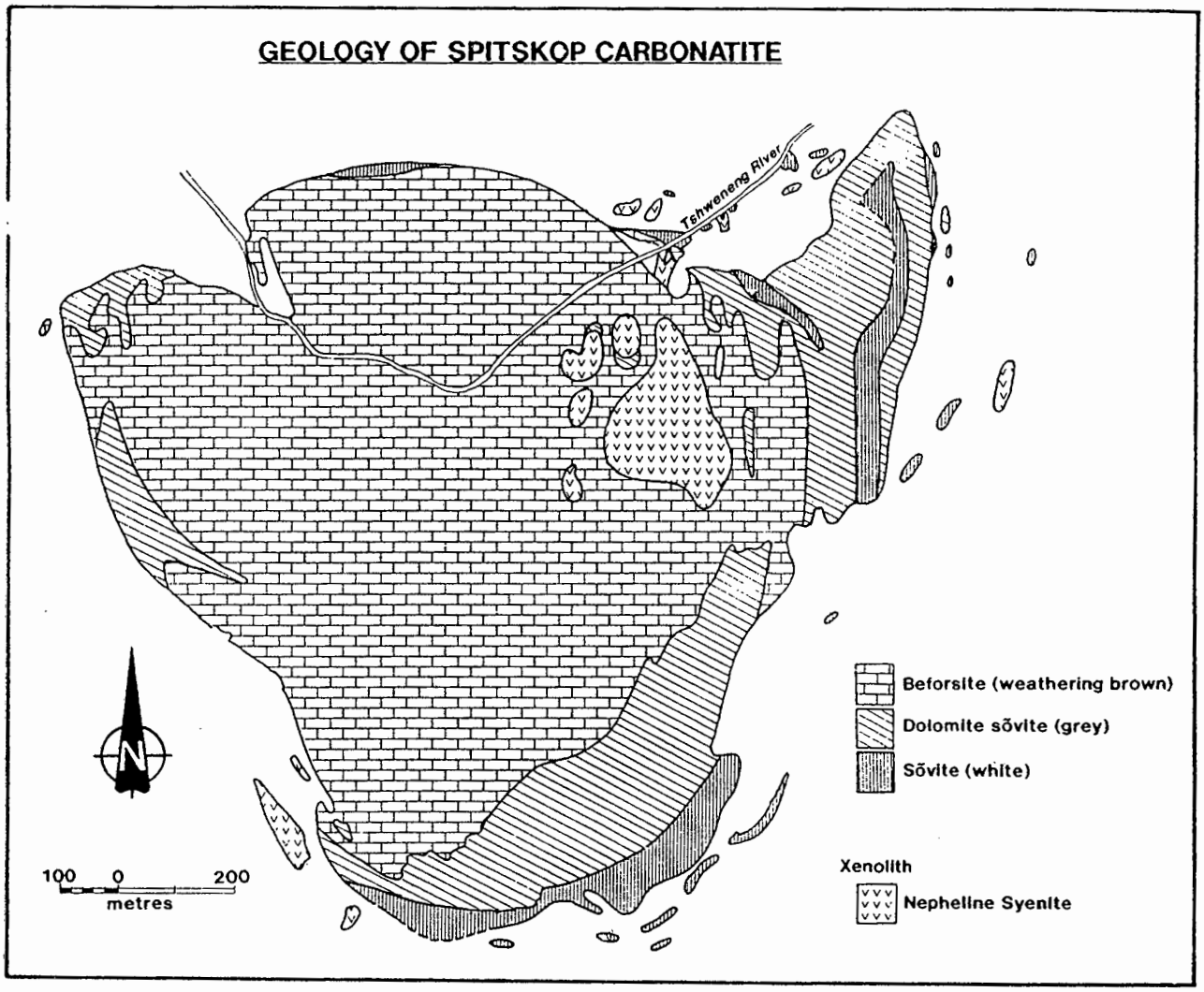

Compiled largely from the map of Verwoerd (1967) with certain xenoliths excluded.

developed in between and along the western margin (Figure 2.2). Strauss and Truter (1950) thought that the central, beforsitic, zone represented an "undecapitated ring dyke" intrusive into the sövite whereas Verwoerd (1967), on the basis of petrographic observations, concluded that the central parts formed by replacement of the outer sövite. Both reports, therefore, regard the beforsite as younger than the sövite.

Woolley and Kempe (1989) proposed that terms such as calcite or dolomite carbonatite (or calcio- and magnesio-carbonatite) be used in preference to sövite and beforsite, respectively. For ease of discussion, reference to the older terms, as originally used by Strauss and Truter (1950) and Verwoerd (1967) will be used to aid discussion of the field relationships and petrography of the carbonatites, but the

terminology recommended by Woolley and Kempe (1989) will be introduced in characterising the carbonatites in the chapter on geochemistry (Chapter 4).

2.5.1. *Calcitic carbonatite ("Sövite")*

Calcitic carbonatite is generally coarser than the dolomitic varieties, carbonate rhombs are commonly 5 to 10 mm across but sparry varieties having crystals up to 25 mm are not uncommon. Two dykes of extremely coarse white carbonatite containing calcite rhombs 4 cm in size cut across the Tshweneng River downstream of the main carbonatite outcrops. More dolomitic carbonate is noted in some samples as a finer-grained, yellowish material filling the interstices between sparry calcite grains.

Non-carbonate constituents generally do not exceed 5-10 percent of the rock by volume, and usually account for less than 1 percent. Concentrations of blue amphibole are noted in the calcitic carbonatite outcrops at the south-eastern edge of the carbonatite body and in the pits of the quarry in the north east.

2.5.2. *Dolomite-calcite carbonatite ("Dolomite Sövite")*

Verwoerd (1967) regarded this variety as an intermediate stage in the "magnesium alteration" of the calcitic- ("sövite") by later dolomitic- carbonatites "beforsite". The "dolomitic sövite" is distinguished by its grey surface colour and grain size from the calcitic and dolomitic carbonatite varieties. Slightly finer-grained than the calcitic variety, sparry carbonate rhombs are still noted and average 3 mm in size.

"Dolomitic sövite" is most abundant in the north-eastern part of the carbonatite body and was well exposed by the quarry-ing operations between 1984-1988. A noteworthy feature of the material revealed in these exposures is the proportion of silicate minerals in the carbonatite: blue amphibole is most common but pyroxene is also noted. The silicates are usually arranged along grain boundaries and may define a foliation in the carbonatite. This fabric was traced by Verwoerd (1967) and shown on his detailed map of the carbonatite outcrop (folder 3; between pages 30,31 in the memoir). Pyrite, magnetite and apatite are also common in this variety and, like the amphibole, are not uniformly distributed through the "dolomitic sövite" but form in patches or streaks, characteristically drawn out into the foliation.

2.5.3. *Dolomitic carbonatite ("Beforsite")*

Dolomite carbonatites are volumetrically the most significant variety and are characterised by finer, and more uniform, grain size in which carbonate grains are typically less than 0.5 mm in size. When fresh, the carbonatite is cream or pale sky-blue but weathers to a distinctive toffee-brown colour.

Blue amphibole is sporadically developed but is less significant than in the previous varieties, usually occurring in irregular clots and patches rather than as persistant streaks. Apatite and magnetite are once again common accessory constituents. Apatite concentrations take the form of schlieren of "..innumerable very thin, closely spaced, microcrystalline streaks.." which define a foliation in the carbonatite (Verwoerd, 1967). Verwoerd (1967) mapped three zones of major apatite concentration within the carbonatite. In the north-central part of the dolomitic carbonatite outcrop, dark apatite schlieren ("..due to contamination with feruginous dust..") are arranged in a continuous circular zone some 400 m in diameter. This zone is particularly well exposed in the banks of the incised Tshweneng River where the structure is seen to be pipe-like with near vertical sides on the north and west, plunging steeply on the south and south-east sides (Plate 2.3d). North of the river this zone is well exposed in a number of large, flat pavements. North of the zone of schlieren, apatite occurs as rounded clots, 2-5 mm across, usually elongated in the foliation direction. These clots are waxy, grey to white, and are characteristically rimmed by fine, darker grey material which appears to be a form of microcrystalline silica. A feature of this zone is the occurrence of euhedral magnetite phenocrysts: these occur as octahedral crystals commonly 5 to 10 mm in diameter and rare examples attain sizes of 15 mm. Magnetite phenocrysts may be concentrated in schlieric lenticular streaks.

Identical apatite clots are abundant near the eastern side of the exposures, to the west of the road between Spitskop and Mare.

2.5.4. *Contact relationships*

Contacts between carbonatite and bounding silicate units are never seen but it is possible to confidently locate the position of the junction in most places to within 5 m. For this reason the essentially smooth and regular outline of the carbonatite, as shown on Verwoerd's (1967) map, is real and noteworthy. Dyke offshoots from the main body are rare and do not penetrate far into the silicates, while brecciation of the

encompassing silicates is never seen. These observations would suggest that the carbonatite was emplaced passively, at least at the currently exposed level in the complex. In addition, there is little detectable change in the local ijolite country rock as the contact with the carbonatite is approached.

Contact relationships are best studied along the north eastern portion of the carbonatite body, on the south eastern slopes of the Mare hill. Here the edge of the carbonatite exposure forms a regular and apparently sharp contact which can be traced continuously for over 400 m (Plate 2.3e). The outer 15 to 25 cms of the carbonatite exposure have a finer grain size and purplish colouration. This feature could simply reflect the action of ground- and rain-water percolating along the carbonate - silicate interface, but probably represents a contact facies of the carbonatite. In places along this northern margin, the dolomitic carbonatite develops an unusual texture which presumably also relates to some contact effect. In place of the generally uniform, fine, granular texture, the carbonate forms sheafs of bladed crystals, generally less than 1 mm in width by 40 mm or more in length, individual blades sometimes separated by a film of soda amphibole (Plate 2.3f). This "spinifex"-like texture is similar to that described by Cooper and Reid (1991) from the Dikker Willem carbonatite, Namibia, and has been found in quenched carbonatites in experimental charges by Sweeney *et al.* (in press).

Verwoerd (1967) described xenoliths of silicate rocks within the borders of the carbonatite: predominantly nepheline syenite, ijolite and a patch of granophyre country rock were also mapped. It is extremely difficult to confirm that these occurrences all represent xenoliths in the carbonatite. Being relatively easily weathered, the carbonatite occupies topographically low areas several tens of metres below the prominant exposures of silicates on Mare and Spitskop. The resistance of the nepheline syenites, and the tendency of nepheline syenite boulder scree to persist across exposed lithological boundaries was described previously. Boulder float of Bushveld granite is commonly discovered throughout the complex and the "granophyre xenolith" is almost certainly float (confirmed by Verwoerd, pers. comm., 1987). Verwoerd (1967) describes the carbonatite foliation wrapping around the patch of nepheline syenite which suggests that this occurrence, at least, does represent a xenolith in the carbonatite.

2.5.5. Intrusions of "Basalt"

The last identifiable phase of magmatic activity in the Spitskop Complex was the intrusion of small, localised bodies of amygdaloidal, very fine-grained, "basaltic"

Figure 2.3: Sketch map of the lower Tshweneng River showing the location of the two basalt plugs.

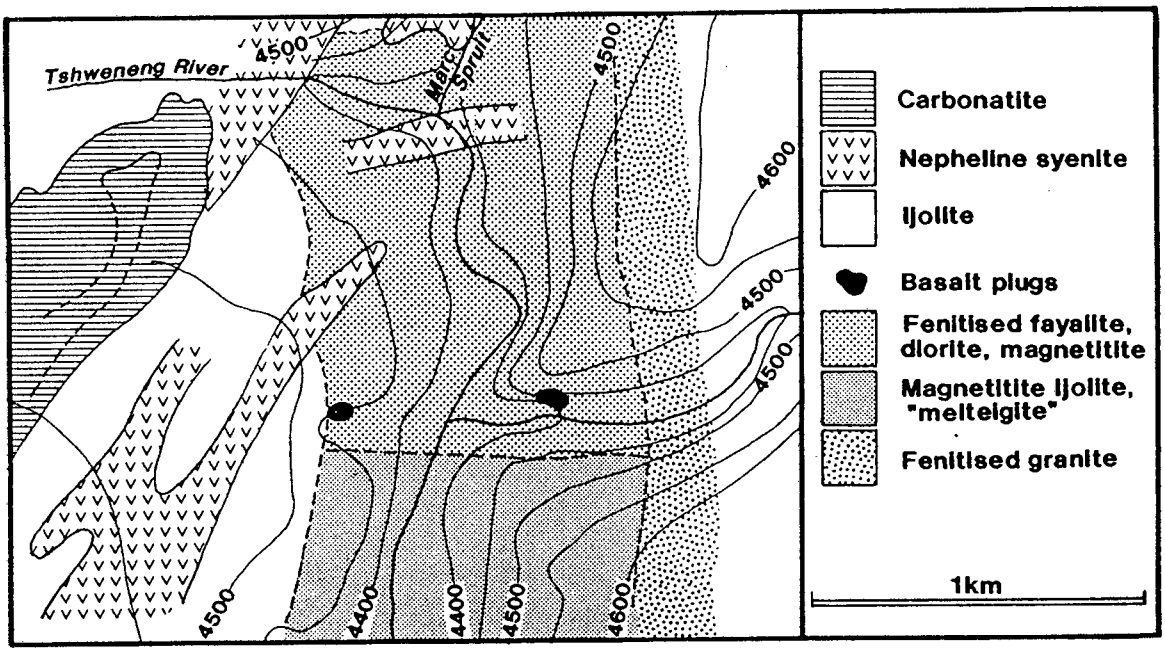

material. While being aware of the terminology problem in using "basalt" for a clearly intrusive magmatic rock, the very fine-grained to glassy nature of much of the material renders the term "dolerite" equally inappropriate. For this reason the terminology used by Strauss and Truter (1950) will be followed.

Two rounded plugs of "soda basalt" were first mapped by Strauss and Truter (1950) on either side of the lower Tshweneng River (Figure 2.3). The western plug is well exposed and is elliptical in form, some 10 by 6 metres in size, and is composed of extremely fresh, blue-grey, fine-grained amygdaloidal material. Finely disseminated pyrite is abundant. The plug is surrounded by grass-covered soil and contact relationships can not be observed (Plate 2.3g) . The eastern plug pierces fenitised fayalite diorites along the tributary stream some 20m upstream of its confluence with the Tshweneng River. Here the plug material is fine-grained, khaki brown in colour, and rather more weathered than in the eastern plug. A distinctly finer-grained, fractured margin, 10-20mm wide, is noted at the contact with the surrounding fenites. Some three dimensional exposure is available at this locality from which the steep, pipe-like form of the intrusion may be established. The occurrence of vesicles and amygdales in the "basalt" of the two plugs would argue a relatively shallow depth of intrusion.

Dykes of "basaltic" material were found cutting the carb-onatite in the pits of the quarry in the north-eastern part of the carbonatite (Plate 2.3h) , and provide evidence that the basalt magmatism postdated the cooling of the carbonatite.

Chapter 3: Petrography of Units of the Spitskop Complex

In this chapter the petrographic character of each of the rock types in the Spitskop Complex are described.

3.1. Pyroxenites

In thin section, the pyroxenite is composed of an interlocking mosaic of anhedral, colourless to faintly green clinopyroxene grains, up to 4 mm in length, with magnetite, brown biotite and apatite as subordinate constituents (Plate 3.1a). In rare sections are the pyroxenes subhedral, in which case the texture may resemble a cumulate rock. Clinopyroxene is typically unzoned and weakly pleochroic: only close to intrusive ijolite do the pyroxenes exhibit zoning to deep green rims. Microprobe measurements (see following chapter) indicate that the clinopyroxene is a low-Ac diopside averaging $Di_{80}Hd_{10}Ac_{10}$.

Biotite generally comprises less than 1 to 2 modal percent, occurring as narrow intergranular fillings, and as small, oriented, prismatic flakes enclosed in the diopside. Magnetite forms as large (over 1 mm), anhedral grains with scalloped margins intergrown with pyroxene, and as small (less than 0.1 mm), subhedral inclusions in the clinopyroxenes. Magnetite inclusions are sometimes arranged in granular clusters. Apatite grains occur as inclusions within the interstitial biotite. Biotite commonly envelopes larger magnetite grains and Strauss and Truter (1950) suggested that a portion of the biotite is a reaction product after magnetite. Where scalloped magnetite grains are bounded by biotite, narrow, discontinuous rinds of titanite intervene along the actual biotite-magnetite contact. Clinopyroxene-biotite contacts are generally sharp and only rarely does biotite occur in irregular, feathery intergrowth with pyroxene suggesting that the mica may be replacing clinopyroxene.

Plate 3.1

Unless otherwise stated, the width of each photomicrograph is equivalent to 4.3mm of section and the photograph was taken in plane polarised light.

3.1a: Photomicrograph of pyroxenite S44. Note the interstitial biotite mica and anhedral magnetite.

3.1b: Photomicrograph of "Type-I" ijolite (S41). Note the zoned clinopyroxene grain (on right) and the large titanite (brown grain on left).

3.1c: Fine-grained "Type-I" ijolite (S51). Note the euhedral square and hexagonal sections of nepheline.

3.1d: Fine-grained granoblastic texture typical of the "Type-II" variety as defined in the text. (Sample S42).

3.1e: Granoblastic, "Type-II" ijolite variety. Photograph is approximately 1mm across. (Sample S52).

3.1f: Type-II ijolite with rounded, clear clinopyroxene in ochrish ("spreustein") matrix. Crossed polars. (Sample S65).

3.1g: Photomicrograph of pyroxene in close proximity to intrusive dykelet of ijolite. Note the good crystal form and strong zoning of pyroxenes. Interstital material is mixture of cancrinite, nepheline and natrolite (Sample S49 from upper Rietfontein Spruit).

3.1h: Photomicrograph of stringer of pyroxenes set in matrix of Type-II, granoblastic ijolite. Such textures are typical of zones where pyroxenite has been extensively mixed with urtite ("nephelinisation" of pyroxenite).

PLATE 3.1

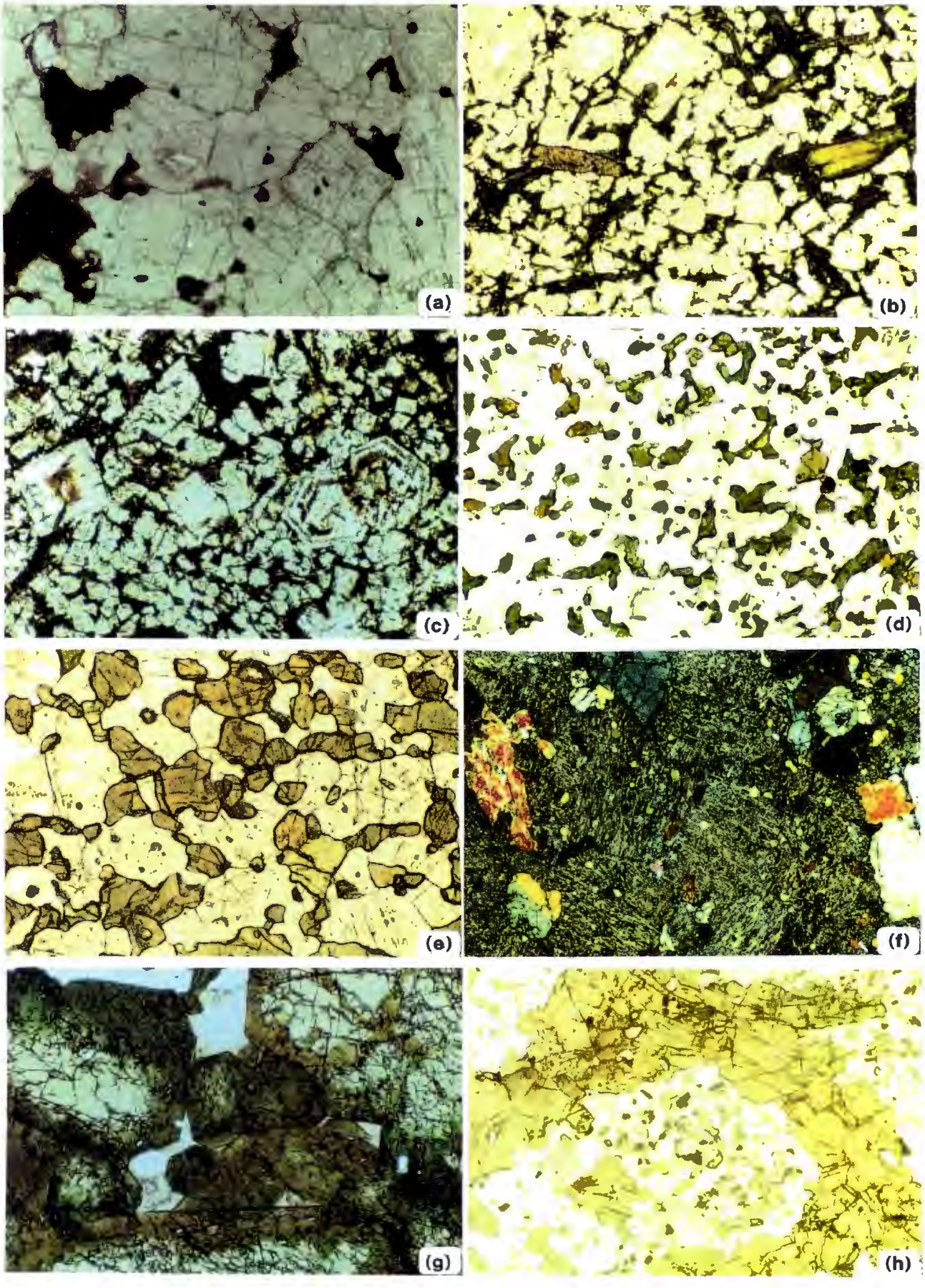

3.2. *Ijolites*

Not surprisingly, the complexities seen in ijolite outcrops translate to an intimidating range of textures in thin section. However, amongst this variation two broad groups of petrographic textures are recognisable.

3.2.1. *Textural Type-I*

Ijolites in this group are characterised by sub- to euhedral, square- or hexagonal-sectioned grains of nepheline set in compact aggregates of prismatic to acicular green clinopyroxene (Plate 3.1b, 3.1c). In finer-grained samples, clinopyroxene aggregates form continuous rims around the nepheline, generating a net-like, or mesh texture. With increasing grain size, or increased modal proportion of neph-eline, the mesh is discontinuous and clinopyroxene aggregates fill the triangular interstices between the nepheline grains. Samples taken from ijolites which show igneous features in out-crop, for example where tabular sheets of ijolite have fine-grained (chilled) margins, always have this "Type-I" texture. Consequently, Type-I ijolites are interpreted as being of igneous origin.

Clinopyroxene is clearly a later crystallising phase than nepheline and is typically green, pleochroic aegirine-augite (Ac_{15}-Ac_{37}). Larger grains are strongly zoned, with paler green cores and deeply coloured rims. Nepheline characteristically contains oriented needles and blebs of pale green pyroxene. The presence of acmite needles is a fairly common feature of plutonic nephelines (Bailey, 1974a) and probably represent an exsolution feature due to the limited solid solution of nepheline in the system nepheline-acmite (Bailey and Schairer, 1966) and do not indicate early crystallisation of clinopyroxene. Titanite is a common accessory in variable proportions and is generally fairly coarse-grained, coarser than the clinopyroxene, and sometimes comparable in size to nepheline (Plate 3.1b). Apatite is an ubiquitous accessory.

Pegmatitic ijolite fractions essentially represent a coarser variant of the "Type I" texture in which the pyroxenes form larger, discrete euhedral grains intergrown with subhedral nepheline rather than as grain clusters. Clinopyroxene is usually zoned from pale green cores to deep green margins. Apatite and large euhedral titanite again comprise the accessories. Cancrinite is very common, particularly in the more nepheline-rich urtite fractions and forms large poikilitic plates enclosing and partially replacing nepheline.

3.2.2. *Textural Type-II*

Many ijolites sampled had textures so clearly distinct from the "Type-I" variety that they could not conceivably share a common genesis with the latter type. Best termed "granoblastic", this texture is typically composed of granular intergrowths of anhedral nepheline and amoeboid clinopyroxene which are characteristically interspersed with zones of polygonal nepheline mosaics which contain rounded, "teardrop-like" individual pyroxene grains set at the triple junctions of adjacent nepheline grains (Plate 3.1d and 3.1e). In its developed form, this texture is reminiscent of that characteristic of granulite facies metamorphic terrains (e.g. as depicted by Moore, 1970). Titanite, either as euhedral wedges or as highly irregular intergrowths with pyroxene, and apatite are ubiquitous accessory phases. Flakes of brown biotite are rare.

Ijolites with this granoblastic texture are typically found in exposures where remnants of pyroxenite are noted.

A sub-class within this textural type is recognised in which unzoned pyroxenes with the typical teardrop form, sometimes arranged in polygranular trails or clusters, occur in a fibrous to amorphous, turbid, ochrish material with moderate birefringence which cannot be completely resolved by the microscope (Plate 3.1f). Cancrinite sometimes forms a narrow clear mantle around the pyroxenes. This feature is reminiscent of "spreustein" alteration as described by Vlasov *et al.* (1966) in the Lovosero Massif of the Kola Peninsular as "..a finely-crystalline mixture consisting mainly of natrolite with an admixture of hydrargillite, diaspore and opaque colloidal matter." This turbid material has clearly not formed through weathering as the clinopyroxenes are perfectly fresh. This sub-type was sampled from the same exposures from which typical type-II ijolites were recovered.

3.2.3. *"Nephelinised" Pyroxenite*

To investigate the influence of the intrusive ijolite sheets on the pyroxenite and to study the "nephelinisation" process envisaged by Strauss and Truter (1950), sections were cut from samples of pyroxenite (S49 and S85) in which 5-10mm wide ijolite dykelets occur.

The most noticeable effect of the ijolite veinlets is that the pyroxenes in the pyroxenite become intensely zoned to darker green margins (Plate 3.1g) which are

significantly more acmitic than the cores (up to Ac_{40}). In addition, patches of felsic components develop in the interstices between clinopyroxenes some distance from the dyke. These patches comprise nepheline variably corroded by cancrinite with scaly aggregates of fine cancrinite and zeolite (?natrolite?). An increase in abundance of cancrinite and zeolite, usually replacing the ijolite nepheline, is also commonly noted at the margins of the ijolite dykelet.

Strauss and Truter (1950) reported a build up of biotite in the pyroxenite near the contact with ijolite. Careful examination of numerous outcrops and thin sections across ijolite-pyroxenite contacts could not confirm this. Indeed, the ijolites are almost completely free of mica or any other potash-bearing phase and so it is difficult to explain the source of the potassium which would be required to generate biotite from clinopyroxene and/or magnetite. Contacts are rather marked by concentrations of *sodic* cancrinite and nepheline. Titanite and apatite also commonly precipitate near this interface. It is more likely that the biotite in the pyroxenite, and the "glimmerite" mica concentrations, are original components in the pyroxenite and were generated prior to the emplacement of the ijolite sheets.

With progressive permeation of ijolite components (essentially nepheline) into the pyroxenite, the pyroxenite disaggregates into stringers of pale green, unzoned clinopyroxene aggregates. The outer margins of the stringers are highly irregular and extensively embayed with small, anhedral nepheline grains, whereas internally, the pyroxene grain contacts are identical to those noted in the pyroxenite. These stringers are dispersed in ijolite having the distinctive Type-II, or "granoblastic", texture (Plate 3.1h).

From these observations Type-II, "granoblastic" textured ijolite varieties may develop through the introduction of the nepheline component from intrusive Type-I ijolite (essentially the addition of urtite) to pyroxenite and subsequent recrystallisation.

3.2.4. Other textural variants

The previous textural types account for about seventy-five percent of the ijolites sampled; the remainder contain textural or mineralogical variations, often subtle, that do not conform completely to either of the groups described above.

A phase of ijolite occurs in the upper Rietfontein Spruit which contains distinct felsic ocelli and millimetre-sized feathery mafic streaks or clots. This unusual

type forms a discontinuous dyke-like unit within the other ijolite types. In thin section the rock is unusual in containing small amounts of biotite distributed throughout the slide. The clinopyroxenes are distinct from the other textural types in occurring as elongate anhedral grains, often intimately intergrown with irregular titanite. Another characteristic is the occurrence of aggregates of intergrown clinopyroxene, biotite and magnetite. These mafic minerals are set in an equigranular mosaic of polygonal nepheline.

Outcrops along the lower Tshweneng River are composed of melanocratic ijolites which commonly contain rounded enclaves of magnetite ranging in size from 10 mm or less up to blocks over 1 m in size. These enclaves appear to represent xenoliths derived from upper zone magnetitites in the underlying Rustenburg Layered Suite and will be discussed in more detail in a later chapter. The surrounding ijolites comprise a complex mix, on the millimetre to metre scale, of ijolite exhibiting the characteristic "Type-I" texture, and magnetite-rich ijolites in which the constituent minerals are all anhedral and irregularly intergrown. Textures are highly variable, even at the scale of one thin section. These dark ijolites were termed "melteigites" by Strauss and Truter (1950).

Plate 3.2

Unless otherwise stated, the width of each photomicrograph is equivalent to 4.3mm of section and the photograph was taken in plane polarised light.

3.2a: Composite photomicrograph of typical schistose nepheline syenite from the Rietfontein sheet composed of fine feldspar laths and interstitial acicular soda clinopyroxene. Note cancrinite (yellow) poikilitically enclosing the other minerals in the portion of the photograph taken under crossed polars.

3.2b: Schistose nepheline syenite showing a micro fold deforming the fabric. (Sample S156; Rietfontein)

3.2c: Composite photomicrograph of "nepheline-phyric" nepheline syenite showing euhedral clinopyroxene grains and generally "knotty" appearance of texture. Patches with high interference colours in crossed polar segmant are pectolite. (Sample S03; Rietfontein).

3.2d: Composite photomicrograph showing interstitial pectolite (high relief, high interference colours) in coarse nepheline syenite (S02).

3.2e: Composite photomicrograph of nepheline phenocrysts in foliated matrix of fine feldspar laths in which euhedral clinopyroxene prisms are identifiable. Note the oriented needles of pale green pyroxene contained within the nepheline (S148, Mare).

3.2f: Composite photomicrograph of trachytic nepheline syenite typical of the "eastern" syenite body. Note characteristic carlsbad-twinned and zoned alkali feldspar phenocrysts.(S105, eastern).

3.2g: Photomicrograph (taken with crossed polars) of dolomitic sövite showing large euhedral sparry calcite surrounded by finer-grained aggregates of more magnesian carbonates (ankerite - dolomite). (Sample S55).

PLATE 3.2

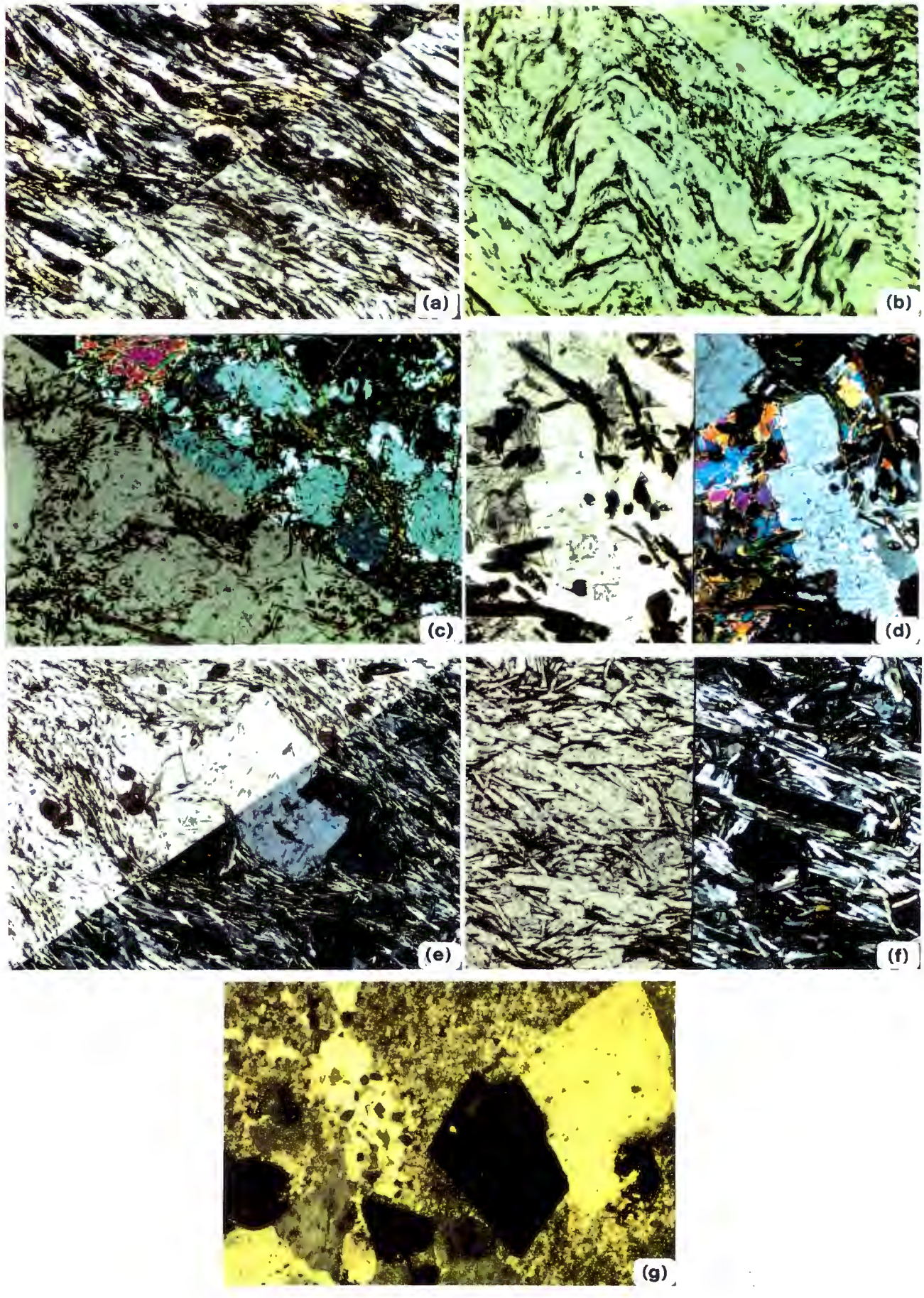

3.3. *Nepheline Syenites*

All varieties of nepheline syenite consist of alkali feldspar, nepheline and green acmitic clinopyroxene with varying amounts of interstitial cancrinite, pectolite, sodalite and natrolite, and accessory titanite. Textural variations are noted between nepheline syenites sampled from the different nepheline syenite bodies and so the petrographic descriptions are ordered by locality.

3.3.1. *Rietfontein*

Schistose varieties of nepheline syenite in the Rietfontein sheet are composed of oriented laths of perthitic potassic feldspar, interspersed with a densely-packed matrix of acicular, often wispy or fibrous, pleochroic, green aegirine-rich clinopyroxene and small, subhedral nepheline. The feldspar has the optical properties of sanidine (no tartan twinning; low, negative 2V). Clinopyroxene sometimes develops in small radial tufts but usually forms aligned fibrous trains wrapping around the feldspar laths (Plate 3.2a) and nepheline. Pectolite is common interstitially. Intergrowths of pectolite and nepheline may form lens-shaped clots. Feldspar laths are sometimes bent and the planar fabric is frequently disturbed and micro folds are seen in some sections (Plate 3.2b). Large plates of cancrinite, some 15-20mm in diameter, are common and poikilitically enclose the major minerals (Plate 3.2b).

Feldspathic streaks and veins contain anhedral feldspar and nepheline, usually extensively corroded, in a matrix of cancrinite, sodalite, granular mosaics of fine grained zeolitic minerals of the natrolite group, and scattered pectolite.

Gradation to coarser varieties in the Rietfontein sheet is marked by an increase in size of the feldspar laths and a tendency to better crystal shape of the nepheline and clinopyroxene. Clinopyroxenes remain typically elongate, however, and the groundmass retains an oriented fabric. Nepheline is almost always the earliest crystallising phase. Only one sample (S31) was found where clinopyroxene appears to be the earliest phase.

Textures in the coarser nepheline syenites are seldom equigranular and are essentially dictated by the nature and habit of the phenocryst phase. When this phase is alkali feldspar, the typically tabular laths have a planar alignment and are surrounded by a matrix of intergrown acicular clinopyroxene, nepheline and smaller feldspars. In samples where nepheline is the coarsest phase, its essentially equant

habit gives the rock a "knotty" appearance in thin section, with the matrix of feldspar laths and clinopyroxene needles wrapping around the square to rounded sections of nepheline (Plate 3.2c).

In all the feldspar-phyric types, the phenocrysts are micro-perthitic and are typically rimmed by albite. As the feldspars increase in size they become subhedral, enclose euhedral insets of nepheline and clinopyroxene, having clearly overgrown earlier crystallised minerals. Perthitic patches are coarser and are more common in the vicinity of nepheline inclusions.

Pectolite and cancrinite are more noticeable in the coarser varieties, mostly due to their larger size rather than a real increase in abundance. The pectolite is in textural equilibrium with the other phases with sharply defined grain margins and is seen to poikilitically enclose euhedral nepheline (Plate 3.2d). Cancrinite generally appears to replace nepheline but in some sections cancrinite is observed in apparent textural equilibrium with nepheline. Sodalite is common as a rim to feldspar and nepheline.

All textural varieties of nepheline syenite in the Rietfontein sheet are hypersolvus: albitic feldspar is only seen in perthitic exsolutions and as narrow borders to the large feldspar macrocrysts.

Banded nepheline syenite

Contiguous sections (S186 a1,a2,b1,b2,c) were cut from a 15cm section of the banded nepheline syenite noted described in Chapter 2. In thin section the banding is defined principally as variations in the relative proportion of clinopyroxene, and as an alternation between nepheline-phyric and feldspar-phyric textures, as described above. Sample S186c is distinctly more feldspar-rich than the others.

3.3.2. Mare

Nepheline syenites from the Mare body are texturally distinct from those on Rietfontein: this distinction is largely the result of a far larger proportion of fine feldspar laths in the matrix than in samples from Rietfontein. The characteristic texture in the Mare nepheline syenites is of early-formed, sub-hedral nepheline crystals, typically 10-15mm in diameter, set in a trachytic matrix of euhedral green pyroxene and small, euhedral tabular sanidine laths which are generally between 0.5mm to 0.7mm in length. The trachytic matrix wraps around the nepheline crystals giving rise to an "augen"-like fabric. Matrix feldspars are typically zoned with

Carlsbad-twinned centres sharply overgrown by an albitic rim. Nepheline commonly contains oriented needles of pale green pyroxene, usually aligned at high angle to the orientation of the fabric in the adjacent parts of the syenite (Plate 3.2e). Where porphyritic feldspar textures occur, the large K-feldspars contain inclusions of nepheline and are generally perthitic with patchy albite. Titanite is an abundant accessory phase.

Late stage auto-metasomatic alteration effects are reflected in the rimming of some nepheline and feldspar by sodalite, corrosion of nepheline by cancrinite, and in one sample, by the apparent replacement of pyroxene by pectolite. In some samples the nepheline phenocrysts may be completely pseudomorphed by granular cancrinite. Auto-metasomatic effects are best developed in the coarser varieties of nepheline syenite.

Samples from the narrow offshoots which cut across the fenites essentially show a finer version of the texture found in the coarser nepheline syenites of the main body. A trachytic texture is more pronounced due to increased abundance of aligned laths of alkali feldspar relative to nepheline. The lack of any secondary alteration in these samples is significant as it implies that the metasomatism of the surrounding mafic fenites occurred before the nepheline syenite sheets were emplaced, or that the fluids effecting the fenitisation were in equilibrium with (derived from?) the syenite magma.

3.3.3. Spitskop

Nepheline syenites from the Spitskop body appear to share textural characteristics with those of both the Mare and Rietfontein bodies. Aligned laths of sanidine are characteristic of the fine-grained marginal facies whereas perthitic feldspar occurs in the coarser, more homogeneous varieties. Schistose types are more feldspathic than those on Rietfontein and the clinopyroxene forms more robust crystals and, although acicular, is not fibrous. Coarser feldspars are perthitic to anti-perthitic and enclose finer, euhedral nepheline. Albite patches tend to concentrate around these inclusions. The margins of the feldspars form complex intergrowths of albite and nepheline. Pleochroic, grey-blue to green, amphibole (arfvedsonite?) was noted in one sample. All textural varieties show evidence of significant late stage, auto-metasomatic alteration of the felsic components. The margins of alkali feldspars may be corroded by natrolite and/or sodalite, whereas nepheline is partly replaced by cancrinite or sodalite. Pectolite and cancrinite are common groundmass components.

3.3.4. *Eastern sheet*

The generally fine-grained nepheline syenites of the eastern sheet are trachytic with euhedral laths of alkali feldspar wrapping around subhedral nepheline "phenocrysts" which are only marginally larger than the feldspars. Clinopyroxenes form densely packed, fine, acicular interstitial fillings between the oriented feldspars (Plate 3.2f).

3.4. *Carbonatites*

As discussed in Chapter 2, the older terminology of "sövite", "dolomitic sövite" and "beforsite" is initially be adopted for calcitic- to dolomitic- ankeritic- carbonatites to simplify comparison with earlier work on Spitskop.

Verwoerd (1967) mapped "dolomite sövite" separately from "pure" sövite largely on the basis of colour in outcrop and grain size. Incipient replacement of calcite in the sövite by more magnesian carbonate was documented and Verwoerd (1967) regarded the "dolomite sövite" as a "..further [stage] in the replacement of sövite by iron-bearing magnesiodolomite..". Verwoerd does not, however, discuss the modal quantity of ankerite/dolomite at which the distinction between "sövite" and "dolomitic sövite" was drawn. In the present study it was found that dolomite is present in almost all samples taken from outcrops of sövite, suggesting that a continuum exists between pure "sövite" and dolomitic sövite. As a result these two carbonatite types are discussed together in this chapter. The beforsites are sufficiently distinct in both outcrop and thin section to be clearly defined.

3.4.1. *Sövite*

Sövites are typically composed of large grains of calcite surrounded by varying amounts of fine-grained dolomite which appears distinctly darker than the calcite in thin section. In some sections, anhedral calcite is noted surrounded by finer-grained mosaics of ankerite. Commonly, however, coarse, euhedral calcite rhombs occur with dolomite filling the interstices with no obvious signs of replacement (see Plate 3.2g). Darker margins to the rhombs suggest that the dolomite accreted to the early rhombs. Indeed, although advocating a replacement relationship, Verwoerd (1967, p33) describes calcite occurring "..mainly in the form of coarse-grained (1-3mm) remnants with rhombohedral outlines"! It is difficult to understand how corroded "remnants"

would retain euhedral "rhombohedral outlines". Verwoerd also made the observation that "Peculiarly enough, places where the replacement process has progressed to the extent that calcite becomes a minor constituent were not encountered" and therefore the "dolomitic sövites" are always compositionally "..closer to that of sövite than [ankeritic] beforsite."

Although replacement of calcite by dolomitic varieties is noted, the textural evidence would be equally consistent with the interpretation that many of the dolomitic sövite varieties represent early-formed calcite "phenocrysts" mixed with variable amounts of later formed ("intercumulus"), dolomitic carbonatite.

Soda amphibole, showing strong pleochroism from lilac to pale blue-green, occurs as fibrous crystals either randomly distributed as tufts, or grouped into veinlets arranged sinuously along grain boundaries. Green to green-brown clinopyroxene also occurs but is less common then the amphibole. Verwoerd (1967) determined that the pyroxene was acmite. Pennine chlorite is noted as an alteration product of clinopyroxene in some sections. Magnetite and apatite are common accessories.

3.4.2. Beforsite

Beforsite is distinguished in thin section by the finer grain size (average 0.2-0.3mm) of the carbonate which generally forms an interlocking mosaic of anhedral grains. Euhedral crystals are rare and occur as rhombohedral grains set in a finer, and darker coloured, matrix of interlocking anhedra. Magnetite is common and usually occurs as dustings of very fine-grained but euhedral crystals. Trails of fine magnetite grains also occur and are sinuously arranged along grain margins. Strongly pleochroic (lilac to pale blue), fibrous amphibole occurs as tufted aggregates or in veinlets (described as "slip-fibre" by Verwoerd, 1967). Brown-green clinopyroxene was rare.

Verwoerd (1967; p35) determined that the main carbonate in the beforsite is ankerite but found that, in places, carbonate grains have iron-bearing dolomite cores surrounded by ankerite. Interestingly, Verwoerd contends that "no replacement relationship seems to exist between the two components"; by implication, then, the ankerite represents a later overgrowth on the dolomite. The dolomite was found by Verwoerd to be the equivalent of that noted interstitially in the sövites.

3.5. *Basalt Intrusions*

Samples from the basalt plugs are extremely fine-grained and appear as brownish devitrified glass in thin section in which crystallites of plagioclase and patches of brown, devitrified glass are discernible. In places the brown material appears to have crystal form, exhibits pleochroism and may be an incipiently-formed amphibole. Rods of this brown material are sometimes seen rimmed by clear feldspar.

Chapter 4: Geochemical Characteristics of the "Igneous" Components of the Spitskop Complex.

4.1. Introduction

In this chapter the salient characteristics of the mineral and whole rock geochemistry of each of the "igneous" components of the Spitskop Complex will be discussed. (Quotes are used in the title because this chapter includes discussion of the Type-II ijolites which are thought to be, at least partly, of metasomatic origin. Fenitisation of the country rocks and of the Bushveld xenolith are specifically excluded, however.) Petrogenetic interpretation of the geochemical data is postponed until Chapters 7 and 8.

All mineral and whole rock major and trace element data are tabulated in Appendix B (Tables B.1 to B.17) along with calculated CIPW normative mineralogy where appropriate. Analytical procedures and comments on data processing (e.g. molecular calculations of minerals, adjustments made for the oxidation state of Fe for the norm calculations, etc.) may be found in Appendix A.

4.2. Mineral Chemistry

4.2.1. Pyroxenites

Available mineral analyses are presented in Table B.1. Only samples demonstrably free of the influence of intrusive ijolite are included; the mineral chemical changes accompanying infiltration by ijolite ("nephelinisation") will be discussed later.

Figure 4.1: Ternary plot of Na- Mg-(Fe^{2+}+Mn) for clinopyroxenes from the pyroxenite.

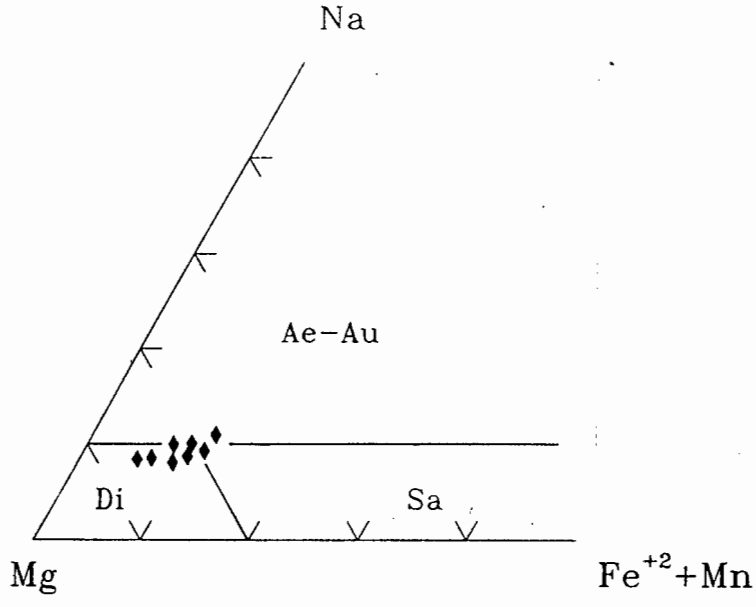

The classification fields are after Jones (1984): Di=diopside; Sa=salite; Ae-Au: aegirine-augite.

The clinopyroxenes comprising the pyroxenite are all diopsidic with low acmite contents and range in composition between $Di_{79}Hd_4Ac_8Sa_9$ and $Di_{69}Hd_{11}Ac_{10}Sa_{10}$. "Sa" refers to "salite" component and is used to denote the sum of "other" components - principally Al, Ti and excess Ca - not accounted for in Ac, Hd and Di. The analyses are plotted on the Na-Mg-(Fe^{2+}+Mn) ternary classification scheme adopted by Jones (1984) in Figure 4.1.

Two analysed micas have atomic Fe:Mg ratios close to 1:2 and hence are near to the boundary between biotites and phlogopites as defined by Deer *et al.* (1966; Fig.74 on page 212).

Figure 4.2: Ternary plot of Na-Mg-(Fe^{2+}+Mn) for clinopyroxenes from Type-I ijolites and urtites.

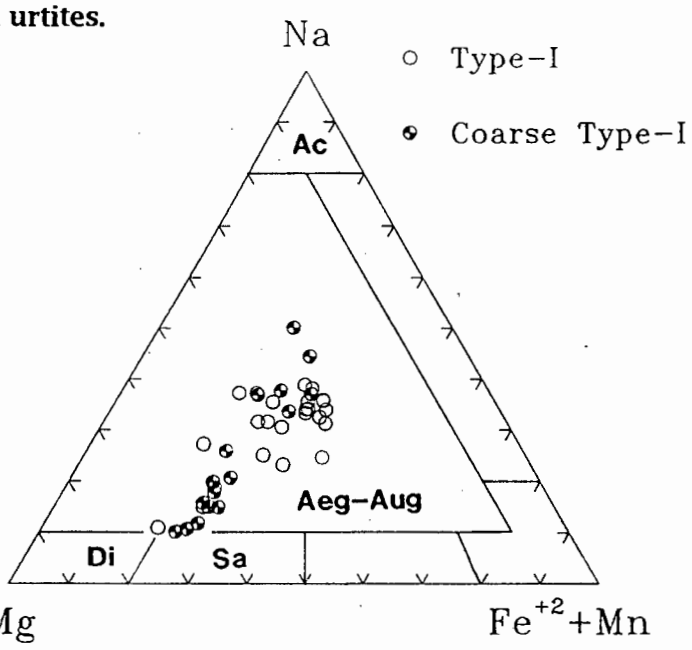

The classification fields are after Jones (1984): Di=diopside; Sa=salite; Ae-Au: aegirine-augite; Ac=acmite.

4.2.2. Ijolites

4.2.2.1. Clinopyroxenes

Clinopyroxene analyses from the Type-I ijolites and urtites are plotted on the Na-Mg-(Fe2++Mn) ternary in Figure (4.2) where it may be seen that the pyroxenes are "aegirine-augite", with three analyses falling on the boundary of the salite field. It is not possible to distinguish the compositions of pyroxenes in the coarse ijolites from those in the finer type.

Clinopyroxenes in the Type-II granoblastic ijolite are also aegirine-augite, but with generally less acmite and more diopside-salite component (Figure 4.3) than in the Type-I variety. In addition, Type II clinopyroxenes include somewhat higher concentrations of non-quadrilateral components, such as Al and Ti (Figures 4.4a and 4.4b).

As noted in Figure 4.4c the principal substitution is between Ca and Na for clinopyroxenes from all ijolite types, the antipathetic 1:1 trend reflecting the relative proportions of salite ($Ca[Mg,Fe]Si_2O_6$) and acmite ($NaFe^{3+}Si_2O_6$) molecules. Both Al and Ti remain in low concentration but show systematic variation (Figure 4.4(d)). Sympathetic variation of Al and Ti is consistent with the hypothetical pyroxene

Figure 4.3:Ternary plot of Na-Mg-(Fe^{2+}+Mn) for clinopyroxenes from Type-II ijolites.

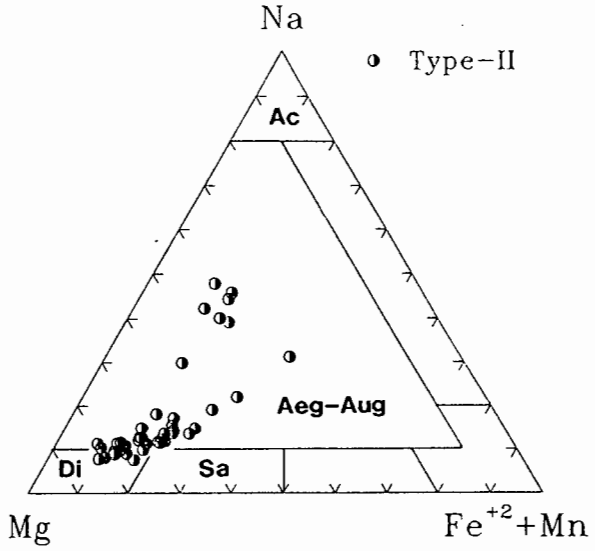

The classification fields are after Jones (1984): Di=diopside; Sa=salite; Ae-Au: aegirine-augite; Ac=acmite.

component $CaTiAl_2O_6$ (Yagi and Onuma, 1967) but, as discussed by Scott (1976), substitutions consistent with this component would produce correlations of 2Al:1Ti. The variation of Al and Ti in the ijolite pyroxenes is closer to 4Al:1Ti, similar to the relationship found for clinopyroxenes from the mafic alkalic volcanics of the Canary Islands by Scott (1976). The lack of any meaningful variation between Ca-(Mg+Fe^{2+}) and Al (Figure 4.5) implies that the higher Al in the Type-II ijolites is not present as $CaAl_2SiO_6$ (Tschermak's molecule).

Figure 4.4: Cation variation (per 6 oxygens) of ijolite clinopyroxenes: (a) Na *versus* Al; (b) Na *versus* Ti; (c) Na *versus* Ca; (d) Al *versus* Ti.

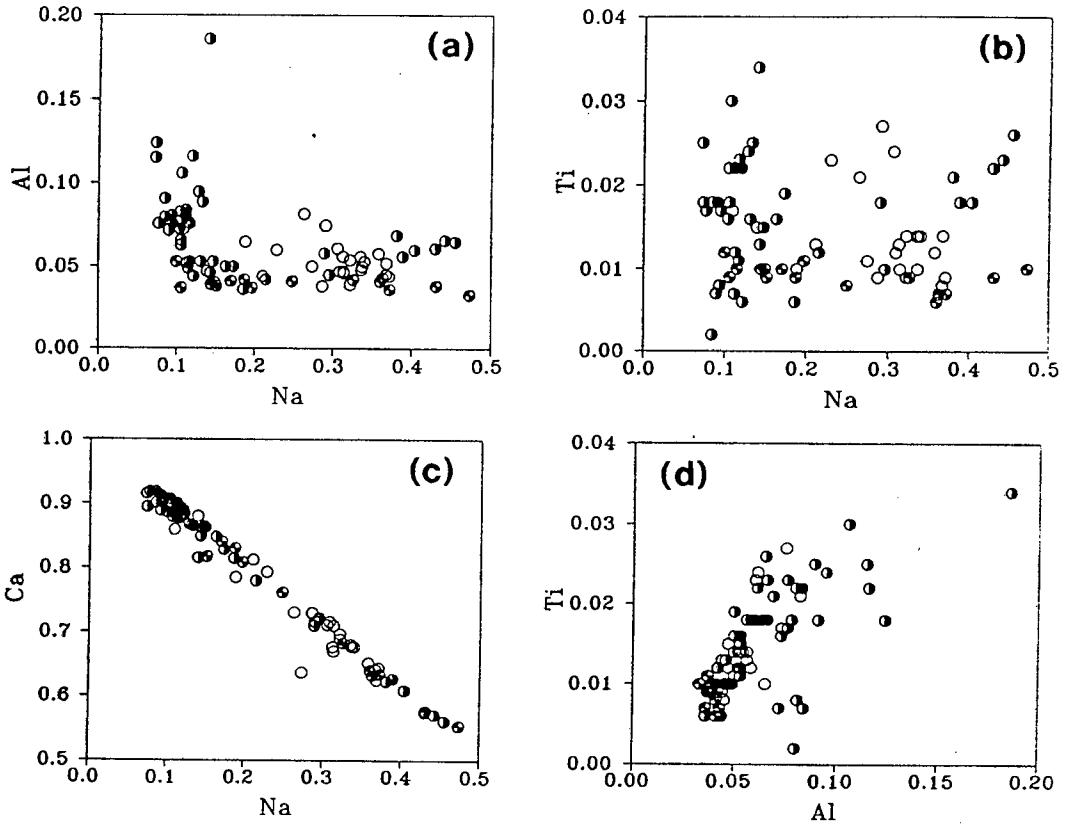

Symbols are as for Figures 4.2 and 4.3.

Figure 4.5: Plot of Ca-(Mg+Fe^{+2}) *versus* Al (per 6 oxygens) for ijolite clinopyroxenes.

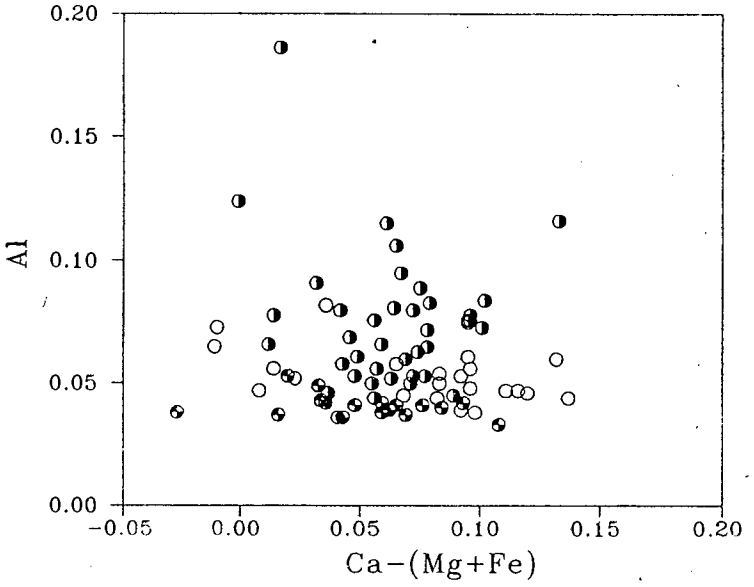

Symbols are as for Figures 4.2 and 4.3

4.2.2.1.1. Changes in clinopyroxene composition accompany-ing "nephelinisation" of pyroxenite

In Chapters 2 and 3 above, the process of "nephelinisation" of pyroxenite by the infiltration of felsic components from intrusive ijolite was discussed.

The petrography of sample S49, a pyroxenite with ijolite dykelets, was described in Chapter 3 above. To study the variations in chemistry of the clinopyroxenes during ijolite/urtite infiltration into the pyroxenite, pyroxene compositions were determined for individual, unzoned grains in the dyke fraction, and for pale green cores and deeper green rims in the pyroxenite fraction, of sample S49. These results are depicted on the Na-Mg-(Fe^{2+}+Mn) ternary in Figure 4.6. As anticipated, cores in the pyroxenite have preserved diopsidic compositions typical of unaffected pyroxenite, whereas the dyke pyroxenes conform to the sodic end of the Type I ijolite compos-itional trend. The rims of the pyroxenite pyroxenes have shifted composition significantly from $Na_{10}Ca_{90}$ to $Na_{30}Ca_{70}$ and are comparable to compositions of clinopyroxenes in the Type-II ijolites.

Figure 4.6: Ternary plot of Na-Mg-(Fe^{2+}+Mn) for clinopyroxenes from sample S49 to show changes due to metasomatic effects of ijolite intrusion.

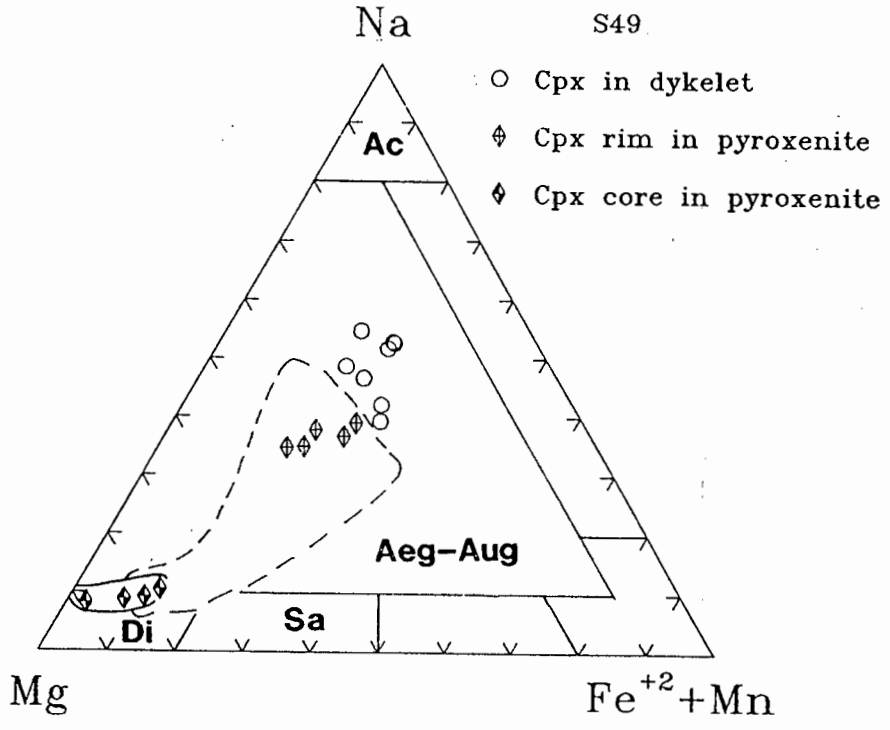

Dashed field marks the compositional variation of Type-II clinopyroxenes.

4.2.2.2. Nepheline

Nepheline analyses from Type-I and Type-II ijolite types are listed in Table B.2 in Appendix B, along with calculated cation proportions on the basis of 32 oxygens and the coordinates of the Q-Ne-Ks ternary projection. Natural nephelines are a solid solution between Na and K end members but always contain more silica and less alumina than indicated by the general formula $(Na,K)AlSiO_4$ (Deer *et al.*, 1966). This feature is demonstrated for the ijolites in Figure 4.7 where it may be noted that nephelines from the granoblastic ijolites generally contain lower Si and higher Al than nephelines of the Type-I variety.

Figure 4.7: Plot of Si versus Al (on the basis of 32 oxygens) for ijolite nephelines.

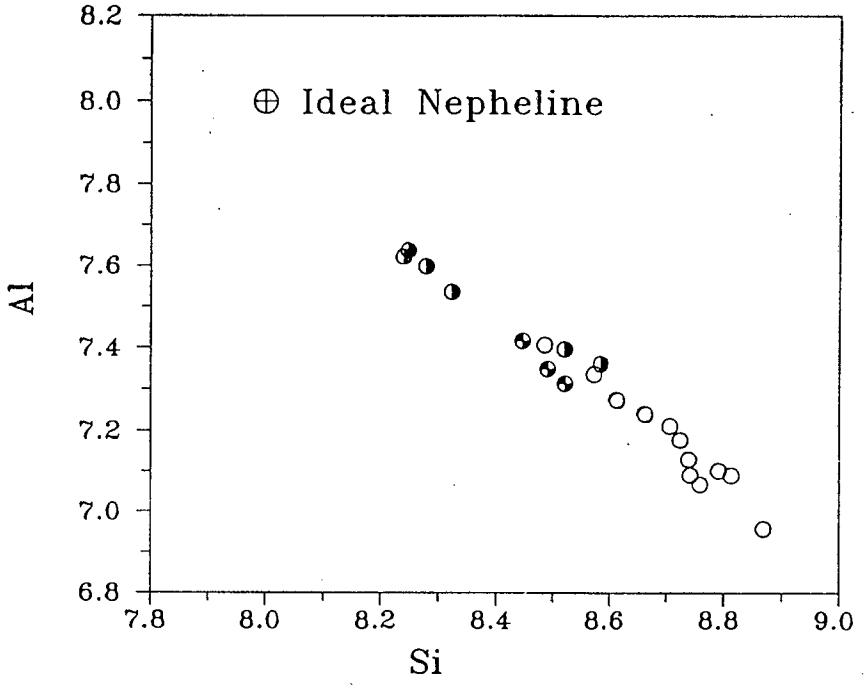

Symbols are those used in Figs 4.2 and 4.3.

The chemistry of natural nephelines was discussed by Tilley (1954), Hamilton and MacKenzie (1960), Hamilton (1961), Carmichael *et al.* (1974), and Gittins (1979), amongst others. Hamilton (1961) investigated the temperature dependence of solid solution in natural nephelines and determined the limits of solid solution at different temperatures. Hamilton proposed that nepheline in equilibrium with silicate liquid could potentially change both its K/Na and Si/Al ratios, whereas in subsolidus, post-magmatic conditions, only the alkalis will move. Subsolidus exchange thus severely limits the application of the nepheline solid solution as a quantitative temperature indicator. Re-equilibration tends to adjust nepheline compositions towards the ideal

Figure 4.8: Q-Ne-Ks projection of ijolite nephelines.

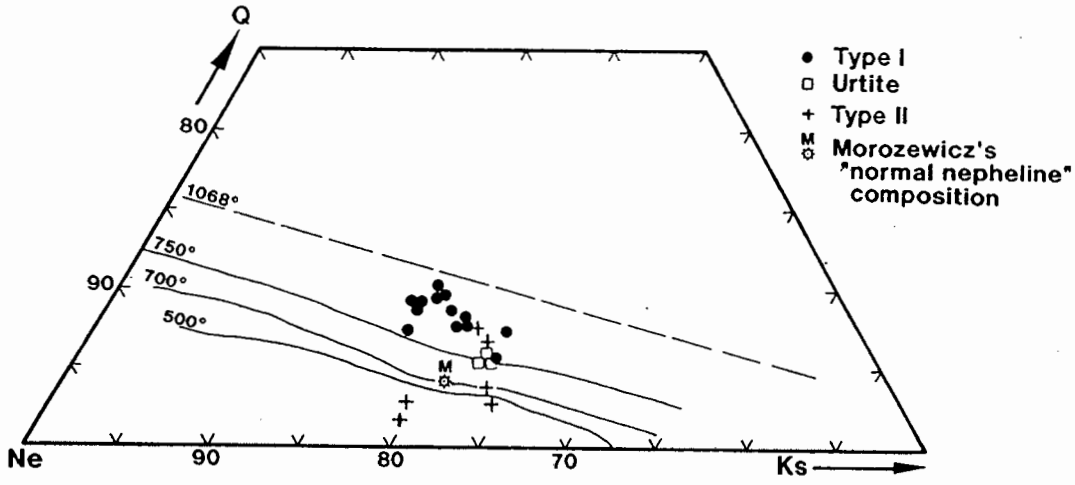

The temperature dependent limits of solid solution are from Hamilton (1961).

$Ne_4Ks_1Q_1$ composition ("Morozewicz's composition"; Tilley, 1954). In Figure 4.8 the ijolite nepheline compositions are compared with the approximate positions of the solid solution limits determined by Hamilton (1961). While the absolute temperatures indicated on Figure 4.8 are not necessarily reliable, it is significant to note that nepheline compositions from the Type-I ijolites consistently preserve higher apparent temperatures relative to the granoblastic, Type-II, ijolite nephelines.

4.2.3. Nepheline Syenites

Available analyses and structural formulae of the principal mineral phases in the syenites are presented in Tables B.1, B.3 and B.4 in Appendix B.

4.2.3.1. Clinopyroxene

In the nepheline syenites the clinopyroxene is Na and Fe rich, and Al and Ti poor, implying a high concentration of the acmite molecule ($NaFe^{3+}Si_2O_6$) and, using the ternary Na-Mg-Fe^{2+}+Mn classification plot, the clinopyroxenes range from aegirine-augite and aegirine-hedenbergite to pure aegirine compositions (Figure 4.9). Pyroxenes from the schistose varieties are consistently high in Na and low in Mg; the massive, nepheline-phyric types are more Mg rich than the schistose; and the porphyritic, feldspar-phyric types trend to lower Na contents than the others.

Inter-element variations once again principally reflect the dominant substitution of Na (acmite) for Ca (diopside) in the structure.

Figure 4.9: Ternary plot of Na-Mg-(Fe^{2+}+Mn) for clinopyroxenes from nepheline syenites.

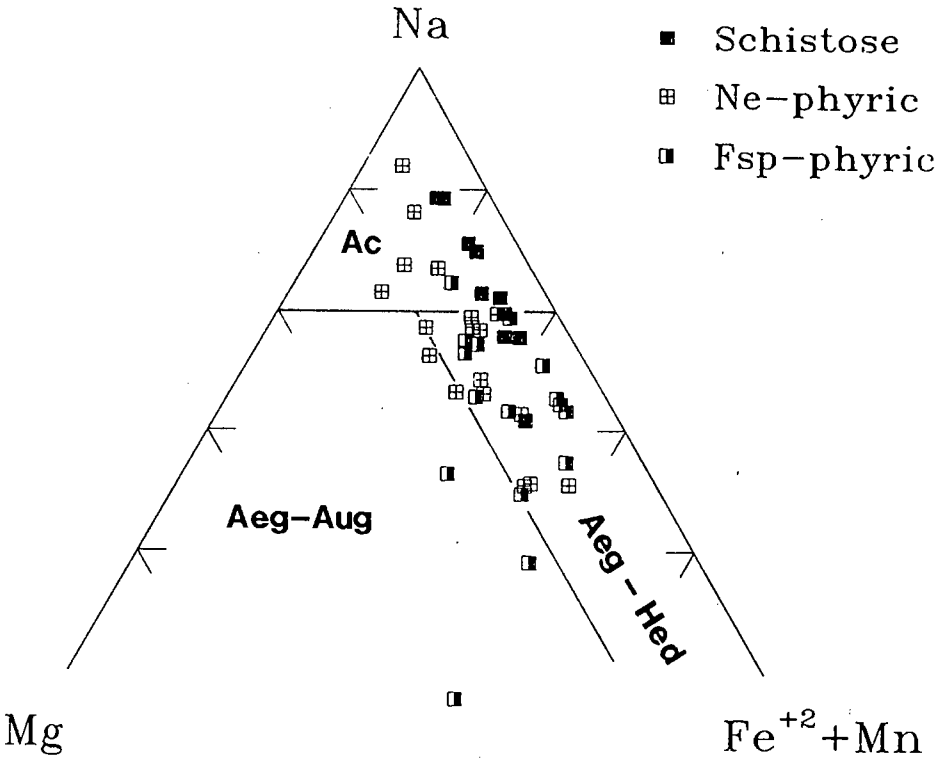

Classification fields are from Jones (1984): Ac=acmite; Aeg-Aug=aegirine-augite; Aeg-Hed: aegirine-hedenbergite.

Figure 4.10: Frequency histogram of normative alkali feldspar compositions calculated from whole rock analyses.

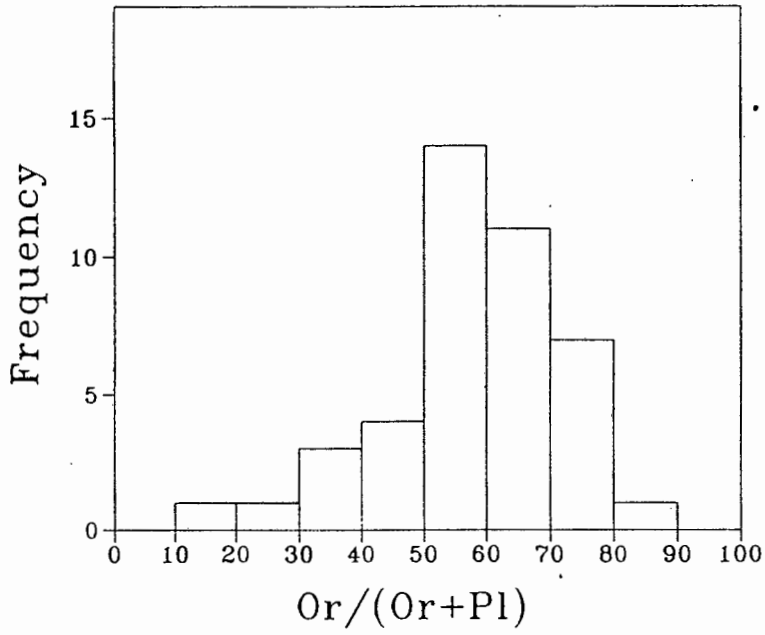

4.2.3.2. Alkali feldspar

Most feldspar grains are perthitic and so it is difficult to ascertain the primary magmatic composition of the alkali feldspar. Most of the coarser grains analysed (Table B.3) are essentially sodic orthoclase and range in composition from $An_{2.1}Ab_{22.6}Or_{75.3}$ to $An_{0.5}Ab_{8.9}Or_{90.6}$. Patches of albitic perthite are almost pure albite containing no An molecule ($Ab_{98.8}$-$Ab_{99.3}$). It is interesting that potassic feldspar patches in perthite contain up to 1.1% BaO whereas Ba could not be detected in albitic patches in the same perthite grain. Strong partitioning of Ba into the Or component in perthite was reported by Mason (1982). Feldspar compositions estimated from whole rock CIPW norms most commonly range from 40-70% Or/(Or+Ab+An), as summarised in Figure 4.10, and suggest more sodic starting compositions than are reflected in the microprobe analyses.

4.2.3.3. Nepheline

Nepheline analyses recast into the normative components Q, Ne and Ks, are plotted in Figure 4.11 along with the limits of solid solution as determined by Hamilton (1961). From these it appears that the analysed nephelines have not suffered extensive low temperature re-equilibration and retain magmatic

Figure 4.11: Q-Ne-Ks projection of nephelines from nepheline syenites.

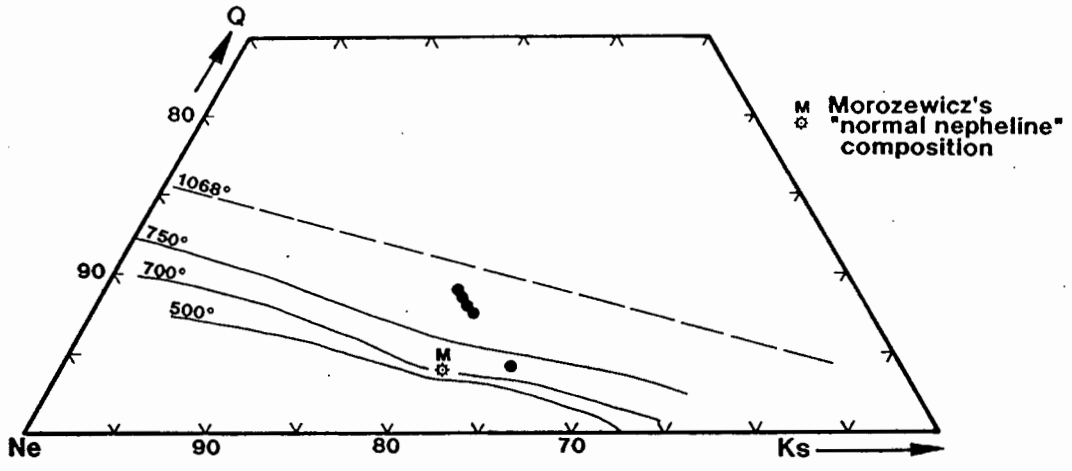

The temperature dependent limits of solid solution are from Hamilton (1961).

compositions: with the exception of one analysed point (from sample S3) all suggest temperatures in excess of 775°C. All the analyses are significantly removed from the so-called Morozewicz's "normal" nepheline convergence composition (Tilley, 1954).

4.2.3.4. Pectolite

Textural relationships argue that the pectolite in the Spitskop nepheline syenites is a primary, though late stage, igneous mineral and not due to subsequent alteration.

Pectolite is generally thought to form at very low temperatures: Deer *et* . (*op. cit.*) indicate that pectolite may be produced by heating its component oxides at 180°C; Leach and Rodgers (1978) reported pectolite forming during metasomatism of serpentinite at 260-350°C; and Craw and Landis (1980) described authigenic pectolite from an ophiolite-derived debris flow. Secondary pectolite after plagioclase was described from the Prospect alkaline diabase-picrite body in Australia by Wilshire (1967) and from veins in gabbros in Japan by Matsubra *et al.* (1979). Pectolite in kimberlite (Kruger, 1982) is thought to relate to the incorporation of foreign, Na-bearing material, or the actions of Na-bearing fluids (Scott Smith *et al.*, 1983).

Pectolite has also been reported from phonolites by Carr *et al.* (1976) who argued from textural relationships that pectolite was a primary constituent of the phonolite. Pectolite is a common accessory constituent in the Lovosero massif, where it is described as a late mineral filling spaces between the main rock forming

minerals, and as inclusions in sodalite (Vlasov *et al.*, 1966; p447). A photomicrograph of pectolite in this publication (Fig. 230 on page 448) shows interstitial pectolite with sharply defined grain boundaries with microcline, albite and aegirine and bears a close resemblance to the mode of occurrence of pectolite at Spitskop. Secondary (late magmatic) pectolite at Lovosero forms "fringes" around eudialyte and microcline (Fig. 231 on page 448). Pectolite has also been described from veins (accompanied by orthoclase and aegirine) traversing fenites in the Tur'ii peninsular, Kola by Kulakov *et al.* (1974). Jones (1980) described manganoan pectolite (15.5% MnO) as a late stage phase in the peralkaline syenites of the Motzfeldt Centre, Igaliko Complex, Greenland.

Pectolite analyses from the cited literature are shown for comparison in Table B.4. It is apparent from the compiled data that the "secondary", low temperature pectolite occurrences have significantly lower concentrations of MnO relative to pectolites of apparently magmatic origin. For this reason pectolite from the nepheline syenites was analysed to compare its MnO content against the published range in composition.

Pectolite was analysed using a defocussed electron beam in the microprobe to reduce volatile loss during analysis. Structural formulae were calculated on the basis of 9 (O+OH) and are consistent with the general formula $(Ca+Mn)_2NaSi_3O_8.(OH)$ as suggested by Deer *et al.* (1966, p144). Results are contained in Table B.4. MnO concentrations range from 2.16% to 4.88% (equivalent to 0.11 to 0.25 atoms of Mn in the structural formula) and are comparable to pectolites of presumed igneous origin.

4.2.4. Comparison of clinopyroxene compositions between rock types

Clinopyroxene is the only mineral common to all the silicate components of the Spitskop Complex and so it is worth investigating whether any systematic compositional variations exist between rock types.

Figure 4.12: Ternary plot of Na-Mg-(Fe^{2+}+Mn) to compare clinopyroxenes from the pyroxenite, ijolites (Type-I) and nepheline syenites.

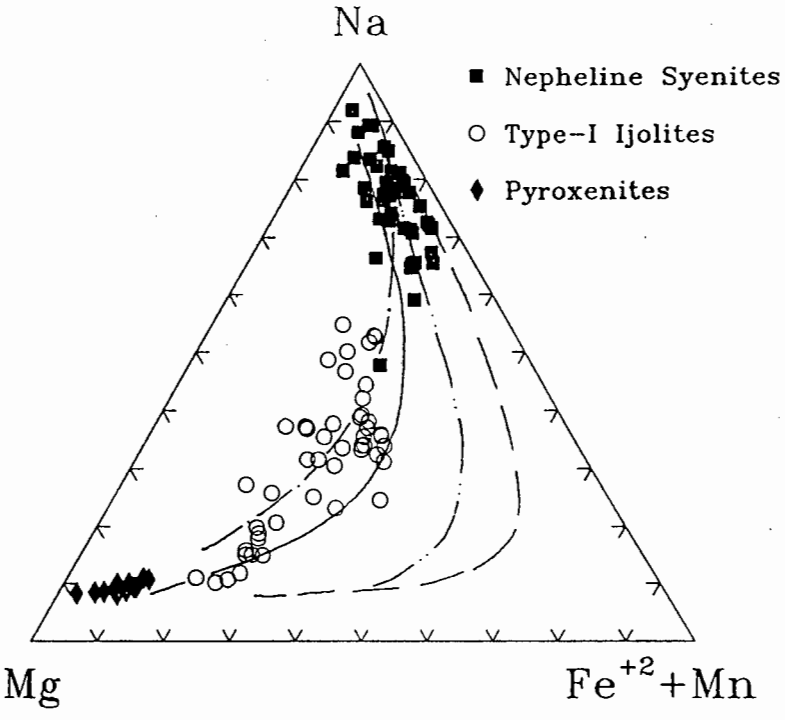

Clinopyroxene crystallisation trends are shown for: Uganda nephelinites (dotted broken line); the Itapirapua Complex, Brazil (solid curve); and the south Qôroq nepheline syenites, Greenland (double-dotted broken line). Trends taken from Jones (1984).

In Figure 4.12 the clinopyroxene compositions from the pyroxenite, Type-I ijolite and nepheline syenites are compared and define what appear to be an evolutionary trend. Clinopyroxene trends from other alkaline complexes are shown for comparison in Figure 4.12 where the variation in the Spitskop clinopyroxenes is more like the trends for the Itapirapua complex, Brazil, and the Uganda nephelinites than the nepheline syenites of South Greenland. The degree of "curvature" of the trend is a function of Fe^{3+}/Fe^{2+} and hence the apparent oxygen fugacity of the system (Stephenson, 1972; Scott, 1976). This observation implies that the Spitskop magmas evolved under rather oxidising conditions. Using Na-Mg as an index of relative evolution (after Stephenson, 1972; Jones, 1984), a progressive increase in the oxidation of Fe is noted through the ijolites and nepheline syenites (Figure 4.13a). A large range in Fe oxidation state is implied for pyroxenes in the pyroxenite but this may partly be an artefact of the low proportions of iron in these pyroxenes: less than 0.3 atoms per unit cell. It must be emphasised that the Fe^{3+}/Fe^{2+} proportions were

estimated following the technique of Droop (1988) which utilises stoichiometry to assign these quantities independently of the concentration of any one element (e.g. Na). The strong correlation between Na and Fe^{3+} is depicted in Figure 4.12b where it can be seen that Na exceeds Fe^{3+} in the aegirine-rich pyroxenes in the nepheline syenites. The oxidation state of iron in magmas is known to be a function of the alkalinity in addition to the f_{O2} of the magma (see review in Carmichael *et al.*, 1974: p282-285) in that increasing Fe^{3+}/Fe^{2+} is favoured by increasing alkalinity and falling temperature. The correlation between Na and Fe^{+3} in the Spitskop pyroxenes may simply be a result of this "alkali-ferric-iron effect" (Carmichael and Nicholls, 1967) and need not necessarily indicate a change in f_{O2}.

Of the minor elements Ti shows a major increase in the clinopyroxenes of the nepheline syenites (Figure 4.13c). Mn increases progressively from the pyroxenites through the ijolites and then decreases in the nepheline syenites (Figure 4.13d). High Ti and "excess" Na has also been noted in aegirines from the nepheline syenites of the South Qôroq (Stephenson, 1972) and Motzfeldt (Jones, 1984) centres of the Igaliko Complex, south Greenland.

4.3. Whole Rock Compositions

4.3.1. Pyroxenite

Three pyroxenite samples were collected which were free of the influence of intrusive ijolite: S44, S47 and S160. To these may be added the three analyses from Nel (1976) which were determined on pyroxenite material from borehole core. In addition sample S85, where dykelets of urtitic micro-ijolite are present, was included to demonstrate the chemical influence of the addition of ijolite material.

Figure 4.13: Chemical variation amongst clinopyroxenes from pyroxenites, ijolites and nepheline syenites: (a) Na-Mg *versus* $Fe^{+3}/\Sigma Fe$; (b) Na *versus* Fe^{+3}; (c) Na-Mg *versus* Ti (d) Na-Mg *versus* Mn.

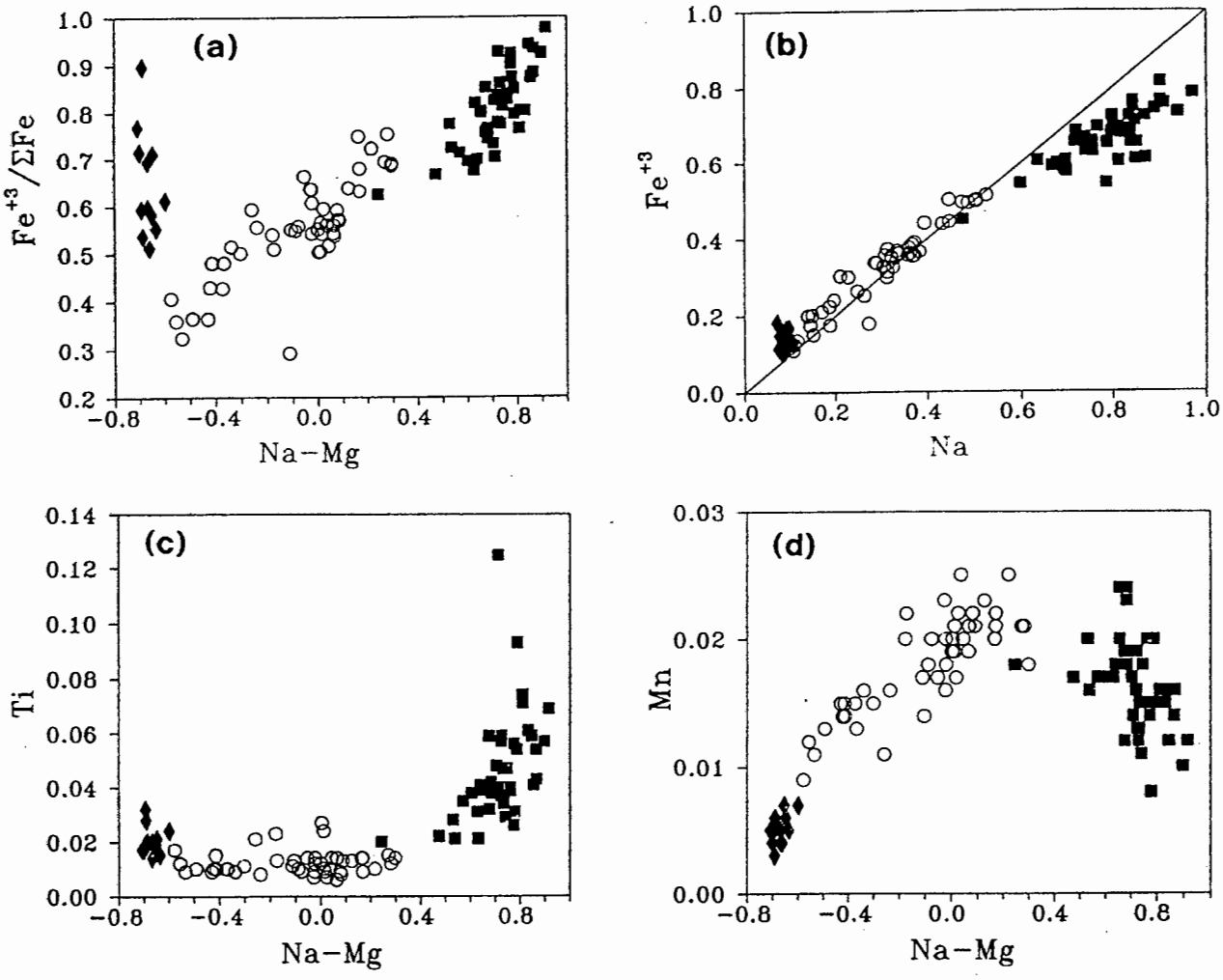

Symbols are those used in Figure 4.12.

Where not influenced by ijolite, the pyroxenites are composed largely of clinopyroxene with minor biotite and magnetite. Being essentially monominerallic, the pyroxenite analyses largely reflect the composition of their diopsidic pyroxenes: low Al_2O_3, high CaO and MgO. It will be noted, however, that the whole-rock analyses of the pyroxenite differ significantly from the compositions of the component clinopyroxene: whole rocks have lower SiO_2 and higher FeO and TiO_2 than the clinopyroxene suggesting the influence of biotite and titaniferous magnetite. The opaque phase in the pyroxenite was, unfortunately, not analysed during the present study. A mass balance calculation using the measured clinopyroxene and mica compositions with stoichiometric magnetite and ulvospinel values suggests that

Figure 4.14: Plot of K_2O versus Total Alkalis to compare Spitskop pyroxenites with selected pyroxenites.

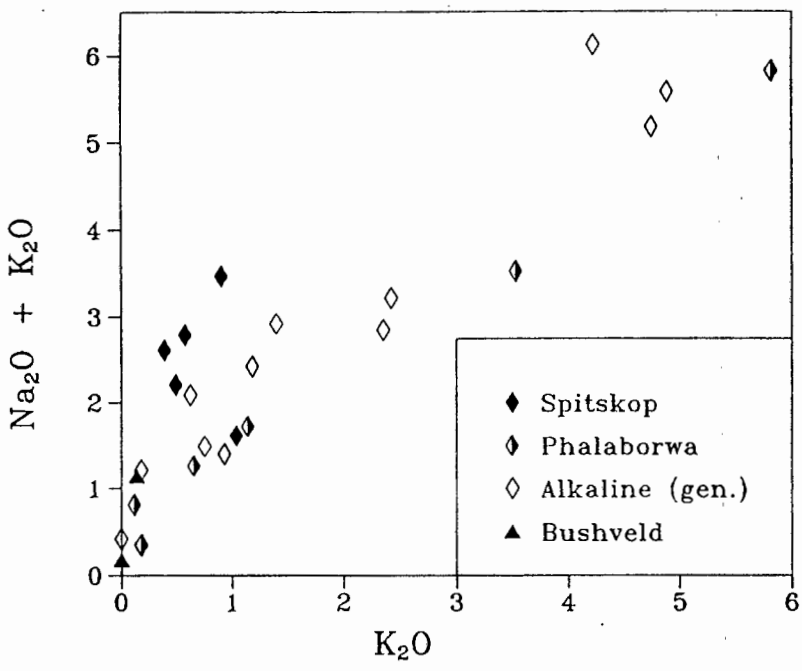

sample S44 is composed of an assemblage of $Cpx_{82}Bi_8Mt_{10}$, the magnetite having the composition $Mt_{73}Ul_{27}$.

The composition of the Spitskop pyroxenites are compared with pyroxenites from other alkaline complexes in Table B.6 and two analyses of pyroxenites from the Bushveld Complex are listed for contrast. Pyroxenites from the Napak carbonatite complex in Uganda have a similar mode of occurrence to those at Spitskop (as xenolithic blocks in ijolite) and are also largely composed of diopsidic clinopyroxene. The tholeiitic Bushveld ortho-pyroxenites are readily distinguished from the alkaline pyroxenites by having higher MgO and SiO_2 contents but lower CaO and total iron. Most of the alkaline pyroxenites from Upton's (1966) compilation have higher TiO_2 than the Spitskop samples, presumably reflecting higher proportions of titano-magnetite and/or titaniferous pyroxene. The Spitskop pyroxenites have elevated Na_2O contents. From Figure 4.14 it may be seen that the total alkali content in world alkaline pyroxenites is largely dominated by K_2O and essentially reflects the modal quantities of mica in the pyroxenite. It is apparent that the Spitskop pyroxenites have amongst the lowest K_2O contents.

No trace element data are provided in the chemical compilations of Upton (1966) and Le Bas (1977). Trace elements are presented for the pyroxenite from the

Figure 4.15: Chondrite-normalised plot of rare earth element concentrations in pyroxenite sample S44.

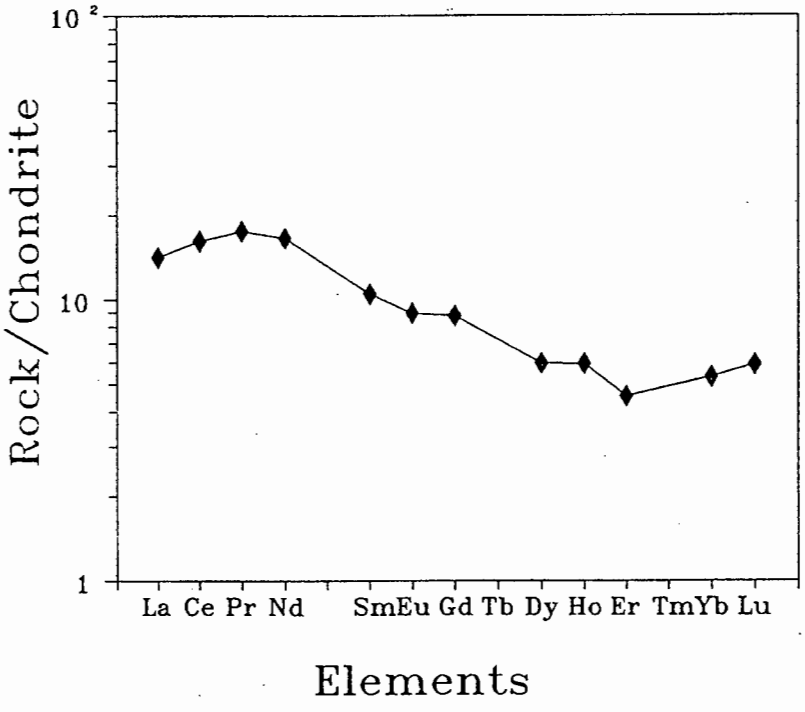

Mbalizi carbonatite (Van Straaten, 1989) but the high LOI for this analysis (11.69%) suggests that significant carbonate is present in the pyroxenite. As a result, the trace element values are unlikely to represent the levels in primary pyroxenite and could reflect modification by carbonatite. Relative to the massive pyroxenites from Phalaborwa, the Spitskop pyroxenites have lower Sr, Y, LREE and Cu contents, but significantly higher concentrations of Ba, Zr, V and Zn. The chondrite-normalised REE pattern for the single analysed Spitskop pyroxenite (S44) has a pronounced "sigmoidal" shape defined by a steep pattern from Nd - Dy with relative depletions in the REE lighter than Nd, and enrichment in the REE heavier than Dy (Figure 4.15). The levels of LREE are low for an alkalic rock: 15-20x chondrite compared to La_N of 380-1150 and Ce_N of 411-880 for the Phalaborwa massive pyroxenites (Eriksson, 1989).

4.3.2. Ijolite

The ijolite samples are grouped into "Type-I" and "Type-II" textural classes as defined in Chapter 3 above, or as "Others" where the texture cannot unambiguously be classed as one or other of these types.

Figure 4.16: Frequency histogram of Mg# values in Type-I ijolites.

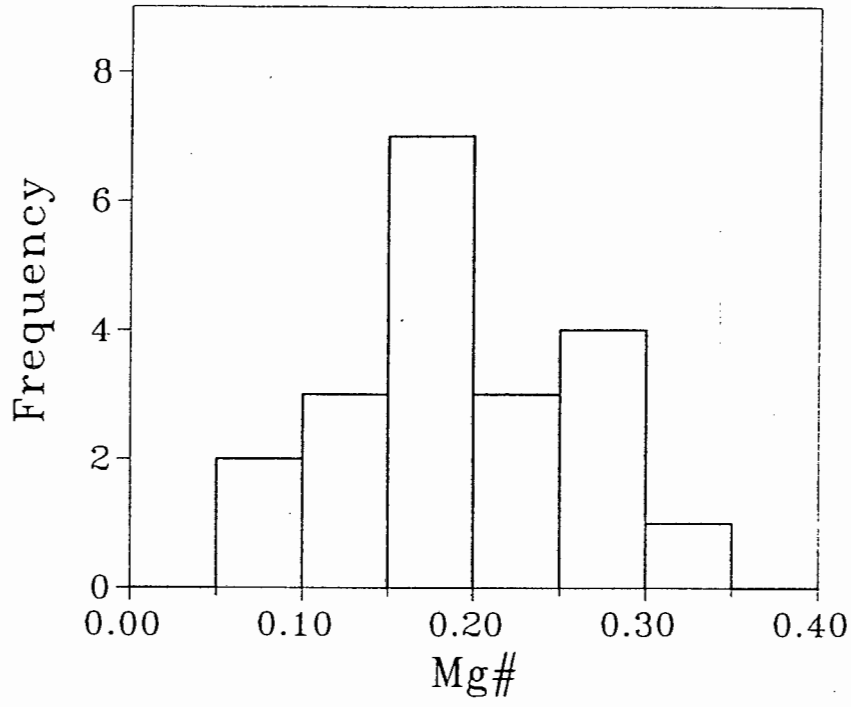

In reviewing the features of ijolites, Bailey (1974a) warned that "It seems likely that the petrology of nepheline-pyroxene rocks will be elucidated only by using the undoubted magmatic rocks as a starting point". With this in mind, it is pertinent to consider the geochemical characteristics of the apparently magmatic "Type-I" ijolites before discussing the relationships between these and those having "granoblastic" textures.

4.3.2.1. Type-I ijolites

Type-I ijolites are evolved rocks with low MgO (1.0-3.5%) and Mg#[1] of 0.1 to 0.3 (Figure 4.16); they have high Na_2O and Al_2O_3, and are peralkaline with Peralkalinity Indices (PI) of 1.1 to 1.2. Although the Spitskop ijolites are clearly not lavas, the analyses have been plotted on the TAS classification diagram (Le Bas *et al.*,

[1]Hughes and Hussey (1976) proposed that "Mg ratio" be reserved for the quantity $100Mg/(Mg+Fe^{+2}+Mn)$, and "*M*" be used where only total Fe has been analysed; i.e. for $100Mg/(Mg+Fe^{+2}+Fe^{+3}+Mn)$. All Fe determinations made for the current study were total iron XRF analyses. Throughout this dissertation "Mg#" is used to refer to the ratio $Mg/(Mg+Fe^{+2}+Fe^{+3})$.

Figure 4.17: SiO_2 - Total Alkalis (TAS) classification plot of Type-I ijolites.

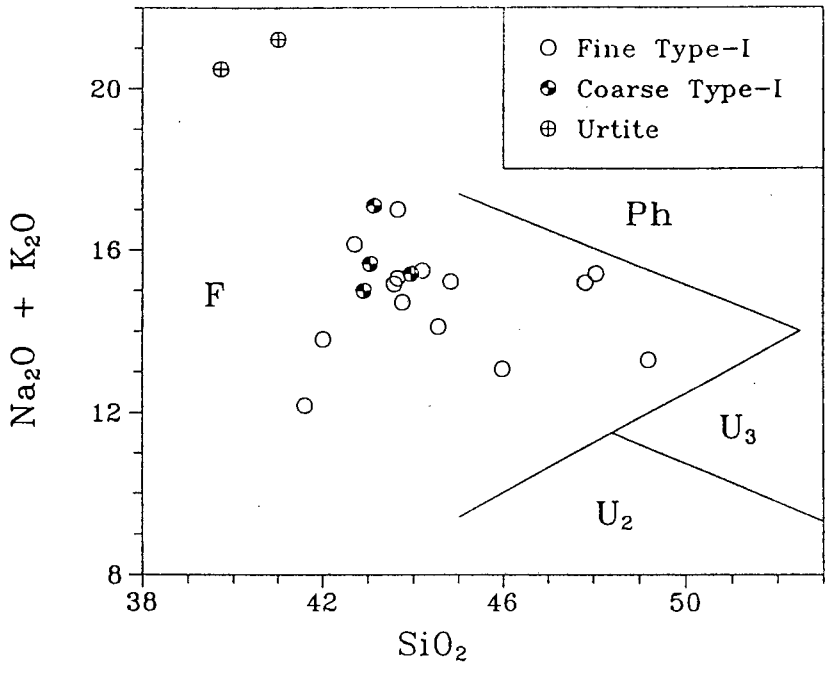

Fields are after Le Bas *et al.* (1986): F=foidite; Ph=phonolite; U_3=tephriphonolite, U_2=phonotephrite.

1986) where they all fall in the "Foidite" field (Figure 4.17). Foidites include nephelinites which are generally regarded as the closest volcanic analogue to ijolites in alkaline complexes (e.g. Bailey, 1974a).

Selected analyses of nephelinite and ijolite from various alkaline complexes are listed for comparison in Table B.9 (Appendix B) along with the mean and standard deviation of the 18 Spitskop Type-I ijolites. It is apparent from this Table and the plots in Figure 4.18 that the Spitskop ijolites generally have higher Na_2O and P.I. with lower CaO.and MgO contents than typical nephelinites and ijolites. Individual ijolite analyses from Napak ("urtite" - N123: King and Sutherland, 1966) and Khibina ("ijolite-urtite" - Kh-11: Gerasimovsky *et al.*, 1974) do occur with Na_2O contents comparable to the Spitskop ijolites but represent leucocratic end-members in each case.

Figure 4.18: Comparison of Spitskop Type-I ijolites with similar rocks from alkaline complexes elsewhere. (a) Na_2O - CaO; (b) Na_2O - FeO^*; (c) Na_2O - MgO; (d) FeO^* - peralkalinity index. Solid line fields mark the compositional variation of Spitskop Type-I ijolites.

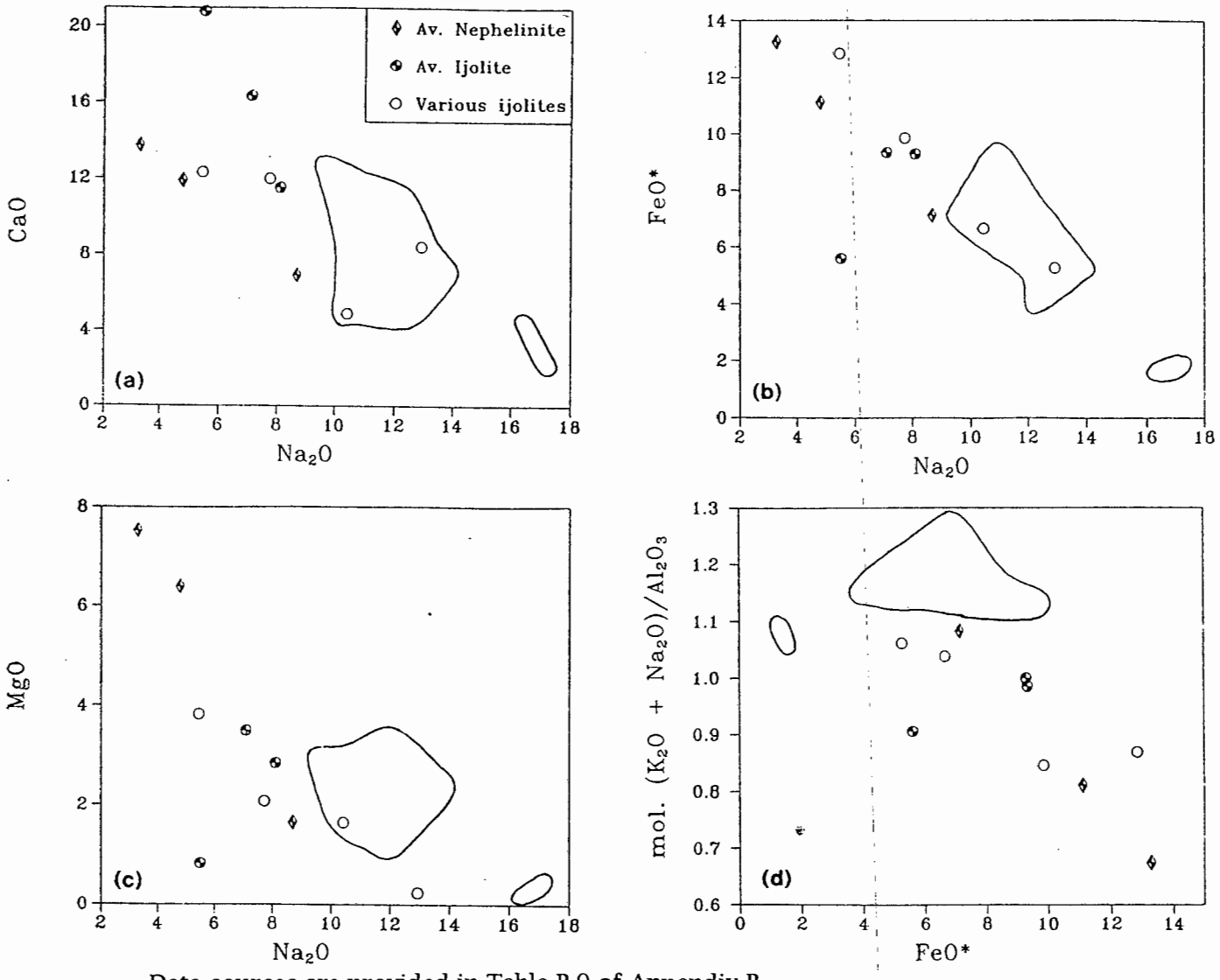

Data sources are provided in Table B.9 of Appendix B.

The chemical variation within the group of Type-I ijolites is depicted in a series of Harker diagrams in Figures (4.19 and 4.20). In the plots of FeO^*[2], CaO and MgO the two urtites analysed appear distinct from the trends defined by the fine- and coarse-grained ijolites. Concentrations of SiO_2 and Al_2O_3 are lower, whereas CaO and Na_2O are higher in samples S67 and S109 than in pure nepheline. This is evidently a reflection of the presence of cancrinite in these urtite samples. The four coarse-grained samples generally fall within the compositional spread of the fine-grained

[2]Throughout this dissertation, FeO^* is used to denote "total iron as FeO".

ijolites with the exception of FeO^*, the coarser samples having distinctly lower FeO contents than the rest.

Figure 4.19: Plots of SiO_2 versus selected major elements for the Type-I ijolites. SiO_2 - (a) Al_2O_3; (b) FeO^*; (c) MgO; (d) Mg#; (e) CaO; (f) Na_2O.

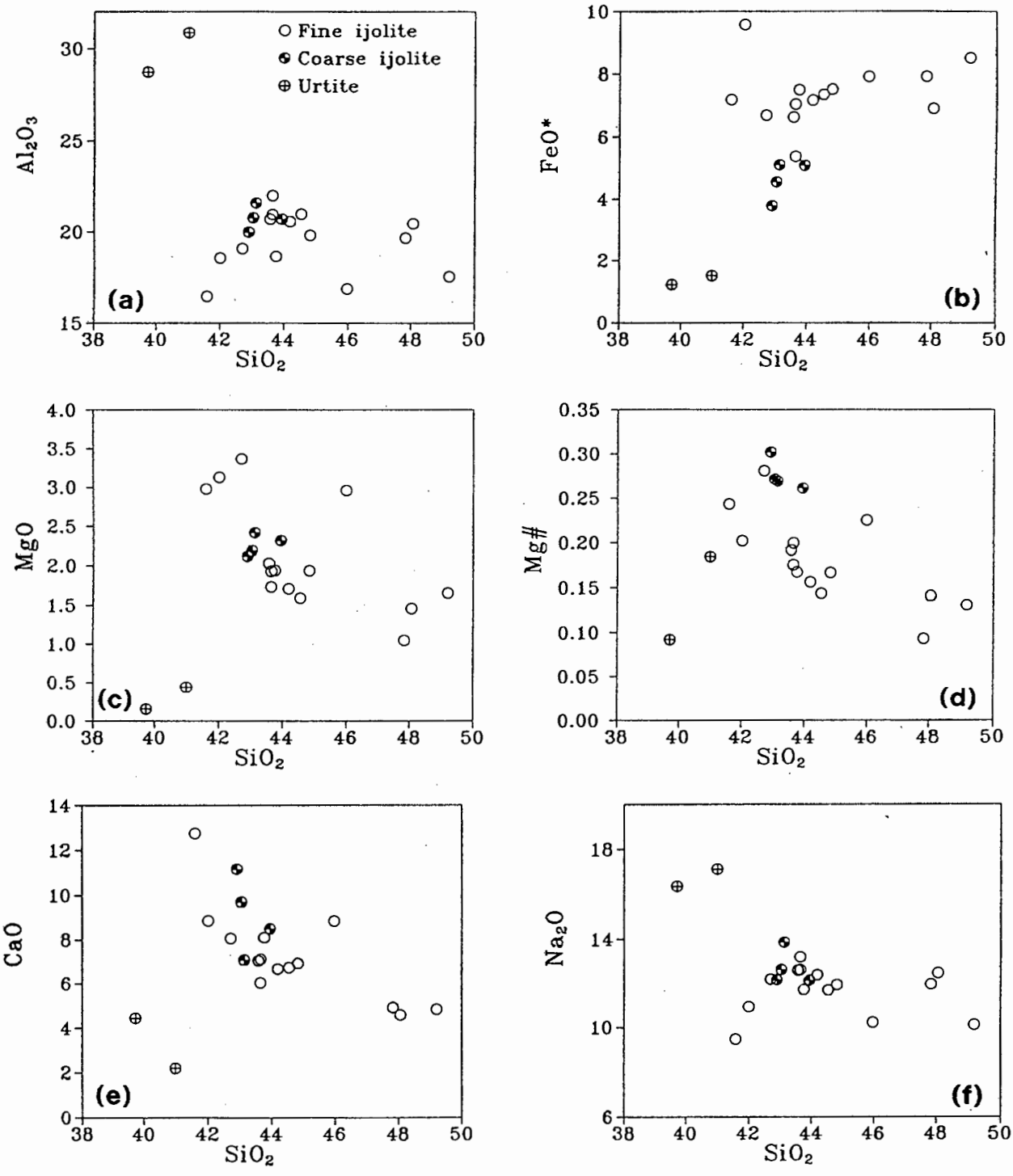

Figure 4.20: Plots of SiO_2 versus selected trace elements for the Type-I ijolites: SiO_2 - (a) Rb; (b) Sr; (c) Ba; (d) Zr; (e) Nb; (f) Y.

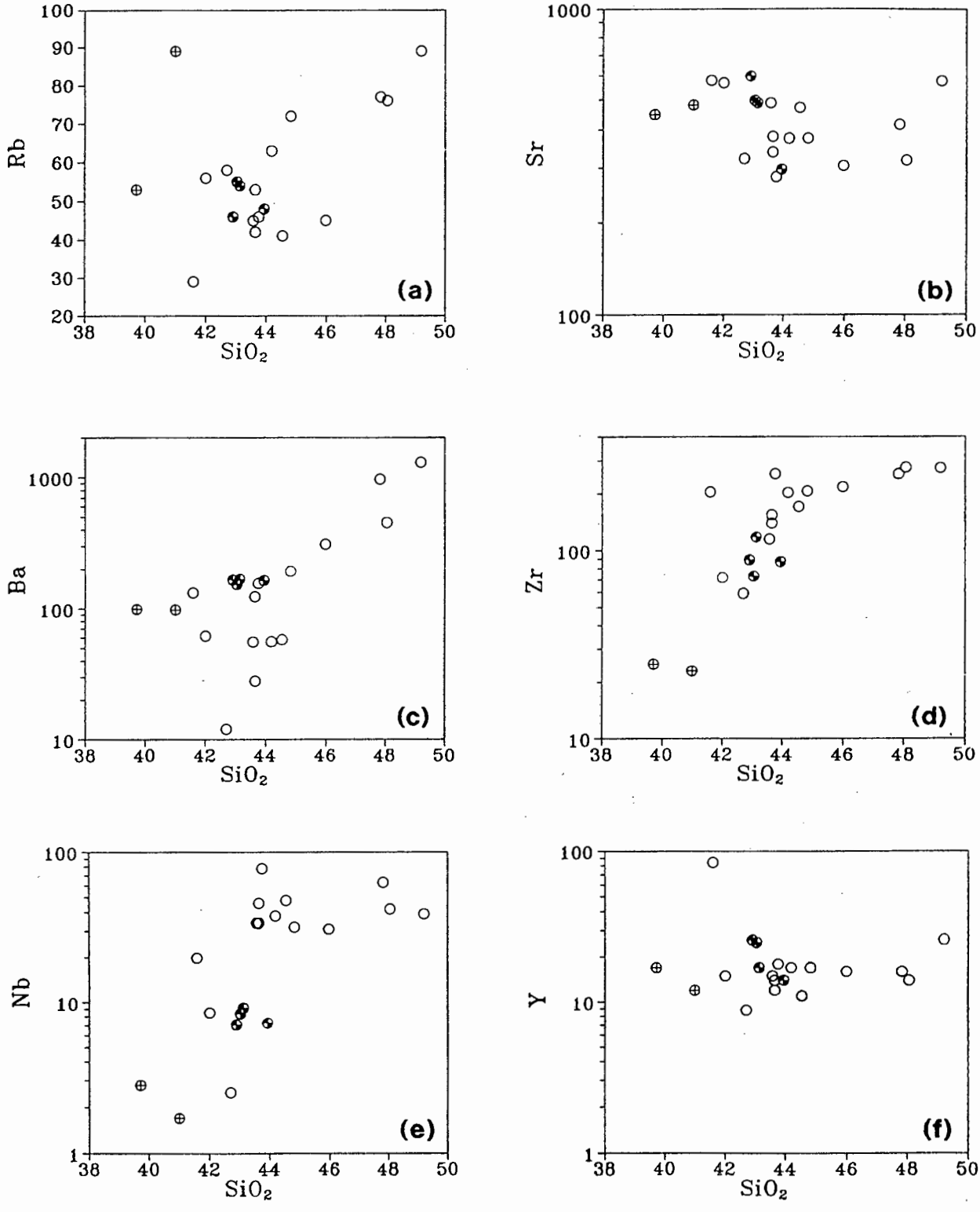

Figure 4.20 (contd) :SiO_2 - (g) Cr; (h) V; (i) Zn; (j) Ce; (k) Zr/Y; (l) Y/Nb.

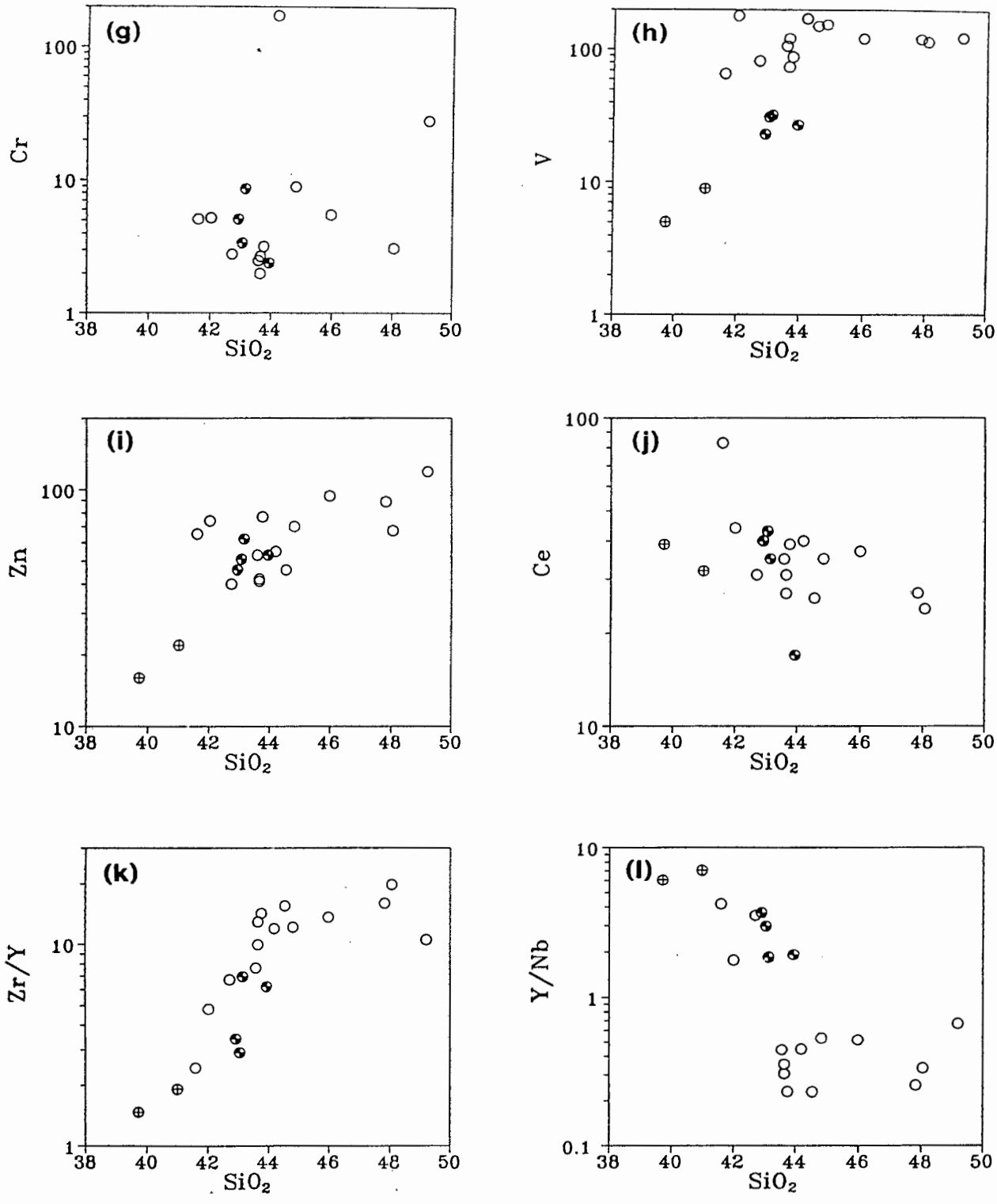

Figure 4.21: Spitskop Type-I ijolites compared with Group-II nephelinites from East Africa: (a) SiO_2 *versus* Mg#; (b) CaO *versus* Na_2O.

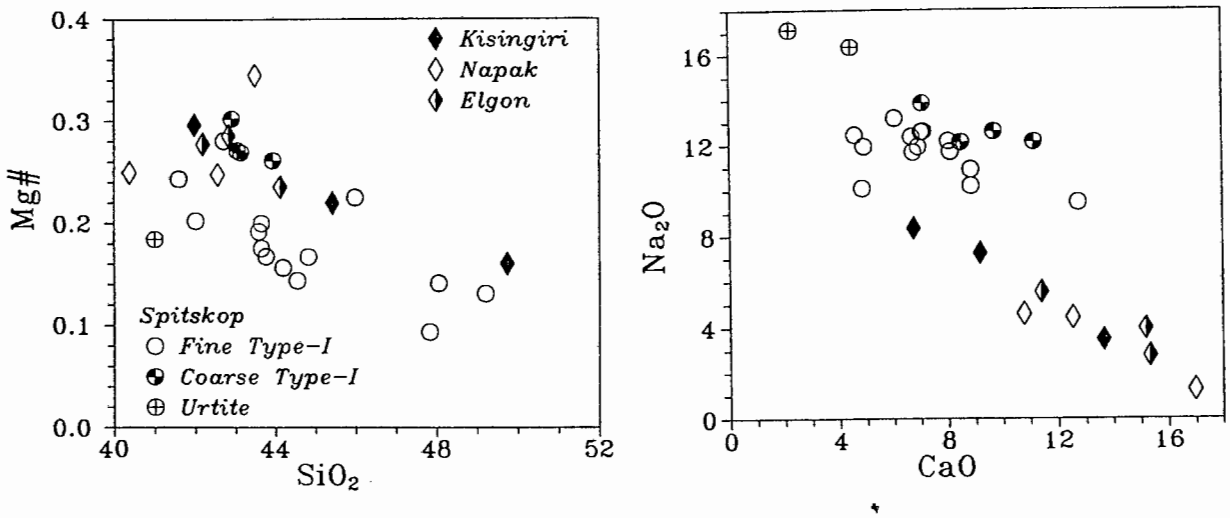

Data from Le Bas (1987; p58)

Figure 4.22: Spidergrams to compare trace element variation in Spitskop ijolites with those in East African nephelinites.

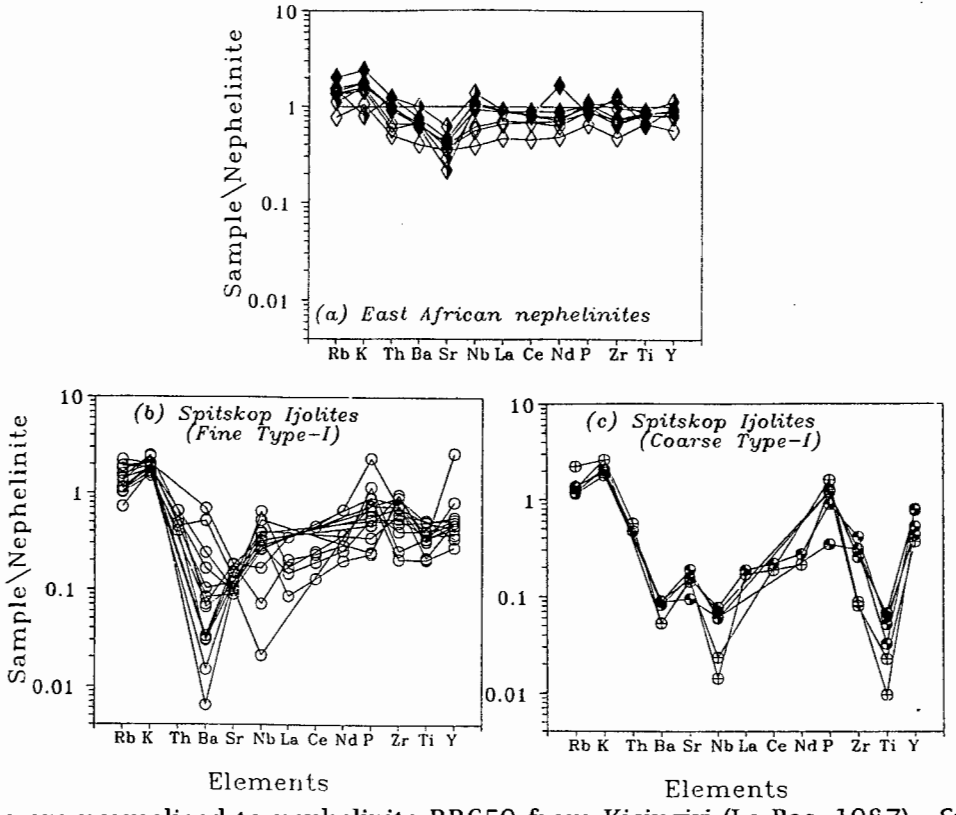

Data are normalised to nephelinite RR659 from Kisingiri (Le Bas, 1987). Symbols are as in Figure 4.21.

Reasonably coherent trends are noted amongst the fine-grained ijolite samples between SiO_2 and FeO^* (positive correlation) and MgO, Mg# and CaO (negative correlation). Amongst the trace elements Zr, Nb, V and Zn have essentially constant concentrations in the fine-grained ijolites and decrease systematically with decreasing SiO_2 in the coarse ijolites and urtites. Ce decreases slightly with increasing silica, whereas Y remains essentially constant with one sample (S18), having significantly higher Ce (89ppm) and Y (84ppm) contents (and La and Nd) than the rest. The similarity in the plots for FeO^* and V is noteworthy. Sr contents range from about 300 to 600ppm but do not show any systematic variation with silica. Ni and Cr are both in very low concentration, generally less than 20 and 10ppm respectively. Samples S79 and S173 have anomalously high Cr contents of 172 and 28ppm, respectively.

Le Bas (1987) distinguished two nephelinite associations: "Group I", or olivine-rich nephelinites, which are commonly associated with alkali basalt and basanite volcanism; and "Group-II", or olivine-poor nephelinites, which can fractionate to phonolite and are commonly associated with carbonatites. In Figure 4.21a,b the Spitskop ijolites are compared with the set of typical East African Group-II nephelinites discussed by Le Bas (1987). In these plots the Spitskop ijolites can be seen to have slightly lower Mg# at equivalent SiO_2 and higher Na_2O at equivalent CaO than the reference set. In Figure 4.22, a range of trace elements in the Spitskop ijolites is compared with the nephelinites using a spidergram with the data normalised to levels in the most primitive nephelinite from Kisingiri (sample RR659 from Le Bas, 1987). In Figure 4.22a progressive differentiation (shown as changing SiO_2, CaO and Na_2O in Figure 4.21) is seen to increase the levels of Rb and K (<2x) and reduce the levels of most other trace elements (to maximum of 0.3x). By contrast, the normalised patterns for the Spitskop ijolites are extremely "spiky" (Figures 4.22b,c). The fine-grained ijolites have lower concentrations of most elements except K and Rb and highly variable Ba and Nb (0.7x to <0.01) contents relative to nephelinite RR659. Sr is less variable at about 0.1-0.2 times the level in RR659. Coarse ijolites (Figure 4.22c) have very pronounced Ti and Nb depletions.

Chondrite-normalised plots of the rare earth elements are shown in Figure 4.23. The ijolites and urtites are LREE enriched (La_N 30-100), with steep traces from La to Dy, but exhibit significant variation in concentration of the REE heavier than Ho. Two samples, S50 and S114, also have relative depletions in La and Ce which produces normalised traces with the "sigmoidal" shape noted for the pyroxenites above. The REE in S18 are distinct in being significantly enriched in the elements Sm to Ho, giving rise to a normalised trace which is convex upwards. This sample has the

highest P_2O_5 concentration (2.07%) and the extreme REE pattern and high Y content may reflect increased contents of cumulus apatite. This will be discussed further in Chapter 7.

Figure 4.23: Chondrite-normalised plot of the rare earth elements in the Type-I ijolites.

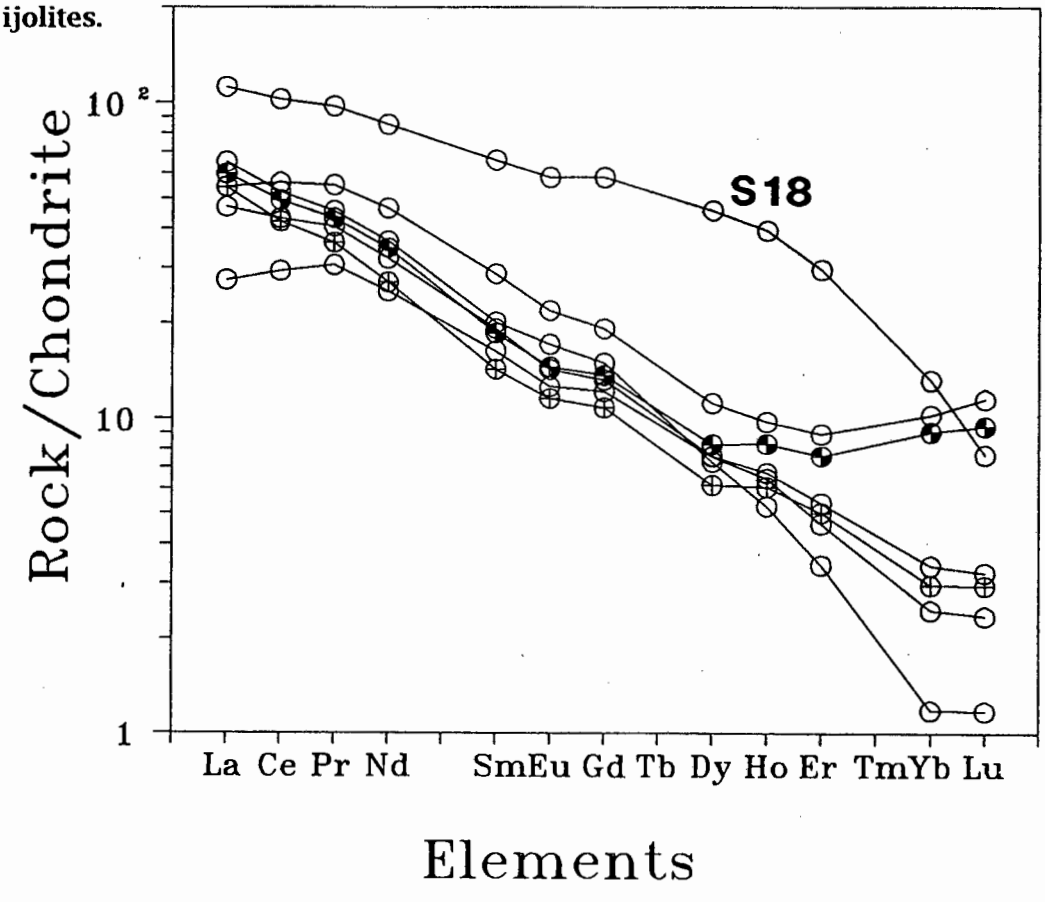

4.3.3. Type-II ijolites

In comparison to the Type-I ijolites, those with granoblastic textures have higher CaO and Mg# values at similar concentrations of SiO_2 (Figure 4.24). All Type-II samples except three are peralkaline: samples S65, S131 and S139 having substantially lower peralkalinity indices of less than 0.7. These three samples all have the "spreustein" groundmass described in Chapter 3.

In view of the higher MgO in the Type-II ijolites, this element has been used to depict the relative concentration levels of selected trace elements in Figure (4.25). Relative to the Type-I ijolites, the granoblastic type has distinctly lower concentrations of Zr, Nb and Y. A group of the Type-II ijolites also contain significantly elevated Ni concentrations which are correlated with MgO.

Figure 4.24: Plots comparing the variation of SiO_2 against selected major elements for the Type-I, Type-II and "Other" ijolite types: (a) Mg#; (b) FeO*; (c) peralkalinity index.

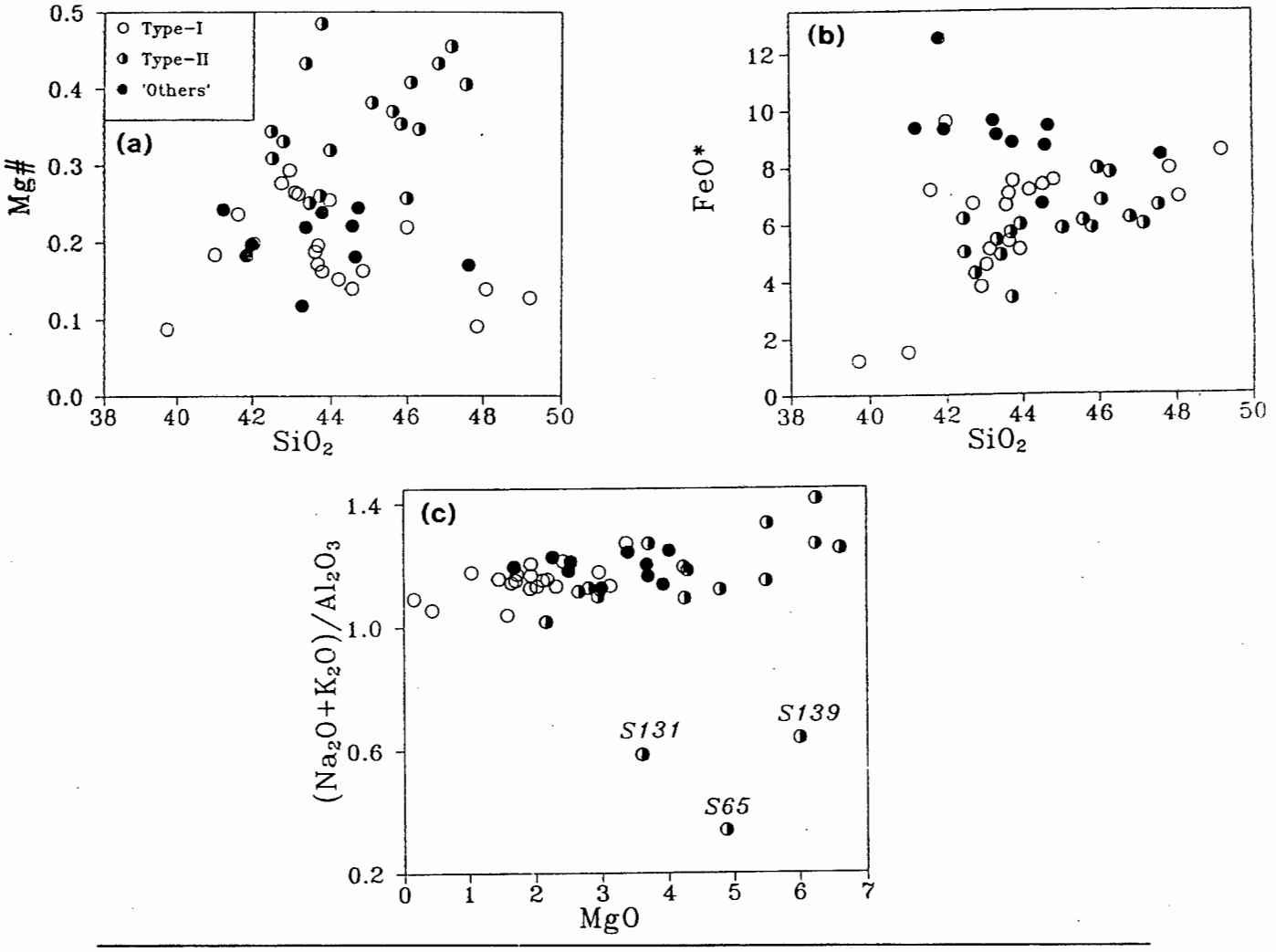

Normalised abundance patterns of the REE in the Type-II ijolites are essentially identical to those noted in the Type-I varieties but the absolute concentrations of the REE are slightly lower in the granoblastic types (Figure 4.26).

4.3.4. "Other" textural types of ijolite

The "Other" ijolites, those which cannot be unambiguously assigned to either of the previous groups, have lower MgO concentrations and Mg# values than Type-II ijolites and are comparable to the Type-I group with respect to these elements (Figure 4.24). The "Other" ijolites are distinguished in having higher FeO^* concentrations than the Type-I and Type-II varieties. Concentrations of Nb, Zr (both higher), and Ni (lower) also differ from those of the Type-II ijolites (Figure 4.25).

Figure 4.25: Plots comparing the variation of MgO against selected trace elements for the Type-I, Type-II and "Other" ijolite types: (a) Zr; (b) Nb; (c) Y; (d) Ni; (e) V

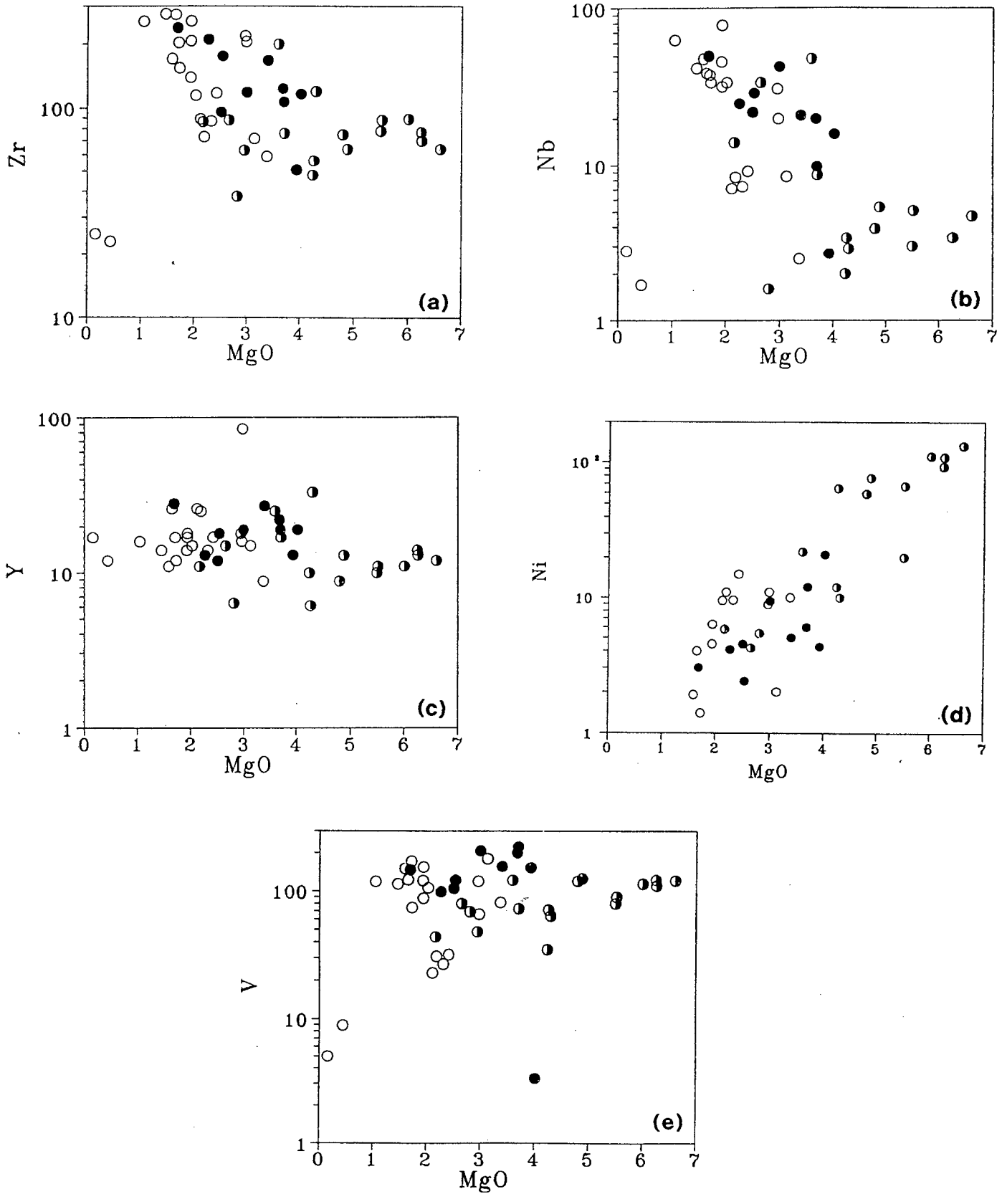

Figure 4.26: Chondrite-normalised plot of the rare earth elements in the Type-II ijolites.

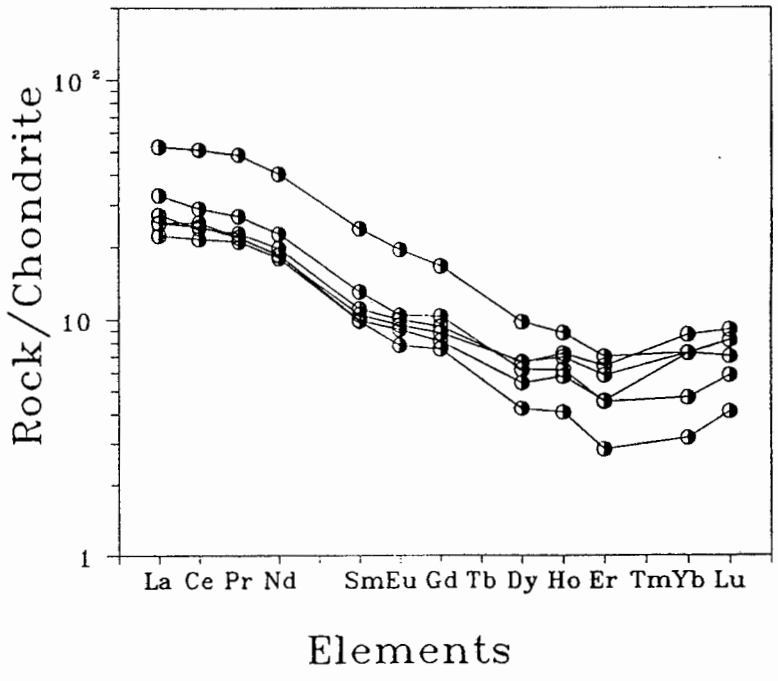

4.3.5. *Nepheline Syenite*

Chemical analyses of the Spitskop nepheline syenites are presented in Table B.10 in Appendix B. All the Spitskop syenites are peralkaline (Figure 4.27a) with peralkalinity indices most commonly in the range 1.1-1.3. This peralkaline character is also reflected in the occurrence of significant *ac* and *ns* in the CIPW norm (Table B.11). The nepheline syenites are felsic, the sum of felsic normative constituents being generally between 70-85% (Figure 4.27b) and are evolved rocks with very low Mg# (Figure 4.27c) of less than 0.3 (mostly <0.15), and Ni and Cr contents close to or below the detection limits for the XRF procedure used (~1.2, 2.5 ppm respectively). A feature of the nepheline syenite analyses is the high volatile contents (expressed as LOI). All samples analysed were totally free of any alteration so the high LOI's are not a secondary feature but reflect the presence of volatile rich phases such as cancrinite, pectolite and sodalite (see petrographic descriptions in Chapter 3).

Figure 4.27: Frequency histograms summarising (a) peralkalinity index; (b) sum of normative felsic constituents; (c) Mg# values in Spitskop nepheline syenites.

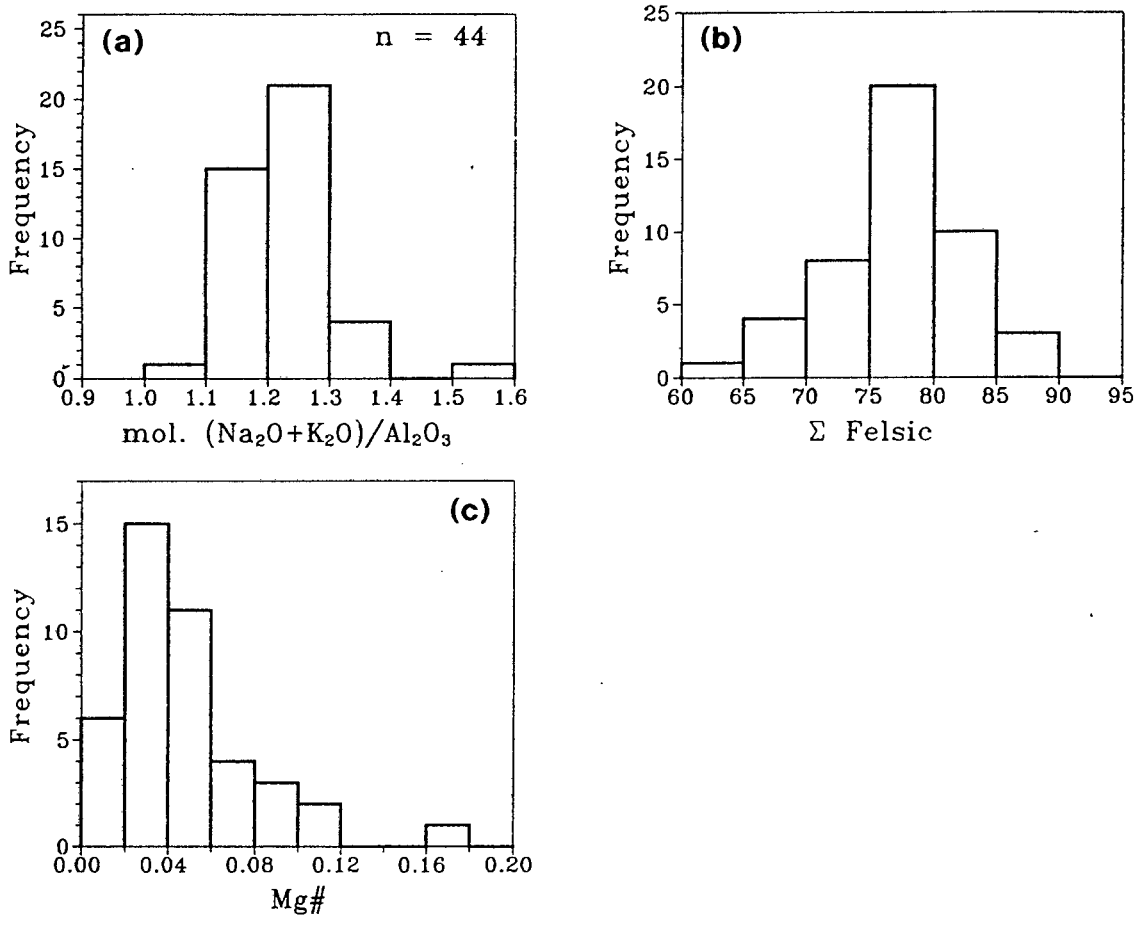

On the TAS classification diagram (Le Bas *et al.*, 1986) in Figure 4.28, all the nepheline syenites plot within the field for phonolites, the volcanic equivalents of nepheline syenites. The compositional ranges of selected elements are shown in a series of Harker diagrams in Figure 4.29 and the mean composition of the Spitskop nepheline syenites is compared to similar rocks from other alkaline complexes in Table B.12 There appears to be little systematic variation in concentration between SiO_2 and the other major and minor elements - only CaO and the alkalis describe definite trends while TiO_2 (not shown) tends to be higher in the lower SiO_2 samples. MgO is consistently low, less than 0.75%, and only sample S31, the single pyroxene-

Figure 4.28: Plot of SiO_2 versus Alkalis for the Spitskop nepheline syenites.

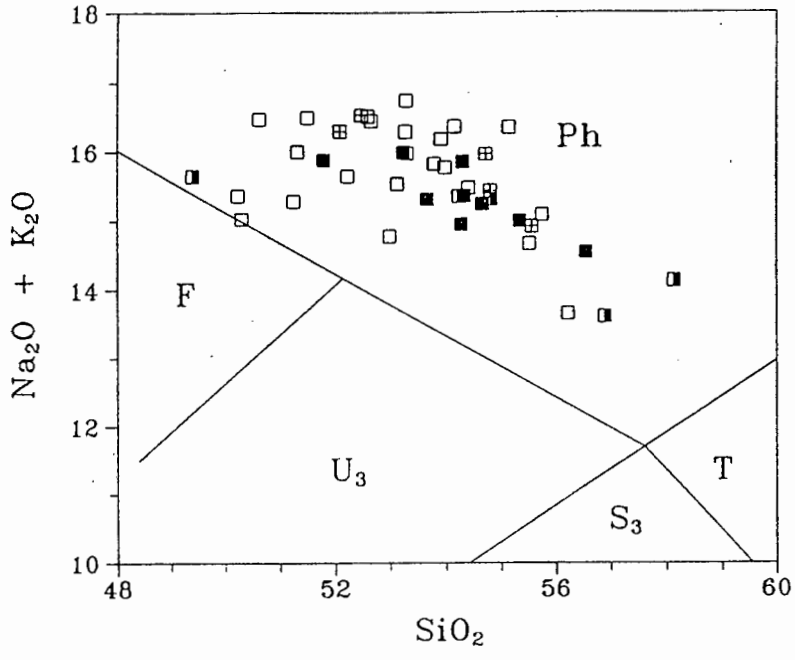

Fields are from Le Bas *et al.* (1986): Ph=phonolites, T=trachytes, F=foidites, U_3=tephriphonolite, S_3=trachyandesite.

phyric nepheline syenite sample in the data set, has a higher MgO concentration (1.71%). P_2O_5 is low, generally less than 0.2%, with, again, S31 having an anomalous value of 0.53%.

Compared to the world average nepheline syenite and phonolite (Le Maitre, 1976) and the average east African phonolite (Le Bas, 1977) the Spitskop nepheline syenites are more peralkaline and have substantially higher Na_2O and lower CaO and K_2O contents. Despite the high degree of peralkalinity of the Spitskop nepheline syenites, the concentrations of Sr and Ba do not exceed 2250 ppm and Zr seldom exceeds 400 ppm. The Spitskop nepheline syenites are therefore not comparable to the truly "agpaitic" (in the restricted useage of the term advocated by Edgar, 1974; 1977) nepheline syenites of Pilanesberg (Lurie, 1973), Lovosero (Gerasimovsky and Kuznetsova, 1966) or Illimaussaq (Ferguson, 1970; Larsen, 1979). Rb exhibits little variation and is largely within the range 100 ±20 ppm. Ba exceeds Sr in most of the Spitskop nepheline syenites: samples from the eastern sheet have Ba contents substantially lower than the other bodies (55-212 ppm) and Ba/Sr less than unity. Samples S31 (pyroxene-phyric) and S153 from Rietfontein, and sample S97 from Mare have Sr concentrations slightly greater than Ba. The trachytic sample from Spitskop, S19, has low Ba/Sr comparable to those of the eastern sheet.

Figure 4.29: Variations of selected major and trace elements in Spitskop nepheline syenites: SiO_2 *versus* (a) Al_2O_3; (b) FeO^*; (c) MgO; (d) CaO; (e) Na_2O

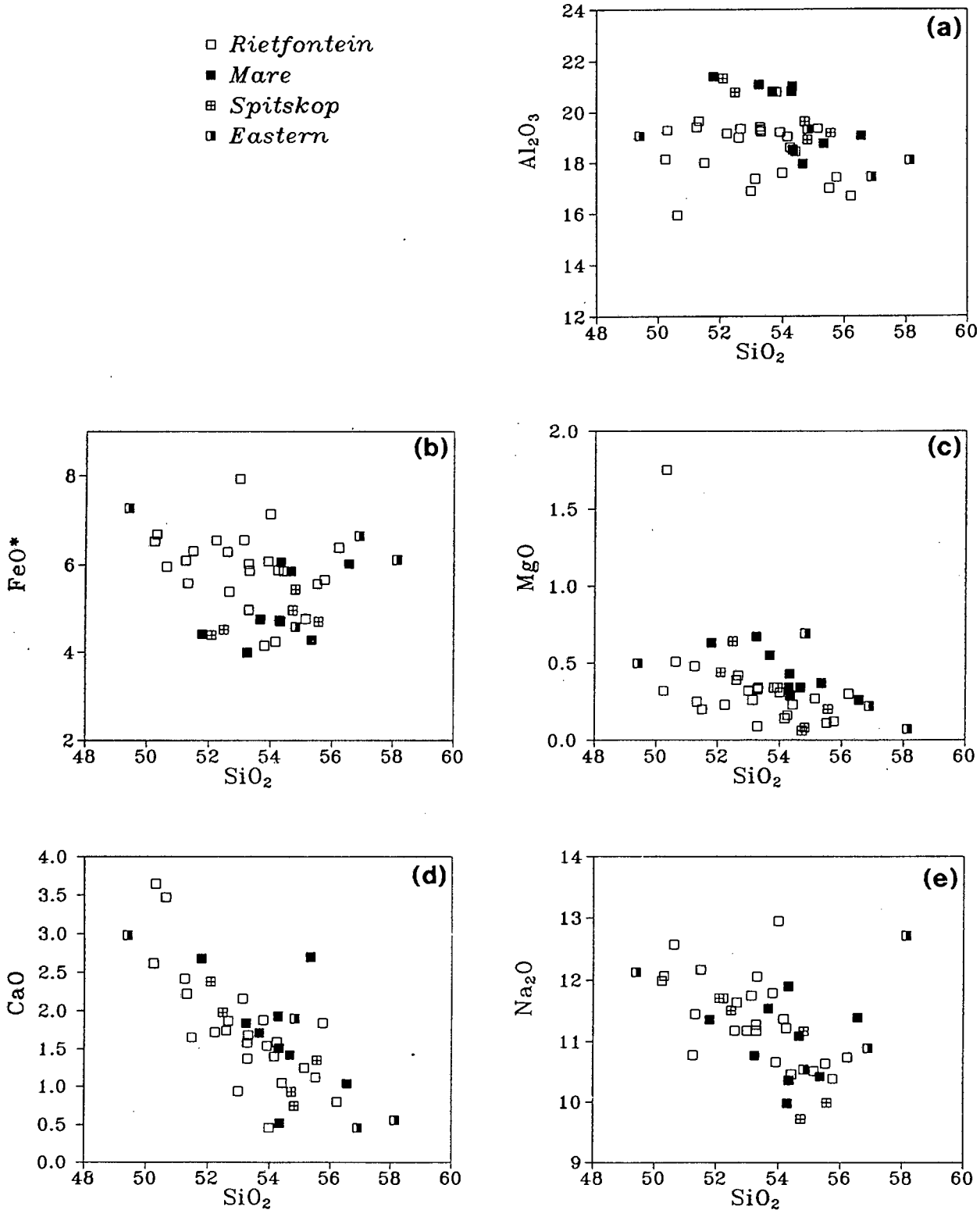

Figure 4.29 (contd): SiO_2 *versus* (f) K_2O; (g) Zr; (h) Ba; (i) Sr; (j) Ce; and (k) histogram of Zr/Nb variations.

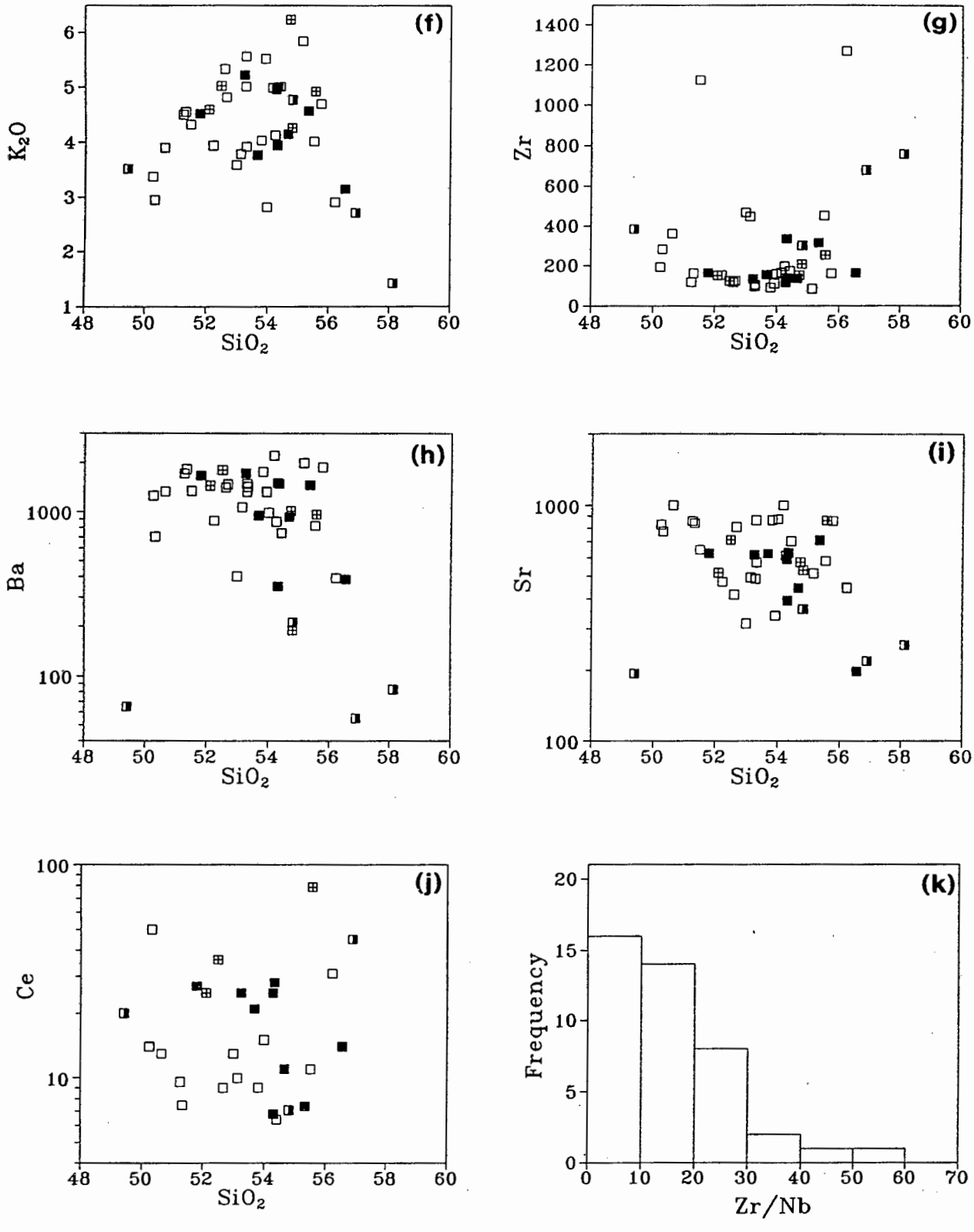

Figure 4.30: Plot of Y+Nb versus Rb for Spitskop nepheline syenites.

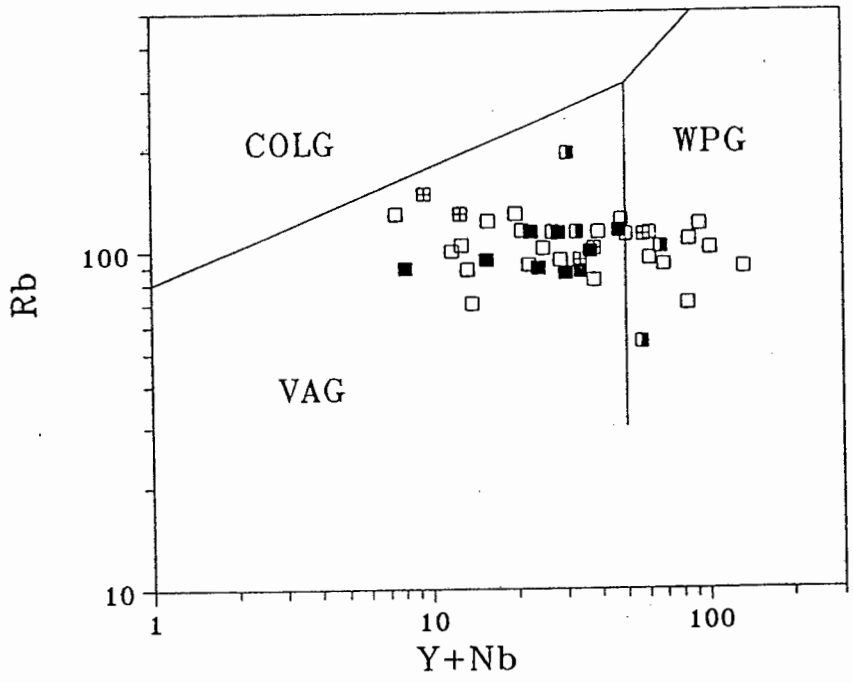

Symbols are those used in Figure 4.29. Fields are from Pearce *et al.* (1984): VAG = Volcanic arc granite; COLG = Syn-collision granite; WPG = Within-plate granite

Figure 4.31: Plot of chondrite-normalised rare earth element abundances in nepheline syenites from the Rietfontein sheet.

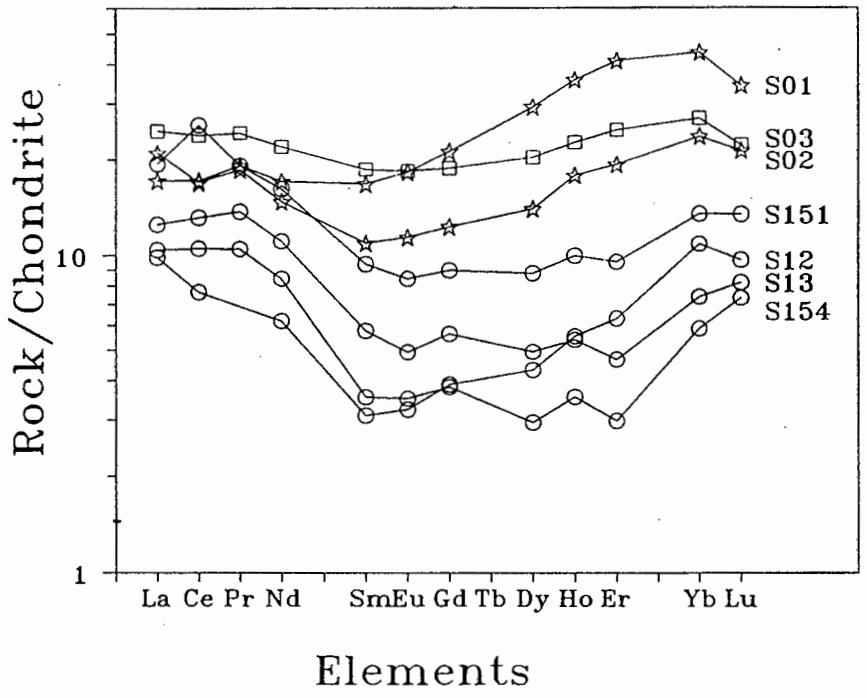

Symbols reflect the textural type: stars=schistose; squares=nepheline-phyric; circles=feldspar-phyric.

Figure 4.32: Chondrite-normalised REE plot comparing Spitskop nepheline syenites with related rocks from other alkaline complexes.

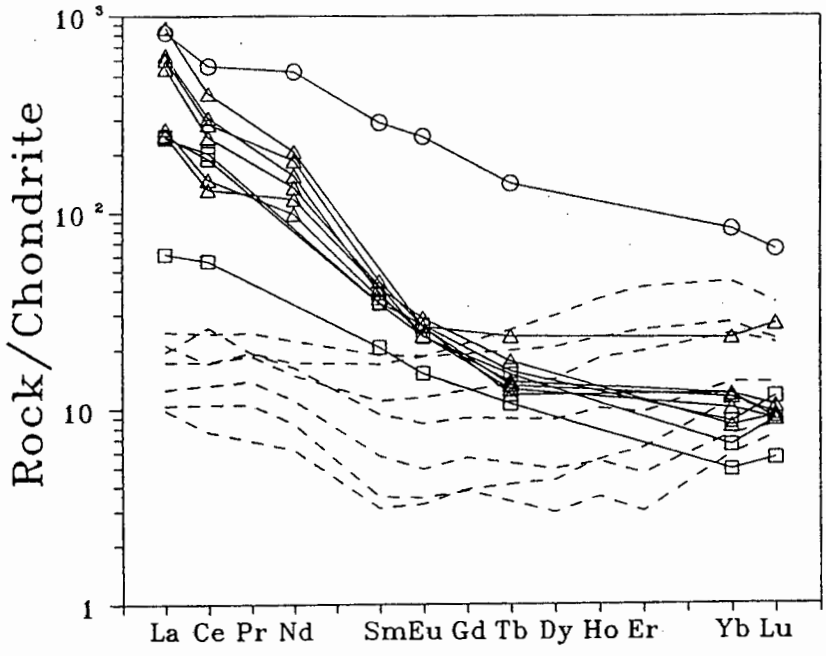

Circle: nepheline syenite from Alnö (Mitchell and Brunfeldt, 1975); Square: nepheline syenite and tinguaite from Fen (Möller *et al.*, 1980); Triangle: phonolite and tinguaite from Kaiserstuhl (Möller *et al.*, 1980).

Both Y and Nb occur in low concentration, with average concentrations of 19 and 21 ppm respectively. Total Nb+Y are also lower than expected for alkalic rocks: indeed, in Figure 4.30, Y+Nb concentrations in the nepheline syenites are lower than the concentrations generally found in within-plate (anorogenic) granites (Pearce *et al.*, 1984)! The LREE are also depleted, many samples having Ce contents below the limits of detection by XRF (ca 6 ppm). Zr/Nb ratios are variable: most have Zr/Nb less than 20 but some range up to 60.

In addition to the low concentrations of the LREE, the chondrite-normalised REE patterns for seven analysed nepheline syenites (all from the Rietfontein sheet) are very unusual (Figure 4.31). Unlike the steep, LREE enriched / HREE depleted, patterns typical of other nepheline syenite complexes (Mitchell and Brunfeldt, 1975; Möller *et al.*, 1980; Price *et al.*, 1985) the Rietfontein syenites have LREE of only 10-20x chondrite, depleted MREE (Sm-Ho) and levels of REE heavier than Ho that are similar to, *or higher than* (S01, S02, S03), the LREE contents! The Spitskop nepheline syenites are compared to nepheline syenites, phonolites and tinguaites from Alnö, Fen, Kaiserstuhl and Mt. Kenya in Figure 4.32. From this plot it may be seen that, while Yb

and Lu are of comparable concentrations, the levels of La,Ce and Nd are depleted by up to two orders of magnitude. In Figure 4.29j, it appears that the LREE concentrations in the Rietfontein syenites tend, on average, to be lower than samples from the other syenite sheets at Spitskop. It would be interesting to analyse the total REE on samples from these other bodies to check whether the unusual REE patterns in the Rietfontein sheet are a feature of all Spitskop nepheline syenites.

4.3.6. Carbonatite

Analyses of carbonatites from Spitskop are shown in Table B.13 in Appendix B.

Samples of carbonatite collected at Spitskop were initially classified on field and petrographic observation as sövite, dolomitic sövite or beforsite following Verwoerd (1967). Woolley and Kempe (1989) proposed a chemical classification of carbonatites based on the relative proportions of CaO, MgO and Fe_2O_3+FeO+MnO (in weight percent) and defined calcio-, magnesio- and ferro-carbonatite fields on a ternary classification plot. The Spitskop carbonatites are shown on such a plot in Figure 4.33(a) where the sövites and dolomite sövites classify as calcio-carbonatites and the beforsites as magnesio-carbonatites.

Figure 4.33: Chemical classification plot of the Spitskop carbonatites after Woolley and Kempe (1989): (a) Weight percent CaO-MgO-FeO*+MnO ternary representation; (b) Binary representation with weight percent CaO/(CaO+MgO+FeO*+MnO) against FeO*/MgO.

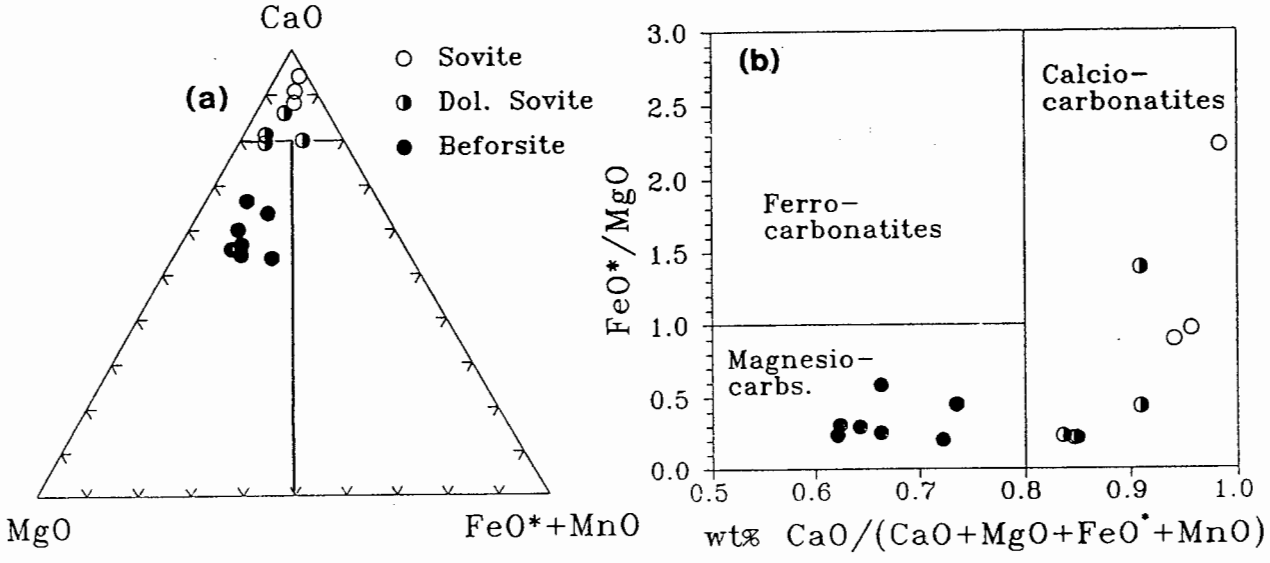

Figure 4.34: Spitskop carbonatite compositions compared with world average Ca- and Mg-carbonatites.

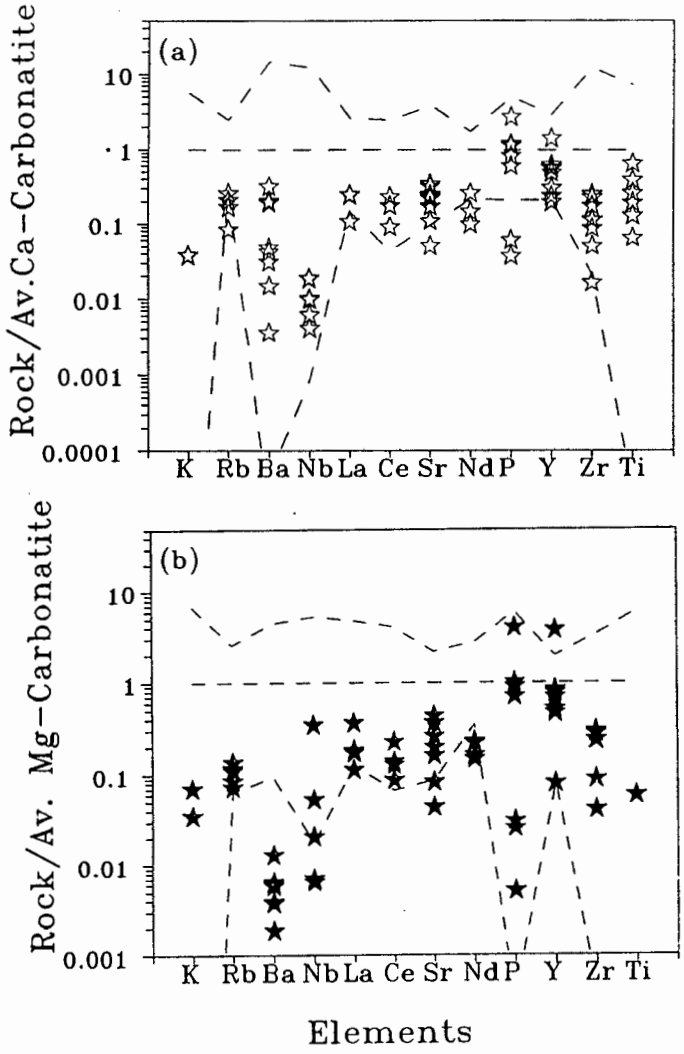

Broken line indicates compositional range of world carbonatites used by Wolley and Kempe (1989) to determine the average values.

The ternary classification may alternatively be represented as a binary plot of weights percent CaO/(CaO+MgO+FeO*) against FeO*/MgO as shown in Figure 4.33(b). A compositional continuum exists between the sövites and dolomitic sövites whereas a clear compositional break (in CaO, MgO and FeO*) separates these carbonatites from the beforsites. In the subsequent discussion the chemical terminology has been adopted: sövites and dolomitic sövites are termed calcio-carbonatite whereas the beforsites are referred to as magnesio-carbonatites.

In its molecular form, the ratio CaO/(CaO+MgO+FeO*) (abbreviated to CCMF) provides a useful index with which to illustrate geochemical compositional changes relative to changing mineralogical character of the carbonatite (i.e. calcite CCMF=1.0;

Figure 4.35: Plot of molecular CaO/(CaO+MgO+FeO*+MnO) ratio against (a) Mg#; (b) Ba; (c) Sr and (d) Nb for the Spitskop carbonatites.

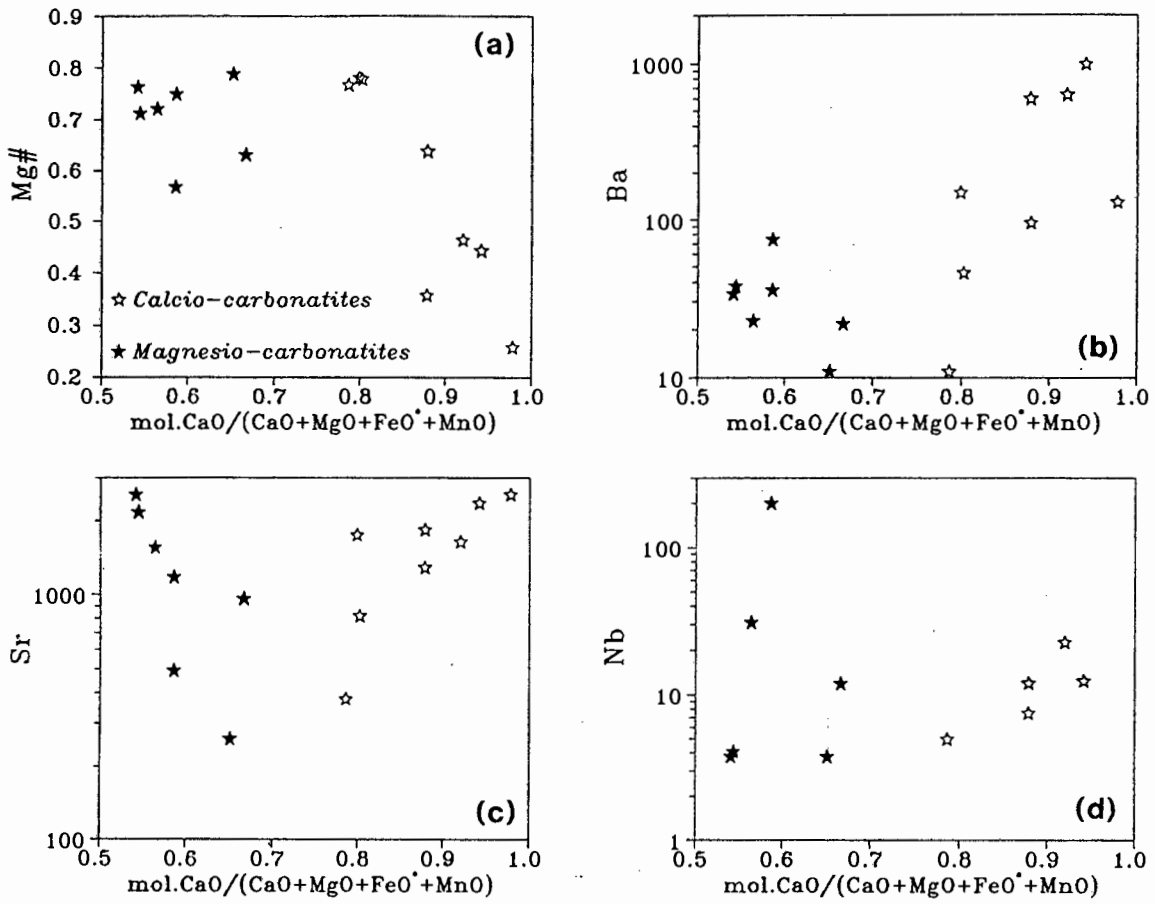

dolomite CCMF=0.5). It has been widely documented (e.g. Le Bas, 1977; 1989) that carbonatite complexes tend to progress from early calcio-carbonatites to late magnesio- and/or ferro-carbonatites. As a result, the CCMF ratio also acts as a crude differentiation index for carbonatites.

In discussing the chemical characteristics of the Spitskop carbonatites, the global average compositions and compositional ranges compiled by Woolley and Kempe (1989) will be used as reference. Care must be exercised in not attaching too much significance to compositional deviations from the Woolley-Kempe average values. In compiling the average values, these authors excluded published analyses where Fe_2O_3 and FeO had not been separately determined or where volatiles were determined as loss on ignition. This effectively excludes most recent XRF-determinations! Wolley and Kempe (1989) also acknowledge that bias remains in their dataset caused by a ".. few analyses with exceptionally high values for certain

elements such as Ba and Nb." Elements which are highly incompatible in basaltic systems commonly form their own minerals in carbonatites (e.g. Nb - pyrochlore; Ba - baryte) or attain elevated concentrations in minerals such as titanite, apatite and amphibole (e.g. Hogarth, 1989). This is reflected in the enormous ranges for certain elements in the Woolley and Kempe data compilation: e.g. in the calcio-carbonatite data set P_2O_5 ranges from 0-10.4%; Nb from 1-15000ppm, Y from 25-346ppm and Zr from 4-2320! The numbers of analyses used to determine the average values are also highly variable, e.g. in the magnesio-carbonatites 51 values were used for P_2O_5, 18 for Nb, 14 for Zr and Ce but only 6 for Nd!

The Spitskop carbonatites are characterised by low FeO^* contents, very low SiO_2, Al_2O_3 and total alkalis. P_2O_5 values are variable and are presumably controlled by the distribution of apatite. High FeO^*/MgO ratios in the calcio-carbonatites are a result of the very low MgO contents in these samples. Mg# values are high, 0.6-0.8, in the magnesio-carbonatites dropping to less than 0.3 in the calcio-carbonatites (Figure 4.35). Of the magnesio-carbonatites, two samples, S06 and S27 have FeO^*/MgO ratios of 0.45 and 0.59 respectively. These iron rich compositions suggest the presence of significant ankeritic carbonate.

A range of minor and trace elements in the Spitskop carbonatites are compared to equivalent values in the Woolley and Kempe world averages in Figure 4.34. In the calcio-carbonatites (Figure 4.34a) concentration levels of all elements are lower than the world average, 3 samples have higher P_2O_5 and one higher Y contents than the average. Nb is consistently low whereas Ba is very variable, ranging from 0.4x down to 0.004x that of the average calcio-carbonatite. Most elements, however, plot within the envelope defined by the compositional range listed in Woolley and Kempe (1989). The magnesio-carbonatites are similar: most elements have lower concentrations than the average but fall within the envelope of compositional variation noted in world Mg-carbonatites. Again, Nb is low whereas the Ba concentrations are all lower than the established global range. P_2O_5 concentrations are highly variable from 0.004x to over 4.0x the global average.

The low Nb concentrations are interesting considering that high Nb is considered a characteristic of magmatic carbonatites, having an average concentration levels of >1200 ppm (range 1-15000!) in calcio- and 600 ppm (range 10-3000!) in magnesio-carbonatites (Woolley and Kempe, 1989). As noted above, the Spitskop ijolites and nepheline syenites have lower Nb contents than equivalent rock types from complexes elsewhere in the world and so low Nb appears to be a characteristic of the Complex as a whole.

The variation of Mg#, Sr, Ba and Nb with changing CCMF ratio is depicted in Figure 4.35. A noteworthy feature of the CCMF *versus* Sr, Ba and Nb plots is the tendency for the "purer" end-member carbonatites - those having CCMF values close to 0.5 or 1.0 - to have the highest trace element concentrations, suggesting a mineralogical control on the distribution of these trace elements.

Concentrations of the elements Ni, Cr, Co and V are all in very low concentration, often below the detection limit of the conventional XRF techniques used (see Appendix A). Zn is generally low in the calcio-carbonatites (10-70ppm) but ranges up to high values of almost 400ppm in the magnesio-carbonatites.

The chondrite-normalised REE profiles (Figure 4.36) generally have the LREE enriched, "steep", patterns typical of world carbonatites (Loubet *et al.*, 1972; Mitchell and Brunfeldt, 1975; Möller *et al.*, 1980; Cullers and Graf, 1984; Woolley and Kempe, 1989). The REE patterns of the calcio-carbonatites overlap those of the magnesio-carbonatites although the latter types exhibit far greater variation in the normalised abundances of the HREE in the range Gd to Lu. Magnesio-carbonatite samples S27 and S54 appear to comprise complementary patterns. The large differences in P_2O_5 in these samples (7.82% in S27; 0.06% in S54) suggest that apatite may be responsible for these variations.

Figure 4.36: Chondrite-normalised plot of REE data for Spitskop carbonatites.

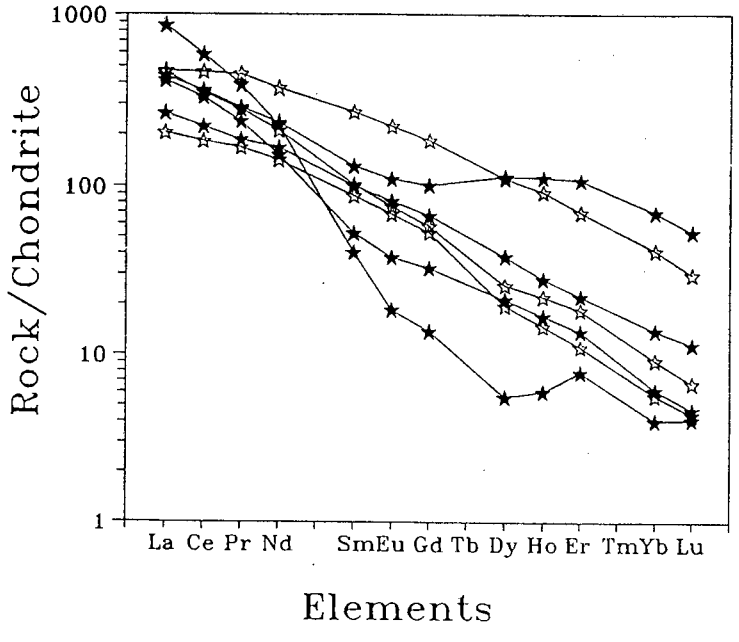

Symbols are those used in Figure 4.35.

4.3.7. *Basalt intrusions*

Two samples of basalt were analysed from the intrusive plugs on either side of the lower Tshweneng River: S74 from the eastern plug and S75 from the western occurrence (analyses are shown in Table B.14 in Appendix B). Other analyses of the basalt plugs have been published by Strauss and Truter (1950; Table 8) and Nel (1976: DA4, referred to as a "latite"!).

In terms of their SiO_2 and alkali contents, and absence of normative nepheline (Table B.14), the analyses indicate that the material in the plugs is sub-alkaline basalt (cf. Le Bas *et al.*, 1986). Strauss and Truter (1950) originally referred to the plugs at Spitskop as "soda basalt" on the basis of their single chemical analysis which is similar to S75 in having very high volatile content and normative Ab>An. Sample S74 has significantly less volatiles and more calcic normative plagioclase compositions. It is possible, then, that Na_2O is not primary and may have been introduced after crystallisation of the basalt. Consequently the prefix "soda-" (or sodic) is not justified for the Spitskop basalts which are, furthermore, clearly not alkaline.

In Table 4.1 the two new analyses (re-calculated volatile-free) are compared to the average Karoo Lesotho basalt composition (Marsh, 1987b). With the exception of the variable CaO and marginally higher MgO, the Spitskop basalts have major element

Table 4.1: Comparison of Spitskop basalt plugs with average basalts.

	S74	S75	Av. Lesotho basalt	Av basalt
SiO_2	50.79	51.16	51.50	49.97
TiO_2	0.92	0.88	0.95	1.87
Al_2O_3	15.80	15.57	15.69	15.99
Fe_2O_3	10.92	10.65	0.96	11.90
MnO	0.22	0.22	0.16	0.20
MgO	7.31	8.02	7.01	6.84
CaO	11.22	8.62	10.69	9.62
Na_2O	2.18	3.84	2.17	2.96
K_2O	0.52	0.89	0.70	1.12
P_2O_5	0.12	0.16	0.16	0.36

Major element compositions of the basalts are re-calculated to 100% anhydrous. Two average values shown for comparison are the average of 49 Karoo basalts from Lesotho (Marsh, 1987b) and the "average basalt" of Le Maitre (1976).

Figure 4.37: Composition of Spitskop Basalt plugs normalised to the average Lesotho basalt (Marsh, 1987b).

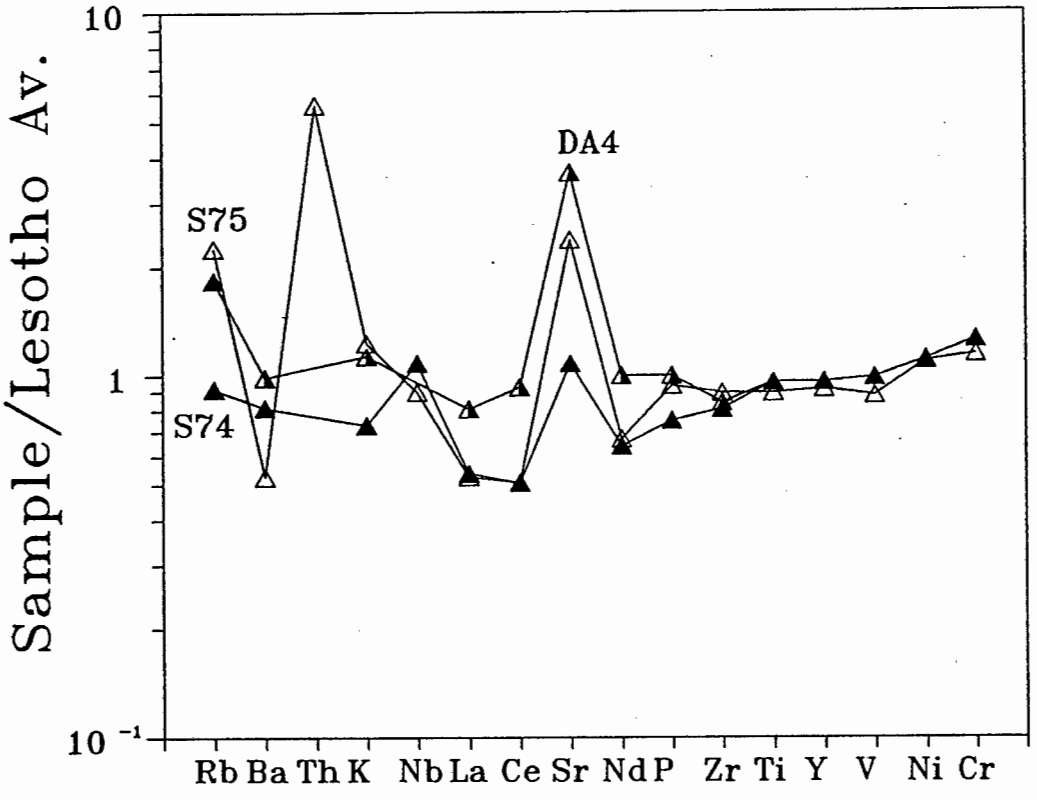

compositions remarkably similar to Karoo basalts from the Central area. In Figure 4.37 the trace element compositions are compared using the normalised variation diagram devised by Marsh (1987b). With the exception of the high Th and Rb concentrations in S75 and the higher, and variable Sr concentrations in all the Spitskop basalts, the Spitskop basalts have closely comparable trace element patterns to Karoo basalts.

As discussed in the field relationships chapter (Chapter 2) earlier, intrusion of the basalt plugs and dykes post-date the solidification of the carbonatite at Spitskop. There is thus no field evidence to prove that the basalts do indeed form part of the Spitskop magmatic event. In view of the major and trace element similarity of the basalts with those of Karoo age, it is equally possible that the basalts may be much younger and unrelated to the petrogenesis of the Spitskop alkaline complex itself.

Chapter 5: Geochronology and Isotope Systematics of the Spitskop Complex.

5.1. *Introduction*

In this chapter, available isotopic data for the igneous rocks of the Spitskop Complex will be presented. New Rb-Sr and Sm-Nd isotopic data were determined on the pyroxenite, ijolites, nepheline syenites and carbonatites and, in addition, Pb and C-O isotopic data were determined for the carbonatites. Sr isotope analyses were also performed on samples of fenitised material but these data are presented and discussed in the chapter dealing with the metasomatic rocks of Spitskop (Chapter 6).

In the first section the Sr isotopic data pertinent to determining the age of the Complex will be discussed. This is followed by a presentation of the remaining radiogenic and stable isotope data which is of broader, more "petrogenetic" interest.

5.2. *Geochronology*

In view of the uncertainty in the age of the Spitskop Complex discussed in Chapter 1, it is of importance to establish whether or not the Spitskop Complex does indeed belong within the suite of Pilanesberg-age alkaline complexes. The purpose of this section, then, is to present and discuss the data on which the dates for Spitskop presented in Table 1.1 are based.

Both the ijolites and nepheline syenites exhibit sufficient variation in Rb/Sr to be suitable for whole rock age determinations using the Rb-Sr system.

Figure 5.1 Isochron plot of magmatic (Type-I) ijolites.

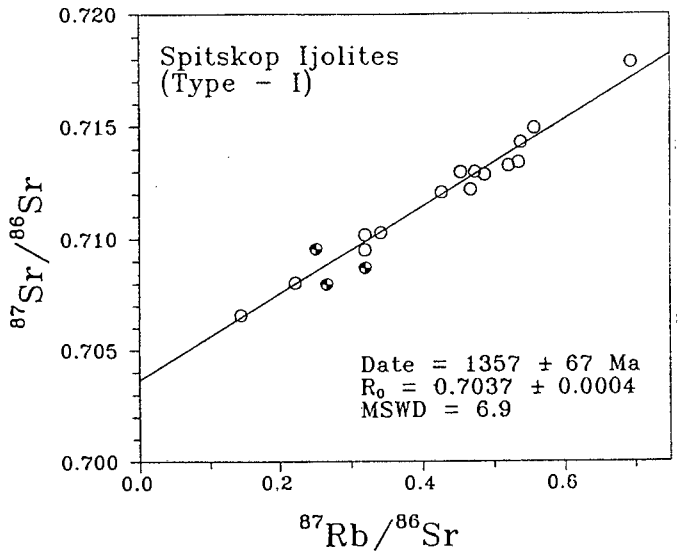

Samples excluded from the regression calculation are ornamented.

5.2.1. *Ijolites*

In view of the complex variations amongst the "Type-II" ijolites described in Chapters 2,3 and 4, only the Sr isotope data on the apparently magmatic, "Type I", ijolite samples were utilised for dating. These 18 samples are depicted on a conventional isochron plot in Figure 5.1. Treating all the points yields a rather poor regression (MSWD = 22) date of 1379 ± 117 Ma, with $^{87}Sr/^{86}Sr_i$ of 0.7034 ±7 (errors enhanced, see Appendix A). Three samples (S41, S82, S83 - differentiated on the plot in Figure 5.1) make significant contributions to this scatter, deviating by 9-12 times the analytical uncertainty in X, and 5-6 times the analytical uncertainty in Y. Excluding these samples significantly reduces the amount of "geological" (i.e. non-analytical) scatter and yields a date of 1357 ±67Ma and initial ratio of 0.7037 ±4. Since the regression line still contains scatter in excess of analytical error (MSWD=6.9; compared to the expected F value of 1.9), the 95% confidence intervals on the parameters were estimated treating analytical and "geological" errors separately (following Harmer and Eglington, 1990; see Appendix).

5.2.2. *Nepheline Syenites*

Regression of all 34 nepheline syenites analysed yields an "errorchron" date of 1437 ±127 Ma. The high MSWD of 43 relative to the expected value (for 34 samples at

Figure 5.2: Isochron plots of nepheline syenites from (a) the Rietfontein body (b) the Mare, Spitskop and eastern bodies.

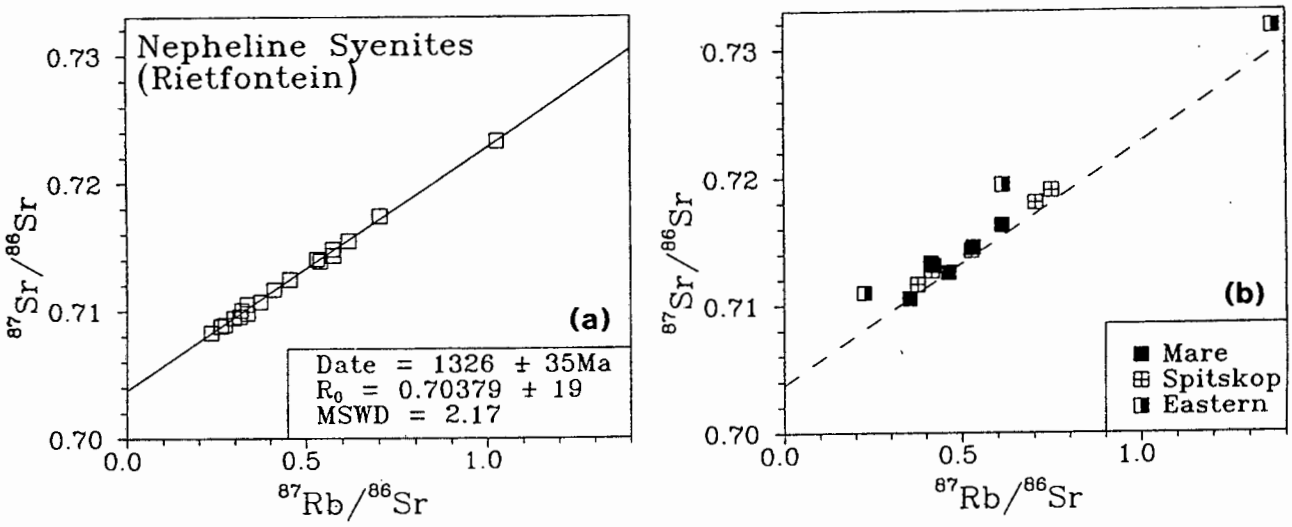

The regression line for the Rietfontein nepheline syenites from (a) is shown as a broken line in (b).

95% confidence) of 1.6 indicates that the data set may contain samples of differing age and/or initial $^{87}Sr/^{86}Sr$. In view of the totally unaltered nature of the samples used (see Chapters 3 and 4), the scatter cannot be attributed to later open system behaviour. If only the 19 nepheline syenites from the Rietfontein sheet are included (Figure 5.2a) in the regression, a date of 1326 ±35 Ma with a $^{87}Sr/^{86}Sr_{(i)}$ of 0.70379 ±19 is obtained with a significantly improved MSWD of 2.17. The expected MSWD for 19 samples at 95% confidence is 1.80, implying that a small amount of "geological" scatter is still present in the data set.

It is concluded that the date of 1326 ±35 is a reasonable estimate of the time of formation of the Rietfontein nepheline syenites. The date and initial $^{87}Sr/^{86}Sr$ are indistinguishable from those determined for the magmatic ijolites.

Data from the other nepheline syenite bodies at Spitskop are plotted in Figure 5.2(b) and all fall above, or within error of, the 1326 Ma isochron line. This suggests that the scatter in the total data set identified above relates more to variations in initial $^{87}Sr/^{86}Sr$ between different nepheline syenite bodies rather than reflecting any real differences in age of formation. The Rietfontein syenite date is consequently accepted as the best available estimate of the age of formation of all the Spitskop nepheline syenites.

5.2.3. Conclusions

The preferred estimates for the dates and initial $^{87}Sr/^{86}Sr$ of the magmatic ijolites and the Rietfontein nepheline syenites are statistically indistinguishable. Because these rock types have similar, i.e. overlapping, Rb/Sr values, the data sets may be regressed together without fear of generating anomalous correlations and spurious dates. The pooled data set of 34 samples results in a combined estimate of 1341 ±37 with $^{87}Sr/^{86}Sr_i$ of 0.70373 ±20 (MSWD=4.1 relative to expected value of 1.64).

This date is thus considered the best estimate for the age of the Spitskop silicate magmatic rocks. With reference to Table 1.1 it may be noted that this age is within error of those listed for the Stukpan complex and all centres within the Pienaars River Complex except Leeuwfontein. There can be no doubt, therefore, that the Spitskop Complex forms part of the widespread alkalic igneous event which gave rise to the Pilanesberg Suite of complexes.

5.3. Isotope Patterns

5.3.1. Introduction

All available isotope data are presented in Tables B.15, B.16 and B.17 in Appendix B. Initial ratios and epsilon values were calculated at 1341 Ma and the errors listed in the table are 95% confidence intervals assuming zero error in the age. The errors thus do not reflect the total uncertainty for each individual estimate but instead relate to the uncertainty applicable in comparing initial isotopic compositions amongst different samples from the complex at the same ("fixed") reference age. Epsilon values were calculated using the model parameters listed in Appendix A.

Discussion of the isotopic data is divided into three parts: the data for the demonstrably magmatic silicate units (pyroxenites, Type-I Ijolite and nepheline syenites) are presented first; these data are then compared to the data for the Type-II and "Other" ijolite types; finally, the carbonatite data are discussed and compared with the silicate units from Spitskop as well as with the available isotopic data for carbonatites elsewhere.

Figure 5.3: Plots of parent/daughter ratios versus initial isotopic ratio: (a) Rb/Sr versus $\varepsilon_{(Sr)}$; (b) Sm/Nd versus $\varepsilon_{(Nd)}$.

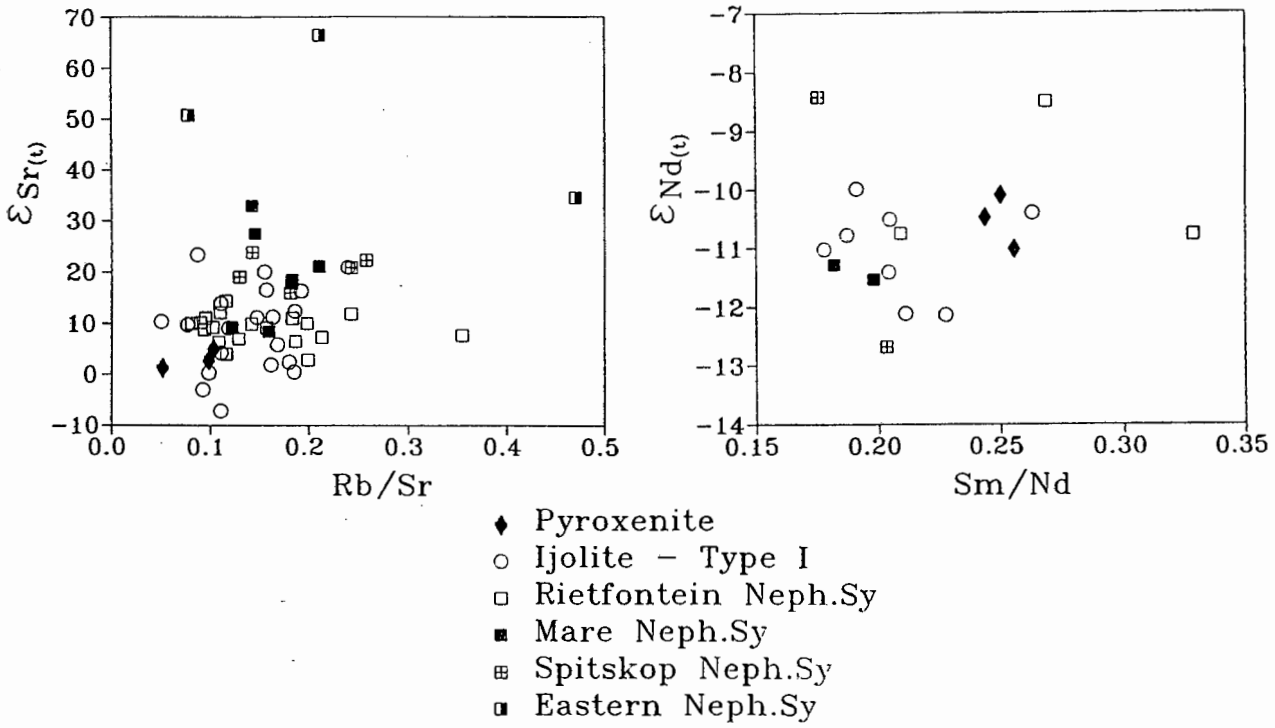

Where possible, discussion of the petrogenetic significance of the isotopic data is postponed until Chapter 7.

5.3.2. Sr and Nd Isotopic composition of the pyroxenite, Type-I ijolite and nepheline syenite

In the discussion of the age of the Spitskop Complex above it was found that the Type-I ijolites had greater variation in $^{87}Sr/^{86}Sr_{(i)}$ than the Rietfontein nepheline syenites, and that the $^{87}Sr/^{86}Sr_{(i)}$ in the syenites from the Rietfontein sheet was lower than, or within error of, those from the other bodies of nepheline syenite.

In Figure 5.3(a) and (b), initial $^{87}Sr/^{86}Sr$ and $^{143}Nd/^{144}Nd$ are plotted against Rb/Sr and Sm/Nd respectively and the lack of any systematic variation is evidence that the adoption of the "compound" date of 1341 Ma does not generate spurious differences in the isotopic data.

The variation in Sr and Nd isotopic composition with changing petrological character may be assessed in Figures 5.4 and 5.6. The three samples of pyroxenite

Figure 5.4: Plot of (a) SiO_2 versus $\varepsilon_{(Sr)}$ and (b) Mg# versus $\varepsilon_{(Sr)}$ for the Pyroxenites, Type-I ijolites and nepheline syenites from Spitskop.

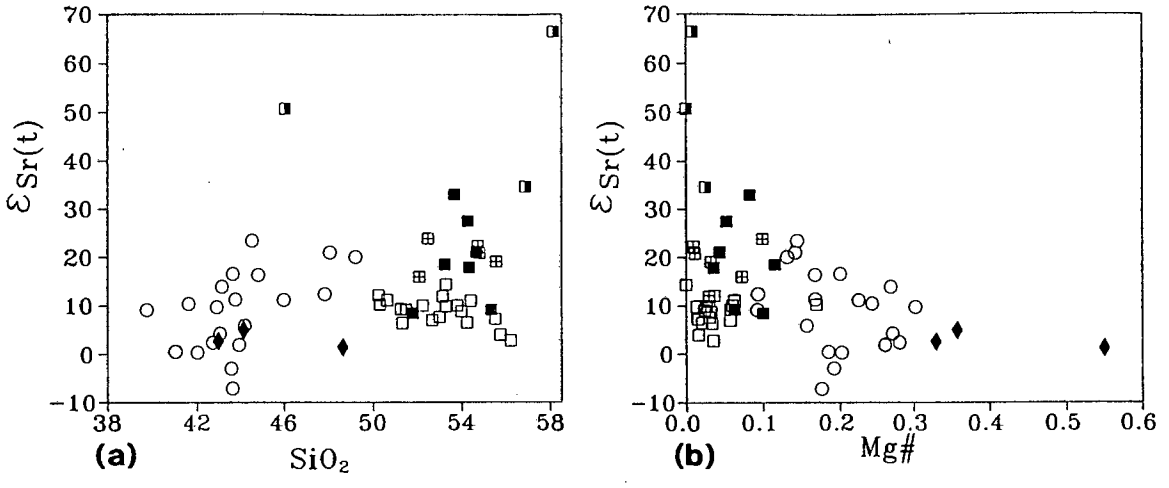

Symbols follow those used in Figure 5.3.

have identical $\varepsilon_{(Sr)}$ and $\varepsilon_{(Nd)}$ values within error of +3 and -10.5, respectively. Amongst the other silicate groups, the variation in $\varepsilon_{(Sr)}$ is somewhat greater than the range in end. The Type-I ijolites have end in the range -10 to -12, while the total variation amongst all the nepheline syenites is from -9 to -13. As indicated from the "near-isochron" relationships discussed above, the Type-I ijolites and the Rietfontein nepheline syenites have similar $\varepsilon_{(Sr)}$ values. Nepheline syenites from the other bodies have $\varepsilon_{(Sr)}$ ranging from +15 to over +60. The range in $\varepsilon_{(Sr)}$ values tends to increase with increasing SiO_2 and decreasing Mg# (Figure 5.4).

In the $\varepsilon_{(Sr)}$-$\varepsilon_{(Nd)}$ plot (Figure 5.6) the Spitskop rocks fall in the "enriched" quadrant of the diagram significantly below the field of Proterozoic carbonatites from Canada. This implies that sources which were enriched in Rb/Sr and Nd/Sm relative to primitive mantle compositions for extended time periods (ca. 1Ga) were involved in the genesis of the Spitskop silicate units. Furthermore, the range in $\varepsilon_{(Sr)}$ within and between the ijolites and the nepheline syenites implies that these rocks could not have been derived through closed-system processes from a common parental magma.

These petrogenetic topics will be dealt with more fully in Chapter 7.

Figure 5.5: Plot of MgO versus $\varepsilon_{(Sr)}$ for Type-I, Type-II and "Other" ijolite varieties.

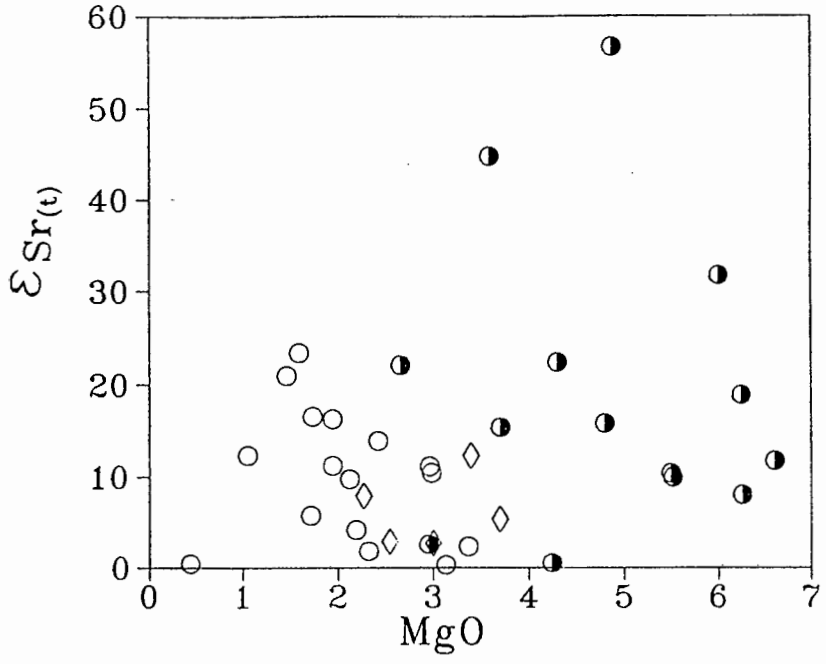

Symbols are: open circle: Type-I ijolites; half-filled circle: Type-II ijolites; open diamond: "other" ijolites.

5.3.3. *Sr isotopic comparison of Type-I, Type-II and "Other" ijolite types*

In Chapter 4 the Type-II ijolites were shown to differ from the Type-I variety in having higher MgO and Mg#. In Figure 5.5 it will be seen that neither the Type-II textural variety nor the "Other" ijolites can be distinguished from the Type-I ijolites on the basis of $\varepsilon_{(Sr)}$. Significantly, the three Type-II samples with $\varepsilon_{(Sr)}>30$ have peralkalinity indices less than unity, high Sr contents and two of these belong to the high-Ni sub-group of the Type-II variety.

5.3.4. *Sr,Nd,Pb,O and C isotopic composition of the carbonatites*

5.3.4.1. *Sr and Nd data.*

Over the past decade, a substantial database has been produced on the Sr-Nd isotopic composition of carbonatites (summarised in Bell and Blenkinsop, 1989; these

Figure 5.6: Plot of Spitskop carbonatite and silicate $\varepsilon_{(Sr)}$-$\varepsilon_{(Nd)}$ data.

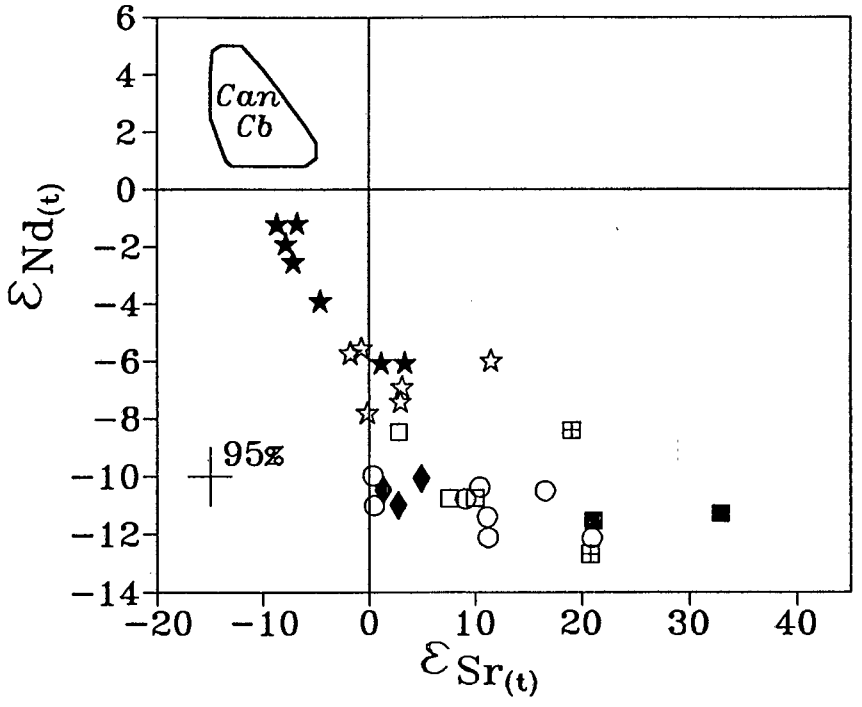

Shown for comparison is the data field for Proterozoic Canadian carbonatites (from Bell and Blenkinsop, 1987a). Open stars are calcio-carbonatites; filled stars magnesio-carbonatites; other symbols follow those in Figure 5.3.

data are more comprehensively discussed in Chapter 9). With very few exceptions, carbonatite complexes of all ages consistently have negative $\varepsilon_{(Sr)}$ and positive $\varepsilon_{(Nd)}$ values and plot within a relatively narrow range in the "depleted" quadrant on the $\varepsilon_{(Sr)}$ *versus* $\varepsilon_{(Nd)}$ plot.

The $\varepsilon_{(Sr)}$-$\varepsilon_{(Nd)}$ data for the Spitskop carbonatites (plotted in Figure 5.6) are variable and are characterised by rather negative $\varepsilon_{(Nd)}$ values of -1 to -7.5 in relation to data for Proterozoic carbonatites from Canada. Although the data ranges overlap, the Spitskop calcio-carbonatites have more extreme $\varepsilon_{(Sr)}$-$\varepsilon_{(Nd)}$ values (i.e. more positive $\varepsilon_{(Sr)}$; more negative $\varepsilon_{(Nd)}$) than the magnesio-carbonatites.

Data for the silicate components in the Spitskop Complex are compared with the carbonatites in Figure 5.6 where it is clear that the silicates have similar or higher $\varepsilon_{(Sr)}$, but lower $\varepsilon_{(Nd)}$ values than the carbonatites.

The petrogenetic implications of this $\varepsilon_{(Sr)}$-$\varepsilon_{(Nd)}$ data will be discussed fully in Chapters 7 and 9.

5.3.4.2. Pb data.

The carbonatite Pb isotopic data are displayed on a conventional $^{207}Pb/^{204}Pb$ - $^{206}Pb/^{204}Pb$ plot in Figure 5.7. Reference 1341 Ma secondary isochrons indicate that significant variation existed in the isotopic composition of Pb in the carbonatites at the time of formation.

Unlike Sr and Nd, variations in initial Pb ratios are more complicated to assess quantitatively in that the U-Pb system seldom remains closed after or during uplift and exposure of rock bodies because of the solubility of U in oxygenated groundwater

Figure 5.7: Plot of Pb isotopic data for Spitskop Carbonatites.

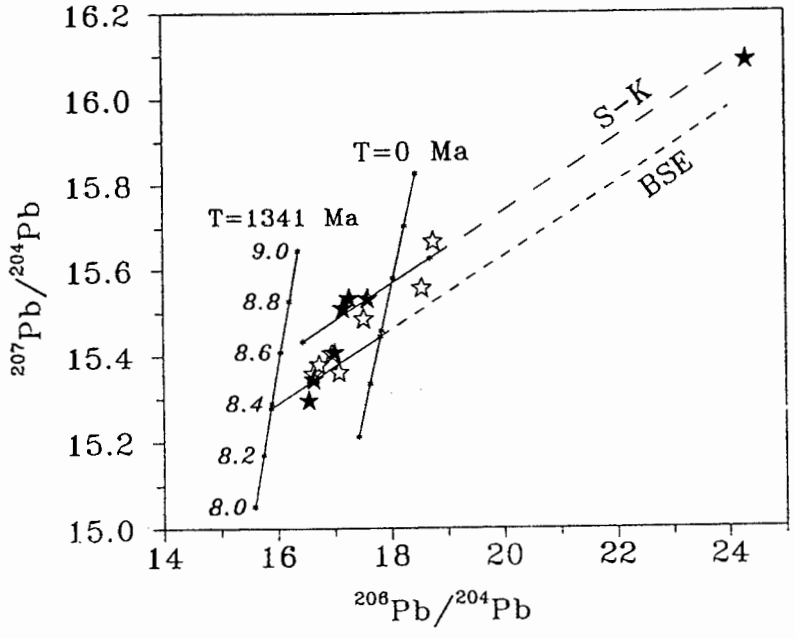

See text for explanation of the primary isochrons "T=1341 Ma" and "T=0", and reference secondary isochrons "S-K" and "BSE".

(e.g. Faure, 1986). The fact that $^{207}Pb/^{204}Pb$-$^{206}Pb/^{204}Pb$ secondary isochrons frequently preserve correct ages whereas whole-rock ^{235}U-^{207}Pb or ^{238}U-^{206}Pb isochrons are seldom obtained implies that in most cases U-Pb mobility was relatively recent (i.e. <10 Ma). Recent U-Pb mobility thus renders the calculation of initial Pb isotope ratios from the measured sample U and Pb concentrations somewhat unreliable.

Where samples are not very radiogenic, it is possible to use modelled source $^{238}U/^{204}Pb$ (μ) as a measure of "relative initial Pb ratio" (discussed further in the Appendix A). In Figure 5.7 two 1341 Ma secondary isochrons are drawn: one for the

Figure 5.8: Plot showing variation of modelled source μ values of the Spitskop carbonatites in relation to world carbonatite data.

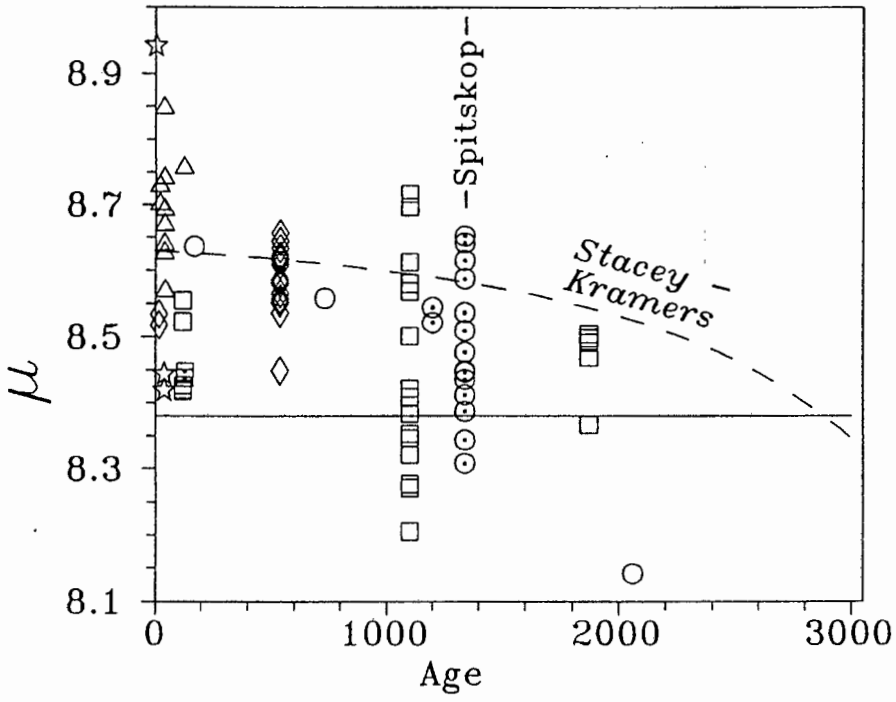

The horizontal solid line depicts the Kwon *et al.* (1989) model bulk earth reservoir used to estimate the individual sample reservoir μ's. The dashed curve represents values for the Stacey and Kramers (1975) Pb evolution model. Sources of world data: Kwon *et al.* (1989); Andersen and Taylor (1988); Nelson *et al.* (1988); Bell *et al.* (1987).

"Bulk Silicate Earth" (BSE) reservoir, a single-stage model derived by Kwon *et al.* (1989); the other for the two-stage model for conformable crustal leads derived by Stacey and Kramers (1975) (S-K). The solid line segments in each isochron link the compositions of Pb at 1341 Ma and 0 Ma according to the parameters of each model.

The BSE reservoir was modelled by Kwon *et al.* (1989) as a simple single stage system starting at 4520 Ma with primordial Pb isotopic compositions (i.e equal to Canyon Diablo Troilite) and a μ of 8.38. This μ value gave the best estimate for the reservoir from which North American carbonatite complexes, ranging in age from 2.7 Ga to 0.1 Ga, were derived. Other Pb reservoirs, generated at the same time with primordial Pb isotopic compositions, but with different μ_{res}'s (e.g. between 8.0 and 9.0) would have Pb isotopic compositions at the time of formation of Spitskop (1341 Ma), which would fall on the straight line labelled "T=1341 Ma" in the diagram. This line is a primary isochron, or 1341Ma "Geochron", for the adopted model and represents the locus of all reservoirs, starting at the same time and with the same initial ratios as BSE, but with differing $^{238}U/^{204}Pb$ (μ). The 1341 Ma primary

isochron has been drawn, and calibrated, only for μ's of 8.0 to 9.0 but is obviously continuous from μ=0.0 (i.e. the primordial Pb starting point) to infinity.

Had the Spitskop carbonatites been extracted from primordial reservoirs which had remained closed systems since 4520 Ma, they would have initial Pb ratios plotting on the primary isochron ("T=1341 Ma"). It is possible, then, to represent the initial isotopic variability in the Spitskop carbonatites numerically by making the assumption that the carbonatites were extracted from reservoirs which formed simultaneously with BSE but had differing μ's, and that any U loss from the samples occurred relatively recently (i.e. <ca.10 Ma). The initial Pb composition of any sample will then be the point of intersection of the 1341 Ma secondary isochron line through the sample point with the 1341 Ma primary isochron for the BSE source. Since this point represents a unique source μ for the selected model, this modelled source μ will be used in the following discussion in preference to the initial ratios themselves. The calculation procedure is derived in Appendix A.2.2.2. This technique is best applied only to samples which are not unduly radiogenic - since the calculation involves an extrapolation, the further the sample point falls from the initial ratio locus for the model, the greater will be the magnitude of the propagated error.

A sample of Pb extracted from either reservoir with sample μ lower than that in the source would plot somewhere on the solid line segment, samples with $\mu_{sample}>\mu_{source}$ would plot on the broken segment, or its extension to higher ratios. All but three of the carbonatites fall to the left of the T=0 locus line for the Kwon *et al.* (1989) model i.e. their present day ratios are less than the present day Pb compositions of all possible μ reservoirs created with primordial compositions at 4520 Ma which have remained closed systems. The carbonatites also plot to the left of "Geochron" for the Stacey-Kramers Pb growth model (not shown). In other words, the Spitskop carbonatite sample U/Pb ratios must have been lower than the reservoirs from which they were extracted.

In Figure 5.7, the positions of the Spitskop carbonatite points relative to the 1341 Ma secondary isochrons of model BSE and Stacey-Kramers indicate that multiple sources, enriched and depleted in U/Pb relative to BSE, were involved in the genesis of the carbonatites. Using calculated model source μ's, the Spitskop carbonatites are compared with published Pb data from carbonatites of different ages in Figure 5.8. In this diagram the trace of the second stage (i.e. 3700 Ma to present) of the Stacey--Kramer two-stage evolution model is drawn as a reference. The Spitskop carbonatites have similar ranges in Pb signature to the 1100 Ma carbonatite complexes of the Canadian Shield, implying contributions from a source with time-integrated μ values

less than the Kwon *et al.* BSE model (i.e. <8.38), and another having U/Pb slightly in excess of the Stacey-Kramers crustal ore lead model (>8.6).

5.3.4.3. $18O$-$13C$ data

Oxygen and carbon isotopes were determined on the carbonate fraction of 11 of the carbonatite samples. These determinations were made on the whole rock powders prepared for geochemical and radiogenic isotope analysis. $\delta^{13}C$ values have a relatively narrow compositional range of -1.7 to -2.9 per mil (relative to PDB) whereas $\delta^{18}O$ values range from +13.5 to +17.2 per mil (relative to SMOW). The compilation of available O-C isotope measurements on sub-volcanic carbonatite intrusions (Deines, 1989) showed that about 50% of the $\delta^{18}O$ values are between +6 and +9 per mil, with a markedly skewed distribution to higher values. The range in $\delta^{13}C$ data is more restricted, the distribution of values more gaussian, with 91% of the analyses falling between -2 and -8 per mil. On average the $\delta^{18}O$ values in carbonatite lavas were higher than in the sub-volcanic carbonatites.

The Spitskop carbonatites are thus somewhat enriched in $\delta^{18}O$ whereas $\delta^{13}C$ values overlap the upper part of the global range.

Deines (1989) noted that the $\delta^{18}O$-$\delta^{13}C$ values are often correlated in complexes having heavy $\delta^{18}O$ values: slopes of the correlations are commonly ± 0.4 whereas data from the Oka carbonatite have a slope of 0.3 and St. Honoré a slope of 0.2. The Spitskop data are poorly correlated (r=0.52) with a slope of 0.25. Alteration was not considered a likely mechanism for generating this correlation by Deines who suggested rather that the correlation "..reflects a process fundamental to carbonatite formation."

The high $\delta^{18}O$ values in the Spitskop carbonatites will be discussed further once the data for the other "Pilanesberg Suite" carbonatite complexes have been presented.

Figure 6.1: Geological sketch map showing the distribution of fenitised rocks along the eastern edge of the Spitskop Complex.

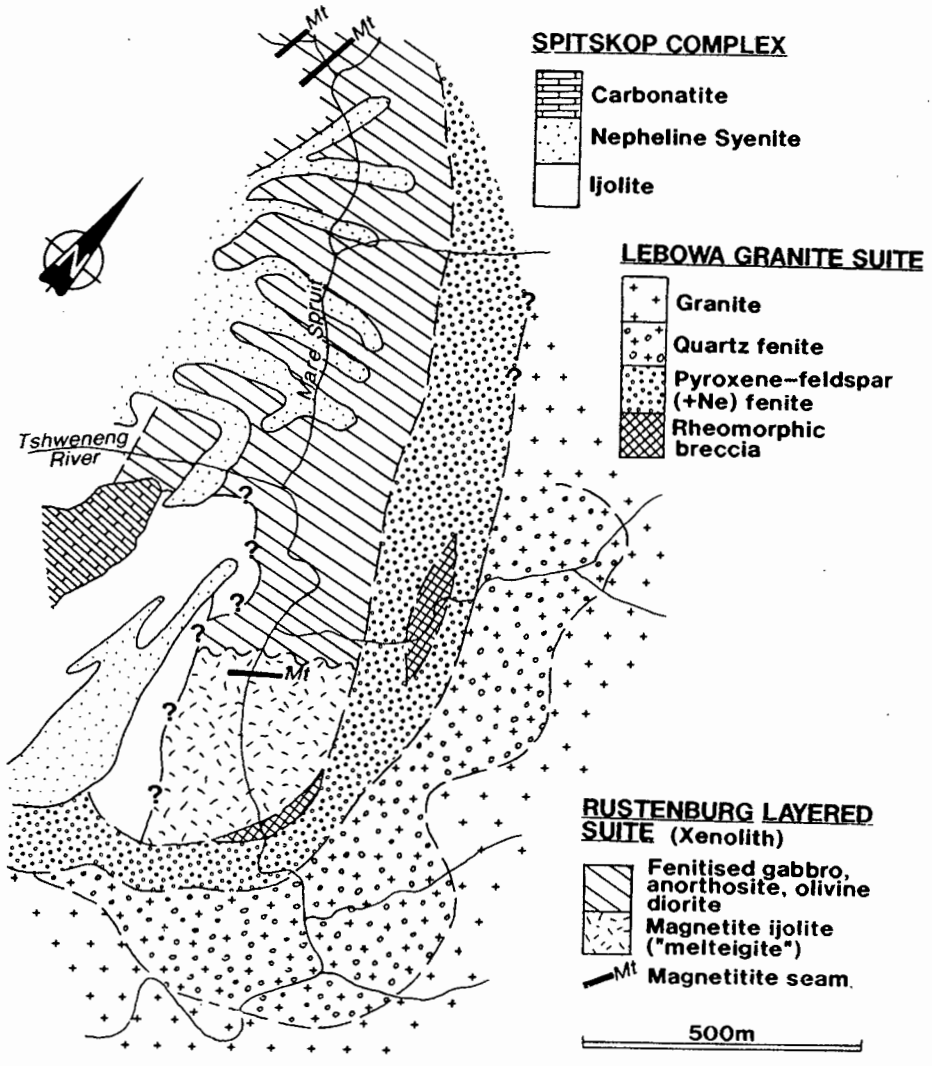

Strauss and Truter used the term "umptekite" to refer to the fenitised Bushveld granites: umptekite is a somewhat outdated igneous rock term and should not strictly be applied to rocks clearly produced by metasomatic processes. Red- and white"umptekites" were mapped by Strauss and Truter (1950) which they regarded as the products of two distinct fenitisation events: an initial lower-grade episode which gave rise to the red variety; and a later, more intense stage resulting in the white"umptekites". They stated that in the red fenites quartz is still present and the feldspars retain the red colouration characteristic of oxidised Bushveld granites. Red fenites are characteristically "cellular" due to the presence of ochre-lined cavities which were regarded as the sites of weathered-out mafic minerals.

Chapter 6: Fenitisation Related to the SpitskopComplex

6.1. Introduction

"Fenite" is here used to denote the products of metasomatic transformation where the metasomatising agent is derived from an alkaline igneous complex, with or without carbonatite, and was first used by Brögger (1921) for such material in the Fen Complex of Norway. The presence of fenitised borders to a carbonatite complex is considered by some workers as unambiguous evidence for the presence of magmatic carbonatite (e.g. Le Bas, 1981).

Two contrasting rock compositions have been fenitised by the intrusion of the Spitskop Complex: granites of the Lebowa Suite which form the country rocks; and mafic cumulates of the Rustenburg Suite which, as discussed in the introductory chapter, occur as a large xenolith in the complex. Strauss and Truter (1950) used igneous terminology to refer to the fenites resulting from these starting compositions, an approach criticised by Verwoerd (1967). Where possible, these igneous terms have been avoided in the present discussion.

The distribution of the metasomatised rocks are shown on the geological map of Spitskop (Figure 2.1), and the Mare Spruit - Lower Tshweneng River outcrops are shown in more detail in Figure 6.1.

6.2. Bushveld granite country rock fenites

The Spitskop Complex is surrounded by country rocks of the Lebowa Granite Suite of the Bushveld Complex. Both the coarse-grained, hornblende granites of the Nebo type, and the medium-grained Klipkloof type (Kleeman and Twist, 1989) are found. Inclusions of granophyre in the Nebo Granite are also reported by Strauss and Truter (1950) and Verwoerd (1964).

Strauss and Truter (1950) were of the opinion that, with the transition to the white variety, the feldspars recrystallised and lost their red pigmentation, while at the same time quartz finally disappeared.

Re-mapping of the fenitised granites has shown, however, that the colour distinction does not always correspond to the final disappearance of quartz.. As the mineralogy is a more faithful reflection of the degree of metasomatic modification, this has been used to draw the boundaries on the map, and forms the basis for the terminology used in the discussion that follows.

At Spitskop, as in other reported fenite occurrences, the degree of metasomatic alteration does not always change in a regionally systematic fashion and is subject to local perturbations. In an investigation of the fenitisation at Fen, Kresten (1988) classified the metasomatised rocks into three geological settings: contact fenites, aureole fenites and vein fenites. Contact types develop close to the source of the metasomatic fluids and are inevitably the product of multiple phases of metasomatism. Aureole fenites cover larger areas than the contact variety and are characterised by more gradual mineralogical changes and, as a result, aureole types may be divided into mappable petrographic zones. Vein fenites superimpose localised irregularities onto the aureole fenite zones where the fenitising agents were concentrated by channelling into fractures and structural heterogeneities.

The zones marked on the map of the Spitskop Complex (Figure 2.1) refer to "aureole" fenites, although the more intensely metasomatised types could perhaps be regarded as "contact" fenites in Kresten's (1988) scheme.

6.2.1. Distribution and Field Relationships

Fenitisation of the Spitskop country rocks is noted to varying degrees at all the exposed contacts of the complex shown on the map (Figure 2.1). A full sequence of metasomatic changes is best preserved at the south eastern border of the complex where the lower Tshweneng River cuts across the contact. Fresh exposures are also found along the eastern tributary to the Tshweneng Spruit (Figure 6.1).

As the complex is approached along the lower Tshweneng River, the first manifestation of metasomatism is the development of a pronounced brick-red colouration in the typically orange-red Nebo granites (Plate 6.1b).

A low-angled jointing, which dips towards the alkaline rocks at 10-20°, is also noted in the granites. Closer to the contact with the Complex the dip of the joint

planes steepens to 40-50°, still oriented towards the centre of the intrusion. The joint pattern developed in the granites close to the margin of the Complex thus has an apparent conical form. Some joints are filled with fine-grained dykelets of ijolite or foyaite. Alongside the dykelets the granite is "bleached" due to the recrystallisation of the red feldspars, and quartz may be totally consumed (Plate 6.1a). Acicular pyroxenes grow to 20 mm and tend to be oriented normal to the margins of the dykelets. Altered zones 10-30 cm wide may form adjacent to fractures 5 mm or less in width, testifying to the passage of significant volumes of material through the fractures before they annealed. The original fractures were thus the site of significant channelling of volatiles and hence localised zones of higher metasomatic "grade" have developed along the fractures.

Exposures in the prominent, southward-pointing loop in the Tshweneng River contain dykes of the finer-grained Klipkloof-type granite within the more common Nebo granites. The Klipkloof-type forms sharply-bounded dykes characteristically 1 to 2 m in width, is aplitic, and is characterised by a lower content of mafic constituents than the Nebo-type. Both varieties of granite fenites are red in outcrop. Quartz is still present in each variety at this locality but in far lower abundance than in typical Bushveld granite. The next exposures, some 10 m further upstream, are of white fenites free of quartz in which both fine (ex Klipkloof) and coarse (ex Nebo) textural types are recognisable.

Quartz-free, white feldspar-pyroxene fenites are fresher and more massive in outcrop than their red, quartz-bearing equivalents (Plate 6.1c). Dykelets and veins of micro-ijolite are ubiquitous. Veins are frequently compositionally banded ("streaky") parallel to their length.

Through all the stages of metasomatism to this point, the fenites, while having recrystallised and lost quartz, still preserve the textural contrast between the Nebo and Klipkloof granite types from which they were derived. The fenites remained competent: brittle fracturing is common and little plastic deformation is detectable.

Passing upstream, the fenites become more pyroxene-rich and the felsic constituents develop a characteristic flesh colour. Growths of new pyroxene form as rosettes of coarsely-crystalline clusters of acicular to bladed crystals resulting in a coarse, "stellate" textured rock (Plate 6.1d). This variety of fenite does not form large, continuous exposures but is found as blocky zones and screens within an abundant meshwork of ijolite sheets. These ijolite sheets were emplaced in several stages, the earliest intrusions often have very diffuse contacts with the fenite

material. "Breccia" zones are noted where the intimate mixture of fenite and ijolite had evidently become plastic (Plate 6.1e): diffuse-bordered fragments of both fine- (ex "Klipkloof") and coarse- (ex "Nebo") grained fenite occur randomly distributed in a matrix of ijolite in which fragments and streaks of feldspar are identifiable. In places it appears that the fenite has rheomorphically injected into the ijolite. A similar zone of jumbled, "rheomorphic breccia" is also noted along the tributary, some 300 m upstream from the confluence (see Figure 6.1), in which fine-grained ijolite, coarse- and fine-grained fenite are set in a streaky matrix of mixed remobilised fenite and ijolite.

Upstream along the Tshweneng River, the proportion of "stellate" fenite decreases in the fenite/ijolite mix and the granitic fenites pass into outcrops of magnetite ijolite, containing sporadic blocks of solid magnetite, intimately mixed with sheets of fine, dark, intrusive ijolite. As will be discussed below, much of the magnetite-bearing ijolitic material is the extensively fenitised end product from xenolithic upper zone Rustenburg Layered Suite material.

6.2.2. Petrography

The coarser granites are typical hornblende-bearing Nebo-type (Kleeman and Twist, 1989), with average grain size of 5 to 7 mm, and composed of anhedral quartz, perthitic alkali feldspar, interstitial pleochroic olive-green hornblende and minor brown biotite. Zircon is an abundant accessory. A slight bluish pleochroism at the margins of some amphibole grains indicates the incipient development of soda-amphibole (?riebeckite, arfvedsonite?), implying that even the apparently fresh and un-metasomatised samples may have been affected by alkaline fluids. Klipkloof-type granites are finer-grained (typically <0.5mm), more even-textured and characteristically contain lower proportions of mafic minerals than the Nebo-type.

Initial signs of fenitisation are the development of strongly pleochroic, deep blue to grey, riebeckitic edges to the hornblende, usually along the contact of this mineral with quartz. Quartz is the first mineral to react: extremely delicate fibres of soda-pyroxene develop which grow from the grain margins into the body of the quartz grain (Plate 6.1f). A zone of more massive pyroxene develops behind the advancing metasomatic front. Tufts of acicular aegirine are also sometimes seen wholly enclosed within a quartz grain. Increased concentration of fluid inclusions occurs in quartz grains where replacement is in progress. Once a quartz grain is totally rimmed by pyroxene, the replacement appears to progress in a more patchy fashion - pyroxene rods and "droplets" form inside the quartz, eventually merging to

a single, polygranular aggregate of pleochroic, green to khaki-coloured, aegirine-rich clinopyroxene in which scattered fragments of quartz may persist (Plate 6.1g).

Stringers of green pyroxene grains, generally euhedral, are commonly noted cutting across fenite samples, apparently marking the site of annealed fluid channel-ways. These stringers are frequently discontinuous. Rarely, and only where the veinlet trace transects quartz grains, perfectly euhedral acicular and prismatic clinopyroxene are found in a matrix of carbonate (Plate 6.1h). An EDAX microprobe examination revealed that the carbonate is calcite and no Na or Mg was detected. Both the good crystal shape and the total absence of any zoning in the pyroxene grains suggest that these zones represent sites of entrapment of the metasomatising fluid. The preservation of the carbonate host in quartz and not feldspar grains is clearly not the result of different reactivities of the host - it has already been noted that quartz was the 'first' phase to react. It seems most likely that the carbonate fluid was able to filter away along the feldspar cleavage but was trapped within the less permeable quartz structure.

The amphibole and biotite are progressively altered to granular aggregates of aegirine-augite and an ore mineral. Feldspars are not noticeably affected although some signs of stress may be seen in the form of recrystallisation trails or the dislocation of twin lamellae. Once all the quartz, hornblende and biotite have been consumed, the fenite comprises a syenitic rock composed of a patchwork mosaic of soda pyroxene and anhedral, perthitic alkali feldspar. Zircon and sphene are minor accessory phases. The feldspars have highly irregular, serrated and sutured margins and often enclose patches of albite and scattered trails of small pyroxene grains. These pyroxene trails appear to represent remnants of original fractures. In some samples a crude banding of components may develop.

Further transformation of the fenites proceeds through:

- an increase in abundance and coarsening of the pyroxene with a tendency to aggregate into grain clusters and rosettes (Plate 6.2a);
- progressive alteration of the feldspar: generally turbid perthite is replaced by aggregates of clear albite and nepheline. These constituents are themselves subsequently replaced by a fibrous white mica (paragonite?) and cancrinite, respectively.
- increase in the abundance of sphene and disappearance of zircon; marked increase in abundance of apatite, frequently intimately intergrown with perthite relics.

The fenitisation process in the granites can thus be divided into two stages: Stage One representing the progressive consumption of quartz and the transformation of the hydrous mafic minerals to produce a feldspar-pyroxene fenite; and Stage Two during which the feldspar is albitised and nephelinitised. Three mineralogical facies may thus be defined: a low grade quartz-fenite facies, an intermediate feldspar-pyroxene facies, and a high grade nepheline facies.

From the mineralogical changes noted in the granite fenites, particularly the replacement of the hydrous phases biotite and hornblende by anhydrous pyroxene, it may be deduced that the fenitising fluid had low a_{H_2O}. The observation of pyroxene-calcite veinlets in the quartz fenites suggests that fluid was likely to have been carbonatitic.

Plate 6.1

6.1a: Micro-ijolite veinlets cutting red quartz fenites derived from Nebo-type granites. Note the light coloured margins to the veinlets. Hammer handle is 750mm long. Outcrops along lower Tshweneng River.

6.1b: Detail of red, quartz fenite derived from Nebo-type granite. Rough surface of outcrop is due to "ochrish cavities" (see text). Pen is 130mm in length. Detail of fenites at same locality as 6.1a.

6.1c: White, feldspar fenite derived from Nebo-type granite. Note fine pyroxene stringers criss-□crossing the fenite and fine ijolite dykelet at right edge of photograph. Pen is 130mm in length. Lower Tshweneng River.

6.1d: "Stellate", nepheline-bearing fenite with dykes of micro-ijolite. Coin is mm in diameter. Lower Tshweneng River.

6.1e: Melange of nepheline fenites derived from both Klipkloof (light coloured block in centre) and Nebo protoliths in matrix of ijolite ("rheomorphic breccia"). Note diffuse borders between blocks and matrix. Blocks on scale bar are 10 mm. Lower Tshweneng River.

6.1f: Photomicrograph of first stages of fenitisation of Nebo granite showing delicate needles of soda pyroxene growing into quartz. Note the strip of more coarsely crystalline pyroxene along the base of the needles. (Sample S118: Long dimension of photograph is 1 mm.)

6.1g: More advanced replacement of quartz by clinopyroxene than Plate 6.1f. "Veins" contain aggregates of acicular soda pyroxene and relic patches of quartz. "Speckled" appearance of quartz grains is due to increased abundance of fluid inclusions. (Long dimension of photograph is 4 mm.)

6.1h: Pyroxene - calcite veinlet in quartz grain in quartz fenite. Note the euhedral shape and absence of zoning in pyroxenes. (Sample S118. Crossed polars; long dimension of photograph is 1 mm).

PLATE 6.1


(a)


(b)

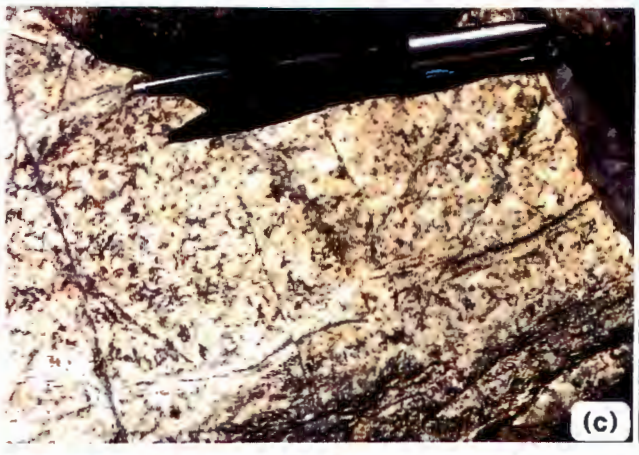
(c)


(d)

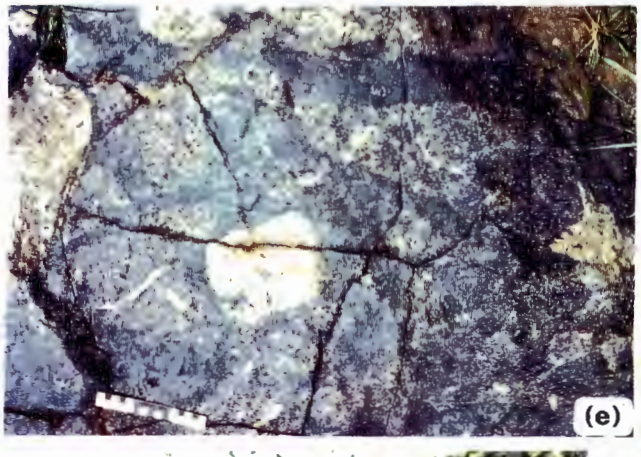
(e)


(f)

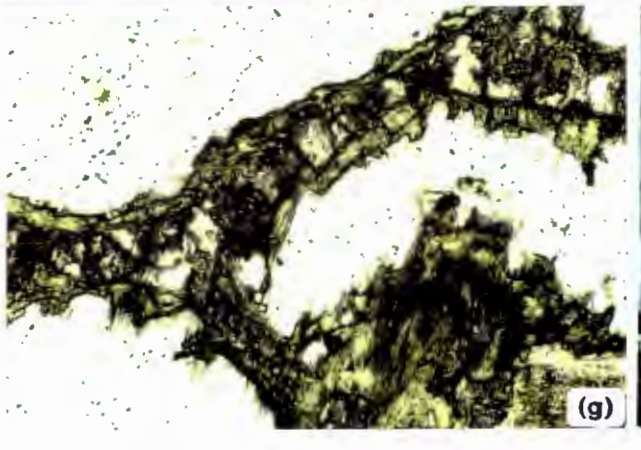
(g)

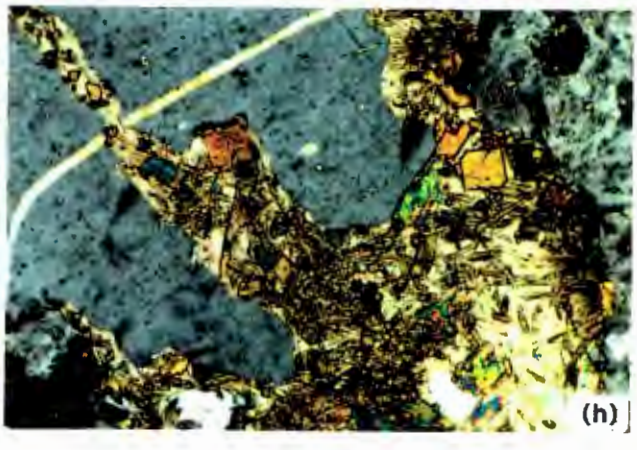
(h)

6.2.3. Geochemistry

Chemical analyses of the granitic fenites are listed in Table B.18.

Strauss and Truter (1950) presented chemical analyses of samples representing the various stages of fenitisation of the granitic country rocks as then recognised (feldspar, amphibole and pyroxene "umptekites"). Harker diagrams were then used to deduce the chemical changes: essentially a progressive decrease in SiO_2 coupled to increasing Na_2O and Al_2O_3, and irregularly increasing Fe_2O_3 with constant total Fe. It was noted that P_2O_5 and TiO_2 were more abundant in the "white fenites". These authors claimed, however, a change in trend in the pyroxene-fenite facies: *decreasing* Na and Al coupled to a sharp increase in Fe^{3+}, Fe^{total} and Ca.

McKie (1966) reviewed the chemical changes during fenitisation at a number of different carbonatitic complexes, including Spitskop, and discussed the potential distortions that result in even qualitative assessments of fenitisation using variation diagrams of oxides in weight percent without first standardising these to equivalent mass units. Following Barth (1952), McKie (1966) proposed the use of cation proportions calculated relative to a "standard cell" of 100 oxygens (or total anions) in fenitisation studies. McKie demonstrated that, when expressed in this form, Strauss and Truters' (1950) analyses show progressive increases in Al, Na, Ca and Fe with decreasing Si i.e. with progressive fenitisation.

In Table B.18, the major elements have been re-cast into the "atoms per 100 oxygen standard cell" form after Barth (1952) and McKie (1966) (for convenience these values are referred to as "standardised" concentrations in the discussion below). In this table the "M-Factor" is calculated after Watson and Harrison (1983) and the variables "q', ne' and ks'" are the values of the projection into the ternary normative quartz-nepheline-kalsilite diagram. Specific gravities (S.G., as g/ml) were determined for some samples.

6.2.3.1. Major elements

The fenite data are projected into the q-ne-ks ternary diagram in Figure 6.2 and the changes in standardised major element concentrations relative to Si are shown in a sequence of plots in Figure 6.3 (a)-(h).

Figure 6.2:Projection of the normative compositions of the granitic fenites onto the q-ne-ks ternary.

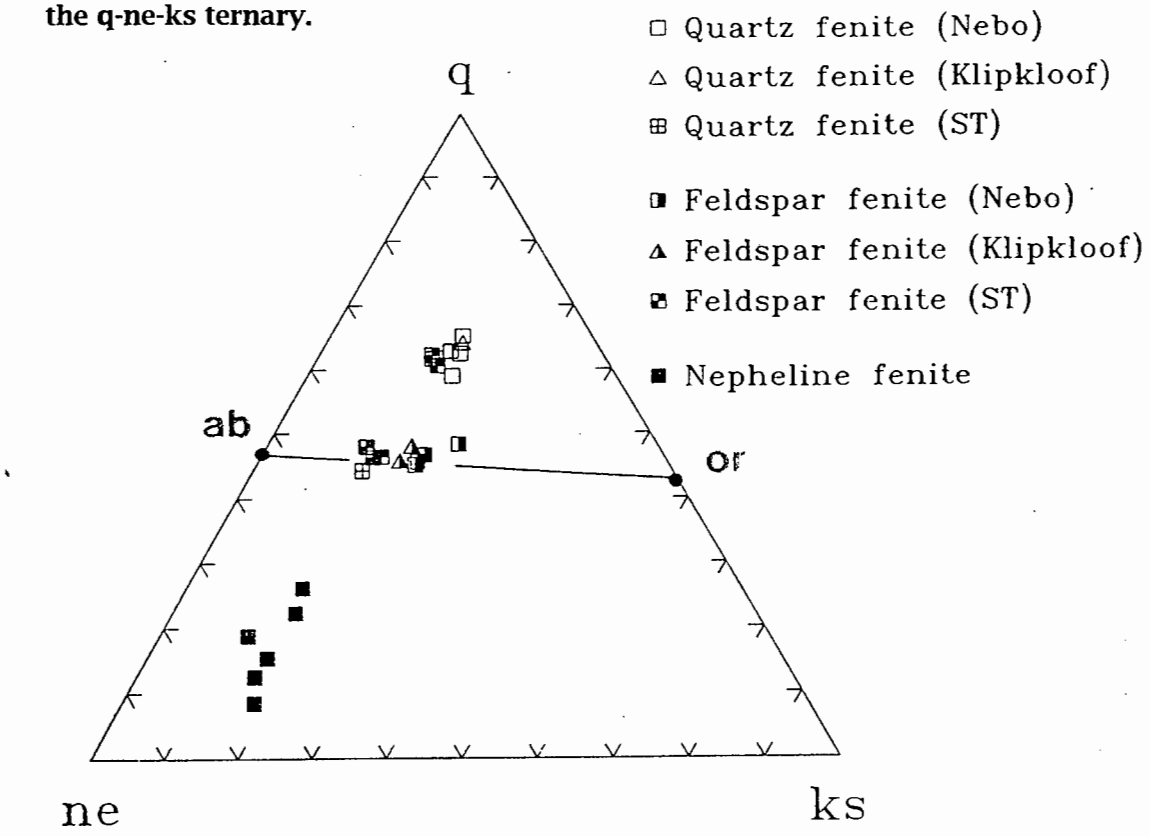

It is immediately apparent that Si decreases progressively, while standardised Al, total Fe, Na and Ca all increase progressively with increasing degree of metasomatism while Mg and Ti increase sharply in the nepheline fenites. All plots show a marked discontinuity at 31-34 %Si, and Al and Fe show wide variations in the feldspar-facies fenites through a narrow Si range at about 35% Si. The variation of K is notably erratic in the fenites with more than 35% Si, whereas P shows very little consistent variation at all.

Figure 6.3: Plots of standardised Si against other major elements for the granitic fenites. All elements are calculated as cations per standard cell of 100 oxygens. See text for explanation. Symbols are the same as those used in Figure 6.2.

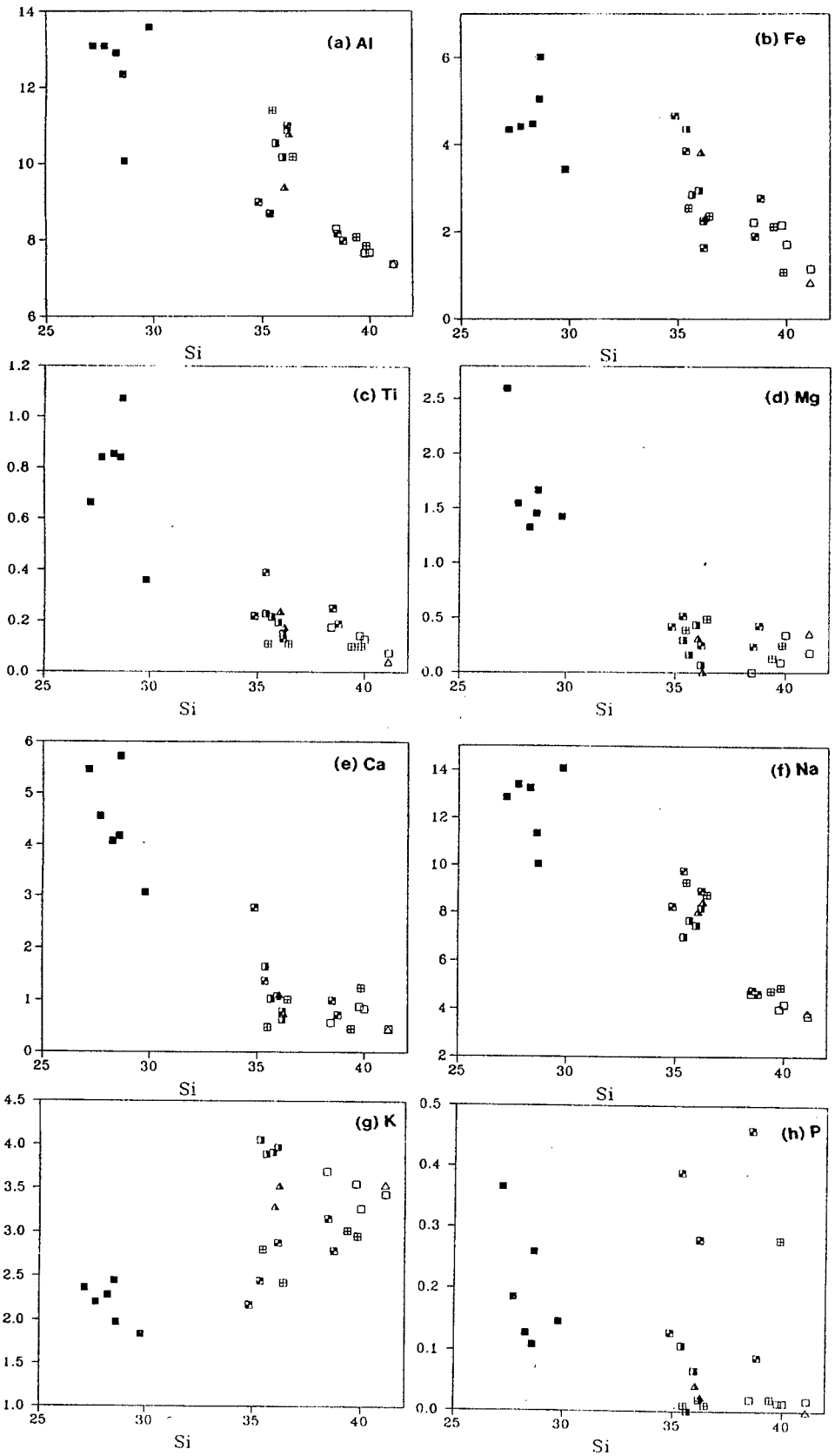

Figure 6.4: Plots of standardised Si against selected trace elements for the granitic fenites. Symbols are the same as those used in Figure 6.2

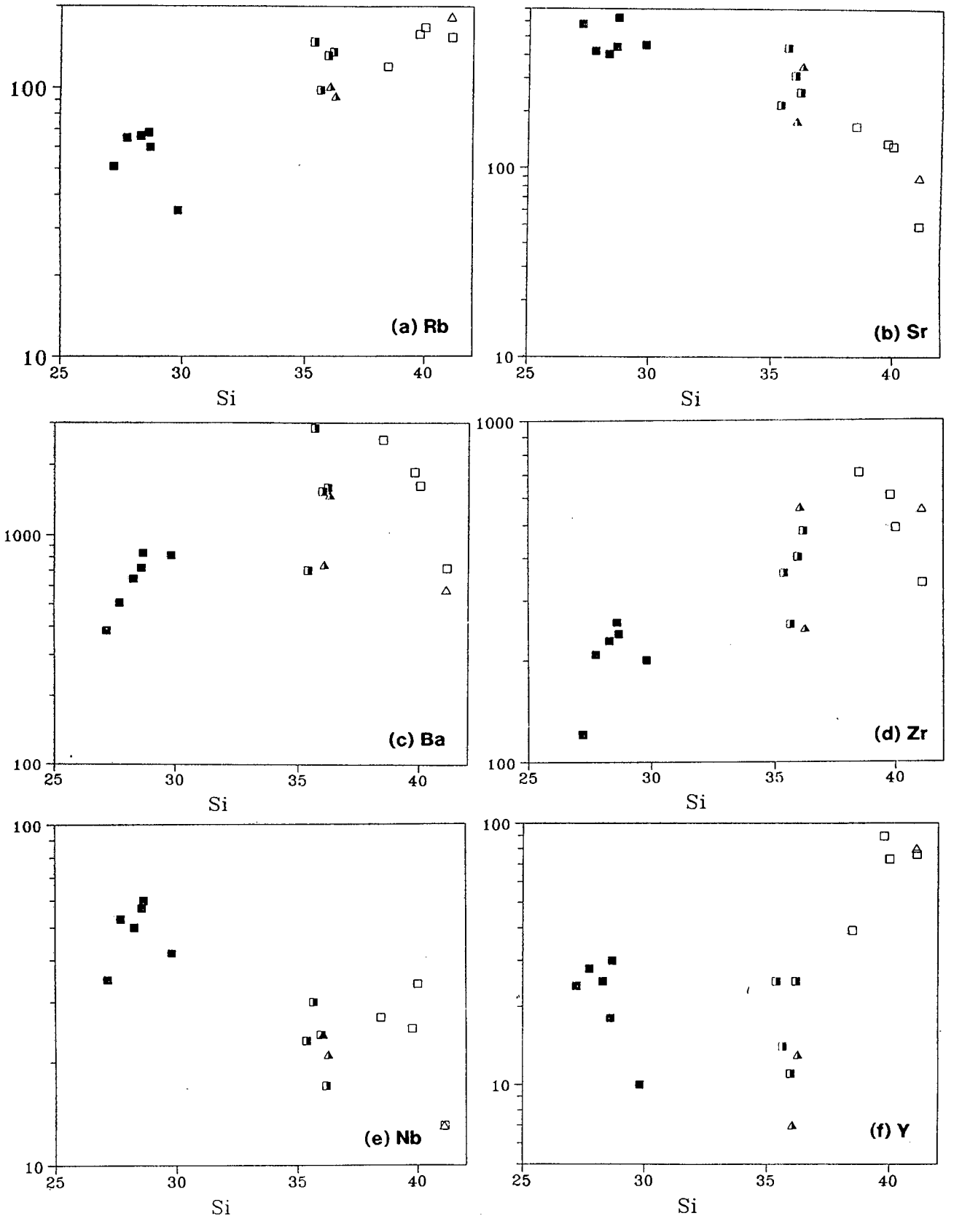

Figure 6.5: Plots of standardised Si against selected element ratios for the granitic fenites.

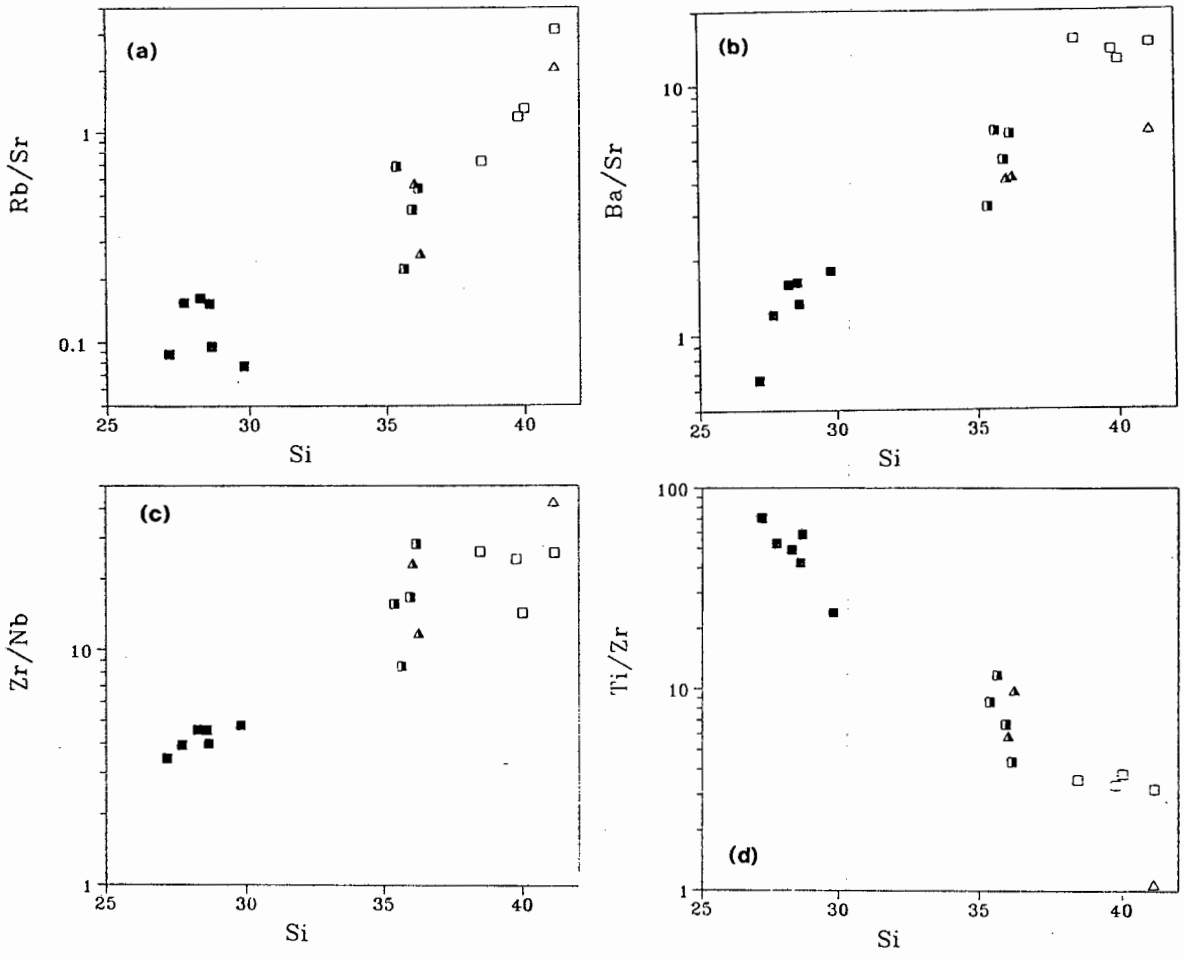

Symbols are the same as those used in Figure 6.2

6.2.3.2. Trace elements

The variation of selected trace elements against standardised Si is depicted in Figure 6.3 (a) to (f). Fenitisation has given rise to gains in Sr and Nb and significant decreases in Rb and Zr. Ba shows no definite variation trend through the quartz- and feldspar- facies fenites, but decreases systematically in the nepheline-facies fenites. Y appears to decrease from the quartz- to the feldspar- facies fenites, yet increases again in the nepheline-facies fenites. The ratios Rb/Sr, Ba/Sr and Zr/Nb all decrease, and Ti/Zr increases progressively with increasing degree of fenitisation (Figure 6.5 a to d). Decreases in Ba and Ba/Sr in the higher grade fenites correlate with the sodification (albitisation) of the granitic microcline feldspar and its replacement by nepheline in the nepheline facies granitic fenites.

Figure 6.5: Plots of chondrite-normalised rare earth element data (a) for selected granitic fenites and (b) for unmetasomatised Nebo granites from Potgietersrus.

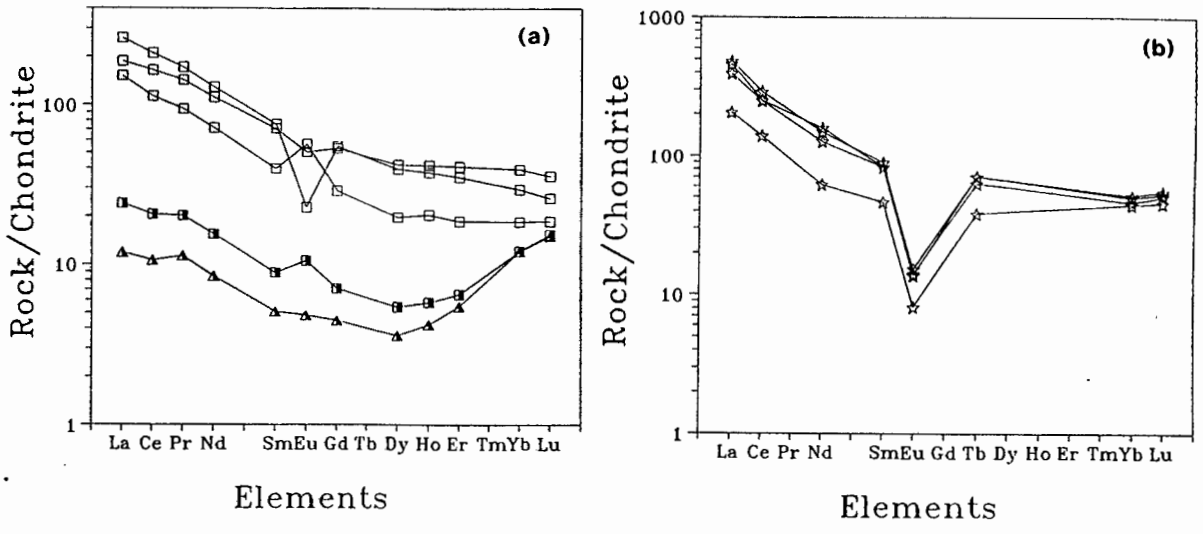

Symbols are the same as those used in Figure 6.2

In Figure 6.6a, the chondrite-normalised REE patterns show that the intermediate grade, feldspar-facies fenites have lost significant quantities of light to middle REE (essentially La-Dy), relative to the quartz-facies samples and the unmetasomatised Nebo granites depicted in Figure 6.6b. The loss of LREE from the granites is unusual as studies of fenitisation elsewhere generally report increases in the total REE, and LREE in particular, (Martin *et al.*, 1978; Morogan, 1989).

Increases in both $(Na_2O+K_2O)/Al_2O_3$ (Figure 6.7) and "M" (Figure 6.8) imply that the fenitising fluids were highly peralkaline and would thus have a high capacity to dissolve zircon. Extrapolating the Watson and Harrison (1983) data at 750°C to higher "M" factors suggests zircon saturation at Zr levels of 174, 406 and 2200ppm for liquids with "M" factors of 2, 3 and 5 respectively (see Figure 6.9). This would suggest that zircon could be dissolved and removed by the fenitising fluids and may explain the decreased Zr levels in the nepheline-facies fenites. Given the high HREE budget in zircon (e.g. compilation in Henderson, 1982; Table 5.2c), dissolution and removal of zircon from the nepheline-facies fenites would lead to depletions in Yb and Lu and would predict that the high grade fenites (not analysed) could show increased normalised LREE/HREE ratios at lower overall REE concentration levels.

Figure 6.7: Plot of standardised Si against peralkalinity index for the granitic fenites.

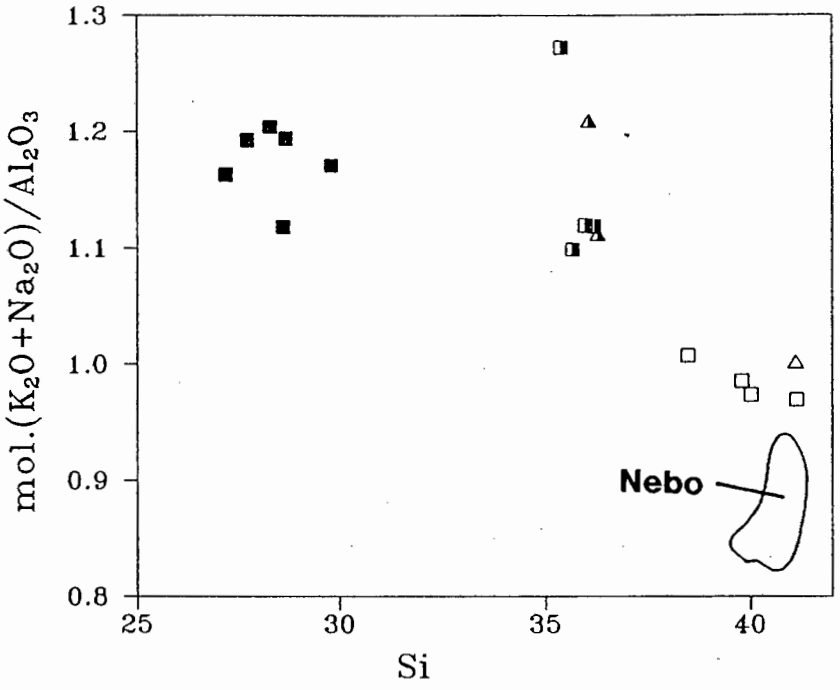

Symbols are the same as those used in Figure 6.2. Field marked is for unmetasomatised Nebo granites (Kleeman, 1985; and unpublished data).

Experiments on REE partitioning between coexisting granitic melts and chloride-rich vapour (Flynn and Burnham, 1978) showed a slight (2-3x) preference of Ce for the vapour relative to Yb. These experiments also showed that CO_2-rich vapours would partition very little REE. A mixed CO_2:Cl fenitising fluid would be consistent with the common occurrence of cancrinite in the nepheline facies fenites.

Figure 6.8: Plot of standardised Si against M-Factor (Watson and Harrison, 1983) for the granitic fenites.

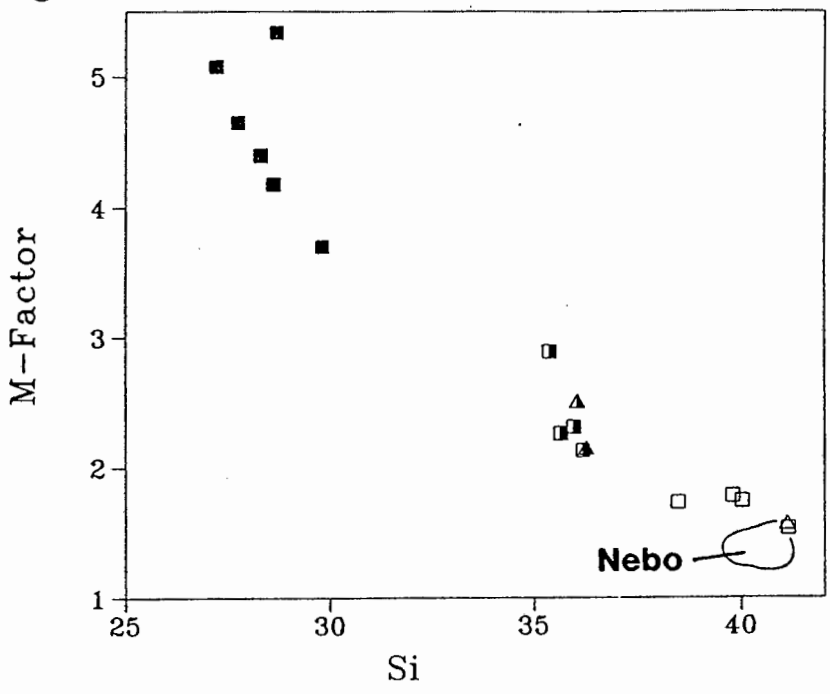

Symbols are the same as those used in 6.2. Field marked is for unmetasomatised Nebo granites (Kleeman, 1985; and unpublished data).

Figure 6.9: Plot of M-Factor (Watson and Harrison, 1983) against Zr for the granitic fenites.

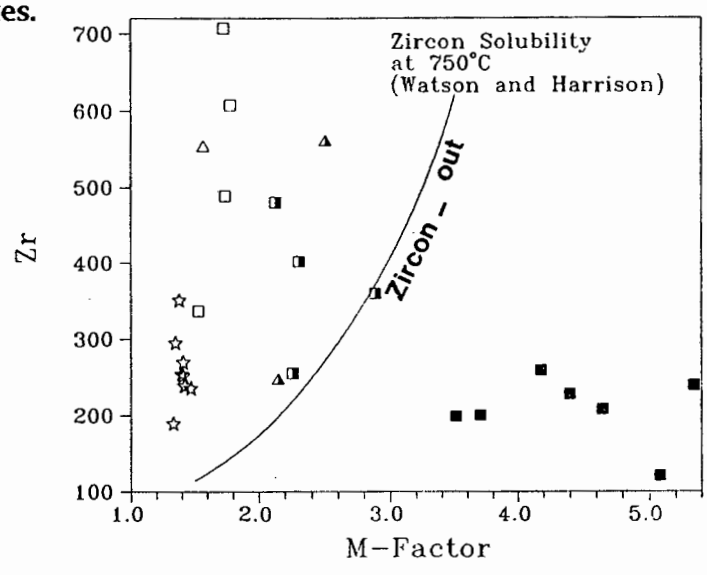

Symbols are the same as those used in 6.2. Open stars are unmetasomatised Nebo granites (Kleeman, 1985; and unpublished data). The curve is the limit of zircon solubility in silicate liquids with different M-Factors extrapolated to higher "M" from the Watson and Harrison 750°C data.

6.2.3.3. A review of "semi-Quantitative" treatments of chemical changes during fenitisation

Appleyard and Woolley (1979) criticized the universal use of the Barth-McKie "standard cell" and demonstrated that this technique makes the implicit assumption that oxygen remained constant during metasomatism. They recommended the use of quantitative mass transfer equations as formulated by Gresens (1967).

Gresens (1967) showed that mass transfer and composition are related by:

$$\delta_{x_i} = W_T\left[F_v c_{i_F}(g_P / g_F) - c_{i_P}\right]$$

where subscripts "P" and "F" denote the "parent" (or "protolith") and "fenite" components, respectively;

δ_{x_i} is the mass loss or gain of component "i", in grams;

F_V is the ratio between the volumes of fenite and parent volumes of the rock mass i.e. $F_V = V_F/V_P$.

g is specific gravity (in g/ml);

c_{iP}, c_{iF} are the weight fractions of "i" in the parent and fenitised samples;

W_T is the mass of the total system. This is most conveniently set to 100g, hence transforming the δ_{x_i} term to grams per 100g, or weight percent.

Gresens' equation has been discussed and modified by Babcock (1973), Grant (1986) and Kresten (1988); and applied in fenitisation studies by, amongst others, Appleyard (1980), Rubie (1982), Kresten (1988) and Morogan (1989). Appleyard and Woolley (1979) argued for the wider application of Gresens' equation in fenitisation studies since it "..forces the evaluation of geological and geochemical factors involved in determining possible geochemical changes".

To analyse metasomatic variations quantitatively requires information on the starting composition(s) of the protolith(s) plus knowledge of the change in volume during fenitisation ($F_V = V_F/V_P$. in the equation). During the early stages of fenitisation parent rock textures are usually preserved which would suggest little change in volume. Constant volume has also been implied in the absence of

extensive brecciation. Once fenitisation is more advanced, however, constant volume assumptions are more difficult to substantiate.

It is clear from the Gresens equation that mass transfers are linearly related to the volume change parameter, F_V. Babcock (1973), Appleyard and Woolley (1979), Morogan and Woolley (1988) and Kresten (1988) made use of "Composition - Volume" plots (Gresens, 1967; Fig. 3) in which F_V factors *versus* mass change, δ_{x_i}, vectors are plotted for each element in a fenitised sample. Changes may then be expressed as the F_V quantity corresponding to no compositional change. If a number of components were immobile during metasomatism, this will be noted as δ_{x_i}-F_V lines intersecting the δ_{x_i}=0 line at nearly equivalent F_V. Appleyard and Woolley (1979) expressed this using a histogram representation of Log(F_V) factors required for zero mass transfer of each element - clustering is then reflected in a unimodal frequency distribution. These authors do warn, however, that well defined clustering may be fortuitous and need not necessarily imply immobility!

Alternatively, if one element can be shown, or is assumed, to have remained constant during metasomatism, F_V may be calculated for this element, and used to solve for δ_{x_i} for all other elements. In discussing the fenitisation of granitic parent rocks at Kisingiri, Rubie (1982) assumed that Al_2O_3 was re-distributed rather than being introduced, and hence remained essentially constant. The validity of this assumption was questioned by Kresten (1988) who pointed out that making an assumption of constant composition of an element also implies that this element was homogeneously distributed in the parent rock.

Kresten (1988) proposed an alternative approach to solving the mass balance equation by making the assumption that the *total mass* change during fenitisation is a minimum. The equation is then solved for F_V by substituting the sum of the components SiO_2, Al_2O_3, $Fe_2O_3^{total}$, MgO, CaO, Na_2O, K_2O and P_2O_5 in the assumed starting composition and fenitised sample for the quantities c_{iP} and c_{iF} respectively. This estimated F_V is then used to solve the mass balance equation for all elements of interest.

In a useful contribution to the understanding of alteration processes, Grant (1986) demonstrated that by transforming the Gresens equation in terms of mass rather than volume, and using concentration units it is possible to express the relationship between components in parent and fenitised rocks as:

$$C_{iF} = M_P/M_F\,(C_{iP} + \delta_{Ci});$$

where:

- subscripts "P" and "F" denote parent and fenite, respectively;
- C indicates concentration;
- M indicates mass and
- δ_{Ci} is the change in concentration of component "i" between fenite and parent rock.

It should be noted that the value of "M_P" essentially defines the concentration unit for the "C" parameters: for M_P = 100g, C=wt%; $M_P = 10^6$g, C=ppm; M_P = SG, C=g/ml; etc.

Figure 6.10: Plot of element concentrations in granite fenite samples (a) S125 and (b) S122 relative to protolith P2 (see text).

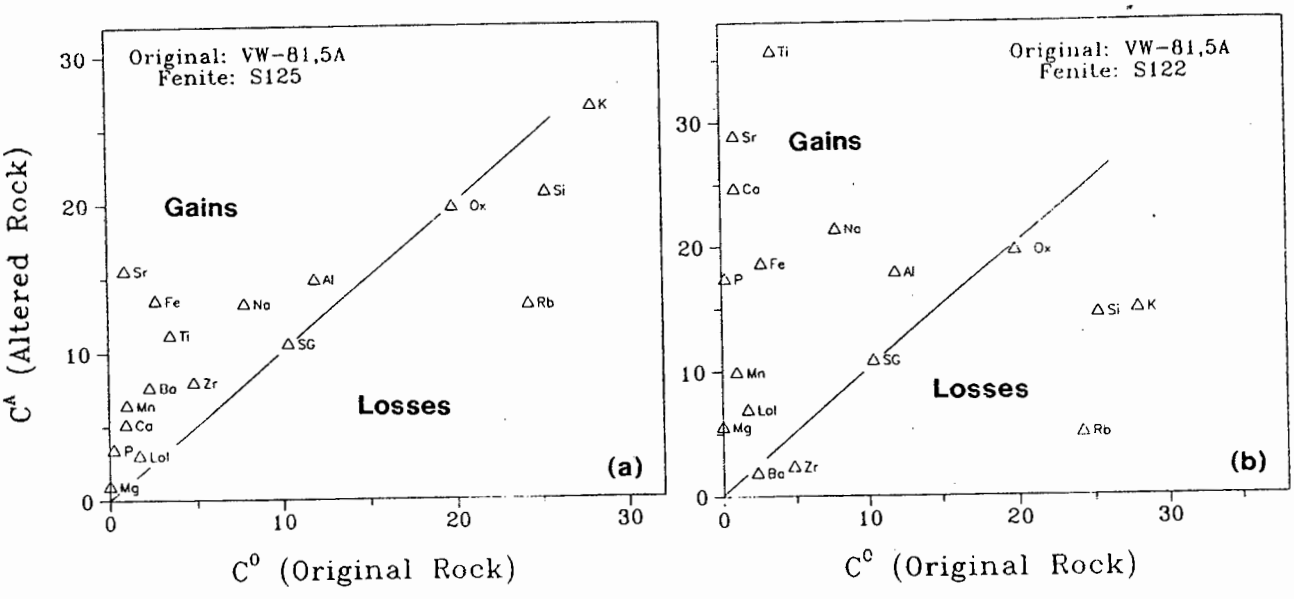

An "isocon line" (Grant, 1986) has been drawn to illustrate the assumption of constant total oxide sum (Kresten, 1988; see text). Certain elements have been scaled. Scaling factors are:

Si/3; Ti x25; Al x1; Fe x2; Mn x50; Mg x2; Ca x3; Na x2; K x5; P x25; LoI x10; ΣOx /5; SG x4; Rb /10; Sr /20; Ba /200; Zr /50

In contrast to the original Gresens (1967) formulation, where the volume change (F_V) must be determined, Grant's equation requires an estimate of the change in mass of the system (F_m=M_P/M_F) during alteration. The significant advantage of Grant's formulation is that it enables most features of metasomatic mass transfer to be depicted on a simple binary plot of C_{iP} vs C_{iF}. By using appropriate (and identical) scaling factors for the parent - fenite pair, major and trace element components of widely differing concentration ranges may be compared on the same plot.

Assumptions made in order to solve the mass balance equations are also more readily evaluated using this approach. Components which were immobile during fenitisation would have δ_{Ci}=0 and hence $C_{iF} = (M_P/M_F)C_{ip}$; consequently groups of immobile elements will define linear trends through the origin on the C_{iP}-C_{iF} diagram. Grant (1986) proposed the term "isocon" to describe these lines. Relative gains and losses of mobile components will be reflected as displacements of data points from the isocon: losses below, gains above. Components which have suffered the same ë□C& plot on linear arrays parallel to the isocon (where no scaling factors are used). Assuming that, for example, Al_2O_3 was immobile during alteration yields an isocon equation of $C_{iF} = (C_{AlF}/C_{AlP})\, C_{iP}$, whereas the assumption of no volume change is reflected by $C_{iF} = (SG_F/SG_P)\, C_{iP}$.

6.2.3.4. An evaluation of mass changes in the Spitskop granitic fenites

A selection of the Spitskop fenites were analysed using each of the above approaches. In all fenitisation studies, the choice of a realistic starting composition is obviously critical. In this regard the Spitskop granitic fenites are more amenable to quantitative treatment than most of the classic fenite occurr□ences in that (i) the country rocks are granites of relatively uniform composition; and (ii) the primary chemical variations in the granites are reasonably well constrained (Kleeman and Twist, 1989). Two suitable granite starting compositions - VW4-71,7A (=P1) and VW4-71,5A (=P2) - were selected from Kleeman's (1985) data by comparing the fractionation trends in the Kleeman data set with the variations in the least modified fenites (see Table B.19). Specific gravities had unfortunately not been determined for the Kleeman samples and so SG's had to be estimated indirectly. Hall's (1938) compilation includes chemical analyses with specific gravity determinations on 6 Bushveld granite samples. These analyses show that the density is strongly correlated with iron content and so the regression line was used to estimate the SG's of P1 and P2 from their FeO contents.

Table 6.1: Volume change (F_V) factors for selected fenites estimated using the approach of Kresten (1988).

	Starting Composition P1	P2	
S104	0.993	0.998	**Quartz fenites**
S117	1.011	1.015	**(low grade)**
S118	1.011	1.015	
S120	0.992	0.996	
S121	1.008	1.012	
Mean	1.003	1.007	
±	0.010	0.009	
S116	1.020	1.024	**Feldspar fenites**
S125	1.020	1.025	**(medium grade)**
Mean	1.020	1.025	
±	-	0.001	
S122	1.057	1.062	**Nepheline fenites**
S123	1.117	1.122	**(high grade)**
S129	1.054	1.059	
Mean	1.076	1.081	
±	0.036	0.036	

In Table 6.1 Kresten's (1988) assumption of constant oxide total was used to estimate the apparent volume change for 10 samples of fenite. Average F_V values are identical whether derived from either P1 or P2 starting compositions and indicate essentially no volume change at low grades (quartz fenite) to a volume increase of +8% at high grade (nepheline facies). These average volume factors were then used in the mass balance equation to quantify the concentration changes for a range of fenite samples (Table 6.2).

In Figures 6.10(a) and (b) the changes in major and selected trace elements between starting composition "P2" and fenite samples S125 and S122 are compared using the "Isocon" approach of Grant (1986). On each of these diagrams density values and total oxide sums are also shown: lines drawn from the origin through these points are graphical representations of the assumptions of zero volume change and zero change in totals (*a la* Kresten), respectively. In neither diagram are potential chemical "isocons" obvious -the linear arrangement of MnO-CaO-TiO_2-Fe_2O_3 in Figure 6.10(a) would imply massive volume increases and is considered fortuitous. Both plots illustrate that making the assumption of constant oxide total

Table 6.2: Quantitative mass balance calculations for selected granite fenites.

	Si	*Ti*	*Al*	*Fe*	*Mg*	*Ca*	*Na*	*K*	*P*	*ΣGain*
					(i) Quartz Fenites					
S120	-0.01	-0.03	-0.34	+0.57	+0.45	+0.46	-0.23	-0.47	-0.01	1.47
S121	-1.45	+0.05	-0.59	+1.27	+0.22	+0.46	-0.44	-0.73	+0.03	2.02
S118	-4.39	+0.18	-0.28	+2.56	+0.41	+1.08	-0.03	-1.02	+0.02	4.25
S117	-5.27	+0.21	-0.38	+3.58	+0.11	+1.15	-0.23	-0.66	+0.02	5.06
S104	-5.69	+0.30	+0.92	+3.87	0.00	+0.66	+0.47	-0.32	+0.03	6.25
					(ii) Feldspar - pyroxene Fenites					
S125	-13.33	+0.32	+3.10	+5.31	+0.51	+1.44	+2.79	-0.26	+0.13	13.60
S116	-13.57	+0.42	+1.85	+7.29	+0.37	+1.48	+3.28	-1.14	+0.08	14.77
					(iii) Nepheline Fenites					
S129	-24.74	+0.69	+7.87	+6.32	+1.64	+4.60	+8.55	-3.12	+0.29	29.96
S123	-30.08	+1.66	+4.88	+9.28	+1.56	+5.92	+5.48	-2.52	+0.20	28.97
S122	-30.62	+1.34	+6.58	+8.11	+2.9	+8.17	+7.13	-2.51	+0.71	34.94

is effectively equivalent to an assumption of constant volume for the fenitisation process under discussion (consistent with the small volume changes calculated earlier using the assumption of constant oxide sum). The chemical changes during the transformation of granite to feldspar-fenite are a significant decrease in SiO_2, increases in CaO, TiO_2, Na_2O, Sr and Fe_2O_3 while Al_2O_3 is marginally enriched and K_2O and LOI essentially remain constant. Developing into the nepheline fenite stage entails significant losses of SiO_2, K_2O, and Rb; large gains of CaO, TiO_2, Na_2O, total Fe_2O_3 and Sr; and smaller increases in Al_2O_3.

Kresten (1988) suggested that the sum of all elements reflecting gains during fenitisation (ΣGain) could be usefully applied as a chemical "Fenitisation Index" (FI): a comparison of the petrographic and chemical variations in the Fen Complex metasomatites indicated the following grade subdivision:

- low grade FI < 6.5
- medium grade 12 > FI > 6.5
- high grade FI > 12.

Fenitisation appears to have been more intense at Spitskop since the petrographic facies correspond to: FI=1.5-6.2 in the quartz-bearing rocks; FI=13.6-14.8 in the quartz- and nepheline-free samples; and FI=29-35 for the nepheline fenites.

Figure 6.11: Plot of Rb/Sr against $^{87}Sr/^{86}Sr_{1341Ma}$ for granite fenites and unmetasomatised Nebo granites.

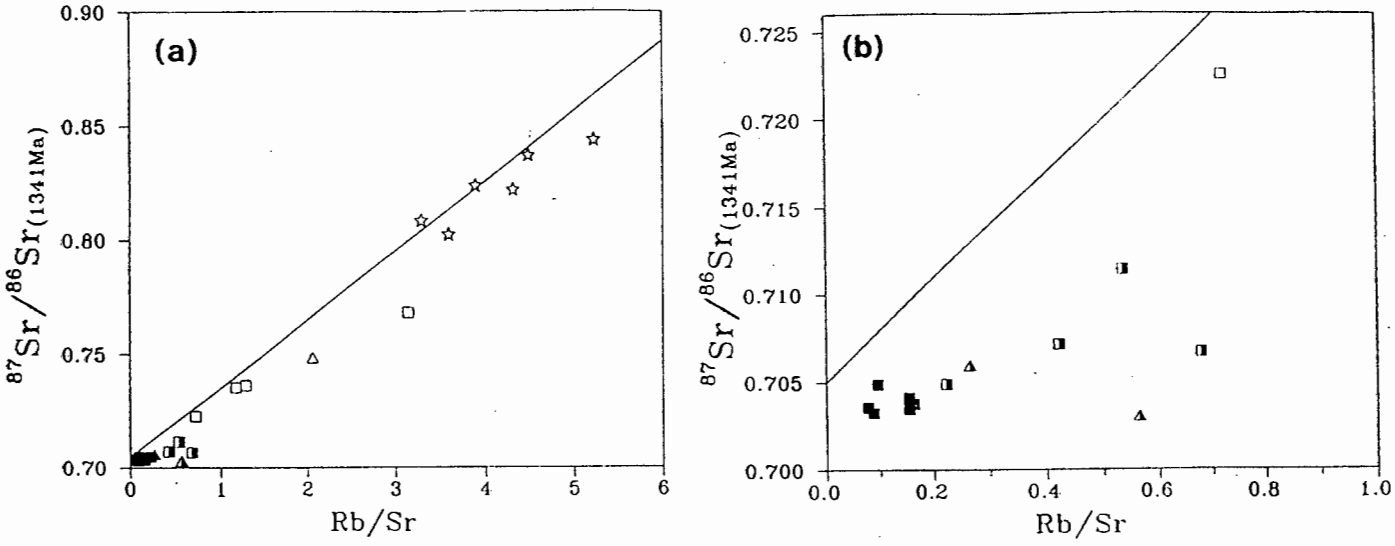

Symbols are the same as those used in Figure 6.2. (a) The Nebo granite data is shown in open stars and is the author's unpublished data. The solid line in the figure is the trace of Nebo granite compositions at 1341 Ma (systems which crystallised with a $^{87}Sr/^{86}Sr$ of 0.705 at 2050 Ma and remained closed). (b) Same plot at expanded scale.

The results of these "quantitative" models essentially confirm that the qualitative trends noted for the Spitskop granitic fenites on the standardised Si-element plots above are not artefacts of mass or volume changes during fenitisation and reflect true compositional changes.

6.2.3.5 Sr isotope systematics

The Lebowa Granite Suite components intruded soon after the emplacement of the mafic rocks of the Rustenburg Layered Suite (Walraven, 1988). In the ca. 700Ma interval between their emplacement and the intrusion of the Spitskop Complex, the extremely high Rb/Sr character of the Nebo granites would have generated large amounts of radiogenic ^{87}Sr. The average Nebo granite composition has 64.5ppm Sr and Rb/Sr of 3.12 (see Table B.19); assuming a $^{87}Sr/^{86}Sr_i$ of 0.705, this ratio would have increased to 0.800 at 1341 Ma. The uncertainty related to the assumption of initial ratio is of little consequence in view of the large Rb/Sr and rapid growth of radiogenic Sr. A large contrast thus existed between the magmas (and associated fluids) of the Spitskop Complex (generally <0.704; see Chapter 5) and the country rocks at the time of intrusion.

Figure 6.12: Plot of 100/Sr against $^{87}Sr/^{86}Sr_{1341Ma}$ for granite fenites.

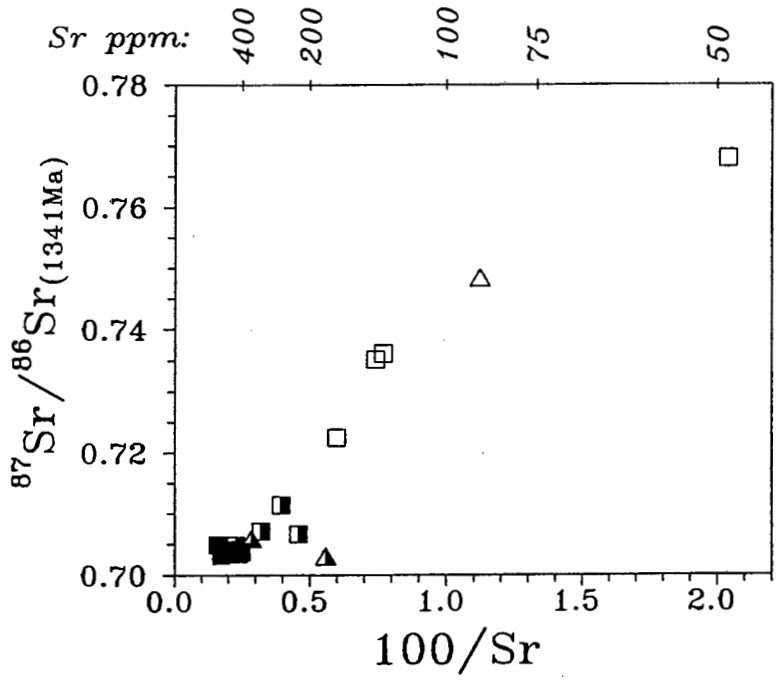

Symbols are the same as those used in Figure 6.2.

Progressive addition of Sr to the granites during fenitisation is suggested by the increase in Sr concentration with falling standardised Si (Figure 6.4). In addition, in the isocon diagram in Figure 6.10(b), Sr plots well above the iso-volume/iso-total "isocon" lines, and above elements such as Na and Fe: as previously discussed, this also indicates that Sr was added to the fenites during metasomatism. Addition of low $^{87}Sr/^{86}Sr$ Sr would progressively change the $^{87}Sr/^{86}Sr$ ratio in the fenites from an original value of ca. 0.80 towards that of the fenitising agent. Consequently, the $^{87}Sr/^{86}Sr$ in the fenitised granites should also provide a sensitive index of progressive fenitisation.

It is important to bear in mind, however, that a primary feature of the Nebo granites is a decrease in Sr content with increasing silica and hence a strong primary correlation exists between SiO_2 and Rb/Sr. As a result, calculating $^{87}Sr/^{86}Sr$ at 1341 Ma for unmetasomatised Nebo granites will generate a correlation between $^{87}Sr/^{86}Sr_{(1341Ma)}$ and both Si content and Rb/Sr which is unrelated to the metasomatic event. In Figures 6.11(a) and 6.11(b) the primary correlation between Rb/Sr and $^{87}Sr/^{86}Sr$ at 1341 Ma is shown as a solid line.

The change in isotopic composition with addition of Sr is demonstrated in Figure 6.12. Two component mixtures describe straight lines on a 1/Sr *versus*

$^{87}Sr/^{86}Sr$ diagram (e.g. Faure, 1986). The deviation from a straight line relationship could be interpreted as: (i) variations in the composition of protolith and/or metasomatising fluid; or (ii) that the metasomatism does not represent a simple binary mixing process.

Changes in $^{87}Sr/^{86}Sr_{(1341Ma)}$ may be utilised to place useful constraints on the amounts and composition of metasomatic agent required to produce the observed change in isotopic composition of the granitic fenites. Faure (1986, p244) provided a formulation to calculate the weight ratio of fluid (F) to rock (R) involved in isotopic exchange required to change the composition of a rock from ε_{Ri} to ε_{Rm}:

$$F/R = \frac{\varepsilon_{R(i)} - \varepsilon_{R(m)}}{\varepsilon_{R(m)} - \varepsilon_{F(i)}} . (Sr_R/Sr_F)$$

where Sr_R and Sr_F refer to the original Sr contents in the initial rock and fluid, respectively.

Replacement of biotite and hornblende by clinopyroxene with progressive fenitisation (see petrography section above) implies that the fenitising agent was not an aqueous fluid. The observation of a calcite-pyroxene veinlet in quartz-fenite S118 suggests that the fenitising agent may have been a carbonate-rich fluid or melt.

In Figure 6.13 the rate of change of $\varepsilon_{(Sr)}$ in an average Nebo granite (Sr=64.5 ppm; $\varepsilon_{(Sr)}$=+1378) is shown in relation to the quantities of a metasomatic agent required with $\varepsilon_{(Sr)}$ of zero and Sr contents of 10, 50, 100, 500, 1000 and 2500ppm. The lower values would be appropriate for aqueous fluids whereas the higher values would probably only be attained in carbonatite melts. Sr contents are not significantly different between calcio- and magnesio- carbonatite samples at Spitskop and mostly range from 1000 to 2600ppm. It is difficult to assess, however, what the Sr concentration would have been in carbonatitic fluids emanating from such a magma. In Table 6.3 fluid/rock ratios are estimated that would be necessary to generate the sequence of fenite samples S121-S125-S122 from protolith "P2" for different fluid compositions. It is clear that substantial quantities of fluid are required to generate the compositions represented in the nepheline facies fenites, prohibitively so for Sr_F concentrations of less than 500 ppm. Note that the tabulated values are weight ratios: since an aqueous or carbonate-rich fluid would certainly have been less dense than the granites, the volume ratios would necessarily have been somewhat higher.

Figure 6.13: Curves depicting change in $\varepsilon_{(Sr)}$ in fenites with different compositions of metasomatic fluid, and changing weight ratios of fluid to rock mass.

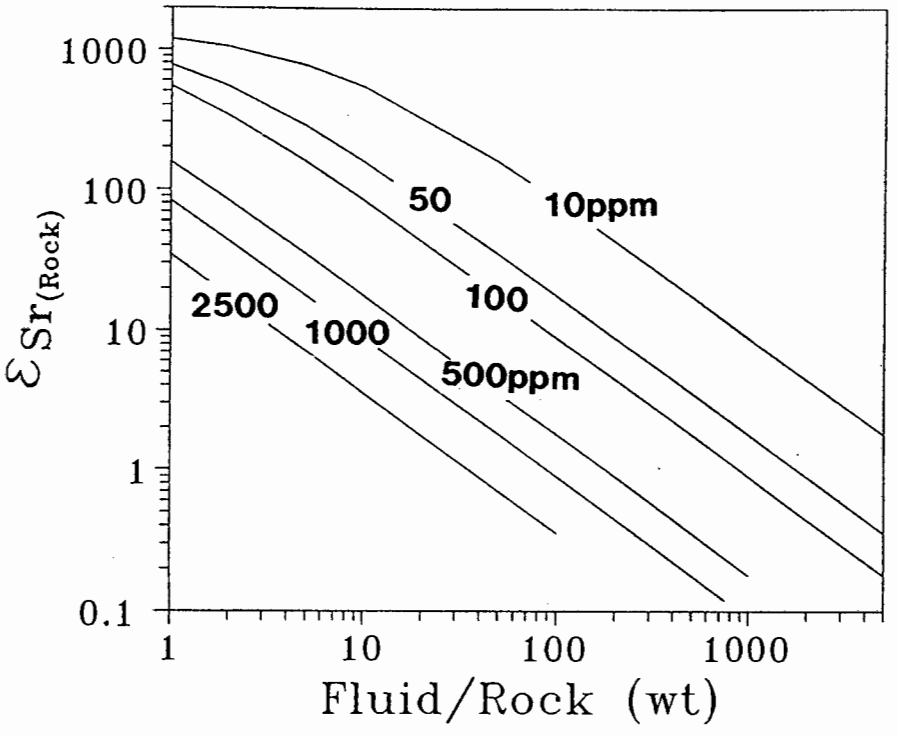

Mineralogical and isotopic constraints both suggest that the metasomatising agent is more likely to have been a carbonate-rich fluid or melt than an aqueous fluid.

Further discussion on the nature of the fenitising agent is offered in the concluding section of this chapter after data for the metasomatism of the Rustenburg Layered Suite xenolith have been presented.

Table 6.3: Fluid/Rock ratios required to generate selected granitic fenites, estimated from $\varepsilon_{(Sr)}$

Sr_R(ppm)=	64.5
ε(Sr)(fluid)=	0.0
ε(Sr)(protolith)=	+1378

	S121	S125	S122
ε(Sr)	+953	+61	+2.9
F/R=	28.8/Sr_F	1393/Sr_F	30584/Sr_F

Sr_F(ppm)	*Fluid/Rock (wt)*		
	S121	**S125**	**S122**
10	2.88	140.0	3058
50	0.6	0 28	610
500	0.06	2.8	61
1000	0.03	1.4	31
2000	0.012	0.56	12

6.3. Fenitised Rustenburg Layered Suite rocks.

These rocks have, perhaps, generated the most controversy in the (limited) literature on Spitskop (Strauss and Truter, 1950; Verwoerd, 1964, 1966, 1967; Nel, 1974). Included in this group are the olivine diorite, various varieties of theralite, as well as the melteigites and jacupirangites of Strauss and Truter. Verwoerd (1966) included a general discussion of these rocks in his communication on the fenitisation of "basic igneous rocks" from various Southern African complexes.

6.3.1. Distribution and Field Relationships

As can be seen on the map (Figure 2.1), these units occur as a well defined tabular block some 3.5 km in length along the north eastern margin of the complex; and as smaller, apparently isolated, patches along the Makpopeng Spruit.

The major exposure occupies much of the river valley from the uppermost Mare Spruit southwards to the significant eastward bend in the lower Tshweneng River. The true lateral extent of this "block" is difficult to ascertain precisely: observations along the tributaries to these rivers were taken in conjunction with air photograph interpretation to fix the outer boundaries marked on the map. Exposures are poor along the inner, south eastern, margin of this zone and this contact is less precisely defined.

An apparent "fenitisation gradient" exists along the length of the block: the degree of metasomatism being far less marked in the upper Mare Spruit exposures than those along the lower Tshweneng River.

Along the upper Mare Spruit and tributaries, lithological successions typical of the upper zone of the Rustenburg Layered Suite of the Bushveld Complex are found. Although deeply weathered, cycles of gabbro, anorthosite, magnetite-gabbro and seams of magnetitite occur invaded by veins and dykes of ijolite and foyaite. These rocks are certainly more extensive than shown on Strauss and Truter's (1950) map and were traced to the uppermost extent of exposure in the Mare Spruit and its western tributary. It is interesting to note that the cultivated soils underlying the ground between these drainage channels are of a dense, dark, clayey type identical to the "turf" characteristic of weathered Bushveld mafic lithologies, and atypical of the soils produced from components of the alkaline complex, or indeed of the surrounding granites.

Plate 6.2

6.2a: High grade, nepheline-bearing fenite showing rosette of acmitic clinopyroxene in perthitic feldspar (turbid) and nepheline (clear). Note micro-veinlet of ijolite at lower right of photomicrograph. (Sample S125. Long dimension of photograph is 1 mm).

6.2b: Block of fenitised "spotted" anorthosite within ijolites along tributary to upper Tshweneng River (cf sample S36). Length of pen is 130 mm.

6.2c: Scapolite (blue interference colours) and calcite (brown) vein replacing plagioclase in fenitised anorthosite sample S94. Width of photomicrograph is 1 mm. (Crossed polars).

6.2d: Cancrinite (cream interference colours; low relief) and calcite (brown) vein replacing plagioclase in fenitised anorthosite sample S94. Width of photomicrograph is 1 mm. (Crossed polars).

6.2e: Narrow rim of vermiform clinopyroxene surrounding primary clinopyroxene in fenitised gabbronorite sample S95. Rectangular outline marked on photograph is approximate field shown in Plate 6.2f. Width of photomicrograph is 4 mm; plane polarised light.

6.2f: Detail of vermiform clinopyroxene intergrown with nepheline (dark background) replacing primary clinopyroxene (red/mauve interference colours) and plagioclase (grey) in fenitised gabbronorite sample S95. Width of photomicrograph is 1 mm; crossed polars.

6.2g: Detail of replacement shells around ortho-pyroxene in sample S95. Brown material along twinning plane in plagioclase is apparently wollastonite (see text). Width of photomicrograph is 1 mm; plane polars.

PLATE 6.2

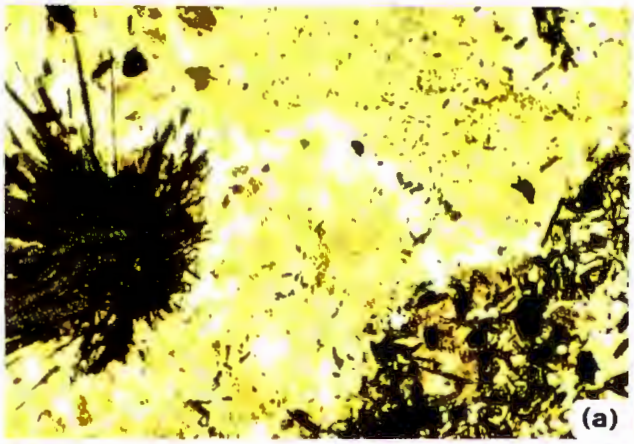
(a)


(b)

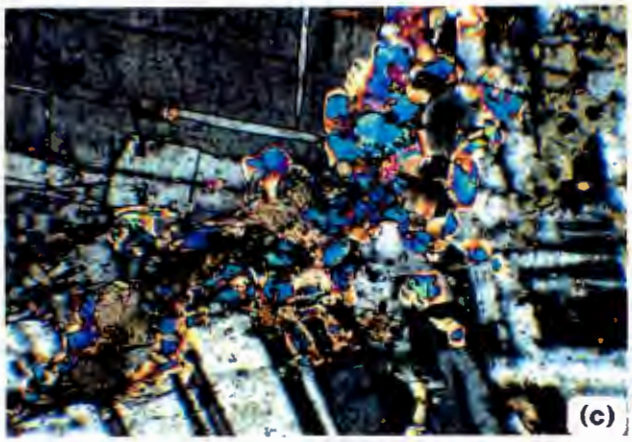
(c)

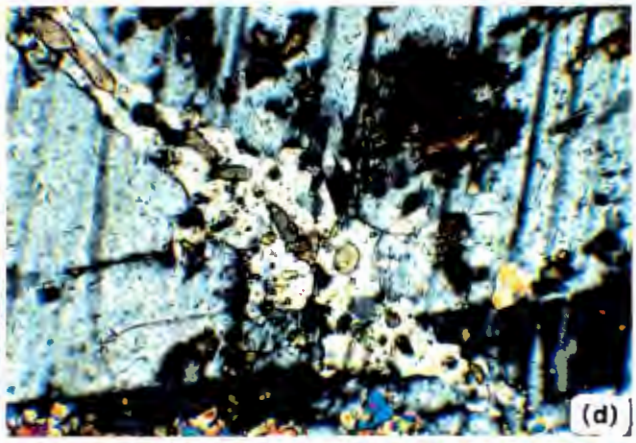
(d)

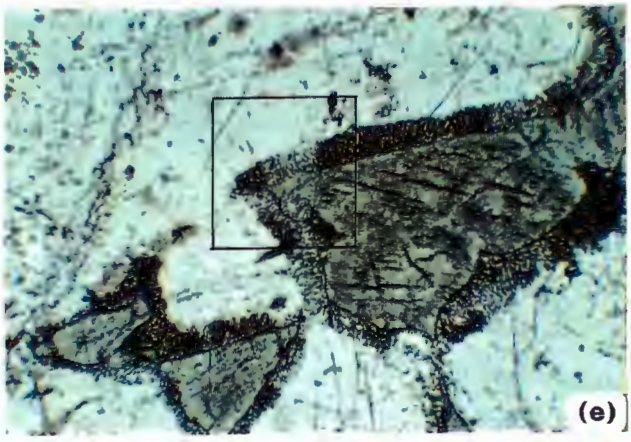
(e)

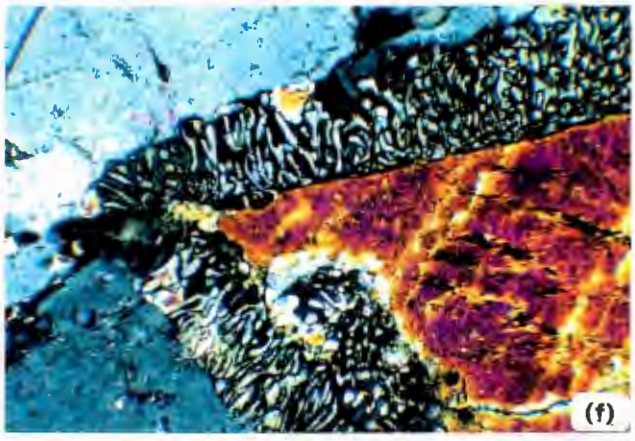
(f)

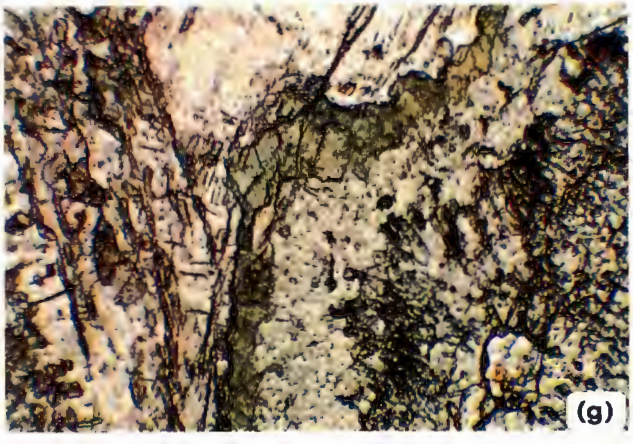
(g)

Anorthositic units commonly exhibit "spotted" to "mottled" textures typical of the Bushveld anorthosites. The strike of the layered succession appears coherent throughout this region at slightly west of north and dips are generally about 50ø upstream, i.e. to the west. Magnetitite seams are generally 20 to 50 cm thick, have sharply defined contacts with anorthosite on the "up dip" side, and are gradational into magnetite gabbro and gabbro on the down-dip margin. Magnetitites of the upper zone of the Bushveld are characterised by a sharp footwall and gradational hangingwall, only magnetite layer #13 showing the opposite relationship (e.g. Molyneux, 1970). These observations imply that the xenolith is inverted at this locality.

Along the Mare Spruit east of Mare hill, the xenolith is "fragmented" by a number of 10 to 30 m wide sheets of foyaite. These sheets characteristically have marginal pegmatoid pockets containing large tabular white feldspars and are typically veined. Magnetitite seams decrease in abundance southwards along the Mare Spruit and in the region of the confluence with the Tshweneng River the succession comprises gabbro mixed with intrusive ijolite and the ubiquitous veins of urtite. The gabbros are weakly foliated, the fabric defined by mineral orientation. As the tributary to the lower Tshweneng River is approached, the degree of metasomatism is sufficiently intense that the boundary between fenitised gabbro and the encompassing ijolite is difficult to establish with confidence, particularly where the intrusive is coarser-grained.

Outcrops along the lower 200 m of the tributary are of intimate mixtures of fenitised gabbro and early intrusive ijolite, extensively veined by urtite (Plate 6.3a) to form an "agmatite" structure (terminology of Mehnert, 1968). Later ijolite sheets, typically 20 to 40 cm in width, cut across and displace the agmatite veining. The later sheets have sharp margins which are emphasised in outcrop by the concentration of nepheline at the contacts in the form of a 2-3 mm "urtite" selvedge.

From the tributary downstream to the contact with the granite fenites, the exposures are of a black, dense magnetite ijolite ("melteigite" of Strauss and Truter, 1950) in which solid blocks and fragments of magnetite are irregularly distributed. These ijolites are distinguishable in outcrop from regular ijolites in that they characteristically develop a brick-red, "rusted" surface with incipient alteration. Dykes of fine ijolite are common and urtite veins and patches are ubiquitous. In some cases ijolite sheets are seen to have finer, chilled margins. Dykes of foyaite and syenite are only rarely noted.

Sheets of white "syenite" pegmatite 20-30 cm wide occur, usually with sharply-defined margins. These are typically composed of large, euhedral, white alkali feldspar interspersed with finer grained matrix. Feldspar grains may attain lengths of 10 cm and are oriented normal to the margin of the sheet, developing a "dog-tooth" texture in places. It is unlikely that these sheets were emplaced as magma: the texture implies that they rather reflect, in part at least, the metasomatic replacement of the host ijolite. As such, they mark sites or zones of fluid passage.

Fragments of magnetitite are characteristic of most exposures along the lower Tshweneng River. Fragments are typically rounded, 1 cm to 10 cm in size, and commonly occur in "swarms" although isolated pieces are also found. A particularly fine exposure is found in the bed of the Tshweneng River some 150 m downstream of the tributary where a metre wide magnetitite seam is preserved in magnetite ijolite (Plate 6.3d). Despite being fractured and disturbed, the seam is laterally continuous across the entire outcrop in the river bed: some 15 m. Although essentially massive magnetite, zones of cumulus plagioclase, now pseudomorphed, are common. The plagioclase grains are always aligned parallel to the margins of the seam. The magnetitite is traversed by narrow, millimetre scale, urtite veinlets: where these veinlets cross zones rich in plagioclase, urtite minerals have pseudomorphed the silicate. Complete replacement of numerous adjacent grains gives rise to "lenses" of new silicate material within the magnetitite. These lenses expanded progressively until the magnetitite was prised apart, ultimately producing disaggregated blocks of magnetitite surrounded by ijolite.

Mafic fenites, macroscopically identifiable as transformed gabbros or anorthosites of Bushveld parentage are also encountered along the Makpopeng Spruit upstream of the tributary leading towards the carbonatite. Here the exposures comprise altered gabbroic and fresher anorthositic material, the plagioclase-rich components are usually distinctly spotted.

Samples of spotted anorthosite in which relict plagioclase is still present, were found amongst the ijolites along the upper reaches of the first Tshweneng River tributary (Plate 6.2b), in the dongas to the east of this locality, and in the ijolites which form a screen in the foyaite exposures on Rietfontein (marked on map in Figure 2.1).

Plate 6.3

6.3a: "Agmatite" structure formed by fenitised olivine diorite cut by veinlets of urtitic ijolite. Note the darker colouration of the fenitised diorite at the contact with the veinlets. Lens cap is ca. 55 mm across. Lower Tshweneng River (at confluence with tributary).

6.3b: Detail of replacement overgrowths on fayalite in fenitised fayalite diorite sample S107. Olivine (high relief, top left) is surrounded by soda clinopyroxene (green) and magnetite, which in turn is partially rimmed by soda amphibole (brown). These shells are surrounded by rodded to vermicular clinopyroxenes intergrown with nepheline. Width of photomicrograph is 1 mm; plane polars.

6.3c: Replacement overgrowth on fayalitic olivine (top left) and rodded cpx/nepheline intergrowth surrounding clino-pyroxene (right margin). Clear material is fine mosaic of nepheline and sodic perthite. Fenitised fayalite diorite sample S107. Width of photomicrograph is 4 mm; plane polars.

6.3d: Fractured seam of magnetitite in magnetite-bearing ijolite ("melteigite"). Lower Tshweneng River. Handle of hammer is 600 mm in length.

6.3e: Replaced cumulus plagioclase within magnetitite seam (see Plate 6.3d). The contact with the magnetite is marked by intergrown titanite and magnetite and the centre of the plagioclase is replaced by a granular mosaic of nepheline and anhedral diopsidic pyroxene. Width of photomicrograph is 1 mm; plane polars. Sample S77c.

6.3f: Magnetite-rich fenite from margins of magnetitite seam along lower Tshweneng River (see Plate 6.3d). Pyroxenes are replaced by fine mosaics of sodic clinopyroxene (green - khaki). Large magnetite grain is rimmed by granular titanite (brown). Width of photomicrograph is 4 mm; plane polars. Sample S77b.

6.3g: Photomicrograph of magnetite ijolite ("melteigite") adjacent to magnetitite depicted in Plate 6.3d. The ijolite is composed of an irregular intergrowth of magnetite (black), usually rimmed by titanite, sodic clinopyroxene (green-khaki) and nepheline (clear). Width of photomicrograph is 4 mm; plane polars. Sample S77a.

PLATE 6.3

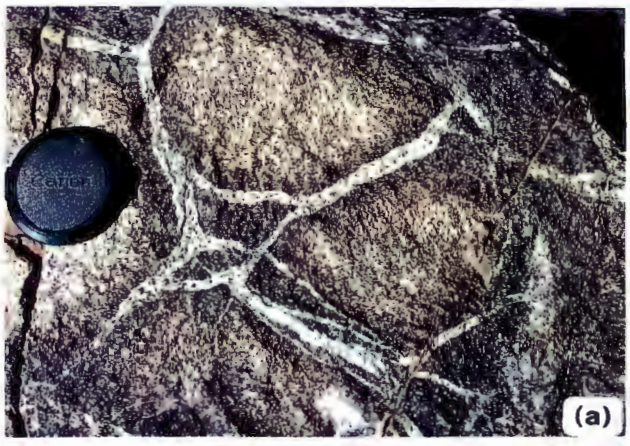
(a)

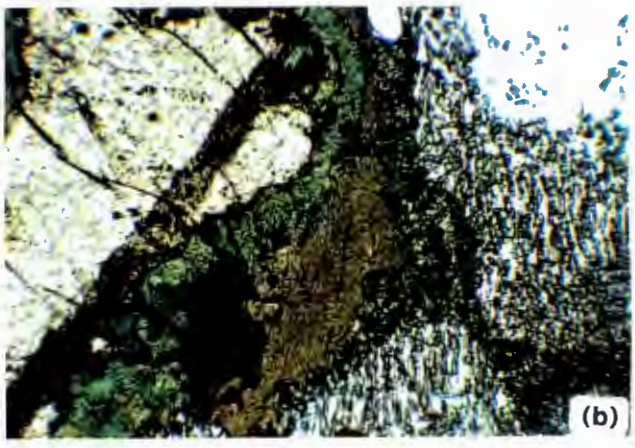
(b)

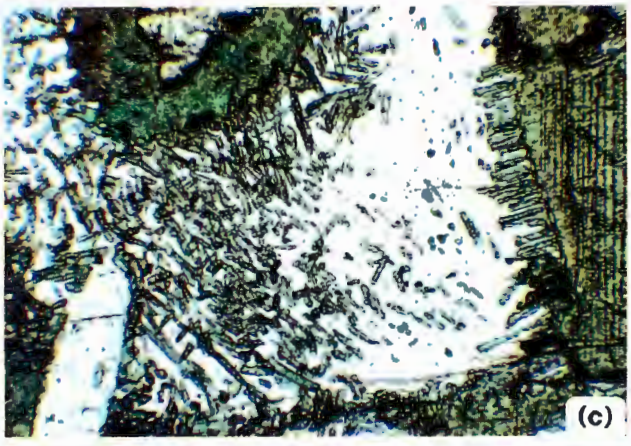
(c)


(d)

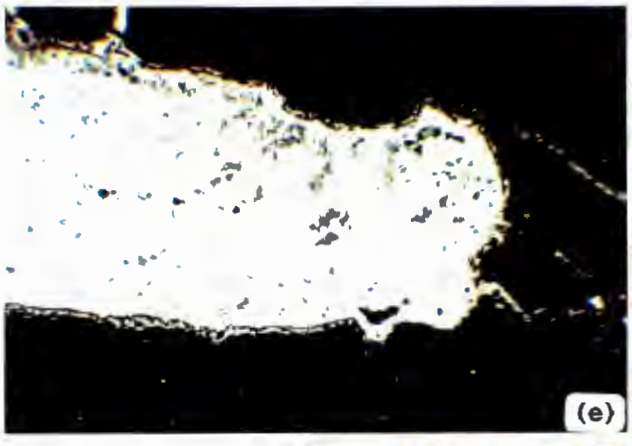
(e)

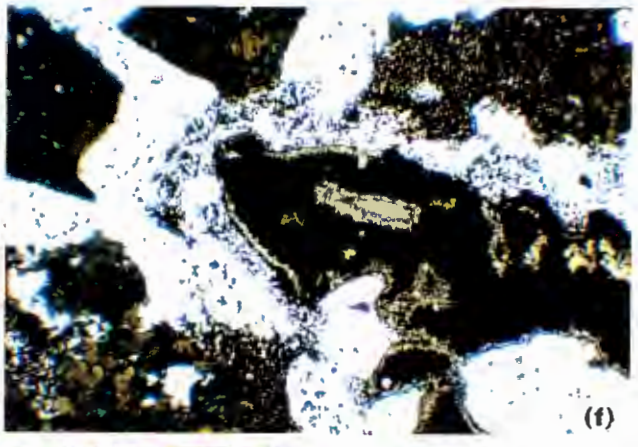
(f)

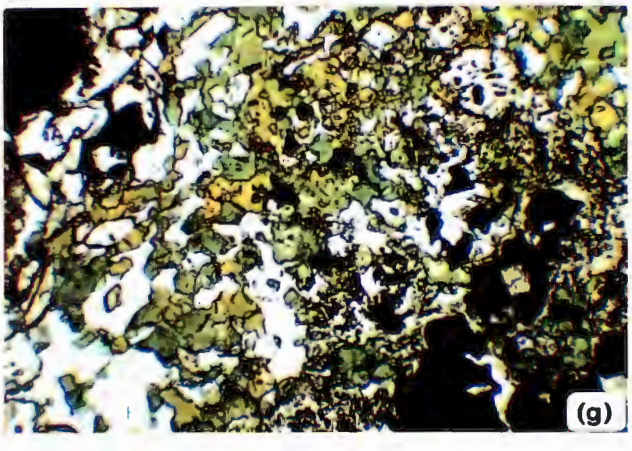
(g)

6.3.2 Petrography

As a rule, the more plagioclase-rich components of the mafic fenite suite are less extensively altered than those containing abundant pyroxene. Plagioclase is totally replaced only at the highest metasomatic grades, and only in the more gabbronoritic starting compositions.

Anorthositic units along the upper Mare Spruit have mosaics of intergrown clear calcic plagioclase grains still showing sharply defined polysynthetic twin lamellae. Early manifestations of alteration are fracturing and a "dusting" in the interior of some plagioclase grains by tufts of a light brown mineral having the appearance of a mica. Where this material is present in larger patches and sheafs it is seen to have a moderate birefringence, length-slow orientation and a low 2V interference pattern. This latter attribute would suggest that the mineral may be paragonite.

Fractures are generally sharply bounded. Broader fractures are filled with veins comprising mixtures of scapolite, carbonate, green clinopyroxene and minor cancrinite (Plates 6.2c, 6.2d). Narrower veins have the appearance of a "bead necklace", individual "beads" consisting alternately of scapolite and carbonate. In places the veins have annealed and their positions are marked by linear trails of scapolite, carbonate, cancrinite and pyroxene grains within the plagioclase mosaic. Alongside these veins, the feldspar may exhibit an increased concentration of brown paragonite "tufts" and under highest magnifications is seen to contain a high concentration of fluid inclusions. In the vicinity of larger veins, wider than 0.2 mm, the boundaries are no longer sharply defined where the plagioclase has altered to intergrown mixtures of paragonite, carbonate and scapolite. Away from the vein contact, isolated and randomly arranged blebs ("teardrops") of cancrinite suggest that the plagioclase has been "soaked" by the metasomatising fluid.

Pyroxenes are more susceptible to alteration and the susceptibility differs markedly between ortho- and clino- pyroxene types. Both varieties develop characteristic reaction haloes or coronas against the bounding plagioclase (Plate 6.2e). Where well developed these coronas are colloform zones: the outer margins smoothly convex into the feldspar, built of delicate, vermiform pale green pyroxene set in a matrix of nepheline or wollastonite. The vermiform pyroxenes are aligned normal to the pyroxene grain margin (Plate 6.2f). Nepheline is clear with low relief, whereas the wollastonite appears turbid pale brown, with a slightly higher (ca. 0.008)

birefringence. Small droplets of scapolite are sometimes observed in the outer parts of the coronas. Where the reaction halo is narrow, it has the appearance of a fuzzy rim around the pyroxene (Plate 6.2e). Haloes expand by growing outwards into the plagioclase and inwards into the pyroxene.

Where alteration haloes surround clinopyroxene, the original pyroxene is largely unaffected: some "dusting" may be present but little noticeable change is apparent. The interface between unaltered pyroxene and vermicular corona is surprisingly sharp; no compositional zoning is evident.

The replacement of orthopyroxene is somewhat more complex. Relict hypersthene is typically surrounded by concentric zones of up to three sets of reaction products. Immediately surrounding the relict orthopyroxene is a zone of granular, anhedral diopsidic clinopyroxene (colourless, high birefringence). Individual grains tend to be elongate and arranged in sheafs, which are disposed in a crude radial orientation. Some opaque intergranular ore grains appear to be produced during this recrystallisation process. A second shell of clear clinopyroxene follows where individual grains are more equant and define a polygranular mosaic. This shell is probably a recrystallised form of the inner reaction zone. The third zone forms a continuous rim around the granular shells and is composed of a distinctly different, pleochroic, green, acmitic clinopyroxene. At the outer edge this green clinopyroxene forms a colloform vermicular corona intergrowth with nepheline and, in places, wollastonite, similar to the coronas noted around original clinopyroxene grains (Plate 6.2g). In the cores of some coarser recrystallised aggregates, where hypersthene is totally replaced, scattered grains of phlogopite are noted.

Similar vermicular reaction intergrowths, albeit involving different mineral species, have been described in fenitised gabbros from Finnmark, Norway (Robins, 1984) and from gabbro xenoliths in the Kannabeam Complex, Namibia (Reid, 1991).

As the degree of metasomatic alteration increases, the vermicular intergrowth coarsens, the pyroxene develops better crystal form, producing oriented rod-like grains.

In the magnetite gabbros and anorthosites in the upper Mare Spruit, reaction haloes develop around the interstitial magnetite in a similar fashion but the haloes are narrower and produce different minerals. Red brown biotite is a characteristic reaction product along with fine-grained titanite and a pleochroic olive-green to brown amphibole. In sample S182, a magnetite gabbro forming the "hanging wall" to one of the magnetitite seams, no biotite is found and the brown amphibole forms the initial

reaction shell on magnetite. The amphibole is zoned to deeper olive to green towards the edge and is surrounded by the typical vermicular intergrowth forming colloform bulges into the surrounding plagioclase.

It has been noted above that the apparent intensity of metasomatism increases southwards along the Mare Spruit and the lower Tshweneng River. Samples from these river sections show far more advanced replacement of the Bushveld assemblages. In general, original pyroxenes are totally replaced by granular aggregates of deeply coloured, strongly pleochroic (khaki to green) clinopyroxene. Only rarely are original clinopyroxene relics preserved. The igneous sub-ophitic texture is still apparent despite the extensive recrystallisation. The compositional character of the original rock types also changes, however, in this direction: the amount of anorthosite decreases and the rocks are largely gabbronorites and olivine diorites along the Tshweneng River. Since plagioclase is apparently less easily metasomatised than the mafic constituents, the increasing alteration of the fenites along the lower Tshweneng River may partly be a reflection of the ease with which the more gabbroic protolith assemblages responded to the metasomatising fluids. A further indication of a change in protolith in this area is the ubiquitous occurrence of apatite which forms as euhedral insets in the mafic minerals suggesting that it was a cumulus component of the original gabbroid.

Fayalitic olivine is observed as corroded relics armoured by a rim of opaque ore intergrown with deep green metasomatic clinopyroxene and/or olive green amphibole (Plates 6.3b, 6.3c). Pyroxene usually forms the innermost reaction shell and is invariably crowded with inclusions of opaque magnetite. Amphibole characteristically forms a discontinuous shell on the pyroxene and is itself bounded by an intergrowth of ore and green pyroxene which passes into the typical rodded to vermiform intergrowth with nepheline. Plagioclase laths are pseudomorphed by fine granular mosaics of nepheline and perthitic alkali feldspar, mixed with rodded pale green clinopyroxene (aegirine augite?) towards the margins of the original feldspar grain which appear to represent the evolved equivalent of the early vermiform intergrowths (see Plate 6.3c).

In magnetite-rich samples, smaller magnetite grains are rimmed by aggregates of intergrown red-brown biotite, green clinopyroxene and irregular titanite. Larger grains are surrounded by a narrow rind of titanite, variably intergrown with nepheline, magnetite and clinopyroxene (Plate 6.3f). In the interior of the magnetitite seams, original cumulus plagioclase has been replaced by a granular mosaic of nepheline

through which are dispersed irregular "droplets" of pale-green pyroxene. A thin rind of titanite is continuously developed along the magnetite (Plate 6.3e).

The final product of the fenitisation of the Bushveld gabbroic to dioritic rocks is an ijolitic rock rich in magnetite and biotite relative to the ijolite types described in Chapter 3. The pyroxenes are more deeply coloured and their grain size distribution is highly irregular: from aggregates of fine grains less than 0.05 mm in size to anhedra over 1.0 mm in diameter (Plate 6.3g).

Fragments of anorthositic fenites sampled from within the Rietfontein foyaite sheet are identical to those from the more massive outcrops along the upper Mare Spruit and contain abundant original plagioclase. The heteradcumulate "mottles" of interstitial clinopyroxene are only slightly affected whereas hypersthene is recrystallised. The spotted anorthosite sampled from ijolite exposures along the tributary to the upper Tshweneng River also retains zones of primary igneous plagioclase. These zones appear as highly fractured remnants between large colloform zones of vermiform intergrowth. An unusual feature of these samples, however, is the occurrence of trails of euhedral, pale brown to lilac-coloured, zoned titan-augite.

6.3.2.1. Fenitisation reactions

In order to better understand the fenitising reactions represented by the assemblages and textures described above, it is useful to construct potential mass balance equations associating the phases involved.

In the anorthositic units plagioclase contains veinlets of scapolite and calcite. Such an assemblage may be described by the reaction well known in metamorphic studies on calc-silicates (e.g Deer *et al.*, 1966):

3 Anorthite + Calcite $\Leftrightarrow$ Scapolite (meionite)

The plagioclase is not, however, pure anorthite molecule but ranges from An_{75} in the anorthosites to An_{50} in the gabbronorites, and even lower values in the olivine diorites. Treating the complete plagioclase composition it is possible to write:

$4\ An_{75}$ + Calcite $\Leftrightarrow$ Scapolite (meionite) + Ab
(3 An + 1 Ab)

$6\ An_{50}$ + Calcite $\Leftrightarrow$ Scapolite (meionite) + 3 Ab
(3 An + 3 Ab)

Transformation of the noritic assemblages can be expressed as:

$(CaAl_2Si_2O_8 + NaAlSi_3O_8) + (MgSiO_3 + FeSiO_3) + 3Na^+ + O_2 \Leftrightarrow$

"Plagioclase" "Hypersthene" "fluid"

$3NaAlSiO_4 + NaFe^{+3}Si_2O_6 + CaMgSi_2O_6$

Nepheline Acmite Diopside

This composite reaction embodies two transformations: the conversion of An+Fs molecules to Ne+Ac, releasing CaO which is accommodated by reaction with the increased En component of the hypersthene to form diopside. Transformation of clinopyroxene is best illustrated through the compound reaction:

$2CaFeSi_2O_6 + NaAlSi_3O_8 + Na_2CO_3 + ½O_2 \Leftrightarrow$

Hd : cpx plagioclase fluid

$2NaFe^{+3}Si_2O_6 + NaAlSiO_4 + 3CaSiO_3 + CO_2$

Ac Ne Wo

Only the ferrous part of the $(Ca[Mg,Fe]Si_2O_6)$ solid solution is significant: the diopside component would persist and simply form a solid solution with acmite. Note that this reaction is dependent on f_{O_2}.

6.3.3. Geochemistry

Analyses of fenites with clearly identifiable Bushveld parentage are listed in Table B.20.

6.3.3.1. Original Stratigraphic position of the xenolith

Mafic fenites along the Tshweneng River section have been noted to contain original fayalitic olivine plus early formed apatite. This assemblage indicates that the original protoliths to these fenites were fayalite diorites of sub-zone C of the upper zone of the Rustenburg Layered Suite (SACS, 1980). Along the upper reaches of the Mare Spruit the fenites comprise anorthosites (mottled and spotted), magnetite gabbro and a series of thin magnetitite seams. Fayalite and apatite are absent. Although it is not possible to precisely identify the stratigraphic level of this succession, it would appear to have been derived from deeper in the upper zone succession than the fenites bearing fayalite relics.

Figure 6.14: Plot of V_2O_5 contents in magnetitite seams from the xenolith at Spitskop compared with variations in upper zone magnetitites.

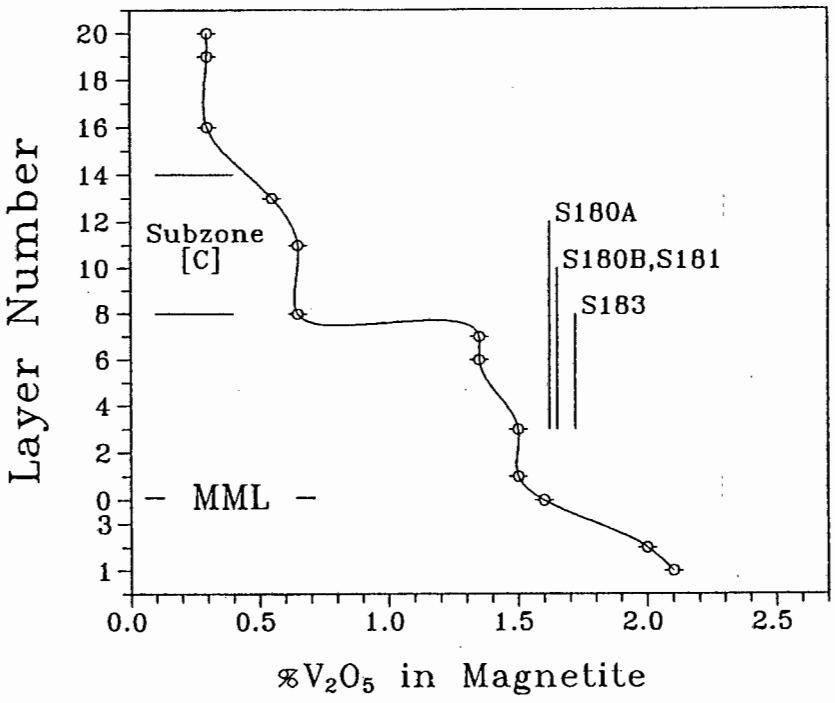

The trend of V_2O_5 compositions in Bushveld magnetitite seams is derived from the data of Molyneux (1970). "MML" = Main Magnetite Layer.

It has long been known that the contents of TiO_2 and V_2O_5 vary systematically through the 21 magnetitite seams found in the upper zone of the Rustenburg Layered Suite (Molyneux, 1970; Cawthorn and Molyneux, 1986): from V_2O_5 values of 1.5 to 2.5% at magnetite layer 1 to less than 0.3% at layer 21. To better constrain the original stratigraphic position of the magnetitite seams in the upper Mare Spruit, 4 samples were analysed from 3 of the seams. Care was taken in preparing the samples for analysis to remove any fracture fill, weathered magnetite or any possible metasomatically introduced material. Samples S180A and S180B were taken from different parts of the same seam to assess the within-seam variation.

The data are plotted in Figure 6.14 in relation to the vanadium contents for the various seam numbers in the Magnet Heights area as established by Molyneux (1970). Clearly, the vanadium contents of the analysed magnetite xenoliths indicate that the magnetitites originated from subzone A, near the base of the upper zone, in the vicinity of the main magnetite layer and associated seams. Data in Molyneux (1970) demonstrate significant along-strike variation in the V_2O_5 contents of the magnetite

seams, although the relative variations between seams remain constant. On the diagram the position of the magnetite seams in Subzone C of the upper zone, the stratigraphic interval deduced for the fayalite diorite fenites, are indicated.

It seems certain, therefore, that the mafic fenites in Spitskop were derived from xenoliths dislodged from different portions of the upper zone and that the zone of mafic fenites along the western margin of the Complex does not represent a single coherent xenolithic block.

Using these observations it is possible to estimate the vertical distance through which the xenoliths were transported by the alkaline magma. In the Magnet Heights area, the Main Magnetite Layer is overlain by some 1300m of cumulates whereas the Subzone C diorites occur some 500-700m below the roof of the Bushveld Complex. At the current erosion level the Spitskop Complex is underlain by at least 200m of Lebowa Suite granite and so transport distances of at least 1500m and 700m are indicated for the upper Mare Spruit and lower Tshweneng River xenoliths, respectively.

6.3.3.2. Chemical changes during metasomatism

An evaluation of chemical changes during metasomatism of the Rustenburg Layered Suite material is obviously more difficult than with the granites because of the much wider range of starting compositions involved and the present sample set is too small relative to the possible range in starting compositions to enable realistic fenite:protolith comparisons to be made. Fayalite diorites are, however, restricted to the upper sub-zones of the upper zone where lithological variation is less marked. The two fenitised diorite samples, S73 and S107, are compared to a mean fayalite diorite composition calculated from the BDS sample suite of M.R. Sharpe (Bushveld Institute, University of Pretoria: unpublished data) on "isocon" diagrams in Figures 6.15(a) and (b). In view of the uncertainties involved in determining the mean reference value, the positions of MgO, TiO_2 and P_2O_5 indicated on the diagrams probably reflect primary differences between the protoliths of S73, S107 and the mean value (e.g. less modal apatite, magnetite in the protoliths) than true losses during fenitisation. The mineral mass balance reactions deduced from the fenite petrography suggest the introduction of Na, and the presence of alkali feldspar would be consistent with increased K and Ba. It is thus unlikely that the Na_2O, K_2O, Rb, Ba and Sr values are due to protolith differences and are more likely to reflect real, and significant, additions during fenitisation.

Figure 6.15: Comparison of compositional differences between fenitised olivine diorite samples (a) S73 and (b) S107 and the mean upper zone fayalite diorite.

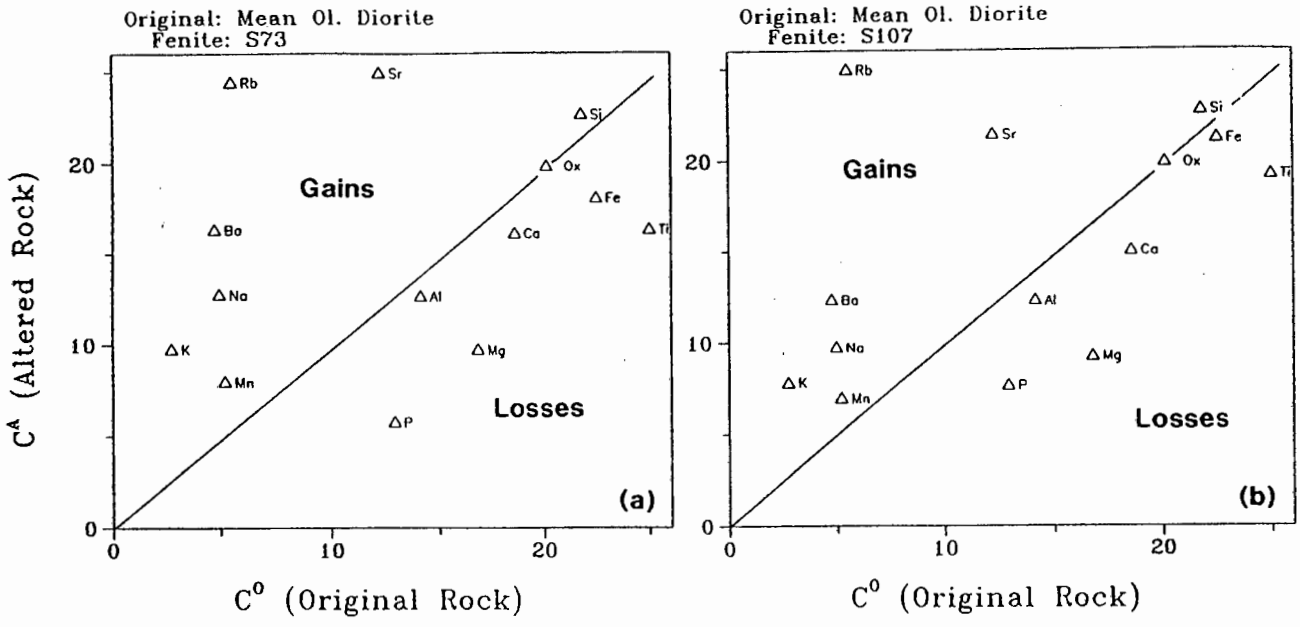

Scaling factors applied to the plots are the same as those used in Figure 6.10 above.

Cumulates of the upper zone of the Bushveld Complex had $^{87}Sr/^{86}Sr_i$ (i.e. at 2050 Ma) of >0.707 (Sharpe, 1985; Cawthorn *et al.*, 1991) coupled to very low Rb/Sr. As a result, these rocks would have had $^{87}Sr/^{86}Sr_{1341}$ of 0.7070-0.7075 at the time of emplacement of the Spitskop Complex. In Table B.20 it may be seen that the anorthosite samples S98, S103, S93 and S99 have essentially retained the primary $^{87}Sr/^{86}Sr$ signature whereas anorthosite S94 and the gabbronorite and fayalite diorite samples all have $^{87}Sr/^{86}Sr$ values lower than the primary magmatic values. Plagioclase is the phase in the fenites which would contain the highest concentrations of Sr. These isotopic relationships are thus consistent with the petrographic observations that plagioclase is the mineral most resistant to the fenitising fluids, and that only where this mineral occurs with significant mafic silicate, i.e. in the gabbronorites and diorites, has the plagioclase been extensively transformed.

6.4. Timing and nature of the fenitising agent(s)

Metasomatic reactions in both the granitic and gabbroic fenites require substantial additions of Na. Progressive metasomatism of the granitic rocks leads to the replacement of the primary hydrous mafic minerals in the granite - hornblende and biotite - with anhydrous sodic pyroxene. In the most intensely fenitised granites birefringent, CO_2-rich, cancrinite is observed replacing nepheline. These mineralogical changes imply that the metasomatising agent was unlikely to be a hydrous fluid but are consistent with the presence of a fluid rich in CO_2. Observation of a carbonate-pyroxene veinlet preserved in quartz grains in one granite fenite is evidence for the existence of CO_2 (or carbonate)- rich fluids during metasomatism. The replacement of calcic plagioclase in the anorthosites by meionitic scapolite is also evidence that carbonate-rich fluids were responsible for at least some of the metasomatic changes.

Le Bas (1977; p270-275) suggested that Na-dominated fenites are produced by fluids in equilibrium with ijolite whereas metasomatism due to carbonatite-related fluids produced potassic fenites. Other authors have attributed differences in the Na/K of fenites to the pressure at which metasomatism took place (e.g. McKie, 1966; Vartiainen and Woolley, 1976) and have argued that high Na/K fenites reflect deeper processes than high K/Na fenites. Rubie and Gunter (1983) showed that temperature, pressure, and the CO_2 and Na/K composition of the fluid are all important factors which determine the ultimate character of the metasomatised product. These authors contend that high-K fenites are only found associated with carbonatites whereas Na-rich fenites may be associated with either silicate (ijolite) or carbonatitic intrusions. Morogan and Woolley (1988) discussed the fenites related to Alnö and suggested that metasomatic fluids related to both ijolite and carbonatitic magmas were responsible for the fenitisation and that some fenites were produced by the superimposition of these fluid types. At Alnö, the ijolitic fluid was more alkaline, had high SiO_2 activity and $X_{H_2O} > X_{CO_2}$ whereas the carbonatite-related fluid had very low SiO_2 activity and $X_{H_2O} > X_{CO_2}$.

Nepheline syenite sheets cutting metasomatised gabbros and anorthosites along the upper Mare Spruit do not show signs of metasomatic alteration (see Chapter 3) and so it may be concluded that the fenitisation of the xenolith must have occurred prior to, or at the same time as, the emplacement of the nepheline syenites. That is, the fenitisation was completed prior to the emplacement of the carbonatite to its present level in the Complex. On the chemical evidence, therefore, the metasomatising fluid appears to have been CO_2 rich, but deduced age constraints

imply that the fluid was derived from the silicate units of the Complex or the precursor to the carbonatite.

It is worth noting that hydrous mafic minerals are never found in the magmatic ijolites or nepheline syenites. At the contacts of intrusive ijolite sheets, localised concentrations of volatiles characteristically give rise to cancrinite. Late stage felsic minerals in the nepheline syenites are typically cancrinite, pectolite and sodalite while the felsic veinlets carry, in addition to these phases, natrolite. Significantly, while some of these minerals are hydrous, aegirine coexists and is never altered to amphibole. Pegmatitic patches noted at some of the nepheline syenite contacts (see Chapter 2) always contain felted masses of aegirine in the groundmass. These observations suggest that residual fluids generated from the crystallisation of the ijolites or the nepheline syenites would have low H_2O activities.

Chapter 7: Petrogenesis of the Spitskop Complex.

7.1. *Introduction*

In this chapter, the geochemical data for the various units of the Spitskop Complex are synthesised and used to evaluate the possible petrogenetic relationships between the different rock units.

The silicate units are dealt with first. Potential causes of the chemical variations between each unit are discussed. This information is then used to investigate the compositional links between the silicate and carbonate components of the Spitskop Complex.

7.2. *The silicate units*

Magmatic silicate components of the Spitskop Complex were emplaced in the time sequence pyroxenite, ijolite and nepheline syenite. Mineral data presented in Chapter 4 indicate that a systematic variation exists in clinopyroxene composition from the pyroxenites through to the nepheline syenites. It is of interest to assess to what extent the silicate units are linked petrogenetically.

7.2.1. *Potential petrogenetic relationships between the pyroxenites and Type-I ijolites.*

As described in Chapter 2, the pyroxenites invariably occur as blocks and zones entirely surrounded by ijolite. The observation of a pyroxenite dyke by Strauss and Truter (1950) would support an intrusive origin for at least some Spitskop pyroxenites. These authors unfortunately do not describe the petrographic features of the dyke material. Textures in the samples collected during the current study

indicate that the pyroxenites are unlikely to reflect liquid compositions and are more likely to represent cumulates (possibly recrystallised).

Pyroxenite xenoliths composed of diopsidic pyroxene are common in the ijolites of many ijolite-carbonatite intrusives in East Africa, particularly the complexes of Napak (King and Sutherland, 1966), Usaki and Sagurume (Le Bas, 1977). Le Bas (1977, p265-268) considered the incorporation of "pyroxene-rich xenoliths ... [a] process common to all ijolite intrusions" and argued that their "texture, structure and position indicate either that [the pyroxenites] are the cumulative product of some early and deep-seated magma chamber of which no evidence .. remains, .. or that they represent the early precipitated and bottom-accumulated fraction of the ijolite magma intrusions."

Neither biotite nor magnetite are ever noted as primary phases in the Type-I ijolites at Spitskop and the clinopyroxenes in the pyroxenites are far more diopsidic than those found in the ijolites. As a consequence, if the pyroxenites do represent

Figure 7.1: Results of model calculations to explain the REE patterns in pyroxenite S44.

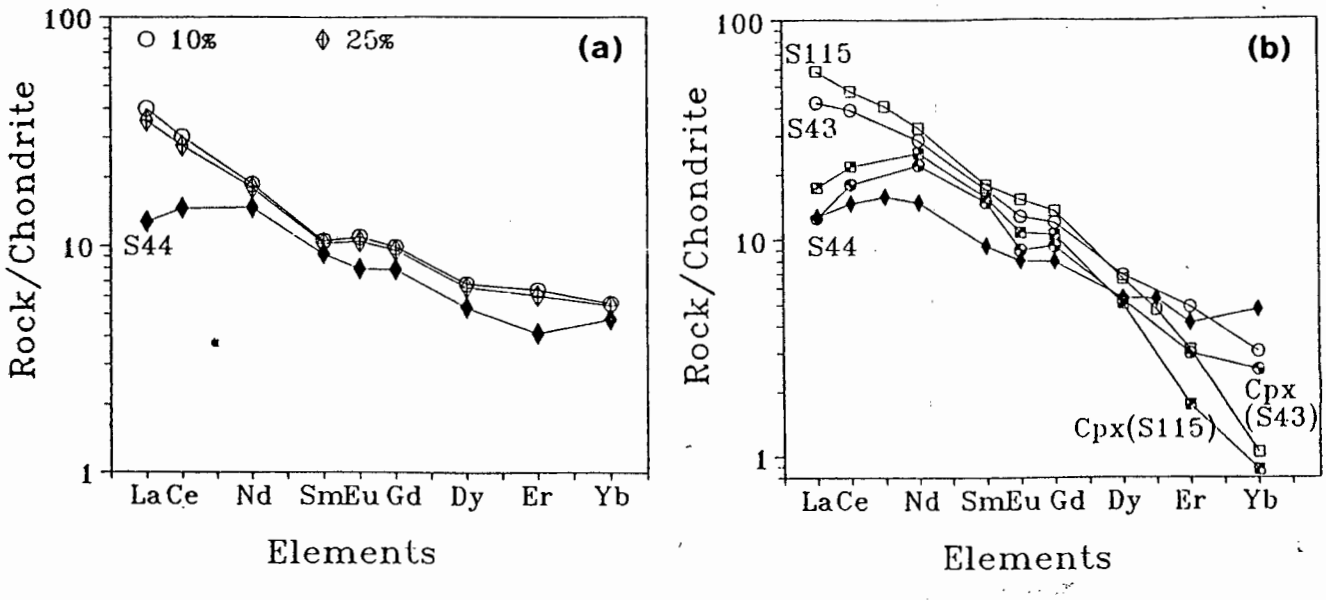

(a) Chondrite-normalised REE traces for liquids in equilibrium with a pure diopside cumulate having REE contents equivalent to sample S44. Equilibrium liquids are calculated assuming that the cumulate represents 10% (upper trace) and 25% (lower trace) crystallisation.
(b) Plot comparing the chondrite-normalised REE patterns in pyroxenite S44 with clinopyroxenes ("Cpx") that could have been produced as cumulates from the fractionation of ijolitic liquids S43 and S115.

cumulates, they must have formed from an earlier, more primitive, magma than that represented by the Type-I ijolites at the present level of erosion in the Spitskop Complex.

The REE pattern of the analysed pyroxenite (S44) is unusual in having a "sigmoidal" shape caused by slight depletions in La, Ce relative to Nd, and enrichments in Yb and Lu relative to Er (see Chapter 4). Similar REE patterns were reported in clinopyroxene cumulates in the syenites of the Ihouhaouene Complex by Bernard-Griffiths *et al.* (1988) who were able to demonstrate that such REE patterns could result from accumulation of clinopyroxene.

As a first approach, if pyroxenite S44 is approximated as a pure diopside cumulate then REE patterns in its parental liquid can be estimated. Results of such calculations using the diopside partition coefficients published by Larsen (1979) are depicted in Table 7.2 and Figure 7.1a. Similar patterns and concentration levels are

Table 7.1: Calculated trace element concentrations (ppm) for parental magma in equilibrium with pyroxenite S44.

			Parental Liquids		*Ijolite*
	D	S44	10%	25%	S115
Rb	0.017	23	1219	1021	56
Sr	0.25	225	833	731	569
Ba	0.024	158	5941	4977	62
Nb	0.025	5.6	202	169	8.5
Zr	0.235	90	351	310	72
Y	0.66	9.7	14.2	14.7	15
La	0.296	4.67	14.67	13.00	21.5
Ce	0.458	13.98	28.87	26.39	45.4
Nd	0.769	10.43	13.25	12.78	23.0
Sm	0.870	2.13	2.42	2.37	4.09
Eu	0.702	0.69	0.95	0.91	1.32
Gd	0.778	2.41	3.03	2.93	4.11
Dy	0.764	2.03	2.59	2.50	2.49
Er	0.615	1.02	1.59	1.50	0.77
Yb	0.831	1.17	1.38	1.35	0.26

Compositions in the parental liquid (=C_O) were estimated using:

$(C_O) = C_S[F(1-D)+D]/D$ (e.g. Henderson, 1982).

Partition data for diopsidic clinopyroxene (D) are from Larsen (1979). Liquid compositions are calculated assuming sample S44 (=C_S) represents 10% (F=0.9) and 25% (F=0.75) crystallisation.

achieved if the pyroxenite is assumed to represent either 10 or 25 percent crystallisation (F=0.9 and 0.75 respectively). Estimated La values are about 40 times chondrite in the model parental liquid with linear normalised LREE patterns from La to Sm. This result indicates that "sigmoidal" REE patterns can be produced in clinopyroxene cumulates from a parental liquid with a linear normalised REE pattern.

Table 7.2: Calculated trace element concentrations in clinopyroxenes in equilibrium with ijolite liquids S115 and S43.

	D_{Cpx}	S115	Cpx_{S115}	S43	Cpx_{S43}	S44
Rb	0.017	56	0.95	53	0.9	23
Sr	0.25	569	142	338	84.5	225
Ba	0.024	62	1.5	123	3.0	158
Nb	0.025	8.5	0.2	34	0.85	5.6
Zr	0.235	72	16.9	155	36.4	90
Y	0.66	15	9.9	12	7.9	9.7
La	0.296	21.47	6.36	15.49	4.59	4.67
Ce	0.458	45.35	20.77	37.41	17.13	13.98
Nd	0.769	22.97	17.66	20.21	15.54	10.43
Sm	0.870	4.09	3.56	3.89	3.38	2.13
Eu	0.702	1.32	0.93	1.10	0.77	0.69
Gd	0.778	4.11	3.20	3.64	2.83	2.41
Dy	0.764	2.49	1.90	2.60	1.99	2.03
Er	0.615	0.77	0.43	1.21	0.74	1.02
Yb	0.831	0.26	0.22	0.75	0.62	1.17

Clinopyroxene REE concentrations are estimated as $D_{Cpx} x C_o$. Partition data (D_{Cpx}) are from Larsen (1979) and Type-I ijolite samples S115 and S43 assumed for the liquid compositions (C_o).

In Table 7.2 and Figure 7.1b REE in pyroxenite S44 are compared with the REE compositions calculated for clinopyroxene in equilibrium with a liquid equivalent to that of Type-I ijolites S115 and S43. Clinopyroxenes crystallising from S115 and S43 would have similar patterns, though higher absolute values, of normalised REE to S44 for the elements La to Dy. High absolute levels of REE calculated for the clinopyroxene are a function of the elevated REE in the ijolites: it was argued earlier that if the pyroxenites at Spitskop are cumulates, then they formed from more primitive liquid compositions, probably having lower LREE contents, than those represented by the Type-I ijolites. Values of Er and Yb in the clinopyroxene in equilibrium with S43 provide a better match to the values in S44 because of the slightly elevated HREE in sample S43 relative to S115.

In Tables 7.1 and 7.2 the same approach has been adopted to model the concentrations of selected trace elements (Rb, Sr, Ba, Nb, Zr, Y). In contrast to the REE, the predicted parental liquids (Table 7.1) do not satisfactorily match the compositions of Ba, Rb, Zr or Nb observed in the Type-I ijolites. In addition, the partition coefficients of Larsen (1979) predict that diopside cumulates forming from ijolitic liquids equivalent to S115 or S43 would have concentrations of Rb, Ba, Zr and Nb much lower than those observed in S44.

7.2.2. An assessment of the petrogenetic relationships between the ijolites and nepheline syenites.

Selected major elements in whole rocks and component mineral phases are depicted on a series of Harker diagrams in Figures 7.2 and 7.3 (a-d) and the variation of minor elements P_2O_5 and TiO_2 against CaO are depicted in Figure 7.3 (e,f).

7.2.2.1. Relationship between Type-I ijolites and nepheline syenites of the Rietfontein sheet

Nephelinites and phonolites are the closest volcanic analogues to ijolites and nepheline syenites, respectively. Le Bas (1977, 1978, 1987) argued that phonolites (and/or nepheline syenites) could be produced as differentiation products of either olivine-poor nephelinites or alkali basalt/basanite parental magmas. Substantial plagioclase fractionation is required to derive phonolite compositions from a basaltic parental magma and this has the effect of depleting the concentrations of both Sr and Ba in the resulting phonolite to levels of 100 ppm or less. As a consequence, phonolites derived from nephelinites may be distinguished in having higher contents of alkalis (ca. 14%), Sr (>1000 ppm) and Ba (>100 ppm) than phonolites produced from alkali basaltic and basanitic parental magmas (Le Bas, 1987). The Spitskop nepheline syenites have Ba and Sr contents of 200-1000ppm and so are compositionally similar to phonolites derived from nephelinites.

Figure 7.2: Plot showing SiO_2 - CaO relationships between the pyroxenites (solid diamonds), Type-I ijolites (open circles) and nepheline syenites (open squares) and component minerals.

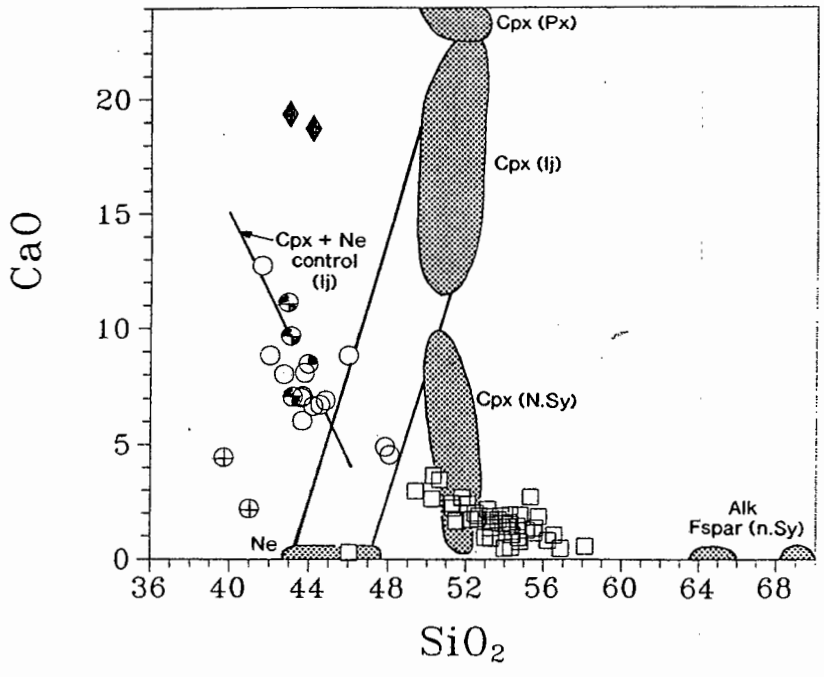

The "Cpx+Ne control" line depicts the possible chemical variations amongst the Type-I ijolites induced by accumulation or fractionation of an assemblage of Ne+Cpx marked by parallel tie-lines between nepheline and clinopyroxene (Cpx(Ij)) compositions analysed in the Type-I ijolites.

Systematic variations between certain major elements in the Harker plots in Figures 7.2 and 7.3 resemble "liquid lines of descent". In addition, the similarity in initial $^{87}Sr/^{86}Sr$ between the Type-I ijolites and the Rietfontein sheet nepheline syenites suggest the possibility that these rock types could be derived from a common parental magma through closed system differentiation processes.

Both their fine-grained nature and their common occurrence as dykes suggest that Type-I ijolites could approximate liquid compositions. With the exception of the schistose variety, most of the Rietfontein nepheline syenites are coarse-grained and are thus less likely to represent liquid compositions. Significant scatter is noted in most SiO_2 - element plots of the nepheline syenite data (see Chapter 4) which suggests that they do not represent a suite of liquids produced by simple closed-system crystal-liquid fractionation.

Figure 7.3: Plots showing variation of (a) Al_2O_3, (b) FeO^*, (c) MgO and (d) alkalis with SiO_2; and (e) TiO_2 and (f) P_2O_5 against CaO for the silicate rocks and component minerals.

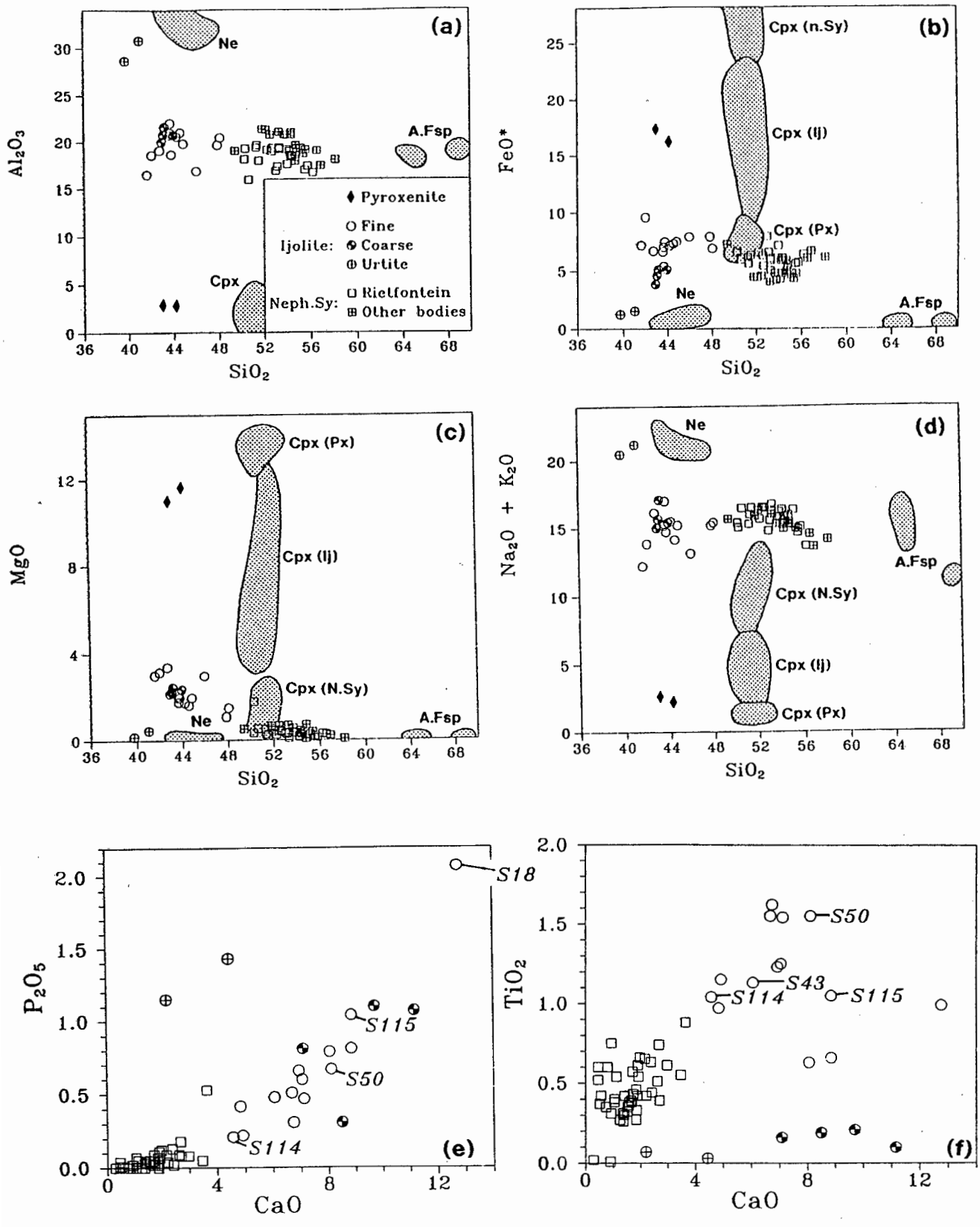

Figure 7.4: Plots showing variation of (a) Rb, (b) Ba, (c) Sr, (d) Zr, (e) Nb and (f) Zr/Nb with SiO_2 amongst the silicate rocks.

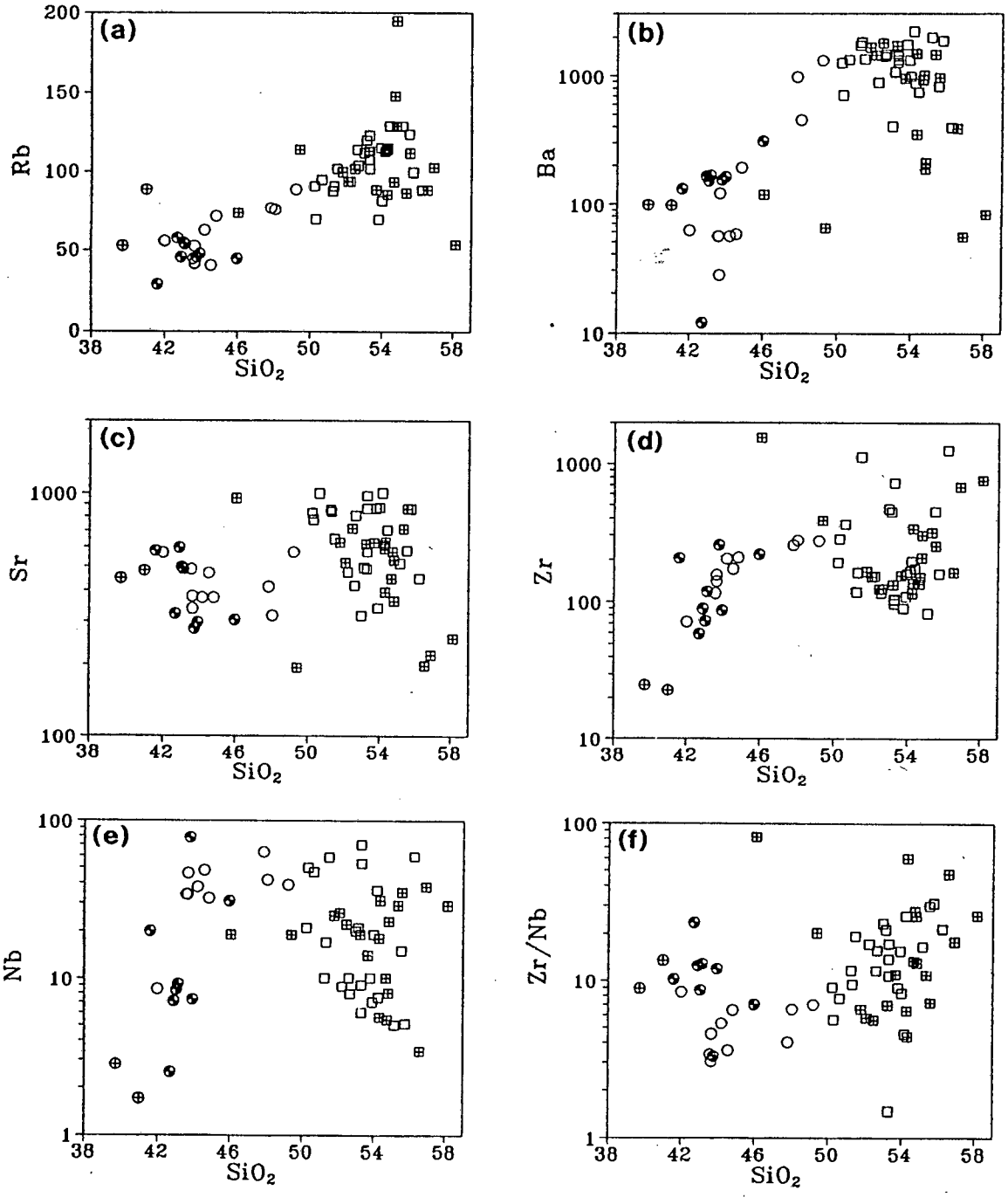

Symbols are as in Figure 7.3(a).

It is clear from the relative positions of whole rock and mineral compositions in Figure 7.2 that the ijolites and nepheline syenites cannot be related by crystal fractionation of their constituent phases (i.e. nepheline, clinopyroxene or alkali

feldspar) from a *single* parent magma. This point is best illustrated with reference to the annotated SiO_2-CaO plot in Figure 7.2. Tie-lines linking the compositional ranges of nepheline and clinopyroxene in the Type-I ijolites lie to the *high*-SiO_2 side of the whole rock compositions. Fractionation of these phases will thus drive the residual liquids to lower SiO_2, i.e. *away* from the compositional field of the nepheline syenites. Accumulation of alkali feldspar in ijolite liquid would be required to link the ijolite and nepheline syenite compositions. However, the total absence of feldspar in the ijolites strongly suggests that feldspar was not a stable liquidus phase in the ijolitic liquids. One or more low-SiO_2 - high CaO fractionating phases would be required to generate the nepheline syenites from the ijolites.

Trace element variations with SiO_2 (depicted in Figure 7.4) also question any single "liquid line of descent" linking the ijolites and nepheline syenites. In general the variation of trace element values with SiO_2 are more scattered in the nepheline syenites (see variation diagrams in Chapter 4). Rb increases with increasing SiO_2 (Figure 7.4a), whereas Ba and Nb increase with increasing SiO_2 in the ijolites but decrease with increasing SiO_2 in the nepheline syenites (Figure 7.4b,e). In Figure 7.4c no systematic variation is discernible between SiO_2 and Sr in ijolites and nepheline syenites. Fractionation of combinations of clinopyroxene, nepheline and alkali feldspar would not be capable of producing large variations in Zr/Nb (using partition coefficient data reported by Larsen, 1979) yet the ijolite and nepheline syenite data exhibit a range in Zr/Nb from about 3 to over 70! The Zr/Nb ratio decreases with increasing SiO_2 in the ijolites and increases with SiO_2 in the nepheline syenites (Figure 7.4f).

Correlations exist between CaO, TiO_2 and P_2O_5 within some of the Type-I ijolites (see Figure 7.3e,f) suggesting that titanite and apatite, common accessory phases in the ijolites (see Chapter 3), may have played a role in determining the final chemistry of the ijolites and nepheline syenites. In Figure 7.3f the low TiO_2 contents in the coarse and urtitic Type-I ijolites (see also the spidergrams in Figure 4.22c) indicate that these are unlikely to have been derived from the same parental liquid as the fine grained ijolites.

Attempts were made to derive the major and minor element contents of the low CaO ijolite S114 from higher-CaO "parent" compositions S50 and S115. No statistically acceptable least-squares mixing models were obtained using any combination of the mineral phases clinopyroxene (both high and low Na members of the Type-I compositional range), nepheline, alkali feldspar, apatite and titanite. In Figures 7.3 (e,f) the range in P_2O_5 and TiO_2 compositions amongst the fine-grained

Type-I ijolites is approximately 0.7% and 0.4% , respectively. These variations would be produced by differences of approximately 2% apatite and 1% titanite (assuming stoichiometric values). Fractionation of these quantities of accessory phases would decrease the CaO content by about 1.6%. Because the CaO variation amongst the Type-I ijolites is over 3.5%, these phases alone cannot adequately explain the observed major element variation. Furthermore, the dramatic effect on the normalised REE patterns of fractionating apatite and titanite from starting liquids S50 and S115 is depicted in Figure 7.5. Sample S114, an "evolved", low-CaO ijolite is plotted for comparison and clearly does not show any marked depletion in the MREE. The partitioning behaviour of Ba and Zr into titanite in alkaline melts (see coefficients determined by Wörner *et al.*, 1983) suggest that residual liquids would be depleted in these elements after titanite crystallisation yet S114 has elevated levels of Zr (4x) and Ba (7x) relative to S115 (Table B.7 in Appendix B). These observations question the significant influence of accessory phases on the overall chemical variation within the Type-I ijolites.

Figure 7.5: Normalised REE plot to show the effect of titanite plus apatite fractionation from Type-I ijolite liquids S50 and S115

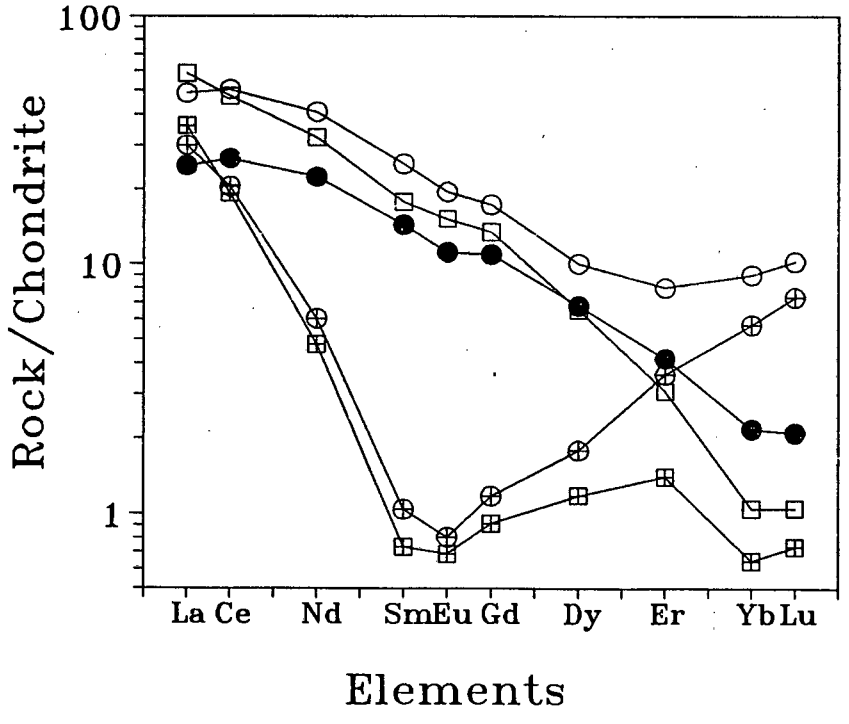

The REE contents in residual liquids (crossed symbols) were calculated after the fractional crystallisation of 1%titanite + 2%apatite from starting liquids with the REE compositions of high-CaO Type-I ijolites S50 and S115 (open symbols). Partition coefficients were from Wörner *et al.* (1983). Low-CaO ijolite S114 is shown for reference (filled circle).

The concave-up REE patterns produced by the apatite-titanite fractionation model discussed above (Figure 7.5) are, however, similar to those noted in the Rietfontein nepheline syenites (Figure 4.31). The low concentrations of both P_2O_5 and TiO_2 in the Rietfontein nepheline syenites are consistent with the removal of these accessory phases. The possible influence of titanite is also reflected in the good positive correlation seen in Figure 7.6 between TiO_2 and the "concavity" of the REE pattern (quantified as Gd/Gd^* in a similar way to Eu/Eu^* - see caption to Figure 7.6) in the Rietfontein nepheline syenites.

In Figure 7.7 the Rietfontein REE patterns are compared to those in the Type-I ijolites. With the exception of S18, the ijolite REE traces approach the "sigmoidal" pattern found in the pyroxenites, and show significant variations in normalised abundances of Yb and Lu (Yb_N=1-12) but less variation in La through Dy (La_N=30-70). Of significance is the fact that, while the LREE in the syenites are depleted relative to the ijolites, most syenites have substantially higher concentrations of Er-Lu! This implies that if titanite fractionation was important in determining the final REE patterns, titanite must have crystallised from liquids with liquids of substantially higher total REE contents than the Type-I ijolites.

Is it possible that the unusual REE contents in the Rietfontein syenites could be the result of selective LREE and MREE loss to an escaped fluid phase produced during crystallisation of the nepheline syenites? Light and middle REE were selectively removed from the metasomatised Bushveld granite country rocks (see discussion in Chapter 6) by the fenitising agent whereas the concentrations of Yb and Lu were little affected. As a result the REE traces of the feldspar fenites bear some resemblance to those noted in the Rietfontein nepheline syenites (compare Figures 4.31 or 7.7 and 6.5a). Arguments were presented in Chapter 6 that fenitisation occurred prior to or during the emplacement of the nepheline syenites. As a consequence, the fenitising fluid could have emanated from the nepheline syenites. Comparison of the nepheline syenite Ce and Yb contents and Ce_N/Yb_N ratio with those in the ijolites and pyroxenite (see Figure 7.8) indicates that the Ce_N/Yb_N ratio in the Rietfontein syenites is controlled by the abundance of the HREE and that the Yb contents are, on average, *higher* than those in the other rock types. This signifies that the REE spectra in the Rietfontein syenites cannot be easily explained by the removal of LREE and MREE: addition of the HREE is also necessary.

Figure 7.6: Plot of TiO_2 *versus* "Gd anomaly", Gd/Gd^*, in the Rietfontein nepheline syenites.

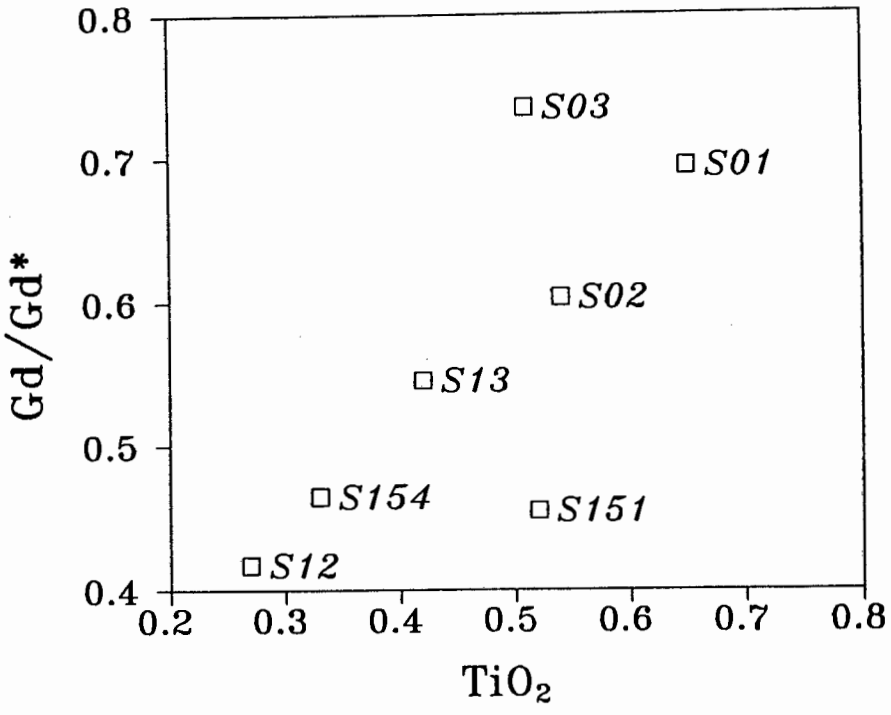

$Gd/Gd^* = Gd_N / 0.5\ (Ce_N + Yb_N)$

Figure 7.7: Comparison of REE contents in the Type-I ijolites (shown as bold line field and S118) and nepheline syenites (squares).

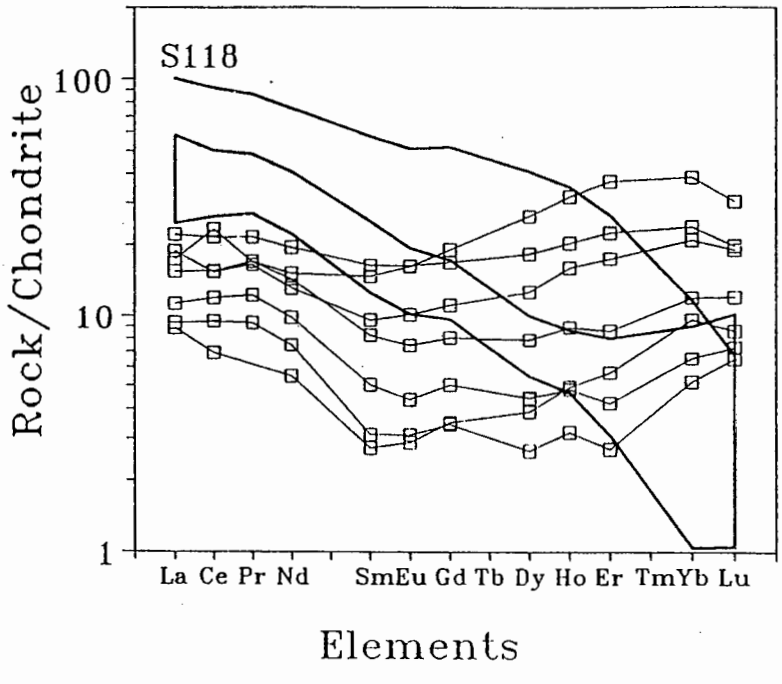

Figure 7.8: Comparison of REE contents in pyroxenite (solid diamond) with those in selected Type-I ijolites (circles) and nepheline syenites (squares).

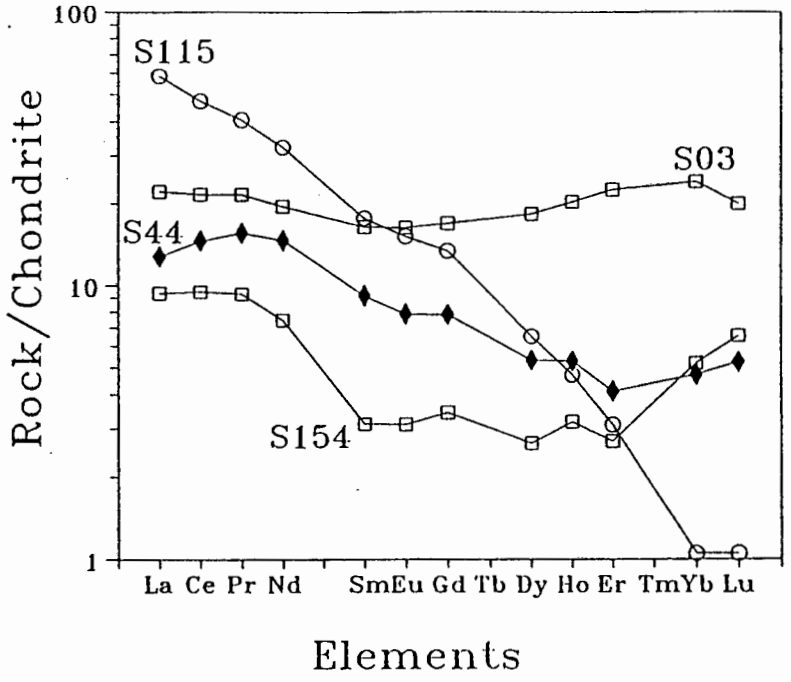

In conclusion, then, it is not possible to relate the major or trace element chemistry in the Type-I ijolites and nepheline syenites through fractionation of their major constituent phases from a single starting liquid. Accessory phases such as titanite and/or apatite possibly influenced the final compositions of some ijolites and the REE of the Rietfontein nepheline syenites but cannot, alone, explain the full range of chemical variation noted between the ijolites and syenites. It is thus unlikely that the ijolites and nepheline syenites were derived from a common parental liquid through closed-system crystal fractionation. Major and trace element variation amongst the ijolites and nepheline syenites is not adequately explained by differentiation processes during emplacement and crystallisation (i.e. processes involving the mineral phases noted in the rocks themselves) and must have been imprinted at an earlier stage.

Figure 7.9: Plot showing correlation between P_2O_5 and La in the Type-I ijolites.

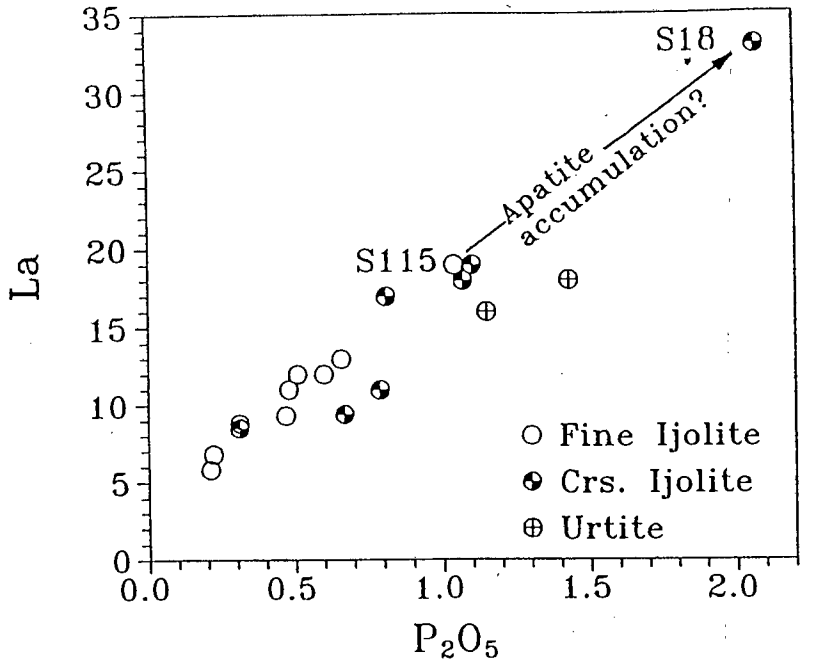

7.2.2.2. The REE in sample S18

Sample S18 differs from the other analysed Type-I ijolites in having elevated concentrations of the REE heavier than Dy. This sample also has the highest P_2O_5 content of the Type-I ijolites and so, considering the abundant apatite observed in thin section and the good correlation between P_2O_5 and LREE (see Figure 7.9), the REE pattern could relate to accumulation of apatite in S18.

CIPW norms listed in Table B.8 suggest that S18 contains about 5 weight percent apatite so REE compositions were calculated for the addition of 5 weight percent of apatite to liquids equivalent in composition to samples S115 and S43. Partition coefficients used were those of Wörner *et al.* (1983). Results are shown in Figure 7.10 where it will be seen that apatite accumulation in either S43 or S115 will enrich the MREE and produce a concave-up REE pattern. The calculations suggest that, if the partition data is applicable, accumulation of 5% apatite will produce a greater MREE enrichment than that seen in S18.

Figure 7.10: Normalised REE patterns for the accumulation of 5% apatite in ijolite liquids S115 and S43.

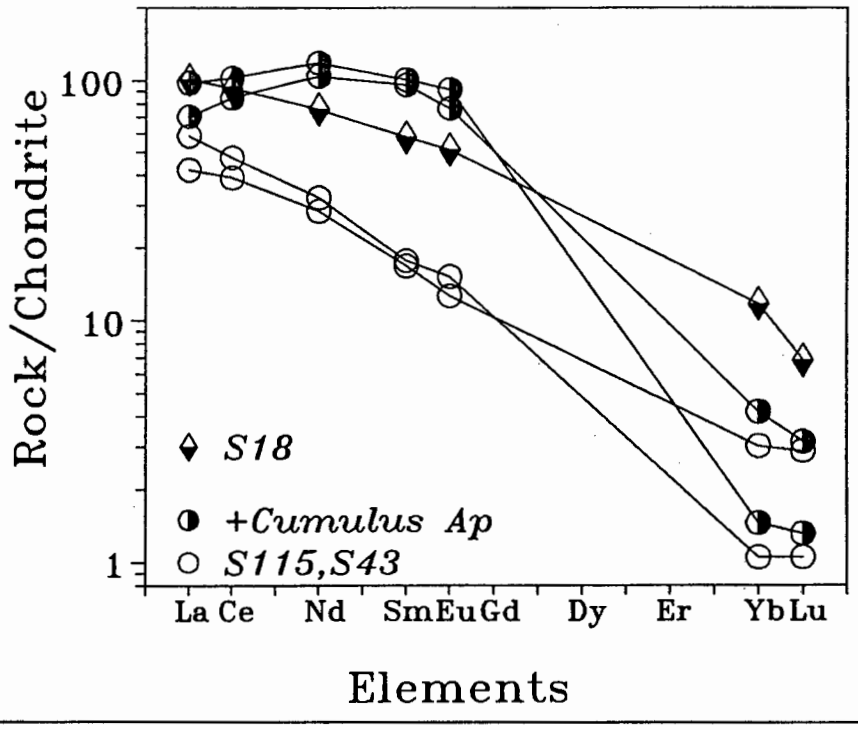

7.2.2.3. Differences between the Rietfontein and other nepheline syenites.

In most of the variation diagrams in Figures 7.3 and 7.4, the other nepheline syenite occurrences have similar compositional ranges to the samples from the Rietfontein sheet, the notable exception being the lower Ba and Sr contents in the Eastern sheet. Syenites from these other sheets differ significantly in their initial $^{87}Sr/^{86}Sr$, however. It is important, then, to assess whether the variable $^{87}Sr/^{86}Sr$ ratios in the other sheets are systematically related to variations in any other elements.

Interaction between intruding nepheline syenitic magma and the high $^{87}Sr/^{86}Sr$ granitic country rocks (see discussion of country rock isotopic compositions in Chapter 6) would generate elevated $^{87}Sr/^{86}Sr$. Elements which are typically enriched in the Bushveld granites are plotted against $\varepsilon_{(Sr)}$ in Figure 7.11a-d. Nepheline syenites from the eastern body have the lowest Sr concentrations and thus would be the most susceptible to contamination. Correlation of high $\varepsilon_{(Sr)}$ and SiO_2 in the two eastern nepheline syenites is consistent with assimilation of granitic country rock, but the low K_2O and Ba contents in these nepheline syenites argue against

simple bulk contamination. Neither the Mare nor Spitskop bodies samples show systematic variation between $\varepsilon_{(Sr)}$ and elements enriched in country rock granites.

It is concluded, therefore, that the higher $\varepsilon_{(Sr)}$ component was introduced at an early stage in the evolution of the magmas injected into the Mare, Spitskop and Eastern bodies and that subsequent magma evolution obscured the elemental signature of the "contamination" event. If this is accepted, then the significant variation in $\varepsilon_{(Sr)}$ preserved in the Mare and Eastern nepheline syenites requires that these bodies were constructed of more than one influx of magma.

Figure 7.11: Plot comparing $\varepsilon_{(Sr)}$ with contents of (a) SiO_2, (b) K_2O, *(c) Ba and (d) 100/Sr* in nepheline syenites from the Rietfontein (open square), Mare (filled square), Spitskop (crossed square) and Eastern (half-filled square) bodies.

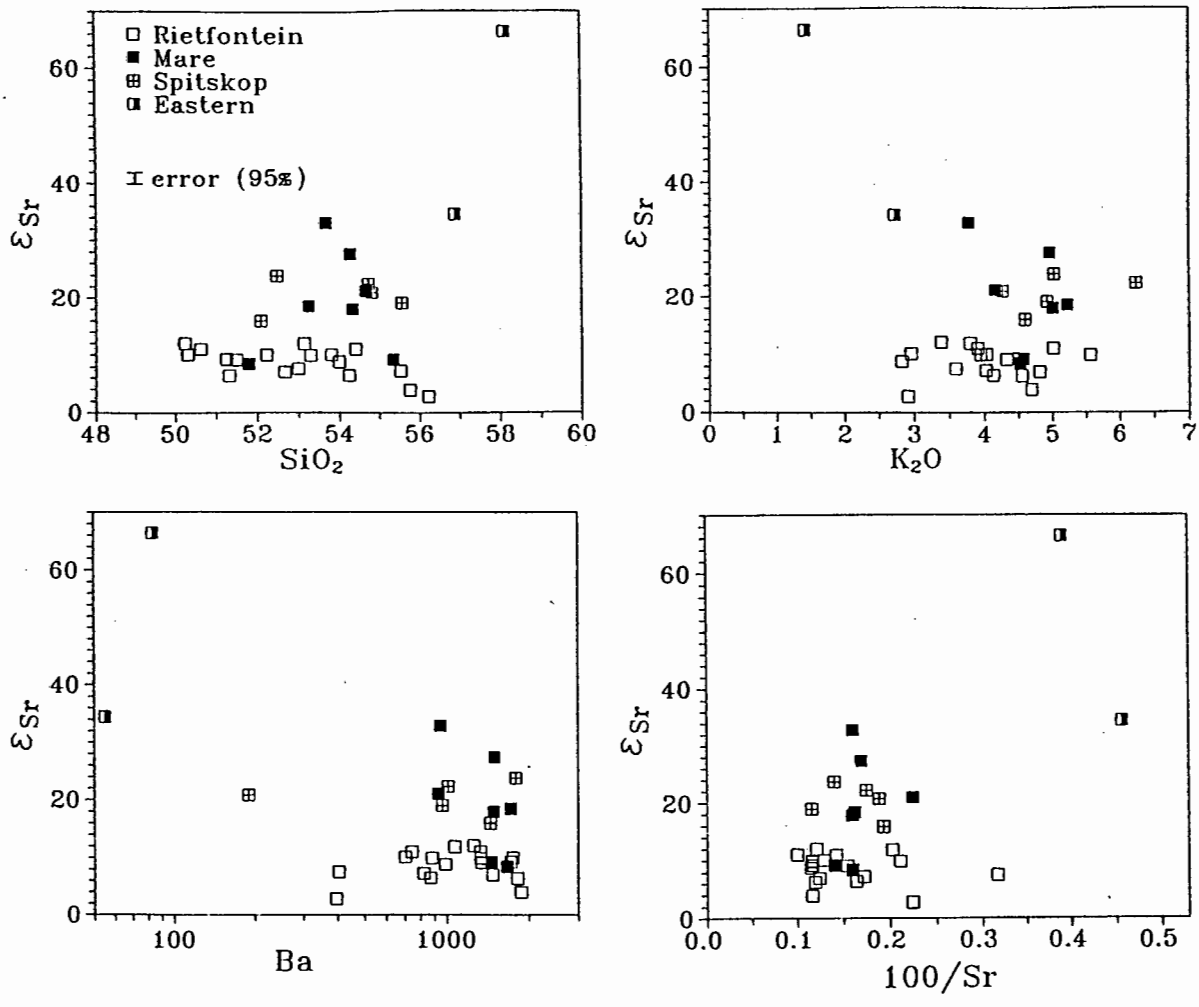

7.2.3. *Petrogenesis of the Type-II ijolites*

Field and petrographic descriptions presented in Chapters 2 and 3 above, suggest that the Type-II ijolites could be derived through "nephelinisation" of the pyroxenite. This process is envisaged as the addition of "urtitic" components, essentially nepheline, to the pyroxenite and subsequent recrystallisation.

It is possible to depict the major element compositional relationships of this process by plotting normative *ac+di* against *ne* (Figure 7.12). Also plotted for reference is sample S85, a pyroxenite containing intrusive ijolite dykelets. All but three of the Type-II ijolites (samples S65, S131 and S139) fall within an array positioned between the pyroxenites and the two nepheline-cancrinite rich, "urtite" samples. This array is consistent with the suggested origin of the Type-II ijolites as mixtures of pyroxenite and nepheline-rich urtitic ijolite.

Figure 7.12: Plot of normative clinopyroxene content (*ac+di*) against (a) normative *ne* and (b) peralkalinity index for the Pyroxenites, Type-I and Type-II ijolites.

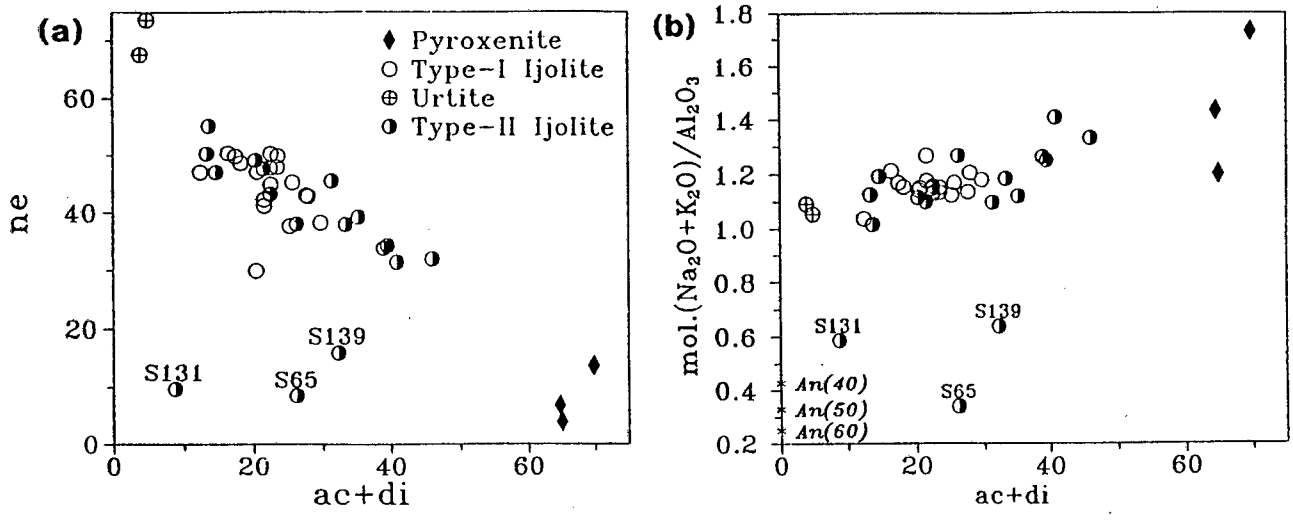

Plotted for reference are the peralkalinity indices appropriate for plagioclase of An_{40}, An_{50} and An_{60}.

Figure 7.13: Plot of MgO against Ni for the Pyroxenites, Type-I and Type-II ijolites.

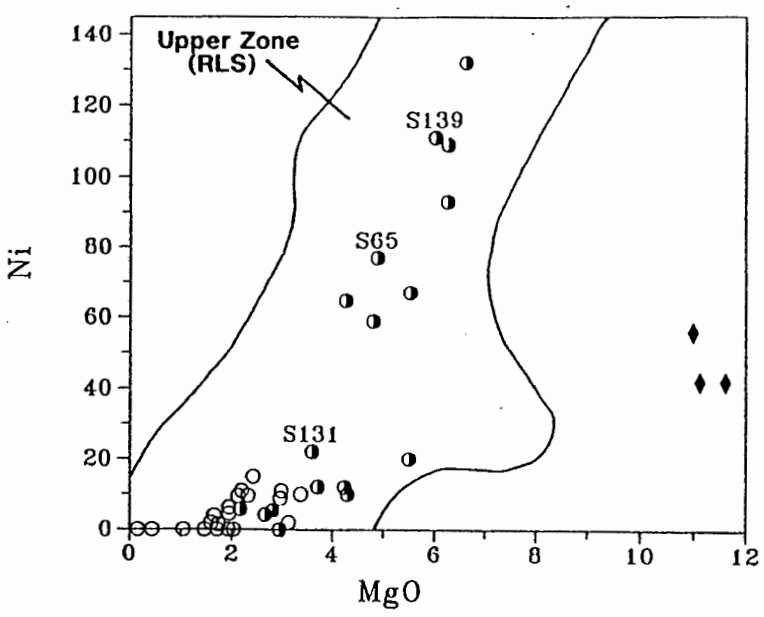

Symbols are as in Figure 7.12. The field within the curves contains the compositions of Rustenburg Layered Suite upper zone cumulates (Sharpe, 1985; unpublished data).

All three low-*ne* samples have low peralkalinity indices (PI) (see Figure 4.24c in Chapter 4) and all contain the "spreustein" groundmass described in Chapter 3. Figure 7.13 depicts the variations in Ni content between the pyroxenites and Type-I and Type-II ijolites. It is clear from this figure that the Ni levels in the high-Ni sub-group of Type-II ijolites (described in Chapter 4) are substantially above the levels attained in the pyroxenites. Two of the low-*ne* ijolites, S65 and S139, also have elevated Ni contents. Neither the high Ni nor the low PI compositions are consistent with a derivation of these Type-II ijolites solely through metasomatism of the pyroxenites. It could be argued that, since only two pyroxenite analyses are available, their Ni contents do not reflect the true range in Ni contents in the pyroxenite body as a whole. It should be remembered that the analysed pyroxenites are taken from xenolithic blocks set in a matrix of Type-I and Type-II ijolites and it is unlikely that their Ni contents are totally unrepresentative. Pyroxenite analyses presented by Nel (1976) unfortunately do not include Ni.

The correlation between MgO and Ni in the high-Ni group (see Figure 7.13) suggests the influence of forsteritic olivine and is similar to the olivine-fractionation trend seen in many mafic magmas (e.g. Hart and Davis, 1978), including those of the

Rustenburg Layered Suite (RLS) of the Bushveld Complex. Peralkalinity indices in the low-*ne* samples are 0.35 and about 0.6, values appropriate for plagioclase of labradorite and andesine compositions, respectively (see values in 7.12b). In Figure 7.13 the Ni-MgO relationships in the Type-II ijolites may be compared those in cumulates from the upper zone of the RLS from the eastern Bushveld Complex. From these figures it is apparent that the high Ni group of Type-II ijolites have MgO-Ni compositions comparable to those seen in upper zone gabbros. It was demonstrated in Chapter 6 that plagioclase was more resistant to metasomatic transformation than pyroxene and that the anorthositic units within the upper zone xenolith were less affected than the associated gabbronorites and olivine diorites. It is significant to note that only fenitised anorthosite and never fenitised norite or gabbro is ever found as relics within ijolite outcrops (see Chapters 2 and 6). As a consequence it is concluded that the high-Ni group of the Type-II ijolites represent the totally metasomatised gabbroidal components associated with these anorthositic units. The "spreustein" groundmass in the low-peralkalinity index ijolites presumably represents an intermediate step in the transformation of plagioclase to nepheline where plagioclase components are still present (as reflected by the low peralkalinity values in Figure 7.12b).

Figure 7.14: Plot comparing initial $^{87}Sr/^{86}Sr$ in pyroxenites, Type-I and Type-II ijolites with the isotopic composition of RLS upper zone rocks (Hamilton, 1977; Sharpe, 1985; Kruger *et al.*, 1987) at 1341 Ma.

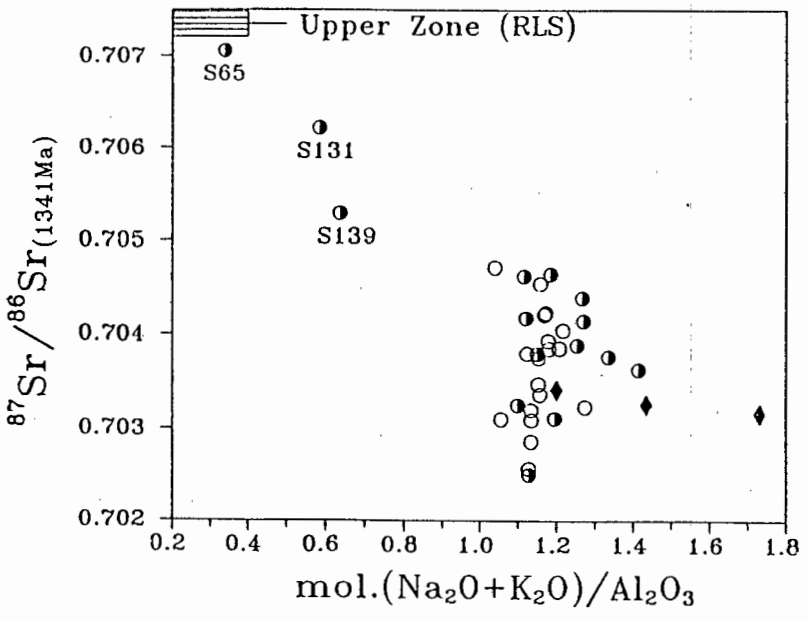

RLS upper zone components had $^{87}Sr/^{86}Sr$ ratios at 1341 Ma of >0.707 (calculated from the data of Hamilton, 1977; Sharpe, 1985; Kruger *et al.*, 1987), significantly higher than those found in the magmatic units of the Spitskop Complex (generally <0.705). Initial $^{87}Sr/^{86}Sr$ ratios in the Type-II ijolites are plotted in Figure 7.14. As a whole, the high-Ni group is not distinguished by $^{87}Sr/^{86}Sr$: only those samples with low peralkalinity indices retain elevated isotopic compositions. Since plagioclase is the most Sr-enriched phase in the gabbroids, it is logical that high $^{87}Sr/^{86}Sr$ would be preserved in those samples where relict plagioclase is cryptically present. Where transformation of plagioclase to nepheline is complete, original Sr has equilibrated with the metasomatic fluids and the isotopic ratios approach those in the magmatic ijolites.

Clearly, then, ijolites with granoblastic texture were not derived through magmatic processes but represent the products of metasomatic alteration of both Spitskop pyroxenite and RLS gabbroidal protoliths.

7.3. Carbonatites

7.3.1. Elemental variations

The carbonatites at Spitskop are composite: an earlier calcio-carbonatite intrusion is itself intruded by magnesio-carbonatite. Petrographic and geochemical data presented earlier indicate that the field distinction between the sövite and dolomite sövite carbonatites (Verwoerd, 1967) is rather ill-defined and the dolomitic sövite appears to be a hybrid phase of calcic and magnesian carbonatite "end-members". Verwoerd (1967) ascribed the dolomitic sövite to replacement of earlier sövite by the later beforsite.

It is important to assess whether the magnesio- and calcio- carbonatite magmas could be petrogenetically linked.

Systematic major element variations between the carbonatites essentially reflect the change in mineralogical composition from calcite-dominant to dolomite-ankerite-dominant carbonatite. Of the minor elements, MnO increases progressively with increasing MgO whereas P_2O_5 and SiO_2 are scattered, reflecting varying accumulations of apatite and interstitial silicate minerals. In a plot of molar CCMF ratio against Sr (Figure 7.15) the trace element contents reach maxima of over 2500ppm at CCMF values near 0.5 and 1.0, i.e. as the whole rocks approach

compositions equivalent to stoichiometric dolomite-ankerite and calcite respectively. Lowest Sr contents (<500ppm) are found in carbonatites with "intermediate" molar CCMF ratios of 0.6-0.8. Other trace elements show similar CCMF-dependent concentration variations: Nb and Ba increase towards the calcite and dolomite compositions whereas Y decreases in the same direction. Concentrations of Ba are markedly lower in the magnesian carbonatites (10-100ppm) relative to the calcic varieties (10-1000ppm).

These trends are difficult to reconcile with the interpretation that the "beforsite" and "dolomitic sövite" represent replacement products of the sövite (Verwoerd, 1967). If the "dolomitic sövite" formed from the alteration of early calcitic carbonatite by a later magnesian magma, the later magma would have to have had a CCMF of about 0.7 with low Sr (<250ppm), rather different to the composition of the magnesio-carbonatites ("beforsite") at Spitskop. Derivation of "dolomitic sövite" through mingling of calcio- and magnesio- carbonatite magmas or of cumulus calcite crystals and magnesio- carbonatite magma are not compatible with the Ba and Sr variation trends.

Variations of Ba, Sr, Nb and Y with CCMF ratio, considered in conjunction with differences in $\varepsilon_{(Sr)}$-$\varepsilon_{(Nd)}$ composition (see Chapter 5, Figure 5.5 and discussion below) require the existence of two discrete carbonatite magmas: one calcio-carbonatite (from which the "sövites" and "dolomitic sövites" crystallised) the other magnesio-carbonatite. Two possibilities are suggested by the Ba and Sr trends in Figures 7.15a 7.15b: (i) that the two magmas evolved from low-Ba,Sr carbonatite magmas with a CCMF in the range 0.7-0.8; or (ii) that two discrete high-Ba,Sr magmas existed which each evolved to intermediate CCMF values through fractionation of dolomite (in the magnesio-carbonatite magma) and calcite (in the calcio-carbonatite magma). Option (i) would require the fractionation of a mineral phase (or assemblage) with low Ba,Sr and CCMF of 0.75. Possible (Ca+Mg)-bearing mineral phases have CCMF ratios of 0.5 (dolomite, diopside) or lower (olivine, pargasite, riebeckite). An assemblage of one or more of these phases plus calcite would thus be necessary: magmatic calcite usually has high Sr contents and so it is unlikely that the crystallising assemblage would have Sr values low enough (<200 ppm) to enrich the residual liquids in Sr. As a consequence, option (ii) is the preferred interpretation (Figure 7.16).

Figure 7.15: Variation of (a) Sr and (b) Ba with molecular CCMF ratio in the various carbonatite types.

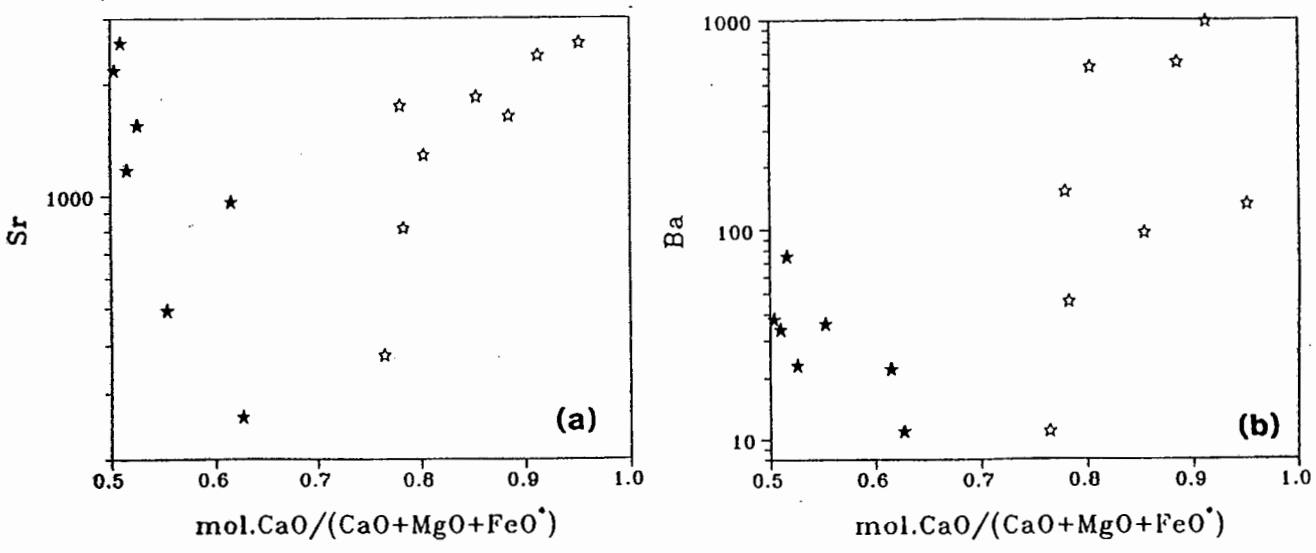

Symbols distinguish the carbonatite varieties: calcio-carbonatites (open star); magnesio-carbonatites (filled star).

Figure 7.16: Cartoon depicting preferred interpretation of Sr and Ba variation in the calcio- and magnesio- carbonatite types.

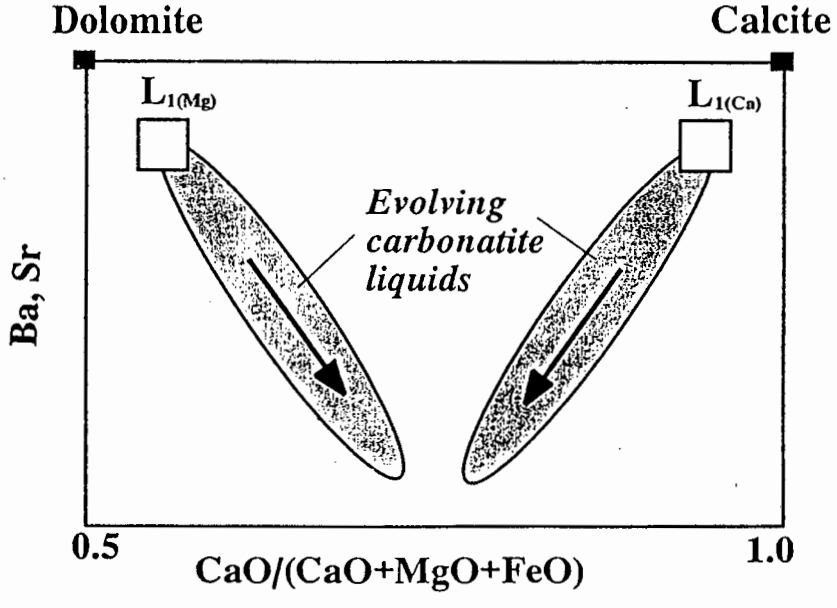

Distinct calcio-carbonatite $L_{1(Ca)}$ and magnesio-carbonatite $L_{1(Mg)}$ starting liquids evolve towards an intermediate CCMF ratio by the fractionation of calcite and dolomite respectively.

7.3.2. *Isotopic variation*

Significant differences in isotopic composition between the Mg- and Ca-carbonatites were noted in Chapter 4: Ca-carbonatites all have $\varepsilon_{(Nd)}$ of -5.0 to -7.5 whereas the Mg-carbonatites have $\varepsilon_{(Nd)}$ ranging from -1.0 to -6.0.

The narrow range in $\varepsilon_{(Sr)}$ and $\varepsilon_{(Nd)}$ in world carbonatites was commented on in Chapter 4 indicating that most carbonatites are consistently derived from a source slightly depleted in Rb/Sr and Nd/Sm relative to model Bulk Silicate Earth (BSE) (summarised in more detail in Chapter 9). Carbonatites from the Spitskop Complex define a trend to negative $\varepsilon_{(Nd)}$ at moderately positive $\varepsilon_{(Sr)}$ values which indicates a component in the Spitskop carbonatites derived from a source which had higher Nd/Sm and Rb/Sr than BSE for geologically significant time periods (i.e. of the order of 1Ga or more). Using the terminology introduced by Zindler and Hart (1986) to categorise global chemical reservoirs, this "component" is comparable to the "EM-I" style of enrichment i.e. a higher fractionation of Sm/Nd (depleted) relative to Rb/Sr (enriched). Two other carbonatite complexes which have "anomalous" isotopic character, Phalaborwa (Eriksson, 1989) and Ihouhaouene (Bernard-Griffiths *et al.*, 1988), both have substantially higher $\varepsilon_{(Sr)}$ relative to $\varepsilon_{(Nd)}$; i.e. they contain components comparable to the "EM-II" reservoir of Zindler and Hart (1986).

In view of the apparent uniqueness of the Spitskop $\varepsilon_{(Sr)}$-$\varepsilon_{(Nd)}$ relationships, it is important to assess whether these isotopic characteristics are primary, i.e. relate to the source from which the carbonatites were derived, or whether they simply represent the imprints of contamination during emplacement.

7.3.3. *Are the carbonatite $\varepsilon_{(Sr)}$-$\varepsilon_{(Nd)}$ values the result of crustal contamination?*

Figure 5.6. in Chapter 5 shows that the most deviant carbonatite isotopic values (i.e. most negative $\varepsilon_{(Nd)}$) are found in the calcio-carbonatites, the first carbonatites to intrude. These carbonatites would have had the greatest opportunity to interact with surrounding continental crust *en route* to the surface, whereas the later magnesio-carbonatites could have been shielded from such interaction by a sheath of calcio-carbonatite.

Figure 7.17: $\varepsilon_{(Sr)}$-$\varepsilon_{(Nd)}$ plot of carbonatite data showing a mixing curve representing bulk contamination of carbonatite S59 with Bushveld granite.

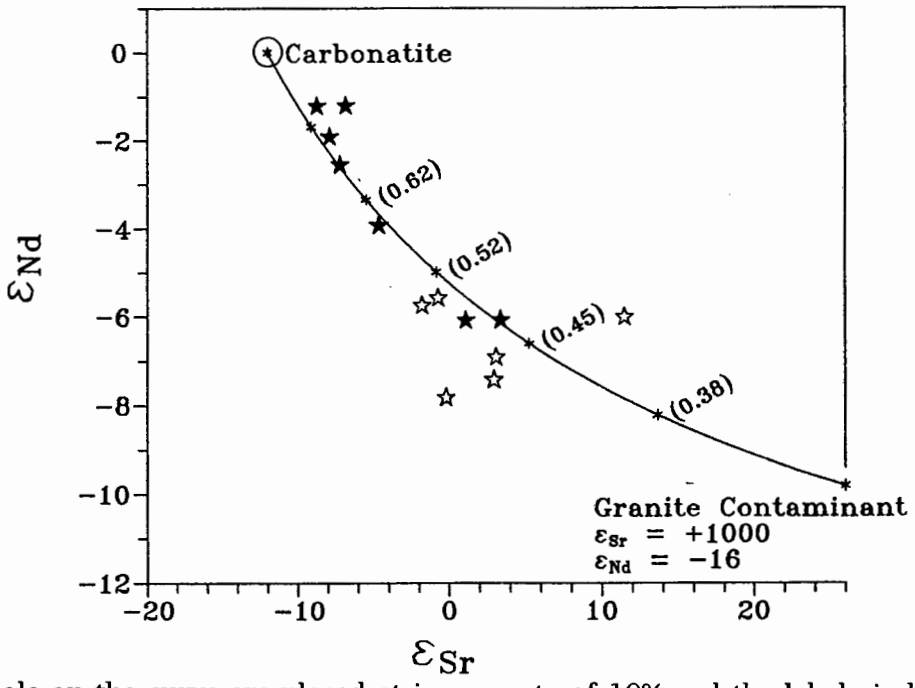

Symbols on the curve are placed at increments of 10% and the labels indicate the predicted Eu/Eu^* in the mix (see text for details). Ca-carbonatites are depicted as open stars; filled stars denote Mg-carbonatites.

In the following sections, the possibilities of crustal contamination of the Spitskop carbonatites through bulk assimilation, assimilation during fractional crystallisation and selective element transfer will be assessed.

7.3.3.1. Bulk contamination

If, as a first approximation, the isotopic signatures are assumed to be the result of bulk contamination, then the trend described by the data on the $\varepsilon_{(Sr)}$-$\varepsilon_{(Nd)}$ plot may be considered a mixing line between a "pristine" carbonatite composition isotopically similar to the Canadian Proterozoic carbonatites ("depleted" component "D"), and an enriched component in the bottom right quadrant of the diagram (component "E"). The shape of mixing lines on an $\varepsilon_{(Sr)}$-$\varepsilon_{(Nd)}$ plot are controlled by the relative Sr/Nd ratios of the two end members: straight mixing lines result when $Sr/Nd_D = Sr/Nd_E$; curved, concave down mixing lines when $Sr/Nd_D < Sr/Nd_E$; curved, concave up mixing lines when $Sr/Nd_D > Sr/Nd_E$ (e.g. Faure, 1986; Chapter 6). The concave-up trend defined by the Spitskop carbonatites, if interpreted as a mixing line, implies that the enriched component had Sr/Nd somewhat lower than the lowest value in the carbonatites i.e. less than 2.0. Such low Sr/Nd are not common but could

Figure 7.18 Plot of $\varepsilon_{(Nd)}$ *versus* europium anomaly (Eu/Eu^*) for Spitskop carbonatites.

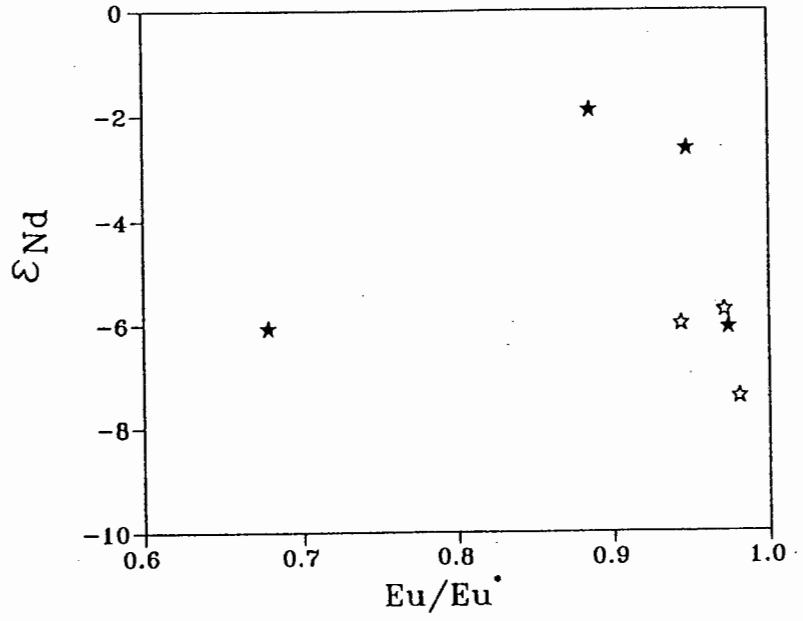

be generated in high-level crustal granitoids which have experienced significant feldspar fractionation.

Bushveld granite country rocks to the Spitskop Complex have experienced substantial feldspar removal (Kleeman and Twist, 1989) and Sr/Nd ratios of less than unity are noted in these rocks. Mixtures of a magnesio-carbonatite liquid having slightly less enriched $\varepsilon_{(Sr)}$-$\varepsilon_{(Nd)}$ than the Spitskop carbonatites ($\varepsilon_{(Sr)}$=-12.0; $\varepsilon_{(Nd)}$=0.0) and Sr and Nd concentrations equivalent to S59 (Sr=2582 ppm; Nd=89.5 ppm) with typical Bushveld granite (Sr=49 ppm; Nd=86.3 ppm; $\varepsilon_{(Sr)}$=+1000; $\varepsilon_{(Nd)}$=-16.0) produces values comparable to the calcio-carbonatite S53 ($\varepsilon_{(Sr)}$=+11; $\varepsilon_{(Nd)}$=-6) at 50% granite component in the mix (Figure 7.17)! This quantity of assimilant is unreasonably large: it is doubtful that a carbonatitic magma, generally considered a rather low temperature melt at shallow crustal levels (Treiman, 1989; Krafft and Keller, 1989; Dawson *et al.*, 1990) would be capable of dissolving such large volumes of granitic material and, if it could, it would no longer be a carbonatite! A partial melt of the granite would, assuming that some feldspar remained in the restite, have lower Sr/Nd but this would not appreciably lower the quantity of assimilant required.

Figure 7.19: Plot of $\varepsilon_{(Nd)}$ *versus* modelled source μ for Spitskop carbonatites.

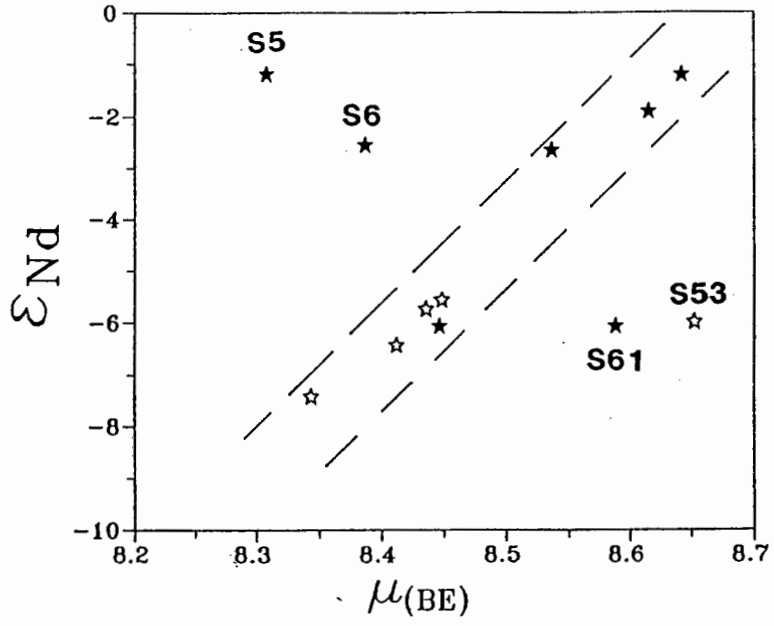

Ca-carbonatites are depicted as open stars; filled stars denote Mg-carbonatites.

Extensive feldspar fractionation has resulted in extreme negative Eu anomalies in the normalised REE patterns of the Bushveld Granites: Eu/Eu^* values (the ratio of the observed normalised Eu value to the value interpolated from Sm and Gd) are frequently <0.2 (e.g. Watterson, 1975). Bulk assimilation of such material should generate a progressive Eu anomaly in the contaminated carbonatite (see labelled tick marks on mixing line in Figure 7.17). No such tendency is evident in Figure 7.18 where most carbonatites have $Eu/Eu^*>0.85$.

Continued magma differentiation subsequent to contamination could mask any isotope-element correlations established during the contamination event. Carbonatite magmas are thought to be characterised by extremely high cation diffusion rates: $5x10^{-5}$ cm^2 sec^{-1} in comparison to $5x10^{-8}$ cm^2 sec^{-1} for basalts (Treiman and Schedl, 1983; Treiman, 1989). The fact that isotopic variations persist amongst the Spitskop carbonatites would imply that the elemental variations induced by the contamination should also be preserved.

A further argument against contamination by Bushveld granite in particular, and upper crustal granites in general, is provided by the Pb isotope data. Bushveld granites are enriched in U and Th (Kleeman and Twist, 1989) and, like model upper crust (e.g. Zartman and Doe, 1981), have highly radiogenic Pb isotope ratios. In Figure

7.19, the bulk of the Pb ratio data in the carbonatites (expressed as μ at 1341 Ma modelled relative to the Kwon *et al.* (1989) reservoir) define a positive correlation when plotted against $\varepsilon_{(Nd)}$ - i.e. the "deviant", low-$\varepsilon_{(Nd)}$ carbonatites have the *lowest* μ's, the opposite of the effect anticipated from upper crustal contamination. Samples S05-S06-S61-S53 possibly describe a crossing trend which would be consistent with an increased upper crustal component in S53 relative to S05 and may identify minor crustal Pb assimilation.

An earth reservoir known to have the combination of negative $\varepsilon_{(Nd)}$, slightly positive $\varepsilon_{(Sr)}$ and unradiogenic Pb is continental lower crust, in particular those portions in the granulite facies (e.g. Weaver and Tarney, 1980; Rogers and Hawkesworth, 1982; Van Calsteren *et al.*, 1986). Contamination of carbonatite with material such as the granulitic xenoliths sampled by Lesotho kimberlites (Van Calsteren *et al.*, 1986) or the Lewisian granulites (Weaver and Tarney, 1980) could potentially produce the anomalous isotopic signatures in the Spitskop carbonatites. The Sr/Nd ratios in these materials are all too high, however, to generate the concave-up trend noted in the carbonatites through bulk assimilation. Menzies and Halliday (1988), however, described *mantle* xenoliths from Loch Roag in Scotland with suitable isotopic signatures, some samples also having low Sr/Nd ratios. Interaction between carbonatite melt with such mantle material would generate the Spitskop isotopic patterns without the involvement of crust.

7.3.3.2. Combined Assimilation - fractional crystallisation (AFC)

From the equations presented by De Paolo (1981) it is possible to show that an isotopically "primitive" carbonatite magma (i.e. with $+\varepsilon_{(Nd)}$ and $-\varepsilon_{(Sr)}$) crystallising and interacting with isotopically "enriched" wallrocks will produce a steep $\varepsilon_{(Sr)}$-$\varepsilon_{(Nd)}$ trend only if the bulk distribution coefficient of the crystallising assemblage for Nd is significantly greater than that for Sr (i.e. Nd is more compatible than Sr). Little is known about crystal-liquid partitioning in carbonatites and even less about liquid-vapour partitioning so this process is difficult to evaluate rigorously. Considering the mineral phases likely to crystallise over significant intervals during the solidification of a carbonatite: olivine, Ca-Mg-Fe carbonates, apatite, soda-amphibole, soda-pyroxene, magnetite; it is difficult to derive a realistic crystallising assemblage that would produce the required relationship in bulk distribution coefficients.

Roden *et al.* (1985) developed an AFC model to explain the isotopic variability in the carbonatites of the Jacupiranga Complex, where the carbonatites are regarded as the final residues produced by the differentiation of mafic and ultramafic silicate

units in a crustal magma chamber. In this model progressive crustal interaction accompanies the fractional crystallisation: as a result the carbonatite residues are isotopically-*enriched* (i.e. higher $\varepsilon_{(Sr)}$, lower $\varepsilon_{(Nd)}$) than the silicate components. Such an AFC solution is clearly untenable for the Spitskop Complex where the carbonatites are *less* isotopically-enriched relative to the ijolites and nepheline syenites (see Chapter 5).

7.3.3.3. Contamination through element-selective transfer processes

"Element-selective material transfer processes" were invoked by Andersen (1987) to explain the enriched isotopic compositions of certain carbonatites (rödbergites) in the Fen Complex, Norway. No details were provided by Andersen as to how these transfer processes acted nor were any attempts made to quantify their effect. If such processes do act, then one could postulate that at Spitskop the transfer agent(s) selectively added upper crustal Nd into the carbonatites but excluded both Sr and Pb.

Evidence for fluids capable of selectively transporting elements *from* the silicate components of the Spitskop complex into the surrounding crustal rocks has been documented in the discussion of the fenitisation in Chapter 6. It is conceivable that any elements dissolved out of the country rocks by these fluids could, in turn, be transported back into the carbonatite and/or silicate units of the Complex. Observations of the element transfers during fenitisation are presented in Chapter 6 and indicate that Nd was indeed partitioned into the metasomatising fluid whereas Sr was partitioned strongly into the fenites. Such selective transfer of Nd relative to Sr could produce enriched $\varepsilon_{(Nd)}$ in the carbonatites without the associated major and trace element trends anticipated for bulk assimilation. The variation of Pb in the fenitised granites (Figure 7.20), however, suggests that Pb would also be leached into the fluid phase and so the correlation between $\varepsilon_{(Nd)}$ and μ in the carbonatites is not consistent with selective contamination from upper crustal rocks. In addition, the LREE and MREE are also partitioned into the fluid and so the Eu anomaly characteristic of upper crustal granites should also have been transferred into the carbonatites along with the Nd.

These observations indicate that element-selective transfers from the country rock granites through the action of the fenitising fluid are not consistent with the isotopic and elemental trends in the carbonatites.

Figure 7.20: Plot of $^{87}Sr/^{86}Sr_{1341Ma}$ versus Pb in progressively fenitised granitic country rocks to the Spitskop Complex.

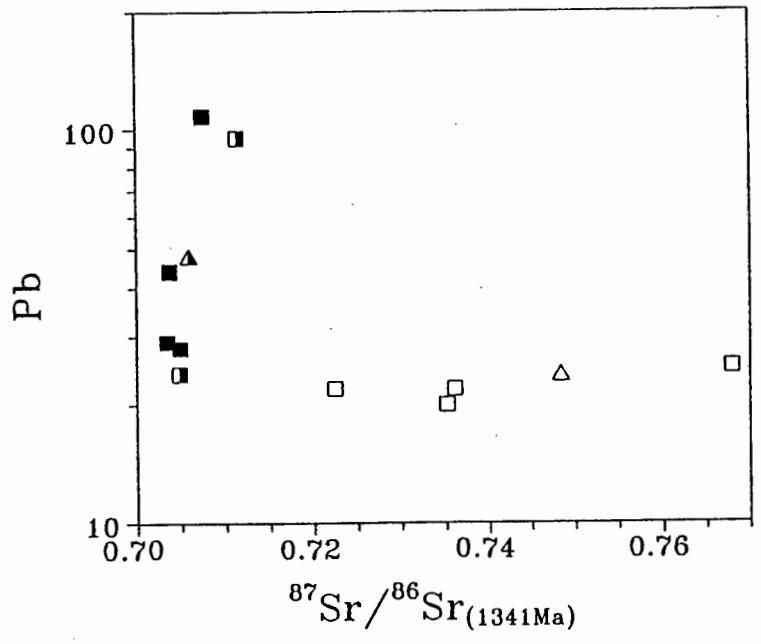

Progressive fenitisation is indicated by decreasing value of $^{87}Sr/^{86}Sr_o$. Open symbols indicate quartz fenites; half-filled symbols feldspar fenites; solid symbols nepheline-fenites.

7.3.3.4. Conclusion

None of the mechanisms considered above offer a totally convincing explanation of the isotopic characteristics of the carbonatites. Element-selective exchange between carbonatite magma and *lower crustal* materials compositionally similar to the Lesotho granulite xenoliths, via the medium of a fluid phase emanating from the carbonatite, could provide a mechanism which satisfies most elemental and isotopic constraints. Alternatively, the isotopic characteristics of the Spitskop carbonatites are primary and reflect the compositional history of their source region. This possibility is favoured and will be investigated further in the concluding chapter of the dissertation after the available data for the other Pilanesberg Suite complexes have been presented.

7.4. The petrogenetic relationship between the silicate and carbonatite units in the Spitskop Complex.

The close spatial association of silicate and carbon-atitic units in the Spitskop Complex provides an excellent opportunity to evaluate the possible petrogenetic links between these chemically disparate rock types. Currently favoured models for the genesis of carbonatites and alkaline rocks involve variations or combinations of essentially three possibilities (Gittins, 1989):

(i) carbonatites form as residues from the fractional crystallisation (at crustal pressures) of a mantle-derived, carbonated parental liquid, usually nephelinite (e.g. Nielsen, 1980; Roden *et al.*, 1985; Wyllie *et al.*, 1990);

(ii) carbonatites and associated nephelinitic and phonolitic silicate rocks represent immiscible fractions of a mantle-derived parental magma (e.g. Le Bas, 1977, 1981, 1987, 1989; Freestone and Hamilton, 1980; Kjarsgaard and Hamilton, 1988, 1989);

(iii) carbonatites represent primary melts from carbonated mantle (Olafsson and Eggler, 1983; Gittins, 1989; Wallace and Green, 1988; Ryabchikov *et al.*, 1990).

A direct petrogenetic relationship between silicates and carbonatites is explicit in models (i) and (ii) but not in (iii).

In the following sections the petrological data from Spitskop will be evaluated in the light of these models.

Figure 7.21: Variation of Mg# and CaO amongst the magmatic components of the Spitskop Complex.

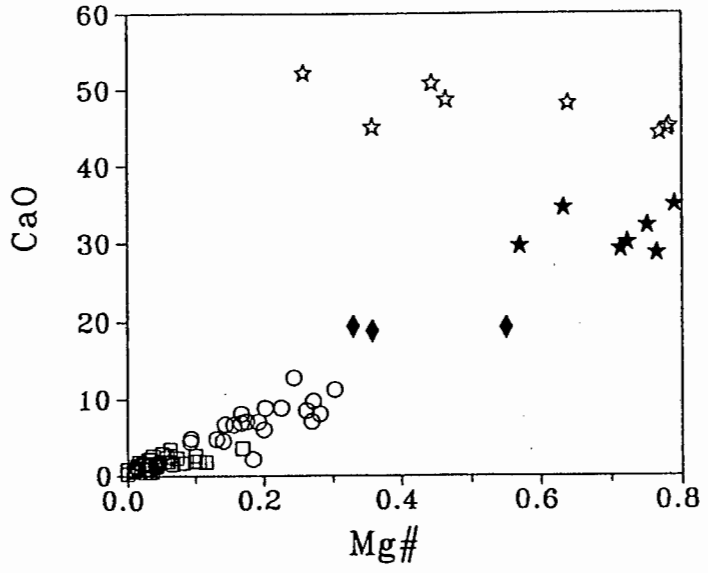

Symbols are: pyroxenites: filled diamonds; open circles: Type-I ijolites; open squares: nepheline syenites; open stars: calcio-carbonatites; filled stars: magnesio-carbonatites.

7.4.1. Carbonatites as residues after fractional crystallisation

Any model of carbonatite genesis must satisfy the universal observation that carbonatites always constitute a late, if not the latest, phase of igneous activity in a carbonatite-silicate igneous complex. Option (i) above satisfies this criterion and has been invoked to explain the carbonatites in the Jacupiranga (Roden *et al.*, 1985) and Gardiner (Nielsen, 1980) Complexes. Gittins (1989) raised several pertinent arguments against the viability of this model. Firstly, Gittins regarded the solubility of CO_2 in nephelinite magmas as insufficient to be able to generate a carbonatitic residue. Also, to produce a carbonatite magma as a residue after differentiation of a nephelinite, Ca, Mg and Fe would have to behave incompatibly, i.e. they should partition towards the residual, CO_2-rich phase. Early crystallising phases in nephelinitic magmas are olivine and clinopyroxene (e.g. Le Bas, 1978; 1987) and so fractional crystallisation should deplete rather than enrich the residue in Ca and Mg.

Data presented in the sections above indicate that the silicate units at Spitskop are not the products of progressive closed-system fractionation of a single parental

magma. Variation of Mg# and CaO in the silicate and carbonatite units of the Spitskop Complex is depicted in Figure 7.21. It is clear from this Figure that MgO and CaO do not vary systematically with age through the units of the Complex. Mg# and CaO decrease progressively with decreasing age of silicate unit, CaO attains its maximum concentration in the calcio-carbonatite whereas MgO is most enriched in the geologically youngest magnesio-carbonatite unit.

If the magmatic evolution of a parental silicate magma to produce a carbonate residue takes place in a closed system, then the Sr, Nd and Pb isotopic ratios should be equivalent in the silicate and carbonatitic fractions. If open system, AFC-like processes operated, the carbonatite would contain a larger proportion of the isotopic signature of the assimilated crustal component than the associated silicate rocks. This relationship is observed in the Jacupiranga carbonatite (Roden *et al.* 1985). At Spitskop, the Sr and Nd isotope relationships show the reverse of this trend: ijolites and nepheline syenites have more enriched $\varepsilon_{(Sr)}$-$\varepsilon_{(Nd)}$ signatures than do the associated carbonatites.

Chemical and isotopic relationships therefore indicate that the carbonatite components at Spitskop cannot represent late stage residues from the differentiation of the silicate magmas.

7.4.2. Carbonatites as immiscible liquids

Formation of carbonatite through immiscible exsolution from phonolitic or nephelinitic magma has been championed by Le Bas in several communications (Le Bas, 1977, 1981, 1987, 1989). Immiscibility in artificial silicate-carbonate systems was first described by Koster van Groos and Wyllie (1966, 1968, 1973) and has been investigated in natural systems by Hamilton and co-workers (Freestone and Hamilton, 1980; Kjarsgaard and Hamilton, 1988, 1989; Hamilton *et al.*, 1989). Most of these experiments were performed at crustal pressures (<7 kbars). Baker and Wyllie (1990) tested immiscibility at upper mantle pressures and argued that "..carbonatitic melts are unlikely to be produced by immiscible exsolution from carbonated silicate liquids at pressures between 20 and 30 kbar."

Partitioning of trace elements between phonolitic and nephelinitic silicate liquids and conjugate sodic to calcic carbonatitic liquids was investigated experimentally by Hamilton *et al.* (1989). Data for Ba and selected REE are shown in Figure 7.22. These data predict that, for immiscible liquid pairs produced over the pressure and temperature range studied (1050-1250°C; 0.8-4 kbars), the Ba/LREE ratio

Figure 7.22: Partition coefficients for Ba and REE between immiscible carbonatite and silicate liquids.

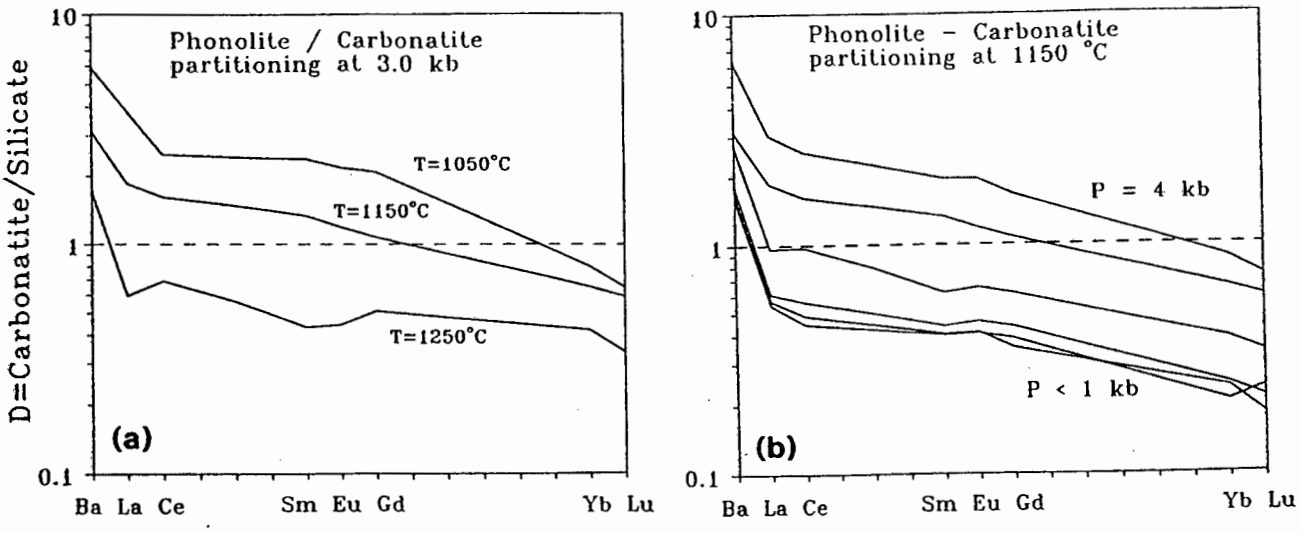

Variations in partition coefficient are shown for (a) changing temperature at 3 kbars; and (b) changing pressure at 1150°C (curves are for 0.8, 0.86, 1, 2, 3 and 4 kbars). Data from Hamilton *et al.* (1989).

should be substantially higher in the carbonatite liquid relative to the silicate liquid. In Figure 7.23 Ba/La increases progressively from the carbonatites through the ijolites to the nepheline syenites. This trend is contrary to that anticipated had the Spitskop carbonatites developed through immiscible exsolution from the ijolites and/or nepheline syenites.

At the point of separation of immiscible liquid fractions, phases in each liquid must be in equilibrium with both carbonate and silicate liquids. This requirement was invoked by Le Bas and Aspden (1981) to contend that the occurrence of fluid inclusions in ijolite apatites compositionally similar to natro-carbonatite was strong evidence in favour of immiscibility. It is obvious that the isotopic composition of the heavier elements (Sr,Nd and Pb) must also be identical in each liquid phase at separation. Immiscible carbonatite and silicate fractions would only have differing isotopic signatures if they interacted with crustal to differing extents after separation. The observation that carbonatites invariably post-date the silicate rocks in alkaline complexes make the mechanics of this process difficult to visualise.

As a consequence, the marked contrast in Sr and Nd isotopic composition between the carbonatites and associated silicates in the Spitskop Complex is considered a strong argument against a derivation through liquid immiscibility.

Figure 7.23: Variation of the Ba/La between the silicate and carbonatitic components of the the Spitskop Complex.

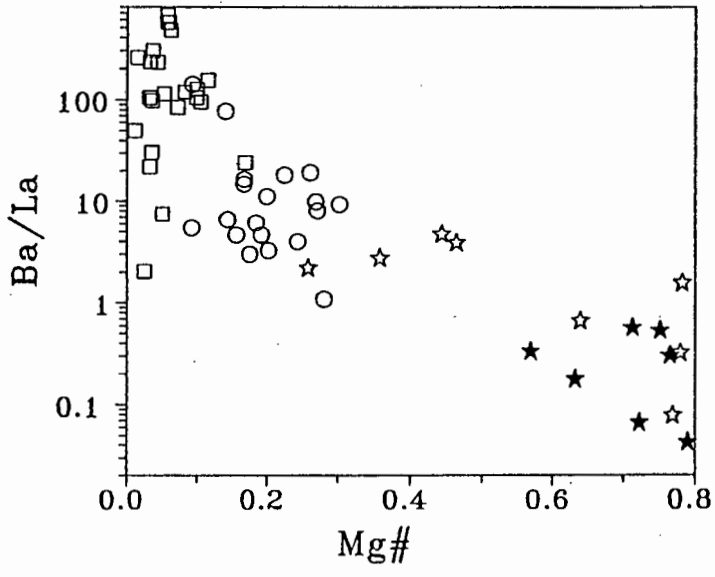

Symbols are as in Figure 7.21.

7.4.3. Carbonatites as primary magmas

Derivation of the Spitskop carbonatites from the silicate units either as residues after fractional crystallisation or through immiscible exsolution may be rejected on geochemical and isotopic grounds. As a consequence, the option that the Spitskop carbonatites may represent differentiates of primary carbonatite magmas must be considered. This option carries the implication that, petrogenetically, the silicate and carbonatite units at Spitskop may be unrelated or related only indirectly.

In a critical review of carbonatite petrogenesis, Gittins (1989) proposed that carbonatite magmas are formed as primary melts of carbonated mantle and undergo extensive differentiation *en route* to the surface. Eggler (1989) argued that carbonatite mantle melts would be dolomitic, have high Mg# (>0.64) and have high concentrations of transition metals, particularly Ni. Gittins (1989) pointed out, though, that carbonatite melts would derive from carbonated peridotite and suggested that during carbonation Ni would be retained in residual olivine in

preference to the carbonate phase. Since melting of the carbonated peridotite would largely involve the carbonated phase, low Ni contents would be anticipated in the partial melt. Wallace and Green (1988) were the first to demonstrate experimentally that carbonatitic liquids could be produced as direct melts of carbonated amphibole peridotite at upper mantle pressures. Carbonatite melt produced in the Wallace and Green (1988) experiments had an Mg# of 0.85 and small but significant amounts of alkalis, SiO_2 and Al_2O_3. Melting studies on mantle materials with P_2O_5 also produced carbonatite melts with Mg# in excess of 0.80 or higher (Ryabchikov *et al.*, 1990; 1991).

In Figure 7.24 the MgO and Mg# values in the magmatic components at Spitskop are compared where it will be noted that the magnesio-carbonatites have Mg# and MgO high enough to be considered primary mantle melts. It is interesting to note that of all the Spitskop rocks, the magnesio-carbonatites have the most "mantle-like" $\varepsilon_{(Sr)}$ and $\varepsilon_{(Nd)}$ signatures. These observations are thus consistent with (but in no way prove) an origin for the Spitskop Mg-carbonatites as near-primary melts from the mantle. The calcio-carbonatites have low MgO contents and Mg# and are thus "evolved" relative to the magnesio-carbonatites.

Further discussion of the possible genetic relationships between carbonate and silicate fractions in alkaline complexes will be presented in the final chapter of this dissertation after presentation of new data from other complexes within the "Pilanesberg suite" of intrusions.

Figure 7.24: MgO-Mg# variations in the Spitskop carbonatites.

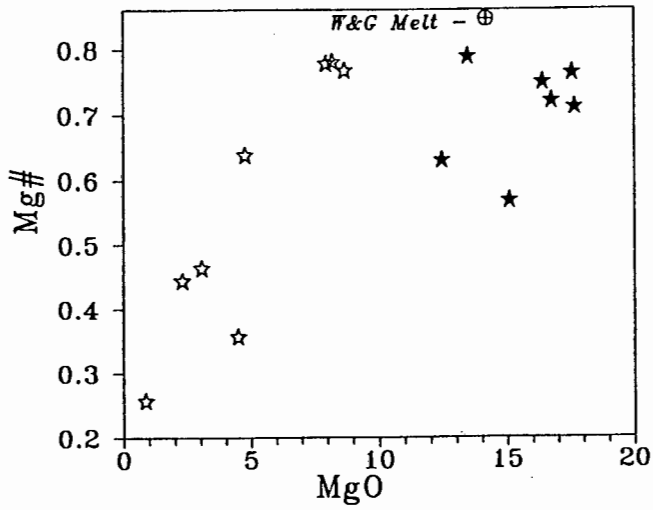

Calcio-carbonatites are shown as open stars; magnesio-carbonatites as filled stars. Circled cross is the composition of carbonatite melt in equilibrium with amphibole lherzolite mantle determined experimentally by Wallace and Green (1988).

7.5. *Concluding summary*

Magmatic activity in the Spitskop Complex started with a silicate phase during which pyroxenite, ijolite and nepheline syenite were sequentially emplaced. These silicate units were then intruded by a compositionally-composite plug of carbonatitic magma.

Chemical relationships between the different silicate units indicate that the pyroxenites, ijolites and nepheline syenites are unlikely to represent the products of progressive differentiation of a single starting magma. The pyroxenites probably represent cumulates from ijolitic magma more primitive than that represented amongst the fine-grained Type-I ijolites. Differences in REE patterns in the ijolites and nepheline syenites can not be explained by separation or accumulation of any plausible combination of the major mineral phases found in the Type-I ijolites and nepheline syenites but suggest a possible role for accessory phases such as apatite or titanite.

In addition, chemical relationships and isotopic differences argue that the carbonatitic units were not derived through magmatic differentiation nor as an exsolved immiscible liquid from the silicates. Variations of trace elements within the

magnesio- and calcio-carbonatites indicate that the carbonatites were derived from the sequential emplacement of two discrete carbonatitic magmas and are not related through low pressure (i.e *in situ*) evolution of a single carbonatite liquid.

Available petrological evidence thus suggests that the different silicate and carbonatitic units in the Spitskop Complex were derived from a number of compositionally distinct magma compositions. With the data now available for the Spitskop Complex, and the current understanding of processes acting in carbonatite-bearing alkaline complexes, it is not possible to derive a quantitative petrogenetic model for the origin and evolution of these different magmas.

The comparative isotopic and geochemical compositions of associated carbonatite and silicate rocks can, however, be usefully applied to evaluate current models to explain the petrogenetic links between these contrasted magma types. Current models for the derivation and evolution of carbonatites and their petrogenetic association with spatially related silicate magmatism will be reviewed in the last chapter and evaluated in the light of the new isotopic and geochemical data from Spitskop and the other Pilanesberg Suite complexes to be presented in the next chapter.

Chapter 8: Other Pilanesberg Suite Intrusives

8.1. Introduction

As discussed in the opening chapter, the Spitskop Complex is one of a number of alkaline complexes which intruded into the central parts of the Kaapvaal Craton in the time period 1200 - 1450 Ma. The general geology and geochemistry of these associated complexes are briefly reviewed in this chapter in order to consider the data from the Spitskop Complex in a more regional context.

In discussing the data from the other Pilanesberg Suite complexes, particular emphasis will be placed on those aspects of the geochemical and isotopic composition of the carbonatitic components of each complex which contribute to an assessment of the petrogenetic models for the origin and evolution of carbonatites and associated silicate rocks which will be reviewed and evaluated in the next chapter.

Geochemical comparisons made in Chapter 7 between the silicate and carbonatite components of Spitskop indicate that the carbonatites are likely to have evolved from mantle-derived primary carbonate magma. The Sr and Nd isotopic data for the Spitskop carbonatites were shown to be somewhat anomalous relative to available data from carbonatites elsewhere and the suggestion was made that these differences may be due to differences in source composition. Data from the other Pilanesberg Suite complexes are important to evaluate whether the anomalous isotopic signatures at Spitskop are a reflection of lithospheric mantle compositions below the whole Kaapvaal Craton during the Proterozoic.

8.2. General Geology of the Complexes

Detailed field and petrographic descriptions of all the carbonatite-bearing complexes are provided by Verwoerd (1967) and only salient features will be

highlighted here. The complexes are considered in sequence from east to west. Carbonatite terminology is that originally used by Verwoerd (1967).

8.2.1.Pienaars River Alkaline Complex.

Components of the Pienaars River Alkaline Complex (PRAC) are arranged in a ca.70 km linear belt trending north-westwards from the Franspoort locality east of Pretoria (see Figure 8.1). The PRAC does not reflect a true stratigraphic "unit" as such but is merely a convenient group term utilised by SACS (1980) to describe a number of alkaline intrusions of widely differing lithologies and ages (Shand, 1921b, 1922; Harmer, 1985).

8.2.1.1.Franspoort nepheline syenite:

This complex was emplaced into the Magaliesberg quartzite to the north of Mamelodi in north-eastern Pretoria. Outcrops are generally poor but, where boulders

Figure 8.1: Locality map showing distribution of the components of the Pienaars River Alkaline Complex.

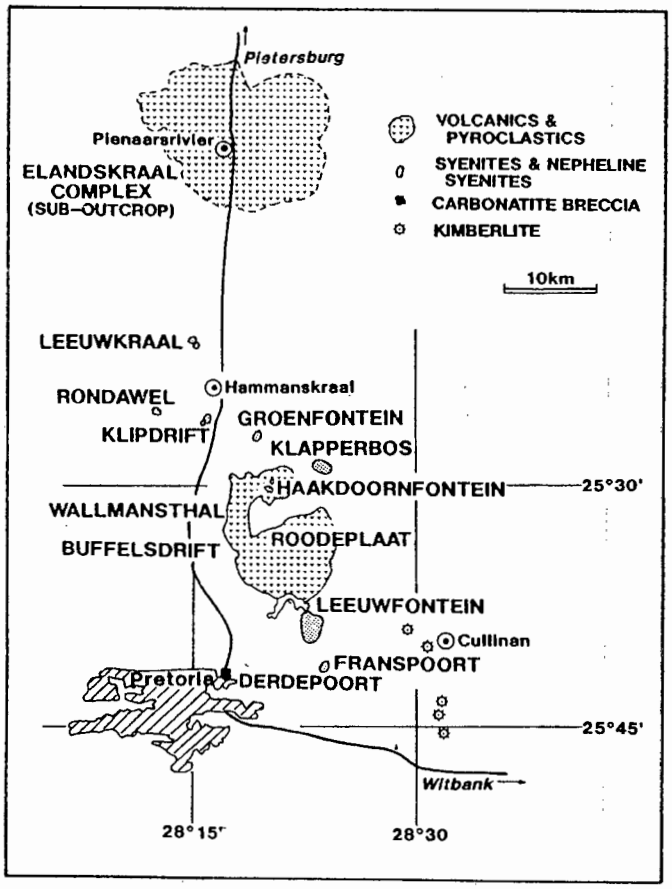

are found, the rocks are extremely fresh. The complex consists of two apparently discontinuous patches of rock: nepheline syenite in the south and related phonolitic lava further north. The syenite consists of perthitic feldspar laths with interstitial nepheline, sodalite and green sodic pyroxene intergrown in classic "foyaitic" texture (as described by Sörensen, 1974).

8.2.1.2.Derdepoort Carbonatite

The position of this carbonatite has given rise to the poort in the Magaliesberg through which the N1 freeway now passes north of Pretoria: the carbonatite forms a low rounded hill on the eastern side of the poort. Outcrops are poor and comprise brown- weathering dolomite-ankerite-carbonatite ("beforsite") with abundant silicate xenoliths of quartzite, sandstone, chloritic mafic material, syenite and lamprophyre. The lamprophyric rock was once prospected because of its close resemblance to kimberlite but analyses reported by Verwoerd (1967) demonstrated that the rock is an alnöite. Two carbonatite samples free of any silicate material were selected for analysis.

8.2.1.3.Leeuwfontein Complex.

Lying south of, and partially covered by, the Roodeplaat Dam, the Leeuwfontein Complex consists of a composite plug of various feldspathic syenites overlain by porphyritic trachytic lavas. No sediments intervene between the lavas and plutonics and the syenites commonly carry xenoliths of the trachytes. It would appear that the complex represents the eroded remnant of a trachytic volcano, where the syenitic sub-volcanic units have risen upwards, stoping into their volcanic roof rocks. A range of syenite types are found: the complex is mostly composed of silica-saturated grey to grey-orange amphibole syenite (syeno-diorite: Toens, 1952), with a core of distinctive, red alkali syenite composed of platy, brick-red feldspars. A body of nepheline syenite is also found along with abundant dyke rocks varying in composition from syenite to "bostonite" (Shand, 1921b; Toens, 1952).

8.2.1.4.Roodeplaat "Caldera" and related subvolcanic plugs

Described as a collapsed caldera structure by Frick and Malherbe (1986), the Roodeplaat volcano consists of an outer rim of trachytic tuffs and lavas with an inner zone of water-lain pyroclastic sediments. The volcanics are intruded by syenite and monchiquite dykes and by late-stage breccias. Plugs of alkaline syenitic material intrude the outer parts of the complex and are thought to be genetically related to the lavas (Frick and Malherbe, 1986). These plugs include the Buffelsdrift Foyaite

(peralkaline, K_2O-rich), Wallmansthal Foyaite, Haakdoornfontein Syenite (composite, silica-saturated syenite) and the Klapperbos Foyaite. Two distinct geochemical fractionation sequences were documented by Frick and Malherbe (1986): a "trachytic" lineage and an "albite-syenite" type, the latter trending to an over-saturated end point. Samples from the Buffelsdrift foyaite and Haakdoornfontein syenites (Harmer, 1985) were analysed during the present study.

8.2.1.5.Klipdrift Syenite

The Klipdrift Syenite is a small plug of a uniform-textured, quartz syenite composed of distinctive, zoned orange alkali feldspar and minor interstitial soda amphibole. These handsome syenites are quarried for facing stone.

8.2.1.6.Rondawel syenite

The Rondawel centre consists of a plug of orange quartz syenite. Xenoliths of trachytic lava in the syenite suggest that the present erosion level is close to the original volcanic / sub-volcanic interface.

8.2.1.7.Leeuwkraal Phonolite

The Leeuwkraal occurrence is poorly exposed but comprises peralkaline phonolite porphyry and lava probably representing a feeder with remnant of associated eruptives (Shand, 1922).

8.2.1.8.Elandskraal Volcano

Drilling of aeromagnetic anomalies near Pienaarsrivier, north of Pretoria, led to the discovery of the Elandskraal "Volcano" structure below cover rocks of Karoo sediments and volcanics. The Elandskraal Volcano is composed of alkali basalts, trachytes and interbedded pyroclastics and thus represents the northern-most component of the Pienaars River Complex (Frick and Walraven, 1985).

8.2.2.Tweerivier

Tweerivier is situated north of Brits (see Figure 1.1) and consists of two carbonatite plugs that represent the eroded conduits of two partially coalesced complexes (Verwoerd, 1967). Although poorly exposed, the essential features were determined by Verwoerd (1967) from a series of boreholes drilled by the Pretoria Portland Cement Company in the 1950's. These borehole cores show that the "conduits" are choked with xenolithic material: the northern body with Transvaal

Sequence meta-sediments; the southern exclusively containing gabbros and magnetitites from the Bushveld. All xenoliths are extensively intruded by dykelets of sövite and minor beforsite. Fenitisation of the surrounding Bushveld granites is noted and testifies to the true magmatic nature of the Tweerivier carbonate (e.g. Le Bas, 1981). Samples for the present study were from boulders of sparry sövite found in the southern part of the complex. Isotope analyses were also performed on the Mintek secondary reference standard S-8, a Tweerivier carbonatite.

8.2.3.Bulhoek

Closely associated with Tweerivier, Bulhoek represents the uppermost level of a carbonatite intrusion. The prominent hill at Bulhoek is due to the more resistant nature of the fenitised granite around the intrusion in relation to normal Bushveld Granite. Outcrops on the western and southern slopes of Bulhoek hill show spectacular breccia zones representing channellways where carbonatite magma has streamed through the granite, disaggregating and metasomatising the country rock. Granite fragments range from <5mm to over 30cm in size; the larger are usually elongate and appear to have been plastically-deformed during the extensive fenitisation. The granite in the Tweerivier-Bulhoek region contains abundant xenolithic fragments of Transvaal quartzite (shown on the 1:250 000 Geological map and on the maps in Verwoerd, 1967) and in places the carbonatite breccias at Bulhoek contain fragments of quartzitic sediments that were freed from the granite matrix during emplacement of the carbonatite. Near the crest of Bulhoek hill dykes of sideritic carbonatite are noted. A large patch of apatite-rich beforsitic carbonatite may be found on the south-eastern part of the complex, below the saddle in the Bulhoek hill.

Samples of carbonatite were collected from dykes near the centre of the complex which were totally free of any macro- or micro-scopic evidence of foreign material.

8.2.4.Kruidfontein

Kruidfontein is a high-level volcanic complex composed of two large concentric rings of pyroclastic breccia, tuffs, siliceous lavas (both intermediate and mafic) and a central mass of carbonatite (Verwoerd, 1967: p153-170). Significant relief affords good exposure of the structure of this complex.

Much of the central carbonatite is a replacement after original siliceous lava and pyroclastics for which Verwoerd (1967) used the term meta-carbonatite It is proposed that the prefix "para-" would be more suitable for these types of "secondary" carbonatite and will be adopted in this discussion. Interbedded with the siliceous pyroclastics are bands of fine-grained, well-bedded, blue carbonate material. Most of these bands were regarded as carbonate replacement zones by Verwoerd but have recently been re-interpreted as primary carbonatite tuffs and pyroclastics (Clarke, 1989; Clarke *et al.*, in press). Calcite and dolomite pseudomorphs after nyerereite ($Na_2Ca(CO_3)_2$, the principle constituent of the east African soda carbonatites such as Oldoinyo L'engai) are discernible in some tuff samples (Clarke, 1989). Primary carbonatites occur as dykes 2 to >10m in width cutting through the beds of tuff and para-carbonatite. Samples for analysis were collected from these dyke carbonatites. Carbonatite analyses presented in Clarke *et al.* were added to the database.

A unique feature of the Kruidfontein Complex is the association of mafic lava ("alkali-basalt"), which occurs as an eccentrically-disposed flow, emplaced prior to the eruption of the pyroclastic material. Clarke (1989) reported the occurrence of similar material as dyke rocks elsewhere in the complex.

8.2.5.Nooitgedacht (SACS proposal: Gelukshoek)

Poorly exposed, Nooitgedacht consists of a sub-volcanic plug of sövite with minor bodies of beforsite and "quartz-parankerite sövite" (Verwoerd, 1967: p102-113). Outcrops of nepheline syenite are found in the country rocks and these presumably represent dykes related to the carbonatite mass.

8.2.6.Pilanesberg

Forming a large circular complex approximately 30 kms in diameter, Pilanesberg is composed of a sequence of cone sheets partially overlain by volcanics and pyroclastics which currently form a thin cover draped over the cone sheets. The plutonics are all agpaitic (i.e. in the sense of Edgar, 1974; 1977: peralkaline with very high concentrations of Zr, Ba, Sr and REE) and range in composition from undersaturated white and green foyaites, including lujavrite (eudialyte-bearing foyaite), to saturated red and white syenites, and a small central plug of riebeckite-granite.

Detailed descriptions of the geology of this complex are provided in Retief (1963), Lurie (1973) and Lurie and Cawthorn (1984).

8.2.7.Goudini (SACS proposal: Ystervarkkop)

Oval in outline, approximately 5.5x4.5 km in size, Goudini represents an eroded volcano structure containing partially carbonated pyroclastics and volcanics (Verwoerd, 1967; p113-152).

Surface exposures largely consist of fine, black tuff, a ring of volcanic breccia and an eccentrically disposed central plug of carbonatitic material. Much of the central carbonate mass is undoubtedly para-carbonatite: the result of near-total carbonation of earlier silicate volcanic and pyroclastic material. That much of the carbonate is secondary after silicate volcanics is spectacularly demonstrated at the peak of the Goudini hill where volcanic pillow structures and inter-pillow matrix and breccia have been totally replaced by dolomite-albite-aegerine para-carbonatite (Verwoerd, 1967; 1990). Rare clasts recovered from the volcanic breccia suggest that the original volcanic material was nephelinitic in composition (Verwoerd, 1990).

Inter-bedded with the tuff beds are zones of carbonate material. These horizons were initially interpreted as carbonate replacements by Verwoerd (1967) but could equally represent carbonatite air-fall tuffs and carbonate precipitates from the intra-crater lake. Soft-sediment deformation structures (load casts) are common features in these carbonate bands.

In the south-central part of the complex a large zone of Bushveld mottled anorthosite occurs, totally enclosed by tuff. The anorthosite is partially metamorphosed by the complex and is interpreted as a large block of country rock which foundered into the vent during the development of the Goudini volcano (Verwoerd, 1967). Intruded into the anorthosite is a spessartite lamprophyric dyke containing strongly zoned titan-augite phenocrysts.

Nelson *et al.* (1988) included two samples from Goudini in their survey of world carbonatites. From the textures and minerals listed in their petrographic description of the samples ("..radial aggregates of green amphibole .. scapolite .. nepheline .. albitised plagioclase ..", etc.) it is obvious that the material was collected from the zone of carbonated breccia and clearly does not represent primary, intrusive, magmatic carbonatite.

8.2.8. Glenover

Poorly exposed and mostly sand covered, the complex comprises a mica-apatite-pyroxenite plug with concentrations of sövite and beforsite towards the centre. This complex was not studied during the current investigation.

8.2.9. Stukpan

Stukpan is the most recently discovered of the Pilanesberg Suite complexes and sub-outcrops below Karoo-aged cover on the farm Stukpan 435, in the general region of the De Bron horst, 20 km east of Bothaville in the OFS. A preliminary description of the discovery and general petrography of the complex was presented by Verwoerd *et al* (1986).

The geology of the carbonatite is known only from geophysical modelling and from intersections in two boreholes. Essentially elliptical in plan, the body is large, measuring approximately 3.1 by 1.7 km and, as such, it represents the largest carbonatite within the Pilanesberg suite. The carbonatite comprises fine- to medium-grained sövite with minor dolomitic (beforsite) bands. Streaks and bands of blue sodic amphibole are common, as are zones of phlogopite and magnetite concentrations, which sometimes reach 20 and 10 mm in diameter, respectively. Apatite is abundant.

One of the exploration boreholes was positioned on the flank of the carbonatite and penetrated the quartzite country rocks. Fenitisation of the quartzite is noted to varying degrees and is reflected by the growth of pink alkali feldspar. The carbonatite also contains blocks of mafic material which were originally logged as "amphibolite" and thought to be an integral part of the intrusion. These blocks are composed of aggregates of pleochroic sodic pyroxene and amphibole which are clearly secondary metasomatic minerals. Isotope data on these "amphibolites" (discussed below) indicate that they are not an integral magmatic part of the Stukpan Complex but represent fenitised xenoliths of earlier volcanics, possibly Ventersdorp Supergroup material.

8.2.10.Bull's Run

Situated in the frontal nappe zone of the Natal Mobile Belt, the Bull's Run intrusion has long been known as a "syenitic complex" (Du Toit, 1931; Charlesworth, 1981). Recent detailed mapping of this area revealed the presence of highly peralkaline nepheline syenites with associated patches of gneissose carbonatite (Scogings and Forster, 1989)! The carbonatites are all calcitic. High concentrations of Sr, Ba, Nb and REE, high LREE/HREE with no Eu anomaly, and the occurrence of pyrochlore suggest a magmatic origin for the carbonatite. The complex has been tectonised and hence predates the final thrusting event in the Tugela region (i.e. is pre-1100Ma: Barton, 1983).

Although geographically removed from the other carbonatite complexes, the Bull's Run occurrence could be grouped with the Pilanesberg Suite complexes on the basis of its age and the fact that it intrudes the margins of the Kaapvaal Craton.

Table 8.1: Preferred dates for the PRAC components.

Grouping	Date	$^{87}Sr/^{86}Sr_{(i)}$	$\varepsilon_{(Sr)}$	MSWD (n)
Quartz Syenites (Rondawel, Haakdoornfontein, Klipdrift)				
all samples:	1464 ± 56	0.7041 ±0.0003	+17 ±5	5.4* (15)
ex H2, H3	1482 ± 33	0.70410 ±0.00019	+17.1 ±2.7	2.1* (13)
Peralkaline syenites (Franspoort, Buffelsdrift, Leeuwkraal)				
all samples:	1332 ± 18	0.70399 ±0.00020	+12.8 ±2.8	0.99 (17)
Leeuwfontein				
"grey syenites":	1431 ± 50	0.70374 ±0.00012	+11.1 ±1.7	1.1 (9)
Leeuwkraal				
phonolites:	1334 ± 22	0.703961 ±0.00022	12.5 ±3.1	0.68 (7)

All errors are expressed as 95% confidence intervals.
* MSWD in excess of that anticipated from analytical uncertain-ties: errors have been augmented to account for the excess scatter using separate estimates for the analytical and "geological" components of the scatter (Harmer and Eglington, 1991).

8.3. Geochronology of the Pilanesberg Suite complexes

Uncertainties in the age relationships of components of the Pilanesberg Suite were raised in earlier chapters. In this section the additional isotopic data of relevance to the age of these complexes is discussed.

8.3.1. Pienaars River Alkaline Complexes

Rb-Sr isotopic data for many of the centres in the PRAC have been published (Harmer, 1985) and demonstrate that the various complexes comprising the PRAC vary significantly in their age. The isotope data for the "grey syenites" of the

Leeuwfontein Complex and the Leeuwkraal phonolites yielded precise dates on their own, whereas the data for the Franspoort, Buffelsdrift, Klipdrift and Haakdoornfontein centres are too restricted in compositional range to yield precise age information. As a result, these data were (somewhat arbitrarily) regressed together as a "younger syenite suite" by Harmer (1985). Data for the Rondawel quartz syenites did not conform to either of these groupings.

Quartz syenites in the Klipdrift, Rondawel and Haakdoornfontein centres are petrographically very similar and are clearly compositionally distinct from the under-saturated and peralkaline rocks from Leeuwkraal, Franspoort and Buffelsdrift. A petrological subdivision of the PRAC units into undersaturated (and peralkaline) and saturated to oversaturated components has consequently been adopted here. Nepheline syenites (sample L14) occur along with the volumetrically more significant saturated syenites in the Leeuwfontein complex and so this complex is treated separately (Harmer, 1985). Dates calculated using this subdivision are listed in Table 8.1). The interpretation based on this "petrological" grouping is preferred since it is more scientifically based and also adequately accounts for the Rondawel data.

Based on this modified interpretation, the PRAC appears to have developed from magmas of progressively higher silica undersaturation and alkalinity with decreasing age. It is interesting to note that this trend is the exact opposite of that of increasing SiO_2-saturation with time reported for the volcanics of the north Kenya Rift by Norry *et al.* (1980).

8.3.2. Kruidfontein, Tweerivier, Bulhoek and Goudini Complexes

Material suitable for age determination is not readily available in any of these carbonatitic complexes. Tweerivier and Bulhoek are composed almost exclusively of carbonatite whereas much of the silicate material at Kruidfontein is pyroclastic or tuffaceous and has been variously carbonated. Four samples of the carbonated basaltic lava at Kruidfontein were analysed but have insufficient variation in Rb/Sr for whole rock dating. The lamprophyre dyke at Goudini has very high Sr and little range in Rb/Sr.

Carbonatite samples from these complexes have sufficient variation in Sm/Nd to achieve an imprecise estimate of the age of the complexes. Regression of 11 carbonatite samples yielded an imperfectly constrained (MSWD=3.6) and imprecise date of 1216 ±203 Ma with initial ratio of 0.51101 ±0.00011 (equivalent to

$\varepsilon_{(Nd)}$=–1.1 ±2.2). This estimate is also consistent with the dates (and 1σ errors) of 1190 ±80 Ma (Sm-Nd) and 1110 ±300 Ma (Pb-Pb) calculated by Nelson *et al.* (1988) for two para-carbonatites from Goudini.

Despite their poor precision, these dates are significant in that they demonstrate that the carbonatites are definitely not Jurassic (Karoo) in age (cf. Verwoerd, 1967; Walraven, 1981).

8.3.3. Pilanesberg Complex

An age of 1250 ±60 Ma has long been accepted for the Pilanesberg Complex, being a K-Ar date determined on biotite from one of the foyaites (Snelling, 1963). This date is consistent with the Rb-Sr dates of 1290 ±180 to 1330 ±80 Ma determined on dykes related to the Pilanesberg Complex (Schreiner and Van Niekerk, 1958; Van Niekerk, 1962).

An attempt was made to obtain age information from Rb-Sr determinations on whole rock samples of selected foyaite units from the Pilanesberg Complex. Green foyaite samples had a restricted range in Rb/Sr and yielded a rather imprecise date of 1195 ±98 Ma, which is within error of the K-Ar date (Figure 8.2a). Some samples rich in eudialyte tended to scatter about the best fit line and were excluded from the regression. White foyaites had a greater compositional range but regression of the 10 data points yielded a very poorly-constrained fit (MSWD=92!!) equivalent to a date of 1119 ±92 Ma (Figure 8.2b).

A more extensive study is required to obtain a precise age for this Complex.

Figure 8.2: $^{87}Sr/^{86}Sr$-$^{87}Rb/^{86}Sr$ isochron plot for (a) the green foyaites and (b) white foyaites from the Pilanesberg Complex.

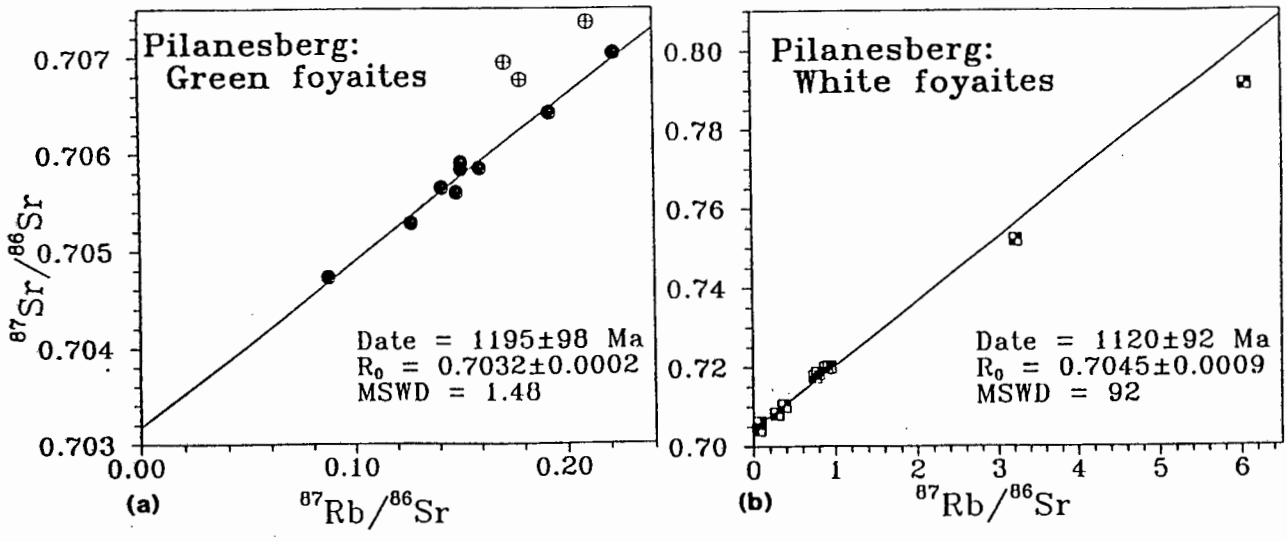

Samples with open symbols in (a) were excluded from the regression calculation.

8.3.4. Stukpan Complex

The association of phlogopite phenocrysts with calcite in the Stukpan carbonatites provides an ideal situation for Rb-Sr geochronology. Separated mica and carbonate fractions (5 each), plotted in Figure 8.3, yielded a date of 1345 ±13 Ma. The MSWD of 3.2 is higher than the value anticipated for 10 samples, 2.1, and thus there is scatter in the data which exceeds the analytical uncertainty. Sample H8m(g) contributes most to this scatter and its exclusion yields a well-constrained regression line (MSWD=1.4) of 1354 ±11 Ma. This date is regarded as the best estimate of the age of crystallisation of the Stukpan carbonatite.

In Figure 8.4, the "amphibolites" are plotted in relation to the carbonatite mineral isochron of 1354 Ma and indicate that this material was clearly not in isotopic equilibrium with the carbonatite and certainly represents xenoliths of older country rock. Model ages (assuming an initial $^{87}Sr/^{86}Sr$ of 0.704) range between 2206 and 3266 Ma. An isochron of 2700 Ma, the age of the Ventersdorp lavas (Armstrong *et al.*, 1986), is shown for reference and suggests that the "amphibolites" could represent fenitised xenoliths of these volcanic rocks.

Figure 8.3: $^{87}Sr/^{86}Sr$-$^{87}Rb/^{86}Sr$ isochron plot for 5 phlogopite (open diamonds) and 4 carbonate (half-filled symbol) fractions separated from the Stukpan Carbonatite.

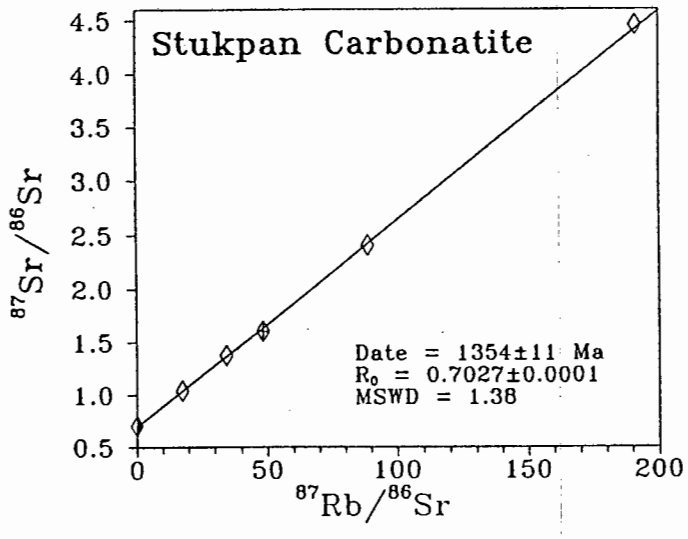

Crossed-diamond symbol denotes phlogopite sample H-8(g) which was excluded from the regression calculation.

8.3.5. Summary

The earliest magmatic activity within the Pilanesberg suite complexes was the emplacement of the quartz syenites (Rondawel, Klipdrift and Haakdoornfontein) of the PRAC at about 1480 Ma. This was followed by the formation of the Leeuwfontein extrusive and intrusive rocks at 1430 Ma. A hiatus of 100 Ma followed after which the Stukpan (1354 Ma) and Spitskop (1341 Ma) carbonatite complexes were emplaced along with the peralkaline components of the PRAC (Leeuwkraal, Franspoort and Buffelsdrift: 1332 Ma). Although not strictly resolvable on the current data set, the carbonatites of the western Transvaal (Nooitgedacht, Kruidfontein, Tweerivier, Bulhoek, Goudini) and the Pilanesberg Complex appear to have been derived during a somewhat later episode at about 1200-1250 Ma. The dating of the Premier kimberlites at 1180 ±30 Ma (Richardson, 1986) suggests that they too may be related to this closing phase of magmatism within the Pilanesberg suite.

It is evident from these dates that there is no systematic change in geographic location as a function of age during the evolution of the Pilanesberg suite magmatism.

Figure 8.4: $^{87}Sr/^{86}Sr$-$^{87}Rb/^{86}Sr$ plot for samples of "amphibolite" from the Stukpan carbonatite.

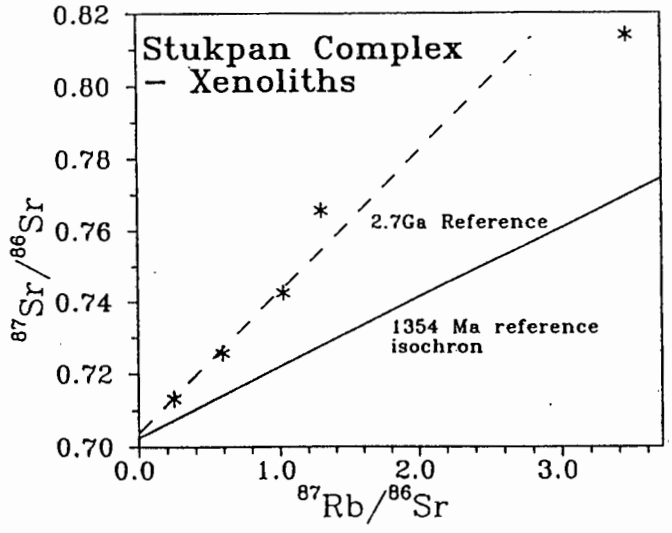

Reference isochrons of 1354Ma (the age of intrusion of the Stukpan carbonatite) and 2700Ma (age of the Ventersdorp volcanic rocks: Armstrong *et al.*, 1991) are shown for comparison.

8.4. Comparative geochemistry amongst the silicate components of the Pilanesberg suite complexes.

An in-depth interpretive discussion of the geochemistry of the Pilanesberg silicate rocks is beyond the scope of the current dissertation. Instead specific aspects only will be highlighted, in particular those of significance to the Spitskop silicate rocks and the aspects related to the petrogenetic association of carbonatite and silicate magmas.

8.4.1. The Pienaars River Complexes

The general chemical characteristics of the Pienaars River Complexes are summarised on a Q-Ne-Ks ternary plot in Figure 8.5 where the subdivision into silica saturated and silica undersaturated groups is apparent. All the silicate rock types are evolved rocks with Mg# below 0.20. It is interesting to note that the peralkaline rock types tend to have lower Mg# (generally <0.1) than the silica saturated rock types (Figure 8.6a) and that SiO_2 and Mg# are positively correlated in the undersaturated syenites but negatively correlated in the saturated group. In terms of the TAS classification (Figure 8.6b) the silica saturated rocks are the compositional equivalents

of trachyandesites to trachytes whereas the peralkaline samples all classify as phonolites. The single nepheline syenite sample from the Leeuwfontein Complex (L14) classifies as a "foidite".

Both the saturated and undersaturated syenites in the PRAC have a more restricted range in Zr/Nb relative to the Spitskop nepheline syenites (Figure 8.7b) despite significant variations in the concentration levels of Zr and Nb (Figure 8.7a). Limited variability in Zr/Nb within individual suites is a common feature of many alkaline complexes (e.g. Weaver *et al.*, 1972; Price *et al.*, 1985; Marsh, 1987a).

8.4.1.1. The undersaturated, peralkaline syenites

The Leeuwkraal phonolites are peralkaline and are indistinguishable in age and initial $^{87}Sr/^{86}Sr$ from the Spitskop nepheline syenites. Compositional variations among the seven samples of Leeuwkraal phonolite are systematic and the possible cause of these variations is evaluated in the next section. Following this, the compositions of all the undersaturated PRAC syenitic bodies are compared with the chemical variation noted in the nepheline syenites at Spitskop.

Figure 8.5: Ternary Q - Ne - Ks of normative data for various components of the Pienaars River Alkaline Complex.

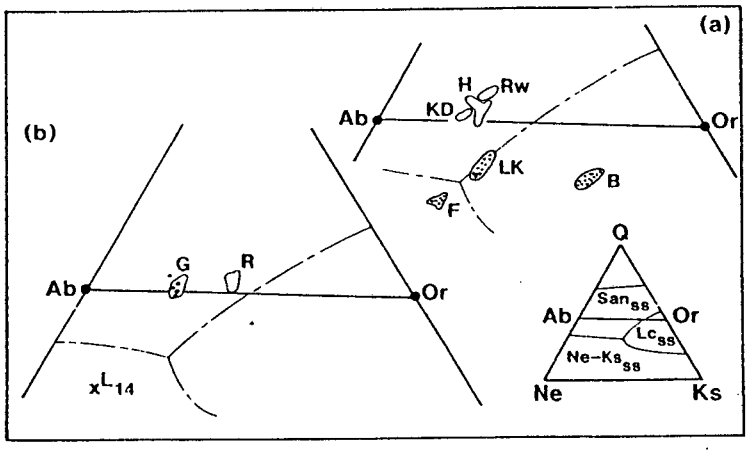

(a) Saturated syenite group: KD: Klipdrift; H: Haakdoornfontein; Rw: Rondawel. Fields for the undersaturated, peralkaline complexes are shaded: F: Franspoort; LK: Leeuwkraal; B: Buffelsdrift.
(b) Data from the Leeuwfontein Complex: G: "grey" syenites and syenodiorites; R: "red" alkali syenites; lavas are shown as dots.
Phase stability fields in small inset diagram are from Hamilton and MacKenzie (1965).

Figure 8.6: Plots of SiO_2 against (a) Mg# and (b) Total Alkalis for the Pienaars River Alkaline Complex.

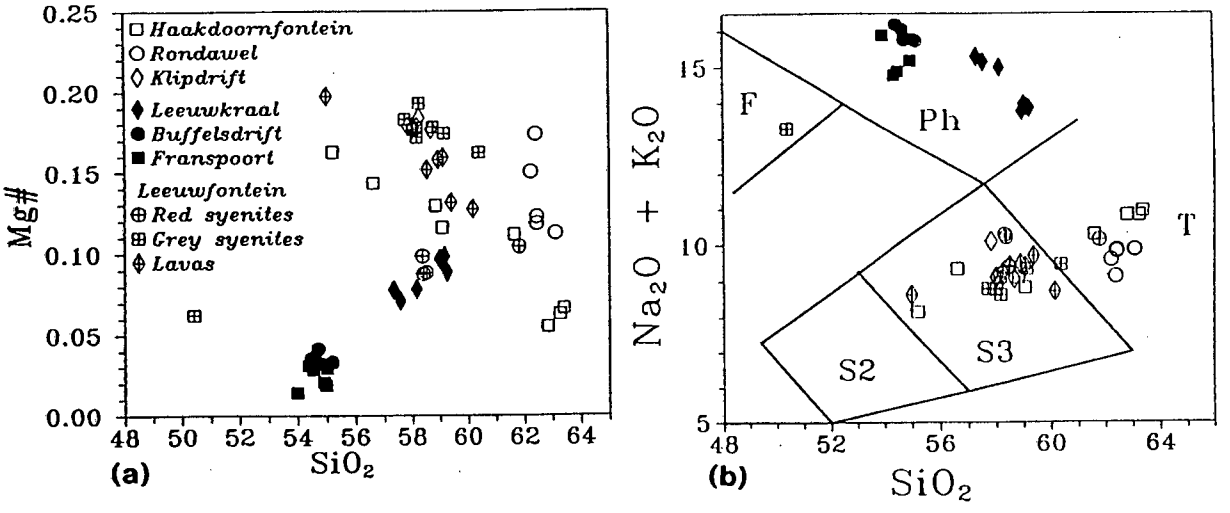

Classification fields in (b) are from Le Bas *et al.* (1986) and refer to:
F: Foidites; Ph: Phonolites; T: Trachyte; S3: Trachyandesite (Na=Benmoreite, K=Latite); S2: Basaltic trachyandesite (Na=Mugearite, K=Shoshonite).

Figure 8.7: Plots showing the Nb - Zr relationships in samples from the Pienaars River Complex.

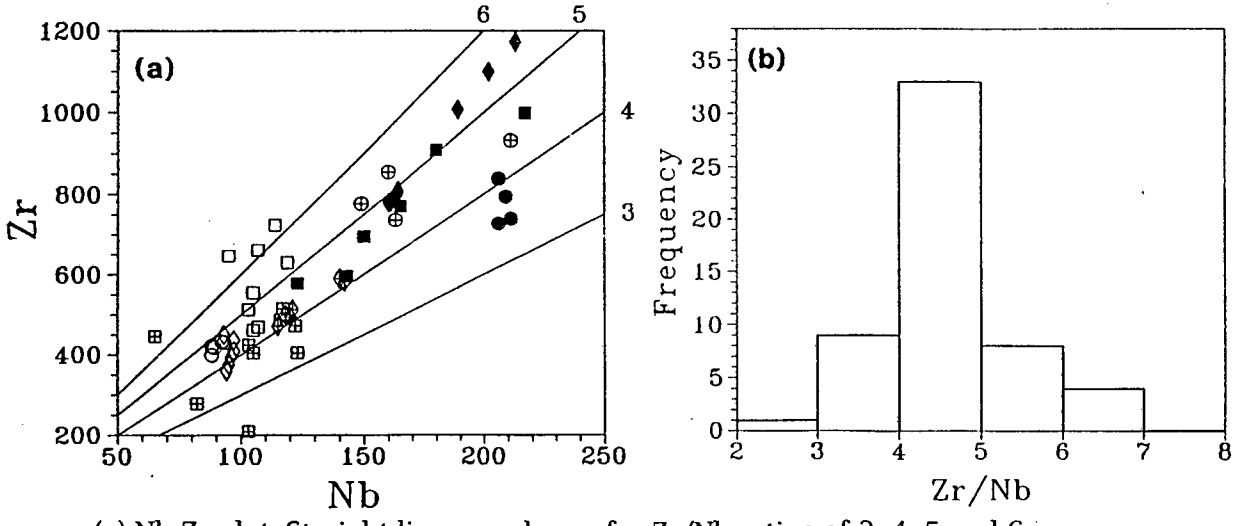

(a) Nb-Zr plot: Straight lines are drawn for Zr/Nb ratios of 3, 4, 5 and 6.
(b) Frequency histogram of Zr/Nb ratios.
Symbols in (a) are the same as in Figure 8.6a.

Figure 8.8: SiO_2 - alkalis plot of Leeuwkraal phonolite data.

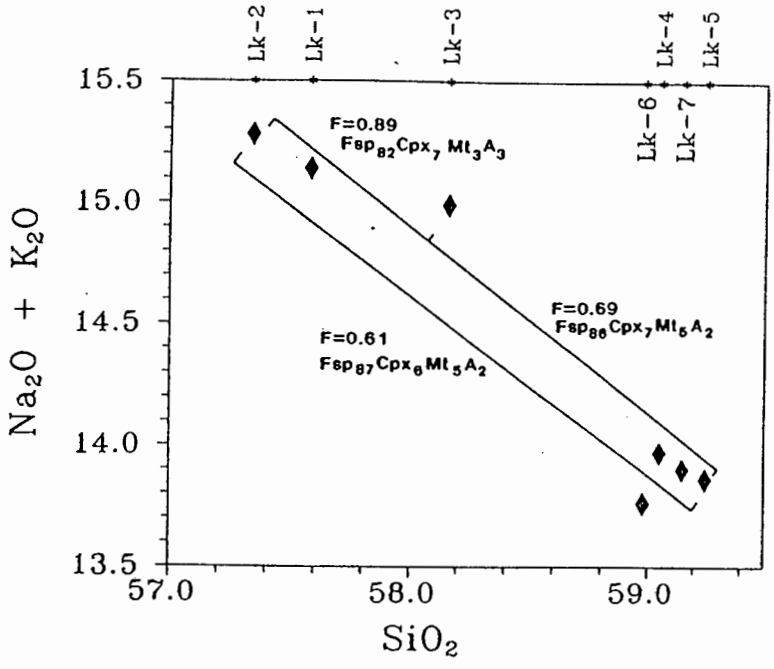

Annotated lines give the results of least square mixing models to match the major element compositions of samples Lk-2, Lk-3 and Lk-5 with the compositions of component mineral phases (see text and Table 8.2 for further details).

Table 8.2: Results of least-squares mix modelling of major elements in the Leeuwkraal phonolites.

	Lk-5/Lk-2	Lk-3/Lk-2	Lk-5/Lk-3
Liquid:	Lk-2	Lk-2	Lk-3
X_{liquid}	0.61	0.89	0.69
$X_{crystals}$	0.39	0.11	0.31
Assemblage[1]	$Fsp_{87}Cpx_6Mt_5A_2$	$Fsp_{82}Cpx_7Mt_3A_3$	$Fsp_{87}Cpx_5Mt_5A_2$
Σr^2	0.08	0.01	0.10

1: "A" denotes accessories: apatite plus titanite, in essentially equal quantities.

8.4.1.2. The Leeuwkraal phonolites

Four of the samples (Lk-4 to Lk-7) are phenocryst-enriched phonolite porphyries whereas the remaining three samples could approach liquid compositions. Least-squares mixing calculations show that the major element compositional variation between samples Lk-2 (lowest SiO_2) and Lk-5 (highest SiO_2) may be attributed to differences in the proportions of alkali feldspar, clinopyroxene and

titano-magnetite (see Table 8.2 and Figure 8.8). Lk-2 may then be regarded as a residual liquid after removal of feldspar, clinopyroxene and titano-magnetite from an initial liquid composition equivalent to Lk-3; porhyry Lk-5 (along with samples Lk4,6,7) is considered a cumulate enriched in the specified cumulus phases.

Trace element variations predicted by the major element mix model were calculated by assuming that Lk-5 is enriched in cumulus alkali feldspar and clinopyroxene which formed in equilibrium with a liquid equivalent to Lk-2. Partition coefficients established by Larsen (1979) were used. In a qualitative sense, the observed variation trends for Rb, Sr, Ba, Nb and Zr (Figure 8.9) are consistent with the model. Concentrations of Ba and Sr in Lk-5 are significantly higher than those estimated but this could simply signify that the true partition coefficients for these elements were larger than those determined by Larson (1979). The model predicts, however, that Ce should be enriched in Lk-2 relative to Lk-5 to the same extent as Nb or Zr whereas a relative depletion of Ce is observed. Approximately 2% of apatite and titanite is predicted in the crystal assemblage in the major element mixing model: if the mis-match in Ce is due to these accessories, then a K_d of about 62 would be required to increase the D_{Ce} to required level (≈1.2). The changes required to the individual partition coefficients of Larsen (1979) in order to perfectly match the compositions of the phonolites (see bulk D's in Table 8.3) are within the known range of variation of K_d's in alkaline rocks.

It is concluded, then, that the systematic chemical variations amongst the Leeuwkraal phonolites could reasonably reflect crystal-liquid fractionation processes.

Figure 8.9: Plots showing the variation of (a) Sr, Ba, Zr (b) Rb, Nb, Ce with SiO_2 in the Leeuwkraal phonolites.

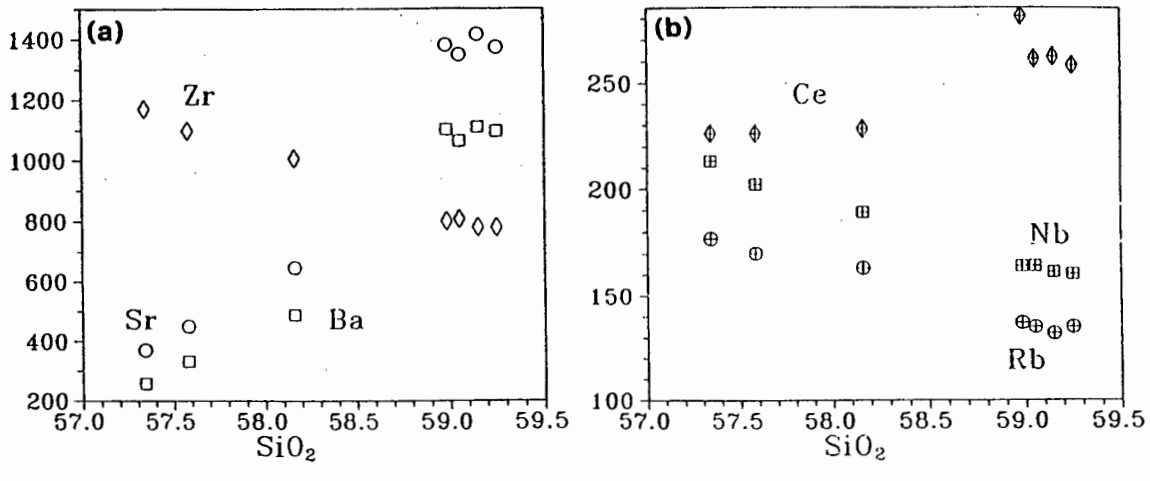

Table 8.3: Table comparing calculated and estimated bulk distribution coefficients required to model the composition of Lk-5.

	Lk2 - Lk5		Lk5 - Lk5	
	calc	est	calc	est
Rb	0.300	0.392	0.446	0.304
Ba	3.191	9.328	5.019	3.225
Sr	2.168	7.958	4.635	2.189
Zr	0.018	0.140	0.270	0.016
Nb	0.005	0.362	0.505	0.005
Y	0.058	0.942	1.157	0.052
La	0.068	0.444	0.690	0.065
Ce	0.066	1.363	1.424	0.062
Nd	0.074	0.668	0.747	0.066

1: Bulk distribution coefficient calculated using mineral K_d's of Larsen (1979).

2: Bulk distribution coefficient required to perfectly match observed trace element concentrations in Lk-5.

8.4.1.2.1. Comparison between undersaturated PRAC syenites and the Spitskop nepheline syenites

Variations of selected elements in the PRAC and Spitskop nepheline syenites are depicted in Figure 8.10. Nepheline syenites from Spitskop have higher levels of FeO^* and Na_2O, and are more peralkaline than the nepheline syenites in the PRAC. SiO_2 is higher in the Leeuwkraal phonolites but the Franspoort and Buffelsdrift units fall within the range of the Spitskop nepheline syenites. The compositional contrast is, however, most marked for the elements Zr, Nb, Ce (and LREE) which are all substantially lower, and more variable, in the Spitskop nepheline syenites. Zr/Nb ratios are more varied and higher in the Spitskop nepheline syenites.

Figure 8.10: Variation diagrams to compare the compositions of the peralkaline nepheline syenites in the PRAC with those in the Spitskop Complex.

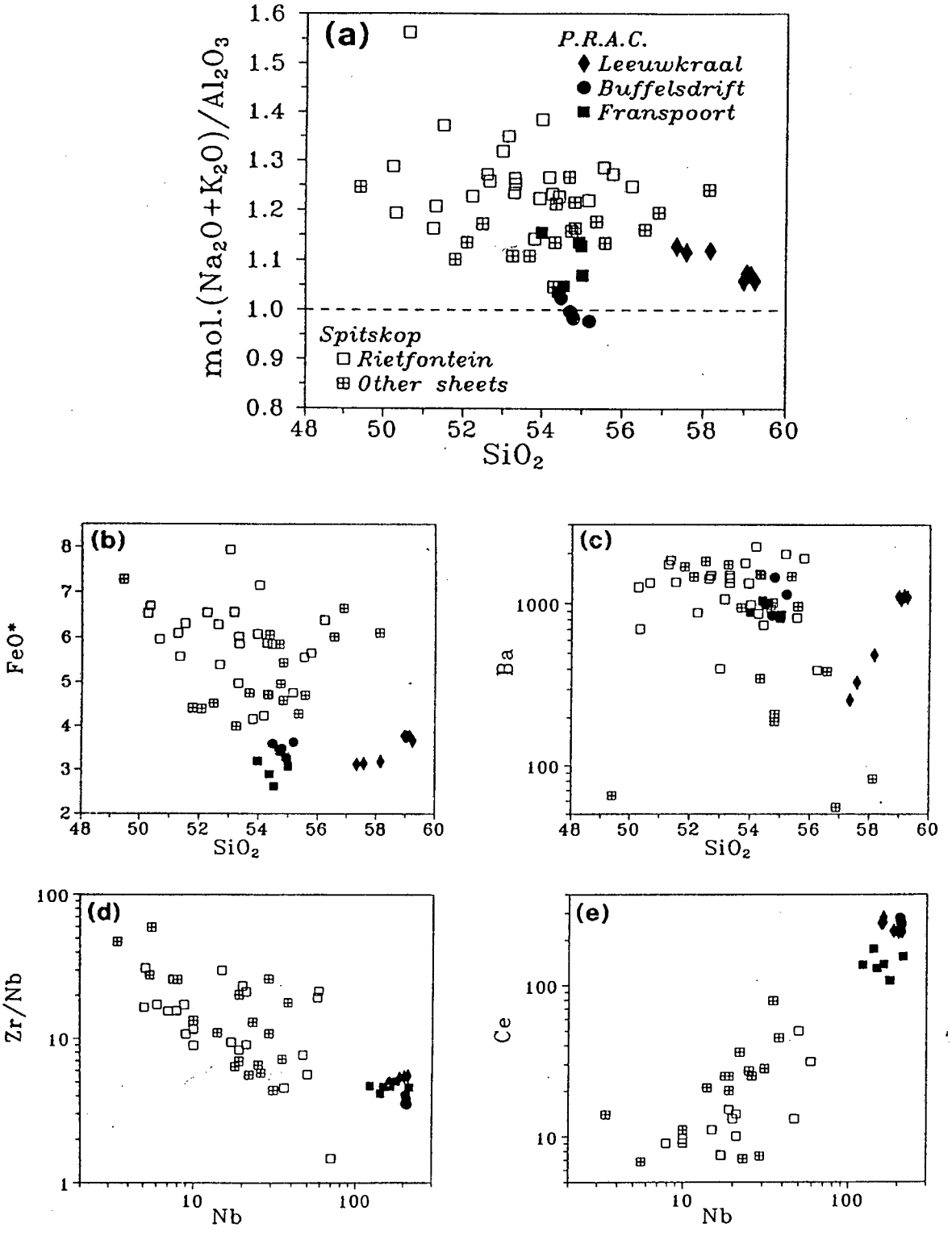

8.4.1.3. The saturated syenites

8.4.1.3.1. Haakdoornfontein syenites

The Haakdoornfontein syenites span a significant range in silica content from 58.6% in H81-8 to 64.5% in H81-4. No microprobe analyses were available for mineral phases in the syenites and so stoichiometric compositions were utilised in mixing calculations. Major element variation could largely be explained by the addition or subtraction of sodic alkali feldspar ($Or_{32}Ab_{65}An_3$) together with minor addition or subtraction of quartz, sodic clinopyroxene and magnetite. Unlike the Leeuwkraal material, the Haakdoornfontein samples are coarse grained so it is not possible to confidently predict which of the samples may approach liquid compositions.

Figure 8.11: SiO_2 - alkalis plot of analyses of basaltic volcanics associated with the carbonatite at Kruidfontein.

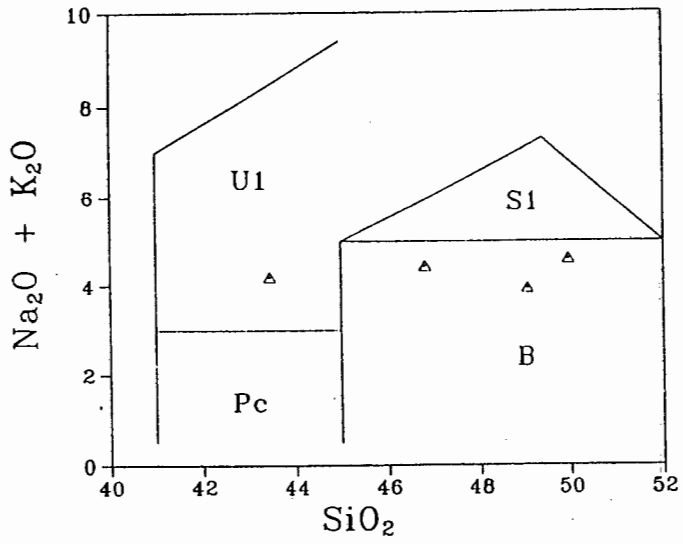

Classification fields are from Le Bas *et al.* (1986) and denote:
U1: basanite (ol>10%) or tephrite (ol<10%); Pc: Picrobasalt; S1: trachybasalt; B: alkali basalt (ne normative) or subalkali basalt (hy, q normative).

8.4.2.The Kruidfontein mafic lavas

The occurrence of mafic lavas and dykes in association with the carbonatites at Kruidfontein was commented on earlier. At Spitskop carbonatites are associated with ijolitic mafic silicates, the intrusive equivalents of nephelinitic volcanics and the original silicate volcanics at Goudini are thought to have been nephelinitic (Verwoerd, 1990; see discussion above). It is of interest, then, to assess whether the Kruidfontein lavas are also nephelinitic. Using the TAS classification plot in Figure 8.11, analyses of the Kruidfontein lavas (re-calc-ulated volatile-free) classify as basalts, only sample K16 plotting in the more basic, U_1, field. None of the lavas are nepheline normative and so are subalkaline. K16 has less than 1% normative olivine and so classifies as a tephrite. Being clearly basaltic in composition, the Kruidfontein lavas are thus not comparable to the undersaturated nephelinitic magmas typically associated with carbonatites (e.g. Le Bas, 1987).

Figure 8.12: Chemical variation diagrams for various Pilanesberg Suite carbonatites.

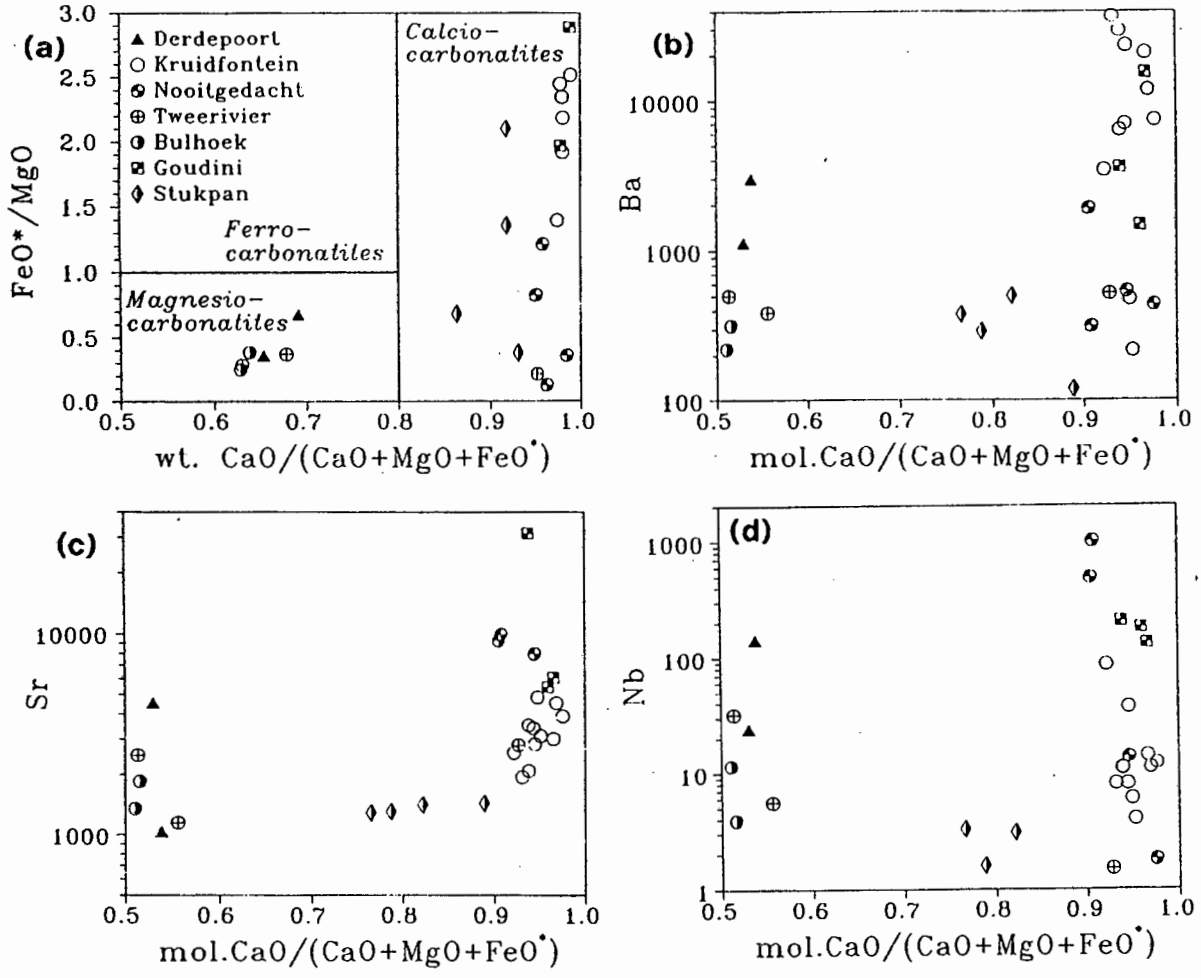

(a) binary representation of the Woolley and Kempe (1989) classification: see Chapter 4; variation of
(b) Ba; (c) Sr; (d) Nb with molar CaO/(CaO+MgO+FeO*).

8.5. Comparative geochemistry of the Pilanesberg suite carbonatites.

All analysed carbonatite samples from the Pilanesberg Suite complexes are plotted on the weight percent CCMF ratio *versus* FeO*/MgO classification plot (modified from Woolley and Kempe, 1989; as discussed in Chapter 4) in Figure 8.12(a). Samples from the Derdepoort and Bulhoek carbonatites are exclusively magnesio-carbonatites whereas both calcio- and magnesio-carbonatites are included from Tweerivier. Samples from Nooitgedacht, Stukpan and Goudini are exclusively calcio-carbonatites.

The tendency noted in the Spitskop carbonatites for certain trace elements to be more abundant in "end-member" carbonatites (i.e. molar CCMF close to 0.5 or 1.0) relative to intermediate compositions is also apparent in the other Pilanesberg Suite carbonatites for the elements Ba, Sr and Nb (Figure 8.12b-d). It is also clear that the concentrations of these elements tend to be higher in the calcio-carbonatites than in the most enriched magnesio-carbonatites. Concentrations of Ba, Sr and Nb are somewhat lower in the Spitskop carbonatites than in the the other Pilanesberg Suite carbonatites. Ni concentrations seldom exceed 10 ppm.

A range of trace elements are compared to relevant global average values determined by Woolley and Kempe (1989) in a series of normalised variation diagrams in Figure 8.13(a-d) following the approach (and provisos!) adopted for the Spitskop carbonatites in Chapter 4. A feature of the Pilanesberg Suite carbonatite data set is the wide variation in concentration level of many trace elements: Nb and Ba, in particular, vary by more than two orders of magnitude. Amongst the magnesio-carbonatites (Figure 8.13a), the Derdepoort carbonatite has higher than average LREE, Y and Zr concentrations while Ba, Nb and Sr are lower. Most elements, and Nb in particular, occur in lower than average concentrations in the Bulhoek and Tweerivier samples. Calcio-carbonatites at Kruidfontein (including analyses from Clarke *etal*, in press) show high levels of Ba, but are variably depletes in Nb and Zr. Calcio-carbonatites from the nearby Nooitgedacht Complex (Figure 8.13c) have Nb_N values ranging from 1.0-0.001! Goudini carbonatites generally have elevated concentrations of most of the trace elements (Figure 8.13d). In contrast, the Stukpan Complex has the most distinct trace element pattern of all the carbonatites with very low LREE contents accompanied by low concentrations of Ba, Nb and Y.

Rare earth elements also show a wide range in concentration although all but the Stukpan carbonatites have the steep, relatively LREE-enriched patterns typical of carbonatites (Figure 8.14). Normalised concentrations of the LREE are highest in samples from the Derdepoort and Goudini (La is close to the upper limit of values within the Woolley and Kempe data set - see Figure 8.13d), attaining values of 9000x chondrite (La>1000 ppm).

Figure 8.13: Normalised variation diagrams comparing the ranges of selected trace elements in the Pilanesberg Suite carbonatites with world carbonatite data from Woolley and Kempe (1989).

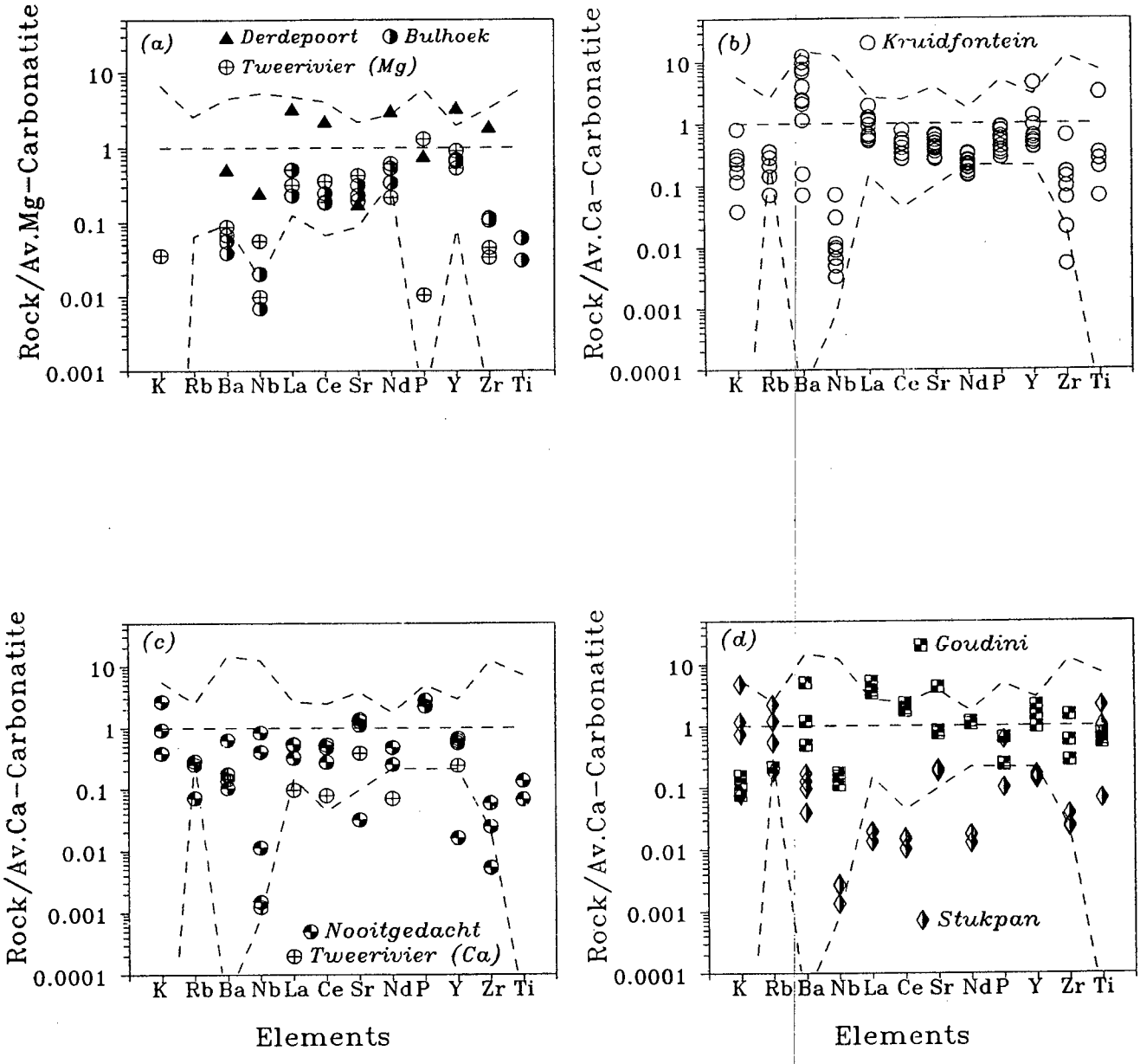

Elements are normalised against the average (a) magnesio- and (b,c,d) calcio-carbonatites from Woolley and Kempe (1989). Broken lines depict the concentration ranges for the global carbonatite dataset.

The Stukpan carbonatite is highly unusual in having low absolute REE concentrations and flat, low LREE/HREE, chondrite-normalised patterns ($La_N \approx 30$). These appear to be amongst the lowest REE contents yet reported from magmatic carbonatites (e.g. see range bounds in Figure 8.13d). The occurrence of typical carbonatite minerals such as soda amphibole and phlogopite, the observation that adjacent quartzites are fenitised and the high concentrations of elements such as Ba and Sr are taken as evidence that the Stukpan Complex is indeed a magmatic carbonatite.

Late-stage, coarse calcite veins at Fen (Sövite-III), reported by Mitchell and Brunfeldt (1975), have LREE concentrations of less than 20 times chondrite and the veins were interpreted to have crystallised after "most of the REE were removed from the magma". The Fen sövite has a slight positive Eu anomaly and Ce_N/Yb_N of about 7. The Stukpan REE patterns have no Eu anomaly and have much lower Ce_N/Yb_N (≈ 3). It is proposed that LREE levels in the Stukpan carbonatite were depleted by the early removal of a LREE-enriched phases such as pyrochlore.

It is apparent that the low (and variable) Nb contents noted in the Spitskop carbonatites (Chapter 4) are a feature of all the carbonatitic bodies within the Pilanesberg Suite of complexes. Low Nb in many of the associated silicate rocks as well suggests that this may be a regional, and possibly source-related(?), feature. Also common to many of the carbonatites is the variability of other trace elements, particularly the REE and Ba, from values equivalent to the Wooley and Kempe (1989) average down to values less than 0.001x. Fractionation of minerals such as apatite, pyrochlore, baryte, strontianite - phases in which these elements are compatible - is possibly responsible for this variability.

Figure 8.14: Chondrite-normalised rare earth element variation diagrams for the Pilanesberg Suite carbonatites.

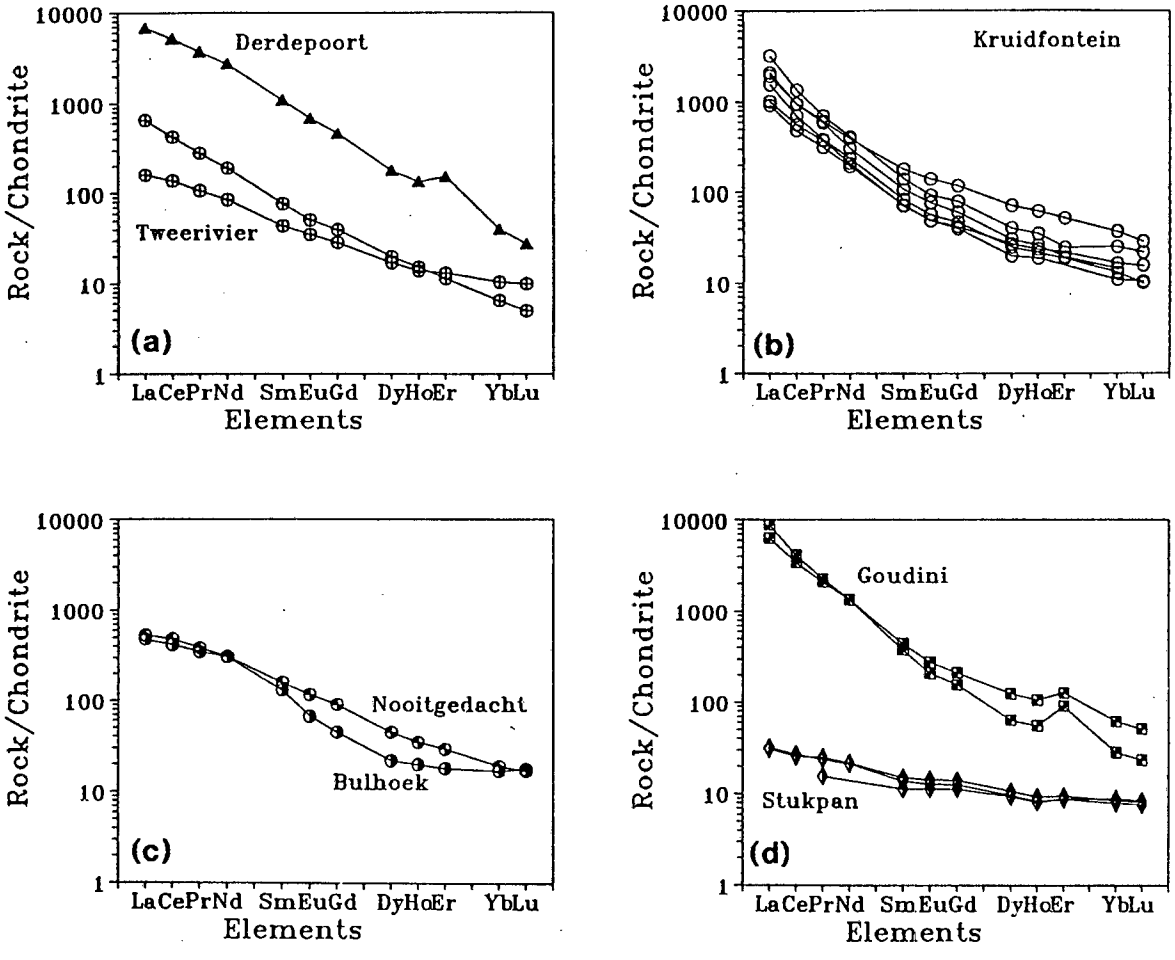

8.6. *Isotope geochemistry of the Pilanesberg Suite complexes.*

8.6.1. Sr-Nd isotopes

8.6.1.1 Carbonatites

The isotopic compositions of Sr and Nd in the Pilanesberg Suite carbonatites are depicted on an $\varepsilon_{(Sr)}$-$\varepsilon_{(Nd)}$ plot in Figure 8.15 and compared with 1.0-1.9Ga carbonatites from North America (Bell and Blenkinsop, 1989).

Figure 8.15: $\varepsilon_{(Sr)}$-$\varepsilon_{(Nd)}$ plot of isotopic data for the Pilanesberg Suite carbonatites.

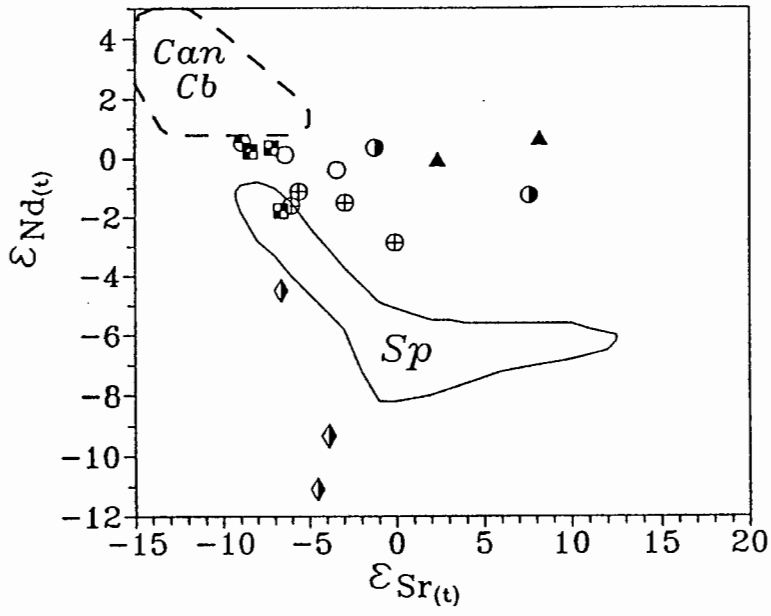

All epsilon data are calculated at the time of crystallisation of each carbonatite. Data from the Spitskop Complex are bounded in the solid line field marked "Sp". The dashed field "Can Cb" includes carbonatites from Canada in the age range 1.0-1.9Ga. Symbols are as in Figure 8.12(a).

The Pilanesberg carbonatites have "enriched" Sr and Nd isotopic values (i.e higher $\varepsilon_{(Sr)}$; lower $\varepsilon_{(Nd)}$) in relation to complexes of comparable age in North America. With the exception of the Stukpan carbonatites, $\varepsilon_{(Nd)}$ data from the other complexes fall in the narrow range -3 to +1 but with $\varepsilon_{(Sr)}$ showing greater variability. One sample from each of the Derdepoort (DP-3) and Bulhoek (BH-2) carbonatites are markedly enriched in $\varepsilon_{(Sr)}$ relative to the carbonatites from the other complexes. As such these complexes describe a trend of shallower slope on the $\varepsilon_{(Sr)}$-$\varepsilon_{(Nd)}$ plot than the Spitskop carbonatite data.

It was noted above that the Stukpan carbonatites have anomalously low concentrations of the LREE (see Figure 8.14) and have the highest Sm/Nd of the carbonatites analysed. If the REE patterns in the Stukpan carbonatite are a primary feature then the Nd isotope systematics in the carbonatite magma would be more susceptible to modification through crustal contamination than the other Pilanesberg suite carbonatites. A negative correlation exists between Nd and $\varepsilon_{(Nd)}$ in the three Stukpan samples, however (Figure 8.17), i.e. the most extreme $\varepsilon_{(Nd)}$ values (-11.2 in H4) are found in samples with highest Nd (14.9 ppm in H4). If $\varepsilon_{(Nd)}$ was changed by

contamination, then Nd must have been *added* to the carbonatite implying that primary Nd concentrations were even *lower* than the present values! The very negative $\varepsilon_{(Nd)}$ values in the Stukpan carbonatite indicate derivat-ion from a source which had had time-integrated depletion in Sm/Nd, i.e. was LREE enriched: this is evidence that the low LREE/HREE in the Stukpan samples is not a source feature but must have been imprinted during petrogenesis.

Figure 8.16: $\varepsilon_{(Sr)}$-$\varepsilon_{(Nd)}$ plot to evaluate the possible role of contamination in the Stukpan Carbonatites.

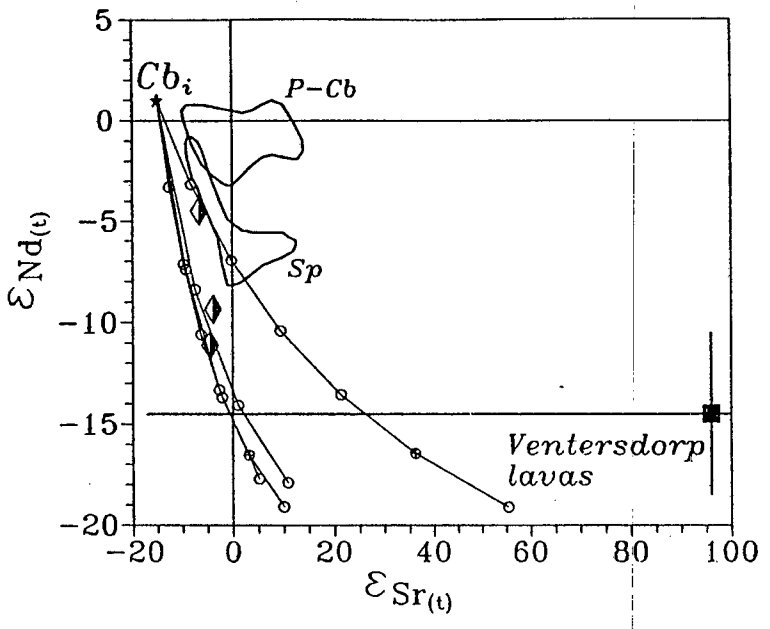

Data for Ventersdorp lavas are taken from Nelson *et al.* (1992) Curves are drawn for mixtures of model primitive Stukpan carbonatite "Cbi" ($\varepsilon_{(Sr)}$=-15, $\varepsilon_{(Nd)}$ =+1; 1400ppm Sr, 15ppm Nd) and various lower crustal granulites from the Vredefort section (Hart *et al.*, 1990). (see text for further details)
Abbreviated data field labels are:
Sp: carbonatites from the Spitskop Complex; P-Cb: carbonatites from the other Pilanesberg Suite complexes.

By contrast, the Stukpan carbonatites have fairly constant $\varepsilon_{(Sr)}$ (-7 to -5) but extremely negative $\varepsilon_{(Nd)}$ values (down to less than -11) and plot to the low $\varepsilon_{(Nd)}$ side of the Spitskop trend.

In the discussion of the Rb-Sr isotopic data for the Stukpan carbonatite above, it was suggested that the "amphibolite" xenoliths in the carbonatite could be highly fenitised Ventersdorp volcanics (see Figure 8.4). With reference to the discussion of the Spitskop carbonatite $\varepsilon_{(Sr)}$-$\varepsilon_{(Nd)}$ in Chapter 7, could the low-$\varepsilon_{(Nd)}$ ratios in the Stukpan carbonatite be the result of exchange with these xenoliths? No $\varepsilon_{(Nd)}$ data are

available for the xenoliths, but Nelson *et al.* (1992) present REE and Sm-Nd isotopic data for volcanics from the Ventersdorp Supergroup indicating that, at 1350 Ma, these volcanics had $\varepsilon_{(Nd)}$ values of -9.1 to -19.4. Assuming that the basaltic components of the Ventersdorp crystallised at 2700 Ma with $^{87}Sr/^{86}Sr$ of 0.701, the samples analysed by Nelson *et al.* (1992) would have had $\varepsilon_{(Sr)}$ of 96 ±103 at 1350 Ma. The very low $\varepsilon_{(Sr)}$ in the Stukpan carbonatite suggests that interaction with Ventersdorp volcanics does not provide an adequate model for the very low $\varepsilon_{(Nd)}$ in the Stukpan carbonatite. The possibility that the Stukpan $\varepsilon_{(Sr)}$-$\varepsilon_{(Nd)}$ may reflect assimilation of lower crustal rocks (see equivalent discussion of Spitskop carbonatite data in Chapter 7) may be assessed in 8.16). Bulk mixing curves are shown between an hypothetical low Nd starting carbonatite ($\varepsilon_{(Sr)}$ -15, $\varepsilon_{(Nd)}$ +1, 1400ppm Sr, 15ppm Nd) and lower crustal granulites from the Vredefort structure (Hart *et al.*, 1990). These mixing curves indicate that assimilation could be responsible for the low $\varepsilon_{(Sr)}$ and $\varepsilon_{(Nd)}$ values in the Stukpan carbonatites but only if the carbonatite had very low primary LREE values and suggest that unrealistically large amounts of granulite (20-30%) would be required.

Implications of the Stukpan $\varepsilon_{(Sr)}$-$\varepsilon_{(Nd)}$ data will be discussed further in the following chapter.

Figure 8.17: Variation of $\varepsilon_{(Nd)}$ with respect to Nd for the Pilanesberg Suite Carbonatites.

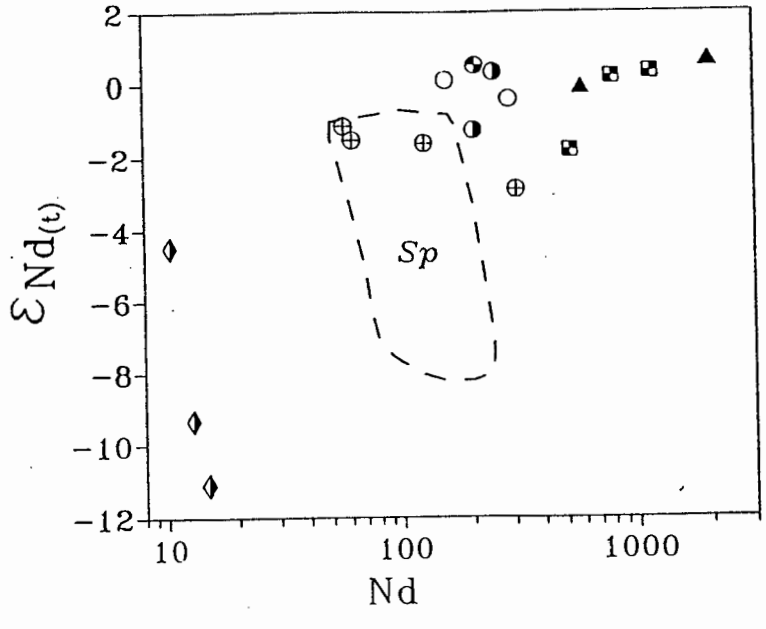

Symbols are as in Figure 8.12(a).

Figure 8.19: $\varepsilon_{(Sr)}$-$\varepsilon_{(Nd)}$ plot to compare the isotopic compositions of the silicate and carbonatite units in the Pilanesberg Suite complexes.

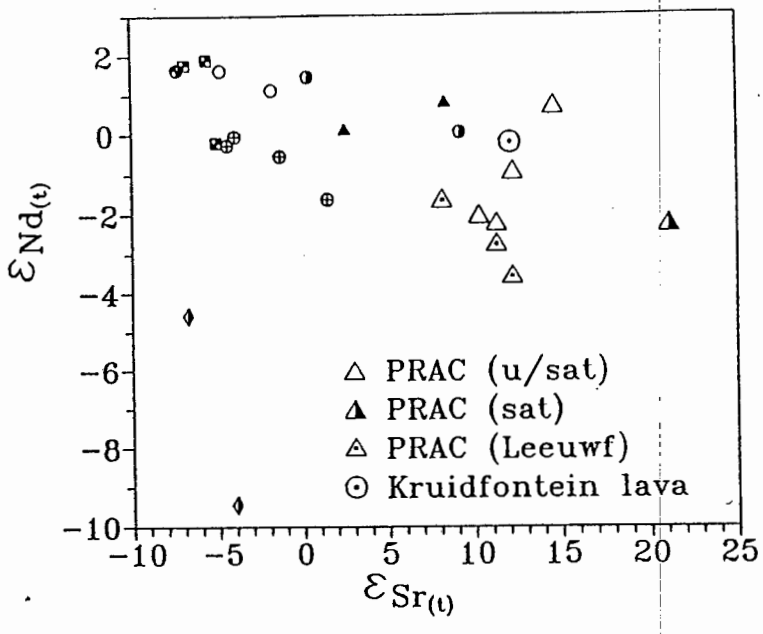

Carbonatite symbols (smaller symbols) are those used in Figure 8.12a.

8.6.1.2. Silicates

Isochron regressions of the various silicate units of the PRAC yield very similar initial $^{87}Sr/^{86}Sr$ ratios: 0.70410 ±19 for the quartz syenites, 0.70374 ±6 for the Leeuwfontein syenites ("grey") and 0.70399 ±20 for the undersaturated syenites. These are equivalent to $\varepsilon_{(Sr)}$ values of 17.1 ±2.7, 11.1 ±1.7 and 12.8 ±2.8 respectively. Green foyaites from the Pilanesberg Complex have a somewhat lower initial $^{87}Sr/^{86}Sr$ of 0.7032 ±2, equivalent to $\varepsilon_{(Sr)}$ of -0.9 ±3.0.

Individual sample $\varepsilon_{(Sr)}$ values for the silicate units of the PRAC and the silicates associated with the Kruidfontein and Goudini carbonatites are compared with the $\varepsilon_{(Sr)}$ values from the carbonatitic units of the complexes on histograms in Figure 8.18. Although some overlap exists, it is clear from this Figure that the silicates have higher $\varepsilon_{(Sr)}$ values than the carbonatites.

Figure 8.18: Frequency histograms comparing the distribution of $\varepsilon_{(Sr)}$ values in the silicate and carbonatite components of the Pilanesberg Suite complexes.

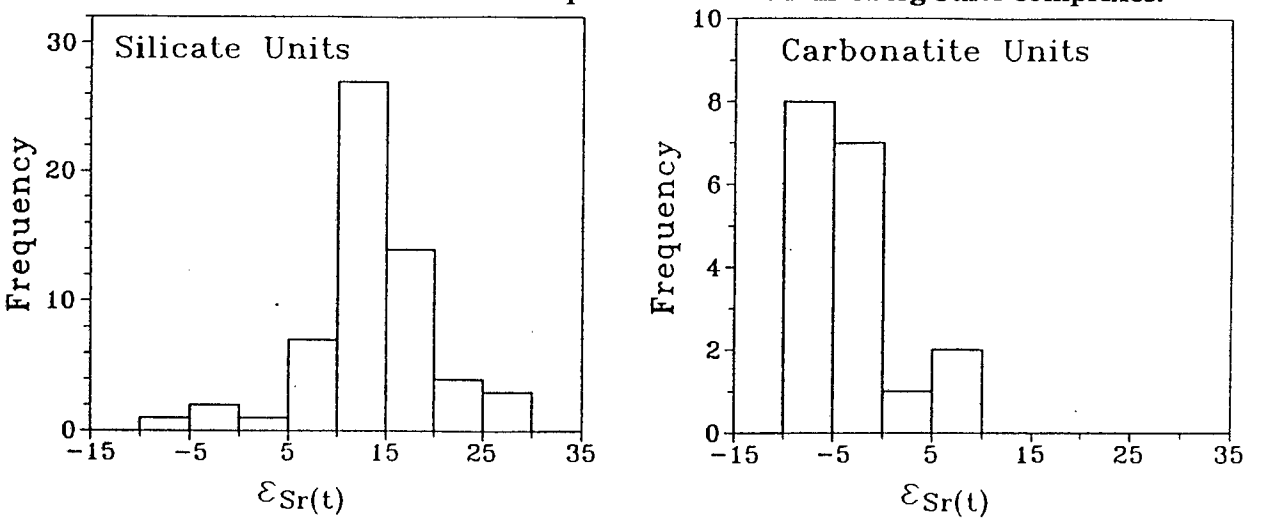

A smaller number of $\varepsilon_{(Nd)}$ data are available for the silicates and these are compared with the carbonatite data on an $\varepsilon_{(Sr)}$-$\varepsilon_{(Nd)}$ plot in Figure 8.19. Differences in $\varepsilon_{(Nd)}$ are not as marked as those for $\varepsilon_{(Sr)}$. Kruidfontein basalt K13 has far higher $\varepsilon_{(Sr)}$ than its associated carbonatites but $\varepsilon_{(Nd)}$ is similar. Amongst the PRAC samples, L15, a trachytic lava from Leeuw-fontein, has similar isotopic composition to the two Derdepoort carbonatites whereas the other PRAC samples group in a field significantly enriched relative to the Derdepoort compositions.

8.6.2. Pb isotopes

Pb isotope data for the carbonatite and silicate units are plotted on a conventional ^{207}Pb-^{206}Pb plot in Figure 8.20. It is significant to note that the Kruidfontein and Goudini carbonatites have less radiogenic Pb than their associated silicate rocks. Most data are bounded by the two reference 1250Ma isochrons drawn for reservoir μ values (relative to the model of Kwon *et al.*, 1989; as used for the Spitskop data in Chapter 5) of 8.2 and 8.8. It is apparent from this diagram that significant scatter exists in the data implying variable initial Pb isotope composition in the carbonatites and silicates both within and between individual complexes. With the exception of the Stukpan samples, the carbonatites exhibit greater variability in $\varepsilon_{(Sr)}$ than $\varepsilon_{(Nd)}$. As a consequence, the implied variability in initial Pb (reflected in μ_2) is depicted against $\varepsilon_{(Sr)}$ in Figure 8.21. No obvious relationship exists between these parameters, indeed the plot emphasises the substantial variation in initial Pb ratios in carbonatites all having negative $\varepsilon_{(Sr)}$.

Figure 8.20: $^{207}Pb/^{204}Pb$ - $^{206}Pb/^{204}Pb$ plot of silicates and carbonatites from the Pilanesberg Suite complexes.

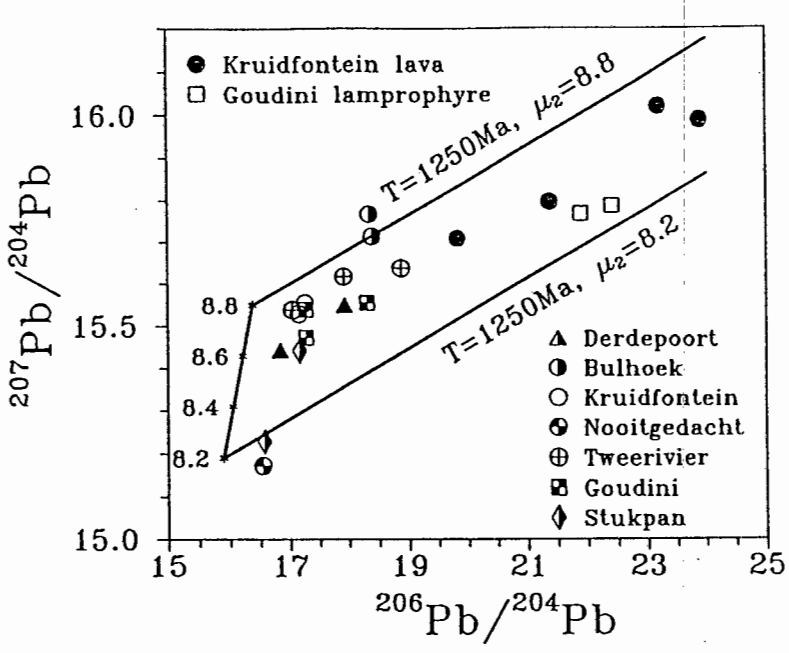

Symbols are the same as those used in Figure 8.20. Two reference 1250Ma secondary isochrons are drawn from initial Pb ratios for model reservoirs (using the Kwon et al. (1989) model parameters) of 8.2 and 8.8.

The highest model μ values (8.8 and 8.9) are found in the two magnesio-carbonatites from Bulhoek. Field observation at Bulhoek indicates that the Bushveld granites were extensively metasomatised by the intrusion of the carbonatite and carbonatite veinlets are noted containing fluidised fragments and clasts of fenitised granite: leaching of radiogenic Pb from the granites into the carbonatites by metasomatic fluids could be responsible for these elevated values. $\varepsilon_{(Sr)}$ in the Derdepoort and Bulhoek carbonatites are somewhat higher than in the other complexes (see Figure 8.19) but the increase of approximately 10 $\varepsilon_{(Sr)}$ units between the two Bulhoek samples is accompanied by a slight *decrease* in model μ. If material transfer from the granites was responsible for the higher μ in the Bulhoek carbonatites, then a significant increase in $\varepsilon_{(Sr)}$ should also be anticipated.

Figure 8.21: Plot showing the relationship between $\varepsilon_{(Sr)}$ and modelled reservoir μ in Pilanesberg Suite carbonatites and silicates.

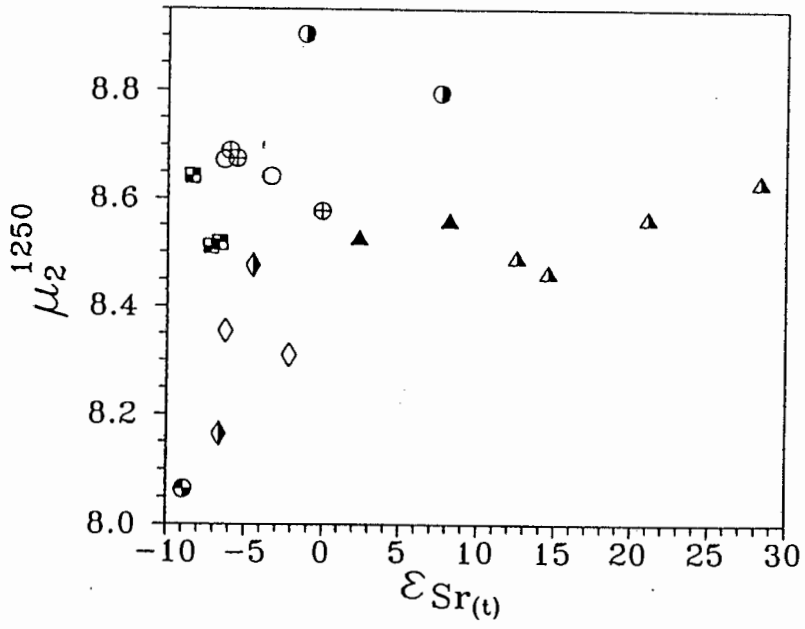

8.6.3. O-C isotopes

Oxygen and carbon isotopes were measured on a small number of selected carbonatite samples. The Stukpan analyses were performed on separated calcite rhombs whereas whole rock powders were analysed for the other complexes. These are plotted in Figure 8.22 along with the data from Clarke *et al.* (in press) for unaltered carbonatites from Kruidfontein and Nooitgedacht. The Goudini samples analysed by Nelson *et al.* (1988) were specifically excluded since they clearly do not represent primary carbonatites. Also shown on the plot is the field of compositions expected for mantle-derived carbonatite magmas (derived from Deines, 1989). With the exception of a single Nooitgedacht sample, the carbonatite data plot out of this field. Most analyses deviate to higher $\delta^{18}O$ values whereas the Stukpan samples show a very narrow compositional range with "mantle-like" $\delta^{18}O$ but with increased $\delta^{13}C$ values. Clarke *et al.* (in press) interpreted the increased $\delta^{18}O$-$\delta^{13}C$ values in the Kruidfontein carbonatites as the result of Rayleigh fractionation effects during crystallisation of the carbonatite magma in the presence of a H_2O-CO_2 vapour phase having a molar H_2O/CO_2 of 0.5.

Figure 8.22: $\delta^{18}O$-$\delta^{13}C$ plot for Pilanesberg Suite carbonatites.

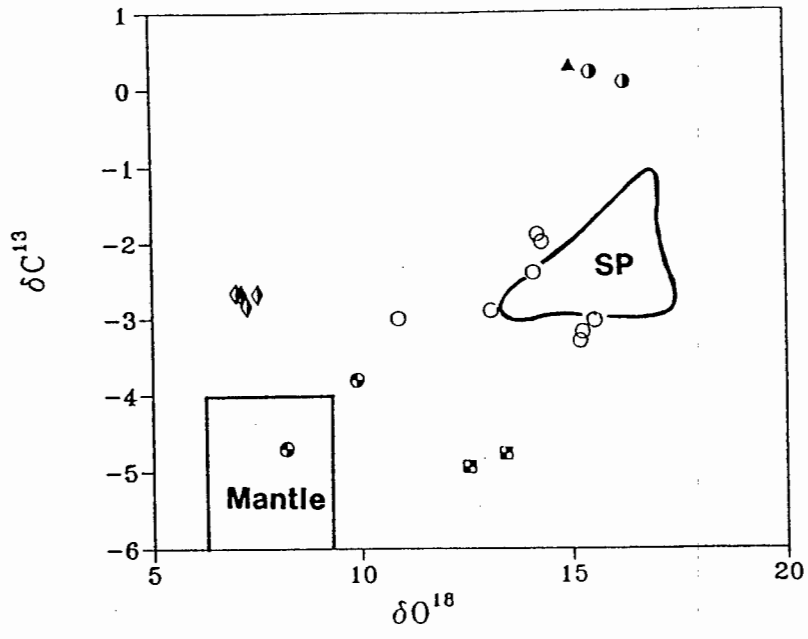

Unmodified $\delta^{18}O$-$\delta^{13}C$ for mantle derived magmas should plot in the rectangular field (after Deines, 1989). Data from the Spitskop Complex carbonatites plot in the irregular field.

A more systematic study is required, particularly analyses of separated carbonate grains, to adequately interpret the $\delta^{18}O$-$\delta^{13}C$ variations in these carbonatites.

8.6.4. Summary

Compared to the $\varepsilon_{(Sr)}$-$\varepsilon_{(Nd)}$ compositions in the Spitskop carbonatites, the Pilanesberg Suite carbonatites in the western Transvaal have less extreme $\varepsilon_{(Nd)}$ but a range in $\varepsilon_{(Sr)}$ values similar to Spitskop. Silicate components in the PRAC have $\varepsilon_{(Sr)}$ which are on average higher than the values noted for the carbonatites. On an $\varepsilon_{(Sr)}$-$\varepsilon_{(Nd)}$ plot, the Kruidfontein lava and the PRAC silicates plot to the high $\varepsilon_{(Sr)}$ and low $\varepsilon_{(Nd)}$ side of the carbonatite data. Carbonatites from Stukpan have similar $\varepsilon_{(Sr)}$-$\varepsilon_{(Nd)}$ signatures to Spitskop but trend to even greater negative $\varepsilon_{(Nd)}$ at negative $\varepsilon_{(Nd)}$ and so have a steeper trend on the $\varepsilon_{(Sr)}$-$\varepsilon_{(Nd)}$ diagram than the Spitskop data.

Chapter 9: Summary and Conclusions : Implications of Pilanesberg Suite Data

9.1. Introduction

The purpose of this chapter is to discuss the implications of the new data on the Pilanesberg suite complexes to the understanding of the genesis of carbonatites in general and in particular to evaluate the genetic relationship, if any, between carbonatites and associated alkaline silicate magmatism.

As discussed in Chapter 7, isotopic and geochemical data from the Spitskop Complex preclude the possibility that the carbonatites originated as a residue after crystallisation of the silicate components or through immiscible exsolution from a silicate parental melt. Carbonatites from the other Pilanesberg suite complexes have, on average, lower initial $^{87}Sr/^{86}Sr$ values than than the silicate components of these complexes. Again, derivation of the carbonatites and silicates from a common silicate parental melt appears unlikely. In addition, geochemical relationships between the ijolite and nepheline syenite units in the Spitskop Complex indicate that these silicate units were not derived through differentiation of a common parental melt. Distinct REE patterns in the nepheline syenites relative to those in the pyroxenites, ijolites and carbonatites argue against a common source for all the components of the Spitskop Complex. These data imply that the different lithological components of the Spitskop Complex were derived from influxes of compositionally (and possibly petrogenetically) distinct magma batches, extracted from different sources.

Figure 9.1: Plot of all $\varepsilon_{(Sr)}$-$\varepsilon_{(Nd)}$ data for carbonatites and silicates from the Pilanesberg Suite Complexes.

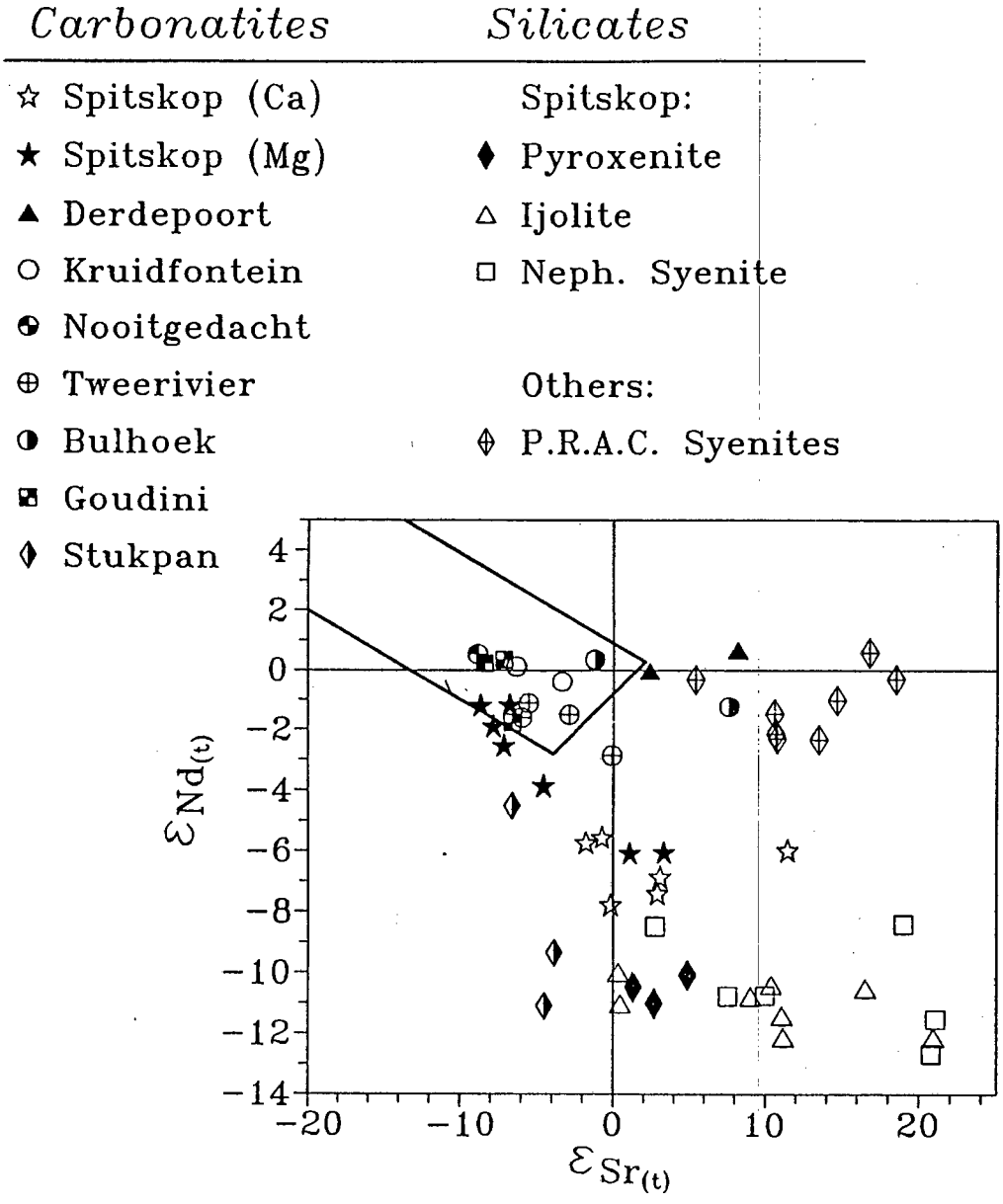

Epsilon values are calculated at the ages of intrusion of each complex. The demarcated field field bounds most world carbonatites and is discussed in Figure 9.3 below.

9.1.1. *Synthesis of the Pilanesberg $\varepsilon_{(Sr)}$-$\varepsilon_{(Nd)}$ data*

Sr and Nd isotopic data for carbonatite and silicate components of the Pilanesberg Suite complexes are summarised in Figure 9.1 where the data describe two trends on the $\varepsilon_{(Sr)}$-$\varepsilon_{(Nd)}$ plot which converge towards carbonatites having $\varepsilon_{(Nd)}$ values close to +1 and $\varepsilon_{(Sr)}$ of about −10. Silicates and carbonatites from the Pienaars

River Complex centres and the Kruidfontein Complex exhibit a greater range of $\varepsilon_{(Sr)}$ values, –1 to +18, relative to $\varepsilon_{(Nd)}$ (+1 to –2) and so define a shallow trend on the diagram. By contrast, the Spitskop and Stukpan carbonatites describe a steeper trend having more variable, and more negative, $\varepsilon_{(Nd)}$ values (–1 to –12). Silicate components of the Spitskop Complex have variable $\varepsilon_{(Sr)}$ (up to +40) at low $\varepsilon_{(Nd)}$ (–9 to –13), and effectively extend the carbonatite variation to more positive values of $\varepsilon_{(Sr)}$.

If the silicate components of the Pilanesberg Suite Complexes represent more primitive melts from which the carbonatites were derived, then these data would imply that the silicates formed from two distinct source reservoirs and coincidentally (and independently) evolved carbonatites with $\varepsilon_{(Sr)}$-$\varepsilon_{(Nd)}$ compositions which converged towards an $\varepsilon_{(Sr)}$ value of about –10 and $\varepsilon_{(Nd)}$ of +1.

9.1.2. A working hypothesis

If it can be demonstrated that carbonatites can exist as discrete melts in the mantle, and that at least part of the Proterozoic sub-Kaapvaal mantle was characterised by depleted $\varepsilon_{(Sr)}$-$\varepsilon_{(Nd)}$ (i.e. negative $\varepsilon_{(Sr)}$ and positive $\varepsilon_{(Nd)}$), then the Pilanesberg Suite $\varepsilon_{(Sr)}$-$\varepsilon_{(Nd)}$ data may be logically interpreted as the result of interaction between a primary carbonatite melt (with depleted mantle $\varepsilon_{(Sr)}$-$\varepsilon_{(Nd)}$ values) and one or more enriched lithospheric (crust or mantle) reservoirs during its evolution and passage to the surface. By implication, then, since the silicate data fall at the enriched ends of the carbonatite trends in Figure 9.1, the Pilanesberg Suite silicate rocks contain a larger proportion of the enriched reservoir(s); i.e. the silicate components are probably derived, in whole or part, from the enriched reservoir(s).

It is therefore proposed that the Pilanesberg Suite data are best explained by a model whereby the carbonatites evolve from primitive carbonatitic mantle melts, whereas the associated silicate magmas are derived from melting of mixtures of enriched lithosphere and trapped carbonatite melt.

In the following sections, available experimental and isotopic data are reviewed and used to argue that discrete carbonatite magmas can occur in the mantle. A brief review is then presented of current models for the origin of the alkaline silicate magma types commonly associated with carbonatites, particularly the felsic varieties which are more common in the Pilanesberg Suite complexes. The hypothesis proposed above is then assessed in the light of this review and a dynamic model is presented for the petrogenetic relationship between the carbon-atite and silicate components of alkaline complexes.

9.2. *Carbonatites as primary mantle melts*

9.2.1. *Experimental evidence*

Derivation of carbonatites as primary melts of carbonated mantle material has long been discussed by experimental petrologists involved in investigating the peridotite-CO_2-H_2O system at mantle pressures (e.g. Wyllie and Huang, 1975; Koster Van Groos, 1975; Olafsson and Eggler, 1983; Wyllie, 1980). The topology of the peridotite-CO_2 system is dominated by a carbonation reaction where peridotite olivine reacts to magnesian carbonate at elevated pressures by the reaction:

$$\underset{\text{olivine}}{2Fo} + \underset{\text{clinopyroxene}}{Di} + 2CO_2 = \underset{\text{orthopyroxene}}{4En} + \underset{\text{dolomite}}{Cd} \qquad [9.1]$$

Solubility of CO_2 increases significantly in partial melts at pressures in excess of this reaction (Wyllie and Huang, 1976a) and this leads to a sharp depression in temperature of the peridotite solidus.

Traces of carbonate liquids were reported in melting experiments on mantle materials (e.g. Wendlandt and Mysen, 1978) but the first experimental demonstration that carbonatite melt could occur in equilibrium with natural mantle material was presented by Wallace and Green (1988). These experiments were performed on fertile peridotite ("Hawaiian pyrolite") under oxidising conditions in the presence of small amounts of CO_2 and H_2O (CO_2 80% of total volatile phase). A P-T field was delineated in which carbonatite melt coexists with amphibole lherzolite (Figure 9.2): carbonatite melt is formed where amphibole remains stable at temperatures above the peridotite solidus. As such, the carbonatite melt "window" is bounded at high temperature and pressure by the amphibole breakdown curve, and at low temperatures and pressure by the volatile under-saturated peridotite solidus. At temperatures and pressures above the amphibole breakdown reaction, CO_2-bearing silicate melts rather than carbonatite melts are formed: olivine nephelinite in the spinel stability field, olivine melilitite in the garnet stability field. As a consequence, mantle containing carbonatitic partial melt will overlie mantle with dispersed melilititic partial melt along any geotherm intersecting the carbonatite stability field.

Figure 9.2: Phase diagram for fertile peridotite ("Hawaiian Pyrolite") solidus relationships under fluid-undersaturated conditions.

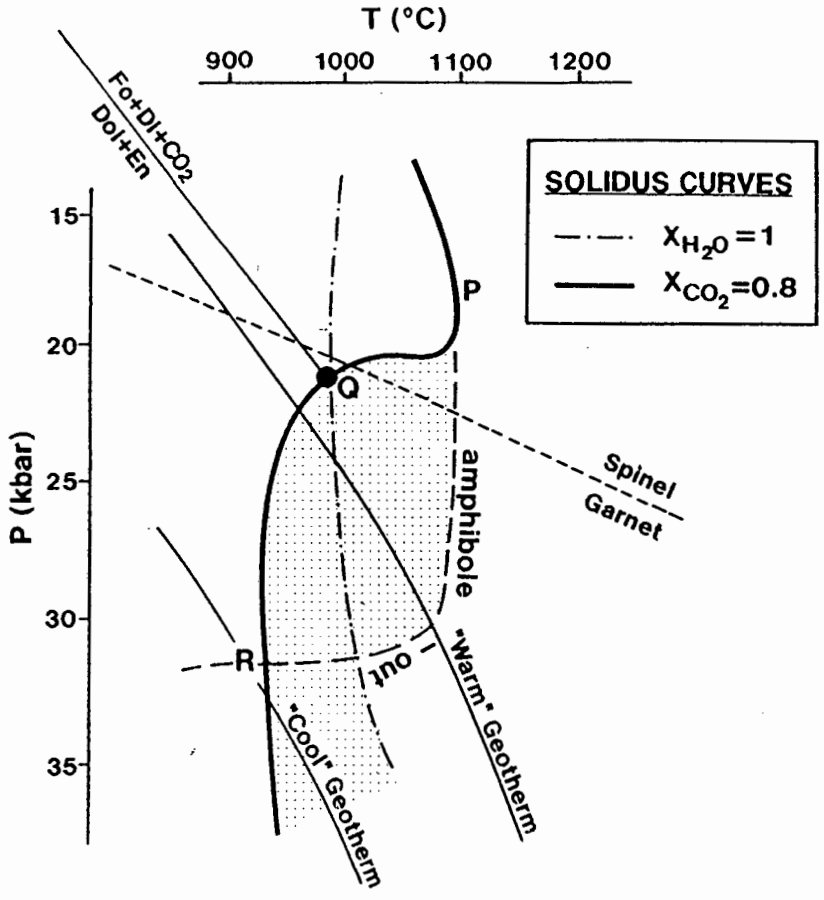

Solidus curves are from Wallace and Green (1988), Green and Wallace (1988) and Fallon and Green (1989). The stippled field marks the P,T conditions under which carbonatite melt exists in equilibrium with mantle peridotite.

Since the presence of amphibole controls the occurrence, size and position of the carbonatite stability field in P-T space, the presence of carbonatite melt is favoured in a fertile peridotite where the mole fraction of water is about 0.4 and is greatly limited in a refractory lherzolite impoverished in Na, Ti and K (Wallace and Green, 1988).

The equilibrium carbonatite melt in the Wallace and Green experiments was magnesian (Mg#=0.845) and contained significant amounts of alkalis (4.99% Na_2O; 0.35% K_2O) and some SiO_2 and Al_2O_3. Magnesio-carbonatite melts were also produced in experiments at 20-30kbars in the peridotite-carbonate-phosphate system by Ryabchikov and co-workers (Ryabchikov *et al.*, 1990; 1991). These experiments also demonstrated that mantle carbon-atite melts extract appreciable amounts of Na

from associated silicate phases and can dissolve large amounts of P_2O_5 and rare earth elements. Mantle carbonatite melts are in equilibrium with residual garnet which would preferentially retain the HREE and thus impart the strong LREE-HREE fractionation on the melt which is a characteristic feature of carbonatites (e.g. Möller *et al.*, 1980; Woolley and Kempe, 1989).

Available experimental data confirm, therefore, that carbonatites can occur as primary melts of carbonated amphibole peridotite and indicate that primitive melts will be magnesium-rich i.e. dolomite- rather than calcite-carbonatites.

9.2.2. Isotopic data

Early investigations of the Sr isotopic geochemistry of carbonatites showed that most carbonatites were characterised by $^{87}Sr/^{86}Sr$ ratios significantly lower than average continental crust (e.g. Powell *et al.*, 1962, 1966) but comparable to $^{87}Sr/^{86}Sr$ in oceanic basalts (Faure and Powell, 1972). As a result of these isotopic data, carbonatites came to be generally regarded as being derived from the mantle (e.g. Faure and Powell, 1972). Up until the late 1980's, though, carbonatites were usually considered "secondary" magmas derived from siliceous mantle melts like nephelinites through fractional crystallisation or immiscible exsolution (e.g. King and Sutherland, 1960; Le Bas, 1977, 1981; Wyllie, 1989; Kjarsgaard and Hamilton, 1989).

Carbonatites have Sr and Nd concentrations which are substantially higher than average crustal rocks (e.g. see average values in Woolley and Kempe, 1989). If these concentration levels are primary features, then carbonatites are less likely to have their isotopic signatures affected through interaction with crustal rocks during emplacement. These attributes have been invoked in several investigations to argue that the Sr and Nd isotopic composition of carbonatites can be utilised to investigate the nature of the sub-continental mantle (e.g. Bell *et al.*, 1982; Bell and Blenkinsop, 1985, 1987a, 1989). Despite the cyclicity inherent in this reasoning, this approach has established a substantial database of $\varepsilon_{(Sr)}$-$\varepsilon_{(Nd)}$ isotope measurements on carbonatites.

An extremely significant implicit assumption in the use of carbonatites as isotopic "windows to the mantle" is that, for the high Sr and Nd concentrations in carbonatites to be an effective barrier against contamination by crustal rocks, carbonatites must exist as discrete magmas at mantle depths, already with the elevated concentrations of incompatible trace elements characteristic of carbonatites sampled at surface.

Figure 9.3: Compilation of $\varepsilon_{(Sr)}$-$\varepsilon_{(Nd)}$ data for world carbonatites younger than 200Ma.

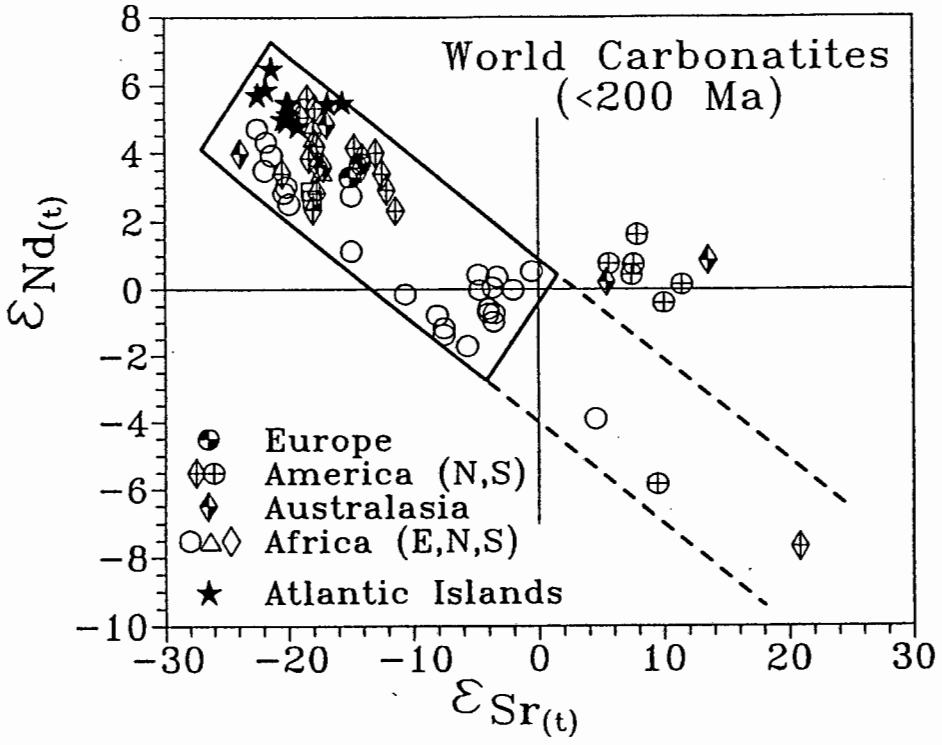

All epsilon values were calculated at the time of emplacement of each carbonatite. The boxed field (heavy solid line) bounds 85% of the carbonatite data and has the coordinates (clockwise from top): (–21.3, 7.3); (1.5, 0.45); (–4.2, –2.7); (–27, +4.1).

Over 120 $\varepsilon_{(Sr)}$-$\varepsilon_{(Nd)}$ and somewhat fewer Pb isotope measurements are currently available for carbonatites ranging in age from present day to 2700 Ma and widely distributed geographically: Europe, North and South America, the Atlantic Ocean, Africa and Australasia. Discussions of the data have been presented by Nelson *et al.* (1988), Bell and Blenkinsop (1989) and Kwon *et al.* (1989).

9.2.2.1. $\varepsilon_{(Sr)}$-$\varepsilon_{(Nd)}$ variations in world carbonatites

To limit potential distortions inherent in comparing ε values from data sets of differing ages, the variations in composition in carbonatite complexes less than 200Ma in age are discussed first. More than 75% of the available data are for carbonatites in this age range.

Figure 9.4: Comparison between $\varepsilon_{(Sr)}$-$\varepsilon_{(Nd)}$ compositions of young carbonatites, Group-I kimberlites and selected oceanic island basalts.

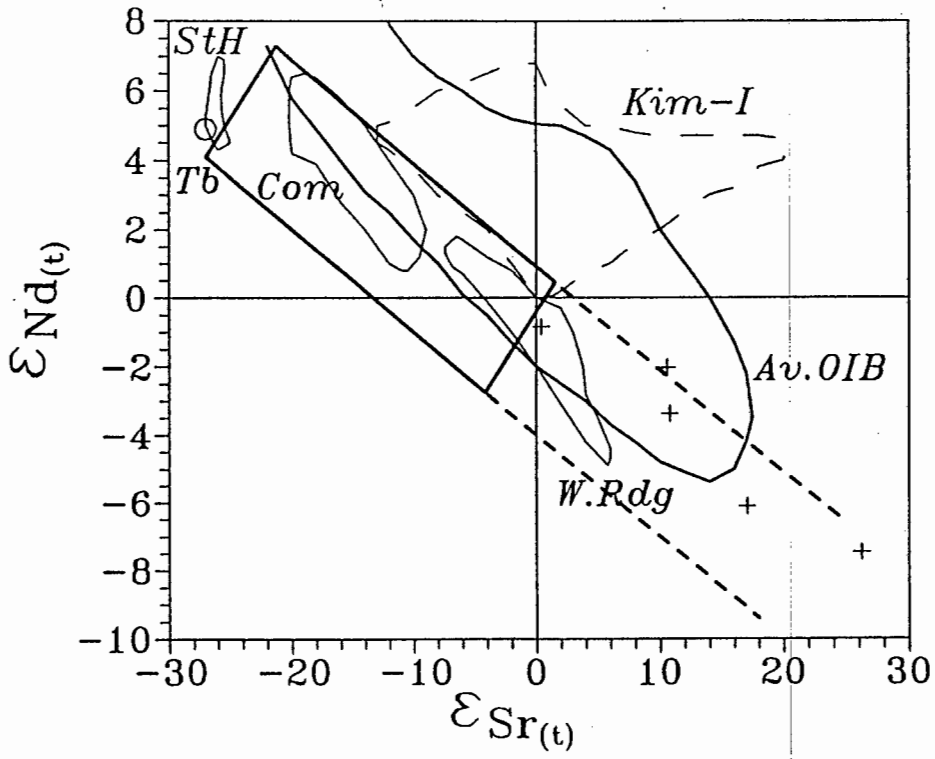

Fields are:

Av.OIB: a "generalised field" enclosing most oceanic island basalts;
StH: Saint Helena Island; Tb: Tubuaii Island; Com: Comores Islands;
W.Rdg: Walvis Ridge; (all fields from Wilson, 1989; Chapter 9);
Kim-I: Group-I Cretaceous kimberlites (Smith, 1983)

Most analyses plotted in Figure 9.3 - including data from widely separated areas including Atlantic Ocean Islands, Canada, New Zealand, Namibia, north Africa, Europe and some east African complexes - plot within a relatively narrow range of –10 to –24 $\varepsilon_{(Sr)}$, and +2 to +6 $\varepsilon_{(Nd)}$. Bell and Blenkinsop (1987b) demonstrated that available $\varepsilon_{(Sr)}$-$\varepsilon_{(Nd)}$ data for African carbonatites define a quasi-linear array trending to increasingly positive $\varepsilon_{(Sr)}$ and negative $\varepsilon_{(Nd)}$ values and referred to this array as the "East African Carbonatite Line". The Homa Bay carbonatite has the most "enriched"[1] signature ($\varepsilon_{(Sr)}$ +4.5; $\varepsilon_{(Nd)}$ –3.9) of the East African carbonatites. The single determination from the Catalào carbonatite of Brazil (Bizzi *et al.*, in press) plots along the extension of this array. Additional data gathered from the East African

[1] In the interests of brevity, positive $\varepsilon_{(Sr)}$ and negative $\varepsilon_{(Nd)}$ values will be referred to as "enriched" (i.e. reflecting time-integrated enrichments in Rb/Sr and Nd/Sm) and "depleted" to denote negative $\varepsilon_{(Sr)}$ and positive $\varepsilon_{(Nd)}$ values (i.e. reflecting time-integrated depletions in Rb/Sr and Nd/Sm).

carbonatites of Oldoinyo Lengai (Nelson *et al.*, 1988; Harmer and Gittins, unpublished data) and Shombole (Bell and Peterson, 1991) trend away from this array to higher $\varepsilon_{(Sr)}$-$\varepsilon_{(Nd)}$ values. Data from Jacupiranga, Brazil (Roden *et al.*, 1985), and Walloway, Australia (Nelson *et al.*, 1988) have $\varepsilon_{(Sr)}$ values which are significantly higher than the other carbonatites. The most extreme carbonatite composition, though, is that reported for the carbonatite at Crazy Mountains, Montana by Dudas *et al.* (1987) which has $\varepsilon_{(Sr)}$ of +20 and $\varepsilon_{(Nd)}$ of –7.

As shown on Figure 9.3, 85% (63 out of 74) of the young carbonatite isotopic analyses are enclosed within a rectangular-shaped field: the base of which corresponds closely to the so-called "East African Carbonatite Line" of Bell and Blenkinsop (1987b); the upper limit drawn parallel to the base to enclose the compositions of the Atlantic Island and Shombole-Lengai carbonatite data. The Catalào and Crazy Mountains carbonatites fall within an extension of the array to higher $\varepsilon_{(Sr)}$. Nelson *et al.* (1988) and Bell and Blenkinsop (1989) commented on the similarity between the $\varepsilon_{(Sr)}$-$\varepsilon_{(Nd)}$ compositions of carbonatites and ocean island basalts (OIB). In Figure 9.4 the "Carbonatite array" compares closely with OIB data from Tubuaii, Saint Helena, Comores and the Walvis aseismic ridge occurrences which fall to the low $\varepsilon_{(Nd)}$ side of the OIB's and define the low $\varepsilon_{(Nd)}$ ("LoNd") array of Hart *et al.* (1986). The similarity in $\varepsilon_{(Sr)}$-$\varepsilon_{(Nd)}$ between carbonatites and OIB indicates that the young carbonatite data set, which consists mostly of carbonatites from continental areas, contains no evidence of isotopic components not present in mantle-derived oceanic basalts.

In Figures 9.5 (a) and (b) the $\varepsilon_{(Sr)}$-$\varepsilon_{(Nd)}$ data for carbonatites older than 200 Ma are compared with the array defined for young carbonatites. Data for the 2.0 Ga Southern African Phalaborwa and North African Ihouhaouene complexes are substantially enriched in $\varepsilon_{(Sr)}$ and plot to the right, and well above, the carbonatite array whereas all the other complexes plot within, and towards the upper end of the array. With the exception of Phalaborwa and Ihouhaouene, then, older carbonatites seem to have been derived from sources with similar Rb/Sr and Sm/Nd fractionation histories, i.e. enrichments or depletions for comparable time periods, to those producing modern carbonatites. The array is thus useful as a reference for Proterozoic carbonatites as well.

Figure 9.5: $\varepsilon_{(Sr)}$-$\varepsilon_{(Nd)}$ data for carbonatites greater than 200Ma in age.

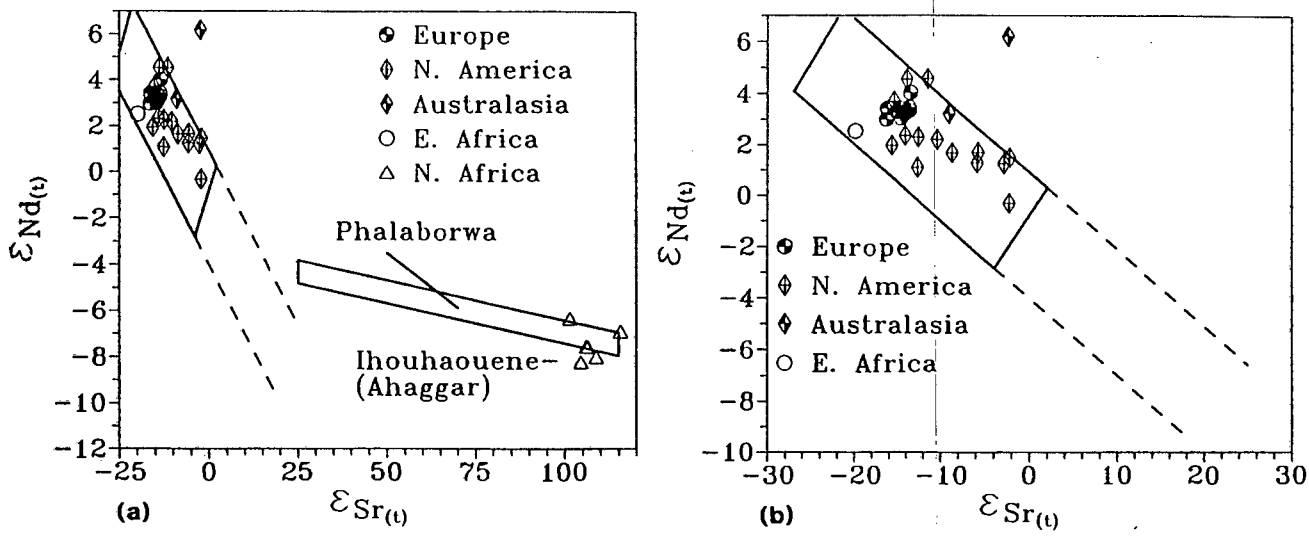

(a) Including data from the extremely $\varepsilon_{(Sr)}$-enriched 2.0Ga Phalaborwa and Ihouhaouene carbonatite complexes.
(b) At expanded scale to show the comparison with the isotopic variations in carbonatites <200Ma in age.
Epsilon values are calculated at the time of intrusion of the individual complexes. Symbols are the same as Figure 9.4.

9.2.2.2. Pb isotopic composition of world carbonatites

Pb isotopic data on carbonatites are less extensive than Nd or Sr and, in many cases, Pb data for a specific complex were not determined on the same samples used for the Sr and Nd measurements (e.g. Kwon *et al.*, 1989). The interpretation of Pb isotopic data for older carbonatites, and comparison between complexes of different ages, is more difficult than for isotopes of Sr and Nd. Kwon *et al.* (1989) showed that ^{206}Pb-^{204}Pb is generally negatively correlated with initial $^{87}Sr/^{86}Sr$ (positively correlated with initial $^{143}Nd/^{144}Nd$) in carbonatites younger than 2700 Ma. Again, young carbonatites have similar Pb isotopic compositions to OIB, many having comparable ratios to data from Saint Helena and Tubaii, islands defining the "HIMU" reservoir discussed by Zindler and Hart (1986).

9.2.2.3. $\varepsilon_{(Sr)}$-$\varepsilon_{(Nd)}$ variations in alkaline silicate rocks associated with carbonatites

A brief review of the relative $\varepsilon_{(Sr)}$-$\varepsilon_{(Nd)}$ variation in these contrasted compositions is of significance in evaluating the possible "primary" status of carbonatite liquids.

Surprisingly few studies have been published on the isotopic relationships between the silicate and carbonatite components of individual alkaline complexes.

Sr isotope ratios in phonolitic lavas associated with the natro-carbonatites of Oldoinyo Lengai are more variable and have higher $^{87}Sr/^{86}Sr$ values than those obtained for the carbonatites (Bell *et al.*, 1973). In the Shombole volcano, nephelinites have comparable $\varepsilon_{(Sr)}$-$\varepsilon_{(Nd)}$ values to the carbonatites whereas the phonolites are isotopically distinct (Bell and Peterson, 1991). Pyroxenites from the 2Ga Phalaborwa Complex have initial $^{87}Sr/^{86}Sr$ in the range 0.7114-0.7124 whereas the associated carbonatites vary from 0.7039 to 0.7068 (Eriksson, 1989).

Sr isotope values are similar in the carbonatites and uncontaminated silicate components (syenite, phonolite, lamprophyre) in the Tamazert complex of Morocco (Bernard-Griffiths *et al.*, 1991) whereas $\varepsilon_{(Nd)}$ values decrease in the sequence lamprophyre-carbonatite-syenite/phonolite. No distinction in isotopic composition is observed between the carbonatites and associated silicates in the Oka Complex, Canada (ijolite, okaite, carbonatite: Wen *et al.*, 1987), the Gardiner Complex, Greenland (nephelinites, carbonatite: Nielsen and Buchardt, 1985), nor for Fuerteventura, Canary Islands (basanite, tephrite, ijolite, nephelinite, carbonatite: Hoernle and Tilton, 1991).

More data are available for carbonatites and silicates associated on a more regional scale, i.e. in volcanic provinces. Carbonatite components of the Miocene Kaiserstuhl complex in Germany have more consistent isotopic signatures ($\varepsilon_{(Sr)}$ of −11 to −15) than the associated silicate volcanics (Schleicher *et al.*, 1990): nephelinites have lower $\varepsilon_{(Sr)}$ (−16 to −12) and higher $\varepsilon_{(Nd)}$ whereas the more felsic phonolites and tephrites have substantially higher $\varepsilon_{(Sr)}$ (−6 to +7). By comparison, Quaternary and Tertiary "mantle-derived and derivitive" mafic silicate rocks from the German volcanic province (Wörner *et al.*, 1986) range in $\varepsilon_{(Sr)}$ from −23 to +6 whereas the more felsic trachytes and phonolites have even higher $\varepsilon_{(Sr)}$ values.

9.2.3. *Discussion*

Experimental evidence indicates that magnesio-carbonatite magmas can be generated by partial melting, under oxidising conditions, of volatile-undersaturated peridotite at upper mantle pressures. The similarity between Sr and Nd isotopic ratios observed in young carbonatites and ocean island basalts is also consistent with carbonatites originating as direct melts of the mantle.

With few exceptions, carbonatites show a limited range in $\varepsilon_{(Sr)}$-$\varepsilon_{(Nd)}$ compositions which are remarkably consistent between continents and over geological time. Pb isotopic values are more variable and tend to correlate with initial $^{143}Nd/^{144}Nd$. These observations indicate that, through time, carbonatites are consistently derived from sources with trace element fractionation histories comparable to the sources of many oceanic island basalts (Nelson *et al.*, 1988; Bell and Blenkinsop, 1989; Kwon *et al.*, 1989). By contrast, many alkaline silicate rocks have more variable isotopic signatures which tend to be similar to, or more enriched (i.e. higher $\varepsilon_{(Sr)}$, lower $\varepsilon_{(Nd)}$) than, the carbonatites.

These relationships are difficult to reconcile with genetic models which consider carbonatite liquids as secondary derivitives of primary silicate melts and rather favour the existence of primary carbonatite magmas at mantle depths. The similarity between the isotopic compositions of Sr-Nd-Pb in OIB and carbonatites, plus the limited range of $\varepsilon_{(Sr)}$-$\varepsilon_{(Nd)}$ compositions for carbonatites emplaced into crustal segments of widely different ages (e.g. Oka - Canadian Shield; Canaries and Cape Verdes - Atlantic oceanic crust) suggests derivation from sub-lithospheric sources, possibly mantle plumes (Nelson *et al.*, 1988).

9.2.3.1. *Are the known field and compositional observations on carbonatites adequately explained by primitive carbonatite melts?*

While experimental investigations provide evidence that magnesio-carbonatites can exist as primary melts in equilibrium with peridotite mantle, they do not establish that such melts are necessarily related to carbonatites as sampled at surface. Indeed, Barker (1989) has asserted that "There is little evidence for a primary carbonatite magma ascending directly from the mantle".

Magnesio-carbonatite quenched liquid droplets have been described in pyroclastics from the carbonatite volcanoes of south-east Zambia (Bailey, 1989,1990;

Ngwenya and Bailey, 1990) which contain dolomite in equilibrium with magnesio-chromite crystals compositionally identical to those found in mantle peridotites and kimberlites (Bailey, 1989). As a consequence, the quenched droplets are interpreted as primary carbonatite mantle melt erupted at high speed (Bailey, 1990). The pyro-clastics are associated with intrusive magmatic magnesio-carbonatites which developed in a "..slow moving (or high level storage) melt system, equilibrated at low pressure" and calcio-carbonatites are common, but no alkaline silicate or alkaline carbonatite magmatism is associated with these Zambian volcanoes (Bailey, 1990).

Calcio-carbonatites are more abundant than magnesio- or ferro-carbonatites in carbonatite complexes worldwide. In addition, where calcio- and magnesio-carbonatites are associated in single complexes, the calcio-carbonatites tend, as at Spitskop, to be earlier (e.g. Le Bas, 1977; Barker, 1989). It is therefore important to assess possible petrogenetic schemes which could generate calcio-carbonatite liquids from dolomitic parental mantle melts. Carbonatites characteristically also contain elevated concentrations of LILE and certain HFSE, in particular Sr, Ba, Nb, P and the LREE. The extent to which the observed levels of these elements are explained by partial melting of mantle material will also be discussed.

Figure 9.6: Variation in composition of carbonatite liquid WG-1 and the liquidus carbonate phase with pressure (Sweeney *et al.*, in press).

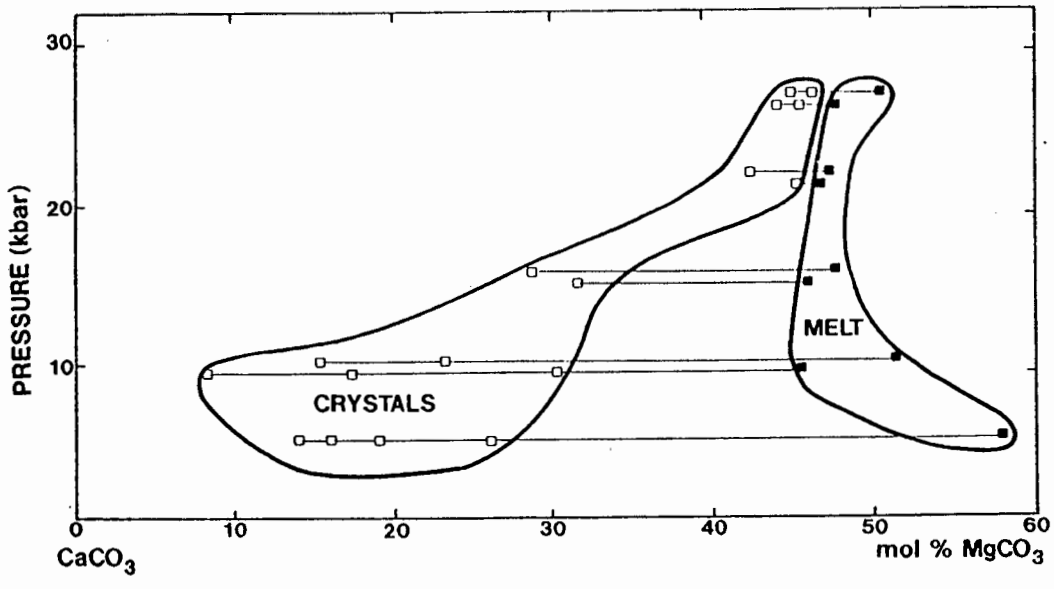

9.2.3.1.1. The evolution from Mg- to Ca- carbonatites

Wallace and Green (1988) established that the liquidus phases of their experimental carbonate mantle melt (for convenience here termed "WG-1") were dolomite, olivine and spinel. Fractionation of forsteritic olivine is an obvious mechanism by which WG-1 could evolve towards a more calcitic composition but crystallisation of olivine (and any other silicate mineral) is limited by the SiO_2 content of the carbonatite melt. Simple mass balance indicates that only seven weight percent of stoichiometric forsterite could crystallize from the WG-1 composition which would reduce the Mg# of the resulting liquid from 0.85 to 0.80 and only increase the CCMF from 0.48 to 0.54. Crystallisation of magnesian spinel is similarly limited by the Al_2O_3 content in the melt.

Wallace and Green (1988) calculated that substantial dolomite fractionation from WG-1 could produce sodic carbonatite equivalent to that described from Oldoinyo Lengai. Sweeney *et al.* (in press) investigated the evolution of the WG-1 carbonatite melt through decreases in pressure and temperature. These experiments confirmed that the principal liquidus phases were carbonate, olivine and spinel but showed that, while the liquid composition remained magnesian, the liquidus carbonate became progressively more calcitic with falling pressure (reproduced in Figure 9.6). As a result, fractionation of the liquidus carbonate phase would drive the residual liquid to more *magnesian* compositions.

It will be noted from 9.2 that the carbonatite melt field is situated below the thermal maximum in the solidus curve: ascending carbonatite melts which remain in equilibrium with their surroundings will therefore encounter the solidus at ca. 20kbars and must freeze by the reaction:

$$4\ Opx + Dol = 2\ Fo + Di + 2CO_2 \qquad [9.2]$$

i.e. the "carbonation" reaction (equation [9.1] above) shown in Figure 9.2 expressed in reverse. The Sweeney *et al.* (in press) experiments thus simulate the ascent of carbonatite melt partially shielded from interaction with surrounding peridotite. These authors suggested that minor reaction between the carbonatite melt and wall rock diopside would shift the melt to more calcic composition by the reaction:

$$\underset{\text{Melt-1}}{Di + 3\ Dol} = \underset{\text{Melt-2}}{2\ Fo + 4\ Cc} + 2\ CO_2 \qquad [9.3]$$

Limited reaction between dolomitic melt and wall rock ortho-pyroxene may also cause a shift to more calcitic melt compositions by:

$$\underset{}{En} + \underset{\text{Melt-1}}{2\,Dol} = \underset{}{2\,Fo} + \underset{\text{Melt-2}}{2\,Cc} + \underset{}{CO_2} \qquad [9.4]$$

The relative proportions of pyroxene ("wall rock") to dolomite ("carbonatite melt") in the reactants of the balanced equations are significant: equation [9.2] has Opx:Dol in the ratio 4:1 and would thus be appropriate to situations where only minor amounts of carbonatite melt is present. Reactions [9.3] and [9.4] have Px:Melt proportions of 1:3 and 1:2 respectively, and so would apply in situations where more substantial quantities of carbonatite melt is available.

Interaction between dolomitic carbonatite melt and pyroxene-bearing wall-rocks is thus a viable alternative mechanism to derive calcic carbonatitic magma from a magnesian primary melt.

The WG-1 composition contains about 5% Na_2O and 0.35% K_2O and processes such as carbonate fractionation and reaction with pyroxene should concentrate the alkalis in the residual melt. Most carbonatites sampled at surface have very low alkali contents - the Woolley and Kempe (1989) averages reflect less than 0.6% total alkalis. Only the rare natro-carbonatites of Oldoinyo Lengai and Shombole have elevated alkali contents. Most carbonatite complexes are surrounded by fenite aureoles where the country rocks have been subjected to metasomatism by Na- and/or K-rich fluids emanating from the carbonatite (e.g. review of McKie, 1966; also references in Chapter 6). Loss of alkalis to a fluid phase at lower pressure could thus explain the discrepancy in alkali budgets between WG-1 and surface carbonatites. Sweeney *et al.* (in press) demonstrated that the WG-1 composition does indeed pass through a melt to melt plus vapour reaction at lower pressure. Alkali halides were identified lining gas cavities in the experimental charges and so Sweeney *et al.* deduced that alkalis would be extracted into a halogen-rich vapour with falling pressure. The reaction occurred at about 13 kbars, 1000°C near to the WG-1 liquidus and at just over 700°C below 1 kbar. Alkali loss, and associated metasomatism, would be expected during the passage of evolving carbonatite melt through continental crust.

9.2.3.1.2. Trace and minor element concentrations in carbonatites

Carbonatites characteristically have elevated levels of Sr, Ba, Nb and the LREE and have very large LREE/HREE. Carbonatite melt of amphibole lherzolite will form in equilibrium with amphibole, garnet and the lherzolite phases. Concentration levels of a selection of elements in 0% (i.e. maximum enrichment attainable by partial melting)

Figure 9.7: Normalised variation diagram to compare trace element concentrations in average magnesio-carbonatite with low degree partial melts of garnet amphibole lherzolite.

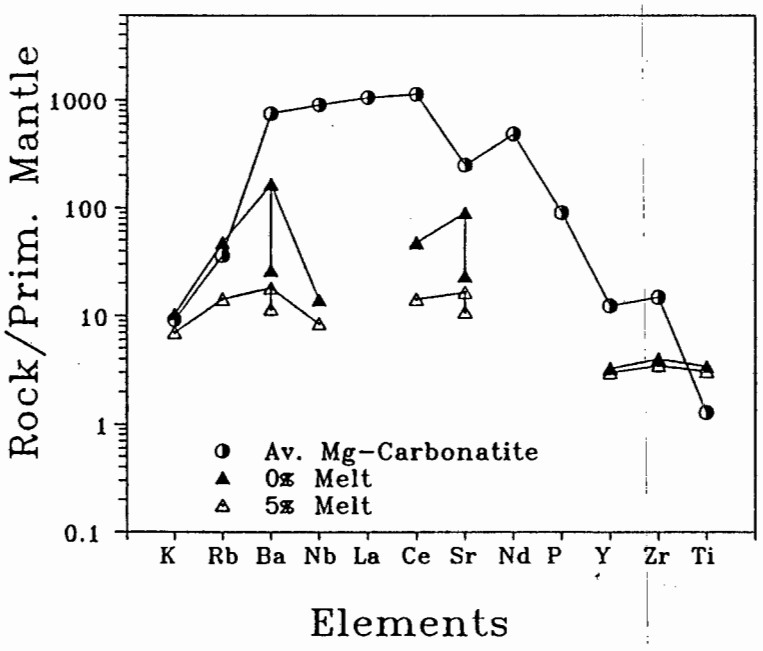

Two values are plotted for Ba and Sr: these reflect differences in the published amphibole-carbonatite melt partition coefficients. See text and caption to Table 9.1 for further details.

and 5% batch melts in equilibrium with a residual garnet-amphibole-lherzolite mineral assemblage are tabulated in Table 9.1 and compared with levels in average magnesio-carbonatite in a spiderdiagram in Figure 9.7.

In Figure 9.7 the maximum enrichment levels are generally somewhat lower than those in the average carbonatite: Nb and the LREE differ by more than one order of magnitude; Ba, Sr, Y and Zr approach the average more closely. Ti is higher in the melts than the carbonatite average. Concentration levels of Rb, Ba, Nb, Ce and Sr fall rapidly with increasing degree of melting. These calculations suggest that some degree of enrichment of the primary melt is required to match the levels attained in average carbonatite. This could be achieved either through prior enrichment of the mantle source or by enrichment during evolution of the melt. Bulk distribution coefficients for all the elements are dominated by the presence of residual amphibole and garnet since individual coefficients for olivine and orthopyroxene are extremely small. During the exchange reactions with wall-rock pyroxene discussed above, Rb, Ba, Nb, Ce, Sr, and Y would be strongly retained in the residual melt and so will become progressively enriched during ascent.

Table 9.1: Enrichment factors (C_l/C_o) in model carbonatitic melts.

	D	$C_l/C_{o(max)}$	$C_l/C_{o(5\%)}$
K	0.097	10.3	7.0
Rb	0.021	47.6	14.3
Ba	0.006 (0.038)	166.7 (26.3)	18.0 (11.6)
Nb	0.071	14.1	8.5
Ce	0.021	47.6	14.3
Sr	0.011 (0.043)	90.0 (23.3)	16.5 (11.0)
Y	0.303	3.3	3.0
Zr	0.247	4.1	3.5
Ti	0.291	3.4	3.1

Enrichment levels were calculated for batch melts in equilibrium with the residual assemblage $Ol_{60}Opx_{20}Cpx_{10}Amph_5Gt_5$. $(C_l/C_o)_{max}$ represents a "0% partial melt" and is equivalent to 1/D. Bulk distribution coefficients were estimated using mineral-carbonatite melt partition coefficients determined by Brenan and Watson (1991) and Sweeney *et al.* (1992), supplemented by those for basaltic melts at high pressure by T.H.Green *et al.* (1989). Large differences exist between the Ba and Sr carbonatite melt - amphibole partition coefficients reported by Sweeney *et al.* and those of Brenan and Watson. Values shown in parenthesis are calculated using the latter values.

9.2.3.2. Conclusion

Magnesio-carbonatites can form as direct melts of mantle peridotite. These primitive melts may evolve to more calcic compositions through interaction with mantle wall rocks during ascent. The levels of elements such as Ba, Sr, LREE and Nb also need to increase during melt evolution to the levels characteristic of carbonatites found at surface.

9.3. Review of current models for genesis of felsic alkaline silicate magmatism.

If carbonatites can be generated directly as melts of peridotite, then the petrogenetic link between carbonatites and associated (spatially and temporally) silicate rocks is less obvious and warrants discussion.

Alkaline magmatism encompasses an extremely wide spectrum of rock types and is too broad a topic for exhaustive treatment here: the discussion will be restricted to those silicate rock types found amongst the Pilanesberg suite complexes and which are commonly associated with carbonatites worldwide. Aspects of this

topic were included in the discussion of the genesis of the Spitskop carbonatites in Chapter 7: nephelinitic magmas in particular are widely favoured as parental magmas from which carbonatites are derived through immiscible exsolution or as residues from fractionation (Le Bas, 1987, 1989; Kjarsgaard and Hamilton, 1989).

More felsic alkaline rock types, phonolites and trachytes, and their coarse-grained equivalents nepheline syenites and syenites, common in the Pilanesberg suite complexes, are frequently associated with carbonatites elsewhere (e.g. Oldoinyo Lengai: Donaldson *et al.*, 1987; Shombole: Bell and Petersen, 1991; complexes of the Chilwa province: Woolley and Jones, 1987; Kaiserstuhl, Germany: Schleicher *et al.*, 1990) and are characteristic magma types in continental rifts and certain oceanic islands (e.g. Carmichael *et al.*, 1974; Wilson, 1989).

9.3.1. Differentiation from alkalic, mantle-derived mafic parental magmas

Phonolitic and trachytic magmas have traditionally been regarded as the products of closed system, low pressure frac-tional crystallisation of undersaturated mafic parental magmas such as alkali basalt, basanite or nephelinite (e.g. Coombs and Wilkinson, 1969; Baker, 1969; Lippard, 1973; Carmichael *et al.*, 1974).

Objections to low pressure fractionation as the sole mechanism producing felsic alkaline magmas include the lack of intermediate compositions between basalt and trachyte (Chayes, 1963; Yoder, 1973; Bailey, 1987) and the disproportionate volume of felsic relative to mafic lavas in some provinces (Goles, 1976). Bailey (1987) has argued that the lack of intermediate compositions is not an artefact of limited exposure, and noted that the most common nodules in felsic volcanics are cognate (i.e. syenite) and, where subvolcanic syenitic plutons are exposed below phonolite or trachyte lavas, these seldom contain intermediate components. It is apparent, then, that "..the case for low-pressure differentiation as a *universal* mechanism for producing felsic magmas can be seen to be without foundation" (Bailey, 1987; p5). Wilkinson and Stolz (1983) also questioned the generation of felsic alkaline rocks solely through low pressure fractionation of nephelinitic parents and proposed that at least some phonolites form as products of upper mantle or deep crustal melting.

9.3.2. Models of D.K. Bailey - the role of metasomatism

Irving and Green (1976) argued that the low $Mg/(Mg+Fe^{+2})$ ratios in phonolitic magmas preclude their derivation as primary melts from peridotitic mantle containing

forsteritic olivine. Despite these arguments, phonolites and trachytes have been reported which contain ultramafic xenoliths of presumed mantle origin (Wright, 1966, 1969; Irving and Price, 1981) suggesting that, under certain circumstances, phonolite and trachyte magmas can exist at mantle depths. Bailey (1987) has pointed out that available experimental data do not preclude the existence of alkali feldspars and nepheline, essential components of felsic alkaline magmas, in the upper mantle. Modelling the geochemistry of a number of lherzolite-bearing phonolitic lavas led Irving and Price (1981) to conclude that "..fractional crystallisation processes at mantle pressures have produced at least some phonolitic liquids which remained essentially unmodified during subsequent ascent to the surface".

In a number of papers, Bailey (1980a, 1980b, 1982, 1986, 1987) has argued that felsic alkaline magmas can be generated as primary melts from lithospheric mantle materials previously modified (metasomatised) by the flux of volatiles.

Alkali basalts are characterised by high absolute LREE abundances and high LREE relative to HREE. While it is possible to generate the LREE/HREE fractionations in low degree partial melts of garnet lherzolite, this process does not generate the necessary absolute abundance levels of LREE (e.g. Mysen, 1983). As a result, the necessity for metasomatism as a precursor to the generation of the trace element enriched alkaline rocks (including carbonatites and kimberlites) has been advocated in many papers over the last 25 years (Lloyd and Bailey, 1975; Carter *et al.*, 1978; Boettcher and O'Neill, 1980; Menzies and Murthy, 1980; Wass and Rogers, 1980; Mysen, 1983; Haggerty, 1989).

9.3.3. Melting of crustal rocks

Some authors have also proposed the lower continental crust as a source for phonolitic and trachytic magmas. The common occurrence of these magma types in oceanic areas precludes this as the only mechanism to generate felsic alkaline rocks, but may be significant in cratonic areas (e.g. Marsh, 1987a). Goles (1976) suggested that the large volume of basaltic magma required to produce the voluminous plateau phonolites of East Africa could also have melted lower crustal rocks which were added to the felsic magmas. The generation of Si-undersaturated melts from generally over-saturated felsic crust does not appear intuitively reasonable. Bailey (1974b) suggested that an influx of alkali-enriched volatiles would supply heat for melting and also enhance the undersaturated nature of the partial melts. Metasomatically-enriched lower crustal xenoliths have been reported in alkaline lavas from the Eifel, Germany (Stosch and Lugmair, 1984) and Marsh (1987a) discussed other

lower crustal xenolith suites which contain nepheline-normative material potentially capable of producing felsic alkaline magmas. Variably fenitised crustal xenoliths (granitic and gabbroic) in the Oldoinyo Lengai carbonatites were described by Morogan and Martin (1985) in which incipient small degree SiO_2-undersaturated peralkaline and SiO_2-oversaturated peraluminous melts were observed.

9.3.4. Conclusion

Clearly, no obvious consensus currently exists in the literature concerning the derivation of felsic alkaline rocks in general, and phonolitic and trachytic magmas in particular. Certainly, the mechanisms reviewed above are not all mutually exclusive and some models invoke a combination of these factors: Price *et al.* (1985) argued that the phonolites and trachytes of Mt. Kenya were derived through low pressure crystal fractionation from a range of alkali basalts which were themselves derived from mantle metasomatised by carbonatitic magmas. It seems reasonable, therefore, that phonolite and trachyte magmas may be generated by different petrogenetic schemes and that no single model satisfies all observations.

It has been demonstrated that phonolite magmas can exist in the mantle. Prior metasomatic enrichment of the mantle or lower crustal source would appear to be necessary to produce those felsic alkaline rocks with high concentration levels of the LILE and HFSE.

Figure 9.8: Plot of Mg# against (a) MgO and (b) molecular CaO/(CaO+MgO+FeO) composition for the Pilanesberg Suite carbonatites.

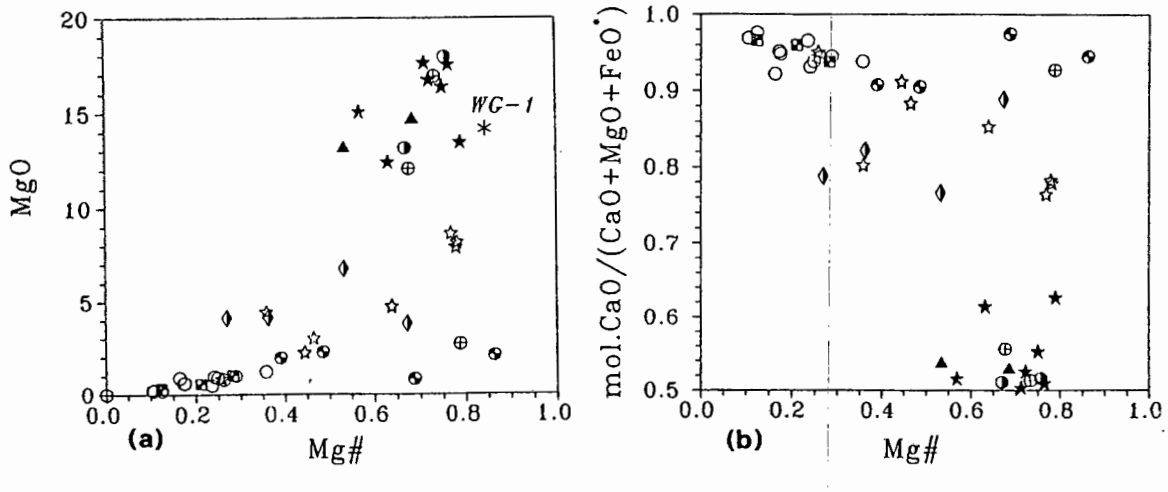

The point marked "WG-1" in (a) is the composition of the experimental melt of Wallace and Green (1988).

Figure 9.9: Plotof $\varepsilon_{(Sr)}$-$\varepsilon_{(Nd)}$ showing potential enriched reservoirs in relation to variations amongst the Pilanesberg Suite carbonatites and associated alkaline silicate rocks.

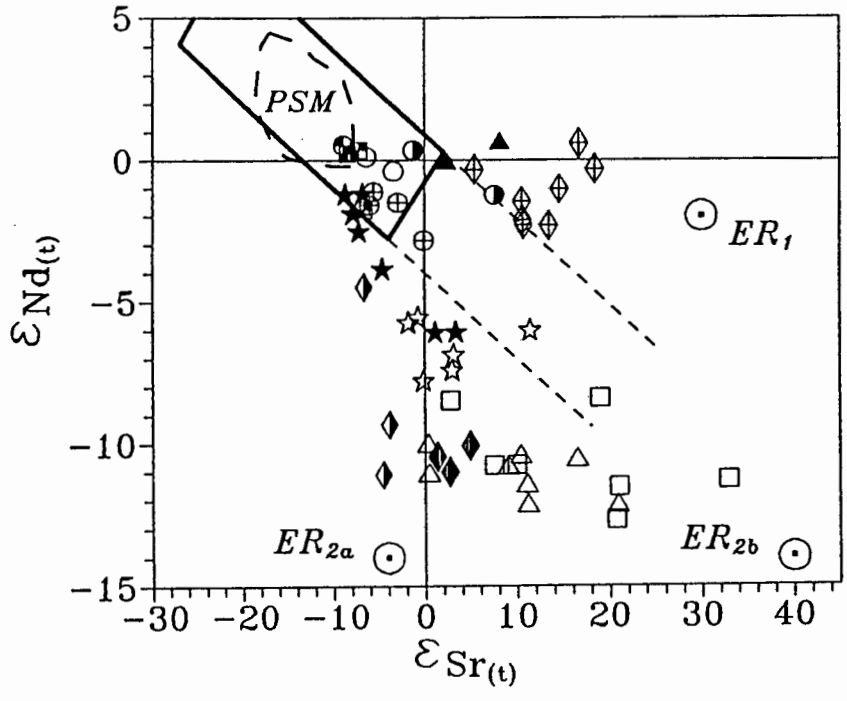

Shown for comparison is the array bounding the compositional variation in young carbonatites (heavy solid and narrow-dashed lines). Analyses of megacrysts recovered from the 1.2Ga Premier and Schuller kimberlites plot within the dashed field labelled "PSM". The compositions of possible enriched reservoirs are labelled ER_1, ER_{2a} ER_{2b} (see text for further details).

9.4. *The isotopic composition of the Pilanesberg Suite carbonatites and silicates*

It was noted in the opening section of this Chapter that the $\varepsilon_{(Sr)}$-$\varepsilon_{(Nd)}$ data for the Pilanesberg Suite carbonatites essentially describe two fundamentally different variation trends. It was proposed that the isotopic variation was the result of primary carbonatitic mantle melts interacting with isotopically enriched reservoirs. An attempt will now be made to better constrain the nature of, and the processes involved in, this "interaction".

9.4.1. Pilanesberg Suite carbonatites : primary or derivitive?

Experimental data discussed above established that primary carbonatite melts of peridotitic mantle would be dolomitic. Figure 9.8 summarises the CCMF, Mg# and MgO relationships in the Pilanesberg Suite carbonatites and indicates that many of the magnesio-carbonatites have Mg# of over 0.65 and MgO exceeding 12%, compositions consistent with those predicted for primary mantle melts (Eggler, 1989).

$\varepsilon_{(Sr)}$-$\varepsilon_{(Nd)}$ isotopic data for all the Pilanesberg Suite carbonatites are compared with the "young carbonatite array" in Figure 9.9. As demonstrated earlier, the solid line portion of the array also bounds all available analyses of 1.0-1.9Ga carbonatites (all from Canada).

Experimental data indicate that carbonatite melts are generated in equilibrium with pargasitic lherzolite and that carbonated silicate magmas form beyond the stability field of amphibole (see Figure 9.2). For the peridotite and volatile compositions studied by Wallace and Green (1988), then, silicate magmas generated in the deep mantle will crystallise pargasite and be transformed into carbonatitic melts on entering the super-solidus amphibole stability field. Megacrysts in kimberlite are generally regarded as having crystallised from a magma (e.g. Mitchell, 1986) and Jones (1987) argued that the Premier megacrysts are "almost certainly derived from magmas which were generated within the asthenosphere" and which were thought to be the alkali picrite precursors to the kimberlite. Consequently, the isotopic composition of the Proterozoic deep subcontinental mantle below the Kaapvaal Craton may conveniently be estimated from megacrysts included the 1.2Ga Premier and Schuller kimberlites (Kramers and Smith, 1983; Richardson, 1986) which were emplaced near the southern end of the array of alkaline complexes making up the Pienaars River Complex (see Chapter 8).

In Figure 9.9 the compositional field ("PSM" = Premier-Schuller megacrysts) for megacrysts from the Premier and Schuller kimberlites (Jones, 1987; Winterburn, 1990; De Bruin, 1991) is shown and corresponds with the central portion of the carbonatite array. One of the three analysed inclusions in Premier diamonds (Richardson, 1986) coincides with the PSM field: the others have somewhat higher $\varepsilon_{(Nd)}$ (+6.3, +8.2).

These data suggest that at 1.2Ga the source for under-saturated alkaline melts (and carbonatites?) in the deep sub-continental lithosphere or upper asthenospheric

mantle below the central Kaapvaal Craton was characterised by depleted $\varepsilon_{(Sr)}$-$\varepsilon_{(Nd)}$ values.

Carbonatites from the Spitskop and Stukpan complexes have unusually negative $\varepsilon_{(Nd)}$ values which imply the involvement of an additional component (lithospheric mantle or crust?) not sampled by the other Pilanesberg carbonatites. It is important to note that for the Spitskop carbonatites the magnesio-carbonatites have less of this component, i.e. they approach the "PSM" values more closely, than the calcio-carbonatites. Considering the isotopic and Mg# relationships in conjunction with the experimental constraints, it is proposed that the Spitskop magnesio-carbonatites represent the more "primitive" of the carbonatites and that the more "evolved" (i.e. more negative $\varepsilon_{(Nd)}$) signature in the calcio-carbonatites was acquired from interaction with enriched wall rocks during magma evolution and ascent. Arguments were presented in Chapter 8 against the involvement of upper crust which suggests that this interaction took place either in the mantle or deep crust. Calcio-carbonatites from other Pilanesberg Suite complexes do not always have "anomalous" isotopic signatures: the Nooitgedacht and Goudini sövites have the most depleted $\varepsilon_{(Sr)}$-$\varepsilon_{(Nd)}$ signatures of the Pilanesberg Suite data set. Clearly, anomalous isotopic signatures will only occur if the evolving carbonatite melt encounters a lithospheric reservoir which had experienced ancient Rb/Sr and Nd/Sm enrichments.

From the data distributions in Figure 9.9 it is apparent that at least two distinct isotopic reservoirs are required to explain the deviations of the carbonatite data from PSM: one with high $\varepsilon_{(Sr)}$ relative to $\varepsilon_{(Nd)}$ as encountered by the Derdepoort and Bulhoek carbonatites (=ER_1); whereas the Spitskop and Stukpan carbonatites require a reservoir with low $\varepsilon_{(Nd)}$ relative to $\varepsilon_{(Sr)}$ (=ER_{2a}). The silicate components of the Spitskop Complex extend the $\varepsilon_{(Sr)}$-$\varepsilon_{(Nd)}$ variation in the carbonatites to higher $\varepsilon_{(Sr)}$ values suggesting the presence of a reservoir characterised by high $\varepsilon_{(Sr)}$ and low $\varepsilon_{(Nd)}$ (=ER_{2b}).

9.4.2. Characteristics of the "Isotopically - Enriched" components in the Pilanesberg Suite carbonatites and silicates

Possible "enriched reservoir" (ER) compositions are labelled on Figure 9.9: ER_1 for the PSM - Bulhoek - PRAC array; ER_{2a} and ER_{2b} as possible enriched components in the Spitskop and Stukpan carbonatite - Spitskop silicate trends respectively.

Table 9.2: Time - fractionation relationships for the generation of the defined enriched mantle reservoirs.

Time of enrichment: (before present)	2.3Ga	2.6Ga	3.2Ga
ER_1 ($\varepsilon_{(Sr)}$ =+30; $\varepsilon_{(Nd)}$=−2)			
f_{Sr}	5.06	4.22	3.17
f_{Nd}	0.81	0.85	0.90
ER_{2a} ($\varepsilon_{(Sr)}$=−4; $\varepsilon_{(Nd)}$=−14)			
f_{Sr}	1.99	1.79	1.53
f_{Nd}	0.37	0.50	0.66
ER_{2b} ($\varepsilon_{(Sr)}$=+40; $\varepsilon_{(Nd)}$=−14)			
f_{Sr}	5.96	4.93	3.65
f_{Nd}	0.37	0.50	0.66

Tabulated data are the fractionation factors in parent:daughter element ratio (as defined in text) required to generate the various ER's from a depleted mantle peridotite (PSM) enriched at 2.3 Ga (i.e. 1Ga prior to the carbonatite magmatism), 2.6 and 3.2 Ga. The isotopic composition of PSM at 1.3Ga ($\varepsilon_{(Sr)}$=−15; $\varepsilon_{(Nd)}$=+3) was assumed to have been generated by element fractionations imprinted on primitive, "Bulk Earth" mantle at 3.5Ga: PSM consequently has Rb/Sr=0.018 and Sm/Nd=0.343.

By assuming that all of these reservoirs are (or were) components of the Proterozoic lithospheric mantle below the Kaapvaal Craton, it is possible to constrain the parent/daughter element fractionations that would be required to generate the isotopic compositions of each "ER" from "PSM"-like mantle through any specified lapsed period of geological time.

In discussing these fractionations the following shorthand will be adopted:

$f_{Nd} = (Sm/Nd)_E / (Sm/Nd)_{PSM}$; and

$f_{Sr} = (Rb/Sr)_E / (Rb/Sr)_{PSM}$;

where "E" refers to the enriched reservoir and "PSM" indicates the starting, or primary mantle reservoir, characterised by the Premier and Schuller material.

Fractionations required to generate the ER_{2a} are similar to those encountered in low degree partial melts of fertile garnet peridotite. A 0.1% melt of garnet peridotite (assuming the melting behaviour of natural peridotite PHN 1611 as determined by Harrison, 1981) would have f_{Sr}=2.43 and f_{Nd}=0.57. Segments of mantle

lithosphere enriched in such small degree melts (nephelinite?, carbonatite?) generated and trapped at 2.6Ga would produce reservoirs having isotopic compositions intermediate between ER_{2a} and ER_{2b} at 1.3Ga (see values in Table 9.2). Enriched $\varepsilon_{(Sr)}$ relative to $\varepsilon_{(Nd)}$ signatures, like ER_1, are common in continental volcanics (e.g. Hawkesworth *et al.*, 1884; 1987), certain lamproites and the Group-II type ("micaceous") kimberlites (Smith, 1983; Fraser *et al.*, 1985) and are rarely reported in carbonatites (Phalaborwa: Eriksson, 1989; Ihouhaouene: Bernard-Griffiths *et al.*, 1988; see Figure 9.5b). The parent/daughter fractionations required for this style of enrichment (see factors for ER_1 in Table 9.2) are difficult to generate through realistic melting models of unmodified peridotite and have been attributed to enrichments by hydrous fluid (Hawkesworth *et al.*, 1984) or K-rich silicate melts such as lamproite (McKenzie, 1989).

A basic assumption in these calculations is that the element concentrations in average basalt, kimberlite, lamproite and carbonatite, as calculated from samples collected at surface, are reasonably representative of the concentration levels in more primitive melts at mantle depths. In the case of the carbonatites at least, this is certainly an oversimplification. The significant alkali contents in the Wallace and Green (1988) experimental melt plus the Na- and K- fenites surrounding most carbonatite complexes indicate that mantle carbonatites would have substantially higher Na, K and Rb contents than are reflected in the Woolley and Kempe averages.

To investigate the isotopic effects on PSM mantle of enrichment by carbonatitic or undersaturated alkaline melts, the isotopic compositions of mixtures of small amounts (2, 5 and 10%) of average alkali basalt, kimberlite, lamproite (averages from Bergman, 1987) and carbonatite (magnesio-carbonatite from Woolley and Kempe, 1989) with modelled PSM mantle were calculated (Table 9.3) and are depicted in Figure 9.10 (see table caption for details). Enriched lithospheric reservoirs such as ER_{2a} and ER_{2b} may thus readily generated by the entrapment of small amounts of undersaturated alkaline silicate melts and/or carbonatite.

Table 9.3: Change in parent:daughter element ratios in depleted mantle (PSM) caused by the addition of small amounts of melt.

Amount melt added :	+2%	+5%	+10%
Alkali Basalt			
Rb/Sr	0.034	0.044	0.051
Sm/Nd	0.266	0.231	0.211
$\varepsilon_{(Sr)}$	+4	+13	+20
$\varepsilon_{(Nd)}$	−7	−11	−14
Kimberlite			
Rb/Sr	0.050	0.066	0.076
Sm/Nd	0.225	0.189	0.172
$\varepsilon_{(Sr)}$	+19	+33	+42
$\varepsilon_{(Nd)}$	−12	−16	−18
Lamproite			
Rb/Sr	0.120	0.149	0.163
Sm/Nd	0.161	0.136	0.126
$\varepsilon_{(Sr)}$	+82	+108	+121
$\varepsilon_{(Nd)}$	−19	−22	−24
Carbonatite			
Rb/Sr	0.007	0.006	0.006
Sm/Nd	0.092	0.079	0.075
$\varepsilon_{(Sr)}$	−20	−21	−21
$\varepsilon_{(Nd)}$	−28	−29	−30

Epsilon values were calculated assuming that the tabulated quantites of the relevant melt was added to PSM mantle at 2.8 Ga (i.e. 1.5Ga prior to the intrusion of the Spitskop and Stukpan complexes).

An evaluation of the true concentration levels of trace elements, particularly the parent and daughter elements to the important isotopic systems, is of great significance in understanding and constraining the petrogenesis of carbonatites and associated alkaline magmatism. If the trace element levels in the averages used in the calculation above are realistic order-of-magnitude estimates of mantle magmas, then the influence of such magmas in modifying the trace element contents in lithospheric mantle is dramatically illustrated by the figures in Table 9.3: e.g. the Rb/Sr in depleted

mantle is increased 6-fold and the Sm/Nd halved by the addition of just 2% lamproite melt.

Figure 9.10: Plot showing the $\varepsilon_{(Sr)}$-$\varepsilon_{(Nd)}$ compositions of depleted mantle enriched by low degree melts.

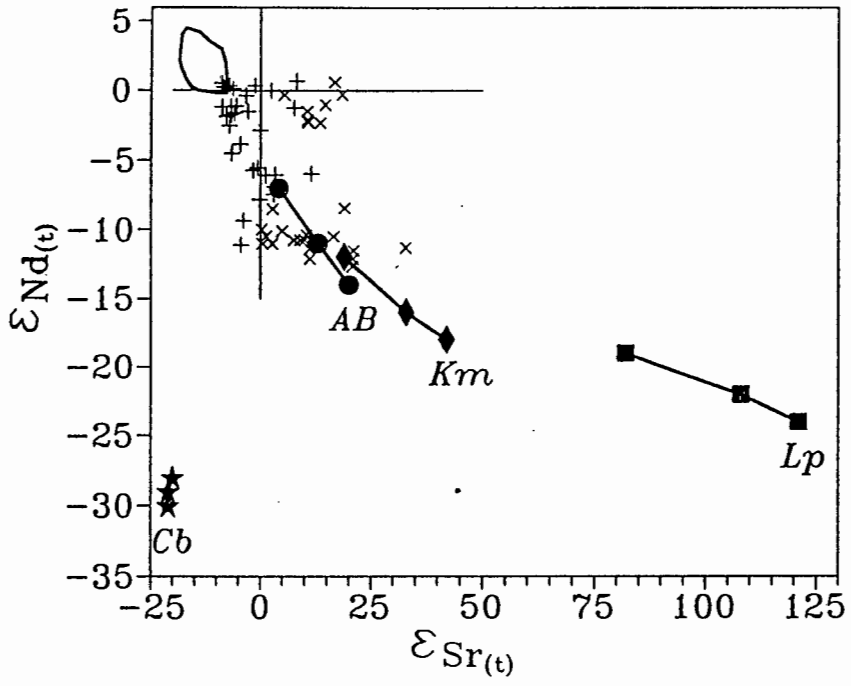

Solid line segments with symbols refer to PSM mantle (enclosed field) enriched at 2.8Ga by the addition 2, 5 and 10 percent of melts having the composition of average magnesio-carbonatite (Cb), alkali basalt (AB), kimberlite (Kb) and lamproite (Lp). Pilanesberg Suite carbonatites (+) and silicates (x) are shown for reference.

These changes in concentration of Sr and Nd in the altered mantle, while substantial relative to average mantle values are, however, small relative to the levels in average carbonatite, kimberlite or lamproite. As a consequence, it would be very difficult to modify the isotopic composition of these mantle melts through "interaction" with parts of the mantle rendered isotopically anomalous due to ancient additions of similar melts. As an example, to change the $\varepsilon_{(Nd)}$ of a carbonatite melt with 630ppm Nd (average magnesio-carbonatite) from a value of +3 (≡PSM) to −10 (≡ Stukpan carbonatites) would require incorporation of 87% of mantle enriched with 10% carbonatite melt as listed in Table 9.3. A lower Nd carbonatite melt, such as S59 (49ppm Nd) would still require the incorporation of almost 40% of the enriched mantle component to reduce $\varepsilon_{(Nd)}$ to −10. The hypothetical "interaction" required to change the Spitskop and Stukpan isotopic compositions is thus likely to have occurred at an early late stage in the evolution of the carbonatite prior to the attainment of the

elevated concentrations of Sr and Nd. Alternatively, the "interaction" process would need to be such that the carbonatite could equilibrate with, or extract anomalous Sr and Nd from, a large volume of the enriched reservoir.

9.5. A model for carbonatite genesis

Any petrogenetic scheme or model to explain the association of silicate and carbonatite components in alkaline complexes in general, and in the Spitskop Complex in particular, must account for the following:

(i) the high abundance of LILE and high LREE/HREE in both silicate and carbonatitic magma types;

(ii) the observation that the carbonatites always intrude later than the silicates;

(iii) the tendency for magnesio-carbonatites to be emplaced later than calcio-carbonatite.

With reference to the association of rock types in the Spitskop Complex, a model must also be consistent with:

(iv) the more anomalous $\varepsilon_{(Sr)}$-$\varepsilon_{(Nd)}$ signatures in the silicates relative to the carbonatite fractions, and

(v) the more anomalous $\varepsilon_{(Sr)}$-$\varepsilon_{(Nd)}$ signatures in the early, calcio-carbonatites relative to the later magnesio-carbonatites.

The model for the generation and evolution of carbonatite melts can be demonstrated with reference to the cartoon sketch of depth sections drawn along a series of geotherms of progressively higher gradient in Figure 9.11.

Given the presence of oxidised volatiles (i.e. CO_2-H_2O) and suitably fertile lherzolite compositions, carbonated silicate partial melts (olivine melilitic) will be present in equilibrium with garnet lherzolite along a "warm" continental geotherm at depths of 120-90 km (left hand side of Figure 9.11). These melts will be overlain by a zone of garnet-amphibole-lherzolite containing traces of sodic magnesio-carbonatite melt.

Extraction of partial melts in the mantle is controlled by the distribution of melt through the host solid and the rate of melt movement through the matrix. The distribution of a fluid phase through a solid medium is controlled by the interfacial tension between the fluid and adjacent solid phases (see reviews by McKenzie, 1985; Watson and Brennan, 1987; Watson *et al.*, 1990). This force is reflected in the dihedral angle (Ø, also termed "wetting" angle) formed between the fluid and adjacent solid phases at textural equilibrium. At Ø=0° the fluid forms an intergranular film; at Ø<60° the fluid is distributed as a continuous, interconnected volume through the solid whereas for Ø>60° the fluid will occur as isolated "pockets" or "islands" through the

solid (well illustrated in Watson *et al.*, 1990). In addition, the rate of movement of an interconnected fluid is controlled by the viscosity of the fluid (McKenzie, 1985) such that highly viscous fluids, even if connected in three dimensions, will not be able to separate from their solid matrix in geologically reasonable time periods.

Figure 9.11: Cartoon representation of depth sections drawn along geotherms of progressively increasing geothermal gradient (see inset).

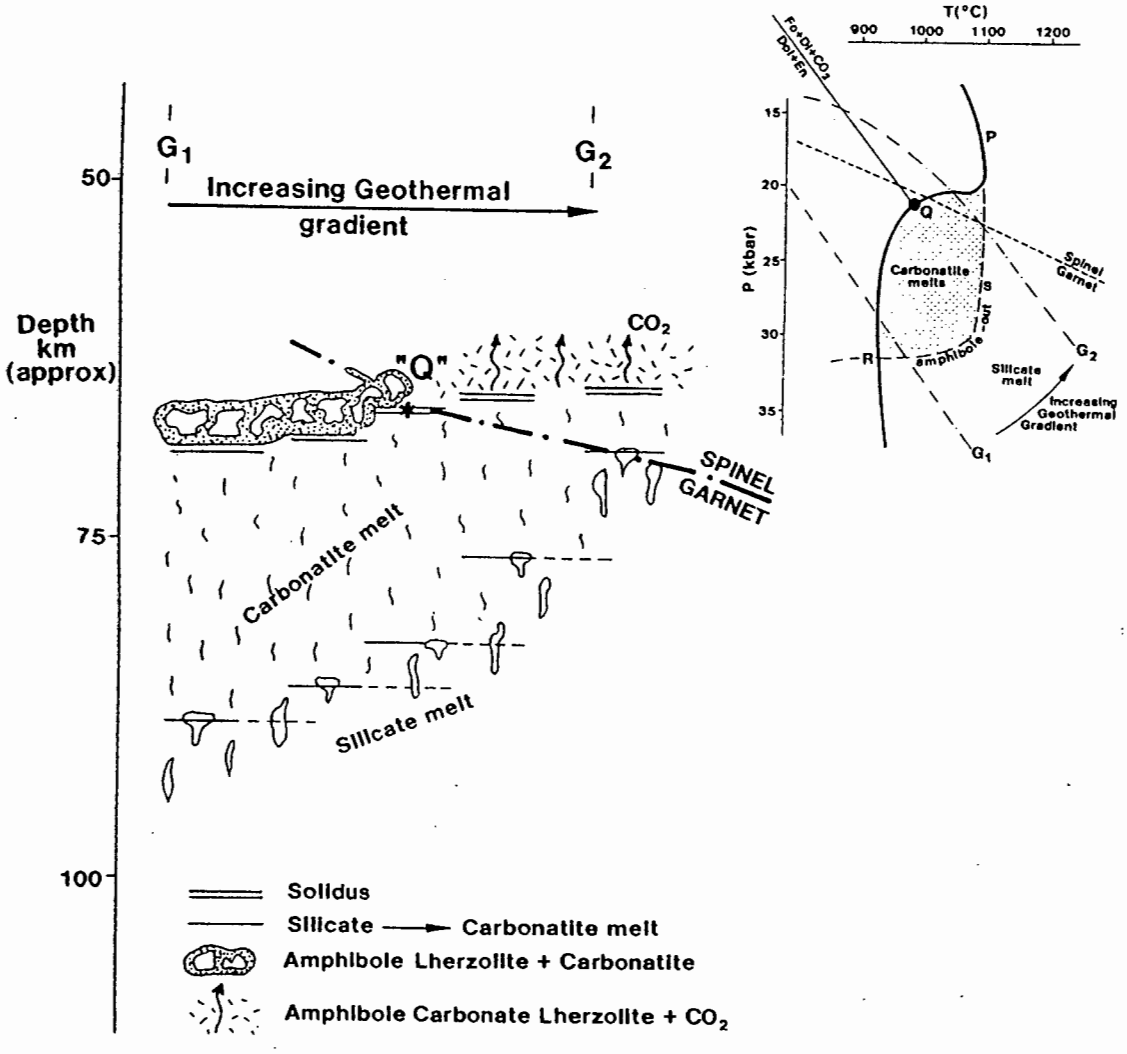

Phase boundaries in the inset are constructed from Wallace and Green (1988), Falloon and Green (1989).

Carbonated melilitite to nephelinite silicate magmas and carbonatite melts have low viscosities (e.g. McKenzie, 1985). Carbonatite melts furthermore form low wetting angles (23-36°) with peridotite minerals (Hunter and McKenzie, 1989; Watson *et al.*, 1990) and will consequently be extremely mobile: McKenzie (1985) calculated that a 0.1% partial melt of carbonatite composition would separate from 100 km

section of mantle in a few million years. In addition, Watson *et al.* (1990) suggested that surface tension forces were capable of inducing infiltration of carbonate melt into peridotite without any additional driving force.

As a result of low viscosity and suitable wetting angles with mantle olivine (McKenzie, 1985; Watson *et al.*, 1990), the melilitic melts will percolate upwards at low degrees of melting (possibly <1%: McKenzie, 1985). Because both the silicate and carbonatitic melts are able to move at low degrees of melting, the melt will remain dispersed through the peridotite and is unlikely to accumulate into discrete magma batches: the melt will thus ascend along the geotherm in equilibrium with its matrix rather then rising along a steeper, adiabatic gradient.

The amphibole stability boundary represents a "silicate melt solidus" where the rising silicate melt will precipitate pargasitic amphibole and change composition to sodic magnesio-carbonatite. Ascending carbonatitic melt will intersect the solidus curve along RQ and freeze generating a mixture of garnet-pargasite-lherzolite plus carbonate.

As the geotherms rise, the "silicate solidus" is intersected at progressively shallower depths with the result that previously precipitated silicate components are re-melted to re-crystallise at shallower depths (see Figure 9.11). Carbonatite melt continues to precipitate at about the same depth level. Once the geotherm passes through the critical point "Q" on the solidus, carbonate will no longer be stable and so carbonatite melt will react with the lherzolite, and by consuming orthopyroxene (see reaction 9.2) progressively alter the peridotite to more clinopyroxene-rich, "wehrlitic" compositions, with the expulsion of CO_2 vapour (Green and Wallace, 1988). Substantial compositional gradients could be anticipated along QP as the trace constituents carried by the carbonatite melt are distributed between the metasomatic clinopyroxene, amphibole and/or phlogopite developed from the H_2O in the melt, and the evolved CO_2 vapour. CO_2 vapour will not easily dissipate since it is less mobile than the melt through a peridotite matrix (see Hunter and McKenzie, 1989; Watson *et al.*, 1990). Depending on the rate of supply of melt, then, a substantial CO_2 vapour - pressure may develop above the solidus section "QP". Increased CO_2 over-pressure may result in hydraulic fracturing of the lherzolite above "QP" (Spera, 1984; Watson and Brenan, 1987; Hunter and McKenzie, 1989) or alternatively, the increased fCO_2 may lead to the breakdown of the pargasitic amphibole (Green and Wallace, 1988).

It is proposed that the repeated cycles of precipitation, re-melting and re-precipitation allow the dispersed melt fractions to accumulate into magma batches of sufficient size to rise adiabatically to the surface. Alternatively, with progressive

enrichment of the zone "QP" the lherzolite will be transformed to an alkali wehrlite which will melt to produce an alkaline silicate magma of nephelinitic composition. Assisted by the CO_2 gas pressure the melt can readily ascend towards the surface.

Subsequent carbonatitic melts will favour, and be focussed towards, the channelway created by the silicate melt(s) which facilitates the collection and aggregation of the small pockets of melt. Successive carbonatite melts will rise through the melt channelway and be shielded from extensive interaction with wall rocks by a conduit lining of the reaction products between earlier melts and mantle. The combination of decreased thermal and chemical contrast between melt and surroundings allows carbonatite to finally reach the surface. The initial carbonatite melts would also form a conduit lining and so subsequent batches of carbonatite would be shielded from interaction with wall rocks to a greater extent.

This sequence of events would normally occur over a relatively short period of geological time through isotopically homogeneous mantle materials, and so isotopically similar silicate and carbonatite components would be produced. If the silicate and carbonatitic melts thus generated proceed to surface without further interaction with crust or isotopically anomalous mantle, then they would have similar isotopic compositions.

The Pilanesberg Suite complexes, though, passed through the sub-Kaapvaal Craton lithospheric mantle, a mantle segment known to have been stabilised to significant depths since at least 3.2Ga (Richardson *et al.*, 1984), and known to be isotopic-ally heterogeneous as a result of several episodes of enrichment through metasomatism or the entrapment of low degree melts (e.g. Richardson *et al.*, 1985; Menzies *et al.*, 1987; Winterburn *et al.*, 1990). Carbonatites from the Phalaborwa Complex, emplaced into the Kaapvaal Craton at 2.0Ga, have some of the most extreme isotope values yet published and are regarded as reflecting derivation from an enriched mantle source (Eriksson, 1989).

As argued by Haggerty (1989), Meen (1987) and Meen *et al.* (1989), the depth interval of the inflection ("ledge") in the solidus for peridotite-CO_2 will be a zone where long lived enrichments are most likely to be preserved. The experimental results of Wallace and Green (1988) suggest that the trace of the amphibole stability boundary at the ambient mantle conditions (P,T,X) during a magmatic / metasomatic event would also be an important zone of enrichment in Ti and alkali elements. By implication then, it is possible that trace element enrichment signatures appropriate for the ER_{2a} and ER_{2b} "reservoirs" could be generated by a single, unerupted, episode of mantle melting: ER_{2a} reflecting slightly shallower mantle levels than ER_{2b}.

Trace element enrichments in the "metasome" zone (Haggerty, 1989) would be largely hosted in carbonate, amphibole and phlogopite along with exotic titanate minerals (Jones, 1989). These phases would be efficiently scavenged by the repeated melting cycles depicted in Figure 9.11 and transferred into the melts which are ultimately trapped at the depth interval equivalent to the solidus section "QP". This scavenging would thus effectively transfer the enriched isotope components towards "QP".

Clearly, the first (silicate) melts to successfully pass through the solidus and reach surface would have more of the enriched component than subsequent melts. Also, the first carbonatite melt to accumulate sufficiently to ascend towards the surface would interact with the conduit wall rocks more than subsequent batches of carbonatite. As a result, the first carbonatite melt to reach surface would tend to be both more calcic and have more enriched isotopic signatures than later batches, exactly as is noted at Spitskop.

The model thus successfully satisfies both the sequence of intrusion and relative isotopic signatures in the components of the Spitskop Complex. This model would predict:
(i) that alkaline silicate magmatism should precede the emplacement of carbonatites; and, if ancient enriched lithosphere is present due to partial melts trapped at the vapour undersaturated peridotite solidus, that
(ii) the carbonatite component in carbonatite-silicate complexes should consistently have less enriched isotopic signatures;
(iii) since interaction between primary carbonatite melt and wall rock pyroxene shifts the melt to more calcic composition, the model also predicts that calcio-carbonatites should be emplaced after magnesio-carbonatite; and that the calcio-carbonatites should have more enriched isotopic signatures than the magnesio-carbonatites.

Woolley (1987) proposed a model for the Chilwa Province alkaline complexes (Malawi) which is conceptually similar to the model outlined above. Woolley argued that it was impossible to derive the range of rock types present in the Chilwa Province by fractional crystallisation from alkali basalt and proposed instead a derivation through melting of lithosphere (crust and mantle) that had been extensively modified through volatile metasomatism. It was envisaged that early in the evolutionary cycle carbonatitic melts were produced at depth as dispersed droplets and that these migrated upwards and froze. Rising geotherms, accompanied by increased "focussing" of volatiles, "would continuously re-melt [the carbonatite] and so enable it to move to successively higher levels, at the same time increasing its volume and

enriching it in alkalis and incompatible elements." Focussing of melts and volatiles produced a "disc" of metasomatised lithosphere which was progressively thickened to shallower levels and into the crust. Trachytic (lower crust), phonolitic (shallow mantle) and carbonatite - nephelinite (deeper mantle) melts were thus derived from progressively deeper portions of the "metasomatised lithosphere disc". Carbonatites were only able to progress to the surface after it had coalesced into sufficiently large melt "batches".

In conclusion, the model proposed earlier satisfactorily accounts for the isotopic variation within the silicate and carbonatitic components of the Pilanesberg Suite complexes. It is proposed that the variable isotopic compositions are a direct result of the maturity of the Kaapvaal Craton mantle lithosphere: having been stable to significant depths since at least 3.2Ga (Richardson *et al.*, 1984), it was subject to several episodes of additions and subtractions of trace elements. Additions of as little as 2 weight percent of undersaturated silicate and/or carbonatite melt some 1.0-1.5Ga prior to the Pilanesberg magma-tism would be sufficient to account for the isotopic signatures in the Stukpan and Spitskop Complexes.

It is proposed that the processes described in the model probably acted during the genesis of many carbonatite complexes: the processes will only be manifest as isotopic variations if the melts proceed through old, thick lithosphere previously subjected to periods of metasomatism and/or melt infiltration.

It is perhaps worth reflecting that the oldest known carbonatites (see compilation by Woolley, 1989) are the 2680 Ma Kaminak Lake body in Canada and similar aged (2650 Ma) Tupertalik complex of Greenland. Commenting on the exponential increase in the number of carbonatite occurrences with time, Woolley (1989) observed that "..the conditions for the production of carbonatite were not only established by the late Archaean, but have become increasingly widespread with time." Is it possibly the ability of mantle lithosphere (oceanic and continental) to trap carbonate-rich partial melts, promoting accumulation and enrichment of the dispersed melt that dictates the appearance of carbonatite magma at the earth's surface?

References

Andersen, T. (1987). Mantle and crustal components in a carbonatite complex, and the evolution of carbonatite magma: REE and isotopic evidence from the Fen Complex, S.E. Norway. *Chem. Geol. Isotope Geosci. section*, **65**, 147-166.

Andersen, T. and Taylor, P.N. (1988). Pb isotope geochemistry of the Fen carbonatite complex, S.E. Norway: Age and petrogenetic implications. *Geochim. Cosmochim. Acta*, **52**, 209-215.

Allsopp, H.L., and Eriksson, S.C. (1986). The Phalaborwa complex; isotopic evidence for ancient lithospheric enrichment. *Joint Ann. Meeting, GAC-MAC.* Carleton University, Ottawa: 40 (Abstract).

Appleyard, E.C. (1980). Mass balance computations in metasomatism: Metagabbro/nepheline syenite pegmatite interaction in northern Norway. *Contrib. Mineral. Petrol.*, **73**, 131-144.

Appleyard, E.C. and Woolley, A.R. (1979). Fenitization: An example of the problems of characterizing mass transfer and volume changes. *Chem. Geol.*, **26**, 1-15.

Armstrong, R.A. (1987). Geochronological studies on Archaeanand Proterozoic formations of the foreland of the Namaqua front and possible correlates on the Kaapvaal Craton. Ph.D. thesis, University of Witwatersrand, Johannesburg, 274pp, unpubl.

Armstrong, R.A., Compston, W., Retief, E.A., Williams, I.S. and Welke, H.J. (1991). Zircon ion microprobe studies bearing on the age and evolution of the Witwatersrand triad. *Precambrian Research*, **53**, 243-266.

Babcock, R.S. (1973). Computational models of metasomatic processes. *Lithos*, **6**, 279-290.

Baertschi, P. (1957). Messung und Deutung relativer Häufigkeitsvariationen von O^{18} un C^{13} in Karbonatgesteinen und Mineralien. *Schweiz. Min. Petr. Mitt.*, **37**, 74-152.

Bailey, D.K. (1974a). Nephelinites and ijolites. in Sörensen, H. (ed.), *The Alkaline Rocks*, Wiley, London, 53-66.

Bailey, D.K. (1974b). Origin of alkaline magmas as a result of anatexis: Crustal Anatexis. in Sörensen, H. (ed.), *The Alkaline Rocks*, Wiley, London, 436-442.

Bailey, D.K. (1980a). Volatile flux, geotherms, and the generation of the kimberlite-carbonatite-alkaline magma spectrum. *Mineral. Mag.*, **43**, 695-699.

Bailey, D.K. (1980b). Volcanism, Earth degassing and replenished lithosphere mantle. *Phil. Trans. R. Soc.*, **A297**, 309-322.

Bailey, D.K. (1982). Mantle metasomatism - continuing chemical change within the Earth. *Nature*, **296**, 525-530.

Bailey, D.K. (1986). Fluids, melts, flowage and styles of eruption in alkaline ultramafic magmatism. *Trans. geol. Soc. S.Afr.*, **88**, 449-457.

Bailey, D.K. (1987). Mantle metasomatism - perspective and prospect. in J.G. Fitton and B.G.J. Upton (eds.), *Alkaline Igneous Rocks*, Geological Society Special Publication No 30, Blackwell, Oxford, 1-13.

Bailey, D.K. (1989). Carbonate melt from the mantle in the volcanoes of south-east Zambia. *Nature*, **338**, 415-418.

Bailey, D.K. (1990). Mantle carbonatite eruptions: Crustal context and implications. *Lithos*, **26**, 37-42.

Bailey, D.K. and MacDonald, R. (1987). Dry peralkaline felsic liquids and carbon dioxide flux through the Kenya rift zone. In: Mysen, B.O. (ed.), *Magmatic Processes: Physicochemical Principles.* Geochem. Soc. Spec. Pub., No. 1, 91-105.

Bailey, D.K. and Schairer, J.F. (1966). The system Na_2O-Al_2O_3-Fe_2O_3-SiO_2 at 1 atmosphere and the petrogenesis of alkaline rocks. *J. Petrol.*, **7**, 114-170.

Baker, I. (1969). Petrology of the volcanic rocks of Saint Helena Island, South Atlantic. *Bull. Geol. Soc. Am.*, **80**, 1283-1310.

Baker, M.B. and Wyllie, P.J. (1990). Liquid immiscibility in a nephelinite-carbonate system at 25 kbar and implications for carbonatite origin. *Nature*, **346**, 168-170.

Barker, D.S. (1989). Field relations of carbonatites. in Bell,K. (ed.), *Carbonatites - Genesis and Evolution*, Allen and Unwin, London, 38-69.

Barker, D.S. and Nixon, P.H. (1989). High-Ca, low-alkali carbonatite volcanism at Fort Portal, Uganda. *Contr. Mineral. Petrol.*, **103**, 166-177.

Barth, T.F.W. (1952). *Theoretical Petrology.* Wiley, New York, 387pp.

Barton, E.S. (1983). *The geochronology of the frontal zones of the Namaqua-Natal Mobile Belt.* Ph.D. Thesis, University of Witwatersrand, 205pp (Unpubl.).

Barton, J.M.B., and Ryan, B. (1977). A review of the geochronologic framework of the Limpopo Mobile Belt. *Bull. geol. Surv. Botswana*, **12**, 183-200.

Barton, J.M.B., Du Toit, M.C., van Reenen, D.D. and Ryan,B. (1983). Geochronologic studies in the Southern Marginal Zone of the Limpopo Mobile Belt, southern Africa. *Spec. Publ. geol. Soc. S. Afr.*, **8**, 55-64.

Basu, A.R., and Tatsumoto, M. (1980). Nd-isotopes in selected mantle-derived rocks and their implications for mantle evolution. *Contr. Mineral. Petrol.*, **75**, 43-54.

Bell, K. and Blenkinsop, J. (1985). Carbonatites - Clues to mantle evolution. *Geological Society of America Abstracts with Programs*, **17**, 151.

Bell, K. and Blenkinsop, J. (1987a). Archaen depleted mantle: Evidence from Nd and Sr initial ratios of carbonatites. *Geochim. Cosmochim. Acta*, **51**, 291-298.

Bell, K. and Blenkinsop, J. (1987b). Nd and Sr isotopic compositions of East African carbonatites: implications for mantle heterogeneity. *Geology*, **15**, 99-102.

Bell, K. and Blenkinsop, J. (1989). Neodymium and strontium isotope geochemistry of carbonatites. *in* Bell,K. (ed.), *Carbonatites - Genesis and Evolution*, Allen and Unwin, London, 617pp, 278-300.

Bell, K., Blenkinsop, J., Cole, T.J.S. and Menagh, D.P. (1982). Evidence from Sr isotopes for long-lived heterogeneities in the upper mantle. *Nature*, **298**, 251-253.

Bell, K., Blenkinsop, J., Kwon, S.T., Tilton, G.R. and Sage, R.P. (1987). Age and isotopic systematics of the Borden carbonatite complex, Ontario, Canada. *Can. J. Earth Sci.*, **24**, 24-30.

Bell, K., Dawson, J.B. and Farquhar, R.M. (1973). Strontium isotope studies of alkalic rocks: the active carbonatite volcano Oldoinyo Lengai, Tanzania. *Geol. Soc. Am. Bull.*, **84**, 1019-1030.

Bell, K. and Peterson, T. (1991). Nd and Sr isotope systematics of Shombole volcano, East Africa, and the links between nephelinites, phonolites and carbonatites. *Geology*, **19**, 582-585.

Bernard-Griffiths, B., Peucat, J-J., Fourcade, S., Kienast, J-R. and Ouzegane, K. (1988). Origin and evolution of 2 Ga old carbonatite complex (Ihouhaouene, Ahaggar, Algeria): Nd and Sr isotopic evidence. *Contrib. Mineral. Petrol.*, **100**, 339-348.

Bernard-Griffiths, B., Fourcade, S. and Dupuy, C. (1991). Isotopic study (Sr,Nd,O and C) of lamprophyres and associated dykes from Tamazert (Morocco): crustal contamination processes and source characteristics. *Earth and Planet. Sci. Lett.*, **103**, 190-199.

Berg, G.W. (1986). Evidence for carbonate in the mantle. *Nature*, **324**, 50-51.

Bergman, S.C. (1987). Lamproites and other potassium-rich igneous rocks: a review of their occurrence, mineralogy and geochemistry. in J.G. Fitton and B.G.J. Upton (eds.), *Alkaline Igneous Rocks*, Geological Society Special Publication No 30, Blackwell, Oxford, 103-190.

Bizzi, L.A., Smith, C.B., De Witt, M.J., Armstrong, R.A. and Meyer, H.O.A. (in press). Mesozoic kimberlites and related alkalic rocks in south-western Sao Francisco Craton, Brazil: A case for local mantle reservoirs and their interaction. in: Proceedings of Kimberlite Conference, Brazil 1991.

Boettcher, A.L. and O'Neill, J.R. (1980). Stable isotope, chemical and petrographic studies of high pressure amphiboles and micas: evidence for metasomatism in the mantle source regions of alkali basalts and kimberlites. *Am. J. Sci.*, **280A**, 594-621.

Brenan, J.M. and Watson, E.B. (1991). Partitioning of trace elements between carbonate melt and clinopyroxene and olivine at mantle P-T conditions. *Geochim. Cosmochim. Acta*, **55**, 2203-2214.

Brey, G., Brice, W.R., Ellis, D.J., Green, D.H., Harris, K.L. and Ryabchikov, I.D. (1983). Pyroxene-carbonate reactions in the upper mantle. *Earth and Planet. Sci. Lett.*, **62**, 63-74.

Bristow, J.W., Armstrong, R.A. and Allsopp, H.L. (1982). A note on the geology and geochronology of the Tsange Gabbros. *Trans. geol Soc. S.Afr.*, **85**, 135-139.

Brögger, W.C. (1921). Die Eruptivgesteine des Kristianiagebietes. IV. Das Fengebiet in Telemark, Norwegen. *Skrifter udgit av Videnskabsselskabet i Kristiania. I. Math.-Nat. Klasse.* **No.9**, 1-408.

Brouwer, H.A. (1910). *Oorsprong en Samenstelling der Transvaalschen Nepheliensyenieten.* Mouton, Gravenhage.

Bryan, W.B., Finger, L.G. and Chayes, F. (1969). Estimating proportions in petrographic mixing equations by least squares approximation. *Science*, **163**, 926-927.

Canil, D. (1990). Experimental study bearing on the absence of carbonate in mantle-derived xenoliths. *Geology*, **18**, 1011-1013.

Carmichael, I.S.E. and Nicholls, J. (1967). Iron-Titanium oxides and oxygen fugacities in volcanic rocks. *J. Geophys. Res.*, **72**, 4665-4687.

Carmichael, I.S.E., Turner, F.J. and Verhoogen, J. (1974). *Igneous Petrology.* McGraw-Hill, New York, 739p.

Carr, G.R., Phillips, E.R. and Williams, P.R. (1976). An occurrence of eudialyte and manganoan pectolite in a phonolite dyke from south-eastern Queensland. *Mineral. Mag.*, **40**, 853-856.

Carter, S.R., Evensen, N.M., Hamilton, P.J. and O'Nions, R.K. (1978). Continental volcanics derived from enriched and depleted source regions: Nd and Sr isotopic evidence. *Earth and Planet. Sci. Lett.*, **37**, 401-408.

Cawthorn, R.G. and Molyneux, T.G. (1986). Vanadiferous magnetite deposits of the Bushveld Complex. *in* Anhaeusser, C.R. and Maske, S. (eds.): *Mineral Deposits of South Africa*, Geol. Soc. S. Afr., Johannesburg, 1251-1266.

Cawthorn, R.G., Meyer, P.S., and Kruger, F.J. (1991). Major addition of magma at the pyroxenite marker in the western Bushveld Complex, South Africa. *Jour. Petrology*, **32**, 739-763.

Charlesworth, E.G. (1981). *Tectonics and metamorphism of the northern margin of the Namaqua Natal Mobile Belt near Eshowe.* Ph.D. thesis (unpubl.), Univ. Natal, Durban, 433p.

Chayes, F. (1963). Relative abundance of intermediate members of the oceanic basalt--trachyte association. *J. Geophys. Res.*, **68**, 1519-1534.

Clarke, L.B. (1989). Ph.D. Thesis, University of Leicester, (Unpubl.).

Clarke, L.B., Le Bas, M.J. and Spiro, B. (in press). Rare earth, trace element and stable isotope fractionation of carbonatites at Kruidfontein, Transvaal, S Africa. in: Proceedings of Kimberlite Conference, Brazil 1991.

Coombs, D.S. and Wilkinson, J.F.G. (1969). Lineages and fractionation trends in undersaturated volcanic rocks from the east Otago volcanic province (New Zealand) and related rocks. *J. Petrol.*, **10**, 440-501.

Cooper, A.F and Reid, D.L. (1991). Textural evidence for calcite carbonatite magmas, Dicker Willem, southwest Namibia. *Geology*, **19**, 1193-1196.

Cox, K.G., Duncan, A.R., Bristow, J.W., Taylor, S.R. and Erlank, A.J. (1984). Petrogenesis of the basic rocks of the Lebombo. *Spec. Publ. geol. Soc. S. Afr.*, **13**, 149-169.

Craw, D. and Landis, C.A. (1980). Authigenic pectolite, stevensite, and pyroaurite in a Quaternary debris flow, Southland, New Zealand. *J. Sed. Petrol.*, **50**, 497-504.

Cullers, R.L. and Graf, J.L. (1984). Rare earth elements in igneous rocks of the continental crust: Predominantly basic and ultrabasic rocks. in Henderson, P. (ed.), *Rare Earth Element Geochemistry*, Elsevier, Amsterdam, 237-274.

Davies, R.D., Allsopp, H.L., Erlank, A.J., and Manton, W.I. (1970). Sr-Isotopic studies on various layered mafic intrusions in Southern Africa. Geol. Soc. S.Africa, Special Publication 1, 576-592.

Dawson, J.B. (1962). Sodium carbonate lavas from Oldoinyo Lengai, Tanganyika. *Nature*, **195**, 1075-1076.

Dawson, J.B. (1989). Sodium carbonatite extrusions from Oldoinyo Lengai, Tanzania: implications for carbonatite complex genesis. in Bell,K. (ed.), *Carbonatites - Genesis and Evolution*, Allen and Unwin, London, 617pp, 255-277.

Dawson, J.B., Pinkerton, H., Norton, G.E. and Pyle, D.M. (1990). Physicochemical properties of alkali carbonatite lavas: Data from the 1988 eruption of Oldoinyo Lengai, Tanzania. *Geology*, **18**, 260-263.

De Bruin, D. (1991). *The megacryst suite from the Schuller kimberlite, South Africa.* Ph.D. thesis (unpubl.), Univ. Cape Town, Cape Town, 250pp.

Deer, W.A., Howie, R.A., and Zussman, J. (1966). *An Introduction to the Rock Forming Minerals.*, Longman, London, 528p.

Deines, P. (1989). Stable isotope variations in carbonatites. in Bell,K. (ed.), *Carbonatites - Genesis and Evolution*, Allen and Unwin, London, 617pp, 301-359.

De Paolo, D.J. and Wasserburg, G.J. (1976). Nd isotopic variations and petrogenetic models. *Geophys. Res. Letters*, 3, 249-252.

De Paolo, D.J. (1981). Trace element and isotopic effects of combined wallrock assimilation and fractional crystallisation. *Earth and Planet. Sci. Lett.*, 53, 189-202.

De Paolo, D.J. (1988). *Neodymium Isotope Geochemistry.* Springer-Verlag, Berlin, 187pp.

Donaldson, C.H., Dawson, J.B., Kanaris-Sotiriou, R., Batchelor, R.A. and Walsh, J.N. (1987). The silicate lavas of Oldoinyo Lengai, Tanzania. *Neues Jahrbuch Miner. Abh.*, **156**, 247-279.

Droop, G.T.R. (1987). A general equation for estimating Fe^{3+} concentrations in ferromagnesian silicates and oxides from microprobe analyses, using stoichiometric criteria. *Mineral. Mag.*, **51**, 431-435.

Dudàs, F.Ö., Carlson, R.W. and Eggler, D.H. (1987). Regional Middle Proterozoic enrichment of the subcontinental mantle sources of igneous rocks from central Montana. *Geology*, **15**, 22-25.

Duncan, A.R., Erlank, A.J. and Betton, P.J. (1984). Appendix 1: Analytical techniques and database descriptions. *Spec. Publ. geol. Soc. S.Afr.*, **13**, 389-395.

Duncan, R.A., McCulloch, M.T., Barsczus, H.G. and Nelson, D.R. (1986). Plume versus lithospheric sources for melts at Ua Poa, Marquesas Islands. *Nature*, **322**, 534-538.

Du Toit, A.L. (1931). *The geology of the country surrounding Nkandla, Natal.*, Expl. Sheet 109, Geol. Surv. S.Afr., 111p.

Edgar, A.D. (1974). On the use of the term "Agpaitic". *Mineral. Mag.*, **39**, 729-730.

Edgar, A.D. (1977). A comment on "Agpaicity revisited: pattern recognition in the chemistry of nepheline syenite rocks" by Dagbert *et al.*. *Geochim. Cosmochim. Acta*, **41**, 439-440.

Eggler, D.H. (1987a). Solubility of major and trace elements in mantle metasomatic fluids: Experimental constraints. *in* Menzies, M.A. and Hawkesworth, C.J. (eds.), *Mantle Metasomatism*, Academic Press, London, 21-41.

Eggler, D.H. (1987b). Discussion of recent papers on carbonated peridotite, bearing on mantle metasomatism and magmatism: an alternative. *Earth and Planet. Sci. Lett.*, **82**, 398-400.

Eggler, D.H. (1989). Carbonatites, primary melts, and mantle dynamics. in Bell,K. (ed.), *Carbonatites - Genesis and Evolution*, Allen and Unwin, London, 617pp, 561-579.

Eglington, B.M. (1987). Field, geochemical and isotope studies of selected areas of Proterozoic crust in south-central Natal. Ph.D. Thesis, University of Natal, 373pp, Unpubl.

Eglington, B.M., Harmer, R.E. and Kerr, A. (1989). Isotope and geochemical constraints on Proterozoic crustal evolution in South-eastern Africa. *Precambrian Res.*, **45**, 159-174.

Eglington, B.M. and Harmer, R.E. (1989). *GEODATE: a program for the processing and regression of isotope data using IBM-compatible microcomputers.* CSIR Manual EMA-H 8901, C.S.I.R., Pretoria, 57pp.

Eriksson, S.C. (1983). *Aspects of the petrochemistry of the Phalaborwa Complex, north-eastern Transvaal, South Africa.* Ph.D. thesis (unpubl.), Univ. Witwatersrand, Johannesburg, 495pp.

Eriksson, S.C. (1984). Age of carbonatite and phoscorite magmatism of the Palabora Complex (South Africa). *Chem. Geol. (Isot. Geosci. Sect.)*, 46, 291-299.

Eriksson, S.C. (1989). Phalaborwa: A Saga of Magmatism, Metasomatism and Miscibility. in Bell,K. (ed.), *Carbonatites - Genesis and Evolution*, Allen and Unwin, London, 617pp, 221-254.

Falloon, T.J. and Green, D.H. (1989). The solidus of carbonated, fertile peridotite. *Earth and Planet. Sci. Lett.*, **94**, 364-370.

Falloon, T.J. and Green, D.H. (1990). Solidus of carbonated fertile peridotite under fluid-saturated conditions. *Geology*, **18**, 195-199.

Farrow, D.J. (1988). An improved chemical method for whole rock Pb separations and its application to the petrogenesis of the Rooiberg Felsites. M.Sc., University of Pretoria, 72pp, (Unpubl.).

Faure, G. (1986). *Principles of Isotope Geology* (Second Edition), Wiley and Sons, New York, 589p.

Faure, G. and Powell, J.L. (1972). *Strontium Isotope Geology*, Springer-Verlag, New York, 188p.

Ferguson, J. (1970). The differentiation of agpaitic magmas: The Illimaussaq intrusion, South Greenland. *Can. Mineral.*, **10**, 335-349.

Ferguson, J. (1973). The Pilanesberg Alkaline Igneous Province. *Trans. geol. Soc. S. Afr.*, 76(3), 249-270.

Flynn, R.T. and Burnham, W.C. (1978). An experimental determination of rare earth partition coefficients between a chloride containing vapor phase and silicate melts. *Geochim. Cosmochim. Acta*, 42, 685-701.

Flohr, M.J.K., and Ross, M. (1989). Alkaline igneous rocks of Magnet Cove, Arkansas: Metasomatized ijolite xenoliths from Diamond Jo quarry. *Am. Mineral.*, 74, 113-131.

Fraser, K.J., Hawkesworth, C.J., Erlank, A.J., Mitchell, R.H. and Scott-Smith, B.H. (1985). Sr, Nd and Pb isotope and minor element geochemistry of lamproites and kimberlites. *Earth and Planet. Sci. Lett.*, 76, 57-70.

Freestone, I.C. and Hamilton, D.L. (1980). The role of liquid immiscibility in the genesis of carbonatites - An experimental study. *Contrib. Mineral. Petrol.*, 73, 105-117.

Frick, C. and Malherbe, S.J. (1986). *The geology of the Roodeplaat Caldera, north-east of Pretoria*, Bulletin geol. Surv. S. Afr., 79, 44p.

Frick, C. and Walraven, F. (1985). The petrology and geochemistry of the pre-Karoo Elandskraal Volcano, South Africa. *Trans. geol. Soc. S. Afr.*, 88, 225-243.

Fryer, B.J. and Edgar, A.D. (1977). Significance of rare earth distributions in coexisting minerals of peralkaline undersaturated rocks. *Contrib. Mineral. Petrol.*, 61, 35-48.

Gerassimovsky, V.I. and Kuznetsova, S.Ya. (1966). Chemical composition of the Lovosero massif. (In Russian). Geochimija, 4, 390-397.

Gerassimovsky, V.I., Volkov, V.P., Kogarko, L.N. and Polyakov, A.I. (1974). Alkaline Provinces: Kola Peninsular. in Sörensen, H. (ed.), *The Alkaline Rocks*, Wiley, London, 206-221.

Gerlach, D.C., Cliff, R.A., Davies, G.R., Norry, M. and Hodgson, N. (1988). Magma sources of the Cape Verdes Archipelago: Isotopic and trace element constraints. *Geochim. Cosmochim. Acta*, 52, 2979-2992.

Gittins, J. (1979). The feldspathoidal alkaline rocks. in Yoder, H.S. (ed), *The Evolution of the Igneous Rocks - Fiftieth Anniversary Perspectives*, 351-390, Princeton University Press, Princeton.

Gittins, J. (1989). The origin and evolution of carbonatite magmas. in Bell,K. (ed.), *Carbonatites - Genesis and Evolution*, Allen and Unwin, London, 617pp, 580-600.

Goles, G.G. (1976). Some constraints on the origin of phonolites from the Gregory Rift, Kenya, and inferences concerning basaltic magmas in the Rift System. *Lithos*, **9**, 1-8.

Grant, J.A. (1986). The Isocon Diagram - A simple solution to Gresens' equations for metasomatic alteration. *Econ. Geol.*, **81**, 1976-1982.

Green, D.H. and Wallace, M.E. (1988). Mantle metasomatism by ephemeral carbonatitic melts. *Nature*, **336**, 459-462.

Green, T.H., Sie, S.H., Ryan, C.G. and Cousens, D.R. (1989). Proton-microprobe determined partitioning of Nb, Ta, Zr, Sr and Y between garnet, clinopyroxene and basaltic melt at high pressure and temperature. *Chem. Geol.*, **74**, 201-216.

Gresens, R.L. (1967). Composition-volume relationships in metasomatism. *Chem. Geol.*, **2**, 47-65.

Grünenfelder, M.H., Tilton, G.R., Bell, K. and Blenkinsop, J. (1989). Lead and strontium isotope relationships in the Oka carbonatite complex, Quebec. *Geochim. Cosmochim. Acta*, **50**, 461-8.

Haggerty, S.E. (1989). Mantle metasomes and the kinship between carbonatites and kimberlites. in Bell,K. (ed.), *Carbonatites - Genesis and Evolution*, Allen and Unwin, London, 546-560.

Hall, A.L. (1911). Annual Report of the Geological Survey of the Transvaal for 1910, Pretoria, 58-60.

Hall, A.L. (1938). Analyses of Rocks, Minerals, Ores, Coals, Soils and Waters from Southern Africa. South African Geological Survey Memoir, **32**, 876p.

Hamilton, D.L. (1961). Nephelines as crystallisation temperature indicators. *Jour. Geol.*, **69**, 321-329.

Hamilton, D.L. and MacKenzie, W.S. (1960). Nepheline solid solution in the system $NaAlSiO_4$-$KAlSiO_4$-SiO_2. *Jour. Petrology*, **1**, 56-72.

Hamilton, D.L. and MacKenzie, W.S. (1965). Phase equilibrium studies in the system $NaAlSiO_4$-$KAlSiO_4$-SiO_2-H_2O. *Mineral. Mag.*, **34**, 214-231.

Hamilton, D.L., Bedson, P. and Esson, J. (1989). The behaviour of trace elements in the evolution of carbonatites. in Bell,K. (ed.), *Carbonatites - Genesis and Evolution*, Allen and Unwin, London, 617pp, 405-427.

Hamilton, P.J. (1977). Sr isotopic and trace element studies of the Great Dyke and Bushveld mafic phase and their relation to early Proterozoic magma genesis in southern Africa. *J. Petrol.*, **18**, 24-52.

Hamilton, P.J., Evensen, N.M., O'Nions, R.K. and Tarney, J. (1979). Sm-Nd systematics of Lewisian gneisses: implications for the origin of granulites. *Nature*, **277**, 25-28.

Harmer, R.E. (1985). Rb-Sr isotopic study of units of the Pienaars River Alkaline Complex, north of Pretoria, South Africa. *Trans. geol. Soc. S. Afr.*, **88**, 215-223.

Harmer, R.E., Eglington, B.M., Farrow, D., Butcher, A.R., Auret, J.M., Stander, Y.Y. and Grosser, E. (1986) Manual of laboratory procedures for isotope analysis. CSIR Report IFIS 21, C.S.I.R., Pretoria.

Harmer, R.E. and Eglington, B.M. (1990). A review of the statistical principles of geochronometry: towards a more consistent approach for reporting geochronological data. *S.Afr. J. Geol.*, **93**, 845-856.

Harrison, W.J. (1981). Partitioning of REE between minerals and coexisting melts during partial melting of a garnet lherzolite. *Am. Mineral.*, **66**, 242-259.

Hart, S.R. and Davis, K.E. (1978). Nickel partitioning between olivine and silicate melt. *Earth and Planet. Sci. Lett.*, **40**, 203-219.

Hart, S.R., Gerlach, D.C. and White, W.M. (1986). A possible new Sr-Nd-Pb mantle array and consequences for mantle mixing. *Geochim. Cosmochim. Acta*, **50**, 1551-1557.

Hart, R.J., Andreoli, M.A.G., Tredoux, M. and De Wit, M.J. (1990). Geochemistry across an exposed section of Archaen crust at Vredefort, South Africa: with implications for mid-crustal discontinuities. *Chemical Geology*, **82**, 21-50.

Hawkesworth, C.J.,Marsh, J.S., Duncan, A.R., Erlank, A.J. and Norry, M.J. (1984) The role of continental lithosphere in the generation of the Karoo volcanic rocks: Evidence from combined Nd- and Sr-isotope studies. *Geol. Soc. S. Afr., Spec. Publ.*, **13**, 341-354.

Hawkesworth, C.J. and Menzies, M. (1987). *Mantle Metasomatism*, Academic Press, London, 342pp.

Hawkesworth, C.J., Rogers, N.W., van Calsteren, P., and Menzies, M. (1984). Mantle enrichment processes. *Nature*, **311**, 331-335.

Hawkesworth, C.J., van Calsteren, P., Rogers, N.W. and Menzies, M. (1987). Isotope variations in recent volcanics: a trace element perspective. in Hawkesworth, C.J. and Menzies, M. (eds), *Mantle Metasomatism*, Academic Press, London, 365-388.

Henderson, P. (1982). *Inorganic Geochemistry.* Pergamon Press, Oxford, 353pp.

Henoc, J., Heinrich, K.F.J. and Myklebust, R.L. (1973). A rigorous correction procedure for quantitative electron probe microanalysis (COR 2). U.S. Bureau of Standards Technical Note 769, U.S. Govt. Printing Office, Washington D.C.

Hoernle, K.A. and Tilton, G.R. (1991). Sr-Nd-Pb isotope data for Fuerteventura (Canary Islands) basal complex and subaerial volcanics: applications to magma genesis and evolution. *Schweiz. Mineral. Petrogr. Mitt.*, **71**, 3-18.

Hofmann, A.W. and White, W.M. (1982). Mantle plumes from ancient oceanic crust. *Earth and Planet. Sci. Lett.*, **57**, 421-436.

Hogarth, D.D. (1989). Pyrochlore, apatite and amphibole: Distinctive minerals in carbonatite. in Bell,K. (ed.), *Carbonatites - Genesis and Evolution*, Allen and Unwin, London, 617pp, 105-148.

Holmes, A. (1958). Spitskop Carbonatite, Eastern Transvaal. *Bull. Geol. Soc. Am.*, 69, 1525-1526.

Hughes, C.J. and Hussey, E.M.(1976). *M* and Mg values in igneous rocks: proposed usage and a comment on currently employed Fe_2O_3 corrections. *Geochim. Cosmochim. Acta*, **40**, 485-486.

Hunter, R.H. and McKenzie, D. (1989). The equilibrium geometry of carbonate melts in rocks of mantle composition. *Earth and Planet. Sci. Lett.*, 92, 347-356.

Irving, A.J. (1978). A review of experimental studies of crystal/liquid trace element partitioning. *Geochim. Cosmochim. Acta*, 42, 743-770.

Irving, A.J. and Price, R.C. (1981). Geochemistry and evolution of lherzolite-bearing phonolite lavas from Nigeria, Australia, East Germany, and New Zealand. *Geochim. Cosmochim. Acta*, **45**, 1309-1320.

Irving, A.J. and Green, D.H. (1976). Geochemistry and petrogenesis of the Newer Basalts of Victoria and South Australia. *J. Geol. Soc. Aust.*, 23, 45-66.

Jones, A.P. (1980). *The petrology and structure of the Motzfeldt Centre, Igaliko, South Greenland.* PhD. Thesis, University of Durham (Unpubl.).

Jones, A.P. (1984). Mafic silicates from the nepheline syenites of the Motzfeldt centre, South Greenland. *Mineral. Mag.*, **48**, 1-11.

Jones, A.P. (1989). Upper-mantle enrichment by kimberlitic or carbonatitic magmatism. in Bell,K. (ed.), *Carbonatites - Genesis and Evolution*, Allen and Unwin, London, 448-463.

Jones, R.A. (1987). Strontium and neodymium isotopic and rare earth element evidence for the genesis of megacrysts in the kimberlites of southern Africa. *in* Nixon, P.H. (ed.) *Mantle Xenoliths*, Wiley, London, 711-724.

Jordan, T. (1988). Structure and formation of the continental tectosphere. *J. Petrol.*, **37**, 11-37.

Keller, J. (1989). Extrusive carbonatites and their significance. in Bell,K. (ed.), *Carbonatites - Genesis and Evolution*, Allen and Unwin, London, 70-88.

King, B.C. and Sutherland, D.S. (1960). Alkaline rocks of Eastern and Southern Africa. *Sci. Prog.*, **47**, 298-321, 504-524, 709-720.

King, B.C. and Sutherland, D.S. (1966). The Carbonatite Complexes of Uganda. in O.F. Tuttle and J. Gittins (eds.), *Carbonatites*, Wiley, London, 73-126.

Kjarsgaard, B.A. and Hamilton, B.D. (1988). Liquid immiscibility and the origin of alkali-poor carbonatites. *Mineral. Mag.*, **52**, 43-55.

Kjarsgaard, B.A. and Hamilton, B.D. (1989). The genesis of carbonatites by immiscibility. in Bell,K. (ed.), *Carbonatites - Genesis and Evolution*, Allen and Unwin, London, 388-404.

Kleeman, G.J. (1985). The geochemistry and petrology of the roof rocks of the Bushveld Complex east of Groblersdal. *Unpublished M.Sc. Thesis, University of Pretoria*, 178pp.

Kleeman, G.J. and Twist, D. (1989). The compositionally-zoned sheet-like granite pluton of the Bushveld Complex: Evidence bearing on the nature of A-type magmatism. *J. Petrol.*, **30**, 1383-1414.

Koster Van Groos, A.F. (1975). The effect of high CO_2 pressures on alkalic rocks and its bearing on the formation of alkalic ultrabasic rocks and the associated carbonatites. *Am. J. Sci.*, **275**, 163-185.

Koster Van Groos, A.F. and Wyllie, P.J. (1966). Liquid immiscibility in the system Na_2O-$Al_2O_3SiO_2$-CO_2 at pressures up to 1 kilobar. *Am. J. Sci.*, 264, 234-255.

Koster Van Groos, A.F. and Wyllie, P.J. (1968). Liquid immiscibility in the join $NaAlSi_3O_8$-Na_2CO_3-H_2O and its bearing on the genesis of carbonatites. *Am. J. Sci.*, **266**, 932-967.

Koster Van Groos, A.F. and Wyllie, P.J. (1973). Liquid immiscibility in the join $NaAlSi_3O_8$-$CaAl_2Si_2O_8$-Na_2CO_3-H_2O. *Am. J. Sci.*, **273**, 465-487.

Krafft, M. and Keller, J. (1989). Temperature measurements in carbonatite lava lakes and flows from Oldoinyo Lengai, Tanzania. *Science*, **245**, 168-170.

Kramers, J.D. (1979). Lead, uranium, strontium, potassium and rubidium in inclusion--bearing diamonds and mantle-derived xenoliths from southern Africa. *Earth and Planet. Sci. Lett.*, 42, 58-70.

Kramers, J.D., Smith, C.B., Lock, N.P., Harmon, R.S. and Boyd, F.R. (1981). Can kimberlites be generated from an ordinary mantle? *Nature*, **291**, 53-56.

Kramers, J.D. and Smith, C.B. (1983). A feasibility study of U-Pb and Pb-Pb dating of kimberlites using groundmass mineral fractions and whole-rock samples. *Isotope Geosc.*, **1**, 23-38.

Kresten, P. (1988). The chemistry of fenitization: Examples from Fen, Norway. *Chem. Geol.*, **68**, 329-349.

Kruger, F.J. (1982). The occurrence of cebollite in kimberlite and included zeolitised crustal xenoliths - a correction and discussion of the occurrence of pectolite. *Mineralogical Magazine*, 46(339), 273-274.

Kruger, F.J., Cawthorn, R.G. and Walsh, K.L. (1987). Sr-isotopic evidence against magma addition into the Upper Zone of the Bushveld Complex. *Earth and Planet. Sci. Lett.*, **84**, 51-58.

Kulakov, A.N., Evdokimov, M.D., and Bulakh, A.G. (1974). Mineral veins in fenites of the Tur'ii peninsular in the Murmansk region. (in Russian). *Zap. Vses. Min. Obshch.*, **103**, 179-191.

Kwon, S.-T., Tilton, G.R. and Grünenfelder, M.H. (1989). Lead isotope relationships in carbonatites and alkalic complexes: an overview. in Bell,K. (ed.), *Carbonatites - Genesis and Evolution*, Allen and Unwin, London, 617pp, 360-387.

Lancelot, J.R. and Allegre, C.J. (1974). Origin of carbonatitic magma in the light of the Pb-U-Th isotope system. *Earth and Planet. Sci. Lett.*, 22, 233-238.

Larsen, L.M. (1979). Distribution of REE and other trace elements between phenocrysts and peralkaline undersaturated magmas, exemplified by rocks from the Gardar igneous province, south Greenland. *Lithos*, 12, 303-315.

Leach, T.M. and Rodgers, K.A. (1978). Metasomatism in the Wairere Serpentinite, King County, New Zealand. *Mineral. Mag.*, 42, 45-62.

Le Bas, M.J. (1977). *Carbonatite-Nephelinite Volcanism.*

Le Bas, M.J. (1978). Are olivine-poor nephelinites a primary melt product from the mantle? *Bull. Volcanol.*, 41-4, 463-465.

Le Bas, M.J. (1981). Carbonatite magmas. *Mineralogical Magazine*, 44, 133-140.

Le Bas, M.J. (1987). Nephelinites and carbonatites. in J.G. Fitton and B.G.J. Upton (eds.), *Alkaline Igneous Rocks*, Geological Society Special Publication No 30, Blackwell, Oxford, 85-94.

Le Bas, M.J. (1989). Diversification of carbonatite. in Bell,K. (ed.), *Carbonatites - Genesis and Evolution*, Allen and Unwin, London, 617pp, 428-447.

Le Bas, M.J. and Aspden, J.A. (1981). The comparability of carb-onatitic fluid inclusions in ijolites with natrocarbon-atitic lava. *Bull. Volc.*, 44, 429-438.

Le Bas, M.J., Le Maitre, R.W., Streckeisen, A. and Zanettin, B. (1986). A chemical classification of volcanic rocks based on the total alkali-silica diagram. *J. Petrol.*, 27, 745-750.

Le Maitre, R.W. (1976). The chemical variability of some igneous rocks. *J. Petrol.*, 17, 589-637.

Le Roux, A.P., Erlank, A.J. and Needham, H.D. (1981). Geochemical and mineralogical evidence for the occurrence of at least three distinct magma types in the FAMOUS region. *Contrib. Mineral. Petrol.*, 77, 24-37.

Linthout, K. (1984). Alkali-zirconosilicates in peralkaline rocks. *Cont. Mineral. Petrol.*, 86, 155-158.

Lippard, S.J. (1973). The petrology of phonolites from the Kenya Rift. *Lithos*, 6, 217-234.

Lloyd, F.E. and Bailey, D.K. (1975). Light element metasomatism of the continental mantle: the evidence and the consequences. *Phys. Chem. Earth.*, 9, 389-416.

Loubet, M., Bernat, M., Jovoy, M. and Allègre, C.J. (1972). Rare earth contents in carbonatites. *Earth and Planet. Sci. Lett.*, **14**, 226-232.

Lurie, J. (1973). *The Pilanesberg: geology, rare element geochemistry and economic potential.* Unpubl. Ph.D. thesis, Rhodes University.

Lurie, J., and Cawthorn, R.G. (1984). Excursion Guidebook: Geokongres '84.

Marsh, J.S. (1987a). Evolution of a strongly differentiated suite of phonolites from the Klinghardt Mountains, Namibia. *Lithos*, **20**, 41-58.

Marsh, J.S. (1987b). Basalt geochemistry and tectonic discrimination within continental flood basalt provinces. *J. Volcanol. Geotherm. Res.*, **32**, 35-50.

Martin, R.F., Whitley, J.E. and Woolley, A.R. (1978). An investigation of rare-earth mobility: fenitized quartzites, Borralan complex, N.W. Scotland. *Contrib. Mineral. Petrol.*, **16**, 69-73.

Mason, R. (1982). Trace element distributions between perthite phases of alkali feldspars from pegmatites. *Mineralogical Magazine*, **45**, 101-106.

Matsubra, S., Kato, A., Tiba, T., and Nomura, M. (1979). Pectolite, analcime, natrolite and thomsonite in altered gabbro from Yani, Shinshiro, Aichi Prefecture, Japan. Memoirs of the National Science Museum, Tokyo, **12**, 13-22.

McKenzie, D. (1985). The extraction of magma from the crust and mantle. *Earth and Planet. Sci. Lett.*, **74**, 81-91.

McKenzie, D. (1989). Some remarks on the movement of small melt fractions in the mantle. *Earth and Planet. Sci. Lett.*, **95**, 53-72.

McKie, D. (1966). Fenitization. In: Tuttle, O.F. and Gittins, J. (Editors), *Carbonatites*, Wiley-Interscience, New York, 261-294.

Meen, J.K. (1987). Mantle metasomatism and carbonatites: An experimental study of a complex relationship. *in* Morris, E.M. and Pasteris, J.D. (eds.), *Mantle Metasomatism and Alkaline Magmatism.*, Geol. Soc. Am. Special Paper **215**, 91-100.

Meen, J.K., Ayers, J.C. and Fregeau, E.J. (1989). A model of mantle metasomatism by carbonated alkaline melts: Trace element and isotopic compositions of mantle source regios of carbonatite and other continetal igneous rocks. *in* Bell,K. (ed.), *Carbonatites - Genesis and Evolution*, Allen and Unwin, London, 464-499.

Mehnert, K.R. (1968). *Migmatites and the Origin of Granitic Rocks.* Elsevier, Amsterdam.

Menzies, M.A. and Murthy, V.R. (1980). Mantle metasomatism as a precursor to the genesis of alkaline magmas - isotopic evidence. *Am. J. Sci.*, **280-A**, 622-638.

Menzies, M.A., Rogers, N.W., Tindle, A. and Hawkesworth, C.J. (1987) Metasomatism and enrichment processes in lithospheric peridotites, an effect of asthenosphere--lithosphere interaction. *in* Menzies, M.A. and Hawkesworth, C.J. (eds.), *Mantle Metasomatism*, Academic Press, London, 313-361.

Menzies, M.A. and Halliday, A. (1988). Lithospheric mantle domains beneath the Archaen and Proterozoic crust of Scotland. *J. Petrol.*, **37**, 275-302.

Meyer, R. and De Beer, J.H. (1987). Structure of the Bushveld Complex from resistivity measurements. *Nature*, 325, 610-612.

Middlemost, E.A.K. (1989). Iron oxidation ratios, norms and the classification of volcanic rocks. *Chem. Geology*, 77, 19-26.

Mitchell, R.H. (1986). *Kimberlites: mineralogy, geochemistry and petrology.* Plenum Press, New York, 442pp.

Mitchell, R.H. and Brunfelt, A.O. (1975). Rare earth element geochemistry of the Fen Complex, Norway. *Cont. Mineral. Petrol.*, **52**, 247-259.

Möller, P., Morteani, F. and Schley, F. (1980). Discussion of REE distribution patterns of carbonatites and alkalic rocks. *Lithos*, **13**, 171-179.

Molyneux, T.G. (1970). Geology of the area in the vicinity of Magnet Heights, eastern Transvaal, with special reference to the magnetic iron ore. *Spec. Publ. geol. Soc. S. Afr.*, **1**, 228-241.

Moore, A.C. (1970). Descriptive terminology for the textures of rocks in granulite facies terrains. *Lithos*, **3**, 123-127.

Morogan, V. (1989). Mass transfer and REE mobility during fenitization at Alnö, Sweden. *Contrib. Mineral. Petrol.*, **103**, 25-34.

Morogan, V. and Martin, R.F. (1985). Mineralogy and partial melting of fenitized crustal xenoliths in the Oldoinyo Lengai carbonatitic volcano, Tanzania. *Am. Mineral.*, **70**, 1114-1126.

Morogan, V. and Woolley, A.R. (1988). Fenitization at the Alnö carbonatite complex, Sweden; distribution, mineralogy and genesis. *Contrib. Mineral. Petrol.*, **100**, 169-182.

Morris, E.M. and Pasteris, J.D. (editors) (1987). *Mantle Metasomatism and Alkaline Magmatism.*, Geol. Soc. Am. Special Paper 215, Geol. Soc. Am., Boulder, 383pp.

Mysen, B.O. (1983). Rare earth element partitioning between (H_2O+CO_2) vapor and upper mantle minerals: Experimental data bearing on the conditions of formation of alkali basalt and kimberlite. *Neues Jahrbuch Miner. Abh.*, **146**, 41-65.

Nel, D.J. (1976) *A petrochemical investigation of the Spitskop Alkaline Complex.* M.Sc. thesis, University of Pretoria (unpubl.).

Nelson, D.R., Chivas, A.R., Chappell, B.W. and McCulloch, M.T. (1988). Geochemical and isotopic systematics in carbonatites and implications for the evolution of ocean-island sources. *Geochim. Cosmochim. Acta*, **52**, 1-17.

Nelson, D.R., Trendall, A.F., De Laeter, J.R., Grobler, N.J. and Fletcher, I.R. (1992). A comparative study of the geochemical and isotopic systematics of late Archaean flood baslats from the Pilbara and Kaapvaal Cratons. *Precambrian Res.*, **54**, 231-256.

Ngwenya, B.T. and Bailey, D.K. (1990). Kaluwe carbonatite, Zambia: an alternative to natrocarbonatite. *Jour. Geol. Soc. London*, **147**, 213-216.

Nielsen, T.F.D. (1980). The ultramafic cumulate series, Gardiner Complex, East Greenland: Cumulates in a shallow level magma chamber of a nephlinitic volcano. *Contrib. Mineral. Petrol.*, **76**, 60-72.

Nielsen, T.F.D. and Buchardt, B. (1985). Sr-C-O isotopes in nephelinitic rocks and carbonatites, Gardiner Complex, Tertiary of East Greenland. *Chemical Geology*, **53**, 207-217.

Noble, S.R., Lightfoot, P.C. and Schärer, U. (1989). A new method for single-filament isotopic analysis of Nd using in situ reduction. Isotope Geoscience, 79, 15-19.

Norrish, K. and Hutton J.T. (1969). An accurate X-ray spectrographic method for the analysis of a wide range of geological samples. *Geochim. Cosmochim. Acta*, **33**, 431-453.

Norry, M.J., Truckle, P.H., Lippard, S.J., Hawkesworth, C.J., Weaver, S.D. and Marriner, G.F. (1980). Isotopic and trace element evidence from lavas, bearing on mantle heterogeneity beneath Kenya. *Phil. Trans. R. Soc. Lond.*, **A297**, 259-271.

Olafsson, M. and Eggler, D.H. (1983). Phase relations of amphibole, amphibole-carbonate, and phlogopite--carbonate peridotite: petrologic constraints on the asthenosphere. *Earth and Planet. Sci. Lett.*, **64**, 305-315.

Oosthuyzen, E.J. and Burger, A.J. (1964). Radiometric dating of intrusives associated with the Waterberg System. *Ann. geol. Surv. S. Afr.*, **3**, 87-106.

Pearce, J.A., Harris, N.B.W., and Tindle, A.G. (1984). Trace element discrimination diagrams for the tectonic interpretation of granitic rocks. *J. Petrol.*, **25**, 956-983.

Phillips, D., Onstott, T.C. and Harris, J.W. (1989). $^{40}Ar/^{39}Ar$ laser-probe dating of diamond inclusions from the Premier kimberlite. *Nature*, **340**, 460-462.

Platt, R.G., Wall, F., Williams, C.T., and Woolley, A.R. (1987). Zirconolite, chevkinite and other rare earth minerals from nepheline syenites and peralkaline granites and syenites of the Chilwa Alkaline Province, Malawi. *Mineral. Mag.*, **51**, 253-263.

Powell, J.L., Hurley, P.M. and Fairbairn, H.W. (1962). Isotopic composition of strontium in carbonatites. *Nature*, **196**, 1085-1086.

Powell, J.L., Hurley, P.M. and Fairbairn, H.W. (1966). The strontium isotope composition and origin of carbon-atites. in O.F. Tuttle and J. Gittins (eds.), *Carbonatites*, Wiley, London, 365-378.

Price, R.C., Johnson, R.W., Gray, C.M. and Frey, F.A. (1985). Geochemistry of phonolites and trachytes from the summit region of Mt. Kenya. *Contrib. Mineral. Petrol.*, **89**, 394-409.

Reid, D.L. (1979). Age relationships within the Mid-Proterozoic Vioolsdrif Batholith, lower Orange River area. *Trans. geol. soc. S.Afr.*, **82**, 205-214.

Reid, D.L. (1991). Alakline rocks in the Kuboos-Bremen igneous province, southern Namibia: The Kanabeam multiple ring complex. *Communs. geol. Surv. Namibia*, **7**, 3-13.

Retief, E.A. (1963). *Petrological and mineralogical studies in the southern part of the Pilanesberg alkaline complex, Transvaal, South Africa.* Unpubl. Ph.D. thesis, Oxford University.

Richardson, S.H. (1986). Latter-day origin of diamonds of eclogitic paragenesis. *Nature*, **322**, 623-626.

Richardson, S.H., Gurney, J.J., Erlank, A.J. and Harris, J.W. (1984). Origin of diamonds in old enriched mantle. *Nature*, **310**, 198-202.

Richardson, S.H., Erlank, A.J. and Hart, S.J. (1985). Kimberlite--borne garnet peridotite xenoliths from old enriched subcontinental lithosphere. *Earth and Planet. Sci. Lett.*, 75, 116-128.

Robins, B. (1984). Petrography and petrogenesis of nephelinized metagabbros from Finnmark, Northern Norway. *Contrib. Mineral. Petrol.*, **86**, 170-177.

Roden, M.F., Rama Murthy, V. and Gaspar, J.C. (1985). Sr and Nd composition of the Jacupiranga carbonatite. *Journal of Geology*, **93**, 212-220.

Rogers, N.W. and Hawkesworth, C.J. (1982). Proterozoic age and cumulate origin for granulite xenoliths, Lesotho. *Nature*, **299**, 409-413.

Rubie, D.C. (1982). Mass transfer and volume change during alkali metasomatism at Kisingiri, western Kenya. *Lithos*, **15**, 99-109.

Rubie, D.C. and Gunter, W.D. (1983). The role of speciation in alkaline igneous fluids during fenite metasomatism. *Contrib. Mineral. Petrol.*, **82**, 165-175.

Ryabchikov, I.D., Baker, M. and Wyllie, P.J. (1990). Phosphate--bearing carbonatite liquids in equilibrium with mantle lherzolites at 30 kbar. *Geochemistry Int.*, , 102-106.

Ryabchikov, I.D., Orlova, G.P., Senin, V.G. and Trubkin, N.V. (1991). Interphase partition of rare earth elements during partial melting in the peridotite-carbonate--phosphate system. *Int. Geology Review*, **33**, 565-573.

Schleicher, H., Keller, J. and Kramm, U. (1990). Isotope studies on alkaline volcanics and carbonatites from the Kaiserstuhl, Federal Republic of Germany. *Lithos*, **26**, 21-35.

Schneider, M.E. and Eggler,D.H. (1986). Fluids in equilibrium with peridotite minerals: Implications for mantle metasomatism. *Geochim. Cosmochim. Acta*, **50**, 711-724.

Schreiner, G.D.L. and Van Niekerk, C.B. (1958). The age of a Pilanesberg dike from the central Witwatersrand. *Trans. geol. Soc. S.Afr.*, **61**, 198-199.

Scogings, A.J. and Forster, I.F. (1989). Gneissose carbonatites in the Bull's Run Complex, Natal. *S.Afr. J. Geol.*, **92**, 1-10.

Scott, P.W. (1976). Crystallization trends of pyroxenes from the alkaline volcanic rocks of Tenerife, Canary Islands. *Mineral. Mag.*, **40**, 805-816.

Scott Smith, B.H., Skinner, E.M. and Clement, C.R. (1983). Further data on the occurrence of pectolite in kimberlite. *Mineral. Mag.*, **47**, 75-78.

Shand, S.J. (1921a). The nepheline rocks of Sekukuniland. *Trans. geol. Soc. S. Afr.*, **24**, 111-149.

Shand, S.J. (1921b). The igneous complex of Leeuwfontein, Pretoria district. *Trans. geol. Soc. S. Afr.*, **24**, 232-249.

Shand, S.J. (1922). The alkaline rocks of the Franspoort Line, Pretoria District. *Trans. geol. Soc. S. Afr.*, **25**, 81--100.

Shand, S.J. (1928). The geology of Pilansberg (Pilaan's Berg) in the Weatern Transvaal: a study of the alkaline rocks and ring-intrusions. *Trans. geol. Soc. S. Afr.*, **31**, 97-156.

Sharpe, M.R. (1985). Strontium isotope evidence for preserved density stratification in the main zone of the Bushveld Complex, South Africa. *Nature*, **316**, 119-126.

Smith, C.B. (1983). Pb, Sr and Nd isotopic evidence for sources of southern African kimberlites. *Nature*, **304**, 51-54.

Snelling, N.J. (1963). Age determination unit. *Ann. Rep. Overseas geol. Surv.*, p30.

Sörensen, H. (1974). Alkali syenites, feldspathoidal syenites and related lavas, in Sörensen, H. (ed.), *The Alkaline Rocks*, Wiley, London, 22-52.

South African Committee for Stratigraphy (SACS) (1980). Stratigraphy of South Africa. Part 1 (Comp. L.E. Kent). Lithostratigraphy of the Republic of South Africa, South West Africa/Namibia, and the Republics of Bophuthatswana, Transkei and Venda. *Handb. geol. Surv. S. Afr.*, **8**, 690pp.

Spera, F.J. (1984). Carbon dioxide in petrogenesis, III. Role of volatiles in the ascent of alkaline magma with special reference to xenolith-bearing mafic lavas. *Contrib. Mineral. Petrol.*, **88**, 217-232.

Stacey, J.S. and Kramers, J.D. (1975). Approximation of terrestrial lead isotope evolution by a two-stage model. *Earth and Planet. Sci. Lett.*, **26**, 207-221.

Stephenson, D. (1972). Alkali clinopyroxenes from nepheline syenites of the South Qôroq Centre, south Greenland. *Lithos*, **5**, 187-201.

Stosch, H.-G. and Lugmair, G.W. (1984). Evolution of the lower continental crust: granulite facies xenoliths from the Eifel, West Germany. *Nature*, **311**, 368-370.

Strauss, C.A. and Truter, F.C. (1950). The alkali complex at Spitskop, Sekukuniland, Eastern Transvaal. *Trans. geol. Soc. S. Afr.*, **53**, 81-125.

Sweeney, R.J., Green, D.H. and Sie, S.H. (1992). Trace and minor element partitioning between garnet and amphibole and carbonatitic melt. *Earth and Planet. Sci. Lett.*, **113**, 1-14.

Sweeney, R.J., Falloon, T.J. and Green, D.H. (in press). Experi-mental constraints on the possible mantle origin of natrocarbonatite. IAVCEI Spec. Publ. on Oldoinyo Lengai.

Tilley, C.E. (1954). Nepheline-alkali feldspar parageneses. *Am. J. Sci.*, **252**, 65-75.

Toens, P.D. (1952). *The Geology around Leeuwfontein north-east of Pretoria.* M.Sc. thesis (Unpubl.), University of Pretoria, Pretoria, 117p.

Treiman, A.H. (1989). Carbonatite magma: properties and processes. in Bell,K. (ed.), *Carbonatites - Genesis and Evolution*, Allen and Unwin, London, 617pp, 89-104.

Treiman, A.H. and Schedl, A. (1983). Properties of carbonatite magma and processes in carbonatite magma chambers. *Jour. Geol.*, **91**, 437-447.

Twyman, J.D. and Gittins, J. (1987). Alkalic carbonatite magmas: parental or derivitive? in J.G. Fitton and B.G.J. Upton (eds.), *Alkaline Igneous Rocks*, Geological Society Special Publication No 30, Blackwell, Oxford, 85-94.

Upton, B.G.J. (1966). Alkaline Pyroxenites. in Wyllie, P.J. (ed.), *Ultramafic Rocks*, 281-288.

Van Calsteren, P.W.C., Harris, N.B.W., Hawkesworth, C.J., Menzies, M.A. and Rogers, N.W. (1986). Xenoliths from southern Africa: a perspective on the lower crust. in Dawson, J.B., Carswell, D.A., Hall, J. and Wedepohl, K.H. (eds),

The Nature of the Lower Crust, Geological Society Special Publication No. 24, p351-362.

Van Niekerk, C.B. (1962). The age of the Gemspost Dyke from the Venterspost gold mine. *Trans. geol. Soc. S. Afr.*, 65, 105-111.

Van Straaten, P. (1989). Nature and structural relationships of carbonatites from southwest and west Tanzania. in Bell,K. (ed.), *Carbonatites - Genesis and Evolution*, Allen and Unwin, London, 617pp, 177-199.

Vartiainen, H. and Woolley, A.R. (1976). The petrography, mineralogy and chemistry of the fenites of the Sökli carbonatite intrusion, Finland. *Geol. Surv. Finland Bull.*, **280**, 1-87.

Verwoerd, W.J. (1964). The significance of fenitised granite--pegmatites in the Spitskop Complex. Trans. geol. soc. S. Afr., **67**, 219-227.

Verwoerd, W.J. (1966). Fenitisation of basic igneous rocks. In: Tuttle, O.F. and Gittins, J. (Editors), *Carbonatites*, Wiley-Interscience, New York, 295-307.

Verwoerd, W.J. (1967). *The carbonatites of South Africa and South West Africa*: Handbk geol. Surv. S. Afr., 6, 452p.

Verwoerd, W.J., Weder, E. and Harmer, R.E. (1986). The Stukpan carbonatite: a new discovery in the Orange Free State goldfield. Geocongress '86, p899-902 (Extended Abstract).

Verwoerd, W.J. (1990). Pillow lava associated with the Goudini carbonatite volcano, South Africa. IAVCEI Congress, Mainz, Germany, (Abstract).

Vlasov, K.A., Kuzmenko, M.V. and Eskova, E.M. (1966). *The Lovosero Alkali Massif* (English Edition), Oliver and Boyd, London, 627pp.

Von Eckermann, H. (1948). *The alkaline district of Alnö Island.* Sver. Geol. Unders., Ca **36**, 176pp.

Wallace, M.E. and Green, D.H. (1988). An experimental deter-mination of primary carbonatite magma composition. *Nature*, **335**, 343-346.

Walraven, F. (1981). *The Geology of the Rustenburg Area: Explanation of Sheet 2526.* Geol. Survey S.Africa, Government Printer, Pretoria, 37p.

Walraven, F. (1988). Notes on the age and genetic relationships of the Makhutso Granite, Bushveld Complex, South Africa. *Chem. Geol. (Isotope Geoscience Section)*, 72, 17-28.

Walsh, J.N., Buckley, F. and Barker, J. (1981). The simultaneous determination of the rare-earth elements in rocks using inductively coupled plasma source spectrometry. *Chem. Geol.*, **33**, 141-153.

Wapstra, A.H. and Bos, K. (1977). The 1977 atomic mass evaluation Part 1. Atomic mass table. *Atomic Data and Nuclear Data Tables*, 19, 177-214.

Wass, S.Y. and Rogers, N.W. (1980). Mantle metasomatism - precursor to continental alkaline volcanism. *Geochim. Cosmochim. Acta*, **44**, 1811-1823.

Watson, E.B. and Green, T.H. (1981). Apatite/liquid partition coefficients for the rare earth elements and strontium. *Earth and Planet. Sci. Lett.*, **56**, 405-421.

Watson, E.B. and Harrison, T.M. (1983). Zircon saturation revisited: temperature and composition effects in a variety of crustal magma types. *Earth and Planet. Sci. Lett.*, **64**, 295-304.

Watson, E.B. and Brenan, J.M. (1987). Fluids in the lithosphere, 1. Experimentally--determined wetting characteristics of CO_2-H_2O fluids and their implications for fluid transport, host-rock physical properties, and fluid inclusion formation. *Earth and Planet. Sci. Lett.*, **85**, 497-515.

Watson, E.B., Brenan, J.M. and Baker, D.R. (1990). Distribution of fluids in the continental mantle. in Menzies, M. (ed.), *Continental Mantle*, Clarendon Press, Oxford, 111-125.

Watterson, J.I.W. (1975). Instrumental neutron activation analysis and the classification of granites from the Bushveld Igneous Complex. Ph.D. Thesis, Univ. Witwatersrand, 360pp (unpubl.).

Weaver, B.L. and Tarney, J. (1980). Continental crust composition and nature of the lower crust: constraints from mantle Nd-Sr isotope correlation. *Nature*, **386**, 342-6.

Weaver, S.D., Sceal, J.S.C. and Gibson, I.L. (1972). Trace element data relevant to the origin of trachytic and pantelleritic lavas in the East African Rift System. *Contrib. Mineral. Petrol.*, **36**, 181-194.

Wen, J., Bell, K. and Blenkinsop, J. (1987). Nd and Sr isotope systematics of the Oka complex, Quebec, and their bearing on the evolution of the sub-continental upper mantle. *Contrib. Mineral. Petrol.*, **97**, 433-437.

Wendlandt, R.F. and Mysen, B.O. (1978). Melting phase relations of natural peridotite + CO_2 as a function of degree of partial melting at 15 and 30 kbar. *Carn. Inst. Wash. Year Book*, **77**, 756-761.

White, B.S. and Wyllie, P.J. (1992). Solidus reactions in synthetic lherzolite-H_2O-CO_2 from 20-30 kbar, with applications to melting and metasomatism. *J. Volcanol. Geotherm. Res.*, **50**, 117-130.

White, W.M. (1985). Sources of oceanic basalts: Radiogenic isotopic evidence. *Geology*, **13**, 115-118.

Wilkinson, J.F.G. and Stolz, A.J. (1983). Low-pressure fractionation of strongly undersaturated alkaline ultrabasic magma: the olivine-melilite--nephelinite at Moiliili, Hawaii. *Contrib. Mineral. Petrol.*, **83**, 363-374.

Willis, J.P.W., Ahrens, L.H., Danchin, R.V., Erlank, A.J., Gurney, J.J., Hofmeyr, P.K., McCarthy, T.S. and Orren, M.J. (1971). Some interelement relationships between lunar rocks and fines and stony meteorites. Proc. Second Lunar Sci. Conf., *Geochim. Cosmochim. Acta*, suppl 2, **2**, 1123-1138.

Willis, J.P.W., Erlank, A.J., Gurney, J.J., Theil, R.H. and Ahrens, L.H. (1972). Major and minor trace element data for some Apollo 11,12,14 and 15 samples, 1269-1273. In: L.D. Heymann (ed.), Proc. Second Lunar Sci. Conf., MIT Press, Boston, 2155pp.

Wilshire, H.G. (1967). The Prospect alkaline diabase-picrite intrusion New South Wales, Australia. *J. Petrol.*, **8**, 97-163.

Wilson, M. (1989). *Igneous Petrogenesis*, Unwin Hyman, London, 466pp.

Winterburn, P.A. (1990). Documentation of isotope analyses and sample collections. CSIR Report EMA-I 9001, Ematek, C.S.I.R., P.O.Box 395, Pretoria.

Winterburn, P.A., Harte, B. and Gurney, J.J. (1990). Peridotite xenoliths from the Jagersfontein kimberlite pipe: 1. Primary and primary metasomatic mineralogy. *Geochim. Cosmochim. Acta*, **54**,

Wood, D.A., Tarney, J., Saunders, A.D., Bougault, H., Joron, J.L., Treuil, M. and Cann, J.R. (1979). Geochemistry of basalts drilled in the north Atlantic by IPOD Leg 49: implications for mantle heterogeneity. *Earth and Planet. Sci. Lett.*, **42**, 77-97.

Woolley, A.R. (1987). Lithosphere metasomatism and the petrogenesis of the Chilwa Province of alkaline igneous rocks and carbonatites, Malawi. *Jour. Afr. Earth Sci.*, 6, 891-898.

Woolley, A.R.(1989). The spatial and temporal distribution of carbonatites. in Bell,K. (ed.), *Carbonatites - Genesis and Evolution*, 15-37, Allen and Unwin, London.

Woolley, A.R. and Jones, G.C. (1987). The petrochemistry of the northern part of the Chilwa alkaline province, Malawi. in J.G. Fitton and B.G.J. Upton (eds.), *Alkaline Igneous Rocks*, Geological Society Special Publication No 30, Blackwell, Oxford, 335-355.

Woolley, A.R. and Kempe, D.R.C. (1989). Carbonatites: nomenclature, average chemical compositions, and element distribution. in Bell,K. (ed.), *Carbonatites - Genesis and Evolution*, 1-14, Allen and Unwin, London.

Wörner, G., Beusen, J.-M., Duchateau, N., Gijbels, R. and Schmincke, H.-U. (1983). Trace element abundances and mineral/melt distribution coefficients in phonolites from the Laacher See Volcano (Germany). *Contrib. Mineral. Petrol.*, **84**, 152-173.

Wörner, G., Zindler, A., Staudigel, H. and Schmincke, H.-U. (1986). Sr, Nd and Pb isotope geochemistry of Tertiary and Quaternary alkaline volcanics from West Germany. *Earth and Planet. Sci. Lett.*, **79**, 107-119.

Wright, J.B. (1966). Olivine nodules in a phonolite of the East Otago alkaline province, New Zealand. *Nature*, 210, 519.

Wright, J.B. (1969). Olivine nodules and related inclusions in trachyte from the Jos Plateau, Nigeria. *Mineral. Mag.*, **37**, 370-374.

Wyllie, P.J. (1974). Limestone assimilation. in Sörensen, H. (ed.), *The Alkaline Rocks*, Wiley, London, 459-474.

Wyllie, P.J. (1978). Mantle fluid compositions buffered in peridotite-CO_2-H_2O by carbonates, amphibole and phlogopite. *Jour. of Geology*, 86, 687-713.

Wyllie, P.J. (1980). The origin of kimberlites. *J. Geophys. Res.*, **85**, 6902-6910.

Wyllie, P.J. (1984). The effect of carbon dioxide on phase relationships for synthetic lherzolite and harzburgite. *Geol. en Mijnbouw*, **63**, 213-219.

Wyllie, P.J. (1987a). Transfer of subcratonic carbon into kimberlites and rare earth carbonatites. in *Magmatic Processes: Physicochemical Principles* (ed. B.O. Mysen), The Geochemical Society Spec. Publ. 1, 107-119.

Wyllie, P.J. (1987b). Discussion of recent papers on carbonated peridotite, bearing on mantle metasomatism and magmatism. *Earth and Planet. Sci. Lett.*, **82**, 391-397, 401-402.

Wyllie, P.J. (1989). Origin of carbonatites: evidence from phase equilibrium studies. in Bell,K. (ed.), *Carbonatites - Genesis and Evolution*, Allen and Unwin, London, 617pp, 500-545.

Wyllie, P.J. and Huang, W.L. (1975). Peridotite, kimberlite, and carbonatite explained in the system $CaO-MgO-SiO_2-CO_2$. *Geology*, **3**, 621-624.

Wyllie, P.J. and Huang, W.L. (1976a). High CO_2 solubilities in mantle magmas. *Geology*, **4**, 21-24.

Wyllie, P.J. and Huang, W.L. (1976b). Carbonation and melting reactions in the system $CaO-MgO-SiO_2-CO_2$ at mantle pressures with geophysical and petrological applications. *Contrib. Mineral. Petrol.*, **54**, 79-107.

Wyllie, P.J., Baker, M.B. and White, B.S. (1990). Experimental boundaries for the origin and evolution of carbonatites. *Lithos*, **26**, 3-19.

Yagi, K. and Onuma, K. (1967). The join $CaMgSi_2O_6$-$CaTiAl_2O_6$ and its bearing on the titanaugites. *J. Fac. Sci., Hokkaido Univ.*, ser. 4, **8**, 463-483.

Yoder, H.S. (1973). Contemporaneous basaltic and rhyolitic magmas. *Am. Mineral.*, **58**, 153-171.

Zartman, R.E. and Doe, B.R. (1981). Plumbotectonics - the model. *Tectonophysics*, 75, 135-62.

Zindler, A. and Hart, S.R. (1986). Chemical Geodynamics. *Ann. Rev. Earth Planet. Sci.*, **14**, 493-571.

Appendix A: Analytical and Calculation Procedures

A.1: Analytical Procedures

A.1.1: Whole rock elemental analyses

A.1.1.1 X-ray fluorescence (XRF) spetrometry

XRF analyses of Spitskop samples were performed on Siemens SRS-1 and Philips PW1400 spectrometers using the routine techniques applied in the Department of Geochemistry, University of Cape Town (UCT), as described in Willis *et al.* (1971, 1972), Le Roux *et al.* (1981) and Duncan *et al.* (1984). Samples from the other Pilanesberg Suite complexes were analysed by Dr. M.R. Sharpe on an ARL 2900 spectrometer in the Geology Department, University of Pretoria. Data reduction procedures closely followed those used at UCT. International rock standards were used for calibrations.

Major elements: Na was determined on pressed powder briquettes whereas the other major elements were determined in duplicate on fused glass discs following the method of Norrish and Hutton (1969). Volatile components were determined gravimetrically by consecutive heating, for periods of 12 hours or more, at 110°C (H_2O^-) and 1000°C (loss on ignition: LOI). It was found that certain nepheline syenites had melted at 1000°C and so LOI's for these rocks were performed at 850°C.

Glass discs were made using the standard Norrish-Hutton recipe of fusing 0.28g of the ashed sample powder with 1.5g of Johnson Matthey Spectroflux 105 and 0.02g of $NaNO_3$. The procedure was modified slightly for the carbonatite samples: LOI's were determined by heating at 1200°C for over 48 hours. Ashed carbonatite powder was mixed with pure SiO_2 (~1:1) before fusing. After analysis, the results were re-calculated to correct for the added SiO_2.

Table A.1: Assessment of major element analyses.

Oxide	Precision	"Accuracy"	LLD
SiO_2	0.140	0.264	0.04
TiO_2	0.008	0.008	0.005
Al_2O_3	0.080	0.079	0.02
Fe_2O_3	0.038	0.064	0.014
MnO	0.008	0.003	0.008
MgO	0.148	0.086	0.07
CaO	0.028	0.030	0.008
Na_2O	0.032	0.067	0.08
K_2O	0.002	0.022	0.002
P_2O_5	0.012	0.018	0.011

From Duncan *et al.*, (1984). "Accuracy" is the average absolute difference (in %oxide) between recommended values for calibration standards and those calculated from the calibration line. LLD is the detection limit (in %oxide at 99% level).

K_α-spectral lines were used for all major elements. Background corrections were performed using "blank" materials fused in the same way as the samples. Backgrounds for the Na powder briquettes were measured either side of the Na K_α line position. Inter-element absorption and enhancement effects were corrected using the approach and "alpha factors" presented by Norrish and Hutton (1969) and corrections were made for crystal fluorescence interferences on Mg. Estimated values for precision and accuracy are listed in Table A.1 (from Duncan *et al.*, 1984).

Trace elements: In view of the high trace element concentrations sometimes encountered in alkaline rocks and carbonatites, a representative suite of samples from Spitskop were analysed at the initiation of the project to assess the potential range of trace elements in these rocks. With few exceptions, the trace element contents were found not to be extreme and were within the compositional range accomodated by the routine XRF analytical procedures adopted by the Geochemistry Department, UCT as applied to the anlayses of Karoo rocks described by Duncan *et al.* (1984).

Table A.2: Summary of trace element analytical parameters used .

Element	Line	Interference	Matrix Correction[1]	Precision (ppm)[2]	LLD (99%)
Nb	K	Y, U, Th	CP	1.2	1.8
Zr	K	Sr, Th, U	CP	1.4	1.4
Y	K	Rb, Th, U	CP	1.0	1.3
Rb	K	U	CP	1.1	1.5
U	L	Rb	CP	2.5	3.5
Sr	K	Th	CP	1.7	1.5
Th	L	Pb	CP	3.1	4.0
Pb	L	Th	CP	3.2	4.5
Zn	K		Calc	1.7	1.4
Cu	K		Calc	2.1	2.9
Ni	K		Calc	1.0	1.2
Ba	L	Ti, Sc	Calc	6.0	3.7
Sc	K		Calc	1.2	1.2
Co	K	Fe	Calc	2.5	4.5
Cr	K	V	Calc	2.1	2.2
V	K	Ti	Calc	3.7	5.5
La	L		Calc	1.7	2.9
Ce	L	Nd	Calc	2.9	6.0
Nd	L	Ce	Calc	1.6	3.6

[1] CP = estimated from intensity of Compton peak of X-ray tube; Calc = calculated from major element concentrations

[2] Precision is typical absolute error in ppm estimated as the 2σ counting error for the concentration range of the samples in this study.

Modified after Duncan *et al.* (1984)

Trace elements were determined on pressed powder briquettes. Similar data reduction procedures were used for analyses performed at UCT (all Spitskop data) and Pretoria U/Rocklabs (other Pilanesberg Suite data). Corrections for background, matrix and spectral interferences (where appropriate), were as described by Duncan *et al.* (1984). Corrections were made for dead time losses, instrumental drift and for variations in count rate at different positions of the sample-holder carousel. Background profiles were established by analysing "blank" samples of differing absorption coefficients (high purity silica and silica-Fe_2O_3 mixtures) whereas spectral interference factors were established with interference standards ("blank" material

with ca.2000ppm of the element of interest added as specpure salt). Corrections for matrix effects for elements with analyte line wavelengths less than the Fe K-absorption edge were made from the intensity of the Mo K_α Compton peak from the Mo-anode X-ray tube. For other trace elements, corrections were made using absorption coefficients calculated from the analysed major element concentrations. Analytical precisions and detection limits (based on counting statistics) are tabulated in Table A.2.

A.1.1.2 ICP-ES determination of rare earth elements

Rare earth elements (REE) were determined in selected samples by Dr. J.N. Walsh at the Royal Holloway and Bedford New College, United Kingdom using ICP emission spectroscopy. Analytical procedures are described in Walsh *et al.* (1981). Precisions (as relative standard deviation) are always below 7% for all the REE and are more typically around 2%.

A.1.2: Mineral Analyses

Minerals were analysed on the UCT Cameca-Camebax electron microprobe. The following instrumental conditions were routinely applied:

40nA beam current and 15kV accelerating voltage;
analysing crystals (K_α analyte lines):

TLAP for Na, Mg, Si and Al;
LiF(200) for Fe, Mg;
PET for Ca, K, Ti and P;

flow counter detectors with Ar/CO_2 gas mixtures.

Corrections for interelement matrix effects were performed using the ZAF procedure (modified after Henoc *et al.*, 1973). Correction for the oxidation state of Fe in clinopyroxenes was made using the approach of Droop (1987).

A.1.3: Isotope analyses

All isotope analyses were performed in the isotope geochemistry laboratories at the CSIR: initially these formed part of the National Physical Research Laboratory and from 1987 the Division of Earth, Marine and Atmospheric Science and Technology. Details of the techniques used have appeared in several publications (Harmer, 1985; Harmer and Sharpe, 1985; Eglington, 1987; Farrow, 1988) and are available as a laboratory manual (Harmer *et al.*, 1986).

A.1.3.1 Chemical processing

A.1.3.1.1 Rb - Sr and Sm - Nd

Rb and Sr concentration measurements for whole rocks were performed by XRF as described above, and for minerals by isotope dilution mass spectrometry (IDMS). All Sm and Nd concentrations were determined by IDMS. Isotopic standards ("spikes") enriched in ^{87}Rb (>95%), ^{84}Sr (>80%), ^{149}Sm (>95%) and ^{150}Nd (>95%) were stored as solutions in 2.5M HCl (Rb,Sr) or 2.0M HNO_3 (Sm,Nd) and periodically calibrated against gravimetrically prepared shelf solutions. Separate dissolutions were carried out to deterimine the Sr and Nd isotopic composition ("natural" run) and for Sm and Nd concentration measurements ("spiked" run).

Whole rock silicate powders or mineral concentrates were allowed to digest in mixtures of concentrated HF and ~8M HNO_3 (ca. 8ml+5ml) in 25ml, screw-top FEP Teflon vials on a hot plate at 80°C for 8-48 hours. The solutions were then slowly evaporat-ed to half volume, a further 5ml 8M HNO_3 added, and evaporated once more. This was repeated once more and the solution evaporated to dryness. 6M HCl was then added and the sealed vial held at ca. 80°C for 2-4 hours. After drying, more 6M HCl was added and the solution checked for signs of remaining fluoride. Solutions were then dried.

A modified procedure was adopted for dissolving carbon-atite samples. Carbonate was initially dissolved in HCL: the sample powder was dampened with H_2O then 2-3ml 2.5M HCl was added and the reaction allowed to proceed. A further 2-3ml 6M HCl was then added and the vial gently warmed. Once all effervescence had subsided the vial was sealed and the solution heated for 30 minutes. After cooling, the solution was transferred to a cleaned FEP or polypropylene centrifuge tube. After centrifuging the clear solution was decanted and the residue repeatedly rinsed with H_2O. Any silicate residue was then dissolved in the centrifuge tube with a few drops of HF and 8M HNO_3. Ultrasoning assisted the solution process. Once dissolved the silicate fraction was transferred to a micro-vial and evaporated to dryness with excess HNO_3. After repeated evaporations in 6M HCl the clear chloride solution was quantitatively added to the carbonate solution and dried.

Rb, Sr and bulk REE were separated using 10mm diameter ion exchange columns packed with 6ml of Bio-Rad AG50W-x12, 200-400# cation exchange resin. Rb and Sr were eluted with 2.5M HCl and the REE collected with 6M HCl. Column resin was washed and regenerated with 6M HCl and pure H_2O.

Nd and, where appropriate, Sm were separated from the bulk REE fraction using reverse phase liquid chromatography on a second, 8mm diameter, column filled with HDEHP (bis-2-ethyl hydrogen phosphate) supported on powdered PTFE teflon (an adaptation of the "Kel-F" technique as used by Richard *et al.,* 1976). Nd was eluted with 0.2M HCl and Sm with either 0.4M or 2.5M HCl. A second pass through the column guaranteed a Nd fraction totally free of Sm.

A.1.3.1.2 Pb - Pb

Sample for Pb analyses were dissolved in the same way as for Sr and Nd but using specially cleaned reagents and vials in a cleaner air environment. The dried, dissolved sample was trans-formed to bromide with 1M HBr. Pb was separated on quartz glass micro-columns packed with ca. 20µl of cleaned AG1x 200-400# anion resin. After cleaning and conditioning of the columns the sample was loaded in 100µl of 0.5M HBr, rinsed with 3x500µl aliquots of 0.5M HBr, and the Pb fraction was stripped with 200µl of H_2O. It was found that the emission during mass spectrometric analysis was improved by purifying the extracted Pb fraction with a second pass through the column.

A.1.3.2 Mass Spectrometry

Mass spectrometric measurements were performed on either a VG MM30 single collector, single focussing, mass spectrometer (MM30) or an automatic VG 354, double-focussing, 54cm radius, spectrometer equipped for simultaneous beam collection on up to 5 faraday collectors (VG354). Data acquisition and spectrometer control software for the MM30 was written by the author. The manufacturer-supplied software for the VG354 was extensively modified by Dr BM Eglington and the author.

Rb: Rb fractions were loaded on the side filament of a double Ta filament assembly and analysed on the MM30. Sr was loaded as the nitrate on single Ta beads and fumed with H_3PO_4. Analysis was by combined multi-collection peak jumping mode on the VG354. Mass fractionation during analysis was corrected by normalising the measured $^{86}Sr/^{88}Sr$ value to 0.1194. Between 100 and 120 normalised $^{87}Sr/^{86}Sr$ ratios were accumulated for each determination.

Sm: Sm was loaded on single Ta beads in the same way as Sr and analysed on the MM30 spectrometer. This procedure produced smooth, steadily increasing ion beams and highly precise measurements could be attained in a short time (generally 40-60 measurements).

Nd: Two approaches were adopted for Nd. Initially, Nd was loaded onto each Ta side filament of a triple Ta-Re-Ta strung filament assembly. This technique supresses the formation of oxide species and generally yielded precise data after the accumulation of 120-140 ratios. As an alternative Nd was loaded on single Re filaments with a suspension of Pt-doped activated carbon to supress oxide creation (as described by Noble *et al.*, 1989). Identical results were achieved on analyses of the standard solution with both loading techniques. The presence of Sm was checked by monitoring mass 147 and where encountered the analysis was aborted. Mass-dependent fractionation during analysis corrected by normalising the measured $^{146}Nd/^{144}Nd$ to 0.7219. During each analysis the $^{145}Nd/^{144}Nd$ was monitored as an internal consistency check.

Pb: Pb was analysed on single Re filament assemblies using the silica gel - phosphoric acid emitter. Once under vacuum in the spectrometer, the bead was raised to a high temperature (ca. 1250-1350°C) for about 30 seconds, then reduced to standard running conditions (1150-1220°C). This allowed the silica gel to melt thoroughly and produced more stable ion beams. This approach was adapted from a technique developed by the late Prof. Hans Welke and Dr. Rich Armstrong at BPI (Geophysics), Wits, at that time (ca. 1985-1987: see Armstrong, 1987). Mass dependent fractionation was corrected using factors determined empirically through analysis of the NBS reference Pb SRM981. It is suspected that the amount of Pb present will effect the degree of fractionation during analysis. Since the carbonatites had widely variable concentrations of Pb, and that the amount of Pb being loaded could only be very crudely controlled, a test was run at the outset of the project to monitor the possible effects of Pb amount on fractionation. Series of 250ng, 500ng and 750ng total Pb loads were analysed together in spectrometer using standard analysing procedures. It was found that the magnitude of the fractionation factor, and the standard deviation on the factors, was not distinguishable between the 250ng and 750ng loads. At least two NBS 981 analyses were performed at the same time as the unknown measurements and these factors used to correct the measurements.

A.1.3.3 Data Quality

In the following discussion, the standard deviation is represented by sigma, "σ ", whereas the standard error of the mean (i.e. $\sigma/\sqrt{n}$) is represented by "σ_m".

A.1.3.3.1 $^{87}Sr/^{86}Sr$

Within-run data quality was monitored by $2\sigma_m$ determined on 100-125 ratio measurements. *Total* data sets were screened and measurements differing by more than $\pm 2\sigma$ from the mean were excluded. Typical within-run precisions ($2\sigma_m$) were below 0.005%.

Long term machine precision and accuracy was monitored by repeated analysis of shelf standard solutions of NBS standard SRM 987 (referred to as "NBS987") and Eimer and Amend ("E&A") standard $SrCO_3$ salts.

During the period of data gathering (ca. 1984 to 1988) a total of 30 analyses of NBS 987 were determined by the author on the VG354 which gave a pooled average of 0.710270 ±26 (1σ); identical to the average on 287 measurements made by all operators of 0.70271 ±30. Repeated determinations of the E&A standard by the author averaged 0.708039 ±28 (n=7) compared with an all-operator average of 0.708008 ±45 (n=14).

To evaluate the replication on real samples, i.e. where dissolution and chromatographic separation are involved, replicate measurements were made on USGS standard basalt BCR-1. Twelve separate determinations average to 0.705039 ±28, a comparable 1σ precision to that achieved for analysis of pure salt solutions.

A.1.3.3.2 $^{143}Nd/^{144}Nd$

No widely analysed international Nd salt standard (e.g. "La Jolla", "Leeds") was available in the CSIR laboratories. Long term spectrometer replication was thus monitored using a solution of Johnson Matthey Specpure Nd_2O_3 (batch number 882589). The ratio $^{145}Nd/^{144}Nd$ was monitored as a useful check of internal consistency of the mass spectrometry.

At the time of commissioning of the VG354 in December 1984, replicate analyses were made of the Nd salt solution then in use at the University of Leeds ("Leeds" standard) and gave the following average values:

$^{143}Nd/^{144}Nd = 0.511111 \pm 4$ (13 separate measurements); and

$^{145}Nd/^{144}Nd = 0.348407 \pm 9$.

Analyses of the CSIR standard solution run at the same time gave:

$^{143}Nd/^{144}Nd = 0.511820 \pm 8$ (7 separate measurements); and

$^{145}Nd/^{144}Nd = 0.348419 \pm 15$.

A compilation of 112 separate analyses performed by all operators in the CSIR laboratory from 1986-1992 averages to:

$^{143}Nd/^{144}Nd = 0.511810 \pm 23$

and

$^{145}Nd/^{144}Nd = 0.348413 \pm 16$;

indistinguishable from the values achieved at commissioning. Thirty-three measurements of the standard performed by the author during the same time period yielded:

$^{143}Nd/^{144}Nd = 0.511819 \pm 18$.

Analyses of the CSIR shelf standard are compiled in Table A1.3 to illustrate the long term stability of the mass spectrometric analyses of Nd over the period during which data was collected for the current study.

Table A1.3: Compilation of Nd isotopic analyses on CSIR shelf standard Nd solution (Johnson Matthey Nd_2O_3).

Time Period	$^{143}Nd/^{144}Nd \pm 1\sigma$	n
1987	0.511827 ±18	10
1988	0.511819 ±17	27
1989	0.511817 ±21	36
1990	0.511814 ±13	10

Accuracy was assessed using replicate analyses of BCR-1. 17 separate determinations by various operators since establishing the facility gave:

$^{143}Nd/^{144}Nd =$ 0.512666 ±33 (0.007%);

whereas 9 replicate measurements of this standard by the author yielded better reproducibility:

$^{143}Nd/^{144}Nd =$ 0.512650 ±19 (0.004%).

These ratios are within error of the accepted ratio for this standard of 0.51264 (for mass spectrometry of metal ions, corrected for fractionation using $^{146}Nd/^{144}Nd$=0.7219).

Long-term reproducibility of $^{143}Nd/^{144}Nd$ measurements by the author is assessed as 0.05%, based on pooled replicates of BCR-1 plus other standards and unknowns.

A.1.3.3.3 Pb isotopes:

Uncertainties in $^{206}Pb/^{204}Pb$ and $^{207}Pb/^{204}Pb$ were assessed to be 0.07 and 0.1% respectively, while the correlation in the errors was calculated as 0.86.

A.1.3.3.4 Rb,Sr,Sm and Nd concentrations

For most samples used in this study, Rb and Sr concentrations were those determined by XRF with an uncertainty in Rb/Sr of 1% (UCT) or 1.5% (University of Pretoria / Rocklabs). A smaller number (Stukpan mineral separates; Pienaars River complexes reported in Harmer, 1985) were measured by isotope dilution mass spectrometry (IDMS) with an uncertainty of 0.8%.

All Sm and Nd concentrations were measured by IDMS with an uncertainty in the $^{147}Sm/^{144}Nd$ of 0.2%.

A.1.3.3.5 ^{18}O and $\delta^{13}C$

The oxygen and carbon isotopic measurements on carbonatites used in this dissertation were determined for the author by Mr AS Talma of the Stable Isotope Facility of EMATek (then NPRL), CSIR. Uncertainties are quoted as 0.03 permil for both $\delta^{18}O$ and $\delta^{13}C$ measurements.

A.2: Conventions, formulae and constants used in isotopic calculations

A.2.1: Calculation of isotopic ratios of parent - daughter elements

The relationships between isotopic and atomic proportions of elements were derived using the isotopic masses of Wapstra and Bos (1977) and are:

$$^{87}Rb/^{86}Sr_{(atomic)} = Rb/Sr_{(ppm)}*(2.692948+0.28304*^{87}Sr/^{86}Sr)$$

$$^{147}Sm/^{144}Nd_{(atomic)} = Sm/Nd_{(ppm)}*(0.531497+0.142521*^{143}Nd/^{144}Nd)$$

A.2.2: Calculation of dates and associated uncertainties

Regressions and age calculations were performed using the GEODATE Version 2.2 computer program (Eglington and Harmer, 1991) which implements the recommendations discussed by Harmer and Eglington (1990).

Goodness - of - fit of the regression lines were assessed by testing the mean sum of the weighted deviates of sample data from the line against an F based on the number of samples regressed (n_S) and analytical uncertainties based on 60 replicates (n_r). All confidence intervals are constructed at the 5% level of significance using n_r=60. Confidence intervals for data sets containing scatter in excess of that attributable to analytical error (i.e. "errorchrons") were constructed using separate "Students-t" multipliers for the "analytical" and "geological" components of the total variation as discussed in Harmer and Eglington (1991).

Decay constants used were:

^{87}Rb : $1.42 \times 10^{-11} a^{-1}$

^{147}Sm : $6.54 \times 10^{-12} a^{-1}$

^{235}U : $9.8485 \times 10^{-10} a^{-1}$

^{238}U : $1.55125 \times 10^{-10} a^{-1}$

A.2.2.1 Epsilon calculations

Epsilon notation follows the definition by De Paolo and Wasserburg (1976) and describes the fractional deviation of the isotopic composition of a sample (Smp) relative to a reference reservoir (Ref):

$$\varepsilon_{(Nd)} = [^{143}Nd/^{144}Nd_{(Smp)}/^{143}Nd/^{144}Nd_{(Ref)} - 1].10^4$$

and

$$\varepsilon_{(Sr)} = [^{87}Sr/^{86}Sr_{(Smp)}/^{87}Sr/^{86}Sr_{(Ref)} - 1].10^4$$

The Bulk Earth reference reservoir used in this dissertation is described by the following parameters:

$^{87}Sr/^{86}Sr_{(p)} = 0.7047$ $\quad$ $^{143}Nd/^{144}Nd_{(p)} = 0.51264$

$^{87}Rb/^{86}Sr = 0.0847$ $\quad$ $^{147}Sm/^{144}Nd = 0.1967$

Errors in the epsilon parameters given in the data tables are based on the 95% confidence intervals estimated for the relevant initial isotopic ratios.

A.2.2.2 Calculation of model - dependent μ

The calculation of initial Pb ratios in old rocks is bedevilled by the fact that the U-Pb system seldom remains closed after or during uplift and exposure of rock bodies due to the solubility of U in oxygenated groundwater (e.g. Faure, 1986). The fact that $^{207}Pb/^{204}Pb$ - $^{206}Pb/^{204}Pb$ secondary isochrons frequently preserve correct ages whereas whole-rock ^{235}U-^{207}Pb or ^{238}U-^{206}Pb isochrons are seldom obtained implies that in most cases U-Pb is a relatively recent (i.e. <10 Ma) phenomenon. Recent U-Pb mobility renders the calculation of initial Pb isotope ratios from the measured sample U and Pb concentrations somewhat unreliable. Th tends to be less mobile than U but facilities for precise and accurate Th concentration measurements were not available during the present study.

Where samples are not overly radiogenic, it is possible to use modelled source $^{238}U/^{204}Pb$ (μ) as a measure of "relative initial Pb ratio".

All U-Pb reservoirs formed at the same time (t_0) with the same $^{207}Pb/^{204}Pb$ (Y_0) and $^{206}Pb/^{204}Pb$ (X_0) ratios will, at a subsequent time (t_1) have Pb isotopic compositions (X_1,Y_1) given by:

$$Y_1 = Y_0 + \mu_{res}/137.88\,(e^{\lambda_5 t_0} - e^{\lambda_5 t_1}) \qquad [1a]$$

$$X_1 = X_0 + \mu_{res}(e^{\lambda_8 t_0} - e^{\lambda_8 t_1}) \qquad [1b]$$

where λ_5 and λ_8 are the decay constants for ^{235}U and ^{238}U respectively, and μ_{res} is the $^{238}U/^{204}Pb$ of the reservoir. Equations [1a] and [1b] describe a straight line in $^{206}Pb/^{204}Pb$ - $^{207}Pb/^{204}Pb$ space which is effectively the locus of Pb isotopic ratios for all possible t_1-age reservoirs produced at t_0.

A sample extracted from a reservoir described by [1a], [1b] will have present day (i.e. t_p=0) Pb ratios defined by:

$$Y_p = Y_1 + \mu_{smp}/137.88\,(e^{\lambda_5 t_1} - 1) \qquad [2a]$$

$$X_p = X_1 + \mu_{smp}(e^{\lambda_8 t_1} - 1) \qquad [2b]$$

The ratios X_1, Y_1 are the "initial ratios" for the sample and can only be reliably determined from the measured present day X_p, Y_p if the sample isotopic system remained closed (i.e. no changes in μ_{smp} or radiogenic Pb since crystallisation). As noted above, though, most surface samples appear to have suffered recent loss of U and/or Pb.

Figure A.1:Pb isotope plot to illustrate the relationship between reservoir μ and initial Pb isotopic ratios in samples.

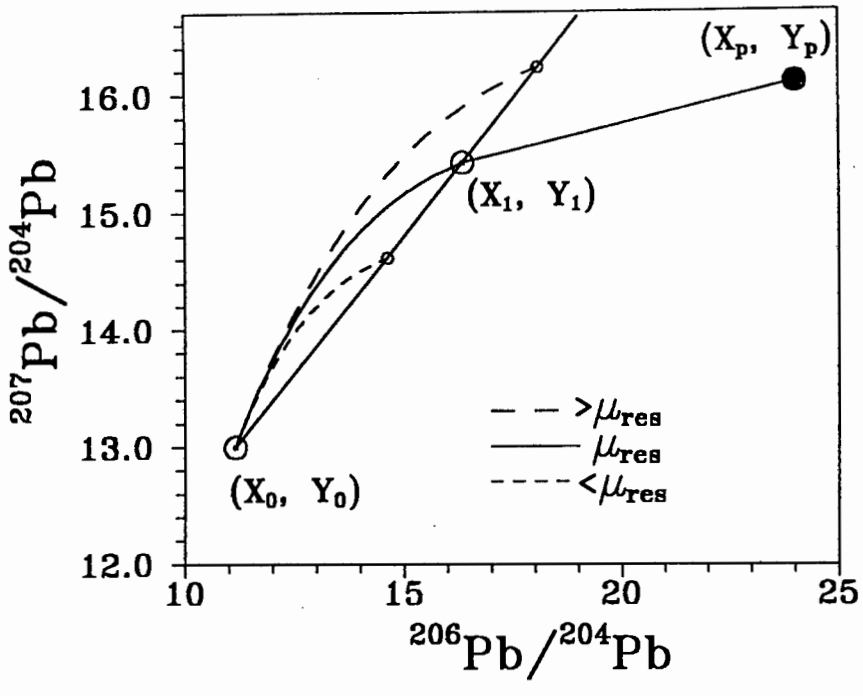

Inspection of equations [1] and [2] above indicates, however, that the sample X_1, Y_1 values are directly proportional to μ_{res} and formation history of their source reservoir. As a result, if a reasonable parental reservoir can be assumed, the modelled μ_{res} will function as an effective quantitative replacement for the unattainable sample initial $^{206}Pb/^{204}Pb$ and $^{207}Pb/^{204}Pb$ values.

From the relationships defined above, it is simple to derive:

$$\mu_{Res} = \frac{m_{smp}(X_0 - X_p) + Y_p - Y_0}{(e^{\lambda_5 t_0} - e^{\lambda_5 t_1})/137.88 - m_{smp}(e^{\lambda_8 t_0} - e^{\lambda_8 t_1})}$$

where m_{smp} is the slope of the sample Pb-Pb isochron:

$$m_{smp} = \frac{(e^{\lambda_5 t_1} - 1)}{137.88(e^{\lambda_8 t_1} - 1)}$$

The formulation discussed above is illustrated in Figure . The solid curved line illustrates the changing isotopic composition in the source reservoir from which

the sample was extracted at t_1. The dashed curves depict two hypothetical reservoirs with μ's which are larger and smaller than the reference reservoir value, μ_{res}.

A.3: General

A.3.1: CIPW Norm calculations

Iron was determined as total Fe_2O_3 by XRF and so a correction for oxidation state was required prior to calculating CIPW normative constituents. The recommendations of Middlemost (1989) were used in all cases and the following iron oxidation ratios (Fe_2O_3/FeO) were assumed:

Basaltic rocks:	0.2
Ijolites	0.4
Syenites, phonolites, nepheline syenites	0.5
Pyroxenites	0.6

A.3.2: Relationship between parent/daughter fractionation and changing ε.

Consider a sample reservoir fractionated from the reference reservoir at time t_f. Using "K" to denote the ratio between parent and daughter isotope, then the isotopic compositions (R) of sample and reference at subsequent time "t_1" are:

$$R_{Smp}(t_f) = R_{Smp}(t_f) + K_{Smp}.M \quad \text{--[1]}$$

$$R_{Ref}(t_f) = R_{Ref}(t_f) + K_{Ref}.M \quad \text{--[2]}$$

where $M = (e^{\lambda t_f} - e^{\lambda t_1})$

Define $f = K_{Smp}/K_{Ref}$, $K_{Smp} = f.K_{Ref}$

Substitute, subtract [2] from [1], and simplify (by definition $R_{Smp}(t_f) = R_{Ref}(t_f)$):

$$R_{Smp}(t_f) - R_{Ref}(t_f) = K_{Ref}.M(f-1)$$

Now $\varepsilon = \dfrac{R_{smp}(t_f) - R_{Ref}(t_f)}{R_{Ref}}$

Therefore:

$$\varepsilon = \frac{K_{Ref} . M(f-1)}{R_{Ref}} 10^4$$

For two sample reservoirs, both separated from the reference reservoir at the same time:

$$\varepsilon_1 - \varepsilon_2 = \frac{K_{Ref} . M}{R_{Ref}} (f_1 - f_2)$$

SAMPLE LOCALITY MAP FOR THE SPITSKOP COMPLEX

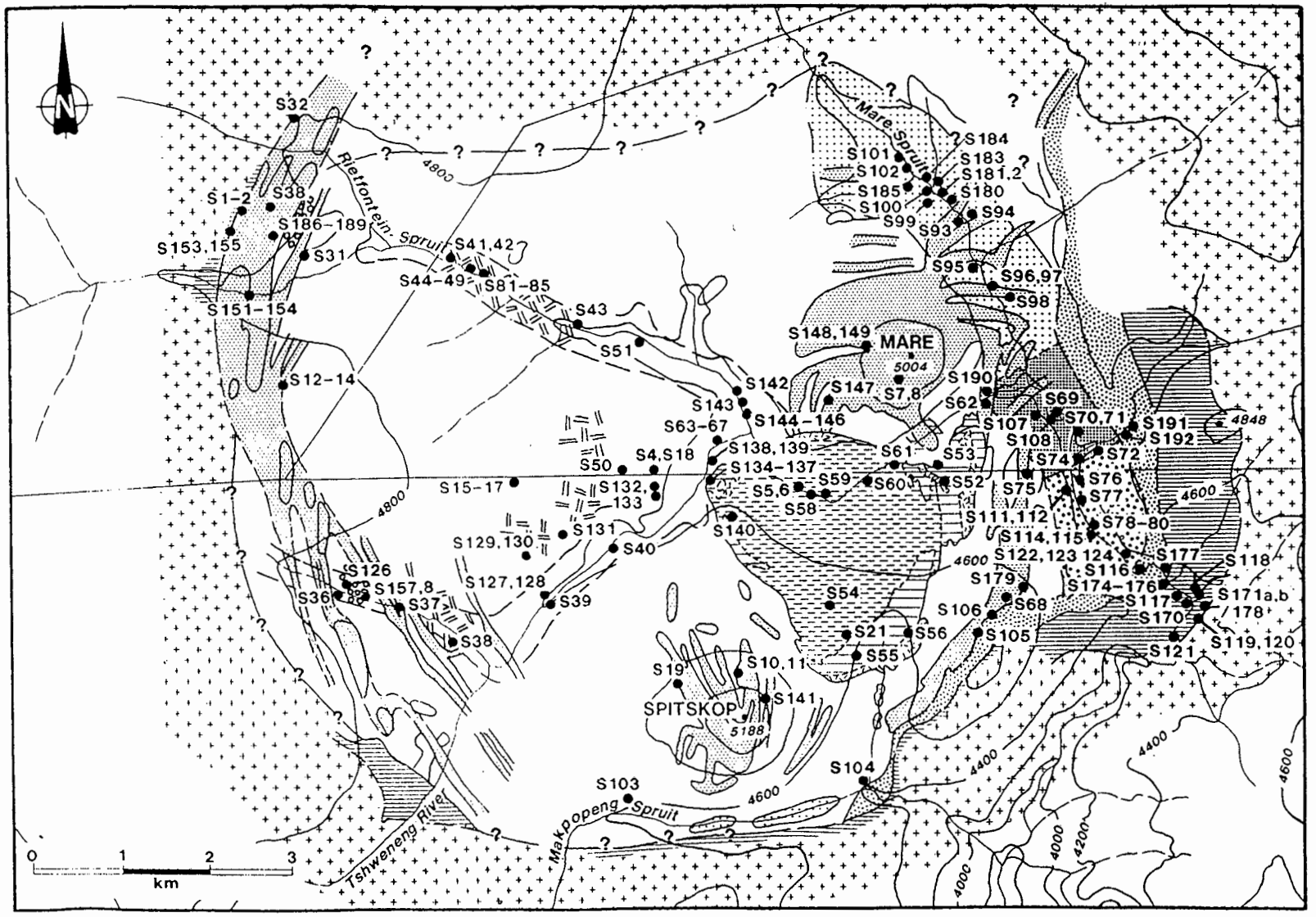

Appendix B:
Data Tables

The following section contains the tables of analytical data determined during the current study as well as tables of data used for reference purposes. Analytical procedures are discussed in Appendix A.

In the tables entries of "0.0" reflect concentrations below the limits of detection (see Tables A.1 and A.2 in Appendix A); elements not analysed for are shown as "-" or are left blank.

Tables

Table B.1: Compositions of clinopyroxenes from the silicate units in the Spitskop Complex.

(a) Pyroxenites

	S44.1	S44.2	S44.3	S44.4	S44.c1	S44.c2	S44.c3	S44.c4
SiO_2	52.66	52.26	52.36	52.10	51.49	51.32	51.50	51.27
TiO_2	0.49	0.54	0.70	0.71	0.76	0.60	0.59	1.13
Al_2O_3	1.16	1.26	1.75	1.87	1.86	1.75	1.36	1.79
Fe_2O_3	4.75	4.66	3.85	3.68	5.93	5.22	5.31	4.06
FeO	2.88	3.37	3.30	2.89	2.17	1.85	1.45	2.52
MnO	0.14	0.15	0.12	0.20	0.19	0.14	0.15	0.16
MgO	13.90	13.37	13.63	13.99	13.41	14.04	14.15	13.86
CaO	22.95	22.52	23.28	23.09	23.53	23.29	23.71	23.51
Na_2O	1.34	1.46	1.23	1.15	1.26	1.09	1.06	1.04
Total	100.27	99.59	100.22	99.68	100.60	99.30	99.28	99.34
Cations per 6 Oxygens								
Si	1.943	1.945	1.933	1.929	1.901	1.911	1.918	1.910
Ti	0.014	0.015	0.019	0.020	0.021	0.017	0.017	0.032
Al	0.050	0.055	0.076	0.082	0.081	0.077	0.060	0.079
Fe^{+3}	0.132	0.130	0.107	0.103	0.165	0.146	0.149	0.114
Fe^{+2}	0.089	0.105	0.102	0.089	0.067	0.058	0.045	0.078
Mn	0.004	0.005	0.004	0.006	0.006	0.004	0.005	0.005
Mg	0.764	0.741	0.750	0.772	0.738	0.779	0.785	0.769
Ca	0.907	0.898	0.921	0.916	0.931	0.929	0.946	0.938
Na	0.096	0.105	0.088	0.083	0.090	0.079	0.077	0.075
Ac	9.6	10.5	8.8	8.3	9.0	7.9	7.7	7.5
Di	76.4	74.1	75.0	77.2	73.8	77.9	78.5	76.9
Hd	8.9	10.5	10.2	8.9	6.7	5.8	4.5	7.8
Sa	5.1	4.9	6.0	5.6	10.5	8.4	9.3	7.8

(b) Type-I ijolites (fine grained)

	S41.1	S41.2	S41.3	S41.4	S41.5	S43.1	S43.2	S43.3	S43.4	S43.5	S43.6	S43.7	S43.8	S50.1	S50.2
SiO_2	49.87	50.09	50.54	50.53	50.99	51.56	51.68	51.29	51.43	51.82	51.23	51.82	52.18	51.41	51.24
TiO_2	0.92	0.83	0.50	0.48	0.50	0.36	0.59	0.36	0.46	0.42	0.49	0.73	0.49	0.31	0.32
Al_2O_3	1.66	1.33	1.19	1.24	1.17	1.44	1.64	1.05	1.24	1.30	1.12	1.86	1.18	0.87	0.84
Fe_2O_3	11.68	11.23	12.07	12.76	12.54	6.15	4.42	10.83	10.38	12.55	12.64	8.94	12.48	12.35	11.81
FeO	10.40	9.95	10.17	9.69	9.71	7.41	5.82	8.05	7.62	6.50	7.39	5.51	5.71	9.41	8.43
MnO	0.61	0.63	0.62	0.64	0.65	0.47	0.27	0.54	0.43	0.50	0.55	0.34	0.53	0.54	0.61
MgO	5.04	5.12	4.87	4.76	4.81	9.89	12.28	7.07	7.35	6.78	6.33	9.34	7.52	5.40	6.42
CaO	17.43	17.18	16.72	16.52	16.54	19.27	21.38	16.30	16.54	16.10	16.61	18.18	15.47	17.10	17.94
Na_2O	3.91	4.08	4.31	4.50	4.59	2.54	1.50	4.22	4.22	4.88	4.57	3.63	5.04	4.37	3.90
Total	101.52	100.44	100.99	101.12	101.50	99.09	99.59	99.72	99.67	100.85	100.93	100.35	100.60	101.76	101.51
Cations per 6 Oxygens															
Si	1.913	1.935	1.945	1.941	1.949	1.963	1.939	1.966	1.966	1.959	1.949	1.944	1.967	1.956	1.947
Ti	0.027	0.024	0.014	0.014	0.014	0.010	0.017	0.010	0.013	0.012	0.014	0.021	0.014	0.009	0.009
Al	0.075	0.061	0.054	0.056	0.053	0.065	0.073	0.047	0.056	0.058	0.050	0.082	0.052	0.039	0.038
Fe^{+3}	0.337	0.327	0.349	0.369	0.361	0.176	0.125	0.313	0.299	0.357	0.362	0.252	0.354	0.354	0.338
Fe^{+2}	0.333	0.321	0.327	0.311	0.311	0.236	0.183	0.258	0.244	0.205	0.235	0.173	0.180	0.299	0.268
Mn	0.020	0.021	0.020	0.021	0.021	0.015	0.009	0.018	0.014	0.016	0.018	0.011	0.017	0.017	0.020
Mg	0.288	0.295	0.279	0.273	0.274	0.561	0.687	0.404	0.419	0.382	0.359	0.522	0.422	0.306	0.364
Ca	0.716	0.711	0.689	0.680	0.677	0.786	0.860	0.670	0.677	0.652	0.677	0.731	0.625	0.697	0.730
Na	0.291	0.306	0.322	0.335	0.340	0.188	0.109	0.314	0.313	0.358	0.337	0.264	0.368	0.322	0.287
Ac	29.1	30.6	32.2	33.5	34.0	17.6	10.9	31.3	29.9	35.7	33.7	25.2	35.4	32.2	28.7
Di	28.8	29.5	27.9	27.3	27.4	56.1	68.7	40.4	41.9	38.2	35.9	52.2	42.2	30.6	36.4
Hd	33.3	32.1	32.7	31.1	31.1	23.6	18.3	25.8	24.4	20.5	23.5	17.3	18.0	29.9	26.8
Sa	8.8	7.8	7.2	8.1	7.5	2.7	2.1	2.5	3.8	5.6	6.9	5.3	4.4	7.3	8.1

Type-I ijolites (fine-grained, contd.)

	S50.3	S50.4	S50.5	S50.6	S50.7	S50.8	S50.9	S50.10	S82.1
SiO_2	51.55	50.55	50.64	50.01	50.57	50.71	50.75	50.54	51.20
TiO_2	0.54	0.33	0.42	0.46	0.80	0.29	0.31	0.36	0.36
Al_2O_3	1.07	1.02	1.04	0.97	1.35	0.99	0.96	1.06	1.08
Fe_2O_3	7.08	12.93	12.40	10.48	10.53	13.18	13.41	12.46	6.06
FeO	6.90	8.96	9.08	9.09	8.05	8.88	8.32	8.80	13.21
MnO	0.48	0.58	0.58	0.67	0.62	0.67	0.66	0.75	0.51
MgO	9.93	5.30	5.41	6.71	7.22	4.96	5.10	5.22	6.59
CaO	21.96	17.28	17.43	19.76	19.61	15.47	15.56	16.45	15.13
Na_2O	1.92	4.23	4.16	2.84	3.13	4.89	4.95	4.49	3.60
Total	101.43	101.17	101.16	100.99	101.89	100.05	100.02	100.13	97.74
Cations per 6 Oxygens									
Si	1.931	1.938	1.940	1.919	1.912	1.960	1.960	1.952	2.012
Ti	0.015	0.010	0.012	0.013	0.023	0.008	0.009	0.010	0.011
Al	0.047	0.046	0.047	0.044	0.060	0.045	0.044	0.048	0.050
Fe^{+3}	0.200	0.373	0.357	0.303	0.300	0.384	0.390	0.362	0.179
Fe^{+2}	0.216	0.287	0.291	0.292	0.255	0.287	0.269	0.284	0.434
Mn	0.015	0.019	0.019	0.022	0.020	0.022	0.022	0.025	0.017
Mg	0.554	0.303	0.309	0.384	0.407	0.286	0.293	0.301	0.386
Ca	0.881	0.710	0.716	0.813	0.794	0.641	0.644	0.681	0.637
Na	0.139	0.314	0.309	0.211	0.229	0.367	0.371	0.336	0.274
Ac	13.9	31.4	30.9	21.1	22.9	36.7	37.1	33.6	17.9
Di	55.4	30.3	30.9	38.4	40.7	28.6	29.3	30.1	38.6
Hd	21.6	28.7	29.1	29.2	25.5	28.7	26.9	28.4	43.4
Sa	9.1	9.6	9.1	11.3	10.9	6.0	6.7	7.9	0.1

(c) Type-I ijolites (coarse - grained)

	S134.1	S134.2	S134.3	S134.4	S134.5	S134.6	S134.7	S134.8	S134.9	S134.10	S134.11	S134.12	S134.13	S134.14	S134.15
SiO_2	51.65	51.93	51.49	51.70	51.47	51.10	52.02	51.69	52.29	52.07	51.86	52.20	51.48	51.40	51.42
TiO_2	0.30	0.33	0.37	0.34	0.35	0.31	0.33	0.24	0.31	0.43	0.37	0.29	0.36	0.35	0.22
Al_2O_3	0.94	0.94	0.84	0.92	0.87	0.83	0.85	0.96	0.83	1.19	1.11	0.92	0.89	0.74	0.90
Fe_2O_3	11.34	7.95	8.48	7.42	6.17	15.16	5.31	12.63	3.88	4.17	4.79	9.30	7.09	17.26	13.05
FeO	8.60	6.76	7.58	7.23	7.38	7.94	8.33	6.48	7.29	6.72	7.52	6.67	6.90	5.99	9.26
MnO	0.63	0.50	0.48	0.40	0.43	0.63	0.47	0.71	0.36	0.37	0.42	0.49	0.45	0.78	0.60
MgO	6.14	9.40	8.86	9.56	10.00	4.56	10.29	6.88	11.39	11.74	10.80	8.69	9.97	4.49	5.20
CaO	16.70	20.65	19.96	20.80	21.18	13.99	20.14	15.45	21.95	22.07	21.72	18.90	21.34	13.55	15.62
Na_2O	4.41	2.57	2.69	2.33	1.96	5.77	2.06	4.91	1.45	1.37	1.58	3.41	2.03	6.39	4.86
Total	100.72	101.03	100.74	100.70	99.81	100.29	99.80	99.95	99.75	100.13	100.17	100.87	100.52	100.95	101.13
Cations per 6 Oxygens															
Si	1.971	1.951	1.949	1.950	1.954	1.968	1.972	1.972	1.971	1.953	1.955	1.964	1.944	1.962	1.966
Ti	0.009	0.009	0.011	0.010	0.010	0.009	0.009	0.007	0.009	0.012	0.010	0.008	0.010	0.010	0.006
Al	0.042	0.042	0.037	0.041	0.039	0.038	0.038	0.043	0.037	0.053	0.049	0.041	0.040	0.033	0.041
Fe^{+3}	0.326	0.225	0.241	0.211	0.176	0.439	0.151	0.362	0.110	0.118	0.136	0.263	0.202	0.496	0.376
Fe^{+2}	0.275	0.212	0.240	0.228	0.234	0.256	0.264	0.207	0.230	0.211	0.237	0.210	0.218	0.191	0.296
Mn	0.020	0.016	0.015	0.013	0.014	0.021	0.015	0.023	0.011	0.012	0.013	0.016	0.014	0.025	0.019
Mg	0.349	0.526	0.500	0.537	0.566	0.262	0.581	0.391	0.640	0.656	0.607	0.487	0.561	0.255	0.296
Ca	0.683	0.831	0.809	0.841	0.862	0.577	0.818	0.632	0.886	0.887	0.877	0.762	0.863	0.554	0.640
Na	0.326	0.187	0.197	0.170	0.144	0.431	0.151	0.363	0.106	0.100	0.115	0.249	0.149	0.473	0.360
Ac	32.6	18.7	19.7	17.0	14.4	43.1	15.1	36.2	10.6	10.0	11.5	24.9	14.9	47.3	36.0
Di	34.9	52.6	50.0	53.7	56.6	26.2	58.1	39.1	64.0	65.6	60.7	48.7	56.1	25.5	29.6
Hd	27.5	21.2	24.0	22.8	23.4	25.6	26.4	20.7	23.0	21.1	23.7	21.0	21.8	19.1	29.6
Sa	5.0	7.5	6.3	6.5	5.6	5.1	0.4	4.0	2.4	3.3	4.1	5.4	7.2	8.1	4.8

(d) Type-II ijolites

	S134.16	S51.1	S51.2	S51.3	S51.4	S51.5	S51.6	S51.7	S42.1	S42.2	S42.3	S42.4	S42.5	S42.6	S42.7
SiO_2	51.78	50.51	50.70	50.71	51.61	49.49	50.93	51.24	50.91	51.16	51.18	51.32	51.46	52.18	52.48
TiO_2	0.26	0.35	0.89	0.80	0.69	0.79	1.08	0.79	0.64	0.62	0.56	0.65	0.63	0.63	0.65
Al_2O_3	0.80	0.99	2.01	1.72	1.14	2.59	2.40	1.89	1.78	1.73	1.66	2.80	1.44	2.08	1.50
Fe_2O_3	12.35	10.93	6.44	6.40	7.31	7.50	5.02	5.47	6.76	6.20	6.27	2.18	5.92	3.69	3.87
FeO	7.57	9.88	6.13	4.45	4.75	5.41	5.97	5.12	3.56	2.58	3.47	5.25	2.33	3.83	4.25
MnO	0.67	0.57	0.32	0.25	0.29	0.29	0.23	0.24	0.21	0.25	0.17	0.16	0.20	0.19	0.22
MgO	6.10	5.43	10.66	11.71	11.17	10.39	11.44	11.85	12.41	13.23	12.54	13.07	13.48	13.61	13.30
CaO	15.45	17.41	21.49	22.10	20.60	21.94	22.18	22.46	22.44	22.79	22.66	22.26	22.42	22.76	22.12
Na_2O	5.01	3.94	1.82	1.61	2.37	1.63	1.48	1.45	1.47	1.32	1.44	1.02	1.47	1.19	1.47
Total	99.99	100.01	100.46	99.75	99.93	100.03	100.73	100.51	100.18	99.88	99.96	98.70	99.35	100.16	99.87
Cations per 6 Oxygens															
Si	1.983	1.956	1.905	1.907	1.938	1.873	1.900	1.912	1.901	1.905	1.912	1.926	1.921	1.929	1.948
Ti	0.007	0.010	0.025	0.023	0.019	0.022	0.030	0.022	0.018	0.017	0.016	0.018	0.018	0.018	0.018
Al	0.036	0.045	0.089	0.076	0.050	0.116	0.106	0.083	0.078	0.076	0.073	0.124	0.063	0.091	0.066
Fe^{+3}	0.356	0.318	0.182	0.181	0.207	0.214	0.141	0.154	0.190	0.174	0.176	0.062	0.166	0.103	0.108
Fe^{+2}	0.243	0.320	0.193	0.140	0.149	0.171	0.186	0.160	0.111	0.080	0.108	0.165	0.073	0.119	0.132
Mn	0.022	0.019	0.010	0.008	0.009	0.009	0.007	0.008	0.007	0.008	0.005	0.005	0.006	0.006	0.007
Mg	0.348	0.313	0.597	0.656	0.625	0.586	0.636	0.659	0.691	0.734	0.698	0.731	0.750	0.750	0.736
Ca	0.634	0.722	0.865	0.891	0.829	0.890	0.887	0.898	0.898	0.910	0.907	0.895	0.897	0.901	0.880
Na	0.372	0.296	0.133	0.117	0.173	0.120	0.107	0.105	0.106	0.095	0.104	0.074	0.106	0.085	0.106
Ac	35.6	29.6	13.3	11.7	17.3	12.0	10.7	10.5	10.6	9.5	10.4	6.2	10.6	8.5	10.6
Di	34.8	31.3	59.7	65.6	62.5	58.6	63.6	65.9	69.1	73.4	69.8	73.1	75.0	75.0	73.6
Hd	24.3	32.0	19.3	14.0	14.9	17.1	18.6	16.0	11.1	8.0	10.8	16.5	7.3	11.9	13.2
Sa	5.3	7.1	7.7	8.7	5.3	12.3	7.1	7.6	9.2	9.1	9.0	4.2	7.1	4.6	2.6

Type-II ijolites (contd.)

	S64.1	S64.2	S64.3	S64.4	S131.1	S131.2	S131.3	S131.4	S131.5	S131.7	S131.8	S131.9	S139.1	S139.2	S139.3
SiO_2	52.16	51.93	51.74	51.80	51.56	51.71	49.72	51.39	51.73	51.94	51.44	52.22	51.93	52.04	51.98
TiO_2	0.20	0.47	0.42	0.57	0.63	0.78	1.22	0.72	0.64	0.82	0.92	0.62	0.57	0.38	0.41
Al_2O_3	0.81	1.05	0.95	1.19	1.31	1.38	4.20	1.53	1.34	1.48	1.46	1.26	1.13	1.20	1.18
Fe_2O_3	6.85	6.10	8.08	5.54	10.32	14.80	5.46	12.61	14.41	14.74	16.09	12.79	6.47	5.37	5.18
FeO	7.77	7.54	8.80	7.30	4.43	4.98	4.43	5.73	3.85	4.98	3.54	5.20	5.83	5.82	6.10
MnO	0.49	0.40	0.54	0.40	0.36	0.40	0.19	0.42	0.35	0.38	0.40	0.31	0.36	0.35	0.38
MgO	9.38	10.32	8.24	10.55	9.35	6.55	11.80	6.97	7.44	6.33	6.60	7.23	10.64	11.39	11.42
CaO	20.13	21.15	19.22	21.54	17.52	14.21	20.29	15.29	15.08	14.16	13.88	15.52	21.12	22.31	22.21
Na_2O	2.54	1.96	2.93	1.80	3.95	5.88	1.92	5.16	5.53	6.05	6.22	5.33	2.24	1.62	1.56
Total	100.33	100.91	100.92	100.69	99.43	100.70	99.23	99.82	100.38	100.88	100.55	100.49	100.30	100.48	100.42
Cations per 6 Oxygens															
Si	1.972	1.949	1.959	1.945	1.951	1.952	1.865	1.955	1.950	1.956	1.940	1.968	1.949	1.946	1.946
Ti	0.006	0.013	0.012	0.016	0.018	0.022	0.034	0.021	0.018	0.023	0.026	0.018	0.016	0.011	0.012
Al	0.036	0.046	0.042	0.053	0.058	0.061	0.186	0.069	0.060	0.066	0.065	0.056	0.050	0.053	0.052
Fe^{+3}	0.195	0.172	0.230	0.156	0.294	0.420	0.154	0.361	0.409	0.418	0.457	0.363	0.183	0.151	0.146
Fe^{+2}	0.246	0.236	0.279	0.229	0.140	0.157	0.139	0.182	0.122	0.157	0.112	0.164	0.183	0.182	0.191
Mn	0.016	0.013	0.017	0.013	0.012	0.013	0.006	0.014	0.011	0.012	0.013	0.010	0.011	0.011	0.012
Mg	0.528	0.577	0.465	0.590	0.527	0.369	0.660	0.395	0.418	0.355	0.371	0.406	0.595	0.635	0.637
Ca	0.815	0.850	0.780	0.867	0.710	0.575	0.816	0.623	0.609	0.571	0.561	0.627	0.849	0.894	0.891
Na	0.186	0.143	0.215	0.131	0.290	0.430	0.140	0.381	0.404	0.442	0.455	0.389	0.163	0.117	0.113
Ac	18.6	14.3	21.5	13.1	29.0	42.0	14.0	36.1	40.4	41.8	45.5	36.3	16.3	11.7	11.3
Di	52.8	57.7	46.5	59.0	52.7	36.9	66.0	39.5	41.8	35.5	37.1	40.6	59.5	63.5	63.7
Hd	24.6	23.6	27.9	22.9	14.0	15.7	13.9	18.2	12.2	15.7	11.2	16.4	18.3	18.2	19.1
Sa	4.0	4.4	4.1	5.0	4.3	5.4	6.1	6.2	5.6	7.0	6.2	6.7	5.9	6.6	5.9

Type-II ijolites (contd.)

	S139.4	S142.1	S142.2	S142.3	S142.4	S142.5	S51.c1	S51.c2	S42.c1	S42.c2	S42.c3	S131.6
SiO_2	51.95	52.41	52.64	52.29	51.77	52.59	50.20	50.79	52.10	51.12	52.23	51.68
TiO_2	0.53	0.29	0.20	0.25	0.24	0.07	0.84	0.78	0.64	0.88	0.63	0.60
Al_2O_3	1.19	1.86	1.00	1.65	1.92	1.83	2.12	1.80	1.79	2.62	1.76	1.48
Fe_2O_3	6.04	4.35	5.10	4.96	5.44	3.77	5.79	4.70	3.79	4.19	4.24	11.79
FeO	6.04	5.15	4.68	3.81	4.37	4.23	6.16	5.81	3.80	2.95	3.34	6.00
MnO	0.31	0.38	0.36	0.33	0.42	0.45	0.28	0.26	0.17	0.17	0.18	0.44
MgO	10.82	12.37	12.28	13.04	11.93	12.96	10.67	11.56	13.70	13.80	13.84	7.40
CaO	21.54	22.85	22.13	23.08	22.54	23.14	21.31	21.63	22.36	23.04	23.28	16.90
Na_2O	2.02	1.31	1.69	1.25	1.55	1.19	1.73	1.52	1.26	1.01	1.08	4.54
Total	100.43	100.97	100.08	100.66	100.18	100.23	99.10	98.85	99.60	99.78	100.58	100.83
Cations per 6 Oxygens												
Si	1.947	1.938	1.962	1.933	1.931	1.948	1.909	1.926	1.935	1.896	1.924	1.949
Ti	0.015	0.008	0.006	0.007	0.007	0.002	0.024	0.022	0.018	0.025	0.017	0.017
Al	0.053	0.081	0.044	0.072	0.084	0.080	0.095	0.080	0.078	0.115	0.076	0.066
Fe^{+3}	0.170	0.121	0.143	0.138	0.153	0.105	0.166	0.134	0.106	0.117	0.117	0.335
Fe^{+2}	0.189	0.159	0.146	0.118	0.136	0.131	0.196	0.184	0.118	0.092	0.103	0.189
Mn	0.010	0.012	0.011	0.010	0.013	0.014	0.009	0.008	0.005	0.005	0.006	0.014
Mg	0.604	0.682	0.682	0.718	0.663	0.716	0.605	0.653	0.758	0.763	0.760	0.416
Ca	0.865	0.905	0.884	0.914	0.901	0.919	0.868	0.879	0.890	0.916	0.919	0.683
Na	0.147	0.094	0.122	0.090	0.112	0.085	0.128	0.112	0.091	0.073	0.077	0.332
Ac	14.7	9.4	12.2	9.0	11.2	8.5	12.8	11.2	9.1	7.3	7.7	33.2
Di	60.4	68.2	68.2	71.8	66.3	71.6	60.5	65.3	75.8	76.3	76.0	41.6
Hd	18.9	15.9	14.6	11.8	13.6	13.1	19.6	18.4	11.8	9.2	10.3	18.9
Sa	6.0	6.5	5.0	7.4	8.9	6.8	7.1	5.1	3.3	7.2	6.0	6.3

(e) "Nephelinised" pyroxenite

	(i) Cores in pyroxenite				(ii) Rims in pyroxenite				(iii) Discrete pyroxenes in dyke						
	S49.4	S49.5	S49.6	S49.c6	S49.7	S49.8	S49.9	S49.c5	S49.1	S49.2	S49.3	S49.c1	S49.c2	S49.c3	S49.c4
SiO_2	52.28	49.98	50.86	50.74	50.77	51.57	51.70	49.81	51.30	51.29	50.94	50.42	50.75	50.06	50.05
TiO_2	0.68	1.02	0.87	0.71	0.43	0.50	0.35	0.47	0.19	0.48	0.49	0.45	0.40	0.43	0.50
Al_2O_3	1.76	2.88	1.96	1.76	1.27	1.22	0.97	1.22	1.20	1.14	1.18	1.10	0.98	1.04	1.05
Fe_2O_3	4.70	6.52	5.94	5.39	13.46	12.99	12.45	12.54	17.30	15.46	17.60	12.44	17.57	15.13	16.80
FeO	3.03	0.69	3.39	2.13	7.14	5.90	5.13	7.11	7.15	6.56	5.33	8.44	5.20	7.72	6.67
MnO	0.22	0.11	0.22	0.16	0.56	0.55	0.57	0.59	0.62	0.67	0.62	0.64	0.63	0.71	0.64
MgO	13.52	13.79	12.52	13.40	6.03	6.79	7.77	5.43	5.61	4.86	4.95	5.05	4.20	4.64	3.69
CaO	23.51	23.97	22.99	23.41	16.63	16.37	17.06	15.95	15.02	14.01	14.45	15.01	12.06	15.05	13.02
Na_2O	1.22	0.99	1.34	1.11	4.60	4.87	4.47	4.78	5.57	6.02	6.05	5.04	6.96	5.23	6.41
Total	100.92	99.95	100.10	98.81	100.89	100.76	100.46	97.90	103.96	100.48	101.61	98.59	98.74	100.01	98.83
Cations per 6 Oxygens															
Si	1.922	1.853	1.897	1.905	1.936	1.952	1.955	1.955	1.963	1.961	1.931	1.969	1.971	1.940	1.957
Ti	0.019	0.028	0.024	0.020	0.012	0.014	0.010	0.014	0.014	0.014	0.014	0.013	0.012	0.013	0.015
Al	0.076	0.126	0.086	0.078	0.057	0.054	0.043	0.056	0.051	0.051	0.053	0.051	0.045	0.048	0.048
Fe^{+3}	0.130	0.182	0.167	0.152	0.386	0.370	0.354	0.370	0.498	0.445	0.502	0.366	0.514	0.441	0.494
Fe^{+2}	0.093	0.021	0.106	0.067	0.228	0.187	0.162	0.233	0.229	0.210	0.169	0.276	0.169	0.250	0.218
Mn	0.007	0.003	0.007	0.005	0.018	0.018	0.018	0.020	0.018	0.022	0.020	0.021	0.021	0.023	0.021
Mg	0.741	0.762	0.696	0.750	0.343	0.383	0.438	0.318	0.205	0.277	0.280	0.294	0.243	0.268	0.215
Ca	0.926	0.952	0.919	0.942	0.680	0.664	0.691	0.671	0.520	0.574	0.587	0.628	0.502	0.625	0.545
Na	0.087	0.071	0.097	0.081	0.340	0.357	0.328	0.364	0.502	0.446	0.445	0.382	0.524	0.393	0.486
Ac	8.7	7.1	9.7	8.1	34.0	35.7	32.8	36.4	50.2	44.5	44.5	36.6	51.4	39.3	48.6
Di	74.1	76.2	69.6	75.0	34.3	38.3	43.8	31.8	20.5	27.7	28.0	29.4	24.3	26.8	21.5
Hd	9.3	2.1	10.6	6.7	22.8	18.7	16.2	23.3	22.5	21.0	16.9	27.6	16.9	25.0	21.8
Sa	7.9	14.6	10.1	10.2	8.9	7.3	7.2	8.5	6.8	6.8	10.6	6.4	7.4	8.9	8.1

(f) Nepheline syenites

	S02.c1	S02.c2	S02.c3	S02.c4	S02.c5	S02.c6	S02.c7	S02.c8	S02.c9	S02.c10	S-03.c2	S-03.c3	S-03.c4	S-03.c5	S-03.c6
SiO_2	51.27	51.33	50.97	50.98	51.33	51.09	51.74	51.39	51.61	52.06	51.93	51.37	51.89	52.31	51.90
TiO_2	2.45	1.99	4.30	1.85	2.13	1.47	1.41	3.22	1.85	2.59	0.90	1.17	2.05	1.62	2.05
Al_2O_3	2.23	3.33	1.23	1.28	4.46	1.61	1.79	1.15	1.32	2.52	1.22	1.43	1.34	1.55	1.74
Fe_2O_3	22.56	25.46	18.81	24.86	21.23	28.20	25.68	22.62	26.46	21.17	26.57	23.45	22.73	23.64	26.46
FeO	4.95	1.85	7.13	3.96	4.72	1.76	3.35	5.22	3.14	5.88	2.58	4.22	3.53	3.43	1.43
MnO	0.48	0.31	0.57	0.45	0.45	0.50	0.49	0.61	0.44	0.45	0.47	0.40	0.58	0.36	0.38
MgO	0.69	0.73	1.28	0.81	0.64	0.61	0.59	0.89	0.65	0.70	1.19	1.17	1.99	1.88	1.12
CaO	3.18	0.92	4.83	4.06	2.09	2.30	2.35	3.64	1.97	3.01	3.94	4.98	5.41	3.45	2.31
Na_2O	11.38	12.62	10.49	11.12	11.71	12.10	11.91	11.27	12.10	11.46	11.36	10.65	10.63	11.31	12.32
Total	99.19	98.55	99.61	99.37	98.76	99.64	99.31	100.01	99.54	99.84	100.16	98.84	100.15	99.55	99.72
Cations per 6 Oxygens															
Si	1.976	1.969	1.966	1.972	1.967	1.964	1.991	1.974	1.985	1.989	1.986	1.991	1.978	1.998	1.978
Ti	0.071	0.057	0.125	0.054	0.061	0.043	0.041	0.093	0.054	0.074	0.026	0.034	0.059	0.047	0.059
Al	0.101	0.151	0.056	0.058	0.201	0.073	0.081	0.052	0.060	0.114	0.055	0.065	0.060	0.070	0.078
Fe^{+3}	0.654	0.735	0.546	0.724	0.612	0.816	0.744	0.654	0.766	0.609	0.764	0.684	0.652	0.680	0.759
Fe^{+2}	0.160	0.060	0.230	0.128	0.151	0.057	0.108	0.168	0.101	0.188	0.083	0.137	0.113	0.109	0.046
Mn	0.016	0.010	0.019	0.015	0.015	0.016	0.016	0.020	0.014	0.015	0.015	0.013	0.019	0.012	0.012
Mg	0.040	0.042	0.074	0.047	0.037	0.035	0.034	0.051	0.037	0.040	0.068	0.068	0.113	0.107	0.064
Ca	0.131	0.038	0.200	0.168	0.086	0.095	0.097	0.150	0.081	0.123	0.161	0.207	0.221	0.141	0.094
Na	0.851	0.939	0.785	0.834	0.870	0.902	0.889	0.839	0.902	0.849	0.842	0.801	0.786	0.837	0.910
Ac	65.4	73.5	54.6	72.4	61.2	81.6	74.4	65.4	76.6	60.9	76.4	68.4	65.2	68.0	75.9
Di	4.0	4.2	7.4	4.7	3.7	3.5	3.4	5.1	3.7	4.0	6.8	6.8	11.3	10.7	6.4
Hd	16.0	6.0	23.0	12.8	15.1	5.7	10.8	16.8	10.1	18.8	8.3	13.7	11.3	10.9	4.6
Sa	14.6	16.3	15.0	10.1	20.0	9.2	11.4	12.7	9.6	16.3	8.5	11.1	12.2	10.4	13.1

Nepheline syenites (contd.)

	S-03.c7	S-03.c8	S-03.c9	S-03.c10	S-154.c1	S-154.c2	S-154.c3	S-154.c4	S-154.c5	S-154.c6	S-154.c7	S-154.c8	S-12.c1	S-12.c2	S-12.c3
SiO_2	51.89	52.11	52.06	51.25	51.93	50.92	52.36	50.91	51.38	51.06	51.76	51.29	51.34	51.05	51.30
TiO_2	1.95	2.08	2.39	1.63	1.39	1.05	1.97	1.29	1.31	1.19	0.71	1.35	1.36	1.66	1.27
Al_2O_3	1.52	1.21	1.56	1.24	1.49	1.12	1.44	1.26	1.17	1.21	1.19	1.19	1.09	1.33	1.12
Fe_2O_3	25.23	24.88	27.35	23.85	23.82	19.77	20.86	19.60	21.55	20.35	23.08	22.57	25.08	21.72	24.05
FeO	1.87	1.77	0.56	4.36	4.15	8.60	5.39	7.77	6.57	7.38	4.57	5.03	4.70	7.18	6.30
MnO	0.44	0.39	0.36	0.54	0.47	0.51	0.58	0.51	0.56	0.53	0.51	0.72	0.61	0.52	0.45
MgO	1.66	2.17	0.97	1.11	1.15	1.13	1.57	1.62	1.22	1.66	1.85	1.51	0.63	0.62	0.55
CaO	3.23	3.80	0.78	4.55	4.06	6.60	3.99	6.44	5.34	7.86	6.43	6.39	5.12	6.25	5.60
Na_2O	11.73	11.49	13.10	10.79	11.10	9.11	10.89	9.19	10.02	8.88	9.90	9.90	10.70	9.86	10.26
Total	99.52	99.90	99.14	99.32	99.55	98.81	99.04	98.59	99.12	100.13	100.00	99.95	100.63	100.19	100.90
Cations per 6 Oxygens															
Si	1.981	1.981	1.988	1.982	1.995	1.998	2.015	1.993	1.997	1.975	1.988	1.976	1.972	1.975	1.972
Ti	0.056	0.059	0.069	0.047	0.040	0.031	0.057	0.038	0.038	0.035	0.021	0.039	0.039	0.048	0.037
Al	0.068	0.054	0.070	0.057	0.067	0.052	0.065	0.058	0.054	0.055	0.054	0.054	0.049	0.061	0.051
Fe^{+3}	0.725	0.712	0.786	0.694	0.689	0.584	0.604	0.577	0.630	0.592	0.667	0.655	0.725	0.632	0.696
Fe^{+2}	0.060	0.056	0.018	0.141	0.133	0.282	0.173	0.254	0.214	0.239	0.147	0.162	0.151	0.232	0.202
Mn	0.014	0.013	0.012	0.018	0.015	0.017	0.019	0.017	0.018	0.017	0.017	0.024	0.020	0.017	0.015
Mg	0.094	0.123	0.055	0.064	0.066	0.066	0.090	0.095	0.071	0.096	0.106	0.087	0.036	0.036	0.032
Ca	0.132	0.155	0.032	0.189	0.167	0.277	0.164	0.270	0.222	0.326	0.265	0.264	0.211	0.259	0.231
Na	0.868	0.847	0.970	0.809	0.827	0.693	0.812	0.698	0.755	0.666	0.737	0.740	0.797	0.740	0.765
Ac	72.5	71.2	78.6	69.4	68.9	58.4	60.4	57.7	63.0	59.2	66.7	65.5	72.5	63.2	69.6
Di	9.4	12.3	5.5	6.4	6.6	6.6	9.0	9.5	7.1	9.6	10.6	8.7	3.6	3.6	3.2
Hd	6.0	5.6	1.8	14.1	13.3	28.2	17.3	25.4	21.4	23.9	14.7	16.2	15.1	23.2	20.2
Sa	12.1	10.9	14.1	10.1	11.2	6.8	13.3	7.4	8.5	7.3	8.0	9.6	8.8	10.0	7.0

Nepheline syenites (contd.)

	S-12.c4	S-12.c5	S-12.c6	S-12.c7	S-12.c8	S-12.c9	S-13.c1	S-13.c2	S-13.c3	S-13.c4	S-13.c5	S-13.c6	S-13.c7
SiO_2	52.17	50.25	50.11	51.36	50.86	52.04	51.56	50.76	52.01	51.05	50.58	50.94	51.77
TiO_2	1.09	1.42	1.35	1.10	1.40	1.01	1.41	0.73	1.29	1.38	0.74	0.70	0.98
Al_2O_3	1.28	0.92	0.86	1.23	1.02	1.43	1.02	1.11	1.23	2.08	1.12	1.09	1.21
Fe_2O_3	26.09	22.27	23.33	22.19	20.72	23.38	22.70	20.83	24.14	23.47	18.54	15.54	20.83
FeO	3.39	6.92	6.46	6.42	8.04	4.84	5.11	7.16	4.29	4.49	8.35	8.38	5.47
MnO	0.26	0.70	0.72	0.36	0.54	0.34	0.62	0.49	0.50	0.43	0.51	0.55	0.62
MgO	1.15	0.59	0.60	1.37	0.99	1.29	1.68	1.70	1.41	1.50	2.13	4.02	2.59
CaO	3.71	6.99	6.96	5.24	7.00	3.99	5.81	8.96	4.69	4.21	9.32	12.52	7.60
Na_2O	11.41	9.43	9.48	10.02	9.22	10.90	10.08	8.45	10.79	10.63	7.88	6.34	9.13
Total	100.55	99.49	99.86	99.29	99.80	99.21	99.99	100.19	100.34	99.24	99.17	100.08	100.20
Cations per 6 Oxygens													
Si	1.987	1.967	1.957	1.993	1.980	2.007	1.983	1.967	1.988	1.969	1.978	1.966	1.983
Ti	0.031	0.042	0.040	0.032	0.041	0.029	0.041	0.021	0.037	0.040	0.022	0.020	0.028
Al	0.057	0.042	0.040	0.056	0.047	0.065	0.046	0.051	0.055	0.095	0.052	0.050	0.055
Fe^{+3}	0.748	0.656	0.685	0.648	0.607	0.678	0.657	0.607	0.694	0.682	0.546	0.451	0.601
Fe^{+2}	0.108	0.227	0.211	0.208	0.262	0.156	0.165	0.232	0.137	0.145	0.273	0.271	0.175
Mn	0.008	0.023	0.024	0.012	0.018	0.011	0.020	0.016	0.016	0.014	0.017	0.018	0.020
Mg	0.065	0.034	0.035	0.079	0.057	0.074	0.096	0.098	0.080	0.086	0.124	0.231	0.148
Ca	0.151	0.293	0.291	0.218	0.292	0.165	0.239	0.372	0.192	0.174	0.391	0.518	0.312
Na	0.843	0.716	0.718	0.754	0.696	0.815	0.752	0.635	0.800	0.795	0.598	0.475	0.678
Ac	74.8	65.6	68.5	64.8	60.7	67.8	65.7	60.7	69.4	68.2	54.6	45.1	60.1
Di	6.5	3.4	3.5	7.9	5.7	7.4	9.6	9.8	8.0	8.6	12.4	23.1	14.8
Hd	10.8	22.7	21.1	20.8	26.2	15.6	16.5	23.2	13.7	14.5	27.3	27.1	17.5
Sa	7.9	8.3	6.9	6.5	7.4	9.2	8.2	6.3	8.9	8.7	5.7	4.7	7.6

Table B.2: Ijolite nepheline compositions.

(a) Type-I Ijolites (Fine-grained)

	S49/1	S49/2	S49/3	S49/4	S49/5	S49/6	S41/1	S41/2	S41/3	S50/1	S50/2	S50/3	S82/1
SiO_2	45.60	45.68	46.81	46.05	47.12	45.54	46.09	46.03	46.43	44.06	43.96	45.58	44.72
Al_2O_3	31.38	30.40	32.08	31.87	32.16	32.64	32.39	32.64	32.41	31.99	32.56	31.20	32.03
Fe_2O_3	1.31	1.19	1.31	1.37	1.33	1.36	1.23	1.36	1.30	1.17	0.97	1.44	1.13
CaO	0.00	0.03	0.00	0.04	0.00	0.05	0.05	0.00	0.05	0.11	0.00	0.00	0.04
Na_2O	15.62	15.34	15.65	15.59	15.63	15.47	15.82	15.97	15.99	14.62	15.34	15.33	16.02
K_2O	5.65	5.43	5.32	5.35	5.21	6.01	4.97	5.08	4.87	6.54	6.79	5.78	5.01
Total	99.56	98.07	101.17	100.27	101.45	101.07	100.55	101.08	101.05	98.49	99.62	99.33	98.95
Ions per 32 Oxygens													
Si	8.742	8.868	8.791	8.739	8.813	8.612	8.706	8.663	8.724	8.572	8.485	8.759	8.614
Al	7.092	6.958	7.103	7.131	7.091	7.277	7.213	7.242	7.179	7.338	7.409	7.069	7.274
Fe+3	0.189	0.174	0.185	0.195	0.188	0.193	0.175	0.192	0.184	0.171	0.140	0.209	0.164
Na	5.806	5.774	5.699	5.737	5.668	5.672	5.794	5.828	5.826	5.515	5.741	5.712	5.983
K	1.382	1.345	1.275	1.295	1.243	1.450	1.198	1.220	1.167	1.623	1.672	1.417	1.231
Ne	72.60	72.15	72.26	72.69	72.14	71.73	73.86	74.06	74.22	69.73	71.26	71.60	75.36
Ks	19.57	19.25	17.99	18.27	17.62	20.41	17.00	17.26	16.56	22.85	23.13	19.99	17.27
Q	7.84	8.59	9.75	9.04	10.24	7.86	9.14	8.69	9.22	7.42	5.61	8.41	7.37

	(b) Type-I Ijolites (Fine-grained)			(c) Type-II Ijolites					
	S134/1	S134/2	S134/3	S51/1	S42/1	S42/2	S64/1	S142/1	S142/2
SiO_2	43.77	44.16	43.74	43.41	42.75	43.16	43.02	45.16	44.90
Al_2O_3	32.14	32.16	32.59	33.35	33.55	33.61	33.80	32.86	33.07
Fe_2O_3	1.40	1.24	1.28	0.90	0.82	0.93	1.27	1.04	1.14
CaO	0.00	0.00	0.00	0.00	0.00	0.05	0.04	0.00	0.00
Na_2O	15.29	15.62	15.35	16.06	17.21	16.89	15.69	15.42	15.39
K_2O	6.54	6.43	6.73	7.09	5.63	5.64	6.93	5.96	6.47
Total	99.14	99.61	99.69	100.81	99.96	100.28	100.75	100.44	100.97
Ions per 32 Oxygens									
Si	8.491	8.521	8.446	8.323	8.239	8.278	8.247	8.584	8.521
Al	7.351	7.316	7.419	7.538	7.623	7.600	7.639	7.363	7.399
Fe+3	0.204	0.181	0.186	0.130	0.119	0.135	0.183	0.149	0.163
Na	5.751	5.844	5.747	5.970	6.431	6.281	5.832	5.683	5.663
K	1.619	1.583	1.658	1.734	1.384	1.380	1.695	1.445	1.566
Ne	71.65	72.47	71.54	73.00	78.72	77.86	72.75	71.86	71.20
Ks	22.53	22.28	22.98	24.29	19.45	19.24	23.54	20.35	21.93
Q	5.82	5.25	5.48	2.70	1.83	2.91	3.72	7.79	6.87

Table B.3: Nepheline Syenite alkali feldspar and nepheline compositions.

Alkali Feldspars (Perthite)

	(a) K-feldspar								(b) Na-Feldspar				
	S02.1	S02.2	S-12.1	S-13.2	S-13.5	S-13.6	S-154.1	S-154.2	S-12.2	S-13.1	S-13.3	S-13.4	S-154.3
SiO_2	64.13	64.85	65.30	64.96	65.32	65.12	65.15	65.15	68.96	68.85	69.07	69.33	69.03
Al_2O_3	18.41	17.90	18.01	18.05	18.20	18.17	17.97	18.22	18.90	18.87	18.85	18.96	18.88
FeO	0.15	0.00	0.27	0.00	0.19	0.36	0.27	0.27	0.00	0.10	0.12	0.14	0.24
Na_2O	2.17	0.21	1.02	1.35	1.56	1.93	1.45	2.38	11.21	11.12	11.09	11.26	11.15
K_2O	13.75	16.45	14.93	14.53	14.29	13.41	12.83	11.38	0.12	0.11	0.10	0.18	0.20
BaO	0.00	0.25	0.54	0.69	1.13	1.07	0.52	1.02	0.00	0.00	0.00	0.00	0.00
Total	98.61	99.66	100.07	99.58	100.69	100.06	98.19	98.42	99.19	99.05	99.23	99.87	99.50
Ions per 32 Oxygens													
Si	11.94	12.06	12.06	12.06	12.03	12.03	12.12	12.09	12.11	12.10	12.12	12.10	12.09
Al	4.04	3.92	3.92	3.95	3.95	3.96	3.94	3.99	3.91	3.91	3.90	3.90	3.90
Fe	0.02	0.00	0.04	0.00	0.03	0.06	0.04	0.04	0.00	0.02	0.02	0.02	0.04
Na	0.78	0.08	0.36	0.49	0.56	0.69	0.52	0.86	3.82	3.79	3.77	3.81	3.79
K	3.27	3.90	3.52	3.44	3.36	3.16	3.04	2.69	0.03	0.03	0.02	0.04	0.05
q	43.06	44.00	2.03	44.35	1.41	44.94	47.91	48.25	47.61	47.83	4.14	47.45	3.25
ne	9.99	0.27	8.73	6.26	13.33	9.04	6.96	11.49	51.98	51.80	95.26	51.94	95.55
ks	46.95	55.73	89.24	49.39	85.26	46.02	45.12	40.26	0.41	0.38	0.60	0.61	1.20

Nepheline

	S-03.n1	S-03.n2	S-13.n1	S-13.n2	S-13.n3	S-154.n1
SiO_2	43.33	43.18	45.46	45.67	45.94	43.96
Al_2O_3	32.94	33.81	31.81	31.82	31.42	33.07
FeO	0.13	0.17	0.63	0.76	0.87	0.42
Na_2O	15.37	15.48	15.40	15.48	15.37	14.93
K_2O	7.15	6.98	5.84	5.95	5.69	5.92
Total	98.92	99.62	99.14	99.68	99.29	98.30
Ions per 32 Oxygens						
Si	8.43	8.14	8.73	8.73	8.80	8.52
Al	7.55	7.52	7.20	7.17	7.10	7.55
Fe	0.02	0.02	0.10	0.12	0.14	0.07
Na	5.80	2.55	5.74	5.74	5.71	5.61
K	1.77	0.00	1.43	1.45	1.39	1.46
q	4.46	4.25	8.04	7.92	8.70	7.62
ne	71.19	71.97	71.97	71.80	71.81	71.59
ks	24.34	23.77	19.99	20.28	19.49	20.79

Table B.4: Pectolite compositions from Spitskop nepheline syenites and selected global occurrences.

	(a) Pectolite in Spitskop nepheline syenites							(b) World pectolites						
	S3.p1	S3.p2	S3.p3	S2.p1	S2.p2	S150	S10	[1]	[2]	[3]	[4]	[5]	[6]	[7]
SiO_2	53.81	53.70	53.78	52.48	52.61	52.72	52.76	51.40	53.40	51.16	51.84	54.98	54.64	54.60
TiO_2	-	-	-	-	-	-	-	-	0.05	0.33	-	-	-	-
Al_2O_3	-	-	-	-	-	-	-	0.82	0.45	0.92	0.87	0.30	0.07	-
Fe_2O_3	-	-	-	-	-	-	-	-	0.72	0.93	0.49	0.24	-	-
FeO	0.73	0.85	0.82	0.56	0.34	0.66	0.95	2.10	0.24	0.00	-	-	0.14	0.10
MnO	2.74	2.80	2.51	4.88	3.50	2.16	3.38	16.30	1.82	0.60	-	0.03	0.09	0.20
MgO	0.00	0.00	0.00	0.00	0.00	0.04	0.04	0.03	-	-	0.11	-	0.02	-
CaO	30.06	29.98	29.95	27.62	29.48	31.16	29.81	17.74	31.34	32.20	33.26	33.51	32.79	33.90
Na_2O	9.10	9.20	9.16	9.01	8.97	9.17	8.40	9.06	8.46	8.00	10.30	8.83	8.62	9.30
Total	96.44	96.53	96.22	94.55	94.90	95.91	95.34	97.45	96.47	94.14	96.87	97.89	96.37	98.10
Atoms per 9 Oxygens														
Si	3.195	3.190	3.198	3.194	3.183	3.160	3.180	3.133	3.167	3.113	3.082	3.189	3.212	3.175
Ti	-	-	-	-	-	-	-	-	0.002	0.015	-	-	-	-
Fe^{+2}	0.036	0.042	0.041	0.029	0.017	0.033	0.048	0.107	0.044	0.043	0.022	0.010	0.007	0.005
Mn	0.138	0.141	0.126	0.252	0.179	0.110	0.173	0.842	0.091	0.031	-	0.001	0.004	0.010
Mg	0.000	0.000	0.000	0.000	0.000	0.004	0.004	0.003	-	-	0.010	-	0.002	-
Ca	1.912	1.908	1.908	1.801	1.911	2.001	1.925	1.159	1.992	2.099	2.119	2.083	2.065	2.112
Na	1.048	1.060	1.056	1.063	1.052	1.066	0.982	1.071	0.973	0.944	1.187	0.993	0.982	1.048

Source of world pectolite analyses:
1-3 are "primary" pectolites from syenitic complexes:
1: Queensland (Carr et al., 1976); 2,3: Tur'ii peninsular, USSR (Kulakov et al., 1974).
4-7 are "secondary" pectolites:
4: veins in gabbro, Japan (Matsubra et al., 1979); 5: kimberlite, Lesotho (Kruger, 1982); 6: diabase-picrite, Australia (Wilshire, 1967);
7: authigenic pectolite from ophiolite debris flow (Craw and Landis, 1980).

Table B.5: Whole rock analyses and CIPW norms of pyroxenites from Spitskop.

(a) Analyses

	S44	S47	S160
SiO_2	44.15	48.64	42.98
TiO_2	1.78	0.58	1.92
Al_2O_3*	2.80	5.29	2.85
Fe_2O_3	18.00	7.85	19.26
MnO	0.27	0.22	0.27
MgO	11.61	11.12	10.98
CaO	18.72	19.23	19.35
Na_2O	1.72	5.35	2.23
K_2O	0.49	0.33	0.39
P_2O_5	0.02	0.14	0.00
LOI	0.44	1.50	0.07
H_2O-	0.05	0.10	0.04
Total	99.49	100.35	99.74
Rb	23	15	21
Ba	158	20	215
Sr	225	289	213
U	5.9	12	0.0
Zr	90	111	84
Nb	5.6	2.6	4.4
Cr	124	252	58
V	246	100	286
Sc	32	22	0.0
Ni	42	42	56
Co	56	35	52
Pb	258	62	4.6
Zn	101	52	99
Cu	6.9	0.0	30
Y	9.7	8.9	9.6

(b) CIPW Norms

	S44	S47	S160
Qz	0.00	0.00	0.00
Z	0.02	0.02	0.02
Or	2.09	0.00	2.02
Pl	0.00	0.00	0.00
Lc	0.00	1.53	0.00
Ne	6.32	13.75	6.77
Ac	2.54	13.05	5.62
Ns	0.00	1.18	0.00
Wo	3.20	0.00	6.14
Di	66.88	54.93	58.99
Hy	0.00	0.00	0.00
Ol	0.00	4.75	0.00
Mt	13.72	0.00	15.32
Il	3.38	1.10	0.58
Hm	0.00	0.00	0.00
Ap	0.05	0.32	0.00
Total	98.85	98.49	97.54
Pl(Ab)	4.43	0.00	0.00
Pl(An)	0.00	0.00	0.00
Di(Wo)	33.46	28.96	31.64
Di(En)	28.91	22.03	27.35
Di(Fs)	0.00	3.94	0.00
Ol(Fo)	0.00	3.97	0.00
Ol(Fa)	0.00	0.78	0.00

(c) Rare earth elements

	S44
La	4.7
Ce	14.0
Pr	2.1
Nd	10.4
Sm	2.1
Eu	0.69
Gd	2.4
Dy	2.0
Ho	0.45
Er	1.0
Yb	1.2
Lu	0.20

Table B.6: Analyses of pyroxenites from selected world occurrences.

(a) Pyroxenites from various alkaline complexes | (b) Pyroxenites from Napak

	Px-1	Px-2	Px-3	Px-4	Px-5	Px-6	Px-7	Px-8	PvS-MbP	Napak-1	Napak-2	Napak-3
SiO_2	38.39	35.42	37.47	40.25	41.20	44.49	43.35	44.39	26.42	39.98	41.39	43.25
TiO_2	4.54	4.05	1.07	4.76	3.63	2.26	4.38	3.91	1.64	3.10	2.55	3.07
Al_2O_3	7.05	9.21	2.86	2.74	3.14	8.72	9.67	6.37	5.54	12.14	4.91	11.49
Fe_2O_3	9.07	8.94	11.77	10.83	9.56	4.54	5.26	5.11	11.74	4.13	10.37	0.39
FeO	6.17	7.17	7.83	7.38	7.70	4.55	2.65	4.86	0.00	8.70	9.77	12.63
MnO	0.32	0.29	0.16	0.16	0.20	0.10	0.09	0.10	0.23	0.25	0.21	0.32
MgO	11.58	7.77	10.12	12.04	12.20	12.38	15.74	14.20	8.73	11.24	10.06	8.41
CaO	19.01	20.83	21.68	20.21	20.22	17.81	12.20	17.02	23.18	17.65	18.02	12.00
Na_2O	0.74	1.47	0.47	0.42	1.03	0.80	0.44	0.50	0.70	1.24	1.52	1.90
K_2O	0.75	0.62	0.93	0.00	0.18	2.42	4.74	2.35	4.88	1.18	1.40	4.22
P_2O_5	0.82	2.23	4.33	0.45	0.00	0.77	0.00	0.26	5.25	0.06	0.02	0.51
LOI	0.65	1.16	1.45	0.53	0.46	0.68	0.63	0.39	11.69	0.35	0.00	1.22
H_2O-	0.14	0.11	0.27	0.46	0.00	0.03	0.07	0.05	0.00	0.00	0.00	0.00
Total	99.23	99.27	100.41	100.23	99.52	99.55	99.22	99.51	100.00	100.02	100.22	99.41

(a) Pyroxenite analyses prefixed "Px" are extracted from the compilation by Upton (1966; Table 9.1)
Px-1: jacupirangite from Jacupiranga (Brazil); Px-2: jacupirangite from Magnet Cove (USA); Px-3: apatite pyroxenite from Libby (USA); Px-4: fine grained pyroxenite from Iron Hill (USA); Px-5: fine grained pyroxenite from Afrikanda (USSR); Px-6: pyroxenite block from Alban Volcano (Italy); Px-7: biotite pyroxenite from Bufumbira (Uganda); Px-8: biotite pyroxenite from Katwe Crater (Uganda).

Sample PvS-MbP is a pyroxenite from the Mbalizi carbonatite (Tanzania); from Van Straaten (1989).

(b) Alkali pyroxenites from the Napak complex (Uganda) from the compilation of Le Bas (1977; p304). The samples are listed as coming from Lokupoi, Napak: Napak-1 is a magnetite pyroxenite (original number: SUN569); Napak-2 (SUN35C); Napak-3 (SUN25).

(c) Phalaborwa pyroxenites

(d) Bushveld Complex pyroxenites

	F25M	F38M	F12F	F67F	F5P	F28P	BDS-130	BDS-66
SiO_2	50.50	48.11	54.51	39.89	39.24	45.86	54.63	52.23
TiO_2	0.18	0.15	0.14	0.21	0.40	0.36	0.11	0.23
Al_2O_3	0.70	0.45	1.00	1.55	3.78	6.02	1.01	6.93
Fe_2O_3	1.91	1.02	0.38	0.81	1.89	2.73	11.26	15.22
FeO	4.05	3.35	2.82	2.31	1.78	4.02	0.20	0.29
MnO	0.22	0.35	0.05	0.29	0.14	0.20	29.67	17.56
MgO	14.77	14.04	13.72	12.76	17.08	20.57	2.13	6.05
CaO	23.88	25.54	22.04	28.41	21.69	10.83	0.18	1.00
Na_2O	0.17	0.69	0.61	0.58	0.00	0.00	0.00	0.14
K_2O	0.18	0.12	0.65	1.14	3.53	5.82	0.00	0.02
P_2O_5	2.72	5.44	4.18	11.44	8.97	0.48	0.00	0.37
LOI	0.56	0.81	0.65	0.72	1.81	2.37	0.00	0.13
H_2O-	0.17	0.04	0.06	0.04	0.09	0.09		
Total	100.01	100.11	100.81	100.15	100.40	99.35	99.19	100.17
Rb	10	6	485	302	71	22	-	4
Ba	2	-	57	126	161	500	-	-
Sr	874	1362	1039	2084	870	289	-	97
Zr	19	18	55	6	21	12	3	20
Nb	3	5	4	3	-	8	-	-
V	47	-	23	-	10	68	103	136
Ni	110	50	44	36	87	48	532	364
Zn	43	16	30	16	32	97	72	110
Cu	94	81	-	-	-	114	-	10
Y	35	54	44	93	62	12	3	8
La	127	378	132	627	208	20	-	-
Ce	356	760	373	1213	646	21	-	-

(c) Alkali pyroxenites from the Phalaborwa Complex (Eriksson, 1989): samples F25M and F38M are massive pyroxenite; F12F and F67F are feldspathic pyroxenite; F5P and F28P are micaceous pyroxenite.
(d) Tholeiitic pyroxenites from the Rustenburg Layered Suite of the Bushveld Complex.
BDS-130 is a feldspathic orthopyroxenite from the lower critical zone of the Rustenburg Layered Suite (within the zone of occurrence of the lower group, "LG", chromitites).
BDS-66 is a sample of the "pyroxenite marker" in the upper parts of the main zone of the Rustenburg Layered Suite.
Both samples are from the definitive sample suite compiled and analysed by M.R. Sharpe (unpublished data: Bushveld Institute, U Pretoria).

Table B.7: Whole rock analyses of ijolites from the Spitskop Complex.

(a) Type-I ijolites (fine-grained)

	S22	S41	S43	S70	S79	S82	S83	S114	S16	S18	S50	S115	S143	S173
SiO_2	44.82	44.54	43.65	47.83	44.19	43.58	43.65	48.06	45.98	41.60	43.76	42.01	42.71	49.20
TiO_2	1.23	1.62	1.13	1.15	1.55	1.25	1.54	1.04	0.66	0.99	1.55	1.05	0.63	0.97
Al_2O_3	19.81	20.99	22.02	19.65	20.58	20.71	20.97	20.45	16.86	16.46	18.64	18.57	19.09	17.53
Fe_2O_3	8.36	8.18	5.98	8.81	7.98	7.38	7.84	7.68	8.80	7.99	8.34	10.66	7.45	9.47
MnO	0.21	0.22	0.13	0.21	0.20	0.17	0.17	0.12	0.25	0.26	0.26	0.19	0.12	0.23
MgO	1.94	1.59	1.73	1.05	1.71	2.03	1.93	1.46	2.96	2.98	1.94	3.13	3.37	1.65
CaO	6.93	6.74	6.06	4.92	6.68	7.05	7.12	4.58	8.85	12.75	8.11	8.85	8.05	4.84
Na_2O	11.93	11.69	13.20	11.95	12.38	12.59	12.61	12.46	10.21	9.47	11.71	10.93	12.18	10.10
K_2O	3.27	2.41	3.79	3.23	3.10	2.56	2.68	2.94	2.87	2.69	2.99	2.86	3.95	3.19
P_2O5	0.66	0.31	0.48	0.22	0.51	0.60	0.47	0.21	0.81	2.07	0.67	1.04	0.79	0.42
LOI	0.37	1.91	1.05	0.73	0.32	2.03	1.50	0.51	1.11	2.11	1.28	0.40	0.52	1.54
H_2O-	0.09	0.31	0.09	0.11	0.07	0.17	0.10	0.08	0.15	0.17	0.10	0.07	0.11	0.08
Total	99.62	100.51	99.31	99.86	99.27	100.12	100.58	99.59	99.51	99.54	99.35	99.76	98.97	99.22
Rb	72	41	53	77	63	45	42	76	45	29	46	56	58	89
Ba	193	58	123	972	56	56	28	452	310	132	156	62	12	1309
Sr	374	470	338	414	374	487	379	317	305	579	281	569	322	573
Th	0.0	4.9	7.9	5.5	0.0	0.0	0.0	0.0	0.0	0.0	5.9	0.0	0.0	-
U	0.0	7.3	7.3	7.0	0.0	0.0	0.0	0.0	0.0	0.0	4.7	0.0	0.0	-
Zr	207	171	155	255	203	115	140	276	218	205	256	72	59	274
Nb	32	48	34	63	38	34	46	42	31	20	78	8.5	2.5	39
Cr	8.9	0.0	2.0	0.0	172	2.5	2.7	3.1	5.5	5.1	3.2	5.2	2.8	28
V	155	151	74	119	172	106	121	114	120	66	88	180	82	123
Sc	1.9	0.0	1.8	1.5	1.8	2.3	2.8	0.0	3.7	4.9	0.0	6.1	4.2	-
Ni	4.5	1.9	1.4	0.0	0.0	0.0	0.0	0.0	8.9	11	6.3	2.0	10	4.0
Co	17	16	13	12	18	18	19	16	21	19	20	28	22	17
Pb	6.4	6.4	0.0	9.0	0.0	0.0	0.0	0.0	0.0	0.0	331	0.0	0.0	24
Zn	70	46	41	89	55	53	42	67	94	65	77	74	40	119
Cu	23	44	0.0	12	16	33	47	14	8.3	0.0	3.9	40	0.0	43
Y	17	11	12	16	17	15	14	14	16	84	18	15	8.8	26
La(x)	13	8.8	11	6.8	12	12	9.3	5.8	17	33	9.4	19	11	0.0
Ce(x)	35	26	27	27	40	35	31	24	37	83	39	44	31	0.0
Nd(x)	23	18	18	20	26	22	20	14	22	57	25	24	18	0.0

	(b) Type-I ijolites (coarse-grained)				(c) Urtites		(d) Type-II ijolites							
	S04	S134	S136	S138	S67	S109	S42	S51	S64	S65	S81	S126	S127	S131
SiO_2	43.94	42.91	43.05	43.14	39.72	41.00	43.33	42.76	45.59	45.05	43.73	42.49	42.46	45.98
TiO_2	0.19	0.10	0.21	0.16	0.03	0.07	0.47	0.42	0.25	0.19	0.27	0.22	0.33	0.96
Al_2O_3	20.71	19.99	20.78	21.61	28.73	30.87	18.34	23.03	17.19	16.53	20.71	20.80	16.35	18.70
Fe_2O_3	5.66	4.22	5.07	5.67	1.36	1.68	6.03	4.74	6.76	6.46	3.80	5.57	6.87	8.79
MnO	0.17	0.16	0.15	0.17	0.07	0.00	0.14	0.13	0.22	0.29	0.08	0.10	0.15	0.17
MgO	2.32	2.12	2.19	2.42	0.16	0.44	5.50	2.81	4.80	4.88	4.24	2.95	4.30	3.60
CaO	8.50	11.16	9.70	7.08	4.45	2.20	10.82	7.23	10.87	17.69	8.96	9.56	13.06	8.08
Na_2O	12.13	12.15	12.61	13.86	16.36	17.12	11.12	12.78	9.84	2.41	12.74	11.68	10.13	4.62
K_2O	3.27	2.83	3.04	3.23	4.13	4.10	2.59	4.58	2.86	1.53	3.52	3.39	2.51	3.10
P_2O5	0.31	1.07	1.10	0.81	1.43	1.15	0.92	0.76	0.25	0.26	1.11	2.69	3.95	0.84
LOI	3.35	2.90	2.23	2.57	2.84	1.67	1.01	0.65	1.34	4.07	1.19	1.09	0.82	4.04
H_2O-	0.16	0.07	0.08	0.10	0.08	0.16	0.09	0.09	0.11	0.22	0.06	0.11	0.06	0.54
Total	100.71	99.68	100.21	100.82	99.36	100.46	100.36	99.98	100.08	99.58	100.41	100.65	100.99	99.42
Rb	48	46	55	54	53	89	45	58	30	28	47	38	45	32
Ba	164	166	153	168	99	98	116	11	36	1721	73	96	121	1010
Sr	297	597	497	488	448	481	372	214	364	838	390	369	866	858
Th	5.7	0.0	0.0	0.0	6.8	0.0	6.2	5.9	6.5	12	0.0	0.0	0.0	0.0
U	8.2	0.0	0.0	0.0	7.5	0.0	6.6	6.8	6.2	9.3	0.0	0.0	0.0	0.0
Zr	87	89	73	118	25	23	78	38	75	64	48	63	120	200
Nb	7.3	7.1	8.4	9.2	2.8	1.7	3.0	1.6	3.9	5.4	2.0	0.0	2.9	48
Cr	2.4	5.1	3.4	8.6	0.0	0.0	56	3.1	14	14	22	3.2	4.5	0.0
V	27	23	31	32	5.0	8.9	80	69	120	125	35	48	64	122
Sc	2.1	3.2	4.4	3.7	0.0	0.0	5.7	3.6	21	22	7.7	3.3	4.0	2.9
Ni	9.6	9.5	11	15	0.0	0.0	20	5.4	59	77	12	0.0	10	22
Co	15	11	14	16	2.0	2.3	22	15	33	37	14	11	20	24
Pb	13	6.8	6.6	0.0	19	5.7	9.8	5.3	96	103	0.0	0.0	0.0	0.0
Zn	53	46	51	62	16	22	34	23	62	87	24	28	49	73
Cu	7.0	1.4	2.0	0.0	1.1	3.9	11	0.0	2.0	19	0.0	0.0	9.2	52
Y	14	26	25	17	17	12	10	6.3	8.8	13	10	18	33	25
La(x)	8.5	18	19	17	18	16	7.6	6.7	5.7	10	12	13	41	15
Ce(x)	17	40	43	35	39	32	18	13	15	19	26	37	94	36
Nd(x)	9.0	25	26	21	24	18	10	8.3	8.0	11	17	24	53	21

Type-II ijolites (contd.)

(e) Mixed pyroxenite-ijolite

	S132	S135	S137	S139	S142	S144	S145	S157	S158	S47	S85
SiO_2	43.70	46.08	46.30	47.54	47.15	43.96	46.81	45.82	43.44	48.64	39.25
TiO_2	1.01	0.25	0.32	0.24	0.23	0.62	0.21	0.17	0.41	0.58	0.51
Al_2O_3	21.63	14.54	13.43	15.86	14.93	17.35	13.74	19.54	23.82	5.29	10.06
Fe_2O_3	6.32	7.56	8.64	7.35	6.62	6.63	6.87	6.49	5.45	7.85	5.74
MnO	0.17	0.21	0.25	0.21	0.18	0.15	0.18	0.16	0.12	0.22	0.12
MgO	2.66	6.25	5.52	6.01	6.61	3.71	6.26	4.26	2.17	11.12	7.29
CaO	7.20	12.17	12.21	12.27	12.09	9.72	11.74	8.81	7.07	19.23	20.08
Na_2O	12.27	9.76	9.74	4.55	9.80	11.18	10.33	11.05	12.32	5.35	8.58
K_2O	3.67	2.20	1.78	2.44	2.41	3.39	2.26	2.98	3.70	0.33	0.59
P_2O5	0.63	0.25	0.32	0.19	0.13	1.21	0.28	0.02	1.16	0.14	5.58
LOI	1.28	1.42	2.09	3.61	0.63	1.03	0.88	0.72	1.04	1.50	2.33
H_2O-	0.11	0.15	0.20	0.27	0.15	0.14	0.09	0.12	0.15	0.10	0.10
Total	100.65	100.84	100.80	100.54	100.93	99.09	99.65	100.14	100.85	100.35	100.23
Rb	32	28	28	35	46	48	45	47	51	15	18
Ba	81	66	108	583	42	48	31	427	199	20	260
Sr	276	434	378	885	296	408	380	179	254	289	1157
Th	0.0	0.0	0.0	6.0	0.0	0.0	0.0	3.1	0.0	5.8	0.0
U	0.0	0.0	0.0	0.0	0.0	0.0	0.0	0.0	0.0	12	0.0
Zr	88	77	88	89	64	76	70	56	86	111	52
Nb	34	0.0	5.1	0.0	4.7	8.7	3.4	3.4	14	2.6	0.0
Cr	3.4	26	25	25	42	2.8	15	22	-	252	98
V	80	122	90	114	121	73	110	71	44	100	73
Sc	3.6	29	18	22	25	5.8	24	-	-	22	14
Ni	4.2	93	67	111	132	12	109	65	5.8	42	30
Co	17	36	31	33	37	22	34	71	64	35	23
Pb	5.8	37	0.0	7.4	0.0	0.0	0.0	3.3	0.0	62	0.0
Zn	64	66	71	64	61	43	63	52	44	52	39
Cu	13	32	24	31	26	0.0	17	9.0	5.7	2.5	3.0
Y	15	14	11	11	12	17	13	6.1	11	8.9	37
La(x)	12	8.1	9.7	7.2	6.7	21	9.3	0.0	-	0.0	50
Ce(x)	37	19	21	18	17	45	23	0.0	-	12	104
Nd(x)	23	11	12	9.3	10	29	14	0.0	-	9.4	65

(f) Unclassified ijolites ("Others")

	S23	S46	S80	S84	S108	S110	S111	S113	S128	S130
SiO_2	41.83	43.33	43.75	44.69	44.61	43.25	41.96	41.22	44.54	47.61
TiO_2	1.58	1.06	1.27	1.04	1.12	1.55	2.36	1.19	0.99	0.55
Al_2O_3	15.18	17.09	15.52	16.01	18.31	17.69	18.41	18.72	20.36	18.19
Fe_2O_3	13.93	10.14	9.84	10.48	9.70	10.69	10.35	10.39	7.44	9.33
MnO	0.27	0.25	0.26	0.20	0.19	0.21	0.15	0.17	0.16	0.19
MgO	3.70	3.40	3.68	4.02	2.54	1.69	3.00	3.93	2.51	2.27
CaO	10.57	8.45	11.27	8.26	7.67	8.91	9.38	9.71	7.51	5.87
Na_2O	9.27	11.41	9.70	10.59	11.44	11.36	11.04	11.23	12.84	11.93
K_2O	2.28	2.31	2.52	2.37	3.14	2.29	2.41	2.65	2.75	2.52
P_2O5	1.01	0.92	1.26	0.71	0.57	1.60	0.76	1.07	0.61	0.46
LOI	0.05	1.14	0.15	1.29	0.07	1.01	0.16	0.24	0.87	0.92
H_2O-	0.11	0.06	0.08	0.10	0.11	0.12	0.11	0.09	0.07	0.09
Total	99.78	99.56	99.30	99.76	99.47	100.37	100.09	100.61	100.65	99.93
Rb	37	40	42	55	60	50	46	51	47	41
Ba	31	109	17	371	256	113	26	25	35	434
Sr	715	661	698	536	486	614	491	373	445	367
Th	0.0	8.1	0.0	0.0	0.0	0.0	0.0	0.0	0.0	0.0
U	0.0	8.7	0.0	0.0	0.0	0.0	0.0	0.0	0.0	0.0
Zr	107	168	124	117	176	238	119	51	96	210
Nb	9.9	21	20	16	29	50	43	2.7	22	25
Cr	20	0.0	7.9	143	5.5	30	6.3	0.0	4.7	5.7
V	224	156	201	3.3	122	147	208	153	105	99
Sc	8.7	5.6	7.3	7.1	4.3	4.8	12	4.1	3.4	1.7
Ni	12	5.0	6.0	21	2.4	3.0	9.4	4.3	4.5	4.1
Co	40	32	35	33	25	22	43	31	19	17
Pb	0.0	0.0	0.0	0.0	0.0	0.0	0.0	0.0	0.0	0.0
Zn	86	103	59	92	75	99	51	53	54	90
Cu	103	78	93	119	61	21	87	16	45	4.7
Y	19	27	22	19	18	28	19	13	12	13
La(x)	22	21	23	14	13	21	15	11	12	8.6
Ce(x)	51	50	58	35	38	61	39	33	31	21
Nd(x)	29	26	36	19	22	36	25	21	18	10

(g) REE compositions of selected ijolites

(i) Type-I ijolites: fine-grained; coarse; urtite

(ii) Type-II ijolites

	S43	S114	S18	S50	S115	S138	S109	S42	S51	S64	S132	S135	S142
La	15.49	9.07	36.99	17.94	21.47	19.71	17.93	10.86	7.37	8.36	17.29	8.99	8.29
Ce	37.41	25.37	88.51	48.33	45.35	42.73	36.57	25.05	18.65	21.92	44.17	20.76	21.17
Pr	4.95	3.73	11.87	6.70	5.56	5.26	4.41	3.29	2.57	2.68	5.94	2.79	2.67
Nd	20.21	15.88	53.69	29.22	22.97	21.87	16.97	14.32	11.33	11.74	25.48	12.46	11.63
Sm	3.89	3.31	13.38	5.83	4.09	3.77	2.90	2.65	2.00	2.02	4.84	2.25	2.12
Eu	1.10	0.97	4.47	1.69	1.32	1.12	0.89	0.80	0.60	0.70	1.50	0.77	0.73
Gd	3.64	3.34	15.99	5.29	4.11	3.76	2.97	2.84	2.07	2.23	4.59	2.57	2.42
Dy	2.60	2.58	15.67	3.82	2.49	2.83	2.10	2.11	1.45	1.86	3.35	2.25	2.28
Ho	0.51	0.49	3.00	0.74	0.40	0.63	0.46	0.47	0.31	0.44	0.67	0.55	0.53
Er	1.21	1.04	6.66	2.00	0.77	1.71	1.13	1.02	0.64	1.03	1.58	1.44	1.32
Yb	0.75	0.54	2.90	2.25	0.26	1.99	0.65	1.04	0.70	1.60	1.61	1.91	1.61
Lu	0.11	0.08	0.26	0.39	0.04	0.32	0.10	0.20	0.14	0.28	0.28	0.31	0.24

Table B.8: Normative mineralogy calculated for the ijolites from the Spitskop Complex.

(a) Type-I ijolites : fine-grained

	S22	S41	S43	S70	S79	S82	S83	S114	S16	S18	S50	S143	S115	S173
Or	0.00	10.86	0.00	19.09	0.00	0.00	0.00	17.37	4.41	0.00	0.00	0.00	0.00	18.85
Pl	0.00	0.00	0.00	2.82	0.00	0.00	0.00	5.22	0.00	0.00	0.00	0.00	0.00	11.87
Lc	15.15	2.65	17.56	0.00	14.36	11.86	12.42	0.00	9.84	12.46	13.85	18.30	13.25	0.00
Ne	45.34	51.22	49.93	43.49	48.00	49.99	50.35	45.29	38.32	37.75	42.92	41.28	43.12	32.79
Kp	0.00	0.00	0.00	0.00	0.00	0.00	0.00	0.00	0.00	0.00	0.00	0.00	0.00	0.00
Ac	6.40	3.85	4.58	6.75	6.11	5.65	6.00	5.88	6.74	6.12	6.39	5.70	8.16	7.25
Ns	2.33	0.00	3.34	2.41	2.15	1.83	1.62	2.31	1.86	0.81	2.93	4.74	0.84	1.12
Wo	0.00	2.45	0.00	0.00	0.00	0.00	0.00	0.00	0.00	0.00	0.00	0.00	0.00	0.00
Di	24.07	21.68	12.88	20.06	21.55	21.45	19.40	18.28	32.42	21.59	23.50	6.55	10.92	18.52
Ol	0.89	0.00	2.60	1.12	0.65	1.13	1.76	1.64	0.90	3.87	0.78	9.85	10.32	3.75
Cs	0.52	0.00	3.60	0.00	1.36	1.74	2.87	0.00	0.00	7.42	2.50	8.34	7.52	0.00
Mt	0.00	1.21	0.00	0.00	0.00	0.00	0.00	0.00	0.00	0.00	0.00	0.00	0.00	0.00
Cm	0.00	0.00	0.00	0.00	0.04	0.00	0.00	0.00	0.00	0.00	0.00	0.00	0.00	0.01
Il	2.34	3.08	2.15	2.18	2.94	2.37	2.92	1.98	1.25	1.88	2.94	1.20	1.99	1.84
Ap	1.53	0.72	1.11	0.51	1.18	1.39	1.09	0.49	1.88	4.80	1.55	1.83	2.41	0.97
Z	0.04	0.03	0.03	0.05	0.04	0.02	0.03	0.06	0.04	0.04	0.05	0.01	0.01	0.06
Total	98.61	97.75	97.78	98.48	98.38	97.43	98.46	98.52	97.66	96.74	97.41	97.80	98.54	97.03
Pl(Ab)	0.00	0.00	0.00	2.82	0.00	0.00	0.00	5.22	0.00	0.00	0.00	0.00	0.00	11.87
Pl(An)	0.00	0.00	0.00	0.00	0.00	0.00	0.00	0.00	0.00	0.00	0.00	0.00	0.00	0.00
Di(Wo)	11.92	10.73	6.44	9.73	10.67	10.69	9.65	8.99	16.19	10.85	11.65	3.31	5.44	9.07
Di(En)	4.40	3.96	2.79	2.29	3.95	4.43	3.87	2.94	6.86	4.99	4.44	1.64	2.21	2.69
Di(Fs)	7.75	6.98	3.65	8.04	6.94	6.33	5.88	6.35	9.37	5.76	7.40	1.61	3.28	6.76
Ol(Fo)	0.30	0.00	1.06	0.23	0.22	0.44	0.66	0.48	0.36	1.70	0.28	4.73	3.92	0.99
Ol(Fa)	0.59	0.00	1.54	0.89	0.43	0.69	1.10	1.15	0.54	2.16	0.51	5.12	6.41	2.76

(b) Type-I ijolites : coarse-grained (c) Type-I:urtite (d) Type-II ijolites

	S04	S134	S136	S138	S67	S109	S42	S51	S64	S65	S81	S126	S127	S131	S132
Or	0.00	0.00	0.00	0.00	0.00	0.00	0.00	0.00	0.00	4.66	0.00	0.00	0.00	18.32	0.00
Pl	0.00	0.00	0.00	0.00	0.00	0.00	0.00	0.00	0.00	29.77	0.00	0.00	0.00	36.65	0.00
Lc	15.15	13.11	14.09	14.97	7.20	7.05	12.00	21.11	13.25	3.43	16.31	15.71	11.63	0.00	17.01
Ne	47.85	47.17	48.73	50.47	67.60	73.65	43.29	50.36	39.27	11.05	47.09	47.73	37.99	12.77	49.20
Kp	0.00	0.00	0.00	0.00	8.65	8.66	0.00	0.08	0.00	0.00	0.00	0.00	0.00	0.00	0.00
Ac	4.33	3.23	3.88	4.34	1.04	1.29	4.62	3.63	5.18	0.00	2.91	4.26	5.26	0.00	4.84
Ns	2.19	2.81	2.87	4.46	2.90	1.73	2.08	2.57	1.14	0.00	4.09	1.37	2.24	0.00	1.75
Wo	0.00	0.00	0.00	0.00	0.00	0.00	0.00	0.00	0.00	3.82	0.00	0.00	0.00	0.00	0.00
Di	16.87	17.79	14.55	9.47	0.00	0.00	15.62	0.00	27.68	38.77	11.66	14.57	26.02	11.47	12.60
Ol	3.14	1.27	3.19	6.10	1.62	2.26	9.38	9.00	4.84	0.00	6.69	4.96	4.41	7.93	4.94
Cs	6.19	8.39	7.31	5.77	3.99	1.11	8.83	9.59	5.74	0.00	7.08	3.81	2.34	0.00	5.09
Mt	0.00	0.00	0.00	0.00	0.00	0.00	0.00	0.00	0.00	2.48	0.00	0.00	0.00	3.37	0.00
Cm	0.00	0.00	0.00	0.00	0.00	0.00	0.01	0.00	0.00	0.00	0.00	0.00	0.00	0.00	0.00
Il	0.36	0.19	0.40	0.30	0.06	0.13	0.89	0.80	0.47	0.36	0.51	0.42	0.63	1.82	1.92
Ap	0.72	2.48	2.55	1.88	3.31	2.66	2.13	1.76	0.58	0.60	2.57	6.23	9.15	1.95	1.46
Z	0.02	0.02	0.01	0.02	0.01	0.00	0.02	0.01	0.02	0.01	0.01	0.01	0.02	0.04	0.02
Total	96.82	96.46	97.58	97.78	96.38	98.54	98.87	98.91	98.17	94.95	98.92	99.07	99.69	94.32	98.83
Pl(Ab)	0.00	0.00	0.00	0.00	0.00	0.00	0.00	0.00	0.00	0.00	0.00	0.00	0.00	15.52	0.00
Pl(An)	0.00	0.00	0.00	0.00	0.00	0.00	0.00	0.00	0.00	29.77	0.00	0.00	0.00	21.13	0.00
Di(Wo)	8.46	8.98	7.31	4.76	0.00	0.00	8.06	0.00	14.14	19.94	6.04	7.38	13.25	5.82	6.37
Di(En)	3.84	4.41	3.42	2.19	0.00	0.00	5.05	0.00	8.02	12.15	3.98	3.79	7.27	3.08	3.19
Di(Fs)	4.57	4.40	3.82	2.52	0.00	0.00	2.51	0.00	5.52	6.68	1.63	3.40	5.49	2.57	3.05
Ol(Fo)	1.36	0.61	1.43	2.69	0.28	0.77	6.06	4.90	2.75	0.00	4.61	2.49	2.41	4.13	2.41
Ol(Fa)	1.78	0.67	1.76	3.41	1.34	1.49	3.32	4.10	2.09	0.00	2.08	2.46	2.00	3.80	2.53

Type-II ijolites (contd.)

(e) Unclassified ijolites ("Others")

	S135	S137	S139	S142	S144	S145	S157	S158	S23	S46	S80	S84	S108	S110	S111
Or	0.00	0.00	14.42	0.00	0.00	0.00	0.00	0.00	0.00	0.00	0.00	0.00	0.00	0.00	0.00
Pl	0.00	0.00	20.20	0.00	0.00	0.00	0.00	0.00	0.00	0.00	0.00	0.00	0.00	0.00	0.00
Lc	10.19	8.25	0.00	11.17	15.71	10.47	13.81	17.14	10.56	10.70	11.68	10.98	14.55	10.61	11.17
Ne	33.88	32.05	18.39	34.33	38.12	31.47	45.46	55.21	35.42	40.65	35.65	37.46	41.55	42.39	44.03
Kp	0.00	0.00	0.00	0.00	0.00	0.00	0.00	0.00	0.00	0.00	0.00	0.00	0.00	0.00	0.00
Ac	5.79	6.62	0.00	5.07	5.08	5.26	4.97	2.05	10.67	7.76	7.53	8.02	7.43	8.19	7.93
Ns	3.14	3.66	0.00	3.21	4.30	5.43	0.92	0.00	0.22	2.95	1.80	2.64	2.72	2.00	0.73
Wo	0.00	0.00	0.00	0.00	0.00	0.00	0.00	0.00	0.00	0.00	0.00	0.00	0.00	0.00	0.00
Di	31.90	38.45	35.92	34.12	21.39	36.22	23.72	14.22	16.58	22.37	27.54	29.93	22.77	26.99	15.09
Ol	6.70	3.90	3.57	5.77	4.42	4.62	5.04	2.89	11.68	6.17	4.29	4.80	3.84	0.93	6.59
Cs	6.09	3.63	0.00	5.28	4.46	3.68	4.57	3.23	8.16	2.89	4.57	0.17	2.31	0.72	7.31
Mt	0.00	0.00	2.82	0.00	0.00	0.00	0.00	1.06	0.00	0.00	0.00	0.00	0.00	0.00	0.00
Cm	0.01	0.01	0.01	0.01	0.00	0.00	0.00	0.00	0.00	0.00	0.00	0.03	0.00	0.01	0.00
Il	0.47	0.61	0.46	0.44	1.18	0.40	0.32	0.78	3.00	2.01	2.41	1.98	2.13	2.94	4.48
Ap	0.58	0.74	0.44	0.30	2.80	0.65	0.05	2.69	2.34	2.13	2.92	1.65	1.32	3.71	1.76
Z	0.02	0.02	0.02	0.01	0.02	0.01	0.01	0.02	0.02	0.03	0.02	0.02	0.04	0.05	0.02
Total	98.77	97.94	96.25	99.71	97.48	98.21	98.87	99.29	98.65	97.66	98.41	97.68	98.66	98.54	99.11
Pl(Ab)	0.00	0.00	4.56	0.00	0.00	0.00	0.00	0.00	0.00	0.00	0.00	0.00	0.00	0.00	0.00
Pl(An)	0.00	0.00	15.65	0.00	0.00	0.00	0.00	0.00	0.00	0.00	0.00	0.00	0.00	0.00	0.00
Di(Wo)	16.37	19.58	18.53	17.61	10.88	18.64	12.08	7.17	8.24	11.19	13.84	15.04	11.30	13.21	7.57
Di(En)	9.77	10.72	11.66	11.10	5.87	11.44	6.66	3.47	3.20	4.86	6.44	6.97	4.37	3.86	3.42
Di(Fs)	5.76	8.15	5.72	5.41	4.64	6.14	4.97	3.58	5.15	6.33	7.26	7.92	7.10	9.92	4.10
Ol(Fo)	4.06	2.12	2.32	3.76	2.36	2.91	2.77	1.35	4.21	2.53	1.91	2.13	1.37	0.24	2.84
Ol(Fa)	2.64	1.78	1.25	2.02	2.06	1.72	2.27	1.54	7.47	3.64	2.38	2.67	2.46	0.69	3.75

Table B.9: Comparison of Spitskop ijolites with ijolites and nephelinites from other alkaline complexes.

	Spitskop Type-I Ijolite (Mean±σ)		Nephelinites			Ijolites						
			LB3	LB4	LMAv	LB1	LB2	W&J1	B7	N23	N123	Kh-11
SiO_2	44.68	±2.3	41.52	47.01	40.60	42.66	40.01	42.30	45.49	42.80	40.94	49.92
TiO_2	1.17	±0.32	2.98	1.22	2.66	1.52	2.38	0.65	0.41	1.82	0.68	2.31
Al_2O_3	19.45	±1.7	10.78	17.53	14.33	16.58	15.25	14.70	11.99	19.08	25.42	21.90
Fe_2O_3	8.21	±1.1	7.95	4.80	5.48	6.45	6.61	4.90	7.08	4.46	4.70	4.00
FeO	-		6.11	2.80	6.17	3.49	3.39	1.19	6.46	5.84	1.02	3.04
MnO	0.20	±0.05	0.23	0.24	0.26	0.25	0.16	0.33	0.35	0.20	0.07	0.19
MgO	2.10	±0.71	7.53	1.65	6.39	2.85	3.50	0.83	3.82	2.08	0.24	1.64
CaO	7.25	±2.1	13.74	6.91	11.89	11.53	16.36	20.82	12.32	11.99	8.41	4.88
Na_2O	11.67	±1.1	3.28	8.68	4.79	8.09	7.10	5.50	5.45	7.73	12.92	10.42
K_2O	3.04	±0.43	1.73	4.36	3.46	3.03	3.10	3.95	1.35	3.17	5.31	5.19
P_2O_5	0.66	±0.47	0.73	0.36	1.07	0.65	0.88	0.82	0.16	0.25	0.64	0.62
LOI	1.10	±0.64	2.80	3.32	2.25	2.58	1.20	3.70	3.95	0.68	0.25	0.74
H_2O-	0.12	±0.06	0.45	1.03	0.54	0.17	0.07	0.10	0.00	0.00	0.00	0.00
Total	99.66		99.83	99.91	99.89	99.85	100.01	99.79	98.83	100.10	100.60	104.85

Nephelinites:
LB3, LB4 : average mela-nephelinite and nephelinite from East Africa (Le Bas, 1977); LmAv: average nephelinite (Le Maitre, 1976).

Ijolites:
LB1, LB2 : average East African micro-ijolite and ijolite (Le Bas, 1977);
W&J1: average Chilwa Island ijolite (Woolley and Jones, 1987); B7: ijolite from Budeda Complex (King and Sutherland, 1966);
N23, N123: ijolite and urtite from Napak Complex (King and Sutherland, 1966);
Kh-11: ijolite-urtite from the Khibina Complex (Gerasimovsky et al., 1974).

Table B.10: Whole rock analyses of nepheline syenites from Spitskop.

Rietfontein Nepheline Syenite Sheet

	S01	S02	S03	S12	S13	S14	S30	S31	S32	S38	S151	S152	S153	S154	S155	S156	S187	S187V	S188
SiO_2	53.13	55.52	50.24	55.75	51.32	51.25	54.24	50.31	52.23	53.80	53.99	50.63	56.22	52.66	54.41	52.99	51.49	53.29	54.16
TiO_2	0.65	0.54	0.51	0.27	0.42	0.44	0.38	0.88	0.43	0.42	0.52	0.55	0.60	0.33	0.40	0.75	0.39	0.01	0.30
Al_2O_3	17.36	16.99	18.15	17.42	19.66	19.41	18.60	19.29	19.16	20.79	17.60	15.94	16.68	19.35	18.44	16.89	18.00	21.89	19.04
Fe_2O_3	7.29	6.18	7.26	6.28	6.20	6.77	6.53	7.44	7.28	4.62	7.94	6.62	7.10	5.99	6.50	8.82	7.01	0.46	4.71
MnO	0.26	0.15	0.32	0.12	0.15	0.12	0.22	0.27	0.20	0.12	0.11	0.20	0.22	0.13	0.13	0.19	0.19	0.03	0.17
MgO	0.26	0.11	0.32	0.12	0.25	0.48	0.16	1.75	0.23	0.34	0.31	0.51	0.30	0.42	0.23	0.32	0.20	0.00	0.14
CaO	2.16	1.12	2.62	1.84	2.22	2.42	1.59	3.65	1.72	1.88	0.46	3.47	0.80	1.87	1.05	0.94	1.65	0.90	1.40
Na_2O	11.75	10.64	11.99	10.39	11.45	10.78	11.22	12.07	11.71	11.79	12.95	12.57	10.74	11.64	10.46	11.18	12.17	12.67	11.37
K_2O	3.79	4.02	3.38	4.69	4.55	4.50	4.13	2.95	3.94	4.03	2.82	3.90	2.91	4.81	5.01	3.59	4.32	5.03	4.99
P_2O_5	0.09	0.05	0.09	0.02	0.04	0.02	0.03	0.53	0.02	0.00	0.04	0.05	0.00	0.02	0.07	0.02	0.02	0.02	0.04
LOI	2.85	4.03	4.20	3.07	2.87	3.14	2.56	0.80	2.12	1.80	2.82	4.63	3.30	2.41	3.26	2.46	3.32	5.38	3.68
H_2O-	0.21	0.22	0.34	0.14	0.22	0.23	0.10	0.07	0.14	0.13	0.12	0.16	0.18	0.13	0.12	0.15	0.19	0.70	0.08
Total	99.80	99.57	99.42	100.11	99.35	99.56	99.76	100.01	99.18	99.72	99.68	99.23	99.05	99.76	100.08	98.30	98.95	100.38	100.08
Rb	120	124	91	100	91	88	114	70	94	70	82	95	89	104	129	112	102	113	113
Ba	1065	823	1255	1876	1823	1719	871	703	883	1752	988	1330	395	1472	743	403	1343	1268	2208
Sr	494	581	827	861	839	857	611	775	474	865	873	999	447	808	703	316	648	977	1002
Th	6.5	5.4	8.3	6.4	5.5	0.0	5.5	12	0.0	0.0	0.0	0.0	6.5	0.0	0.0	0.0	10	0.0	0.0
U	6.5	6.9	6.4	7.7	3.2	0.0	8.1	7.1	0.0	0.0	0.0	0.0	5.9	0.0	0.0	0.0	0.0	0.0	0.0
Zr	447	450	191	159	161	117	195	282	152	90	158	361	1268	124	172	467	1124	733	164
Nb	21	15	21	5.1	17	10	7.5	50	8.8	10	19	47	59	7.9	0.0	20	58	53	36
Cr	0.0	0.0	0.0	0.0	0.0	0.0	0.0	0.0	0.0	0.0	0.0	3.0	0.0	0.0	0.0	1.9	25	0.0	16
V	41	8.5	55	38	67	77	37	91	50	34	71	40	4.5	48	14	17	40	0.0	35
Sc	0.0	0.0	0.0	55	0.0	0.9	0.0	2.1	0.0	0.0	0.0	0.0	0.0	0.0	0.0	0.0	0.0	0.0	0.0
Ni	0.0	0.0	0.0	0.0	0.0	0.0	0.0	0.0	0.0	0.0	0.0	0.0	0.0	0.0	0.0	0.0	2.0	5.0	0.0
Co	5.8	2.5	5.9	3.9	5.9	4.7	4.2	16	5.0	3.1	7.8	7.5	7.5	5.8	4.9	7.6	74	5.0	5.0
Pb	36	17	21	10	6.8	0.0	15	15	15	0.0	0.0	0.0	12	0.0	0.0	6.4	12	0.0	28
Zn	95	114	153	0.0	63	51	75	146	87	29	78	138	131	56	71	74	114	118	187
Cu	0.0	0.0	0.0	0.0	0.0	0.0	0.0	3.2	0.0	0.0	0.0	0.0	0.0	0.0	0.0	0.0	7.0	6.0	5.0
Y	72	33	48	6.8	5.2	3.5	32	34	20	4.0	19	14	75	5.0	7.5	30	43	26	25
La(x)	0.0	3.2	4.2	0.0	0.0	2.6	0.0	29	0.0	3.1	4.2	2.8	13	2.6	0.0	0.0	-	-	-
Ce(x)	10	11	14	0.0	7.5	9.6	0.0	50	0.0	9.0	15	13	31	9.0	6.4	13	-	-	-
Nd(x)	7.1	6.8	12	0.0	4.2	6.6	3.3	21	0.0	7.0	8.9	7.5	16	5.8	4.4	8.0	-	-	-

Rietfontein Nepheline Syenite Sheet (contd.)

	S189	S186.a1	S186.a2	S186.b1	186.b2	S186.c
SiO_2	53.29	52.60	53.31	53.92	53.28	55.14
TiO_2	0.26	0.43	0.38	0.35	0.36	0.27
Al_2O_3	19.31	18.99	19.23	19.21	19.42	19.35
Fe_2O_3	5.52	6.99	6.52	6.75	6.69	5.29
MnO	0.11	0.15	0.14	0.14	0.15	0.13
MgO	0.09	0.39	0.34	0.34	0.33	0.27
CaO	1.37	1.74	1.68	1.54	1.58	1.25
Na_2O	11.18	11.18	12.06	10.66	11.28	10.51
K_2O	5.56	5.33	3.92	5.52	5.01	5.84
P_2O_5	0.00	0.04	0.05	0.05	0.04	0.00
LOI	3.24	1.30	1.41	0.98	1.39	1.41
H_2O-	0.05	0.16	0.25	0.11	0.16	0.18
Total	99.98	99.30	99.29	99.57	99.69	99.64
Rb	123	114	102	115	108	129
Ba	1328	1410	1424	1325	1484	1989
Sr	865	418	573	340	487	514
Th	0.0	0.0	0.0	0.0	0.0	0.0
U	0.0	0.0	0.0	0.0	6.0	6.0
Zr	97	116	104	109	103	83
Nb	9.0	10	6.0	7.0	70	5.0
Cr	45	16	0.0	0.0	0.0	0.0
V	37	88	69	63	65	51
Sc	9.0	4.4	9.0	4.6	0.0	4.6
Ni	0.0	0.0	0.0	0.0	0.0	0.0
Co	6.0	94	74	41	51	56
Pb	19	0.0	0.0	0.0	0.0	11
Zn	66	70	62	65	65	58
Cu	8.0	6.0	5.0	6.0	5.0	6.0
Y	7.0	17	19	14	15	15
La(x)	-	-	-	-	-	-
Ce(x)	-	-	-	-	-	-
Nd(x)	-	-	-	-	-	-

	Mare Nepheline Syenite Sheet									Spitskop Nepheline Syenite Sheet				
	S07	S08	S96	S97	S102	S147	S148	S149	S150	S10	S11	S17	S19	S141
SiO_2	54.28	51.79	56.55	54.31	55.34	53.67	53.24	54.66	54.33	52.09	55.56	54.72	54.80	52.48
TiO_2	0.54	0.74	0.38	0.32	0.39	0.57	0.46	0.42	0.37	0.63	0.31	0.31	0.35	0.66
Al_2O_3	20.81	21.40	19.07	21.01	18.76	20.80	21.08	17.95	18.51	21.33	19.18	19.63	18.90	20.78
Fe_2O_3	5.25	4.90	6.69	5.23	4.76	5.28	4.44	6.50	6.73	4.88	5.22	5.51	6.04	5.02
MnO	0.14	0.13	0.08	0.09	0.10	0.09	0.11	0.10	0.11	0.15	0.20	0.12	0.13	0.08
MgO	0.34	0.63	0.26	0.43	0.37	0.55	0.67	0.34	0.29	0.44	0.20	0.06	0.08	0.64
CaO	1.93	2.68	1.04	1.51	2.70	1.71	1.84	1.42	0.52	2.38	1.35	0.93	0.75	1.98
Na_2O	9.98	11.36	11.39	11.90	10.42	11.54	10.77	11.09	10.36	11.71	9.99	9.72	11.17	11.51
K_2O	4.96	4.52	3.15	3.95	4.57	3.77	5.22	4.15	5.00	4.59	4.92	6.24	4.26	5.02
P_2O_5	0.07	0.18	0.00	0.05	0.08	0.09	0.07	0.03	0.01	0.13	0.03	0.00	0.00	0.12
LOI	2.07	1.02	0.46	1.36	1.63	1.81	0.70	0.68	2.30	1.06	3.17	1.66	3.07	1.27
H_2O-	0.14	0.12	0.08	0.10	0.11	0.14	0.10	0.10	0.16	0.13	0.26	0.13	0.14	0.11
Total	100.51	99.47	99.15	100.26	99.23	100.02	98.70	97.44	98.69	99.52	100.39	99.03	99.69	99.67
Rb	86	100	89	114	87	89	113	94	115	94	112	148	129	102
Ba	1500	1666	388	351	1458	949	1720	930	1485	1446	964	1012	190	1800
Sr	591	626	198	394	712	624	617	446	628	518	863	573	531	713
Th	4.7	7.1	0.0	0.0	0.0	0.0	0.0	0.0	0.0	8.6	11	4.4	5.7	0.0
U	0.0	8.2	0.0	0.0	0.0	0.0	0.0	0.0	0.0	7.8	0.0	6.8	5.1	0.0
Zr	115	164	162	335	315	154	132	134	136	150	252	150	207	123
Nb	18	25	3.4	5.6	29	14	19	10	31	26	35	5.4	8.0	22
Cr	0.0	0.0	0.0	0.0	0.0	0.0	0.0	0.0	1.8	0.0	0.0	0.0	0.0	0.0
V	51	62	30	17	36	42	49	0.0	40	58	33	36	18	44
Sc	0.0	0.0	0.0	0.0	0.0	0.0	0.0	0.0	0.0	0.0	0.0	0.0	0.0	0.0
Ni	0.0	0.0	0.0	0.0	0.0	0.0	0.0	0.0	0.0	0.0	0.0	0.0	0.0	0.0
Co	4.1	7.6	8.4	6.2	3.8	7.9	9.3	0.0	6.8	7.7	2.7	3.9	3.2	6.6
Pb	24	12	0.0	0.0	0.0	22	0.0	0.0	18	18	35	9.8	8.4	6.2
Zn	48	37	43	43	55	34	30	0.0	65	53	137	36	46	55
Cu	1.4	0.0	0.0	0.0	0.0	0.0	0.0	0.0	9.5	0.0	0.0	0.0	0.0	0.0
Y	12	12	4.7	17	5.0	10	9.3	5.8	16	7.9	23	4.1	4.8	16
La(x)	13	13	3.7	0.0	0.0	7.9	11	4.0	15	17	44	0.0	3.8	17
Ce(x)	25	27	14	6.8	7.4	21	25	11	28	25	79	0.0	0.0	36
Nd(x)	11	14	5.6	3.3	3.2	10	15	6.1	13	11	31	0.0	0.0	19

"Eastern" Nepheline Syenite Sheet

	S68	S105	S106	S179	S179V
SiO_2	56.89	49.40	54.81	58.13	46.05
TiO_2	0.60	0.61	0.61	0.42	0.02
Al_2O_3	17.44	19.06	19.32	18.08	27.58
Fe_2O_3	7.39	8.09	5.09	6.79	0.51
MnO	0.20	0.18	0.12	0.11	0.03
MgO	0.22	0.50	0.69	0.07	0.00
CaO	0.46	2.98	1.90	0.56	0.29
Na_2O	10.89	12.13	10.54	12.71	16.23
K_2O	2.72	3.52	4.77	1.42	2.27
P_2O_5	0.01	0.08	0.11	0.00	0.00
LOI	1.94	1.10	2.33	1.85	7.29
H_2O-	0.16	0.11	0.19	0.07	0.12
Total	98.92	97.76	100.48	100.21	100.39
Rb	103	114	195	54	74
Ba	55	65	212	83	119
Sr	219	194	362	256	951
Th	8.2	0.0	0.0	0.0	0.0
U	7.2	0.0	0.0	0.0	0.0
Zr	678	385	300	757	1561
Nb	38	19	23	29	19
Cr	0.0	2.2	0.0	14	45
V	0.0	4.4	12	30	0.0
Sc	179	0.0	0.0	0.0	0.0
Ni	0.0	0.0	0.0	0.0	0.0
Co	5.0	8.1	7.2	0.0	4.0
Pb	51	9.2	5.5	9.0	20
Zn	0.0	68	87	41	78
Cu	0.0	0.0	0.0	0.0	3.0
Y	29	14	7.6	28	99
La(x)	27	8.7	2.2	-	-
Ce(x)	45	20	7.1	-	-
Nd(x)	17	7.5	3.8	-	-

Note: (1) Samples suffixed with "V" refer to feldspathic veins extracted from the nepheline syenite.
(2) La(x),Ce(x) and Nd(x) were measured by XRF.

Rare Earth Element Analyses of samples from the Rietfontein Nepheline Syenite Sheet

	S01	S02	S03	S12	S13	S151	S154
La	5.7	6.9	8.1	3.3	4.1	6.4	3.4
Ce	15	15	21	6.6	11	22	9.1
Pr	2.3	2.3	3.0	0.0	1.7	2.3	1.3
Nd	11	9.3	14	3.9	7.0	10	5.3
Sm	3.4	2.2	3.8	0.6	1.2	1.9	0.7
Eu	1.4	0.9	1.4	0.3	0.4	0.6	0.3
Gd	5.8	3.4	5.2	1.1	1.5	2.5	1.0
Dy	10	4.8	7.0	1.5	1.7	3.0	1.0
Ho	2.7	1.4	1.7	0.4	0.4	0.8	0.3
Er	9.3	4.4	5.6	1.4	1.0	2.1	0.7
Yb	9.6	5.2	6.0	2.4	1.6	3.0	1.3
Lu	1.2	0.7	0.8	0.3	0.3	0.5	0.3

Table B.11: CIPW normative mineralogy calculated for nepheline syenites from Spitskop.

CIPW normative mineralogy of nepheline syenites.
(a) Rietfontein sheet

	S01	S02	S03	S12	S13	S14	S30	S31	S32	S38	S151	S152	S153	S154	S155	S156	S187	S188	S189
Or	22.40	23.76	19.97	27.71	26.89	26.59	24.41	17.43	23.28	23.81	16.66	23.05	17.20	28.42	29.61	21.21	25.53	29.49	32.86
Pl	25.07	36.71	18.18	29.35	14.30	14.37	27.40	15.97	21.06	24.16	35.63	14.48	45.47	16.55	25.56	30.06	17.70	23.23	16.53
Ne	23.36	15.33	30.53	18.50	33.31	32.73	24.53	36.20	30.10	32.69	21.23	24.81	13.07	30.44	22.42	19.95	27.54	25.42	28.08
Kp	0.00	0.00	0.00	0.00	0.00	0.00	0.00	0.00	0.00	0.00	0.00	0.00	0.00	0.00	0.00	0.00	0.00	0.00	0.00
Ac	6.54	5.55	6.52	5.64	5.57	6.08	5.86	6.68	6.54	4.15	7.13	5.94	6.37	5.38	5.84	7.92	6.29	4.23	4.96
Ns	5.54	4.36	4.54	4.20	3.44	2.22	3.63	2.74	3.50	2.46	6.20	9.16	3.27	4.57	3.47	4.36	6.35	4.95	4.80
Wo	0.00	0.00	0.00	0.00	0.00	0.00	0.00	0.00	0.00	0.00	0.00	0.00	0.00	0.00	0.00	0.00	0.00	0.00	0.00
Di	9.25	4.94	11.36	8.55	10.01	10.89	7.13	12.67	7.70	8.67	2.20	15.20	3.68	8.46	4.51	4.15	7.53	6.57	6.51
Hy	0.00	0.00	0.00	0.00	0.00	0.00	0.00	0.00	0.00	0.00	0.00	0.00	0.00	0.00	0.00	0.00	0.00	0.00	0.00
Ol	2.69	3.15	2.19	2.09	1.54	2.08	2.97	4.10	3.44	0.86	6.14	0.28	4.84	2.41	3.98	5.97	3.24	1.59	2.19
Mt	0.00	0.00	0.00	0.00	0.00	0.00	0.00	0.00	0.00	0.00	0.00	0.00	0.00	0.00	0.00	0.00	0.00	0.00	0.00
Il	1.23	1.03	0.97	0.51	0.80	0.84	0.72	1.67	0.82	0.80	0.99	1.04	1.14	0.63	0.76	1.42	0.74	0.57	0.49
Hm	0.00	0.00	0.00	0.00	0.00	0.00	0.00	0.00	0.00	0.00	0.00	0.00	0.00	0.00	0.00	0.00	0.00	0.00	0.00
Ap	0.21	0.12	0.21	0.05	0.09	0.05	0.07	1.23	0.05	0.00	0.09	0.12	0.00	0.05	0.16	0.05	0.05	0.09	0.00
Total	96.29	94.95	94.47	96.60	95.95	95.85	96.72	98.69	96.49	97.60	96.27	94.08	95.04	96.91	96.31	95.09	94.97	96.14	96.42
Pl(Ab)	25.07	36.71	18.18	29.35	14.30	14.37	27.40	15.97	21.06	24.16	35.63	14.48	45.47	16.55	25.56	30.06	17.70	23.23	16.53
Pl(An)	0.00	0.00	0.00	0.00	0.00	0.00	0.00	0.00	0.00	0.00	0.00	0.00	0.00	0.00	0.00	0.00	0.00	0.00	0.00
Di(Wo)	4.38	2.33	5.40	4.03	4.75	5.22	3.37	6.28	3.65	4.16	1.04	7.30	1.75	4.05	2.14	1.97	3.56	3.11	3.06
Di(En)	0.38	0.11	0.54	0.19	0.45	0.81	0.20	2.34	0.27	0.68	0.10	1.21	0.17	0.61	0.18	0.17	0.24	0.22	0.12
Di(Fs)	4.48	2.51	5.42	4.33	4.81	4.87	3.56	4.05	3.78	3.83	1.06	6.69	1.76	3.80	2.19	2.01	3.73	3.25	3.32
Hy(En)	0.00	0.00	0.00	0.00	0.00	0.00	0.00	0.00	0.00	0.00	0.00	0.00	0.00	0.00	0.00	0.00	0.00	0.00	0.00
Hy(Fs)	0.00	0.00	0.00	0.00	0.00	0.00	0.00	0.00	0.00	0.00	0.00	0.00	0.00	0.00	0.00	0.00	0.00	0.00	0.00
Ol(Fo)	0.19	0.12	0.18	0.08	0.12	0.27	0.14	1.41	0.21	0.12	0.47	0.04	0.40	0.31	0.28	0.44	0.18	0.09	0.07
Ol(Fa)	2.50	3.03	2.01	2.01	1.42	1.81	2.83	2.69	3.22	0.74	5.67	0.24	4.44	2.10	3.70	5.53	3.06	1.50	2.12

Rietfontein sheet (contd.)

(b) Mare

	S187V	S186.a1	S186.a2	S186.b1	S186.b2	S186.c	S07	S08	S96	S97	S102	S147	S148	S149	S150
Or	29.72	31.50	23.16	32.62	29.61	34.51	29.31	26.71	18.61	23.34	27.01	22.28	30.85	24.52	29.55
Pl	23.04	13.67	23.76	17.17	17.59	20.39	22.31	13.98	40.00	26.10	26.66	26.31	16.71	29.81	26.67
Ne	33.34	29.43	28.89	27.58	29.47	25.26	30.94	38.42	21.97	32.49	24.05	32.34	33.95	21.35	22.05
Kp	0.00	0.00	0.00	0.00	0.00	0.00	0.00	0.00	0.00	0.00	0.00	0.00	0.00	0.00	0.00
Ac	0.41	6.28	5.85	6.06	6.01	4.75	4.42	4.40	6.01	4.70	4.27	4.74	3.99	5.84	6.04
Ns	5.16	4.53	4.26	3.55	3.87	3.85	0.00	1.45	2.10	2.16	2.86	1.46	1.69	4.19	3.13
Wo	1.59	0.00	0.00	0.00	0.00	0.00	0.00	0.00	0.00	0.00	0.15	0.00	0.00	0.00	0.00
Di	0.98	7.69	7.43	6.74	7.05	5.93	8.38	10.84	4.66	6.40	11.33	7.15	7.88	6.29	2.65
Hy	0.00	0.00	0.00	0.00	0.00	0.00	0.00	0.00	0.00	0.00	0.00	0.00	0.00	0.00	0.00
Ol	0.00	3.42	3.07	3.59	3.40	2.59	1.33	0.46	4.09	2.55	0.00	2.21	1.62	3.41	5.05
Mt	0.00	0.00	0.00	0.00	0.00	0.00	0.14	0.00	0.00	0.00	0.00	0.00	0.00	0.00	0.00
Il	0.02	0.82	0.72	0.66	0.68	0.51	1.03	1.41	0.72	0.61	0.74	1.08	0.87	0.80	0.70
Hm	0.00	0.00	0.00	0.00	0.00	0.00	0.00	0.00	0.00	0.00	0.00	0.00	0.00	0.00	0.00
Ap	0.05	0.09	0.12	0.12	0.09	0.00	0.16	0.42	0.00	0.12	0.19	0.21	0.16	0.07	0.02
Total	94.31	97.43	97.26	98.09	97.77	97.79	98.02	98.09	98.16	98.47	97.26	97.78	97.72	96.28	95.86
Pl(Ab)	23.04	13.67	23.76	17.17	17.59	20.39	22.31	13.98	40.00	26.10	26.66	26.31	16.71	29.81	26.67
Pl(An)	0.00	0.00	0.00	0.00	0.00	0.00	0.00	0.00	0.00	0.00	0.00	0.00	0.00	0.00	0.00
Di(Wo)	0.46	3.67	3.54	3.21	3.35	2.83	4.01	5.28	2.21	3.07	5.44	3.46	3.85	3.00	1.26
Di(En)	0.00	0.46	0.42	0.36	0.37	0.32	0.60	1.41	0.20	0.53	0.92	0.76	1.09	0.36	0.13
Di(Fs)	0.52	3.56	3.47	3.17	3.32	2.79	3.76	4.14	2.25	2.79	4.97	2.92	2.94	2.93	1.26
Hy(En)	0.00	0.00	0.00	0.00	0.00	0.00	0.00	0.00	0.00	0.00	0.00	0.00	0.00	0.00	0.00
Hy(Fs)	0.00	0.00	0.00	0.00	0.00	0.00	0.00	0.00	0.00	0.00	0.00	0.00	0.00	0.00	0.00
Ol(Fo)	0.00	0.36	0.30	0.34	0.31	0.25	0.17	0.11	0.31	0.38	0.00	0.42	0.41	0.34	0.42
Ol(Fa)	0.00	3.07	2.77	3.25	3.08	2.35	1.16	0.35	3.78	2.17	0.00	1.79	1.21	3.06	4.63

	(c) Spitskop					(d) "Eastern" sheet				
	S10	S11	S17	S19	S141	S68	S105	S106	S179	S179V
Or	27.12	29.07	36.87	25.17	29.66	16.07	20.80	28.19	8.39	13.41
Pl	14.60	29.04	19.34	31.20	14.44	48.14	11.70	25.45	55.78	12.85
Ne	37.68	22.87	25.40	22.92	34.94	14.31	36.16	25.66	15.88	63.04
Kp	0.00	0.00	0.00	0.00	0.00	0.00	0.00	0.00	0.00	0.00
Ac	4.38	4.69	4.95	5.42	4.51	6.63	7.26	4.57	6.10	0.46
Ns	2.32	1.85	2.42	3.46	3.11	2.34	3.71	2.60	3.62	1.77
Wo	0.00	0.00	0.00	0.00	0.00	0.00	0.00	0.00	0.00	0.21
Di	9.88	6.14	4.44	3.49	8.25	2.03	12.52	7.59	2.55	1.12
Hy	0.00	0.00	0.00	0.00	0.00	0.00	0.00	0.00	0.00	0.00
Ol	0.59	2.36	2.92	3.77	1.61	5.59	2.48	2.14	4.68	0.00
Mt	0.00	0.00	0.00	0.00	0.00	0.00	0.00	0.00	0.00	0.00
Il	1.20	0.59	0.59	0.66	1.25	1.14	1.16	1.16	0.80	0.04
Hm	0.00	0.00	0.00	0.00	0.00	0.00	0.00	0.00	0.00	0.00
Ap	0.30	0.07	0.00	0.00	0.28	0.02	0.19	0.25	0.00	0.00
Total	98.07	96.68	96.93	96.09	98.05	96.27	95.98	97.61	97.80	92.90
Pl(Ab)	14.60	29.04	19.34	31.20	14.44	48.14	11.70	25.45	55.78	12.85
Pl(An)	0.00	0.00	0.00	0.00	0.00	0.00	0.00	0.00	0.00	0.00
Di(Wo)	4.77	2.91	2.09	1.64	4.02	0.96	5.99	3.70	1.20	0.53
Di(En)	0.95	0.25	0.06	0.05	1.06	0.07	0.83	0.99	0.03	0.00
Di(Fs)	4.16	2.97	2.30	1.79	3.17	1.00	5.71	2.90	1.32	0.60
Hy(En)	0.00	0.00	0.00	0.00	0.00	0.00	0.00	0.00	0.00	0.00
Hy(Fs)	0.00	0.00	0.00	0.00	0.00	0.00	0.00	0.00	0.00	0.00
Ol(Fo)	0.10	0.17	0.06	0.10	0.38	0.33	0.29	0.51	0.10	0.00
Ol(Fa)	0.49	2.19	2.85	3.67	1.24	5.26	2.19	1.64	4.58	0.00

Table B.12: Comparison of mean Spitskop Nepheline Syenite with world averages and selected nepheline syenites and averages from East Africa.

	Mean Spitskop Ne.Sy	1 Mean East African	2 Mean Neph. Syenite	3 Mean Phono-lite	4 MtK4	5 MtK9	6 MtK8	7 MtK11	8 WJ-36	9 WJ-44
SiO_2	55.22	55.41	56.10	57.43	53.19	53.90	55.23	57.09	53.84	57.17
TiO_2	0.48	0.52	0.61	0.63	1.46	0.86	0.80	1.17	0.42	0.00
Al_2O_3	19.54	20.79	21.38	19.46	18.84	20.16	19.84	18.57	20.54	20.57
Fe_2O_3	6.42	3.51	2.30	2.85	3.00	3.24	3.15	1.89	4.10	4.74
FeO	0.00	1.50	2.09	2.07	4.10	2.06	2.18	3.31	1.68	0.13
MnO	0.16	0.20	0.15	0.17	0.27	0.25	0.24	0.23	0.31	0.28
MgO	0.37	0.45	0.79	1.09	1.30	0.90	0.96	0.96	0.13	0.06
CaO	1.73	2.88	2.36	2.78	2.41	1.41	1.48	1.84	3.28	0.58
Na_2O	11.59	9.15	8.40	7.96	9.21	9.31	10.63	8.95	9.41	11.93
K_2O	4.42	5.49	5.69	5.36	5.03	7.43	4.86	5.42	6.25	4.49
P_2O_5	0.07	0.10	0.13	0.18	1.18	0.50	0.64	0.56	0.04	0.05
Rb	105	-	-	-	130	180	172	126	188	150
Ba	1116	-	-	-	1116	763	759	1381	480	50
Sr	601	-	-	-	1088	435	458	548	2456	16
Zr	270	-	-	-	913	705	1019	920	1191	2400
Nb	21	-	-	-	262	369	332	269	270	200
Y	19	-	-	-	35	28	42	38	96	30
La	11	-	-	-	108	90	89	103	-	-
Ce	21	-	-	-	176	134	121	172	-	-
Nd	10.0	-	-	-	-	-	-	-	-	-

Sources of data:
1: average East African nepheline syenite (Le Bas, 1977); 2,3: world averages, from Le Maitre (1976);
4,5,6,7: syenites from Mt. Kenya (Price et al., 1985);
8: nepheline syenite from Chilwa (Woolley and Jones, 1987); 9: aegerine-cancrinite phonolite from Chaone (Woolley and Jones, 1987)

Table B.13: Whole rock analyses of carbonatites from Spitskop.

(a) Calcio-carbonatites

	Sövites			Dolomitic Sövites				
	S57	S86	S87	S21	S53	S55	S56	S91
SiO_2	1.46	3.33	2.51	0.21	1.51	0.53	0.51	4.16
TiO_2	0.01	0.06	0.04	0.02	0.03	0.00	0.01	0.10
Al_2O_3	0.30	0.05	0.07	0.04	0.03	0.04	0.09	0.16
Fe_2O_3	2.13	3.04	2.47	2.26	2.33	1.95	1.98	6.94
MnO	0.50	0.74	0.69	0.78	0.99	0.62	0.61	0.59
MgO	0.86	3.06	2.29	8.70	4.78	7.98	8.23	4.49
CaO	52.37	48.79	50.94	44.42	48.23	44.95	45.30	45.15
Na_2O	0.00	0.73	0.63	0.00	0.00	0.00	1.09	0.93
K_2O	0.01	0.01	0.00	0.00	0.00	0.00	0.00	0.00
P_2O_5	0.08	2.58	1.76	0.13	1.29	2.44	2.49	5.85
LOI	41.03	38.30	39.32	44.21	41.30	41.51	39.64	32.84
H_2O-	1.25	0.02	0.01	0.00	0.02	0.28	0.02	0.15
Total	100.00	100.71	100.73	100.77	100.51	100.30	99.97	101.36
Rb	3.7	-	1.2	2.4	2.4	3.0	3.0	-
Ba	130	633	989	11	96	46	150	597
Sr	2571	1645	2381	380	1851	822	1756	1294
Th	15	1.2	1.2	6.1	9.9	12	8.0	3.3
U	11	-	-	5.6	5.7	8.6	6.0	-
Zr	49	17	3.2	9.8	44	22	34	22
Nb	-	23	13	5.0	7.6	-	-	12
Cr	-	32	48	-	-	-	-	25
V	9.0	25	27	7.2	22	5.7	4.5	79
Sc	-	-	-	-	-	-	-	-
Ni	-	2.7	3.1	-	-	-	-	3.6
Co	5.6	1.9	3.1	-	3.9	3.5	4.3	7.8
Pb	27	13	16	42	25	22	35	27
Zn	24	26	25	30	58	12	24	78
Cu	-	20	28	-	-	-	-	20
Y	24	71	60	29	37	173	68	76
La(x)	58	160	205	139	141	141	95	212
Ce(x)	140	218	345	249	260	361	203	117
Nd(x)	98	154	223	102	142	273	117	215

(b) Magnesio-carbonatites

	Beforsites						
	S05	S06	S27	S54	S58	S59	S61
SiO_2	0.00	0.38	0.12	2.41	0.32	0.00	0.16
TiO_2	0.00	0.02	0.00	0.00	0.00	0.00	0.00
Al_2O_3	0.03	0.00	0.02	0.02	0.08	0.03	0.01
Fe_2O_3	5.55	9.85	6.26	3.10	6.14	4.66	4.70
MnO	1.20	1.70	1.62	1.39	1.38	1.13	0.85
MgO	16.75	15.10	12.47	13.48	17.66	17.56	16.40
CaO	30.12	29.73	34.62	35.05	29.28	28.78	32.27
Na_2O	0.00	0.00	0.00	0.00	0.00	0.00	0.00
K_2O	0.00	0.02	0.00	0.01	0.01	0.00	0.01
P_2O_5	1.75	1.95	7.82	0.06	0.05	0.01	1.37
LOI	42.90	40.83	37.84	43.29	44.94	45.51	43.57
H_2O-	0.18	0.01	0.19	0.01	0.01	0.00	0.01
Total	98.48	99.59	100.96	98.82	99.87	97.68	99.35
Rb	2.3	3.5	-	3.7	4.3	2.7	2.7
Ba	23	75	22	11	38	34	36
Sr	1561	1181	965	261	2181	2582	495
Th	19	17	24	8.6	12	8.5	8.2
U	5.4	26	12	11	12	6.5	7.9
Zr	-	50	-	6.9	40	47	15
Nb	31	201	12	3.8	4.1	3.8	-
Cr	-	-	-	-	-	-	-
V	-	18	3.1	7.0	6.0	3.7	6.1
Sc	15	13	4.4	-	10	14	-
Ni	-	-	-	-	-	-	-
Co	-	4.9	-	-	5.4	-	-
Pb	16	72	21	75	35	36	24
Zn	248	384	60	30	119	56	22
Cu	-	-	-	-	-	-	-
Y	43	48	235	5.0	32	29	52
La(x)	343	222	123	256	66	111	67
Ce(x)	526	329	280	425	132	220	160
Nd(x)	186	111	159	142	63	87	113

(c) Carbonatite Rare Earth Element Data

	Sövite	Dolomitic Sövite		Beforsite			
	S57	S53	S55	S27	S54	S59	S61
La	68	152	155	145	285	136	88
Ce	158	305	401	312	507	286	194
Pr	21	34	55	35	48	29	23
Nd	90	134	235	148	143	96	106
Sm	18	21	55	27	8.3	11	21
Eu	5.3	5.8	17	8.5	1.4	2.9	6.3
Gd	15	16	51	28	3.8	9.0	18
Dy	6.7	8.9	38	39	1.9	7.3	13
Ho	1.1	1.7	7.0	8.6	0.5	1.3	2.1
Er	2.5	4.1	16	24	1.8	3.1	5.0
Yb	1.3	2.0	9.2	15	0.9	1.4	3.1
Lu	0.1	0.2	1.0	1.8	0.1	0.2	0.4

Table B.14: Chemical analyses and CIPW norms of "basalts" from the Spitskop Complex.

(a) Whole rock geochemistry

	S74	S75
SiO2	50.06	49.35
TiO2	0.91	0.85
Al2O3	15.57	15.02
Fe2O3	10.76	10.27
MnO	0.22	0.21
MgO	7.21	7.74
CaO	11.06	8.32
Na2O	2.15	3.70
K2O	0.51	0.86
P2O5	0.12	0.15
LOI	1.29	2.91
H2O-	0.86	0.80
Total	100.72	100.18

(b) Trace elements

	S74	S75
Rb	11	27
Ba	144	93
Sr	207	455
Th	-	7.1
U	6.2	11
Zr	76	84
Nb	5.3	4.4
Cr	356	324
V	237	211
Sc	37	32
Ni	104	103
Co	49	45
Pb	7.0	11
Zn	85	82
Cu	86	79
Y	23	22
La(x)	5.3	5.2
Ce(x)	12	12
Nd(x)	8.3	8.7

(c) CIPW norms

	S74		S75	
	(a)	(b)	(a)	(b)
Qz	0.65	6.38	0.00	0.00
Or	3.01	3.01	5.08	5.08
Pl	49.52	49.52	53.14	53.14
(Ab)	18.19	18.19	31.31	31.31
(An)	31.33	31.33	21.84	21.84
Di	18.69	15.96	15.18	12.80
(Wo)	9.54	8.56	7.78	6.87
(En)	5.38	7.40	4.55	5.94
(Fs)	3.77	0.00	2.85	0.00
Hy	21.40	10.56	2.04	11.81
(En)	12.58	10.56	1.25	11.81
(Fs)	8.82	0.00	0.78	0.00
Ol	0.00	0.00	15.95	1.07
(Fo)	0.00	0.00	9.44	1.07
(Fa)	0.00	0.00	6.51	0.00
Mt	2.38	0.00	2.27	0.00
Cm	0.08	0.08	0.07	0.07
Il	1.73	0.45	1.61	0.43
Hm	0.00	10.76	0.00	10.27
Sp	0.00	1.66	0.00	1.53
Ap	0.28	0.28	0.35	0.35

The CIPW normative mineralogy was calculated with Fe oxidation state
(a) corrected to $Fe_2O_3/FeO=0.2$ after Middlemost (1989) and
(b) all Fe set to Fe_2O_3

Table B.15: Isotopic data for pyroxenites, ijolites and "basalts" from the Spitskop Complex.

	Pyroxenites			Type-I ijolites										
	S44	S47	S160	S22	S41	S43	S70	S79	S82	S83	S114	S16	S18	S50
Rb (ppm)	23.2	15.0	20.9	72.0	41.0	53.0	77.0	63.0	45.0	42.0	76.0	45.0	29.0	46.0
Sr (ppm)	224.6	289.0	212.7	374.0	470.0	338.0	414.0	374.0	487.0	379.0	317.0	305.0	579.0	281.0
$^{87}Rb/^{86}Sr$	0.299	0.150	0.284	0.557	0.252	0.454	0.538	0.488	0.267	0.321	0.694	0.427	0.145	0.474
$^{87}Sr/^{86}Sr$	0.709163 ±0.000013	0.706050 ±0.000008	0.708727 ±0.000014	0.714931 ±0.000009	0.709570 ±0.000030	0.712960 ±0.000030	0.714290 ±0.000010	0.712851 ±0.000010	0.708001 ±0.000015	0.708731 ±0.000015	0.717891 ±0.000010	0.712062 ±0.000009	0.706589 ±0.000007	0.712969 ±0.000009
$^{87}Sr/^{86}Sr_o$	0.70342 ±0.00017	0.70316 ±0.00017	0.70326 ±0.00022	0.70421 ±0.00035	0.70472 ±0.00020	0.70423 ±0.00030	0.70394 ±0.00034	0.70348 ±0.00032	0.70286 ±0.00021	0.70257 ±0.00023	0.70454 ±0.00042	0.70385 ±0.00028	0.70380 ±0.00016	0.70386 ±0.00031
ϵ_{Sr}	4.9 ±2.4	1.3 ±2.4	2.7 ±3.1	16.3 ±5.0	23.4 ±2.9	16.5 ±4.2	12.3 ±4.9	5.8 ±4.5	-3.0 ±3.0	-7.2 ±3.3	20.9 ±6.0	11.1 ±4.0	10.4 ±2.3	11.2 ±4.4
Sm (ppm)	2.09	1.93	1.90			4.10					3.37	3.96	13.32	5.24
Nd (ppm)	8.34	7.91	7.45			20.04					14.79	19.39	50.64	24.80
$^{147}Sm/^{144}Nd$	0.151	0.148	0.155			0.124					0.138	0.123	0.159	0.128
$^{143}Nd/^{144}Nd$	0.511725 ±0.000012	0.511671 ±0.000020	0.511706 ±0.000012			0.511460 ±0.000015					0.511499 ±0.000016	0.511411 ±0.000011	0.511777 ±0.000018	0.511412 ±0.000017
$^{143}Nd/^{144}Nd_o$	0.51039 ±0.00005	0.51037 ±0.00005	0.51034 ±0.00005			0.51037 ±0.00005					0.51029 ±0.00005	0.51033 ±0.00005	0.51038 ±0.00005	0.51029 ±0.00005
ϵ_{Nd}	-10.1 ±1.0	-10.5 ±1.0	-11.0 ±1.0			-10.5 ±1.0					-12.1 ±1.0	-11.4 ±1.0	-10.4 ±1.0	-12.1 ±1.0

Type-I ijolites (contd.)

	S143	S115	S04	S67	S109	S134	S136	S138	S173
Rb (ppm)	58.0	56.0	48.0	53.0	89.0	46.0	55.0	54.0	89.0
Sr (ppm)	322.0	569.0	297.0	448.0	481.0	597.0	497.0	488.0	573.0
$^{87}Rb/^{86}Sr$	0.521	0.285	0.468	0.342	0.536	0.223	0.320	0.320	0.450
$^{87}Sr/^{86}Sr$	0.713263 ±0.000013	0.708569 ±0.000014	0.712195 ±0.000007	0.710291 ±0.000013	0.713401 ±0.000013	0.708042 ±0.000018	0.709523 ±0.000012	0.710204 ±0.000012	0.713122 ±0.000012
$^{87}Sr/^{86}Sr_o$	0.70324 ±0.00033	0.70309 ±0.00022	0.70320 ±0.00030	0.70371 ±0.00024	0.70310 ±0.00034	0.70376 ±0.00019	0.70337 ±0.00023	0.70405 ±0.00023	0.70448 ±0.00030
ϵ_{Sr}	2.4 ±4.7	0.3 ±3.1	1.8 ±4.3	9.1 ±3.5	0.5 ±4.8	9.7 ±2.7	4.2 ±3.3	13.9 ±3.3	20.0 ±4.2
Sm (ppm)		4.50		5.26	3.27				
Nd (ppm)		23.56		28.15	18.41				
$^{147}Sm/^{144}Nd$		0.115		0.113	0.107				
$^{143}Nd/^{144}Nd$		0.511414 ±0.000009		0.511352 ±0.000013	0.511290 ±0.000016				
$^{143}Nd/^{144}Nd_o$		0.51040 ±0.00005		0.51036 ±0.00005	0.51034 ±0.00005				
ϵ_{Nd}		-10.0 ±1.0		-10.8 ±1.0	-11.0 ±1.0				

Type-II ijolites

	S42	S51	S64	S65	S81	S126	S127	S131	S132	S135	S137	S139	S142	S144
Rb (ppm)	45.0	58.0	30.0	28.0	47.0	38.0	45.0	32.0	32.0	28.0	28.0	35.0	46.0	48.0
Sr (ppm)	372.0	214.0	364.0	838.0	390.0	369.0	866.0	858.0	276.0	434.0	378.0	885.0	296.0	408.0
$^{87}Rb/^{86}Sr$	0.350	0.785	0.238	0.097	0.349	0.298	0.150	0.108	0.336	0.187	0.214	0.114	0.450	0.340
$^{87}Sr/^{86}Sr$	0.710530 ±0.000020	0.717590 ±0.000040	0.708767 ±0.000009	0.708916 ±0.000010	0.709814 ±0.000011	0.708983 ±0.000014	0.707535 ±0.000011	0.708295 ±0.000029	0.711074 ±0.000019	0.707984 ±0.000015	0.707888 ±0.000012	0.707499 ±0.000013	0.712538 ±0.000012	0.710696 ±0.000014
$^{87}Sr/^{86}Sr_o$	0.70380 ±0.00025	0.70250 ±0.00047	0.70418 ±0.00020	0.70706 ±0.00015	0.70311 ±0.00025	0.70325 ±0.00022	0.70464 ±0.00017	0.70622 ±0.00015	0.70462 ±0.00024	0.70439 ±0.00018	0.70377 ±0.00019	0.70530 ±0.00016	0.70389 ±0.00030	0.70415 ±0.00024
ϵ_{Sr}	10.4 ±3.5	-8.1 ±6.8	15.8 ±2.8	56.7 ±2.2	0.5 ±3.5	2.6 ±3.2	22.4 ±2.4	44.8 ±2.2	22.1 ±3.4	18.8 ±2.5	9.9 ±2.7	31.7 ±2.2	11.6 ±4.2	15.3 ±3.4
Sm (ppm)														
Nd (ppm)														
$^{147}Sm/^{144}Nd$														
$^{143}Nd/^{144}Nd$														
$^{143}Nd/^{144}Nd_o$														
ϵ_{Nd}														

	Type-II ijolites (contd.)	"Other" Ijolites							Basalts	
	S145	S23	S46	S84	S108	S111	S113	S128	S130	S75	S74
Rb (ppm)	45.0	37.0	40.0	55.0	60.0	46.0	51.0	47.0	41.0	27.0	11.0
Sr (ppm)	380.0	715.0	661.0	536.0	486.0	491.0	373.0	445.0	367.0	455.0	207.0
$^{87}Rb/^{86}Sr$	0.343	0.150	0.175	0.297	0.357	0.271	0.396	0.306	0.323	0.172	0.154
$^{87}Sr/^{86}Sr$	0.710223 ±0.000013	0.706327 ±0.000007	0.707300 ±0.000008	0.707319 ±0.000013	0.710144 ±0.000009	0.708474 ±0.000012	0.709554 ±0.000010	0.708888 ±0.000029	0.709844 ±0.000010	0.712350 ±0.000009	0.706776 ±0.000035
$^{87}Sr/^{86}Sr_o$	0.70363 ±0.00024	0.70345 ±0.00017	0.70393 ±0.00017	0.70161 ±0.00022	0.70327 ±0.00025	0.70326 ±0.00021	0.70195 ±0.00027	0.70301 ±0.00023	0.70363 ±0.00023	0.70905 ±0.00017	0.70382 ±0.00017
ϵ_{Sr}	8.0 ±3.5	5.4 ±2.4	12.3 ±2.5	-20.8 ±3.2	2.9 ±3.6	2.7 ±3.0	-16.0 ±3.8	-0.8 ±3.2	7.9 ±3.3	85.0 ±2.4	10.7 ±2.4
Sm (ppm)											
Nd (ppm)											
$^{147}Sm/^{144}Nd$											
$^{143}Nd/^{144}Nd$											
$^{143}Nd/^{144}Nd_o$											
ϵ_{Nd}											

Table B.16: Isotopic data for nepheline syenite bodies at Spitskop

Nepheline Syenites : Rietfontein

	S01	S02	S03	S12	S13	S14	S30	S31	S32	S38	S151	S152	S153	S154
Rb (ppm)	120.0	124.0	91.0	100.0	91.0	88.0	114.0	70.0	94.0	70.0	82.0	95.0	89.0	104.0
Sr (ppm)	494.0	581.0	827.0	861.0	839.0	857.0	611.0	775.0	474.0	865.0	873.0	999.0	447.0	808.0
$^{87}Rb/^{86}Sr$	0.703	0.618	0.318	0.336	0.314	0.297	0.540	0.261	0.574	0.234	0.272	0.275	0.576	0.373
$^{87}Sr/^{86}Sr$	0.717430 ±0.000020	0.715460 ±0.000140	0.710040 ±0.000050	0.709810 ±0.000040	0.709550 ±0.000040	0.709430 ±0.000040	0.713908 ±0.000009	0.708807 ±0.000011	0.714805 ±0.000007	0.708275 ±0.000009	0.708915 ±0.000012	0.709137 ±0.000014	0.714348 ±0.000013	0.710721 ±0.000013
$^{87}Sr/^{86}Sr_o$	0.70391 ±0.00043	0.70358 ±0.00038	0.70392 ±0.00023	0.70335 ±0.00024	0.70352 ±0.00023	0.70372 ±0.00022	0.70352 ±0.00034	0.70378 ±0.00021	0.70377 ±0.00036	0.70377 ±0.00020	0.70369 ±0.00021	0.70384 ±0.00021	0.70327 ±0.00036	0.70356 ±0.00026
ϵ_{Sr}	11.9 ±6.1	7.2 ±5.5	12.0 ±3.3	3.9 ±3.4	6.3 ±3.3	9.2 ±3.2	6.4 ±4.9	10.1 ±2.9	9.9 ±5.1	10.0 ±2.8	8.8 ±3.0	11.0 ±3.0	2.8 ±5.1	6.9 ±3.7
Sm (ppm)										1.24			3.80	
Nd (ppm)										5.94			14.15	
$^{147}Sm/^{144}Nd$										0.126			0.162	
$^{143}Nd/^{144}Nd$										0.511471 ±0.000012			0.511904 ±0.000014	
$^{143}Nd/^{144}Nd_o$										0.51036 ±0.00005			0.51047 ±0.00005	
ϵ_{Nd}										-10.8 ±1.0			-8.5 ±1.0	

Nepheline Syenites : Rietfontein (contd.)						Nepheline Syenites : Mare						
	S155	S156	S187	S187V	S189	S07	S08	S102	S147	S148	S149	S150
Rb (ppm)	129.0	112.0	102.0	113.0	123.0	86.0	100.0	87.0	89.0	113.0	94.0	115.0
Sr (ppm)	703.0	316.0	648.0	977.0	865.0	591.0	626.0	712.0	624.0	617.0	446.0	628.0
$^{87}Rb/^{86}Sr$	0.531	1.027	0.456	0.335	0.412	0.421	0.462	0.354	0.413	0.530	0.610	0.530
$^{87}Sr/^{86}Sr$	0.714055 ±0.000012	0.723347 ±0.000013	0.712468 ±0.000017	0.710514 ±0.000015	0.711674 ±0.000015	0.713100 ±0.000030	0.712550 ±0.000030	0.710512 ±0.000014	0.713323 ±0.000012	0.714561 ±0.000014	0.716285 ±0.000012	0.714519 ±0.000012
$^{87}Sr/^{86}Sr_o$	0.70384 ±0.00034	0.70360 ±0.00061	0.70371 ±0.00030	0.70408 ±0.00024	0.70376 ±0.00028	0.70500 ±0.00028	0.70366 ±0.00030	0.70371 ±0.00025	0.70539 ±0.00028	0.70437 ±0.00034	0.70455 ±0.00038	0.70433 ±0.00034
ϵ_{Sr}	11.0 ±4.8	7.6 ±8.7	9.1 ±4.2	14.3 ±3.4	9.8 ±3.9	27.5 ±4.0	8.4 ±4.3	9.1 ±3.5	32.9 ±3.9	18.4 ±4.8	21.1 ±5.4	17.9 ±4.8
Sm (ppm)		1.53							1.75		0.81	
Nd (ppm)		4.66									4.09	
$^{147}Sm/^{144}Nd$		0.199							0.110		0.120	
$^{143}Nd/^{144}Nd$		0.512106 ±0.000010							0.511298 ±0.000012		0.511372 ±0.000011	
$^{143}Nd/^{144}Nd_o$		0.51036 ±0.00005							0.51033 ±0.00005		0.51032 ±0.00005	
ϵ_{Nd}		-10.8 ±1.0							-11.3 ±1.0		-11.5 ±1.0	

Nepheline Syenites : Spitskop — Eastern sheet

	S10	S11	S17	S19	S141	S68	S179	S179V
Rb (ppm)	94.0	112.0	148.0	129.0	102.0	103.0	54.0	74.0
Sr (ppm)	518.0	863.0	573.0	531.0	713.0	219.0	256.0	951.0
$^{87}Rb/^{86}Sr$	0.525	0.376	0.748	0.704	0.414	1.364	0.611	0.225
$^{87}Sr/^{86}Sr$	0.714290 ±0.000030	0.711630 ±0.000020	0.719020 ±0.000020	0.718059 ±0.000009	0.712706 ±0.000014	0.731715 0.000010	0.719487 ±0.000016	0.710971 ±0.000020
$^{87}Sr/^{86}Sr_o$	0.70419 ±0.00034	0.70441 ±0.00026	0.70464 ±0.00046	0.70453 ±0.00043	0.70475 ±0.00028	0.70549 ±0.00080	0.70774 ±0.00038	0.70664 ±0.00019
ϵ_{Sr}	15.9 ±4.8	19.0 ±3.7	22.3 ±6.5	20.8 ±6.1	23.8 ±3.9	34.4 ±11.3	66.4 ±5.4	50.8 ±2.7
Sm (ppm)		4.61		0.53				
Nd (ppm)		26.29		2.59				
$^{147}Sm/^{144}Nd$		0.106		0.123				
$^{143}Nd/^{144}Nd$		0.511411 ±0.000011		0.511341 ±0.000017				
$^{143}Nd/^{144}Nd_o$		0.51048 ±0.00005		0.51026 ±0.00005				
ϵ_{Nd}		-8.4 ±1.0		-12.7 ±1.0				

Table B.17: Isotopic data for Spitskop carbonatites.

(a) Sr and Nd: Calcio-carbonatites

	S57	S21	S53	S55	S56	S87	S91
Rb (ppm)	3.7	2.4	2.4	3.0	3.0	1.2	0.0
Sr (ppm)	2571.0	380.0	1851.0	822.0	1756.0	2380.5	1293.6
$^{87}Rb/^{86}Sr$	0.004	0.018	0.004	0.011	0.005	0.001	0.000
$^{87}Sr/^{86}Sr$	0.703026 ±0.000009	0.703640 ±0.000040	0.703950 ±0.000040	0.703480 ±0.000030	0.703115 ±0.000017	0.703179 ±0.000014	0.703059 ±0.000015
$^{87}Sr/^{86}Sr_o$	0.70295 ±0.00014	0.70329 ±0.00014	0.70388 ±0.00014	0.70328 ±0.00014	0.70302 ±0.00014	0.70315 ±0.00014	0.70306 ±0.00014
ϵ_{Sr}	-1.8 ±2.0	3.1 ±2.0	11.5 ±2.0	2.9 ±2.0	-0.7 ±2.0	1.1 ±2.0	-0.2 ±2.0
Sm (ppm)	16.91	10.22	18.23	53.40	18.42		30.61
Nd (ppm)	82.68	84.82	107.93	241.56	104.67		148.43
$^{147}Sm/^{144}Nd$	0.124	0.073	0.102	0.134	0.106		0.125
$^{143}Nd/^{144}Nd$	0.511704 ±0.000011	0.511198 ±0.000011	0.511501 ±0.000012	0.511706 ±0.000018	0.511561 ±0.000010		0.511608 ±0.000016
$^{143}Nd/^{144}Nd_o$	0.51062 ±0.00005	0.51056 ±0.00005	0.51060 ±0.00005	0.51053 ±0.00005	0.51062 ±0.00005		0.51051 ±0.00005
ϵ_{Nd}	-5.7 ±1.0	-6.9 ±1.0	-6.0 ±1.0	-7.4 ±1.0	-5.6 ±1.0		-7.8 ±1.0

(b) Sr and Nd: Magnesio-carbonatites

	S05	S06	S27	S54	S58	S59	S61
Rb (ppm)	2.3	3.5	0.0	3.7	4.3	2.7	2.7
Sr (ppm)	1561.0	1181.0	965.0	261.0	2181.0	2582.0	495.0
$^{87}Rb/^{86}Sr$	0.004	0.009	0.000	0.041	0.006	0.003	0.016
$^{87}Sr/^{86}Sr$	0.702676	0.702732	0.702747	0.704096	0.702570	0.702577	0.703453
	±0.000004	±0.000004	±0.000035	±0.000008	±0.000015	±0.000022	±0.000010
$^{87}Sr/^{86}Sr_o$	0.70259	0.70257	0.70275	0.70331	0.70246	0.70252	0.70315
	±0.00014	±0.00014	±0.00014	±0.00014	±0.00014	±0.00014	±0.00014
ϵ_{Sr}	-6.8	-7.2	-4.6	3.4	-8.7	-7.9	1.1
	±2.0	±2.0	±2.0	±2.0	±2.0	±2.0	±2.0
Sm (ppm)	20.70	12.24	24.19	7:77	8.54	10.63	19.23
Nd (ppm)	162.76	98.78	134.68	123.84	56.55	89.50	95.11
$^{147}Sm/^{144}Nd$	0.077	0.075	0.109	0.038	0.091	0.072	0.122
$^{143}Nd/^{144}Nd$	0.511524	0.511438	0.511667	0.510932	0.511650	0.511443	0.511674
	±0.000012	±0.000011	±0.000013	±0.000012	±0.000008	±0.000009	±0.000009
$^{143}Nd/^{144}Nd_o$	0.51085	0.51078	0.51071	0.51060	0.51085	0.51081	0.51060
	±0.00005	±0.00005	±0.00005	±0.00005	±0.00005	±0.00005	±0.00005
ϵ_{Nd}	-1.2	-2.5	-3.9	-6.1	-1.2	-1.9	-6.1
	±1.0	±1.0	±1.0	±1.0	±1.0	±1.0	±1.0

(c) Pb,O,C: Calcio-carbonatites

	Sövites			Dolomitic Sövites			
	S57	S86	S87	S21	S53	S55	S56
$^{206}/_{204}Pb$	16.734	18.546	17.524	16.636	18.753	17.089	16.958
$^{207}/_{204}Pb$	15.381	15.559	15.488	15.360	15.669	15.363	15.407
$^{208}/_{204}Pb$	36.738	37.978	39.184	36.176	40.329	37.360	36.510
$\delta^{18}O$	13.50	14.35	13.95	15.47	15.44	16.64	14.14
$\delta^{13}C$	-2.83	-2.83	-2.89	-2.88	-2.86	-2.93	-2.86

(d) Pb,O,C: Magnesio-carbonatites

	Beforsites						
	S05	S06	S27	S54	S58	S59	S61
$^{206}/_{204}Pb$	16.552	16.638	24.326	17.005	17.272	17.156	17.593
$^{207}/_{204}Pb$	15.298	15.347	16.088	15.410	15.536	15.512	15.535
$^{208}/_{204}Pb$	36.326	36.206	40.818	36.393	36.916	36.617	36.889
$\delta^{18}O$	15.97	-	-	-	16.63	16.85	17.17
$\delta^{13}C$	-1.84	-	-	-	-1.54	-1.27	-2.81

Spitskop Complex: Geochemical data for the fenitised rocks.

Table B.18: Major, trace element and Sr isotopic composition of fenitised Bushveld Granites surrounding the Spitskop Complex.

(i) Major elements

(a) Quartz-fenites (b) Feldspar-fenites

	Nebo				Klip-kloof	Nebo				Klipkloof	
	S104	S117	S118	S121	S120	S125	S170	S171A	S172	S116	S178
SiO_2	68.97	71.29	72.45	75.43	74.85	62.31	60.33	62.80	61.86	62.54	63.62
TiO_2	0.42	0.34	0.31	0.18	0.10	0.45	0.52	0.35	0.50	0.55	0.41
Al_2O_3	12.59	11.63	11.77	11.46	11.40	14.94	12.56	16.01	15.50	13.80	16.05
Fe_2O_3	5.28	5.13	4.12	2.81	2.04	6.79	9.89	5.19	6.57	8.83	5.42
MnO	0.06	0.10	0.08	0.04	0.00	0.13	0.21	0.12	0.12	0.20	0.11
MgO	0.00	0.11	0.42	0.22	0.44	0.51	0.34	0.08	0.19	0.37	0.01
CaO	0.95	1.47	1.41	0.78	0.76	1.74	2.62	1.02	1.67	1.80	1.21
Na_2O	4.30	3.69	3.92	3.51	3.62	6.67	6.15	7.33	6.87	7.21	7.66
K_2O	5.18	4.98	4.63	4.93	5.05	5.31	5.42	5.40	5.29	4.47	4.85
P_2O_5	0.04	0.03	0.03	0.04	0.00	0.14	0.22	0.04	0.00	0.09	0.05
LOI	1.14	0.32	0.36	0.30	0.48	0.31	0.70	0.40	0.60	0.15	0.32
H_2O-	0.21	0.10	0.13	0.15	0.19	0.19	0.05	0.09	0.12	0.17	0.04
Total	99.14	99.19	99.63	99.85	98.93	99.49	99.01	98.83	99.29	100.18	99.75
S.G.	2.55	2.62	2.63	2.63	2.56	2.65	-	-	-	2.67	-
	Cations per 100 anions:										
Si	38.48	39.79	40.02	41.13	41.10	35.96	35.38	36.18	35.65	36.05	36.26
Ti	0.18	0.14	0.13	0.07	0.04	0.19	0.23	0.15	0.22	0.24	0.18
Al	8.28	7.65	7.66	7.37	7.38	10.16	8.68	10.87	10.53	9.38	10.78
Fe	2.22	2.15	1.71	1.15	0.84	2.95	4.36	2.25	2.85	3.83	2.33
Mn	0.03	0.05	0.04	0.02	0.00	0.06	0.10	0.06	0.06	0.10	0.05
Mg	0.00	0.09	0.35	0.18	0.36	0.44	0.30	0.07	0.16	0.32	0.01
Ca	0.57	0.88	0.83	0.46	0.45	1.08	1.65	0.63	1.03	1.11	0.74
Na	4.65	3.99	4.20	3.71	3.85	7.46	6.99	8.19	7.68	8.06	8.46
K	3.69	3.55	3.26	3.43	3.54	3.91	4.06	3.97	3.89	3.29	3.53
P	0.02	0.01	0.01	0.02	0.00	0.07	0.11	0.02	0.00	0.04	0.02
M-Factor	1.73	1.78	1.74	1.53	1.57	2.31	2.89	2.13	2.26	2.51	2.15
q'	58.89	62.41	62.79	65.13	64.11	46.63	48.27	45.12	45.62	48.07	45.75
ne'	21.71	18.90	19.95	17.19	17.72	31.46	26.18	33.46	32.91	32.44	35.20
ks'	19.40	18.69	17.26	17.69	18.17	21.90	25.55	21.42	21.47	19.50	19.05

(c) Nepheline-fenites

	S122	S123	S129	S174	S175	S176	S177
SiO_2	44.03	46.85	49.76	46.88	45.43	45.13	46.59
TiO_2	1.43	1.83	0.80	2.33	1.83	1.59	1.87
Al_2O_3	17.98	17.16	19.24	13.97	18.19	18.71	18.03
Fe_2O_3	9.36	11.03	7.61	13.06	9.63	9.34	9.82
MnO	0.20	0.25	0.17	0.28	0.24	0.26	0.21
MgO	2.82	1.60	1.60	1.83	1.70	1.41	1.47
CaO	8.26	6.38	4.78	8.73	6.98	10.12	6.26
Na_2O	10.74	9.60	12.12	8.48	11.33	4.70	11.26
K_2O	3.00	3.14	2.40	2.53	2.83	2.75	2.95
P_2O_5	0.70	0.21	0.29	0.50	0.36	0.29	0.25
LOI	0.70	1.01	0.63	1.07	1.04	4.18	1.02
H_2O-	0.08	0.13	0.07	0.07	0.05	0.13	0.06
Total	99.30	99.19	99.47	99.73	99.61	98.61	99.79
S.G.	2.73	2.87	2.73	-	-	-	-
	Cations per 100 anions:						
Si	27.19	28.60	29.80	28.67	27.72	26.50	28.28
Ti	0.66	0.84	0.36	1.07	0.84	0.70	0.85
Al	13.09	12.35	13.58	10.07	13.09	12.95	12.90
Fe	4.35	5.07	3.43	6.01	4.42	4.13	4.49
Mn	0.11	0.13	0.09	0.14	0.12	0.13	0.11
Mg	2.60	1.46	1.43	1.67	1.55	1.23	1.33
Ca	5.46	4.17	3.07	5.72	4.56	6.37	4.07
Na	12.86	11.36	14.07	10.06	13.40	5.35	13.25
K	2.36	2.45	1.83	1.97	2.20	2.06	2.28
P	0.37	0.11	0.15	0.26	0.19	0.14	0.13
M-Factor	5.08	4.18	3.70	5.34	4.65	3.51	4.40
q'	8.41	22.26	18.79	26.10	12.41	34.15	15.31
ne'	73.54	60.97	69.19	58.12	71.47	46.09	68.32
ks'	18.05	16.77	12.02	15.78	16.11	19.76	16.37

(d) Data from Strauss and Truter (1950; Tables 1, 2)

	D	C	J	K	B	I	A	H	G
SiO_2	72.50	71.40	69.99	70.20	64.80	64.40	62.20	60.90	60.00
TiO_2	0.25	0.25	0.45	0.60	0.25	0.30	0.25	0.90	0.50
Al_2O_3	12.10	12.38	12.20	12.60	15.35	16.60	16.97	12.70	13.12
Fe_2O_3	2.60	5.11	6.63	4.59	5.59	3.87	5.91	8.81	10.71
MnO	0.09	0.08	0.08	0.10	0.09	0.06	0.04	0.20	0.32
MgO	0.30	0.16	0.52	0.30	0.58	0.30	0.46	0.60	0.48
CaO	2.10	0.77	1.22	1.70	1.68	1.30	0.78	2.20	4.45
Na_2O	4.60	4.46	4.33	4.50	8.04	8.20	8.40	8.70	7.33
K_2O	4.20	4.28	3.93	4.50	3.37	4.00	3.83	3.30	2.93
P_2O_5	0.60	0.05	0.19	1.00	0.03	0.60	0.02	0.80	0.26
LOI	0.30	0.61	0.41	0.50	0.50	0.40	0.49	0.30	0.25
H_2O-	0.16	0.15	0.12	0.06	0.15	0.08	0.21	0.42	0.11
Total	99.80	99.70	100.07	100.65	100.43	100.11	99.56	99.83	100.46
Cations per 100 anions:									
Si	39.86	39.41	38.81	38.54	36.44	36.19	35.49	35.36	34.85
Ti	0.10	0.10	0.19	0.25	0.11	0.13	0.11	0.39	0.22
Al	7.84	8.06	7.97	8.16	10.17	11.00	11.41	8.69	8.98
Fe	1.08	2.12	2.77	1.90	2.36	1.64	2.54	3.85	4.68
Mn	0.04	0.04	0.04	0.05	0.04	0.03	0.02	0.10	0.16
Mg	0.25	0.13	0.43	0.24	0.49	0.25	0.39	0.52	0.42
Ca	1.24	0.45	0.72	1.00	1.01	0.78	0.48	1.37	2.77
Na	4.90	4.77	4.65	4.79	8.76	8.93	9.29	9.79	8.26
K	2.95	3.01	2.78	3.15	2.42	2.87	2.79	2.44	2.17
P	0.28	0.02	0.09	0.46	0.01	0.28	0.01	0.39	0.13
M-Factor	1.93	1.59	1.68	1.85	2.20	2.09	2.01	3.07	3.19
q'	61.59	61.69	62.16	60.48	47.97	46.24	44.23	46.38	47.84
ne'	23.00	22.50	22.73	22.81	38.63	38.59	41.01	37.35	38.50
ks'	15.41	15.82	15.11	16.71	13.41	15.16	14.76	16.27	13.66

D: "Granophyre" (Klipkloof); C: "Red Granite" (Nebo); J,K: "Amphibole-bearing granite"; B: "Red quartz syenite";
I: "Fine-grained pyroxene umptekite"; A: "Cellular, red umptekite"; H: "Coarse-grained, pyroxene umptekite";
G: "Fine-grained pyroxene umptekite"

(ii) Trace elements and isotopic compositions

(a) Quartz-fenites

(b) Feldspar-fenites

	Nebo				Klip-kloof	Nebo				Klipkloof	
	S104	S117	S118	S121	S120	S125	S170	S171A	S172	S116	S178
Rb	120	158	167	154	183	132	148	136	98	101	93
Ba	2547	1862	1634	719	581	1543	704	1606	2847	746	1489
Sr	167	135	130	49	89	312	218	254	439	179	351
Zr	707	608	489	337	555	402	360	480	255	562	248
Nb	27	25	34	13	13	24	23	17	30	24	21
Pb	22	20	22	25	24	0	908	95	24	0	48
Y	39	89	73	76	80	11	25	25	14	7	13
La	50.15	61.85	-	86.34	-	7.92	-	-	-	3.92	-
Ce	97.82	142.78	-	182.65	-	17.76	-	-	-	9.16	-
Pr	11.48	17.50	-	21.02	-	2.46	-	-	-	1.38	-
Nd	44.94	70.02	-	81.64	-	9.73	-	-	-	5.32	-
Sm	8.05	14.39	-	15.32	-	1.80	-	-	-	1.03	-
Eu	4.35	3.88	-	1.74	-	0.81	-	-	-	0.37	-
Gd	7.89	14.55	-	15.01	-	1.94	-	-	-	1.23	-
Dy	6.71	14.37	-	13.44	-	1.85	-	-	-	1.23	-
Ho	1.54	3.16	-	2.85	-	0.44	-	-	-	0.32	-
Er	4.17	9.18	-	7.87	-	1.46	-	-	-	1.23	-
Yb	4.05	8.62	-	6.45	-	2.65	-	-	-	2.65	-
Lu	0.63	1.21	-	0.88	-	0.52	-	-	-	0.51	-
$^{87}Sr/^{86}Sr$	0.762652 ±0.000018	0.800834 ±0.000019	0.808221 ±0.000020	0.946810 ±0.000022	0.864471 ±0.000019	0.730685 ±0.000016	0.744536 ±0.000010	0.741262 ±0.000010	0.717281 ±0.000013	0.734470 ±0.000014	0.720673 ±0.000019

(c) Nepheline-fenites

	S122	S123	S129	S174	S175	S176	S177
Rb	51	68	35	60	65	78	66
Ba	383	718	816	835	506	4447	644
Sr	579	442	453	627	420	947	405
Zr	121	259	200	239	208	199	228
Nb	35	57	42	60	53	44	50
Pb	0	0	0	28	29	108	44
Y	24	18	10	30	28	24	25
La	-	-	-	-	-	-	-
Ce	-	-	-	-	-	-	-
Pr	-	-	-	-	-	-	-
Nd	-	-	-	-	-	-	-
Sm	-	-	-	-	-	-	-
Eu	-	-	-	-	-	-	-
Gd	-	-	-	-	-	-	-
Dy	-	-	-	-	-	-	-
Ho	-	-	-	-	-	-	-
Er	-	-	-	-	-	-	-
Yb	-	-	-	-	-	-	-
Lu	-	-	-	-	-	-	-
$^{87}Sr/^{86}Sr$	0.708136 ±0.000012	0.712654 ±0.000016	0.707866 ±0.000019	0.710200 ±0.000013	0.712055 ±0.000021	0.712105 ±0.000011	0.712811 ±0.000012

Table B.19: Comparison between least-fenitised granite fenite S121 and potential protolith compostions.

	Mean Nebo ±1σ (n=29)	VW4-71,7A =P1	VW4-81,5A =P2	Fenite S121
SiO_2	73.40 ±1.8	75.26	75.85	75.43
TiO_2	0.25 ±.09	0.17	0.13	0.18
Al_2O_3	11.82 ±.36	11.65	11.89	11.46
Fe_2O_3	3.78 ±1.0	2.29	1.50	2.81
MnO	0.06 ±.02	0.03	0.02	0.04
MgO	0.02 ±.04	0.00	0.00	0.22
CaO	0.96 ±.38	0.70	0.31	0.78
Na_2O	3.68 ±.18	4.18	3.90	3.51
K_2O	5.08 ±.32	5.24	5.59	4.93
P_2O_5	0.03 ±.01	0.01	0.01	0.04
H_2O-	0.21 ±.06	0.14	0.17	0.30
LOI	0.49 ±.16	0.33	0.50	0.15
Total	99.78	100.00	99.87	99.85
Zn	-	53	49	
Nb	28 ±6	26	33	13
Zr	401 ±127	270	241	337
Y	78 ±27	80	61	76
Sr	65 ±45	37	19	49
Rb	201 ±47	229	242	154
U	6.7 ±2.6	7.0	6.0	
Th	29 ±11	41	33	
Pb	22 ±4	21	21	25
Ba	1041 ±693	527	462	719
La	87 ±41	177	36	86
Ce	169 ±81	317	68	183
Nd	100 ±41	153	43	82

Average Nebo and selected Nebo compositions VW4-71,7A and VW4-81,5A are from the data of Kleeman (1985).

Table B.20: Table of chemical analyses of fenitised Rustenburg Layered Suite lithologies.

	Anorthosites				Magnetite-Anorthosites		Gabbronorites			Fayalite Diorites	
	S94	S98	S103	S36	S93	S99	S95	S100	S101	S73	S107
SiO_2	50.71	50.01	51.66	45.93	45.50	49.89	49.49	47.95	48.80	45.45	45.65
TiO_2	0.10	0.29	0.19	0.05	1.60	0.44	0.14	0.15	0.14	1.64	1.93
Al_2O_3	26.57	25.63	25.66	26.42	23.50	25.82	17.74	21.83	21.59	12.71	12.35
Fe_2O_3	2.39	3.05	1.44	2.56	11.14	4.04	6.39	4.43	4.71	18.17	21.25
MnO	0.04	0.00	0.00	0.03	0.06	0.00	0.13	0.14	0.12	0.40	0.35
MgO	0.84	0.87	0.16	2.69	0.83	0.84	8.20	4.07	3.74	1.95	1.86
CaO	12.26	10.90	9.84	13.85	9.89	10.83	13.30	13.37	12.17	8.10	7.54
Na_2O	5.48	5.83	6.99	7.28	5.63	5.96	3.61	6.26	6.27	8.54	6.52
K_2O	0.61	0.87	0.79	0.47	1.09	0.60	0.22	0.57	0.40	1.96	1.57
P_2O_5	0.03	0.04	0.05	0.00	0.04	0.02	0.01	0.06	0.05	0.58	0.77
LOI	0.94	1.64	3.35	1.59	1.23	1.45	0.66	1.13	1.53	0.08	-0.60
H_2O-	0.14	0.18	0.20	0.05	0.21	0.17	0.14	0.12	0.17	0.08	0.09
Total	100.11	99.31	100.33	100.92	100.72	100.06	100.03	100.08	99.69	99.66	99.28
Rb	8.3	10	12	6.1	14	9.5	11	13	8	49	50
Ba	194	148	335	323.2	166	124	123	381	344	820	619
Sr	513	450	593	325.8	404	414	288	534	602	625	537
Zr	10	15	20	14.3	30	28	19	16	29	205	137
Nb	0.0	2.5	3.6	2.3	2.8	2.8	0.0	3.2	8.8	55	16
Cr	24	0.0	10	165.2	67	11	270	55	14	5.0	0.0
V	40	78	5.3	40.7	758	113	91	65	58	51	4.7
Sc	8.4	7.4	3.6	0.0	10	6.3	30	19	17	29	46
Ni	11	0.0	0.0	49.1	104	1.4	156	65	78	0.0	0.0
Co	9.8	13	3.8	12.8	40	18	43	24	27	19	32
Pb	8.0	0.0	0.0	3.2	7.1	7.3	0.0	11	13	14	14
Zn	32	22	16	26.2	52	22	44	43	58	171	173
Cu	35	16	8.3	5.0	368	17	0.0	13	91	25	27
Y	3.7	5.7	6.9	1.6	6.0	4.4	6.2	9.7	13	26	36
La	6.7	4.5	5.7	-	4.4	3.3	3.2	12	11	20	28
Ce	10	9.7	11	-	13	9.9	9.6	19	17	45	67
Nd	5.4	4.0	5.8	-	5.8	5.0	3.3	9.8	8.1	27	38
$^{87}Sr/^{86}Sr$	0.707610 ±0.000015	0.708725 ±0.000012	0.708599 ±0.000014	-	0.709486 ±0.000013	0.708827 ±0.000018	0.708098 ±0.000015	0.707100 ±0.000019	0.707058 ±0.000021	0.708695 ±0.000020	0.711550 ±0.000019

Magnetitites

	S180A	S180B	S181	S183
SiO_2	0.17	0.36	0.80	0.52
TiO_2	13.25	13.55	13.90	13.12
Al_2O_3	3.44	2.49	3.79	3.76
Fe_2O_3	79.86	80.60	77.80	78.21
MnO	0.24	0.26	0.27	0.23
MgO	1.63	1.23	1.93	1.62
CaO	0.58	0.52	0.38	0.23
V_2O_5	1.62	1.65	1.65	1.72
Total	100.79	100.66	100.52	99.41

Geochemical data for the other Pilanesberg Suite Complexes.

Table B.21: Analytical data and CIPW normative constituents for the mafic lavas at Kruidfontein.

	K13	K14	K15	K16
SiO_2	47.57	45.03	43.48	39.13
TiO_2	4.66	4.43	4.67	4.52
Al_2O_3	11.48	10.45	11.31	10.65
Fe_2O_3	17.75	15.44	16.36	14.90
MnO	0.20	0.23	0.20	0.24
MgO	3.29	3.43	2.93	4.13
CaO	5.00	9.42	8.36	12.04
Na_2O	3.35	3.13	3.56	2.63
K_2O	1.04	0.50	0.57	1.15
P_2O_5	0.96	0.81	0.92	0.89
LOI	4.63	8.16	6.91	9.78
H_2O-	0.16	0.14	0.12	0.14
Total	100.09	101.17	99.39	100.20
Rb	16	6.0	9.7	18
Ba	821	455	4832	3586
Sr	437	580	1093	1010
Th	11	11	5.2	5.0
U	7.2	-	5.7	-
Zr	508	477	533	501
Nb	107	88	95	89
Cr	203	198	223	195
V	301	305	348	341
Sc	34	39	31	25
Ni	84	92	86	92
Co	84	56	51	60
Pb	13	4.6	8.1	12
Zn	128	111	114	114
Cu	50	35	53	30
Y	35	35	40	34
La(x)	65	75	55	25
Ce(x)	287	112	198	151
Nd(x)	173	160	151	116

	K13	K14	K15	K16
Qz	5.28	2.13	0.00	0.00
Z	0.10	0.10	0.11	0.10
Or	6.15	2.95	3.37	6.80
Pl	41.56	39.47	43.32	23.66
Ne	0.00	0.00	0.00	6.75
Ac	0.00	0.00	0.00	0.00
Ns	0.00	0.00	0.00	0.00
Di	4.75	24.10	19.93	34.18
Hy	21.08	9.22	7.74	0.00
Ol	0.00	0.00	2.23	3.87
Mt	3.93	3.41	3.62	3.29
Cm	0.04	0.04	0.05	0.04
Il	8.85	8.41	8.87	8.58
Ap	2.22	1.88	2.13	2.06
Total	93.97	91.72	91.36	89.34
Pl:(Ab)	28.35	26.49	30.12	9.80
(An)	13.22	12.99	13.20	13.86
Di:(Wo)	2.35	12.00	9.85	17.16
(En)	0.84	4.85	3.54	7.87
(Fs)	1.56	7.25	6.54	9.15
Hy:(En)	7.36	3.70	2.71	0.00
(Fs)	13.72	5.53	5.02	0.00
(Fo)	0.00	0.00	0.73	1.69
(Fa)	0.00	0.00	1.50	2.17

CIPW normative values were calculated with the Fe_2O_3/FeO adjusted to 0.2 (following Middlemost, 1989).

Table B.22: Analytical data for carbonatites and silicates from western Transvaal complexes.

	K6	K9	N1	TW-1	T5	T6	BH2	BH8	GD2	GD4	GD1A	GD1B	GD5
	Carbonatites		Carb.	Carbonatites					Lamprophyres		Carbonatites		
SiO_2	11.68	8.10	0.06	0.10	22.43	6.71	23.34	0.13	45.54	45.35	3.65	3.47	3.75
TiO_2	0.04	0.03	0.01	0.00	0.00	0.00	0.02	0.01	3.44	3.31	0.08	0.09	0.11
Al_2O_3	0.16	0.08	0.06	0.06	0.07	0.02	0.03	0.07	13.14	12.19	0.32	0.18	0.15
Fe_2O_3	1.91	2.11	0.29	0.64	4.97	5.30	5.59	4.96	11.52	11.74	1.83	2.25	1.89
MnO	0.71	0.96	0.22	0.20	0.82	0.77	0.72	0.83	0.17	0.19	1.62	1.03	1.28
MgO	1.23	0.99	2.11	2.75	12.09	16.92	13.17	17.95	4.91	6.32	0.57	1.03	0.31
CaO	46.49	49.42	54.22	54.42	25.42	28.76	23.21	30.30	9.67	8.25	49.76	45.68	49.83
Na_2O	0.09	0.00	0.00	0.00	0.24	0.14	0.00	0.02	5.21	4.68	0.38	0.39	0.21
K_2O	0.03	0.00	0.00	0.00	0.00	0.01	0.00	0.00	0.21	0.18	0.02	0.04	0.03
P_2O_5	0.78	0.70	0.00	0.00	2.46	0.02	0.00	0.00	1.02	0.89	0.49	0.51	1.35
LOI	36.00	35.99	42.71	42.57	32.10	41.52	33.91	45.10	4.57	7.00	38.63	38.61	37.39
H_2O-	0.03	0.03	0.03	0.06	0.08	0.07	0.03	0.06	0.20	0.15	0.02	0.02	0.00
Total	99.15	98.41	99.71	100.80	100.68	100.24	100.02	99.43	99.60	100.25	97.37	93.30	96.30
Rb	0.0	0.0	0.0	0.0	0.0	0.0	0.0	0.0	1.8	4.9	3.0	0.0	0.0
Ba	6376	23331	539	520	387	501	221	318	345	508	1494	3616	15531
Sr	3505	2819	7956	2792	1148	2494	1351	1848	1071	1685	5433	31338	6055
Th	8.1	48	0.0	4.5	6.4	55	40	16	14	25	38	52	0.0
U	0.0	0.0	0.0	0.0	0.0	0.0	0.0	0.0	14	0.0	1.2	9.4	0.0
Zr	31	18	0.0	0.0	5.5	7.4	19	17	925	672	110	52	285
Nb	11	37	14	1.5	5.6	32	12	3.9	123	96	181	207	133
Cr	58	29	67	63	0.0	15	19	24	67	310	31	0.0	33
V	72	255	0.0	0.0	25	0.0	51	44	237	251	279	305	325
Sc	0.0	0.0	0.0	0.0	0.0	0.0	0.0	0.0	30	22	0.0	0.0	0.0
Ni	9.2	7.8	3.9	4.3	4.4	8.0	1.5	1.0	62	130	11	15	16
Co	3.4	6.5	6.4	7.3	56	21	15	4.0	38	42	3.2	1.3	1.2
Pb	113	129	12	5.6	2.3	17	22	106	17	10	354	243	168
Zn	161	21	5.8	5.8	18	55	315	300	143	134	377	478	297
Cu	48	39	78	33	13	29	13	23	85	93	59	303	73
Y	57	113	66	29	55	32	40	42	46	55	115	177	257
La(x)	565	1335	168	-	392	232	189	387	224	130	2705	2059	2192
Ce(x)	507	1311	422	-	783	469	315	537	280	226	3325	2928	2983
Nd(x)	94	372	246	53	388	181	311	340	238	154	871	1043	1131

(contd)

	K6	K9	N1	TW-1	T5	T6	BH2	BH8	GD2	GD4	GD1A	GD1B	GD5
	Carbonatites		Carb.	Carbonatites					Lamprophyres		Carbonatites		
La	576.3	1184.3	195.2	58.6	-	241.3	175.2	-	-	-	3240.5	-	2322.0
Ce	679.9	1306.0	460.3	132.1	-	410.0	398.3	-	-	-	3908.6	-	3263.2
Pr	53.1	96.8	52.7	14.80	-	38.72	47.80	-	-	-	309.3	-	286.6
Nd	169.3	294.5	220.4	61.4	-	136.9	217.3	-	-	-	951.0	-	948.1
Sm	19.03	32.15	36.87	10.26	-	18.00	30.38	-	-	-	87.5	-	102.4
Eu	4.92	7.98	10.19	3.09	-	4.49	5.85	-	-	-	18.17	-	24.03
Gd	14.17	23.82	27.78	8.80	-	12.23	13.78	-	-	-	47.88	-	65.1
Dy	9.45	15.21	17.19	6.49	-	7.63	8.37	-	-	-	24.24	-	47.55
Ho	1.83	2.96	2.98	1.18	-	1.30	1.70	-	-	-	4.71	-	9.03
Er	4.61	6.13	7.35	3.27	-	2.83	4.52	-	-	-	22.68	-	31.71
Yb	3.26	6.25	4.74	2.58	-	1.61	4.23	-	-	-	6.96	-	15.28
Lu	0.38	0.84	0.65	0.38	-	0.19	0.68	-	-	-	0.89	-	1.94

Table B.23: Analytical data for carbonatites from the Stukpan Complex.

(a) Major elements

	H3	H4	H11	H17
SiO_2	2.03	5.76	0.24	1.53
TiO_2	0.15	0.10	0.01	0.32
Al_2O_3	0.38	1.66	0.07	0.27
Fe_2O_3	6.31	5.14	1.60	9.65
MnO	0.21	0.22	0.21	0.19
MgO	4.17	6.81	3.82	4.13
CaO	47.13	42.79	51.51	46.48
Na_2O	0.01	0.45	0.00	0.02
K_2O	0.30	1.24	0.02	0.19
P_2O_5	0.00	1.26	0.21	0.00
LOI	38.32	35.08	42.11	36.50
H_2O-	0.01	0.11	0.38	0.02
Total	99.02	100.62	100.18	99.30

(b) Trace elements

	H3	H4	H11	H17
Rb	17	31	2.5	7.5
Ba	505	379	119	292
Sr	1412	1285	1438	1303
Th	-	-	-	-
U	2.9	-	-	-
Zr	4.3	7.1	-	4.6
Nb	3.1	3.3	-	1.6
Cr	57	75	61	68
V	126	90	45	222
Ni	6.7	17	-	4.9
Co	23	19	6.6	33
Pb	12	10	4.9	10
Zn	22	28	6.0	30
Cu	29	29	15	32
Y	17	17	20	16
La	11.70	-	11.30	8.10
Ce	25.70	-	24.34	17.05
Pr	3.25	-	3.43	2.14
Nd	15.10	-	15.50	11.10
Sm	3.20	-	3.47	2.62
Eu	1.12	-	1.25	0.99
Gd	3.87	-	4.31	3.45
Dy	3.67	-	4.09	3.53
Ho	0.71	-	0.79	0.69
Er	2.17	-	2.36	2.20
Yb	1.96	-	2.08	2.21
Lu	0.29	-	0.31	0.32

Table B.24: Isotopic data for selected nepheline syenites (foyaites) from the Pilanesberg Complex.

Sample	Rb[1]	Sr[1]	$^{87}Rb/^{86}Sr$	$^{87}Sr/^{86}Sr$[2]	
"White" Foyaites					
P82-1	146.8	5445	0.078	0.70598	(2)
P82-11	130.8	406.5	0.932	0.72030	(3)
P82-12	122.3	398.6	0.889	0.71997	(4)
P82-13	128.3	491.3	0.756	0.71780	(3)
P82-14	135.1	495.9	0.789	0.71858	(5)
P82-19	333.3	2559	0.377	0.71030	(4)
P82-20	279.9	2844	0.285	0.70829	(4)
P82-21	155.3	7001	0.064	0.70435	(6)
P82-22	412.4	198.6	6.06	0.79127	(5)
P82-23	368.3	331.4	3.23	0.75198	(4)
"Green" Foyaites					
P82-2	139.9	4641	0.087	0.70473	(3)
P82-3	180.0	3455	0.151	0.70590	(4)
P82-4	160.3	3659	0.127	0.70528	(4)
P82-5	191.2	3471	0.159	0.70584	(6)
P82-6	219.0	3298	0.192	0.70642	(3)
P82-7	229.1	4451	0.151	0.70583	(5)
P82-8	205.9	4014	0.148	0.70559	(3)
P82-9	222.8	2902	0.222	0.70704	(4)
P82-15	209.7	3532	0.172	0.70694	(6)
P82-16	215.3	4409	0.141	0.70564	(2)
P82-17	206.6	2847	0.210	0.70736	(4)
P82-18	237.1	3834	0.179	0.70676	(5)

1 : Analyses by IDMS. Uncertainty is 0.8%.
2 : Precisions are 2 standard errors of the mean and refer to the least significant figures. Analyses on MM30 single collector mass spectrometer. Analytical uncertainty is 0.01%.

Table B.25: Isotopic data for the complexes of the western Transvaal and Stukpan.

	K13	K14	K15	K16	K6[1]	K9[1]	N1	TW-1	T5	T6[1]	S-8	BH2[1]	BH8[1]
$^{87}Sr/^{86}Sr$	0.705983 ±0.000013	0.704742 ±0.000014	0.705635 ±0.000012	0.705562 ±0.000017	0.702735 ±0.000025	0.702945 ±0.000015	0.702558 ±0.000012	0.702791 ±0.000012	0.703176 ±0.000014	0.70276 ±0.00003	0.702978 ±0.000013	0.703719 ±0.000013	0.703098 ±0.000016
Nd (IDMS)	112.00	-	-	-	156.60	289.23	209.25	56.847	307.12	125.93	61.590	205.10	249.91
Sm (IDMS)	18.213	-	-	-	17.745	31.743	35.312	9.753	45.810	16.847	11.519	29.032	42.380
$^{143}Nd/^{144}Nd$	0.511763 ±0.000026	-	-	-	0.511594 ±0.000032	0.511550 ±0.000014	0.511890 ±0.000009	0.511819 ±0.000020	0.511619 ±0.000009	0.511607 ±0.000016	0.511765 ±0.000009	0.511664 ±0.000010	0.511885 ±0.000011
$^{206}Pb/^{204}Pb$	21.361	23.879	23.166	19.810	17.251	17.143	16.539	17.038	18.869	17.909	-	18.388	18.341
$^{207}Pb/^{204}Pb$	15.795	15.988	16.020	15.707	15.554	15.529	15.172	15.538	15.636	15.617	-	15.713	15.766
$^{208}Pb/^{204}Pb$	41.637	44.113	43.031	40.610	36.719	37.521	37.262	37.217	43.392	38.506	-	42.013	39.166
$\delta^{18}O$	-	-	-	-	15.55	15.26	-	-	-	-	-	15.50	16.30
$\delta^{13}C$	-	-	-	-	-3.03	-3.18	-	-	-	-	-	0.20	0.07

	GD2[1]	GD4[1]	GD1A[1]	GD1B[1]	GD5[1]	H3	H4	H11	H17
	Lamprophyres		Carbonatites						
$^{87}Sr/^{86}Sr$	0.702830 ±0.000012	0.703180 ±0.000010	0.702619 ±0.000013	0.702678 ±0.000025	0.702716 ±0.000013	0.703440 ±0.000013	0.704102 ±0.000016	0.702825 ±0.000013	0.702915 ±0.000013
Nd (IDMS)	-	-	796.25	1148.4	524.50	12.873	14.908	-	10.345
Sm (IDMS)	-	-	86.45	123.93	52.63	2.981	3.280	-	2.699
$^{143}Nd/^{144}Nd$	-	-	0.511576 ±0.000012	0.511579 ±0.000011	0.511432 ±0.000020	0.511658 ±0.000017	0.511506 ±0.000013	-	0.512063 ±0.000010
$^{206}Pb/^{204}Pb$	21.887	22.404	17.265	18.302	17.272	-	17.162	-	16.568
$^{207}Pb/^{204}Pb$	15.766	15.785	15.539	15.554	15.473	-	15.442	-	15.228
$^{208}Pb/^{204}Pb$	41.242	43.381	37.089	36.707	37.493	-	36.506	-	35.972
$\delta^{18}O$	-	-	-	13.43	12.57	7.27	7.13	7.01	7.53
$\delta^{13}C$	-	-	-	-4.77	-4.94	-2.83	-2.67	-2.66	-2.67

[1]: Samples analysed under the author's supervision as part of an Honours project by R.L.Stedman, 1987.

Table B.26: Isotopic data for mineral separates and xenoliths from the Stukpan carbonatite.

Sample	Rb[1]	Sr[1]	$^{87}Rb/^{86}Sr$	$^{87}Sr/^{86}Sr$[2]	
Phlogopite					
H3m	253.4	22.76	34.31	1.374910	(60)
H4m	261.5	9.943	88.80	2.40748	(13)
H8m(g)	282.8	18.45	48.25	1.60625	(7)
H8m(p)	284.2	5.864	191.1	4.4530	(2)
H17m	264.5	45.20	17.50	1.0393	(9)
Calcite					
H3c	0.106	1558	0.0002	0.702613	(24)
H4c	0.372	1681	0.0006	0.702748	(23)
H8c	0.0330	1592	0.0002	0.702619	(17)
H11c	0.0196	1594	0.0000	0.702720	(33)
H17c	0.784	1571	0.0014	0.702632	(15)

Sample	Rb[1]	Sr[1]	$^{87}Rb/^{86}Sr$	$^{87}Sr/^{86}Sr$[2]	
"Amphibolite" xenoliths					
H1x	184.4	520.2	1.0292	0.742545	(14)
H12x	45.52	101.9	1.3000	0.765715	(12)
H13x	115.3	97.42	3.4600	0.814078	(15)
H18x	60.89	298.2	0.5918	0.725702	(14)
H19x	32.30	379.0	0.2464	0.713167	(14)

1 : Analyses by IDMS.
2 : Precisions are 2 standard errors of the mean and refer to the least significant figures.